The International Conference on Energy and Sustainable Futures (ICESF)

Nottingham Trent University, Nottingham, 9 to 11 September 2019
In collaboration with University Alliance and Doctoral Training Alliance for Energy

Edited by
Amin Al-Habaibeh, Abhishek Asthana, Vladimir Vukovic

Nottingham Trent University: Publications

Published by Nottingham Trent University: Publications
Nottingham Trent University, 50 Shakespeare Street, Nottingham NG1 4FQ

2019
ISBN 978-1-912253-01-2 (paperback)
ISBN 978-1-912253-02-9 (eBook)

Production of the ICESF 2019 proceedings is sponsored by

UKUD®

www.ukud.co.uk

Supporting Students into Higher Education

Preface

The effect of global warming and the increase in the levels of greenhouse gases can no longer be ignored. In the summer of 2019 the heat wave in Europe has caused an increase in temperatures in many countries reaching above 40^{o}C. 2019 continues to be globally the hottest June on record, and in July 2019, the UK's highest temperature on records has been officially recorded in Cambridge. Improving the way energy is produced, transported and consumed is becoming very important if we want to have a sustainable and environmentally friendly style of living.

The motivation to reduce carbon emission and global pollution has attracted many countries to adopt renewable energy as a future energy strategy, combined with sustainable consumption behaviour. Most countries aim to reach zero net emissions of greenhouse gases by the second half of this century. This means significant research is needed in a wide range of energy disciplines to achieve such an ambitious target.

Research in academia and industry is evolving to deliver the sustainability and energy requirements for the future. The International Conference on Energy and Sustainable Futures (ICESF) organised by Nottingham Trent University (NTU) in collaboration with Doctoral Training Alliance for Energy (DTA-Energy) and University Alliance presents some of the state-of-the-art research that is being done in this field. The conference is intended for experts in energy and sustainability from industry and academia, research students and early career researchers. This proceedings includes multi-disciplinary papers focused on academic research, industrial applications, and energy innovations and it includes a wide range of energy and sustainability themes such as renewable and clean energy, energy storage, energy management, transportation technology, internet of things, sustainable and resilient cities, condition monitoring and artificial intelligence.

I hope the International Conference on Energy and Sustainable Futures will inspire and motivate our readers to play an important role in future development in the energy and sustainability sector.

Amin Al-Habaibeh

International Conference on Energy and Sustainable Futures

ICESF

Nottingham | UK | 9–11 September 2019

Organised by

NTU NOTTINGHAM TRENT UNIVERSITY

DTA Doctoral Training Alliance Energy

UA University Alliance Doctoral Training Alliance

In collaboration with

Teesside University

University of South Wales

uclan University of Central Lancashire

Manchester Metropolitan University

Coventry University

UNIVERSITY of GREENWICH

UNIVERSITY OF PORTSMOUTH

The Open University

University of Brighton

University of Salford MANCHESTER

University of Hertfordshire UH

Sheffield Hallam University

energy institute Learning Affiliate

Kingston University London

Knowledge Transfer Network

Conference Executive Committee

Amin Al-Habaibeh

Arijit Sen

Deepti Mahajan

George Milev

Giorgio Cucca

Sherna Salim

Conference Organising Committee

Abhishek Asthana, Sheffield Hallam University

Amin Al-Habaibeh, Nottingham Trent University

Arijit Sen, Nottingham Trent University

Ashfaque Alam, Sheffield Hallam University

Babatunde Giwa, University of Greenwich

Ben Diette, University Alliance

Delano Henry, Kingston University

Deepti Mahajan, Nottingham Trent University

Gavin Gillmore, Kingston University

George Milev, Nottingham Trent University

Giorgio Cucca, Nottingham Trent University

Hua Zhong, Nottingham Trent University

Ifrah Mussa, Kingston University

James Eales, Sheffield Hallam University

Jennie Eldridge, University Alliance

Jessica Rigby, Sheffield Hallam University

Martina Bella, University of Greenwich

Matthias Pilz, Kingston University

Nneka Daniel, University of Greenwich

Olatunde Olide, Coventry University

Prince Rautiyal, Sheffield Hallam University

Sam Capp, Manchester Metropolitan University

Sherna Salim, Nottingham Trent University

Supattra Maneen, University of Greenwich

Ukairo Okorie, Kingston University

Vladimir Vukovic, Teeside University

Conference Scientific Committee

Prof Amin Al-Habaibeh, Nottingham Trent University

Dr Amir Nourian, University of Salford

Dr Andrew Oyen Arewa, Coventry University

Dr Anastasios Georgoulas, University of Brighton

Dr Antonios Kanellopoulos, University of Hertfordshire

Dr Chris Ennis, Teesside University

Dr Daniel Shin, Nottingham Trent University

Prof David J Timson, University of Brighton

Dr Dong-Wook Kwak, Coventry University

Dr Fengge Gao, Nottingham Trent University

Dr Georgios Pissanidis, University of Hertfordshire

Dr Helen Roby, Coventry University

Dr Iosif Mporas, University of Hertfordshire

Dr Jonathan Nixon, Coventry University

Dr Jovana Radulovic, University of Portsmouth

Dr Kary Thanapalan, University of South Wales

Dr Luluwah Al-fagih, Kingston University

Dr Michael Short, Teesside University

Dr Olivier Haas, Coventry University

Dr. Ruchira Yapa , Uclan University

Dr Seyed Mohammad Shariatipour, Coventry University

Dr Will Eadson, Sheffield Hallam University

Dr Yehdego Habtay, University of Greenwich

Table of Contents

Nottingham | UK | 9–11 September 2019

iWindCR: A remote corrosion detection and monitoring system for offshore wind turbine structures

N. Bausch [3], J.I. Ahuir-Torres [2], A. Farrar [1], S. Webb [1], S. Simandjuntak [2], J.I. Ahuir-Torres [2], A. Nash [4], B. Thomas [4], J. Muna [5], C. Jonsson [5], D. Mathew [5]

[1] *School of Energy and Electronic Engineering*

[2] *School of Mechanical and Design Engineering*

[3] *School of Energy and Electronic Engineering, University of Portsmouth, Anglesea Road, Portsmouth, PO1 3DJ, United Kingdom*

[4] *Avonwood Developments Ltd, Bournemouth, BH21 7ND, UK*

[5] *Avanti Communications PLC, London, EC4V 6EB, UK*

nils.bausch@port.ac.uk

Abstract

Remote location and arrangement of offshore wind turbines severely limits the application of in-situ non-destructive corrosion detection methods such as ultrasound, acoustic emission and X-Ray. A Real Time Remote Sensing (RTRS) system has been developed to implement autonomous detection and monitoring, providing exhaustive and detailed information on the corrosion process. Utilising the concept of Internet of Things (IoT) through the integration with satellite and terrestrial mesh network communication, *iWindCr,* a technology development project funded by the Innovate UK, aims to design a Wireless Sensor Network (WSN) of smart miniaturised sensors for corrosion detection and monitoring of the offshore wind turbine structures.

Keywords: Offshore, wind turbine, corrosion sensor, electrochemical techniques (OCP and ZRA), Wireless Sensor Network (WSN), Real Time Remote Sensing (RTRS), IoT

1. Introduction

Wind energy is recognised worldwide as a proven technology to meet an increasing demand in electricity, with its added benefit of being renewable. The UK's geographical location makes it ideal for wind energy, accounting for its status as a world leader in the sector (>£21bn estimated invested by 2020, UKTI 2014) [1-4]. The offshore wind turbine (WT) structures and the choice of materials for those structures such as the foundation, platform and tower as well as the turbine parts or nacelle (gearbox and generator) have to consider the harsh conditions generated from the environment that they will be subjected and exposed to [4-8].

The remote geographical locations and positioning of critical parts of a WT, for example its nacelle and blades, makes it unique and challenging for the servicing and maintenance. For example, the environment inside the nacelle of the offshore WTs is different to that of onshore WTs. Robinson, et al. [11] mentioned that the combined total failures of rotors, air brakes and mechanical brakes for onshore WTs make up for up to 22% of the total of subassembly failures, which could be initiated and/or accelerated by the corrosion process.

The work reported on was part of the *iWindCr* project, which was a technology development project funded by Innovate UK. *iWindCr* aimed to design a wireless smart miniaturised sensor network (WSN) for corrosion detection and monitoring. It utilised the concept of Internet of Things (IoT) to integrate the WSN with satellite and terrestrial communication networks, providing a guaranteed data backhaul from remote wind-farm sites to a control room. By monitoring the backhauled data, the output data can then be used as an indication and reference to identify event time and corrosion type.

This conference paper has three sections. The first section presents the corrosion detection techniques that were identified to be of use on WTs. The second part discusses the rationales and challenges around the design of the sensor interface system. The final section reports on the database created and used in the *iWindCr* project.

2. Corrosion processes and detection methods selected for iWindCR

Due to their specific operating conditions and exposed environment, the offshore WT structures would be more likely to experience wet corrosion. From the type of attack, [14] wet corrosion can be classified as uniform or localised. The uniform attack is considered less harmful for metallic materials because it commonly generates a non-uniform or loose oxide or passive film that could slow down further corrosion of the bulk material.

The uniform corrosion is easily identifiable due to its wider attack area. The localised corrosion is more difficult to detect due to its confined nature on a metal surface and the ability to penetrate deeper through the thickness of the parts producing sharply defined holes.

Autonomous techniques and solutions are needed to provide exhaustive and detailed information on the corrosion process that are reliable and cost effective. The application of Real Time Remote Sensing (RTRS) technology would have the means to perform such tasks [6,9,10,12,13,15]. The electrochemical analysis techniques can therefore be adapted onto the sensor system in order to measure the changes for example through the measurements of current, resistance or the electrode potential between the surface of the metals (cathode) and a certain standard reference which could well be another metal (anode). The selected techniques therefore are the Open Circuit Potential (OCP), and the Zero Resistance Ammeter (ZRA) [13,14,16,17].

The **OCP** is often referred to as the equilibrium potential or the rest potential. A passive sensor detects and responds to the input from the physical environment without the need of an external power source to operate. This method can be used to determine the potential distribution on the corroding surfaces that can be used to distinguish whether the corrosion system is in an active or in passive state. The OCP method measures the electrode potential, as a function of temperature and concentration of the oxidised and reduced solutions.

The **ZRA** is a non-destructive and passive electrochemical technique that can measure directly the current density in the corrosion system by only considering the stable current density measurements.

3. Designing *iWindCr* WSN: Rationales and Challenge

Many studies on maintenance strategies of the WTs that have been conducted used the historical failures of certain structures/parts as references, from which the approach of many WT operators currently is based on, i.e. to go through maintenance (repair) about two times a year [18,19,20]. The Dutch Agency for Energy and Environment, for example, has proposed a targeted service demand of a visit once per 12-18 months [18], to reduce costs. The *iWindCr* WSN is therefore aiming for a design life of 3-5 years.

Considering the *iWindCr* deployment plan, see Figure 1, access to and locating a power source for the WSN are relatively difficult. To ensure a reliable and safe operation, the Original Equipment Manufacturer (OEM) is normally very specific and strict with respect to the installation and operation of their parts/products [7,11,18]. It is therefore the *iWindCr* WSN chose for a stand-alone system that would not interfere with the other WT systems. The use of a small battery was considered to provide enough power to each WSN system node over a defined period of operation (i.e. 3-5 years).

After several design iterations, the prototype of the sensor interface was created, taking into account a component selection that favoured low power requirements for conducting the measurement i.e. taking a number of readings at certain time intervals and for sending the data to the communication gateway that will in turn relay the data to a backend database via satellite and finally present the data through a user interface. Lab experiments were used to determine the optimum number of data points needed to collect per measurement for the OCP and ZRA analysis. The tests showed that stable outputs could be obtained by the sensor when using OCP with a minimum of 30 readings per one measurement and with the acquisition time in the area of 120 seconds. With the current design and power, the WSN could take up to 12 measurements per day, but due to corrosion being a relatively slow process, this was then reduced to one measurement of each method per day.

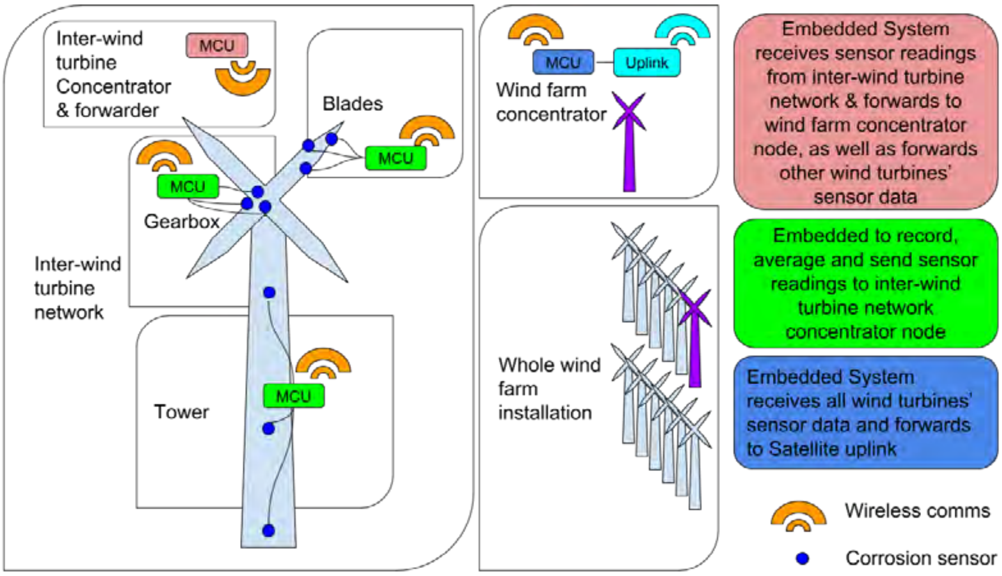

Figure 1: iWindCr WSN system for corrosion detection and monitoring – Deployment diagram.

4. Corrosion outputs/parameters database

The database for *iWindCR* consists of the corrosion parameter outputs or threshold values to provide end users with a benchmark for corrosion detection and monitoring purposes. The database will also be integrated in the data analytics of the *iWindCr* user interface. With this information, the type of corrosion as well as corrosion rate or remaining life of a monitored component can be determined. The outputs OCP and ZRA can then be used to inform the WT end-users when a general corrosion or localised corrosion takes place. In addition, using the ZRA provided data, the measured current can be used to evaluate the rate of material loss due to corrosion and therefore aid in life prediction calculations.

5. Conclusion

The *iWindCr* project aimed to design an IoT WSN system for autonomous corrosion detection and monitoring of offshore WTs. This was achieved through the implementation of a Real Time Remote Sensing (RTRS) technological implementation utilising electrochemical sensor as there are limitations with the use of in-situ techniques with regards to the access for operators and to a power source. The electrochemical sensors instead would allow to remotely monitor the physical and electrochemical changes that take place on the metallic materials. The non-destructive and passive electrochemical techniques such as OCP and ZRA are integrated into the sensor interface of the WSN. Choosing these passive techniques helped reduce the power requirements.

In addition a database of the corrosion parameter outputs and threshold values of the metallic alloys and their relevant environments specific to offshore WTs structures has been created and is used as a benchmark for the corrosion detection and monitoring by the end-users.

Although the work reported here mainly focuses on offshore WT structures, the proposed WSN should be feasibly applicable for other engineering structures in other sectors such as oil and gas, marine, automotive and aeronautics.

Acknowledgments

This work was supported by the Innovate UK *iWindCr* Project (Grant Number 103504) and co-funded by the commercial partners Avonwood Development Ltd and Avanti Communication Plc. The authors would like to acknowledge the Faculty of Technology and the School of Mechanical and Design Engineering, University of Portsmouth, for their support.

References

1 Estate C. A guide to an offshore wind farm. Power. 2010:1-g0.

2. Government U. UK Offshore Wind: Opportunities for trade and investment. In: Trade DfI, ed. UKTI. 2015.

3. Government U. Overview of Support for the Offshore Wind Industry. In: Government H, ed. https://www.gov.uk/government/publications?official_document_status=command_and_act_papers. 2014.

4. Higgins P, Foley A. The evolution of offshore wind power in the United Kingdom. Renewable and Sustainable Energy Reviews. 2014;37:599-612.

5- Janssen L, Lacal-Arántegui R, Brøndsted P, et al. Scientific Assessment in support of the Materials Roadmap enabling Low Carbon Energy Technologies: Wind Energy. JRC Scientific and Technical Reports No. EUR. 2012;25197.

6. Pawsey C. Corrosion Protection for Offshore Wind, Prevention and Aftercare: Meet the Industry Players. 4th International Conference Corrosion Protection for Offshore Wind; 2016; Berlin, Germany.

7. Van Bussel G, Henderson A, Morgan C, et al. State of the art and technology trends for offshore wind energy: operation and maintenance issues. Paper presented at: Offshore Wind Energy EWEA special topic conference. 2001.

8. DNVGL-RP-0416. Corrosion protection for wind turbine. Norway, DNV GLMarch, 2016.

9. Zaher A, McArthur S, Infield D, Patel Y. Online wind turbine fault detection through automated SCADA data analysis. Wind Energy. 2009;12(6):574-593.

10. Schlechtingen M, Santos IF. Comparative analysis of neural network and regression based condition monitoring approaches for wind turbine fault detection. Mechanical systems and signal processing. 2011;25(5):1849-1875.

11. Robinson C, Paramasivam E, Taylor E, Morrison A, Sanderson E. Study and development of a methodology for the estimation of the risk and harm to persons from wind turbines. Report, MMI Engineering Ltd, UK. 2013.

12. Hossain ML, Abu-Siada A, Muyeen S. Methods for Advanced Wind Turbine Condition Monitoring and Early Diagnosis: A Literature Review. Energies. 2018;11(5):1309.

13. Agarwala VS, Reed PL, Ahmad S. Corrosion detection and monitoring-A review. Paper presented at: CORROSION 2000.2000.

14. Uhlig HH, Revie RW. Uhlig's corrosion handbook. Vol 51: John Wiley & Sons; 2011.

15. Márquez FPG, Tobias AM, Pérez JMP, Papaelias M. Condition monitoring of wind turbines: Techniques and methods. Renewable Energy. 2012;46:169-178.

16. Gabrielli C, Keddam M. Review of applications of impedance and noise analysis to uniform and localized corrosion. Corrosion. 1992;48(10):794-811.

17. Papavinasam S. Electrochemical Techniques for Corrosion Monitoring. Corrosion Monitoring Techniques," L. Yang, Ed., Woodhead Publishing, Success, UK. 2008.

18. Scheu M, Matha D, Hofmann M, Muskulus M. Maintenance strategies for large offshore wind farms. Energy Procedia. 2012;24:281-288.

19. Van Bussel G, Zaaijer M. Reliability, availability and maintenance aspects of large-scale offshore wind farms, a concepts study. Paper presented at: Proceedings of MAREC. 2001.

20. Seyr H, Muskulus M. Value of information of repair times for offshore wind farm maintenance planning. Paper presented at: Journal of Physics: Conference Series. 2016.

ICESF
Nottingham | UK | 9–11 September 2019

A Novel Approach for the Assessment of Thermal Insulation in Buildings Using Infrared Thermography and Artificial Intelligence

Arijit Sen [1,3] and Amin Al-Habaibeh [2]

[1,2,3] *Innovative and Sustainable Built Environment Technologies Research Group (iSBET)*
Nottingham Trent University, UK,

arijit.sen2016@my.ntu.ac.uk

Abstract

Buildings consume high energy for space and water heating, and thereby contribute largely to greenhouse gas emission. Improving thermal insulation of buildings' envelop can significantly reduce energy consumption for space heating as well as decrease greenhouse gas emission. However, prior to the retrofitting of a building it is required to evaluate the current level of wall insulation to estimate the additional requirements. Infrared thermography is an effective tool in evaluating building's thermal performance when there is a reasonable temperature gradient between indoor and outdoor temperatures. This paper presents a novel approach of using low-resolution infrared camera with a single point heating system from which the thermal conductivity and thermal insulation of building's wall can be categorised and estimated. An experimental study has been conducted on different sample wall sections and Artificial Neural Network is used to analyse the infrared images of walls for categorisation based on the level of wall insulation. The results show significant accuracy in categorising the wall types based on their level of insulation from a set of infrared images.

Keywords: U-value, Artificial intelligence, Neural Network, Infrared Thermography, Insulation.

1. Introduction

It is necessary to develop strategies for reducing the energy consumption due to space heating of residential buildings. Retrofitting an existing building with improved wall insulation can reduce heat loss through the building's walls and consequently energy consumption for space heating. However, before the retrofitting, it is necessary to identify the current level of insulation, which is the U-value of the building's wall. The designed U-value of a building's wall is calculated as the reciprocal of the summation of thermal resistances of different layers of the wall [1].

$$U = \frac{1}{R_i + \frac{d_1}{k_1} + \frac{d_2}{k_2} + \cdots \ldots\ldots\ldots + R_e} \qquad (1)$$

Here, U is the U-value of the wall, k is the thermal conductivity of the materials in different layers of the wall, d is the thickness of the wall layers, R_i and R_e are the thermal resistance of air at internal surface and external surface respectively. To determine the U-value of an existing building's wall using equation (1), thermal conductivities of different layers of the wall are required to be determined. It can be done by conducting laboratory test on the samples collected by drilling the walls; which is a damaging process. There are several devices available to measure U-values of test specimen in laboratory; however, these often differ as high as 30% from the in-situ U-value [2]. There are two non-invasive methods existing for in-situ U-value measurement namely Heat Flux Meter (HFM) method and Infrared Thermovision Technique (ITT). Both techniques have their own limitations in relation to accuracy, time and environmental conditions. To overcome the limitations this paper proposes a novel approach for the categorisation of buildings' wall insulation based on the U-value by combining thermal images of walls and artificial intelligence with the application of single point heat source.

2. Methodology

An uninsulated wall has a high U-value and most of the applied heat will pass through it. Conversely, an insulated wall has a low U-value and most of the applied heat will disperse over the internal surface. The difference in the thermal response, while applying a point heat in the internal side of a test wall for a certain period, can be observed by monitoring the wall using a low-resolution infrared camera. The schematic diagram of the experimental set up is shown in Figure 1-a. The thermal profile generated from the infrared images is used to train an Artificial Neural Network (ANN) for categorisation of the wall type. ANN consists of neurons organised in layers which mimic the thinking process of a human brain. ANN can be trained to learn certain features of a data set, and based on the learning it can predict the output of a similar unknown input. Figure 1-b shows the architecture of a typical ANN. The experiment work is conducted twice on each wall type so that the data obtained from the first run of experiment could be used for training the ANN and the data obtained from the second run of experiment can be used to test the network performance.

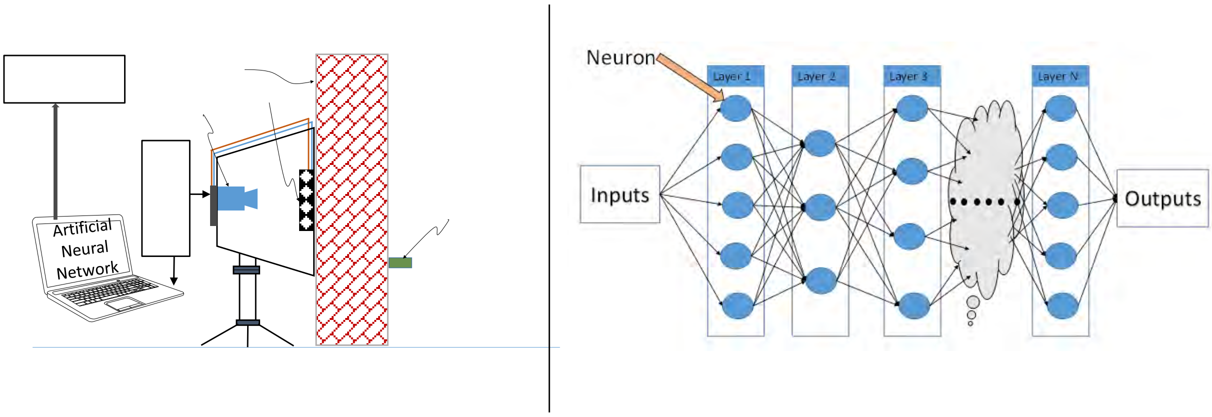

Figure 1: (a) Schematic diagram of experimental set up. (b) The architecture of a typical ANN

3. Experimental work

The experiments are conducted on four different wall samples made of brick, brick with external insulation, concrete block and concrete block with external insulation. EcoTherm board with a thickness of 100 mm is chosen as the external insulation for these walls. A plastic box fitted with a diesel engine glow plug attached to the internal side of the wall is used, combined with IRISYS 1002 infrared camera as in Figure 1-a. The glow plug acts as a point heat source and the infrared camera is set to capture 16x16 pixel infrared images at five seconds interval for about an hour. The glow plug's tip temperature as well as the ambient temperature are recorded with a K-type thermocouple and NI USB-TC01 data acquisition system at one second interval.

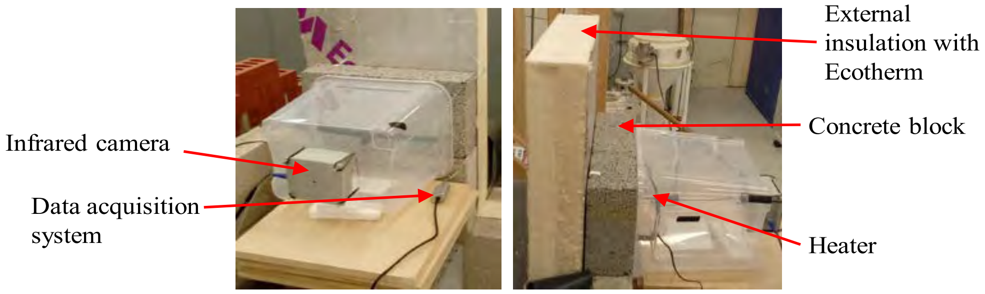

(a) (b)

Figure 2: Experimental work on C1 sample wall

Figure 2-a and Figure 2-b show the experimental work on one of the samples. The sample walls are represented as A1, B1, C1 and D1 for the first run of experiment and A2, B2, C2 and D2 for the second run of experiment. The properties of the sample walls are presented in Table 1. The U-value of the sample walls are calculated using equation (1) where the values of R_i and R_e is considered as 0.13 and 0.04 respectively [3]. The thermal conductivity of brick wall is taken as 0.27 W/mK [4], the thermal conductivity of concrete block is considered as 1.5 W/mK [5] and the thermal conductivity of the Ecotherm is 0.022 W/mK [6].

Table 1: Properties of wall sample used in the experiments.

Sample Number	Material	Thickness (mm)	Thermal Conductivity (W/mK)	U-value (W/m^{2}K)	Schematic view of sample wall
A	Brick	100	0.27	1.86	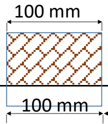
B	Brick insulated externally with Ecotherm	100+100 =200	0.27 & 0.22	1.01	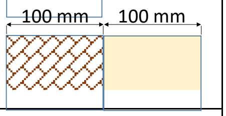
C	Concrete block	95	1.5	4.29	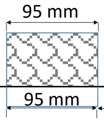
D	Concrete block insulated externally with Ecotherm	95+100 = 195	1.5 & 0.22	1.45	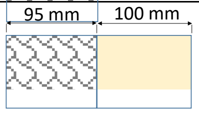

4. Results and Discussion

Sample D1 and D2 has lower U-values than sample C1; therefore, it is expected that the temperature profile of D1 and D2 will be higher than that of C1. The temperature profile of D2 is clearly higher than that of C1 in Figure 3-a. However, the temperature profile of D1 is marginally higher than that of C1 in Figure 3-b, because the ambient temperature was higher during the time of conducting experiment on C1 than on D1.

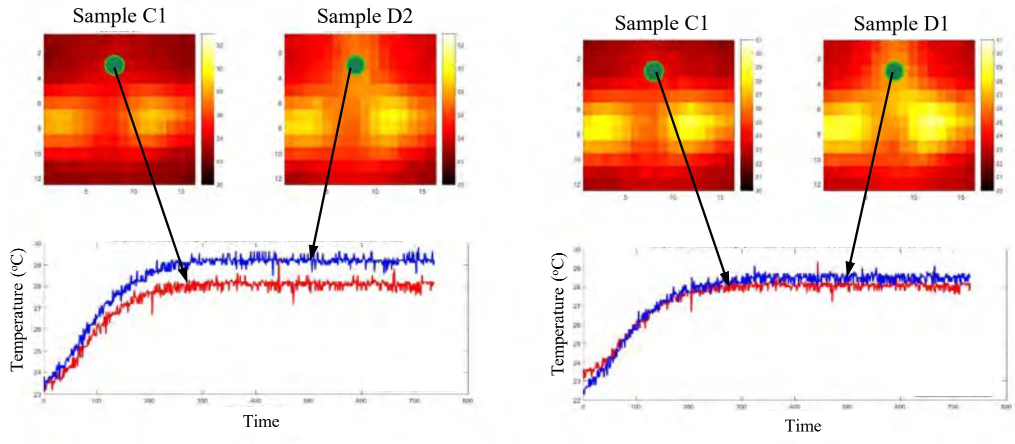

(a) (b)

Figure 3: Comparison of temperature profiles (a) sample C1 and D2, (b) C1 and D2

It is also found that the rate of temperature increase with time is higher in sample D1 and D2. Therefore, it is assumed that ambient temperature has a significant influence on the thermal profile and derivative of thermal profile is a key parameter to identify the characteristics of the thermal profile. Considering these assumptions, three modified profiles namely T^a, T^b and T^{ab} are developed, which are presented in equation (2), (3) and (4)

$$\boldsymbol{T}^{a}_{(i,j,k)} = \boldsymbol{T}_{(i,j,k)} - \boldsymbol{T}^{ext}_{k} \quad (2)$$

$$\boldsymbol{T}^{b}_{(i,j,k)} = \sum_{1}^{k}\left[\boldsymbol{T}_{(i,j,k+1)} - \boldsymbol{T}_{(i,j,k)}\right] \quad (3)$$

$$\boldsymbol{T}^{ab}_{(i,j,k)} = \sum_{1}^{k}\left[\boldsymbol{T}^{a}_{(i,j,k+1)} - \boldsymbol{T}^{a}_{(i,j,k)}\right] \quad (4)$$

Here $T_{(i,j,k)}$ is the original temperature value at pixel *(i,j,k)* on infrared image, $T^{a}_{(i,j,k)}$ is the modified temperature value of pixel *(i,j,k)* on infrared image, $T^{b}_{(i,j,k)}$ is the cumulative temperature difference at pixel *(i,j,k)*, $T^{ab}_{(i,j,k)}$ is the cumulative temperature difference of profile T^a and T^{ext}_{k} is the external temperature at the time of capture of the corresponding infrared image. A feed forward neural network with *softmax* layer is developed using pattern recognition app of MATLAB to categorise the wall types with profile T^b, T^{ab} and their standard deviations as the input parameters and wall type as the output parameters.

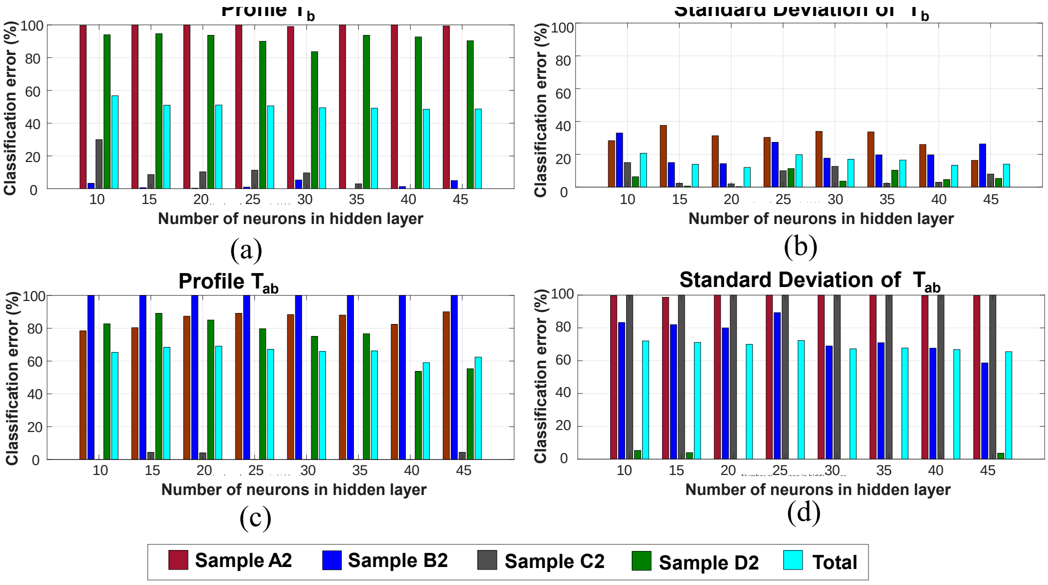

(a) (b) (c) (d)

Figure 4: Percentage error of categorisation

Figure 4-a to Figure 4-d represent the percentage error in categorising the samples A2, B2, C2 and D2 with 10 ,15, 20, 25, 30, 35, 40 and 45 neurons in hidden layer. It is found that the standard deviation of profile Tb shows the least percentage error compare to other profiles. The probable reason for that is the standard deviation represents the dispersion in thermal profile more significantly than the profile itself. Profile Ta was developed by deducting the ambient temperature from the original temperature profile, which probably reduced the variation that characterise the temperature profile; and hence the percentage error in categorisation from profile Tab and the standard deviation of Tab become very high. It is also found from Figure 4-b that ANN with 20 neurons in hidden layer gives the lowest total error which is 12% with the error in detecting A2, B2, C2 and D2 are 31%, 14%, 2% and 0.33% respectively.

5. Conclusion

Retrofitting of residential buildings with improved wall insulation could significantly reduce the energy consumption for space heating; however, in-situ U-value of walls should be considered before retrofitting as over insulation could be expensive with low payback period. The existing methods of U-value estimation have some limitations. Therefore, a novel approach is proposed to categorise a building's wall based on the U-value by combining thermal image and ANN with the application of point heat. The result shows the suitability of feed forward neural network in categorisation of walls from thermal profile developed by analysing thermal images. ANN with 20 neurons in hidden layer achieved 88% overall classification accuracy with a minimum 69% for any particular wall type.

References

[1] Gaspar K, Casals M and Gangolells M (2016) A comparison of standardized calculation methods for in situ measurements of façades U-value. Energy and Buildings 130: 592–599.

[2] Doran S (2001) DETR Framework Project Report :Safety and Health Business Plan Field investigations of the thermal performance of construction elements as built [Online]. Available: http://projects.bre.co.uk/uvalues/U-values.pdf. [Accessed: 17-Feb-2017].

[3] Anderson B (2006) Conventions for U-value calculations, 2006 edition. BRE Press, Scotland UK.

[4] Antoniadis K D, Assael M J, Tsiglifisi C A and Mylona S K (2012) Improving the Design of Greek Hollow Clay Bricks. International Journal of Thermophysics 33 (12): 2274–2290.

[5] ISO 10456 (2007) Building materials and products — Hygrothermal properties — Tabulated design values and procedures for determining declared and design thermal values. [Online]. Available: http://www.superhomes.org.uk/wp-content/uploads/2016/09/Hygrothermal-properties.pdf. [Accessed: 14-May-2018].

[6] EcoTherm (n.d) EcoTherm Rigid Thermal Insulation Boards. [Online]. Available: https://www.ecotherm.co.uk/about-us/features-benefits. [Accessed: 29-Apr-2019].

Nottingham | UK | 9–11 September 2019

Resources Management for Urban Sustainability in the Global South

Yesmeen Khalifa [1], Dr Sharon George [1], Dr Philip Catney[2]

[1]*School of Geography, Geology and the Environment, Keele University, Staffordshire, UK , ST5 5BG*

[2]*School of Politics, Philosophy, International Relations and Environment, Keele University, Staffordshire, UK , ST5 5BG*

y.a.khalifa@keele.ac.uk

Abstract

In order to be truly effective, the strategies pursued to achieve sustainable development must be tailored to fit with the unique characteristics in which they are being developed and implemented. This paper examines the potential for measuring the flow of materials for the creation of robust urban sustainability strategies for a fast-growing city. To this end, we examine complex issues of resources management in Cairo (Egypt) as an example of such challenges in a rapidly urbanizing Global South's city. The research considers cities both as consumers of primary resources (renewable and non-renewable resources) and producers of secondary resources (waste and wastewater). In terms of policy practice and academic research, the ability to measure, assess and control these resources is crucial for improving the sustainability performance of developing countries. Yet a key challenge to this ambition is the lack of reliable data and the difficulty of tracking the flow of materials in the Global South, particularly in rapidly urbanizing cities with significant growth of unplanned, informal settlements. The proposed study examines these resources by utilizing two principal data gathering methods: 1) a quantitative data collection to fill an existing indicator set; and 2) qualitative interviews with representatives from public authorities and site visits. This tests the applicability of the existing tool to understand the unique characteristics of Cairo, drivers and barriers to sustainable resources management.

Keywords: Resource management, Sustainable development, Urbanization, Urban metabolism, Informal flow of materials.

1. Introduction

For the first time in history, the percentage of the urban population exceeded the rural population in 2007 [1]. The urban population will continue to grow and is projected to reach seventy percent within the next thirty years; this presents a significant challenge [2]. Yet the urbanization process is unevenly spread, being particularly concentrated in the Global South and in particular city-regions. All types of cities are projected to increase, and the number of megacities will reach 41 by 2030, of which 27 will be located in the Global South [2]. Such intense urbanization adds urgency to focus on ways of making such cities more sustainable, specifically the ones located in the Global South.

The challenges in cities in middle and low-income countries in Africa and Asia are daunting with rapid and uncontrolled growth of urban populations leading to increased land use without parallel social and economic growth. Such trends hamper the ability of these cities to absorb these growth pressures [1]. These issues are compounded by the additional challenges of resource scarcity and climate change. Both present considerable challenges for urban sustainability in the Global South. Such states and cities lacking the resources necessary to accommodate the expansion of existing cities or to build new cities to meet the demands placed upon them. They also lack the capacity to effectively manage resources and their greenhouse gas emissions, contributing to significant environmental impacts.

Effective resource management is crucial for these countries to reduce their use of primary resources (such as fossil fuels), environmental impacts and maximize the use of renewable energy and secondary resources (such as solid waste and wastewater). Resource management requires quantifying, assessing, and controlling the flow of materials and energy resources. In the Global South's cities, policy practitioners and academic researchers alike are confronted by the problems of tracking the flow of materials due to the uncontrolled growth of cities, the lack of reliable data at the city level, and the methods of data collection which are not consistent [3].

2. Case study: Cairo, Egypt

This study is focused on how to develop strategies to improve resources management in Cairo as an example of a rapidly urbanizing Global South's city, and to understand the potential limits to the uptake arising from its governance issues. The population of the Cairo Governorate is 10 million inhabitants and it is located in the heart of the Greater Cairo Metropolitan Area of more than 20 million [4] (see figure 1).

Figure 1: Map of Egypt [5].

As a developing country, Egypt is facing massive challenges due to its rapid urbanization. National and local authorities in Egypt struggle to provide the basic requirements of the city's inhabitants and adequate services to absorb its rapid rate of growth. The consequences of the largely unchecked rapid urbanization have been a persistent shortage of housing, the growth of informal settlements, increased waste production and excessive use of resources such as water. Altogether added more pressure on the country's fragile infrastructure, exacerbated social inequalities, and further degraded environmental quality contributes to the unsustainability of the city-region.

3. Research aim and methodology

This study outlines the potential of measuring the flow of materials for the creation of robust urban sustainability strategies for a fast-growing city, Cairo. Cities are both consumers of primary (input) resources (for example, energy, electricity, and water) and producers of secondary (output) resources (for example, solid waste and wastewater). Secondary resources will increase due to the growth of human activities and urbanization [6]. These resources are examined in this study by using an existing "multi-layered indicator set" tool [7] which involves collecting and inputting existing published data from government documents and filling gaps and providing context to published data with interviews with appropriate leaders in Egypt and site visits (low, medium and high-density settlements). To further understand the challenges of the Cairo Governorate, the same data was collected for Giza and Qalyubia Governorates. The three governorates are the constituents of the Greater Cairo Region. Additionally, the data of the three governorates have been compared with the whole country (Egypt), to ascertain and quantify, where possible, specific challenges and differences. This tests the suitability and applicability of the existing tool to understand the unique characteristics of Cairo, drivers, and barriers to sustainable resources management.

4. Results and Discussion

The total area of the Greater Cairo Region is almost 3.3 thousand square kilometres of which 48% is located in the Cairo Governorate, 47% in Giza and 5% in Qalyubia as shown in figure 2 [8].

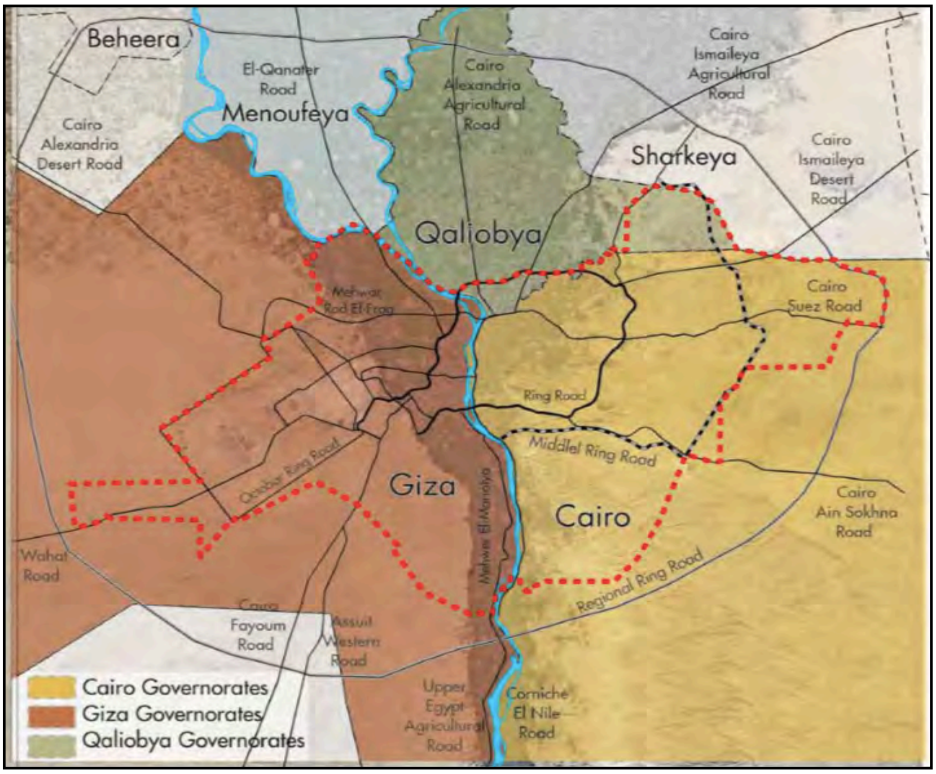

Figure 2: Cairo, Giza, Qalyubia & the boundaries of the Greater Cairo Region (GCR) [8].

In 2016, the total population of Egypt was more than 90 million, with a quarter of the population living in Cairo (10%), Giza (9%) and Qalyubia (6%). The average annual population growth rates of the three governorates and Egypt from 2001 to 2016 were calculated to compare the rates of growth. Giza (3.17%) and Qalyubia (2.77%) have the highest growth rates and the Cairo Governorate (1.91%) is below the average growth rate of Egypt (2.55%). The overall growth rates of the three governorates and Egypt are considered high compared to cities in developed countries. For example, the average annual growth rate of Tokyo is 0.6%, New York and Los Angles is 0.3% over the 16-year period from 2000 to 2016 [9]. If the Cairo and Giza Governorates continue to grow current rates, both will become megacities within the next few years. This only adds more pressure on the existing infrastructure and resources consumption. Although the average annual growth rate of the Cairo Governorate was the lowest from 2001 to 2016, it has the highest inhabited density (population/sq.km) compared to Giza, Qalyubia and the overall average of Egypt (fig.3).

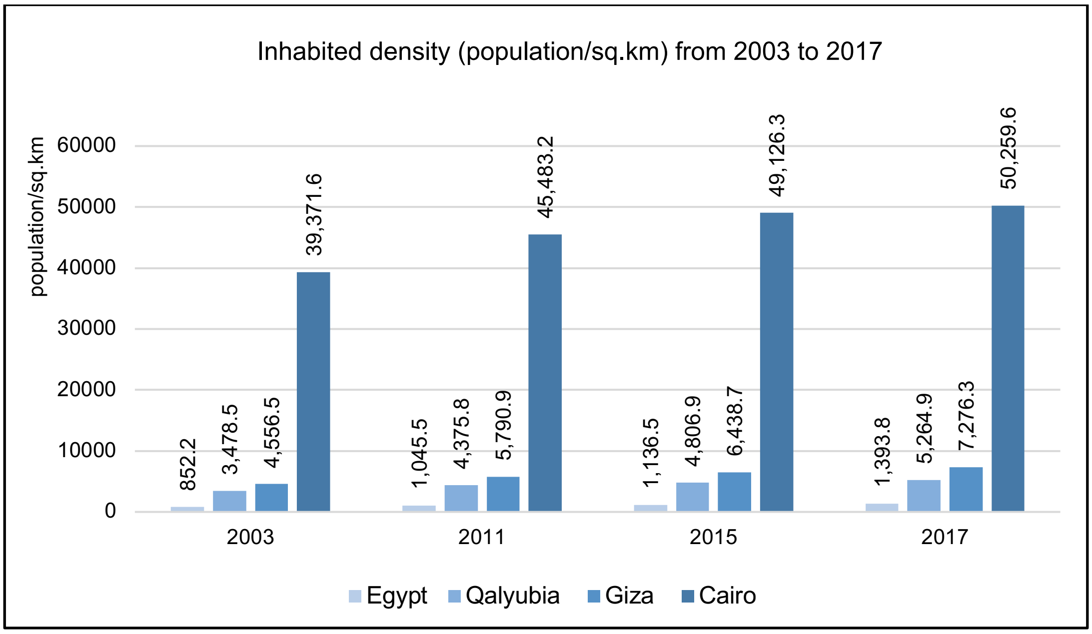

Figure 3: The inhabited density (population/sq.km) of the three governorates and Egypt from 2003 to 2017.

This explains the high percentage of resources consumption in the Cairo Governorate as its electricity consumption was 17% of the total consumption of Egypt in 2015-2016, 22% of the drinking water consumption in 2015-2016, 26% of the solid waste production in 2012 (the most recent and accurate data) and 26% of wastewater production in 2011 (the most recent and accurate data). Additionally, with the Cairo Governorate being the capital of Egypt, the percentages of the coverage of basic services is high compared to the average coverage of Egypt. An additional challenge for the Cairo city-region is its extensive informal settlements, which are not connected to the main electricity grid and drinking water network, or are connected illegally. These informal connections weaken the existing infrastructure and increase the loss of electricity and water resources. The Cairo Governorate is similar to most of the cities in developing countries as it mainly relies on one or two types of traditional fuels with a low share of renewable energy. The Cairo Governorate does not produce any type of energy and relies on other governorates to meet its energy demand. To be able to transform the Cairo Governorate into a self-sustaining city, the secondary resources (solid waste and wastewater) need to be upgraded and fed back into the city to reduce the use of primary resources and reduce the environmental impacts of the secondary resources when left without treatment. Additionally, the share of renewable energy resources must be increased. However, the urban density and the nature of urban form has to be considered because the distributed systems (PV and solar panels) are not suitable for the urban settlements in the Cairo Governorate.

5. Conclusion

Sustainable development requires tailored strategies to fit successfully in a particular place, as each region, country or city has its own characteristics that differ from one place to another and shapes its unique identity. These characteristics must be understood and considered to promote effective sustainable development strategies. To overcome the lack of reliable and accurate data, multiple sources of data are required to measure and assess the flow of materials and the informal flow of materials in the Global South must be considered. The customized tool developed from this research could be used in other countries to explore the flow of resources in different contexts and scales (neighbourhood, local, national, regional or global).

References

1. United Nations 2014, World Urbanization Prospects, the 2014 Revision, United Nations, New York.
2. United Nations 2016a, October-last update, The New Urban Agenda - Habitat III. Available: http://habitat3.org/the-new-urban-agenda/ [2019, 26 January].
3. Currie, P.K. & Musango, J.K. 2017, "African Urbanization: Assimilating Urban Metabolism into Sustainability Discourse and Practice", Journal of Industrial Ecology, vol. 21, no. 5, pp. 1262-1276.
4. CAPMAS 2019, Current Population. Available: https://www.capmas.gov.eg/ [2019, 26 January].
5. United Nations 2012, March-last update, General maps, Egypt. Available: https://www.un.org/Depts/Cartographic/map/profile/egypt.pdf [2019, 22 May].
6. Agudelo-Vera, C., Mels, A., Keesman, K. & Rijnaarts, H. 2012, "The Urban Harvest Approach as an Aid for Sustainable Urban Resource Planning", Journal of Industrial Ecology, vol. 16, no. 6, pp. 839-850.
7. Kennedy, C., Stewart, I.D., Ibrahim, N., Facchini, A. & Mele, R. 2014, "Developing a multi-layered indicator set for urban metabolism studies in megacities", Ecological Indicators, vol. 47, pp. 7-15.
8. GOPP 2012, Greater Cairo Urban Development Strategy, Part 1: Future Vision and Strategic Direction, The General Organisation for Physical Planning, Egypt.
9. United Nations 2016b, The World's Cities in 2016, United Nations, New York.

Nottingham | UK | 9–11 September 2019

Comparing Methane Yields of Washed and Unwashed Summer- and Spring Harvested *Sargassum muticum*

A. Supattra Maneein[1], B. Dr. John Milledge[1], C. Dr. Birthe Nielsen[1]

[1]*Algae Biotechnology, University of Greenwich, Chatham Maritime, ME4 4TB, UK*

sm8149w@gre.ac.uk

Abstract

Biogas production from Sargassum muticum (SM), an invasive seaweed species, is limited by low methane (CH4) yields which could be partly due to the presence of potential inhibitors of anaerobic digestion (AD). The impact of washing spring and summer harvested SM with water on CH4 yield was investigated. There was no statistical significance between washed and unwashed spring and summer SM at the end of a 28-day biochemical methane potential test. However, washing increased the rate of CH4 production after 10 days of AD for summer harvested SM, while decreasing the initial rates for spring harvested SM. Hence, initial removal of potential inhibitors in summer SM using water prior to AD could present a favourable biorefinery approach.

Keywords: Seaweed; biogas; biofuels; water extraction; washing.

1. Introduction

Sargassum muticum (SM) is an invasive brown seaweed species that poses economic and environmental issues [1]. Seaweeds are known to contain high-value products such as polysaccharides and polyphenols with pharmacological value [2]. Hence, the valorisation of this seaweed can have positive implications.

Anaerobic digestion (AD) for biofuel production is a versatile and suitable method of obtaining biofuels from wet biomass such as seaweed [1]. However, methane (CH_4) yields currently obtained from SM is 17% of the theoretical CH_4 yield [1]. This could be due to the recalcitrance of seaweed to hydrolysis during AD and/or possible inhibitors of AD present in seaweed, including high contents of polyphenols and proteins [3,4].

Extractions of high-value products that also results in an increase in CH_4 yield can increase the economic favourability of this process in a biorefinery approach, with water being an ideal solvent, for food grade purposes, and has been used to extract polyphenols [5,6]. The effects of water washing, rather than extraction, on CH_4 yields and recovery of potential high-value products have rarely been investigated [7]. This research aims to determine the effect of extensive washing of spring and summer harvested SM using water on AD.

Furthermore, although seasonal differences in CH_4 yields and composition have been revealed in seaweeds [3], differences in the effects of washing between the two seasons have not been shown. Hence, this research aims to elucidate any differences in CH_4 yields between washed and unwashed spring and summer harvested SM.

2. Experimental Method

2.1. Seaweed Collection and Treatment

Spring-harvested SM was collected in April 2018 (Ramsgate, UK) while summer-harvested SM was collected in July 2018 (Broadstairs, UK) (herein referred to as spring SM and summer SM, respectively). SM from both seasons were rinsed with distilled water to remove sand and any residues from the seawater. The thallus of SM was stored at -18 ℃ before freeze-drying (FD) at -55 ℃ for 48 hours. FD SM was ground using a coffee grinder to a fine powder.

10 g of summer and spring SM was mixed in 100 mL deionised water (dH_2O) and centrifuged (3,900 rpm, 20 minutes). The supernatant was collected and the procedure was repeated on the pellet 5 times to ensure a thorough wash.

2.2. Biochemical methane potential (BMP) determination

BMP tests are used to calculate CH_4 production potential of different substrates [3]. The inoculum was collected from an anaerobic digester treating paper-making waste at Smurfit Kappa Townsend Hook Paper Makers, Kent, United Kingdom. It was 'degassed' at 37 ℃ for three days. The inoculum was homogenised using a handheld blender prior to use.

The Automatic Methane Potential Test System II (AMPTS II) was used to measure CH_4 production. This system contains 500 mL reactors in a temperature controlled water bath with a CO_2 capturing unit and a gas measuring device. 3 replicates were made with each reactor containing 1 g volatile solid (VS) content of each biomass type (summer FD, washed summer SM, spring FD, washed spring SM), inoculum to make an inoculum-to-substrate (I/S) ratio of 5, and made up with water to 400 g. A blank with only inoculum and water was made to calculate net CH_4 production from the SM biomass. Reactors were mixed continuously at 75% power and incubated at 37 °C. CH_4 volumes were recorded daily over 28 days, and corrected to water vapour content at 0 ℃, 101.325kPa.

2.3. *Dry weight and ash content*

All biomass types were dried in a vacuum oven at 105 °C overnight to determine its dry weight (DW) and moisture content [8]. Ash and volatile solid (VS) content were determined using the muffle furnace at 250 °C for 1 hour followed by 550 °C for 2 hours [9].

2.4. *Statistical Analysis*

Excel (2016) was used for student's t-test and IBM SPSS version 25 was used for one-way, two-way and three-way ANOVA analysis. Statistical significance is determined by $p < 0.05$. Dependent variable: cumulative CH_4 yield; daily CH_4 production. Independent variables: treatment (washed, unwashed), season (spring, summer), day (time after incubation).

3. Results and Discussion

3.1. *Dry weight, volatile solids and Ash content*

Washing of SM significantly reduces ash content (student's t-test) (Table 1). Summer washed and spring washed SM showed 48.7% and 53.9% ash reduction relative to their unwashed counterparts, respectively, resulting in a higher VS content for washed SM.

Table 1: Volatile solids and ash content of SM biomass used (n=3)

	% VS DW	**% Ash DW**
Summer	73.5 ± 0.7	26.5 ± 0.7
Summer washed	86.4 ± 0.4	13.6 ± 0.4
Spring	73.1 ± 0.0	26.9 ± 0.0
Spring washed	87.6 ± 0.3	12.4 ± 0.3

3.2. *Effect of season on CH_4 yield*

Table 2: Net cumulative CH_4 production after 28 days (n=3)

	Net CH_4 Yield (mL CH_4 g^{-1} VS)
Summer	118.7 ± 30.1
Summer Washed	159.3 ± 4.4
Spring	139.7 ± 39.0
Spring Washed	154.7 ±16.2

Net CH_4 production at the end of the BMP test (28 days) is shown in Table 2. One-way ANOVA showed that differences in the mean CH_4 potential produced by each SM biomass type after 28 days were not statistically significant. Notably, unwashed SM has a significantly higher variance of 25 mL CH_4 g^{-1} VS relative to washed summer SM. Nevertheless, these results are in contrast to most reported in literature [3,10], showing differences in cumulative CH_4 yields between summer and spring harvested seaweed. These differences could be attributed to species and location of harvest [11].

Cumulative CH_4 production over 28 days shows significant differences in the rate of production between washed and unwashed SM and between spring and summer SM (Figure 1). In a two-way ANOVA, differences in seasonality as well as the interaction between seasonality and day after incubation show a statistical difference in cumulative CH_4 yields ($p < 0.05$). Summer seaweed shows a delay of up to 6 days for unwashed SM and 7 days for washed SM before an increase in rate of CH_4 production; producing up to 85.2 mL CH_4 g^{-1} VS and 63.9 mL CH_4 g^{-1} VS lower yield compared to unwashed spring SM and washed spring SM, respectively.

Spring seaweed shows a rapid increase in CH_4 yields in the first three days of incubation, indicating differences in composition of summer and spring SM as shown by Adams *et al*. (2011) [10]. In the absence of a statistical difference in ash content between the two seasons (student's t-test) which can impact CH_4 yield [3], CH_4 yield differences are likely due to differences in the composition of the organic fraction. Spring SM may contain more easily metabolised monomeric substrates such as glucose that can be readily converted to CH_4, with *Sargassum wightti* showing higher soluble carbohydrate content in spring than summer [12]. Summer SM may require adaptation of microorganisms within the inoculum to SM's

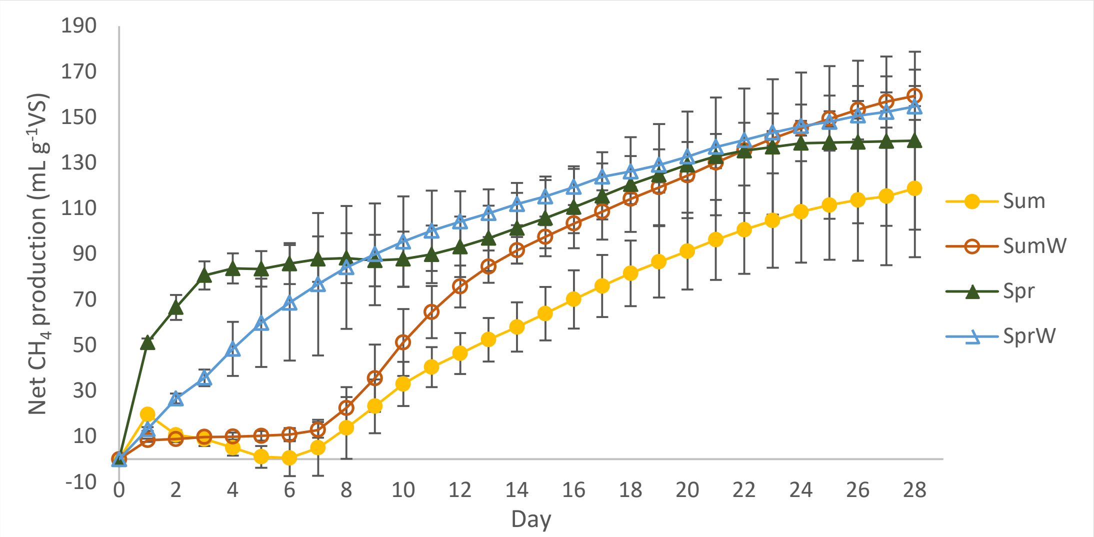

Figure 1: CH_4 production over the BMP test (28 days). Error bars represent standard deviation (SD). Sum: Summer FD SM; Spring FD SM; SumW: Summer washed SM; SprW: Spring washed SM.

substrates and/or require the hydrolysis of more complex substrates before its conversation to CH_4 [10].

3.3. *Effect of washing on CH_4 yield*

Washing of spring SM did not show a statistically significant interaction between day, treatment and season on CH_4 yields ($p > 0.05$). Washed and unwashed spring SM only showed statistical differences between days 1-4, with washed SM having a mean yield of up to 44.9 mL CH_4 g^{-1} VS lower than unwashed SM within these days ($p < 0.05$). The result for spring SM show similarities with freshwater washing of SM [7], attributed to the removal of soluble carbohydrates such as mannitol and glucose, and/or of hydrolytic bacteria with washing.

In contrast, washing of summer SM showed a statistically significant interaction between day, treatment and season on CH_4 yields in a three-way ANOVA. This statistical difference started from day 12 to the end of the BMP test. Additionally, differences in CH_4 production per day between washed and unwashed summer SM was most pronounced on day 10, with washed summer SM producing 5.9 mL CH_4 g^{-1} VS higher than unwashed summer SM. A statistical significance in the interaction between day, treatment and season on daily CH_4 production also highlights the importance of time required for substrate hydrolysis and their conversion to CH_4.

Therefore, it is proposed that washing removes inhibitory compounds that act to limit hydrolysis of complex substrates from summer SM. These compounds could be polyphenolic compounds that have been extracted from *Sargassum* by water and have been associated with limiting hydrolysis of complex substrates and CH_4 yields of *Aschophyllum nodosum* [3,6,13]. Unwashed spring SM and washed summer SM have 72% and 80% lower phenolic content compared to unwashed summer SM (unpublished data), respectively. High polyphenolic content was also detected in other summer-harvested seaweed and is associated with photoprotective properties due to higher light intensity and irradiation in summer [11,14].

These potential inhibitory compounds could either be absent or not in sufficient concentrations within spring SM to have a significant impact on CH_4 production and yield. It was indicated that growing tissues of SM, occurring in the ‘spring growth phase’, would have lower soluble polyphenolic content than older, non-growing parts [14,15], which is likely to be present in higher proportions in summer than spring seaweed. Nonetheless, further analysis of the carbohydrate, protein and lipid composition of the washed liquid and the biomass are required to fully understand the differences in CH_4 yield.

4. Conclusion

CH_4 production over 28 days from summer and spring SM indicate differences in composition. Washing of summer SM increases the rate of CH_4 production after 10 days, while washing spring SM decreases the initial rates of CH_4 production relative to their unwashed counterpart. However, the final CH_4 potential of all SM types were not affected. Washing of summer SM may remove compounds that may limit CH_4 production, resulting in a faster rate of production. Hence, initial removal of potential inhibitors in summer SM using water before AD could present a favourable biorefinery approach.

Acknowledgements
The author would like to acknowledge the financial support of the University of Greenwich and the Doctoral Training Alliance.

References

1. Milledge, J. J.; Harvey, P. J. Ensilage and anaerobic digestion of Sargassum muticum. *J. Appl. Phycol.* **2016**, *28*, 3021–3030.
2. Austin, C.; Stewart, D.; Allwood, J. W.; McDougall, G. J. Extracts from the edible seaweed, Ascophyllum nodosum, inhibit lipase activity in vitro : contributions of phenolic and polysaccharide components. *Food Funct.* **2018**, *9*, 502–510.
3. Tabassum, M. R.; Xia, A.; Murphy, J. D. Seasonal variation of chemical composition and biomethane production from the brown seaweed Ascophyllum nodosum. *Bioresour. Technol.* **2016**, *216*, 219–226.
4. Mhatre, A.; Gore, S.; Mhatre, A.; Trivedi, N.; Sharma, M.; Pandit, R.; Anil, A.; Lali, A. Effect of multiple product extractions on bio-methane potential of marine macrophytic green alga Ulva lactuca. *Renew. Energy* **2018**, *132*, 742–751.
5. Agregán, R.; Munekata, P. E. S.; Franco, D.; Dominguez, R.; Carballo, J.; Lorenzo, J. M. Phenolic compounds from three brown seaweed species using LC-DAD–ESI-MS/MS. *Food Res. Int.* **2017**, *99*, 979–985.
6. Rastian, Z.; Mehranian, M.; Vahabzadeh, F.; Sartavi, K. Antioxidant Activity of Brown Algae Sargassum vulgar and Sargassum angustrifolum. *J. Aquat. Food Prod. Technol.* **2007**, *16*, 17–26.
7. Milledge, J. J.; Nielsen, B. V; Sadek, M. S.; Harvey, P. J. Effect of Freshwater Washing Pretreatment on Sargassum muticum as a Feedstock for Biogas Production. *Energies* **2018**, *11*, 1771.
8. BSi. Solid biofuels - Determination of moisture content - Oven dry method. Part 2: Total moisture - Simplified method. In *BS EN 14774-2:2009*; BSi: UK, 2009.
9. BSi. Solid biofuels - Determination of ash content. In *BS EN 14775:2009*; UK, 2009.
10. Adams, J. M. M.; Toop, T. A.; Donnison, I. S.; Gallagher, J. A. Seasonal variation in Laminaria digitata and its impact on biochemical conversion routes to biofuels. *Bioresour. Technol.* **2011**, *102*, 9976–9984.
11. D'Este, M.; Alvarado-Morales, M.; Ciofalo, A.; Angelidaki, I. Macroalgae Laminaria digitata and Saccharina latissima as Potential Biomasses for Biogas and Total

Phenolics Production: Focusing on Seasonal and Spatial Variations of the Algae. *Energy and Fuels* **2017**, *31*, 7166–7175.

12. Kumar, S.; Sahoo, D.; Levine, I. Assessment of nutritional value in a brown seaweed Sargassum wightii and their seasonal variations. *Algal Res.* **2015**, *9*, 117–125.
13. Milledge, J. J.; Nielsen, B. V.; Harvey, P. J. The inhibition of anaerobic digestion by model phenolic compounds representative of those from Sargassum muticum. *J. Appl. Phycol.* **2019**, *31*, 779–786.
14. Gorham, J.; Lewey, S. A. Seasonal changes in the chemical composition of Sargassum muticum. *Mar. Biol.* **1984**, *80*, 103–107.
15. Koivikko, R.; Loponen, J.; Honkanen, T.; Jormalainen, V. Contents of soluble, cell-wall-bound and exuded phlorotannins in the Brown Alga Fucus vesiculosus, with implications on their ecological functions. *J. Chem. Ecol.* **2005**, *31*.

Nottingham | UK | 9–11 September 2019

Optimisation of low grade Thermal Energy Storage systems with Phase Changing Materials

Law Torres Sevilla [1], Jovana Radulovic [1]

[1] *Anglesea Building, Anglesea Road, Portsmouth, United Kingdom, PO1 3DJ*

law.torressevilla@port.ac.uk

Abstract

The use of phase changing materials (PCMs) for energy storage has been in the focus of scientific research for a while, primarily focusing on building cooling/heating applications due to favourable melting temperature ranges. In this paper we simulated the suitability of encapsulated Paraffin Wax on a small scale in a low temperature thermal energy storage system using COMSOL Multiphysics. Heat absorption and heating dynamics were analysed for different inlet designs and velocities, and the thermal gradient was evaluated across the tank geometry in a number of charging scenarios. The influence of the material properties and the inlet/outlet geometry were studied to inform the optimal tank design.

1. Introduction

Energy storage is an essential component of any renewable energy system due to the intermittent character of these technologies. In times of high demand, where the sun is not shining and the wind is not blowing, the existence of a backup energy supply with easy and fast access is necessary. Thus, Thermal Energy Storage (TES) systems are presented as a suitable solution. The majority of research focuses on sensible heat and latent heat, or the combination of the two. Latent heat TES offers several advantages, such as greater density and narrower operational temperature range [1].

Latent heat focuses on usage of Phase Changing Materials (PCMs) to store energy, where the most common types in research are the solid-liquid ones [2], which have been used extensively and include paraffin types and fatty acids, amongst others. Fatty acids are used in low grade TES and paraffins are suited for both due to their flexibility in extending their polymer chains for different melting temperatures.

Sharma et al. comment on the suitability of capric acid, lauric acid, myristic acid, palmitic acid and stearic acid as PCMs for a 2D theoretical model using a shell and tube heat exchanger. They state fatty acids have favourable properties such as melting congruency, good chemical stability and non-toxicity [3]. Fauzi et al. combine various fatty acids to create two kinds of eutectic mixtures to be cycle tested experimentally for their thermal reliability. The mixtures are myristic acid/palmitic acid/sodium myristate (MA/PA/SM) and myristic acid/palmitic acid/sodium palmitate (MA/PA/SP), and the authors claim these show good performance applicable for TES in domestic usage such as domestic water heating [4].

Kousksou et al. present an analysis of six paraffin types, with air as a working fluid, for a cylindrical tank which is 1.5m in height and 0.06m in diameter. They conclude that the efficiency of the system increases with increasing the inlet velocity and decreasing the melting temperature of the PCMs [1]. Aldoss et al. also provides a study involving the combination of three paraffin types with increasing melting temperatures in a packed bed. These paraffins are waxes denoted as PCM40, PCM50 and PCM60 based on their phase change temperatures. They propose the use of multi stage PCM designs to increase the performance of the system and conclude that, whilst adding a second stage to the TES significantly increases the melting temperature distribution in the charging process, three or more stages provide a less significant improvement. From a practical and economical point of view it is deemed not advisable [5].

In this paper, the suitability of paraffin wax as a low grade temperature TES is considered. Water was chosen as the heat transfer fluid (HTF) due to its suitable thermodynamic properties and the system operating temperature range. A packed bed design containing PCMs in encapsulated spheres was simulated, and the heating dynamics and influence of the various thermal and design parameters were evaluated.

2. Methodology

2.1 System Parameters

The system consists of a symmetrical single cylindrical tank, of 0.5m in height and length, packed with a set of 19x17 encapsulated spheres containing the selected PCM. The tank frame is 0.025m thick and the capsule is considered thin and negligible, with the sphere radius of 0.0125m. The HTF enters the system at a constant temperature of 90°C. The inlet velocities studied were 0.1m/s, 0.05m/s and 0.01m/s. The system initially starts with still water inside the tank at an ambient temperature of 20°C.

The main area of interest is the heating dynamics of the system and how it is affected by tank design, HTF velocity and PCM material properties. Two different designs were analysed, shown in Figure 1, where the PCMs are denoted as the blue square, the inlet is the top light blue line and the outlet is the bottom green line. Design A consists of a single inlet and outlet, both 0.12m in length. Design B consists of two inlets and a single outlet, all with dimensions 0.12m.

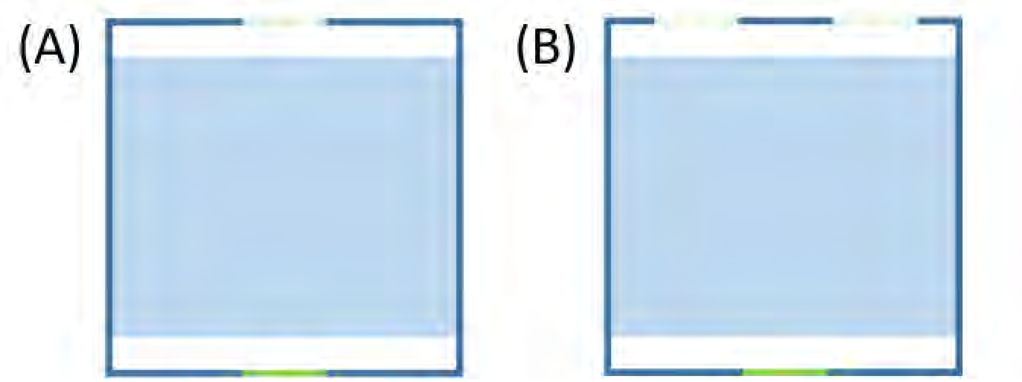

Figure 1: The two design types which are analysed in this paper

The temperatures were monitored at three selected positions: at the centre sphere, the top left sphere and the bottom left sphere, and the overall thermal gradient was recorded across the tank.

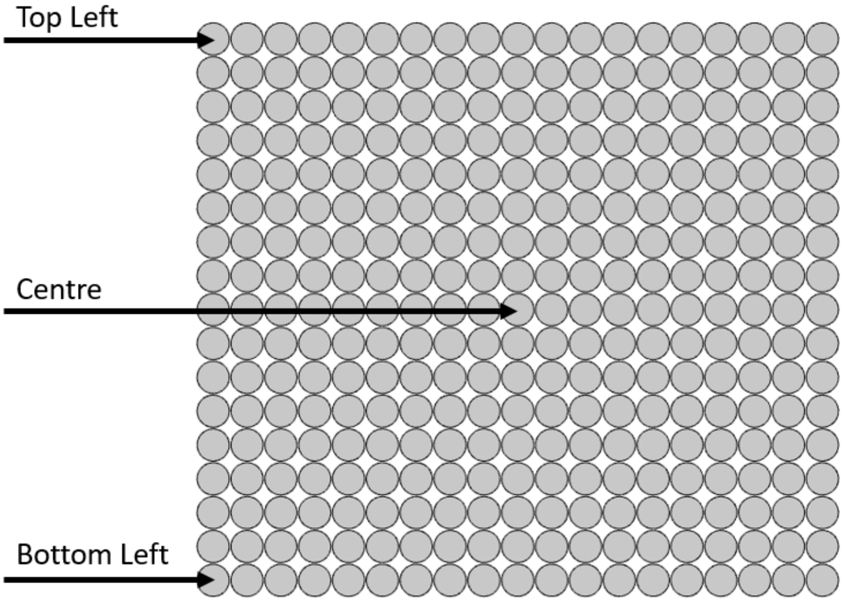

Figure 2: Three positions across the tank where the temperature will be recorded

2.2 Boundary conditions and assumptions

The 2D simulation is run in COMSOL Multiphysics for 10 simulation minutes at 5 second intervals. The model uses the “Laminar Flow” and “Heat Transfer in Fluids” physics, alongside the “Nonisothermal Flow” multi-physics. The mesh was approximately 140,000 mesh elements, mostly triangular prisms. The heat transfer problem was solved using the heat equation for non-uniform isotropic mediums and Fourier’s law:

$$\rho C_p \frac{\partial T}{\partial t} + \rho C_p u \cdot \nabla T + \nabla \cdot q = \mathrm{Q} + \mathrm{Q}_p + \mathrm{Q}_{vd} \qquad \text{(Equation 1)}$$

$$q = k\nabla T \qquad \text{(Equation 2)}$$

Where ρ is density, Cp is heat capacity at constant pressure, T is temperature, t is time, u is velocity, q is heat flux, Q is the heat source, Qp is heat pressure work, Qvd is heat viscous dissipation and k is thermal conductivity.

The boundary conditions in the wall are no slip and the tangential velocity is equal to zero. The inlet boundary condition is set to velocity and the outlet is set to pressure, where initial pressure is zero and the model suppresses backflow. The HTF is modelled as laminar and incompressible, and materials are assumed to be homogeneous and isotropic. There are no heat transfers or losses due to radiation and the outside of the tank is perfectly insulated. Lastly, the spheres are modelled as circles that do not undergo deformation.

The tested PCM was Paraffin Wax. The relevant properties are presented in Table 1:

Table 1: Selected PCM for the study and its relevant properties [6]

Phase Changing Material (PCM)	**Melting point (T_m) °C**	**Latent Heat of Fusion (L) kJ/kg**	**Density Solid / Liquid (ρ_s/ρ_l) kg/m^3**	**Thermal Conductivity Solid / Liquid (k_s/k_l) W/mK**	**Specific Heat Capacity Solid / Liquid (c_{ps}/c_{pl}) J/kgK**
Paraffin Wax	55.55	190.0	825/755	0.230/0.200	2200/2100

3. Results and Discussion

3.1 System Design

As the HTF enters the tank, the spheres closest to the inlet will naturally heat up the fastest. The difference in temperature between the top, centre and bottom spheres after 10 minutes is almost negligible and their heating dynamics follow the same shape. This is the same for both designs, A and B. Nevertheless, with the addition of an extra inlet the charging time of the system is improved by less than 1%, which concludes that a single inlet is simpler and cost effective design. Figure 3 and 4 below shows a both designs for set and varying velocities:

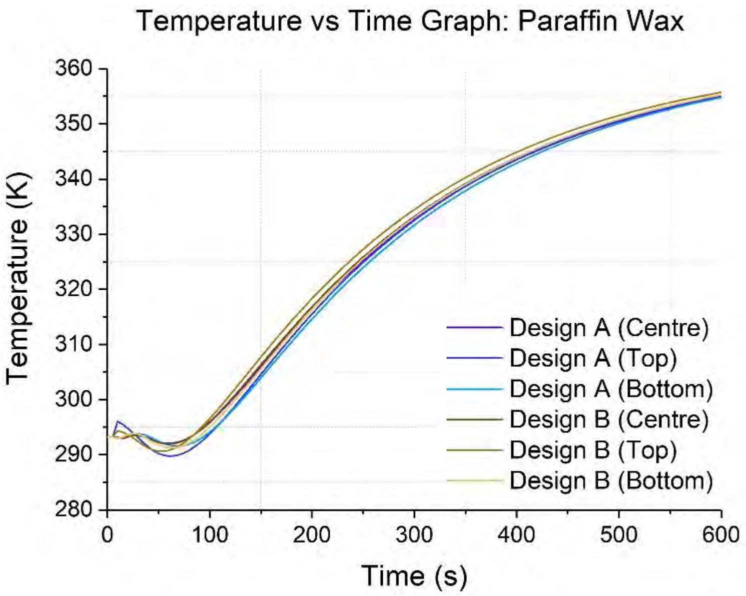

Figure 3: Temperature vs time graphs for both designs at a velocity of 0.1m/s

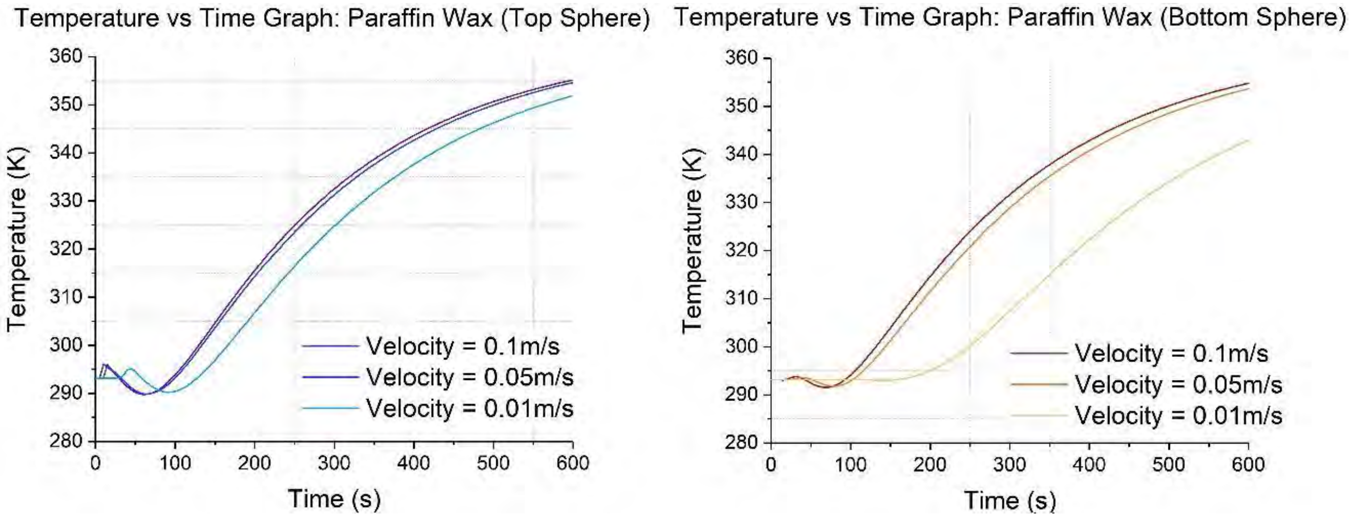

Figure 4: Temperature vs time graphs for all velocities, for Design A, for two positions

3.2 Effect of inlet velocity

Higher inlet velocity results in higher heating dynamics (Figure 4). Changing the inlet velocity from across the tested range led to a temperature decrease of less than 1% (roughly 4°C) for the top sphere, whereas for the bottom sphere it was diminished by ~3% (approximately 12°C). Lower inlet velocities compromise the total heat absorption, particularly for Design A. The minimum and maximum amounts of heat uptake for individual spheres were

1kJ/kg and 25kJ/kg for Design A, respectively. However, for Design B, these were significantly more moderate: 3kJ/kg and 8kJ/kg, respectively. The data suggests that the addition of a second inlet provides a higher heat transfer rate throughout the tank which causes less extreme temperature differences between the top and bottom spheres. This is probably due to the HTF entering and spreading across the tank in a more distributed manner.

Conclusion

From the presented study, the following conclusions can be derived:

- An addition of a second inlet to the system yields higher final temperatures and improves the distribution of the HTF, allowing a better heat transfer rate.
- A higher velocity at the inlet improves the heat transfer rate and allows for higher temperatures and higher heat absorption.

References

1. Kousksou T, Strub F, Castaing Lasvignottes J (2007) Second law analysis of latent thermal energy storage for solar system. Solar Energy Materials & Solar Cells 91: 1275-1281. doi:10.1016/j.solmat.2007.04.029
2. Fallahi A, Guldentops G, Tao M, Granados-Focil S, Van Dessel S (2017) Review on solid-solid phase change materials for thermal energy storage: Molecular structure and thermal properties. Applied Thermal Engineering 127: 1427-1441. doi: 10.1016/j.applthermaleng.2017.08.161
3. Sharma A, Dong Won L, Buddhi D, Un Park J (2005) Numerical heat transfer studies of the fatty acids for different heat exchanger materials on the performance of a latent heat storage system. Renewable Energy 30: 2179-2187. doi:10.1016/j.renene.2005.01.014
4. Fauzi H, Metselaar H.S.C, Mahlia T.M.I, Silakhori M, Chyuan Ong H (2015) Thermal characteristics reliability of fatty acid binary mixtures as phase change materials (PCMs) for thermal energy storage applications. Applied Thermal Engineering 80: 127-131. doi: 10.1016/j.applthermaleng.2015.01.047
5. Taha K. Aldoss, Muhammad M. Rahman (2014) Comparison between the single-PCM and multi-PCM thermal energy storage design. Energy Conversion and Management 83: 79-87. doi: 10.1016/j.enconman.2014.03.047
6. Belen Zalba, Jose Ma Marin, Luisa F. Cabeza, Harald Mehling (2003) Review on thermal energy storage with phase change: materials, heat transfer analysis and applications. Applied Thermal Engineering 23: 251-283. doi: 10.1016/S1359-4311(02)00192-8

Appendices

Table 2: Final temperature reached by spheres for all simulations

Velocity	**Final temperature reached after 10minutes (K)**					
	Design (A)			**Design (B)**		
	Centre	*Top Left*	*Bottom Left*	*Centre*	*Top Left*	*Bottom Left*
0.1m/s	354.97	355.16	354.77	355.23	355.73	355.27
0.05m/s	354.28	354.62	353.63	353.13	353.88	353.04
0.01m/s	350.66	351.87	342.95	352.58	354.66	351.24

Table 3: Final temperature percentage difference between all simulations

Velocity	**Final temperature percentage difference (%)**					
	Design (A)			**Design (B)**		
	Centre	*Top Left*	*Bottom Left*	*Centre*	*Top Left*	*Bottom Left*
0.1 – 0.05m/s	0.19%	0.15%	0.32%	0.59%	0.52%	0.63%
0.05 – 0.01 m/s	1.02%	0.78%	3.02%	0.16%	-0.22%	0.51%
0.1 – 0.01m/s	1.21%	0.93%	3.33%	0.75%	0.30%	1.13%

Table 4: Total final internal energy for all simulations

Velocity	**Total final internal energy (kJ/kg)**					
	Design (A)			**Design (B)**		
	Centre	*Top Left*	*Bottom Left*	*Centre*	*Top Left*	*Bottom Left*
0.1m/s	133.24	133.66	132.81	133.80	134.88	133.89
0.05m/s	131.78	132.49	130.39	129.32	130.91	129.13
0.01m/s	124.04	126.62	107.55	128.13	132.59	125.27

Table 5: Total final internal energy percentage difference between all simulations

Velocity	**Total final internal energy percentage difference (%)**					
	Design (A)			**Design (B)**		
	Centre	*Top Left*	*Bottom Left*	*Centre*	*Top Left*	*Bottom Left*
0.1 – 0.05m/s	1.10%	0.88%	1.82%	3.35%	2.94%	3.56%
0.05 – 0.01 m/s	5.87%	4.43%	17.52%	0.92%	-1.28%	2.99%
0.1 – 0.01m/s	6.90%	5.27%	19.02%	4.24%	1.70%	6.44%

ICESF
Nottingham | UK | 9–11 September 2019

Exploring the Sustainable Economy and Energy For Libya's Future

Ahmed M A Mohamed[1], Sherifa M.I Elabar[2], Bubaker H M Shakmak[3],
[4]Amin Al-Habaibeh

[1]*International and Development research Group (IDERG)*
[1]*Libyan Audit Bureau and*
[1,3,4]*Innovative and Sustainable Built Environment Technologies Research Group (iSBET)*
[2] *Benghazi University- Libya*

ahmed2004amer@yahoo.co.uk

Abstract

Libya during the past decades has made strategic plans for diversification of resources and the development of the economy with partial independence from traditional sources of energy (oil and natural gas). However, oil and natural gas have continued to play a major role in Libya's economy as the main source of revenues and energy.

In the last decade, the production of Libya's oil has been shut down unexpectedly due to the political tension and was significantly interrupted for much of 2011-2018. At the same time, the oil prices rebounding caused the economy to shrink accompanied by the decrease of per-capita income. Furthermore, inflation rates have jumped at a record level and still continuing.

This study is aimed to explore the effect of the price and production quantity of oil on Gross Domestic Product (GDP) and per-capita income. The researchers have conducted a comprehensive survey that included the reports of many originations and institutions to show the impact of fluctuations in oil prices on per capita income.

The study has found that there is an urgent need to develop a strategy to find other energy resources to cope with the high development rates of the economy. Moreover, the study has shown that encouraging the private sector to find alternative resources other than oil and gas by the utilisation of renewable energy technologies will ensure the increase the income per capita and the improvements in the economic, health and educational situations.

1. Introduction

Libya as a member of the Organization of Petroleum Exporting Countries (OPEC) holds the largest proven oil and gas reserves [1] and has one of the highest Gross Domestic Product per capita in Africa [2], [3]. It is located in the middle of North Africa. It has a large coast, 1900 Km long on the Mediterranean Sea with six neighbours: Tunisia, Algeria, Niger, Chad, Sudan and Egypt. It is also situated on the cancer orbit line (Geographic coordinates 25.00 N, 17.00 E). It is exposed to the sunlight during the year and all day long. Most of Libya’s surface consists of coastal plains, plateaus and mountains. The desert extends deep into the south with scattered villages and small towns. The climate is Mediterranean; it is warm in summer and mild in winter. The desert climate in the South is very hot in summer with extreme diurnal temperature ranges. The average temperature is between 15°C throughout the winter and 35°C during the summer time [4], [5]. Libyan's economy is dependent on oil as the main source of energy. Oil export revenues are very important to the economic development of Libya as they represent 96% of the total revenue [5], which provided approximately 95% of all export revenue [6].

In 2011, Libya went through political instability, during which oil production was disrupted which resulted in a GDP contraction of over 40 %. However, it is expected that with the recovery of the oil industry, the high rates of growth will be back [3]. However, the continuous growth in energy demands is one of the important challenges facing energy policymakers in Libya. The exploitation of renewable energy in Libya is becoming important to sustain people’s lifestyle as well as sustaining energy resources. Libya, similar to other countries, is seeking to boost its economy, increase and maintain its sources of income, encouraging investment, and creating new employment opportunities. In addition, the Libyan government started to address issues such as oil reserves and environmental pollution. This paper will explores the sustainable economy and energy for Libya's future and highlight efforts needed to achieve this. In order to gather data for this paper, the researcher conducted a comprehensive survey that has included the reports of World Bank, the United

Nations, Central Bank of Libya, Organization Petroleum Export Countries (OPEC), United States Energy Information Administration (EIA), Central Intelligence Agency (CIA), Index Mundi, various papers, and books related to the subject of the research.

2. Libyan economy background

This part gives an understanding of the importance of the discovery of petroleum on the Libyan's economic sector through providing a summary of government operations, revenues and budgets and at the same time, the effect of this change on both Gross Domestic Product (GDP) and per capita income in Libya.

It could be argued that prior to the year 1960 It was difficult to express any development of the Libyan economy due to the country was poorly baled with skilled and educated manpower, additionally the lack of water and other natural resources. However, the country was relying heavily on advisors including technicians from the UK, USA and UN [7], [8]. In 1951, the average per capita income was less than $30 per year while by 1960 it increased to $100 per year. Previous to the discovery of petroleum in 1959 and the beginning of production in 1961, Libya was one of the poorest countries in the world [9]. In 1955, the GDP was £L15 million Libyan pounds. However, post 1958, GDP had elevated to £L52 million [7], [8]. Prior to the petroleum discovery, the country became dependent on the aid from foreign states and payments for the use of military bases, particularly the UK and USA [10]. Throughout this time, Agriculture was the important mainstay of Libyan society and economy. Unlike the agriculture, the industrial sector was limited, due to lack of capital investment, power and raw materials, although the early years of 1951 the main export was scrap metal salvaged from the debris of the Second World War [10]. The Esso company discovered the commercial oil in Zelten oil field in 1959 [7], [8]. The oil field of Zelten started to produce oil in August 1961 after which the production rose rapidly. Libya was the second largest producer by the year 1969 in North Africa and Middle East region [11]. The Libyan economy has had improved widely as the oil production and revenues rose at a huge rate for the first time by petroleum producer. Per capita income and GDP increased considerably as petroleum revenues rose. Meanwhile, the National Income rose in the year 1962 from £LM131 (131 Million Libyan pounds) to £LM798 in the year 1968 [7].

Oil and natural gas contributed 65.3 % to the real GDP and approximately 95% to Libya's export revenue in 1980 [12]. In the 1980s, the Libyan economy was affected by the low petroleum prices. The petroleum revenues decreased at $5 billion in 1988 from $23.2 billion in 1980 [13], [14].

3. The economic challenge

Oil is the main source of revenue in Libya, where accounts for about 95% of the state's total income, about 65% of GDP and oil exports accounted for 96% of the total Libyan exports [15]. Since 2003, lifting international sanctions, Libya has maintained high levels of economic growth, taking advantage of rising world oil prices and growth in non-economic sectors. Real GDP growth averaged about 7.5% per annum in 2004-2007, driven by a 10% growth rate in non-oil sectors. And with the collapse of oil prices in late 2008.GDP growth rate dropped to 3.8%. Domestic real GDP continued to decline to about 2% in 2009 due to a 1.5% decline in oil production and oil revenues fell by 36%. The sharp drop in oil prices in 2009 also led to a decline in the total public finance surplus to about 10% and the current account balance to about 17% from GDP. Despite huge investments in the agricultural sector and non-oil-related industries, the share of oil in GDP remained the main factor. Diversification of economic activity remains the biggest challenge to sustainable development in Libya[5]. Moreover, Libya's economic situation is unsteady. Oil and gas typically represent 70% of Libya's GDP. In 2012, the decline in oil exports from $60.9 billion to $8.4 billion in 2015, has severely impacted government income, devastating public services, in particular, the education and health systems. Increasingly erratic power supply, high inflation and food shortages became common. In 2016, suspension of some subsidies, mainly on food contributed to a sharp increase in prices, particularly in remote regions and the capital city [16]. In 2017, real per capita GDP growth in Libya, increased by just 1.8% and projected to increase by just 2.3% and 2.9% in 2018 and 2019.TheGDP rose 55.1% (GDP annual growth rate)in 2017 after declines in previous years of economic contraction, however, the output remained about a third lower than the period before the Libyan uprising in 2011.GDP grew in 2017,(See Figure -1), due to the significant increase in oil production. With the sharp decline in oil prices accompanied by the awful security, political, and humanitarian condition, real GDP in 2014 contracted more than 50% in Libya and continued to shrink through 2015 and 2016, although at a slower rate. Accompany of the OPEC agreement to cut oil production to 32.5 million barrels a day, which started early 2017, oil prices increased slightly and fluctuated between $52 and $60 from August to November 2017. In fact, exempt from this agreement, Libya rose oil production substantially toward the end of 2016 and throughout 2017, boosting forecasted growth in real GDP for 2017 and 2018. The economic attitude remains highly uncertain and dependent on progress in achieving stability and fluctuating oil prices.

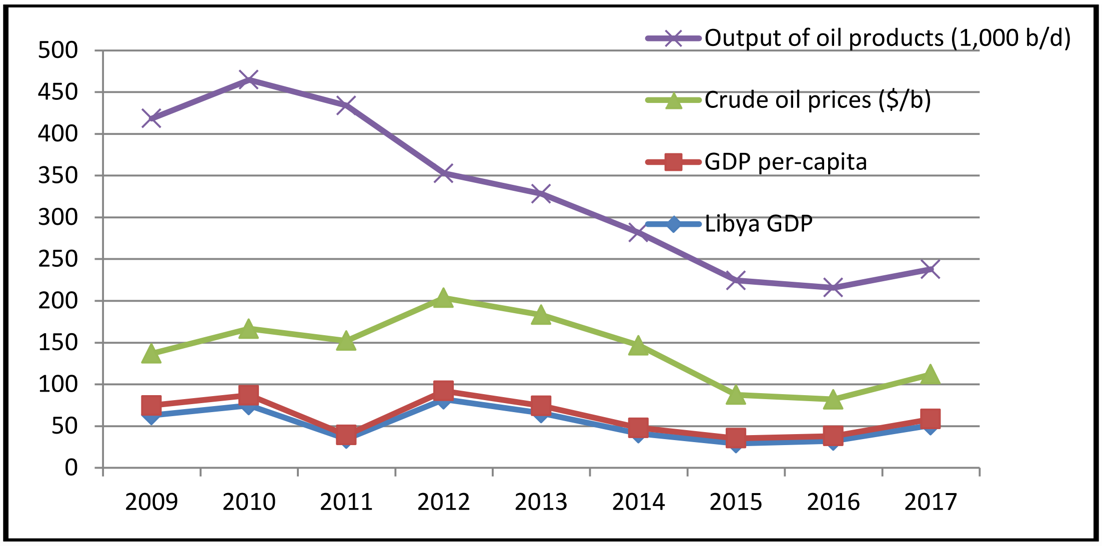

Figure 1 : Libyan GDP, Libyan GDP Per-capita, Crude oil price and output oil products.
Source: OPEC: Annual Statistical Bulletin (2013 &2018).

Figure 1: clarifies the relationship between Libyan GDP, Libyan GDP Per-capita, Crude oil price and output oil products, whereas, the increase in oil production or oil price have a significant impact on the Libyan economy. However, other sectors, for example, industry and agriculture outputs had continued at low levels, although the huge investment in these sectors to increase their share of the GDP, and to obtain the self-sufficiency target.

Oil Sector More Resilient to Instability

Instability of oil production in Libya has been a theme in Libya since the events of 2011. Many distinct phases since then have been reflected in the changes in Libya's oil output.

Mid-2011 and mid-2013, a time of relative stability allowed the quick recovery of majority oil output missing throughout the war. The events of 2011 had inflicted little damage to energy production and economic growth back to more than 1.4Mb/d was attained in little more than six months. It was an astonishing recovery and witness on the wealth of professional expertise within the Libyan energy sector. This was not the last instant that the resilience of the country's oil industry would surprise outside analysts.

From September 2013 to September 2016, a political split in the country was visible in several ways. Shut down the ports of the Sirte Basin’s oil, the closure lasted until September 2016.Libya’s economy struggled in throughout this time, making efforts to build a post-revolutionary landscape more difficult [2].

The oil production, from a daily average of about 400,000 barrels a day (b/d) in2016 to 900,000 in September 2017, enhanced economic performance. The Libyan budget deficit is expected to turn into a surplus of 1.8% of GDP in 2017, with an estimated increase in exports of 62.5% and an estimated boost of 4% in imports, which have been falling with the decline in foreign reserves. After peaking in 2015 at 126.6% of GDP, the budget deficit dropped to an estimated 43% of GDP in 2017[3], [17], [18].

After 2017, oil production has dipped periodically since then due to disruptions but has also rebounded strongly so that in October 2018, output was at 1.25mb/d. Once more, the resilience of Libya’s oil sector revived and hopes that a period of sustained stability would underpin the next phase to come, in which can deliver on plans to regain 2011 output levels of 1.6Mb/d in 2019 and push towards 2mb/d by 2022. [2].

4. **Conclusions**

From the literature review and secondary data, it has been found that the growth of both GDP and Per Capita Income in Libya were due to a rise in the petroleum revenue since 1962. Therefore, there is a strong relationship between economic growth and oil production and prices. The Libyan economy is heavily dependent on the oil sector, it is the main source of income for all Libyan sectors. In fact, this study has also found that the oil is the important factor affecting GDP growth, for that reason the increasing GDP results in an increased standard of living and a decrease in the unemployment rate. Estimating this factor, provides policymakers and researchers with a better understanding of the Libyan economy and the basis for developing plans and strategies for improving the standard living within the country. Libya, similar to other countries, is looking to enhance its economy, increase and maintain its sources of income, encouraging investment, and creating new employment opportunities. The continuous growth in energy demands is one of the important challenges facing the energy policymakers in Libya. Exploitation of renewable energy in Libya is becoming important to sustain people’s lifestyle and sustaining energy resources.

References

[1] A. M. A. Mohamed, A. Al-Habaibeh, and H. Abdo, “An investigation into the current utilisation and prospective of renewable energy resources and technologies in Libya,” *Renew. Energy*, vol. 50, 2013.

[2] A. M. Etelawi, K. A. Blatner, and J. Mccluskey, “Crude Oil and the Libyan Economy,” no. May, 2017.

[3] “Libya GDP Annual Growth Rate,” *TRADING ECONOMICS*, 2019. [Online]. Available: https://tradingeconomics.com/libya/gdp-growth-annual. [Accessed: 20-May-2019].

[4] U. S. D. of S. Staff, “U.S. Relations with LIbya,” *U.S. Department of State*, 2013. .

[5] A. M. A. Mohamed, “Investigation into the Feasibility of the Utilisation of Renewable Energy Resources in Libya,” Nottingham Trent University, 2016.

[6] T. Meyer, “5 Most Oil-Dependent Economies in the World,” *Investopedia*, 2016. [Online]. Available: https://www.investopedia.com/articles/investing/011216/5-most-oildependent-economies-world.asp. [Accessed: 19-May-2019].

[7] A. A. OMAR, “AN EVALUATION OF LOW INCOME HOUSING PROJECT IN DEVELOPING COUNTRIES CASE STUDY: TRIPOLI-LIBYA,” University of Salford, 2003.

[8] A. Bait-Elmal, “The role of management control systems in Libyan organisations: a Libyan development policy case study with special reference to the industrial sector.,” *Structure*, no. January 2000, 2000.

[9] D. Vandewalle, *Libyan Since Independence: Oil and State-Building.* Cornel University Press. Ithaca. Published in the UK in 1998 by I.B.Tauris & Co Ltd., 1998.

[10] W. Abbas, H, “Industrial Development and Migrant labour in Libya.,” Manchester University, 1987.

[11] A. Giurnaz, “Economic of Oil: A Case of Libya,” University of Keele, 1985.

[12] G. Charles, “A Preliminary Assessment of the Distribution of Non-hydrocarbon Minerals.,” in *Planning and Development in Modern Libya.*, S. M. G. and K. S. M. M. M. Burn, Ed. 178-93, London: Menas, 1985, 1985.

[13] . Fishr, W. B, *Libya, The Middle East and North Africa Report.*, 36 th Edit. European Publications limited, London, 1990.

[14] S. Ghanem, “The Oil Industry and the Libyan Economy: the Past, the Present and the Likely Future.,” in *Khader, B. & El- Wifati, B. (Eds), The Economic Development of Libya.*, Croom Helm, London, 1987.

[15] loops, “The reality of Libyan oil in 2016,” Libya, 2016.

[16] U. N. D. Programme, “UNDP in Libya,” *sustainable development goals*, 2019. [Online]. Available: http://www.ly.undp.org/content/libya/en/home/about-us.html. [Accessed: 19-May-2019].

[17] A. A. Adesina, *African Economic Outlook.* African Development Bank Group, 2018.

[18] M. Rpser, “Economic Growth,” *Our World in Data*, 2019. [Online]. Available: https://ourworldindata.org/economic-growth. [Accessed: 19-May-2019].

ICESF
Nottingham | UK | 9–11 September 2019

Neural network based models for online SOC estimation of $LiFePO_4$ batteries used in Electric Vehicles

M. Anjum [1], K. Thanapalan [2], J. Williams[1]
[1]Centre for Automotive & Power Systems Engineering (CAPSE), Faculty of Computing, Engineering & Science, University of South Wales, Pontypridd CF37 1DL, UK
[2]Department of Aeronautical & Mechanical Engineering, Faculty of Computing, Engineering & Science, University of South Wales, Pontypridd CF37 1DL, UK
E-mail: Muhammad.anjum@southwales.ac.uk

Abstract

Several battery chemistries such as Lead-acid, Nickel-metal-hydride (Ni-MH), Nickel-cadmium (Ni-Cd) and Lithium-ion (Li-ion) are the predominant power source in Electric Vehicle and Hybrid Electric Vehicles (EVs/HEVs). Li-ion batteries are currently the favoured power sources in this regard, due to their operative advantages over other battery chemistries. However, it is challenging to determine the battery's current capacity state. Contributing factors to these challenges arise due to battery ageing along with the effects of complex electro-chemical reactions. A critical measure to estimating battery capacity is State of charge (SOC), which identifies when a battery reaches its maximum/minimum potential and therefore remaining capacity. This paper presents a comparative study and performance analysis of different artificial neural network (ANN) based State of charge (SOC) estimation models of Lithium-ion batteries. Beneficially the proposed technique does not require knowledge of the battery's internal parameters or electrochemical/mathematical models. Alternatively, it eliminates the highly skilled knowledge requirement by utilising readily available external parameters, such as the battery's voltage, charge/discharge current at ambient temperature to estimate SOC. Test results show that proposed ANN models achieve higher accuracy, despite ageing and temperature variation effects are not considered. These ANN based SOC models may be used to analyse the effect of operating conditions and energy demand of EVs.

Keywords: Lithium-ion Battery, Electric vehicle, State of charge estimation, Machine learning, Neural network, Comparative study

1. Introduction

Increasing concern over global warming, rising oil prices, CO_2 emissions, ocean pollution, habitat destruction and rapid exhaustion of fossil fuels have driven a major shift for research in energy storage systems. To address this alternative battery systems have been proposed for various applications, one of such steps is utilising battery-powered vehicles on an increasingly larger scale. Continual research on improving battery systems for Electric and Hybrid Electric vehicles (EV's and HEV's) has a critical role in this regard [1-2].

Li-ion batteries are rapidly becoming favorable power sources for EVs due to several operational advantages such as high nominal cell & specific voltage, energy density, cycle life, lightweight, low maintenance and more. Additionally, they have greater energy density when compared to other battery chemistries, thus making them a more suitable option when portability is of relevance. However, it should be recognized that these batteries come with certain restrictions; for instance: they operate at specific temperature and voltage ranges. Furthermore, similar to any other battery chemistry, the accuracy in their capacity estimation also requires improvement; as effects of aging and complex electro-chemical reactions due to battery chemistry undermine battery's performance and capacity. Analogous to other battery chemistries, Li-ion battery's performance and capacity is influenced by factors such as: temperature, current rate, voltage, cycle ageing and charge/discharge regimes. Hence, constant variance of external factors such as temperature, voltage and current, may highly affect the battery's capacity. Therefore, SOC estimation accuracy is directly affected by external conditions prevalent to EV's batteries [1].

Historically, SOC estimation models have primarily used methods which require knowledge of internal battery parameters. Using internal parameters in SOC estimation method may align the model with ageing effects but their measurement method is expensive. Besides, such online SOC estimation of an EV battery would require additional setup in the EV. Hence, SOC estimation models, which rely entirely on machine learning (ML) methods, such as ANN, can surpass the requirement of the battery's internal parameter values. Instead, they can be trained on the battery's external parameters such as charge/discharge current, voltage and temperature to estimate SOC. The use of an ANN based SOC estimation model is proposed for online SOC estimation of EV batteries in this paper. The paper's contribution is two-fold: a) it assesses the operational feasibility of an ANN based model, by using external battery parameters (charge/discharge current, voltage and temperature) which are readily available to an EV's BMS; b) it also sets basis for exploring the generalised specifics of ANN's internal parameters by presenting a comparative analysis of six individual ANN models. These models are designed to generalise the estimation on training data and avoid overfitting, so that online SOC estimation may be achieved with increased accuracy on unseen data.

2. Background

Conventional SOC estimation methods are relatively simple to implement but they typically disregard the effects of aging, temperature and other external factors. Additionally, OCV based conventional methods need rest time which increases their temporal cost [3]. Furthermore, these methods are also affected by inaccuracy errors in parameters measurements and initial states of the battery, such as Coulomb Counting [4, 5] and model based methods [6, 7]. On the other hand, some estimation methods, such as adaptive filter algorithm based methods, may offer higher precision but suffer from heavy computational mathematical analysis [8]. Hence, they require high processing power, which in turn raises the estimation cost or otherwise the computation time. On the contrary, model-based estimation methods may not be heavy on the computation side, but they require internal battery parameters to estimate SOC. Acquiring internal battery parameters is a cost intensive process and each model requires different or more parameters than the other [9,10]. Whereas, machine-learning algorithms as shown in [11] do not require internal battery parameter to reach desirable estimation accuracy. They are also capable of consideration to aging, and external factors such as temperature and noise, but an initial heavy computational cost comes inherently attached with them. This in turn requires heavy initial processing capabilities and large memory to store the training data and build learning model. On the bright side, once a ML model is built, SOC estimation is neither a time-consuming nor processing and memory intensive process. Additionally, ML models like ANN do not involve extensive mathematical computations using internal battery parameters to estimate the unknown states [12].

3. Experimental design and setup

An experiment was designed to assess the operational feasibility of ANN based online SOC estimation model for EV batteries. The other aim of this study was to work towards developing a simple model, which generalises well over training data so that estimation accuracy on unseen data is achieved within a desirable range. The experiment is designed to assess impact of using different non-linear activation functions with a range of ANN's other hyper parameters settings, including only number of layers and neurons in each layer. Works such as [13] have incrementally increased the training iterations and epochs to achieve the desired accuracy. While, there is a high probability that such incremental increase in training iterations and epochs may render the final model highly over fit to the training data. Therefore, in order to avoid high estimation accuracy at the cost of an over fit model, our design explores the efficiency of various activation functions of MLPs while comparing each MLP's performance on three different sets of hidden layer configurations, $S_h = \{S_{h1}, S_{h2}, S_{h3}\}$. Table 1 presents each of these configuration sets; the total number of elements in a set S_{hi} represents the number of hidden layers it has and the value at each index represents the number of neurons for that particular hidden layer. All of these configuration sets were used once each, to train backpropagation MLPs with hyperbolic tangent and rectifier activation functions individually; hence a total of six MLP SOC estimation models were trained.

3.1. Cell specifications and test equipment

$LiFePO_4$ cells were chosen for this experiment due to following characteristics: good thermal stability, high current rating, long life span, higher energy density and low cost as compared to other Li-ion battery materials. The basic parameters of these cells are summarised in Table 2. Five new cells were kept at

	Hidden layer configurations
S_{h1}	$\{20,17,15,13,10\}$
S_{h2}	$\{15,13,10,7\}$
S_{h3}	$\{10,7,5\}$

Table 1 Hidden layer configuration sets

Properties	Values
Dimensions (mm)	7.25 × 160 × 227
Weight (g)	496
Capacity (Ah)	20
Nominal voltage (V)	3.3
Energy density (Wh/L)	247
Operating Temperature (°C)	-30 to 55

Table 2 $LiFePO_4$ cell specification

Figure 1 Lithium pouch cell on test

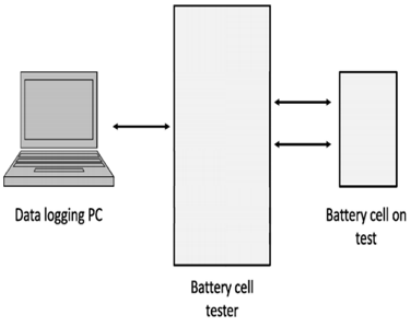

Figure 2 Block diagram of capacity test setup

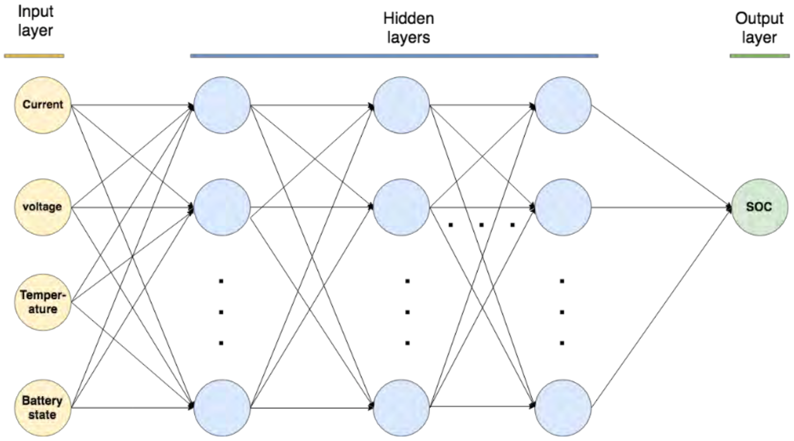

Figure 3 Abstract representation of proposed MLP online SOC estimation model

ambient temperature and passed through capacity test using a battery cell tester in facilities at CAPSE Laboratory of University of South Wales.

3.2. Model parameter extraction

The experimental data, including input parameters for MLP, namely: charge/discharge current, voltage, and temperature, was collected using a battery test bench. Figure 1 & Figure 2 show a cell on test and block diagram of test bench respectively. The battery tester is used to charge and discharge the cell; a thermal chamber provides and maintains the required ambient temperature; and the host computer is used for test control and data storage. The tests on each cell was performed at a 0.1 Hz sampling rate with an ambient temperature of 25°C. A constant current was applied to charge the battery cells to its upper cut-off voltage i.e. 3.6 V, at 0.3 C-rate. After a rest time of ten minutes, the battery cell was discharged to its lower cut-off voltage i.e. 2.0 V. The measured parameters include voltage in volts, current in amperes, temperature in degree Celsius and charged capacity in ampere hours.

3.3. SOC estimation

After successful data collection from all five battery cells, the data was divided into two partitions: 70% for training the MLPs, and 30% for testing the trained MLP models on SOC estimation. The output parameter, i.e. SOC, of the estimation model was appended into original dataset by using charged capacity in Ah, extracted during battery cell testing. The SOC was calculated at each row of the data using Equation 1 as follows:

$$SOC\% = \frac{Q_n}{Q_m} \times 100\% \qquad (1)$$

Where Q_m is the maximum available capacity of the battery cell, and Q_n is the available charged capacity. The battery parameters fed as input to estimation models included: charge/discharge current, voltage, ambient temperature, and battery state (i.e. charge/discharge/rest). Figure 3 depicts a high level representation of proposed MLP online SOC estimation model. The activation function and number of layers and neurons varied for each of the six models as described in previous section and is shown in Table 3. Each model took ~45 minutes on an average to train on training data obtained from one charge/discharge cycle of battery cells. Every model was provided with quantile regression loss function, as the estimation problem at hand is regressive.

4. Results and Discussion

The performance of each model was assessed by applying mean absolute error (MAE) metric on actual SOC as calculated by using charged capacity and estimated SOC. Equation 2 shows the formula used to calculate MAE for the estimation model:

$$MAE = \frac{1}{N}\sum_{i=1}^{n}\left|SOC_{i_a} - SOC_{i_e}\right| \qquad (2)$$

Where SOC_{i_a} represents the actual SOC calculated at observation i from the dataset and SOC_{i_e} represents the estimated SOC value for the same observation. It can be seen in Table 3 that hyperbolic MLPs have generally performed better then rectified MLPs, as for each pair of these MLPs models, trained with same ANN hidden layer configuration set, the error metric has a lower value for hyperbolic MLPs. Model 1, which is a hyperbolic MLP has the lowest value for error metric, i.e. 4.511. It can also be observed from the results that a general trend of improved performance is observed with an increase in number of layers and neurons of MLP models. This observation may indicate that the complex nature of data can be better understood by deeper neural network configurations. Additionally, it can be seen in Figure 4 and Figure 5 shows that the model's performance apart from a subset of actual SOC values less than ~50 ($S_{\sim 50}$), has been satisfactory. That particular subset has been predicted too high as compared to actual value, which is reflected in the error metrics value as well. Further experiments were conducted to see whether manually setting high epoch and iterations values would improve the performance. The results of those experiments had increased the performance of our model as high as MAE's equal to 1.5. However, the cost attached with this lowered MAE was overfitting the model.

Model id	Activation function	Loss function	Hidden layer	Hidden layers and neurons	Mean absolute error
1	hyperbolic	quantile	5	20,17,15,13,10	**4.511**
2	rectifier	quantile	5	20,17,15,13,10	4.556
3	Hyperbolic	quantile	4	15,13,10,7	5.184
4	Rectifier	quantile	4	15,13,10,7	5.767
5	Hyperbolic	quantile	3	10,7,5	4.965
6	Rectifier	quantile	3	10,7,5	*5.990*

Table 3 MLP models performance

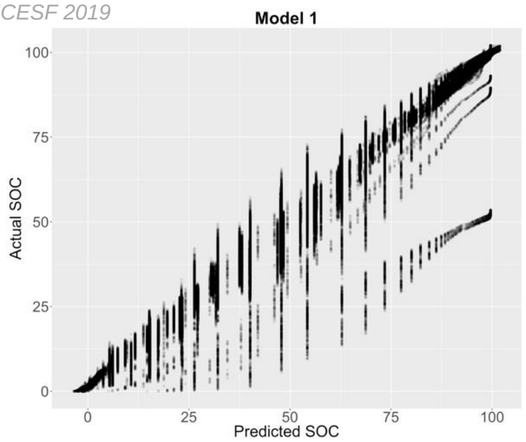

*Figure 4 Model 1's performance plot actual **vs** predicted SOC values*

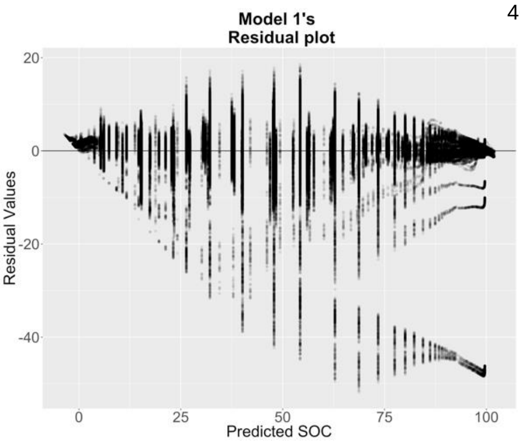

*Figure 5 Model 1's residual plot, difference in actual and estimated SOC **vs** actual SOC*

5. Conclusion

It can be concluded from the experimental results that creating an ANN based online SOC estimation model can be achieved by simply using battery's external parameters (charge/discharge current, voltage, and temperature). The hiccup in model's performance on $S_{\sim 50}$ could be due to lack of range of cycling and calendar aging covered in battery cells data. As discussed in results section, the error could have been brought down but the aim of the experimental setup was to prove that such techniques, as used in some of the recently proposed ANN based estimation models, create overfit models. Additionally, the importance of training data's nature, i.e. battery data extraction over different aging ranges can be assessed undoubtedly from the model's performance on $S_{\sim 50}$. Therefore, it is critical for an ANN based online SOC estimation model to be trained on an extensive amount of various cycle and calendar aging data to consolidate the effects of internal electrochemical reaction caused as the battery/cell ages.

6. References

[1]. Linden F, Reddy T B. Handbook of batteries. McGraw Hill Book Co. 1984;1:3-5

[2]. Herrmann F, Rothfuss F. Introduction to hybrid electric vehicles, battery electric vehicles, and off-road electric vehicles. Adv Batter Technol Electr Veh 2015:3–16.

[3]. Zheng L, Zhang L, Zhu J, Wang G, Jiang J. Co-estimation of state-of-charge, capacity and resistance for lithium-ion batteries based on a high-fidelity electrochemical model. Appl Energy 2016;180:424–34

[4]. Ng KS, Moo CS, Chen YP, Hsieh YC. Enhanced coulomb counting method for estimating state-of-charge and state-of-health of lithium-ion batteries. Appl Energy 2009;86:1506–11.

[5]. Zhang Y, Song W, Lin S, Feng Z. A novel model of the initial state of charge estimation for LiFePO 4 batteries. J Power Sources 2014;248:1028–33.

[6]. Lu L, Han X, Li J, Hua J, Ouyang M. A review on the key issues for lithium-ion battery management in electric vehicles. J Power Sources 2013;226:272–88.

[7]. Waag W, Sauer DU. Adaptive estimation of the electromotive force of the lithiumion battery after current interruption for an accurate state-of-charge and capacity determination. Appl Energy 2013;111:416–27.

[8]. Ting TO, Man KL, Lim EG, Leach M. Tuning of Kalman Filter Parameters via Genetic Algorithm for State-of-Charge Estimation in Battery Management System;2014; 2014.

[9]. Hu X, Li S, Peng H. A comparative study of equivalent circuit models for Li-ion batteries. J Power Sources 2012;198:359–67.

[10]. Di Domenico D, Fiengo G, Stefanopoulou A. Lithium-ion battery state of charge estimation with a Kalman Filter based on a electrochemical model. Control Appl 2008 CCA 2008 IEEE International Conference:702–707; 2008.

[11]. Rui-hao L, Yu-kun S, Xiao-fu J. Battery state of charge estimation for electric vehicle based on neural network. 2011 IEEE 3rd Int Conf Commun Softw Netw 2011:493–6.

[12]. Chen Y, Long B, Lei X. The battery state of charge estimation based weighted least squares support vector machine. Power Energy Eng Conf (APPEEC), 2011 Asia- Pac 2011;1:1–4.

[13]. Ephrem Chemali, Phillip J.Kollmeyer, MatthiasPreindl, AliEmadi State-of-charge estimation of Li-ion batteries using deep neural networks: A machine learning approach, Journal of Power Sources Volume 400, 1 October 2018, Pages 242-255: Elsevier.

Nottingham | UK | 9–11 September 2019

Multi-Voltage Level Operation of DC Loads in a 3-Pole PV-Based DC Microgrid

Babatunde Giwa [1], Yehdego Habtay [2]

[1]*University of Greenwich, b.a.giwa@gre.ac.uk, United Kingdom*
[2]*University of Greenwich, Y.T.Habtay@gre.ac.uk, United Kingdom*

Abstract: This paper proposes 3-pole PV-based dc microgrid with a single stage dc link. The proposed microgrid is operated in grid-connected mode and consists of a photovoltaic source, fixed/slowly changing dc loads operating at different voltage levels. The interface between the utility grid and the microgrid is bi-directional three-level Voltage Source Converter (*3L-VSC*). The architectural design of the *3L-VSC* aided by two equal centre-tapped capacitors serially connected on the dc link is leveraged on to conceptualise the idea of operating dc loads at lower voltage level without the use of additional dc-dc converter. The essence of this idea is to minimise cost for construction, reduce dynamic stability issue and improved power quality of the system. The central control strategy employed comprises of a newly modified Perturb &Observe Maximum Power Point Tracking (P&O *MPPT*) technique for PV model optimum performance and obeying the set conditions for desirable operation of the proposed microgrid. The microgrid model was developed and simulated in *MATLAB*/Simulink, using a realistic PV system model having used the real date form a solar weather station at Wolfson Centre. The functionality of this proposed system was tested under fixed/slowly changing distributed dc loads. The simulation results showed that the system performance is comparable to alternative approach, but with reduced number of components required for microgrid design and some improvement on the dc link voltage quality. This has led to significant reduction in complexity of the microgrid operation.

1. Introduction

The frequency of adoption of Power Electronics Technology (PET) in promoting the use of Renewable Energy Resources (RES) as replacement for conventional power sources is incontrovertible. This has largely given rise to different types of small-scale Distributed Generation (DG) units such as Photovoltaics (PVs), Battery Energy Storage System (BESS) and wind [1] whose penetration has steadily increased in low voltage microgrid [2]. The outputs of these DG units could originally be of either AC or DC that require to be converted to dc before dc load such as dc motors, computers and data centres could be desirably operated. Hence, making dc microgrid, a popular discrete energy system network. More so, reduced power losses during power transfer from source to loads in dc microgrid has contributed to its preferability to ac microgrid [3-6]. The reliability challenge of RES-Based DC Microgrid caused by intermittent nature of RES has been greatly reduced with aggregated RES when operated in islanded mode, but further reduction is certainly achieved in grid-connected mode of operation.

The popular power electronic interface that is responsible for grid-connected mode of operation of dc microgrid, especially with three-phase utility is called three-level Voltage Source Converter (3L-VSC) [7]. This type of converter has many advantages over its preceding version (two-level (2L)-VSC) for the following reasons: improved harmonic performance, less voltage stress on switches and reduced electromagnetic noise [8-11]. DC-DC converter is another power electronics device used in dc microgrid in operating dc loads at a lower or higher voltage other than that at which the primary sources in dc microgrid generate electricity. However, in a given application, bulky capacitors needed to support the operation of dc-dc converter, stability, signal-integrity and EMC issues are major challenges of dc-dc converter [12]. The three-three input-output terminals of 3L-VSC seem a potential characteristic that could be explored for reducing operational cost of grid-connected DC microgrid especially for distributed dc loads

The objective of this paper is to propose the conceptualisation of the idea of operating slowly changing/even distributed dc loads at lower voltage level without the use of dc-dc converter. This will be exhibited within a 3-pole PV-based dc microgrid by leveraging on the three-three input-output terminals feature of 3L-VSC. Section II studies the basis of 3-pole dc microgrid as the concept further leveraged on the two-equal centre-tapped capacitors serially connected on the dc link. Section III explains the operation of the microgrid from modelling to how the PV source data are generated. Section IV gives details of the model simulation viz-a-viz different scenarios considered. Simulation results are presented in section V while analysis of the simulation results is given section V1. The concluding part gives the compendium of the importance and successful performance of this type of microgrid.

2. Conceptualisation of 3-Pole DC Microgrid

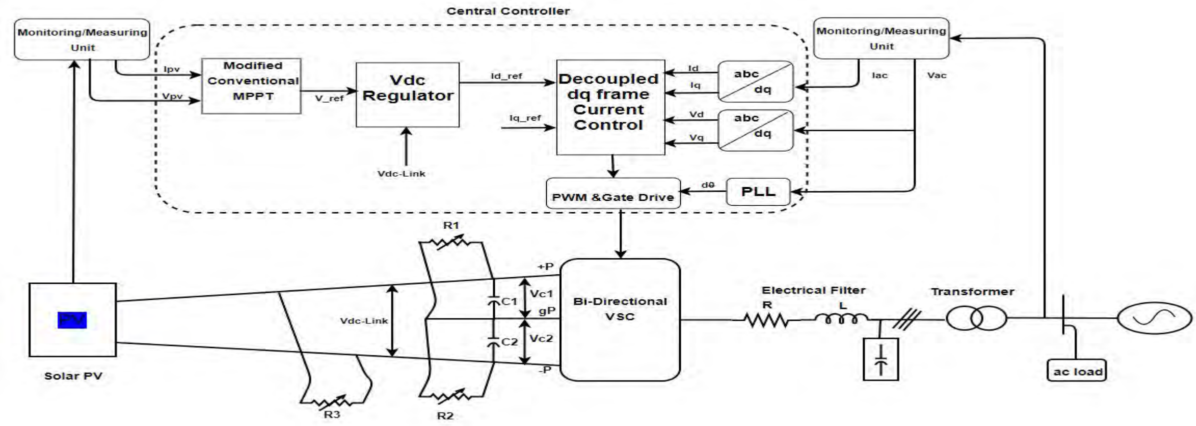

Fig.1: Proposed 3-Pole PV-Based DC Microgrid

The idea of 3-pole DC microgrid as shown in figure 1 is conceived in order to mimic the three-phase operational features of ac system network at distribution level where transformer is not required to operate loads either in phase voltage (Vp) or line voltage (Vline). Same idea is employed in 3-Pole DC microgrid where distributed dc loads (R1, R2 and R3) are directly connected to operate at different voltage levels without the use of dc-dc converter. As stated in section I, 3L-VSC unique features of three-three out-input terminals and the two serially connected capacitors facilitate the establishment of 3-Pole DC microgrid. The three dc side terminals of 3L-VSC represent positive pole (+P), ground pole (gP) and negative pole (-P) while other three terminals are connected to the utility grid. As the power source within the dc microgrid is directly connected to (+P) and (-P), creating a voltage level (Vpp or Vdc-link), the two serially connected capacitors and the ground pole form two equal lower voltage levels (Vgp). These two equal lower voltage levels are directly proportional to Vpp for effective harmonic performance of 3L-VSC. With this concept, the three dc loads R3, R1 and R2 can now respectively be operated at voltage level Vpp, Vgp1 or Vc1 and Vgp2 or Vc2 as shown in fig. 1. Comparatively, (1) gives the relationship between Vp and Vline while (2) gives that between Vpp and Vgp. Irrespective of the numerical values of R1 and R2, (3) must be adhered strictly to in order to avoid putting the 3L-VSC under undue voltage stress as well as undermining its improved harmonic performance over its preceding version (two-level VSC).

$$\mathrm{Vphase} = \frac{\mathrm{VLine}}{\sqrt{3}} \qquad \text{(I)}$$

$$\mathrm{Vgp} = \frac{\mathrm{Vpp}}{2} \qquad \text{(2)}$$

where
$\mathrm{Vgp} = \mathrm{Vc1} = \mathrm{Vc2}$
$\mathrm{Vpp} = \mathrm{Vdc\_link}$

$$\mathrm{Vc1} \approx \mathrm{Vc2} \approx \frac{\mathrm{Vdc\_link}}{2} \approx \frac{\mathrm{Vc1} + \mathrm{Vc2}}{2} \qquad \text{(3)}$$

3. Summary of 3-Pole DC Microgrid Model and Operation

The 3-Pole PV-Based DC Microgrid model shown in figure 1 was developed in MATLAB as a low voltage microgrid network with a single stage dc link that is operable in grid-connected mode via a bi-directional 3L-VSC. The only renewable energy source in the model is an aggregation of Photovoltaic (PV) panels. 250V, 250V and 500V are respectively chosen as the nominal operating voltages for R1, R2 and R3. Modified Perturb & Observe Maximum Power Point Tracking (P&O MPPT) algorithm in figure 2a for all level of solar irradiance ranging from 0-1000W/m^2 was employed to ensure a drift from these nominal voltages fall within UK bilateral acceptable voltage tolerance [13]. With this, the dc loads will be in desirable and continuous operation. The output of the modified-P&O MPPT algorithm is an integral part of the central controller. It will serve as voltage reference (V_ref) of the feedback loop control for the Vdc-link regulation and to ensure 3L-VSC produces only active power (Id_ref) that corresponds to v_ref as shown figure 2b during its operational modes.

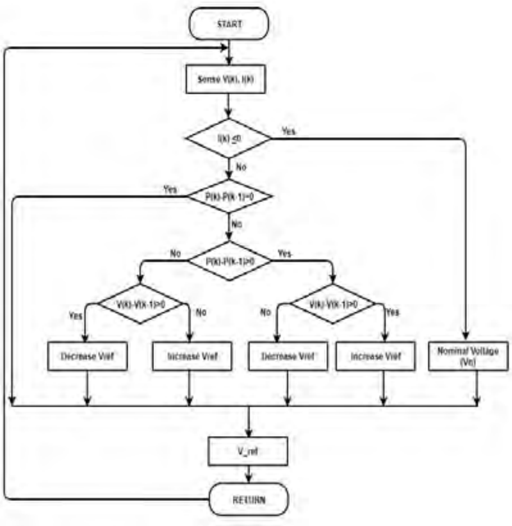

Fig.2a: Modified P&O MPPT Algorithm

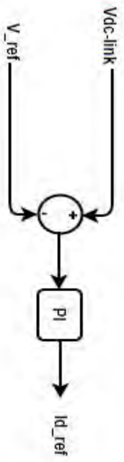

Fig.2b: DC Link PI Controller

To have desirable quality of power exported or imported from the grid, a feedforward loop control is employed for complete decoupling of dq frame current (Id_ref and Iq_ref) while the phase lock loop is used to fulfil the synchronisation of the dc microgrid with the grid. The PV model was inputted with information extracted from the rooftop solar irradiance profile (see figure 3) database at Wolfson Center. The profile clearly show intermittent nature of the solar array at different level of solar insolation over 24 hours.

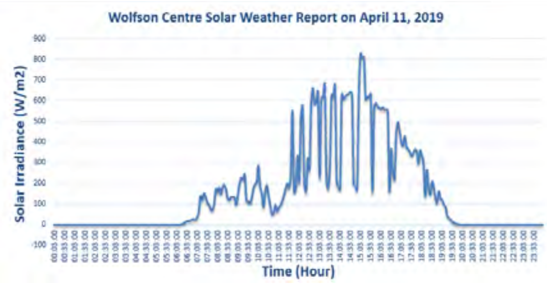

Fig 3. A-Day Solar Irradiance Profile

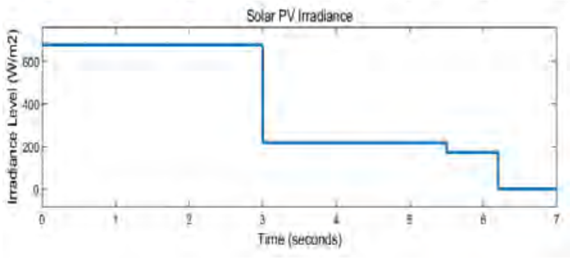

Fig 4. Simulation Solar Irradiance Profile

4. Model Simulation

The developed model of 3-Pole PV-Based DC Microgrid in figure 1 was simulated in MATLAB/Simulink over a range of slowly and rapidly changing irradiance in figure 4. This simulation irradiance profile in figure 4 was a replica of mid-day to mid-night of the irradiance profile in figure 3. The simulation was then carried out with the adoption of the modified P&Q MPPT technique viz-a-viz different dc load values for R1, R2 and R3. The same model was separately prepared for simulation but this time around with the conventional P&Q MPPT algorithm for

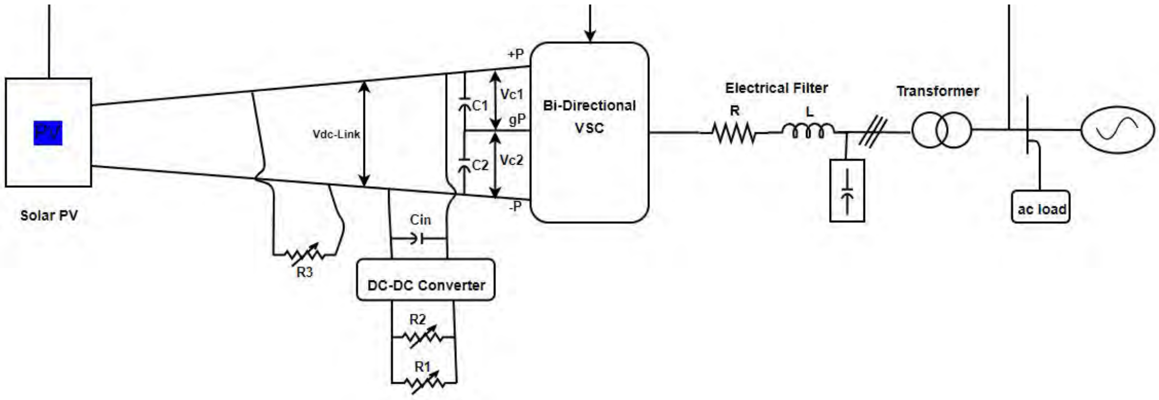

Fig.5: Conventional Grid-Connected DC Microgrid

An alternative model shown in figure 5, a grid-connected PV microgrid was also developed and simulated in MATLAB/Simulink but with the service of dc-dc converter for the operation of R1 and R2. The simulation of this alternative model was done with the conventional P&Q MPPT algorithm and the dc-dc converter is modelled with a feedback control system to ensure that R1 and R2 are operated at nominal voltage of 500V. The use of dc-dc converter or not and type of P&O MPPT employed have defined different scenarios considered during simulation as tabulated below.

TABLE I. SCENARIOS CONSIDERED UNDER SIMULATION

DC LOADS	P&O MPPT (Q) and DC-DC Converter (D)				
	Conventional Q + D not used	Modified Q + D not used	Modified Q + D not used	Unmodified Q + D used	Unmodified Q + D used
R1	5Ω	5Ω	4Ω	5Ω	4Ω
R2	5Ω	5Ω	5Ω	5Ω	5Ω
R3	1Ω	1Ω	1Ω	1Ω	1Ω

5. Simulation Results

The results shown below are the output of the parametric study of the model in Fig. 1 and Fig. 5.

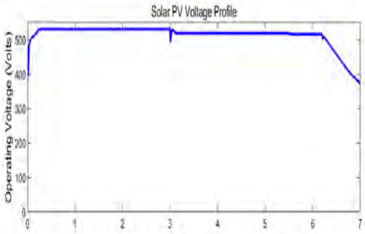

Fig.6a. Solar PV Output voltage with Conventional P&O MPPT under R1=R2=5Ω and R3=1Ω

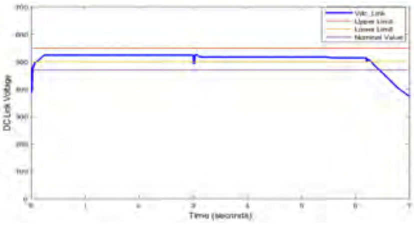

Fig.6b. DC Link Voltage across R3=1 Ω with Conventional P&O MPPT

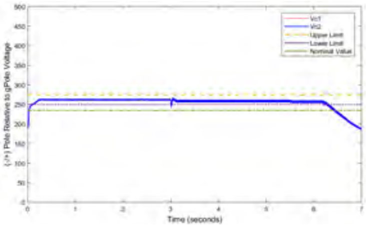

Fig.6c. Pole Voltages across R1=R2=5Ω with Conventional P&O MPPT

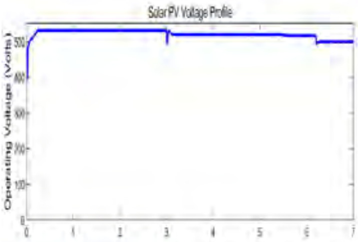

Fig.7a. Solar PV Output voltage with Modified P&O MPPT under R1=R2=5Ω and R3=1Ω

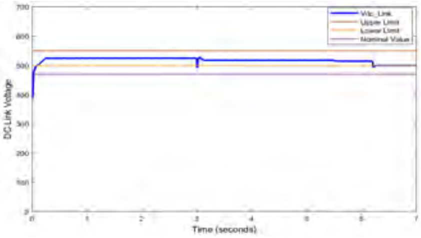

Fig.7b. DC Link Voltage across R3=1 Ω with Modified P&O MPPT

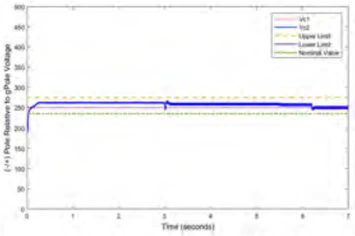

Fig.7c. Pole Voltages across R1=R2=5Ω with Modified P&O MPPT

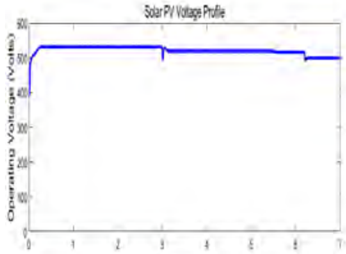

Fig.8a. Solar PV Output voltage with Modified P&O MPPT under R1= 4 Ω, R2=5Ω and R3=1Ω

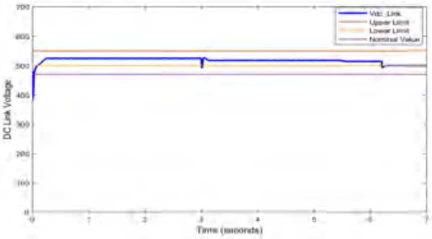

Fig.8b. DC Link Voltage across R3=1 Ω with Modified P&O MPPT

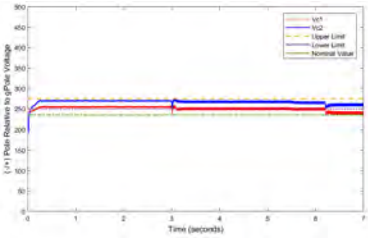

Fig.8c. Pole Voltages across R1=4 Ω, R2=5Ω with Modified P&O MPPT

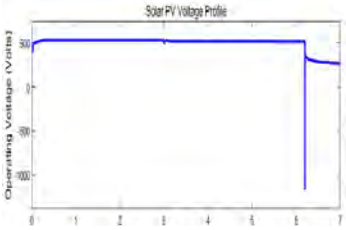

Fig.9a. Solar PV Output voltage with Conventional P&O MPPT + DC-DC Converter under R1= R2=5Ω and R3=1Ω

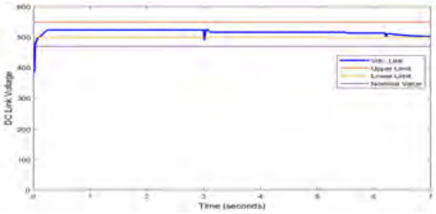

Fig.9b. DC Link Voltage across R3=1 Ω with Conventional P&O MPPT

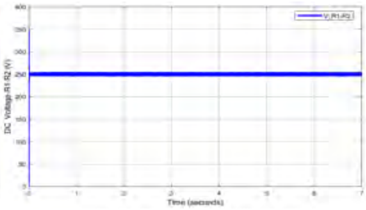

Fig.9c. Pole Voltages across R1= R2=5Ω with Conventional P&O MPPT

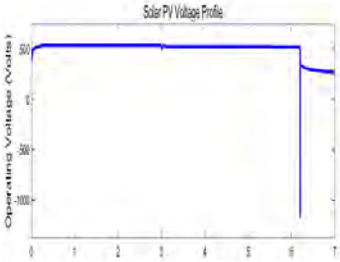

Fig.10a. Solar PV Output voltage with Conventional P&O MPPT + DC-DC Converter under R1= 4 Ω, R2=5Ω and R3=1Ω

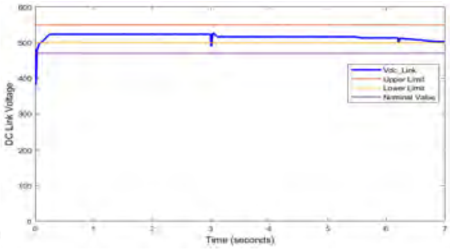

Fig.10b. DC Link Voltage across R3=1 Ω with Conventional P&O MPPT

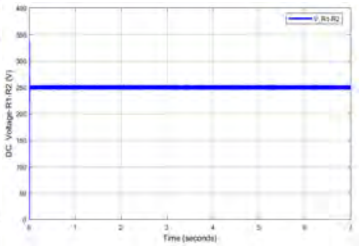

Fig.10c. Pole Voltages across R1=4 Ω and R2=5Ω with Conventional P&O MPPT

6. Discussion

The simulation of the 3-pole PV based dc microgrid in figure 1 under balanced distributed loads R1=R2 (5Ω) but with conventional/unmodified P&Q MPPT led to the undesirable operating voltages across the dc loads (R1, R2 and R3). This is clearly shown in figure 6b and 6c as Vdc-link, Vc1 and Vc2 fell out of the nominal voltage tolerance range (94%-110%) recommended in UK [13]. This fall out is attributed to rapid drop in the PV operating voltage (see figure 6a) caused by rapid change in the solar irradiance of the PV from 200W/m^2 to 0W/m^2 as shown in figure 4. The inadequacy of this conventional P&O MPPT led to the employment of modified version of P&Q MPPT algorithm shown in figure 2a. Consequently, the simulation carried out under same dc load conditions (R1=R2=5Ω and R3=1Ω) and modified MPPT algorithm showed that R1, R2 and R3 are desirably operated, owing to Vdc-link, Vc1 and Vc2 been kept within upper and lower voltage limit as shown in figure 8b and 8c. In additional to this, appreciable improvement was recorded during irradiance level of 0W/m^2 on the Total Harmonic Distortion (THD) of the dc link voltages (Vdc-link, Vc1 and Vc2) relative to dc component. The THD of the voltages across R3, R1 and R3 were respectively reduced from 2.96% to 0.08%, 3.18% to 1.30% and 3.22% to 1.30%.

A clear observation of the dc link voltage signals (Vdc-link, Vc1 and Vc2) as shown in figure 8b and 8c showed that even with slight difference in the distributed dc load resistances (R1≠R2), the modified P&O MPPT proved to be robust enough in ensuring desirable operation of the three dc loads as their operating voltages are within specified limit. Though the quality of grid current might be affected due to the slight mismatch between Vc1 and Vc2, this concern is out of the scope of this research. Despite the observed voltage mismatch, the THD of dc link voltages for Vdc-link, Vc1 and Vc2 remained respectively at 0.16%, 1.42% and 1.22%. These percentages conform to the harmonic standard limit recommended by IEEE 519-1992 [14].

Alternative approach shown in figure 5 was taken to operate the two of the dc loads (R1 and R2) at desirable voltage, with the employment of dc-dc converter and conventional P&O MPPT. Under both R1=R2 and R1≠R2, the dc link voltages Vc1 and Vc2 across R1 and R2 were precisely equal to the nominal voltage of 250V as shown in figure 9c and 10c. With this, the operation proved more desirable for R1 and R2 compare to what was obtained when the R1 and R2 were directly operated on the dc link of the proposed 3-Pole PV Based DC Microgrid. However, the employment of dc-dc converter is expected to increase system cost and distortion in the system. This increased distortion is clearly observed as considerable increase of THD of output voltage of the dc-dc converter fed on R1 and R2 was recorded at 3.2% compared to about 1% recorded in the proposed 3-Pole PV Based DC Microgrid.

7. Conclusion

This paper has presented an implementable concept of operating dc loads at desirable different voltage levels without the employment of dc-dc converter in a novel type of grid-connected dc microgrid called 3-Pole PV Based DC Microgrid. Modified P&O MPPT algorithm developed together with 3L-VSC were leverages for this novel idea that was implemented in Simulink/MATLAB under different scenarios of distributed dc loads and changing solar irradiance. The simulation results have shown comparatively, desirable dynamic performance of the microgrid with reduced number of design components and improved THD of the dc link voltages relative to the dc component. Non-utilisation of dc-dc converter as a sub-system in the operation of these dc loads is anticipated to improve the efficiency of the proposed microgrid and reduce operational cost when compared with the alternative approach.

References

[1] A. Adib, J. Lamb and B. Mirafzal, "Ancillary Services via VSIs in Microgrids With Maximum DC-Bus Voltage Utilization," in IEEE Transactions on Industry Applications, vol. 55, no. 1, pp. 648-658, Jan.-Feb. 2019.

[2] S. Skarvelis-Kazakos, B. A. Giwa and D. Hall, "Microgrid power balancing with redox flow batteries," IEEE PES Innovative Smart Grid Technologies, Europe, Istanbul, 2014, pp. 1-6.

[3] H. Kakigano, M. Nomura, T. Ise, “loss evaluation of DC distribution for residential houses compared with AC system,” The 2010 International Power Electronics Conference-ECCE Asia-(IPEC-Sapporo), 22A1-3, 2010, pp.480-486.

[4] K.Yukita, K.Ban, Y.Goto, K.Ichiyanagi, K.Hirose, T.Ushirokawa, Y.Okui and H.Takabayashi “Power supply system of DC/AC micro grid system,” 8th International Conference on Power Electronics - ECCE Asia, IEEE, pp. 228-234, May 30-June 3, 2011.

[5] Lie Xu, Dong Chen “Control and operation of a DC microgrid with variable generation and energy storage,” IEEE transactions on power delivery, vol. 26, pp. 2513-2522, October 2011.

[6] J. Lee, B. Han, N. Choi, “DC micro-grid operational analysis with detailed simulation model for distributed generation,” Energy Conversion Congress and Exposition (ECCE), IEEE, pp. 3153 -3160, 12-16 Sept. 2010.

[7] F. Sebaaly, H. Vahedi, H. Y. Kanaan, N. Moubayed and K. Al-Haddad, "Design and Implementation of Space Vector Modulation-Based Sliding Mode Control for Grid-Connected 3L-NPC Inverter," in IEEE Transactions on Industrial Electronics, vol. 63, no. 12, pp. 7854-7863, Dec. 2016.

[8] U. M. Choi, H. H. Lee, and K. B. Lee, “Simple neutral-point voltage control for three-level inverters using a discontinuous pulse width modulation,” IEEE Trans. Energy Convers., vol. 28, no. 2, pp. 434–443, Jun. 2013.

[9] N. V. Nguyen, B. X. Nguyen, and H. H. Lee, “An optimized discontinuous PWM method to minimize switching loss for multilevel inverters,” IEEE Trans. Ind. Electron., vol. 158, no. 9, pp. 3966–3968, Sep. 2011.

[10] A. R. Haitham, H. Joachim, R. Jose, and B. M. Ge, “Medium voltage multilevel converters: State of the art, challenges and requirements in industrial applications,” IEEE Trans. Ind. Electron., vol. 57, no. 8, pp. 2581–2596, Aug. 2010.

[11] M. Narimani and G. Moschopoulos, “Analysis and design of a single-stage three-level PFC AC-DC converter,” in Proc. IEEE Appl. Power Electron. Conf., 2012, pp. 1134–1141.

[12] D. J. Nguyen, S. l. Harris, I. Novak, ”Emerging Challenges of DC-DC Converters” DesignCon2007, Santa Clara, CA, January 29-31, 2007. Available: http://www.electrical-integrity.com

[13] J. Whitefield, A. Hay-Ellis ‘The Electrician’s Guide to the 17th Edition of the IET Wiring Regulations BS 7671:2008 Incorporating Amendment 3:2015 and Part P of the Building Regulations’ 2015, p. 120.

[14] S. M. Halpin, "Comparison of IEEE and IEC harmonic standards," *IEEE Power Engineering Society General Meeting, 2005*, San Francisco, CA, 2005, pp. 2214-2216 Vol. 3.

Nottingham | UK | 9–11 September 2019

Dynamic Performance of Tank-Circuited 3-Pole PV-Based DC Microgrid under Stochastic DC Loads Distribution

Babatunde Giwa [1], Yehdego Habtay [2]

[1]*University of Greenwich, b.a.giwa@gre.ac.uk, United Kingdom*
[2]*University of Greenwich, Y.T.Habtay@gre.ac.uk, United Kingdom*

Abstract: This paper presents the operational stability of 3-pole PV-based dc microgrid with unbalanced distributed dc loads. This type of grid-connected dc microgrid model was developed with solar power plant, utility ac grid and bi-directional three-level voltage source converter (3L-VSC). The 3L-VSC serves as an interface between the microgrid and the utility grid through a single-stage dc link. The structural design of the 3L-VSC alongside two equal centre-tapped capacitors in series connection on the dc link have created connecting points for operating variable distributed dc loads at lower voltage level without the employment of additional voltage converter. However, operation of these variable dc loads has resulted into unbalanced pole-to-pole voltage which undermine the stability, power quality of the dc link and normal operation of 3L-VSC. A distributed PWM based algorithm was developed to coordinate the operation of 2-in-1 tank circuit in balancing the pole-to-pole voltages. More so, the employed central controller for PV output power optimisation and regulation of measured ac parameters showed some inefficiency in performance. As such, Perturb & Observe Maximum Power Point Tracking (P&O MPPT) algorithm which is part of the central controller was improved to address the inefficiency. The PV model used was developed with real data from solar weather station at Wolfson Centre. Parametric study was carried out using MATLAB/Simulink on the dynamic performance of the model over a daily solar irradiance profile. The results obtained clearly show that the set conditions for desirable operation of the microgrid together with the loads are successfully met.

1. Introduction

In Renewable Energy Sources (RES) based microgrid, most especially dc microgrid, there is often use of dc-dc converter for operation of dc loads at desirable voltage level [1]. However, there are a number of issues associated with the operation of dc-dc converter in a given application [2], among which are EMC, signal-integrity and stability issues. Within a dc microgrid, not much research has been done on how dc loads could be operated at a specific desirable voltage level without the use of dc-dc converter. But the structural design of 3L-VSC has got unique three-three output-input terminals feature that could be explored for achieving this specific lower voltage level. This possibility could also be supported by two equal centre-tapped capacitors in series connection on the dc link of grid-connected dc microgrid where 3L-VSC is used as interface between the grid and the microgrid.

In the normal operation of 3L-VSC, the voltage across the two aforementioned capacitors needs to be equal so as to have less voltage stress on the switching devices present in the system as well as better quality of its output waveform [3-6]. In [7], dc link capacitance differential, unbalanced three-phase operation and irregularity in switching devices pattern accounted for the voltage imbalance across the two capacitors. This has led to increase in Total Harmonic Distortion (THD) of both the dc link voltage and the grid ac current. In solving this problem of voltage imbalance, several strategic space vector modulation methods have been proposed in [8-14] to address this imbalance mainly for improving the quality of the output waveforms of 3L-VSC. Aside the perspective of these proposed methods, none of them has addressed both the quality of the dc link parameters and voltage balancing in relation to 3-Pole DC microgrid where dc loads are directly operated in parallel with the dc link two capacitors.

The objective of this paper is to propose a simple distributed PWM based algorithm controlled 2-in-1 tank circuit and modified P&O MPPT technique to achieve a desirable dynamic performance of a 3-pole PV-based dc microgrid. This performance is to be examined under a stochastic distributed dc loads and over 24 hours solar irradiance profile while ensuring balancing of the dc link pole-to-pole voltages. Section II explains the concept of 3-pole DC microgrid using the special feature of 3L-VSC. Section III gives details of the microgrid model, simulation results and how the dc microgrid power source data are generated. Analysis of the simulation results in relation to different scenarios considered are given in section IV.

2. Modelling and Operation of Proposed Tank-Circuited 3-Pole DC Microgrid

The section gives an insight into the design model and operation of 3-Pole DC Microgrid as depicted in figure 1. Description of the microgrid model, source of solar irradiance profile, control and embodiment of the tank circuit at the dc link are emphasised here.

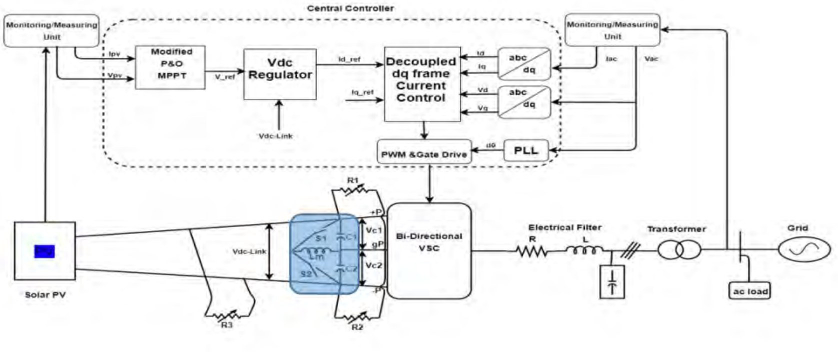

Fig 1. Operational Control of Tank-Circuited 3-Pole PV-Based DC Microgrid

The tank-circuited 3-Pole PV-Based DC Microgrid shown in figure 1 was modelled in MATLAB as a low voltage grid-connected microgrid. Distributed disproportionate dc loads ((R1, R2 and R3) are directly connected to the PV via a single state dc link while the microgrid is connected to the grid via 3L-VSC. The provision of dc-dc converter is not required to safely and desirably operate the aforementioned dc loads. This is owing to the required voltage levels created by three poles (positive pole (+P), ground pole (gP) and negative pole (-P)) via the two equal centre-tapped serially connected capacitor C1 and C2. The three dc loads R1, R2 and R3 are to be desirably operated respectively across the poles on voltages Vpp, $\mathrm{Vc1}$ and $\mathrm{Vc2}$ as shown in fig. 1 or within 94% to 110% of their nominal voltages (Vppn, $\mathrm{Vc1n}$ and $\mathrm{Vc2n}$) [15]. The conditions set for safe and desirable operation of 3L-VSC is (1) while that for the dc loads are (2), (3) and (4) respectively for R1, R2 and R3.

$$\mathrm{Vc1} \approx \mathrm{Vc2} \approx \frac{\mathrm{Vdc-link}}{2} \approx \frac{\mathrm{Vc1+Vc2}}{2} \tag{1}$$

$$0.94\mathrm{Vc1n} \leq \mathrm{Vc1} \leq 1.1\mathrm{Vc1n} \tag{2}$$

$$0.94\mathrm{Vc2n} \leq \mathrm{Vc2} \leq 1.1\mathrm{Vc2n} \tag{3}$$

$$0.94\mathrm{Vppn} \leq \mathrm{Vpp} \leq 1.1\mathrm{Vppn} \tag{4}$$

where

$\mathrm{Vpp = Vdc - link}$

$\mathrm{Vc1n = 250V}$

$\mathrm{Vc2n = 250V}$

$\mathrm{Vppn = Vn = 500V}$

However, stochastic nature of these dc loads especially R1 and R2 could violate the set conditions. To prevent this violation, the dc link is tank-circuited through inductor Lm and Switches, S1 and S2.

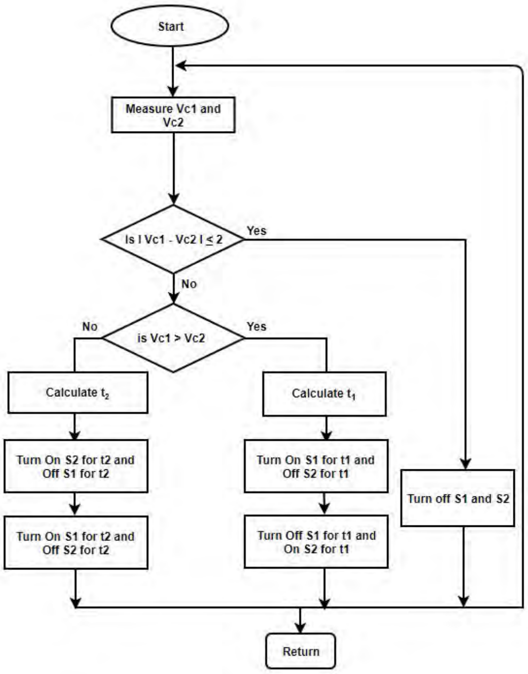

Fig. 2. Distributed Pulse Width Modulation (d-PWM) Algorithm

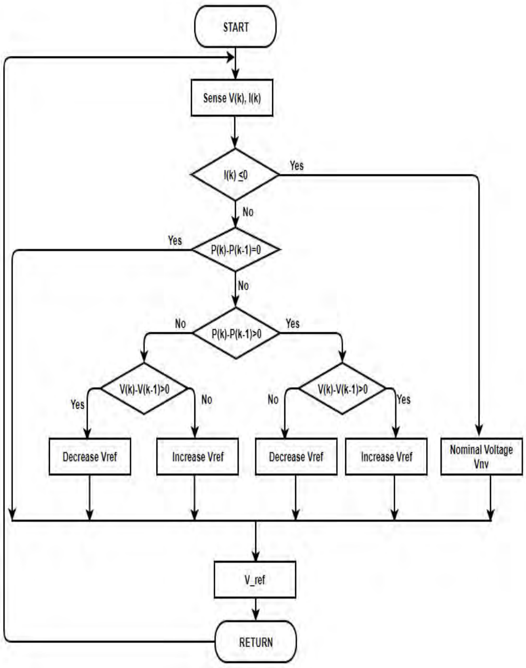

Fig.3. Modified P&O MPPT Algorithm

The tank circuiting part is highlighted in figure 1 and is seamlessly achieved through the developed distributed Pulse Width Modulation (d-PWM) algorithr

If $\mathrm{Vc1} = \mathrm{V1};\ \mathrm{Vc2} = \mathrm{V2}$ and $\mathrm{V1} > \mathrm{V2}$

For (1) *to be met*, (3) *must be valid*

$$(\mathrm{Vm} + \mathrm{V1}) = \frac{\mathrm{V1} + \mathrm{V2}}{2} \qquad (5)$$

Since Lm forms tank circuit with either C1or C2

$$\mathrm{I_{LM}} = \mathrm{I_C} \qquad (6)$$

$$\sqrt{\frac{\mathrm{K(V1 + V2)}}{\mathrm{V1 - V2}}} = t_1 \qquad (7)$$

$$\sqrt{\frac{\mathrm{K(V1 + V2)}}{\mathrm{V2 - V1}}} = t_2 \qquad (8)$$

$$\mathrm{K} = \mathrm{LC} \qquad (9)$$

Where

t_1 and t_2 *are equal and On and Off time for both* S1 and S2

$$\text{Switching Frequency} = \frac{1}{t_1 + t_2}$$

$$\mathrm{L} = \mathrm{Lm}$$

$$\mathrm{C} = \mathrm{C1} = \mathrm{C2}$$

More so, modified version of Perturb & Observe Ma algorithm was developed as shown in figure 3 to fulfil extracted.

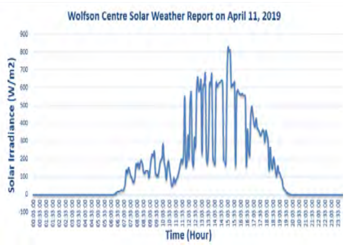

Fig.4. One Day Solar Irradiance Profile

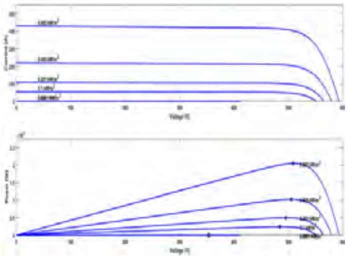

Fig.5.Physical Solar Array Voltage and Power Profile

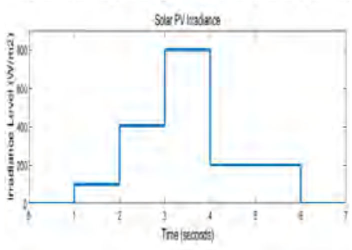

Fig.6 Simulation Solar Irradiance Profile.

3. Simulation of Model

The developed model of 3-Pole PV-Based DC Microgrid was simulated in MATLAB/Simulink for 7 minutes with simulation solar irradiance levels in figure 6. This simulation irradiance levels is a representation of the one-day solar irradiance profile in figure 4. The simulation was run with the chosen value of K (0.0541) and specified value of C (0.541F) was used using (9) to establish the value of Lm. The scenarios considered under simulation is tabulated below.

Table I. Simulation Scenarios under Distributed Stochastic DC Loads

DC LOADS	**P&O MPPT (Q) and Tank-Circuit (T)**			
	Conventional Q + T not used	Modified Q + T used	Conventional Q + T not used	Modified Q + T used
R1	5Ω	5Ω	8Ω	8Ω
R2	8Ω	8Ω	5Ω	5Ω
R3	1Ω	1Ω	1Ω	1Ω

4. Simulation Results

The results of the parametric study of the proposed microgrid are comparatively shown below.

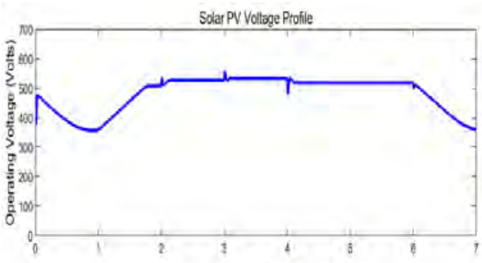

Fig.7a. Solar PV Output voltage with Conventional P&O MPPT under R1≠R2 and R3=1Ω

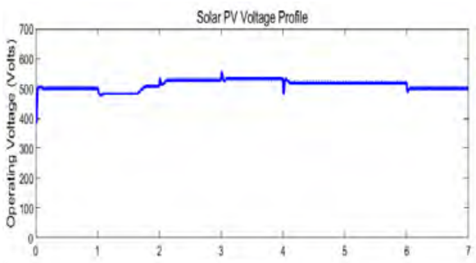

Fig.7b. Solar PV Output voltage with Modified P&O MPPT under R1≠R2 and R3=1Ω

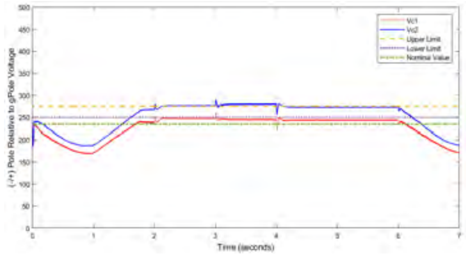

Fig.8a. Pole-to-Pole Voltages Vc1 and Vc2 with Conventional P&O MPPT under R1= 5Ω. R2=8Ω and R3=1Ω

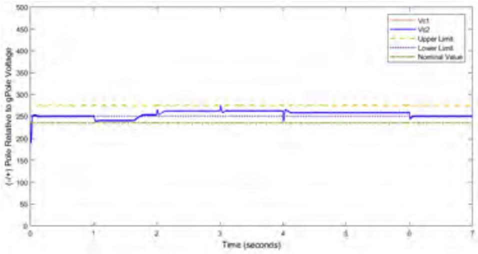

Fig.8b. Pole-to-Pole Voltages Vc1 and Vc2 with Modified P&O MPPT and Controlled T under R1= 5Ω. R2=8Ω and R3=1Ω

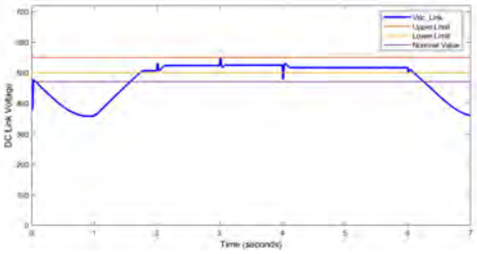

Fig.9a. DC Link Voltage (Vdc_link) with Conventional P&O MPPT under R1= 5Ω. R2=8Ω and R3=1Ω

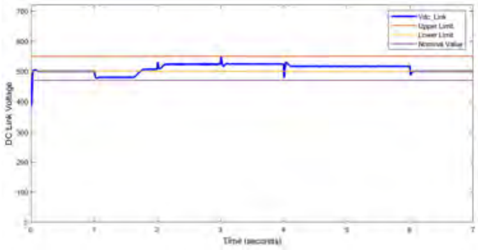

Fig.9b. DC Link Voltage (Vdc_link) with Modified P&O MPPT and Controlled T under R1= 5Ω. R2=8Ω and R3=1Ω

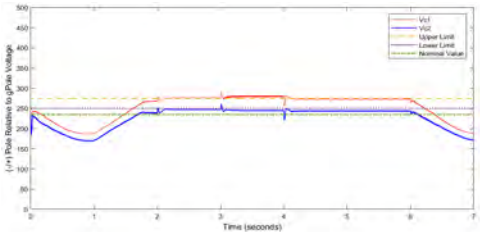

Fig.10a. Pole-to-Pole Voltages Vc1 and Vc2 with Conventional P&O MPPT under R1= 8Ω. R2=5Ω and R3=1Ω

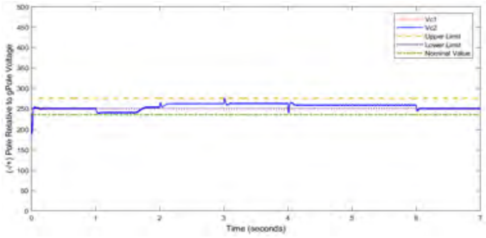

Fig.10b. Pole-to-Pole Voltages Vc1 and Vc2 with Modified P&O MPPT and Controlled T under R1= 8Ω. R2=5Ω and R3=1Ω

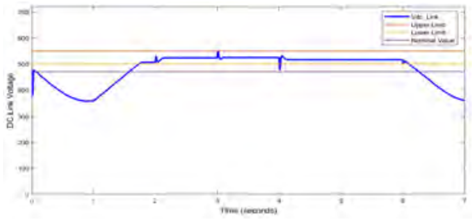

Fig.11a. DC Link Voltage (Vdc_link) with Conventional P&O MPPT under R1= 8Ω, R2=5Ω and R3=1Ω

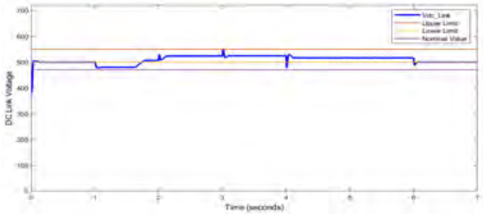

Fig.11b. DC Link Voltage (Vdc_link) with Modified P&O MPPT and Controlled T under R1= 8Ω, R2=5Ω and R3=1Ω

Simulation of the model with conventional P&O MPPT techniques have it in figure 7a that the operating voltage of the PV at maximum power point (V_ref) will promote the violation of the condition set in (4). Owing to the single stage dc link of the model that makes V_ref equals Vdc-link, the violation is so obvious especially during early morning and night when the solar irradiance has dropped to 0w/m2. The replacement of this techniques with the modified P&O MPPT algorithm show in figure 7b that the set condition in (4) is unlikely to be violated as V_ref falls within the set values.

With the following dc loads (R1=5Ω and R2=8Ω), the simulation run with conventional Q and without tank-circuiting has put both Vc1 and Vc2 out of the set values in (2) and (3). The set conditions were gravely violated as shown in figure 8a during the zero irradiance level and solar irradiance transient state. However, the employment of modified Q and tank-circuiting of the dc link show in figure 8b that the conditions set for safe and desirable operation of 3L-VSC and the dc loads are met. For R3, (4) was only violated during zero irradiance level as shown in 9a but this violation was corrected when run with T and modified Q.

Comparatively, the results of the simulation follow similar pattern when R1=8Ω and R2=5Ω (see 10a and 11a) with what were obtained when R1=5Ω and R2=8Ω. Similarly, the employment of modified Q and tank-circuiting of the dc link has helped as shown in figure 10b and 11b to return the Vdc-link, Vc1 and Vc2 within the set values, and this has ensured safe and desirable operation of 3L-VSC. With all scenarios under which the model was simulated, variability of dc load R3 has not contributed to the violation of set conditions (1)-(3), except to (4) during zero irradiance level.

5. Conclusion

This paper has presented simple novel techniques in addressing the challenges faced in operating stochastic distributed dc loads at desirable lower voltage levels without the provision of dc-dc converter in a 3-Pole PV-Based DC Microgrid. This newly conceived type of grid-connected dc microgrid experiences voltage mismatch on the dc link that is undesirable for the operation of VSC. The embodiment of distributed-PWM controlled tank-circuit on the dc link has brought the mismatch to nearly zero. In addition to that, violated set conditions for safe and desirable operation of the stochastic distributed dc loads were corrected through employment of modified P&O MPPT techniques. The concept adopted in solving the aforementioned challenges was developed and implemented in MATLAB/Simulink. The examination of the results over varying factors such as rapidly varying solar irradiance show good dynamic performance and confirm the robustness of the tank-circuit control mechanism.

References

[1] N.Femia, G.Petrone, G.Spagnuolo, M.Vitelli, “Optimization of Perturb and Observe Maximum Power Point Tracking Method,” IEEE Trans. Power Electron, vol. 20, no. 4, pp. 963–973, Jul. 2005.

[2] D. J. Nguyen, S. l. Harris, I. Novak, ”Emerging Challenges of DC-DC Converters” DesignCon2007**,** Santa Clara, CA, January 29-31, 2007. Available: http://www.electrical-integrity.com

[3] Lyu, Jianguo & Hu, Wenbin & Wu, Fuyun & Yao, Kai & Wu, Junji. (2016). A Neutral-Point Voltage Balance Controller for the Equivalent SVPWM Strategy of NPC Three-Level Inverters. Journal of power electronics. 16. 2109-2118. 10.6113/JPE.2016.16.6.2109.

[4] C. C. Wang and Y. D. Li, “Analysis and calculation of zero-sequence voltage considering neutral-point potential balancing in three-level NPC converters,” IEEE Trans. Ind. Electron., Vol. 57, No.7, pp. 2262-2271, Jul. 2010.

[5] J. Lyu, W. Hu, F. Wu, K. Yao, and J. Wu, “A new DPWM method to suppress the low frequency oscillation of the neutral-point voltage for NPC three-level inverters,” Journal of Power Electronics, Vol. 15, No. 5, pp. 1207-1216, Sep. 2015.

[6] U. M. Choi and K. B. Lee, “Space vector modulation strategy for neutral-point voltage balancing in three-level inverter systems,” IET Power Electronics, Vol. 6, No. 7, pp. 1390-1398, Aug.2013.

[7] U. Choi, H. Lee and K. Lee, "Simple Neutral-Point Voltage Control for Three-Level Inverters Using a Discontinuous Pulse Width Modulation," in *IEEE Transactions on Energy Conversion*, vol. 28, no. 2, pp. 434-443, June 2013

[8] J. S. Lee and K. B. Lee, “New modulation techniques for a leakage current reduction and a neutral-point voltage balance in transformerless photovoltaic systems using a three-level inverter,” IEEE Trans. Power Electron., Vol. 29, No. 4, pp. 1720-1732, Apr. 2014.

[9] U. M. Choi, J. S. Lee, and K. B. Lee, “New modulation strategy to balance the neutral-point voltage for three-level neutral-clamped inverter systems,” IEEE Trans. Energy Convers., Vol. 29, No. 1, pp. 91-100, Mar. 2014

[10] U. M. Choi, H. H. Lee, and K. B. Lee, “Simple neutral-point voltage control for three-level inverters using a discontinuous pulse width modulation,” IEEE Trans. Energy Convers., Vol. 28, No. 2, pp. 434-443, Jun. 2013.

[11] C. C. Wang and Y. D. Li, “Analysis and calculation of zero-sequence voltage considering neutral-point potential balancing in three-level NPC converters,” IEEE Trans. Ind. Electron., Vol. 57, No.7, pp. 2262-2271, Jul. 2010.

[12] N. Celanovic and D. Boroyevich, “A comprehensive study of neutral-point voltage balancing problem in three-level A Neutral-Point Voltage … 2117 neutral-point-clamped voltage source PWM inverters,” IEEE Trans. Power Electron., Vol. 15, No. 2, pp. 242-249, Mar. 2000.

[13] U. M. Choi and K. B. Lee, “Space vector modulation strategy for neutral-point voltage balancing in three-level inverter systems,” IET Power Electronics, Vol. 6, No. 7, pp. 1390-1398, Aug.2013.

[14] W. Song, X. Feng, and K. M. Smedley, “A carrier-based PWM strategy with the offset voltage injection for single-phase three-level neutral-point-clamped converters,” IEEE Trans. Power Electron., Vol. 28, No. 3, pp. 1083-1095, Mar. 2013.

[15] J. Whitefield, A. Hay-Ellis ‘The Electrician’s Guide to the 17th Edition of the IET Wiring Regulations BS 7671:2008 Incorporating Amendment 3:2015 and Part P of the Building Regulations’ 2015, p. 120.

Nottingham | UK | 9–11 September 2019

Yeast cell stress: impacts on fermentation and methods for tolerance engineering

Joshua Eardley[1] and David J Timson[1],

[1]*School of Pharmacy and Biomolecular Sciences, University of Brighton, Huxley Building, Lewes Road, Brighton, BN2 4GJ. UK.*

j.eardley@brighton.ac.uk

Abstract

Environmental benefits and increased energy security are associated with the substitution of fossil-derived fuels with biofuels. The commercial viability of biofuels including bioethanol is limited by factors including its uncompetitive price, with policy also favouring the adoption of second-generation or advanced biofuels. Higher costs and energy intensive production steps associated with advanced biofuel production need to be addressed. Obtaining maximum yields from an alcohol fermentation also remains a technical challenge, despite advanced bioprocessing techniques being available. High stress tolerance is considered a favourable phenotypic trait for industrial microorganisms, with chaotropicity being suggested as the major limiting stress factor affecting biofuel production. Budding yeast (*Saccharomyces cerevisiae*) remains the principle yeast utilized for bioethanol production and an outstanding model system for elucidating cellular stress mechanisms. Strategies for biofuel related stress mitigation are of importance to biofuel economics and it is expected that the emergence of novel genetic tools and other strategies for improving fermentation performance will lead to further industry development.

Keywords: Bioethanol; chaotropicity; kosmotropicity; fermentation; biofuel yield; compatible solute; cell stress

1. Introduction

Bioethanol possesses commercial value in multiple forms, including as a biofuel or antimicrobial [1]. Benefits associated with the use of biofuels include increased energy security, air quality, and reduced greenhouse gas emissions [2]. Food-security and land-use-change concerns have shifted policy in favour of the adoption of advanced biofuels [2].

Breakthroughs in second-generation bioethanol production are expected to increase commercial adoption [2], with subsequent chemical conversion having the potential to fulfil other market demands [3]. Factors including higher cost and energy intensive pre-processing steps in comparison to first-generational bioethanol must be addressed however [4]. Yeast and other biofuel producing microorganisms are also “stressed” throughout a fermentation, which renders the bioprocess inefficient and reduces final obtainable titres [5].

2. *Saccharomyces cerevisiae*

Saccharomyces cerevisiae can be found naturally thriving in sugar-rich habitats, with the term ‘archetypical weed species’ previously utilized to describe its dominant nature from an ecological context [5]. *S,cerevisiae* has remained instrumental to baking and alcoholic beverage production since ancient times and is the principle yeast employed for industrial bioethanol production worldwide [6]. Being the first Eukaryotic genome to be fully sequenced, this yeast is considered an indispensable model system for studying genetics, molecular biology, cell physiology, and even the ongoing development of systems biology [6]. The high genetic tractability of this microorganism allows for the manipulation of metabolic pathways, with biofuel researchers often minimizing carbon fluxes to natural metabolic by-products, for the maximisation of ethanol productivity [7]. Re-routing carbon fluxes towards advanced biofuels including isoprenoids and isobutanol is also achievable, with other high value products including pharmaceuticals, nutraceuticals and bulk chemicals (e.g. succinic acid) [7, 8] being produced using *S.cerevisiae*.

3. Yeast fermentation stresses and responses

The microbial production of bioethanol is often limited by feedstock impurities, contaminant microorganisms and undesired side products [9]. Inherent fermentation stress factors include osmotic and oxidative stress, caused by high initial sugar concentrations. This is especially common for first-generation bioethanol, due to high sugar containing feedstocks utilized [10]. Osmotic and cell turgor stress triggers intracellular activities including the central [HOG] high-osmo-glycerol pathway, leading to the increased production of osmolytes. These mediate cellular adaptation through their stabilising effects on cellular constituents [11]. Also termed a ‘compatible solute,’ glycerol is inversely synthesised to ethanol for the maintenance of redox balance, whilst possessing protective functions including serving in cell turgor, heat and oxidative stress [12]. Regulation of channel proteins in the cell membrane and intracellular organelles including the vacuole compensates for osmotic stress [13]. Second-generation bioethanol fermentations also regularly contain high sodium salt concentrations due to the pre-treatment methods utilized, with inhibition of microbial and enzymatic biocatalysts being consequential [14]. The presence of multiple different ions has been hypothesised to influence factors including sugar uptake, with divalent ions including Mg^{2+} also being of importance as a cofactor during fermentation and ethanol protectant [15].

Fermentation processes are exergonic, with high temperature gradients causing yeast to release protective heat-shock proteins (Hsps) and chaperones for the mitigation of heat stress-related effects. Thermally damaged proteins are known to be prevented from aggregating, with some Hsps unfolding aggregated and refolding damaged proteins. Other Hsps target damaged proteins for efficient degradation [16].

Main limiting factor -Chaotropicity

Product-induced inhibition, also termed chaotropicity in the context of a bioalcohol fermentation, has been suggested as the major limiting fermentation factor on biofuel yields [1]. The chaotropic activity of fermentation products including ethanol and vanillin have been quantified using a gel-agar model system (+5.93, +174 kJ kg^{-1} mole added $compound^{-1}$ respectively). Chaotropes increase the entropy of macromolecular systems and cause adverse effects on proteins, phospholipid bilayers and other hydrated cell components. This results in a plethora of effects including reduced cell viability, growth and lower ethanol yields [1, 17].

Like the other primary volatiles, the chaotropic solute ethanol freely diffuses across cell membranes at high concentrations, causing increased membrane fluidity. It has also been found that ethanol tolerant yeasts possess altered ratios in their membrane lipid constituents, causing decreased fluidity in the presence of ethanol in comparison to less tolerant yeasts [18]. Deregulation of membrane ion fluxes by the chaotrope ethanol affects proton-motive force, reducing nutrient uptake. Increased membrane permeability to protons promotes intracellular acidification. Ethanol causes alterations in mitochondrial membrane structure and lowers respiratory rates, leading to reduced ATP levels and the production of reactive oxygen species (ROS). DNA damage, lipid peroxidation and oxidative stress are consequences, which leads to a reduction of cell viability [19].

4. Engineering stress tolerance

The advent of systems biology has allowed for mechanisms underlying stress tolerance in *Saccharomyces cerevisiae* to become well elucidated. This has given rise to numerous rational genetic and metabolic engineering strategies for improved fermentation performance under environmental stress conditions [6, 19]. Another common approach deployed for the development of desirable traits includes directed experimental evolution. In this approach, natural selective pressures imposed on the microorganism promote genetic mutations and the eventual emergence of stress tolerance. Several stress tolerance traits including ethanol and multi-stress resistance have been achieved through evolutionary engineering [19]. Repetitive batch cultivations in the presence of lignocellulosic hydrolysates has previously evolved strains displaying increased tolerance to all inhibitors present [20]. Other strategies advocated for achieving increased ethanol tolerance improvement include engineering cell membrane lipid constituents for decreased membrane fluidity [19]. The emergence of novel tools including genome shuffling and global transcription engineering have also successfully bred stress tolerant yeast [19]. Novel, precise gene editing technologies including CRISPR-Cas9 have also allowed for the development of industrially relevant phenotypic traits [21].

Conclusion

Saccharomyces cerevisiae is considered a robust and versatile microorganism and outstanding model for elucidating cell stress biology. Stresses incurred to yeast throughout a bioethanol fermentation impact on metabolism and reduce final titres. Yeast possess a plethora of stress mechanisms and mitigating cell stress impacts on industrial fermentations has the potential to improve the economics of biofuel production.

Acknowledgments

JE thanks the University of Brighton and the Universities Alliance Doctoral Training Alliance for a PhD studentship. DJT acknowledges his long-standing collaboration with Dr John E Hallsworth (Queen's University, Belfast) who first encouraged him to think about problems of chaotropicity in cellular systems.

References

1. Cray JA, Stevenson A, Ball P, Bankar SB, Eleutherio EC, Ezeji TC, Singhal RS, Thevelein JM, Timson DJ, Hallsworth JE. (2015). 'Chaotropicity: a key factor in product tolerance of biofuel-producing microorganisms.' Curr Opin Biotechnol 33:228-2591.

2. Timilsina, GR. (2014). ‘Biofuels in the long-run global energy supply mix for transportation.’ Philosophical Transactions of the Royal Society A: Mathematical, Physical and Engineering Sciences, 372.

3. das Neves MA, Kimura T, Shimizu N, Nakajima M. (2007). ‘State of the Art and Future Trends of Bioethanol Production’. Dyn Biochem Process Biotechnol Mol Biol 1:1-14

4. Robak, K. and Balcerek, M. (2018). ‘Review of Second-Generation Bioethanol Production from Residual Biomass’. Food Technology and Biotechnology, 56(2).

5. Cray JA, Bell AN, Bhaganna P, Mswaka AY, Timson DJ, Hallsworth JE. (2013). ‘The biology of habitat dominance; can microbes behave as weeds?’ Microbiol Biotechnol 6:453-492

6. Petranovic, Dina, and Goutham N. Vemuri. (2009). 'Impact of yeast systems biology on industrial biotechnology', Journal of Biotechnology, 144: 204-11.

7. Macedo, Nicholas, and Christopher J Brigham. (2014). 'From Beverages to Biofuels: The Journeys of Ethanol-Producing Microorganisms', International Journal of Biotechnology for Wellness Industries, 3: 79-87.

8. Turanlı-Yıldız, B., Hacısalihoğlu, B. and Çakar, Z. (2017). ‘Advances in Metabolic Engineering of Saccharomyces cerevisiae for the Production of Industrially and Clinically Important Chemicals’. Old Yeasts - New Questions.

9. Beckner, M., M. L. Ivey, and T. G. Phister. (2011). 'Microbial contamination of fuel ethanol fermentations', Letters in Applied Microbiology, 53: 387-94.

10. Bertrand E, Vandenberghe LPS, Soccol CRet al. (2016). ‘First generation bioethanol. In: Green Fuels Technology, Springer International Publishing, Switzerland’. 2016, 175–212.

11. Tamás MJ, Rep M, Thevelein JMet al. (200). ‘Stimulation of the yeast high osmolarity glycerol (HOG) pathway-evidence for a signal generated by a change in turgor rather than by water stress’. FEBS Lett;472:159–65.

12. Ansell R, Granath K, Hohmann S, Thevelein JM, Adler L. (1997). The two isoenzymes for yeast NAD+-dependent glycerol 3-phosphate dehydrogenase encoded by GPD1 and GPD2 have distinct roles in osmoadaptation and redox regulation. EMBO J;16: 2179–87. pmid:9171333

13. Saxena, A. and Sitaraman, R. (2016). 'Osmoregulation in Saccharomyces cerevisiae via mechanisms other than the high-osmolarity glycerol pathway'. Microbiology, 162(9), pp.1511-1526.

14. Jönsson, L. and Martín, C. (2016). 'Pretreatment of lignocellulose: Formation of inhibitory by-products and strategies for minimizing their effects'. Bioresource Technology, 199, pp.103-112.

15. Walker, G. and Maynard, A. (1997). 'Accumulation of magnesium ions during fermentative metabolism in Saccharomyces cerevisiae'. Journal of Industrial Microbiology and Biotechnology, 18(1), pp.1-3.

16. Verghese, J., Abrams, J., Wang, Y. and Morano, K. (2012). 'Biology of the Heat Shock Response and Protein Chaperones: Budding Yeast (Saccharomyces cerevisiae) as a Model System'. Microbiology and Molecular Biology Reviews, 76(2), pp.115-158

17. Cray JA, Russell JT, Timson DJ, Singhal RS, Hallsworth JE. (2013). 'A universal measure of chaotropicity and kosmotropicity'. Environ Microbiol 15:287-296

18. Charoenbhakdi, S., Dokpikul, T., Burphan, T., Techo, T. and Auesukaree, C. (2016). 'Vacuolar H^+-ATPase Protects Saccharomyces cerevisiae Cells against Ethanol-Induced Oxidative and Cell Wall Stresses'. Applied and Environmental Microbiology, 82(16), pp.5057-5057.

19. Deparis, Q., Claes, A., Foulquié-Moreno, M. and Thevelein, J. (2017). 'Engineering tolerance to industrially relevant stress factors in yeast cell factories.'. FEMS Yeast Research, 17(4).

20. Almeida, J., Modig, T., Petersson, A., Hähn-Hägerdal, B., Lidén, G. and Gorwa-Grauslund, M. (2007). 'Increased tolerance and conversion of inhibitors in lignocellulosic hydrolysates by *Saccharomyces cerevisiae*'. Journal of Chemical Technology & Biotechnology, 82(4), pp.340-349.

21. Akhmetov, A., Laurent, J., Gollihar, J., Gardner, E., Garge, R., Ellington, A., Kachroo, A. and Marcotte, E. (2018). 'Single-step Precision Genome Editing in Yeast Using CRISPR-Cas9'. BIO-PROTOCOL, 8(6).

Nottingham | UK | 9–11 September 2019

An investigation into the current household energy consumption mix in Nigeria.

Daminabo Pokubo[1] and Amin Al-Habaibeh[2]

[1]*School of Architecture design and built environment, Nottingham Trent University, Nottingham NG1 4BU, UK*

[2]*School of Architecture design and built environment, Nottingham Trent University, Nottingham NG1 4BU, UK*

Daminabo.pokubo2016@my.ntu.ac.uk

Abstract

Energy in any national economy is considered as a fundamental asset required for sustainable development and improvement of living standards. Within the context of developing countries, energy plays an even more significant role, as it is needed to meet up with the energy demands associated with rising economic growth, rising population and large-scale urbanisation. Being one of the leading African economies, Nigeria faces huge sustainability challenges associated with rising energy consumption. Much of the country's population relies on fossil fuel-based energy and solid fuels for energy generation and consumption. For which, the utilisation of these fuels is often considered as contributors to rising carbon footprints and diseases associated with household air pollution. This study, therefore, examines the current energy consumption mix in relation household energy use and its likely effects on the environment and health of Nigerians. Findings emerging from the study indicated that electricity, firewood, charcoal and liquified petroleum gas are the main household energy sources in Nigeria. The study also recommends that increased awareness on the health and environmental impacts of dependence on conventional energy sources would not only improve energy consumption trends amongst households but will enhance energy security and Nigeria's final energy consumption patterns.

Keywords: Renewable energy, Sustainability, Energy consumption, Energy mix, Household consumption, Nigeria.

1. Introduction

Energy plays a crucial role in the development of any country and is considered as a major driver of economic and socio-economic development in any nation. Energy contributes not only to economic growth but acts as a propeller for sectoral development in any country especially the household sector [4]. Energy, being an essential necessity forms an important household ingredient required to perform various household activities including electrification, heating, cooking, transportation and communication [6]. Nevertheless, recent global attention on rising carbon dioxide (CO_2) emissions leading to global climate change have resulted in sustainability concerns as regards the impacts of global energy consumption on the environment and human health, especially sustainability concerns for household energy consumption [13].

In Nigeria, the household sector accounts for the highest share of primary energy consumption when compared to other economic sectors. Studies reveal that the Nigerian household sector accounts for about 78% of the country's total energy consumption [9]. However, much of Nigeria's household energy consumption mix is mainly dominated by fossil fuels and traditional solid biomass, which are often regarded as contributors to rising CO_2 emissions, environmental pollution and respiratory diseases in humans [7,14]. Therefore, creating severe sustainability concerns associated with the likely effects of increased consumption of fossil fuels and traditional solid biomass used to meet the energy demands of Nigeria's one hundred and ninety-two million (192,000,000) citizens [3]. Hence, this study seeks to examine current household energy consumption trend in Nigeria and its likely impact on the ecological balance and health of Nigerians.

2. Status of Household Energy Consumption in Nigeria

Nigeria being one of the leading developing economies in Africa boasts of a huge wealth of energy reserves comprising huge amounts of renewable and non-renewable energy reserves. The energy reserves shown in table 1, have being of immerse benefits to the Nigerian economy in-terms of inflow of foreign investments and socio-economic development attributable to energy being the major export commodity for revenue generation in Nigeria [1].

Table 1: Nigerian Energy Reserves

Energy resources		Reserves
Non-Renewables	Crude oil	37.1 billion barrels
	Natural gas	187 trillion cubic feet
	Coal	2.7 billion tonnes
	Tar sand	31 billion barrels
Renewables	Solar	4-6 kWh/m^2/day
	Wind	2-4m/s at 10m above land
	Hydropower	11,250 MW

Source: Reproduced from Shaaban and Petinrin [12].

Despite the abundant energy potentials in Nigeria, household access to energy supply is low, while some of the resources shown in table 1 remain largely untapped resulting in an overdependence on other resources particularly fossil fuels [10-12]. Thus, creating the need for energy diversification to ensure energy security and increase access to modern energy supply for households. Energy consumption in Nigeria is distributed across various economic sectors of the country but rising population growth, increasing living standards and gradual rural migration to urban cities has led to increased household energy consumption in Nigeria [10,12]. Studies show that about 80% (99.3 million tonnes of oil equivalent Mtoe) of the country's annual energy consumption is derived from combustible solid biomass fuels [7]. Since the household sector has the highest share of energy consumption, it implies that about 80% of the 99.3 Mtoe of total energy consumed annually is consumed by the household sector and derived from solid biomass fuels utilised for various domestic activities. Consequently, raising sustainability concerns linked with deforestation, acute respiratory infections (ARI) and household air pollution (HAP) from the combustion of firewood and charcoal.

However, fuel types utilised in Nigerian households ranges from petrol, diesel, kerosene, electricity, LPG, firewood, charcoal and crop residue. Nevertheless, the consumption of firewood and charcoal surpasses the consumption other fuels. Studies reveal that about 70.7% of Nigerian households (152,000,000 people) use firewood and charcoal mainly for cooking and heating purposes [8]. Resulting in over 43.4 million metric tonnes of wood consumed annually leading to rapid rates of deforestation and about 64,000 deaths annually due to HAP from incomplete combustion of firewood and charcoal in poorly ventilated kitchens despite governmental efforts to increase household access to modern fuel such as LPG and electricity [12]. Despite these governmental efforts recurrent electricity shortages, inadequate gas supply coupled with other factors have resulted in an overreliance on personal generators for household electricity generation and firewood for cooking [5]. From the above review it can be observed that the need to diversify household energy sources to aid transition towards the introduction of cleaner renewable energy sources has become expedient and paramount.

3. Study Approach and Methodology

This study adopted a quantitative survey-based approach to examine patterns of Nigerian household energy consumption and influencers of household choice of fuel. A total of 746 survey questionnaires are distributed for this study, of which 740 responses are considered valid (n=740). The survey as a research instrument was divided into themes to provide clear and insightful guidance to the target population on how to answer the questionnaire. In order to ensure non-overlapping of sample groups, a random sampling technique was adopted.

4. Findings and Discussion

Drawing on data collated during the field-study, a descriptive analysis of the all actors in the field is presented below. All correctly filled surveys were analysed for incomplete and missing responses, resulting in 98% response rate.

4.1. Main Source of Household Energy

Results from the survey indicates that electricity as the major energy source for most respondent’s households as 65.64% of respondents indicated electricity as their main source of energy. While electricity constitutes as the main energy source for most households, about 36.02% of respondents show that their main source of electricity is from the national grid, which indicates governmental efforts to increase household access to electricity in Nigeria. Whereas 29.62% of respondents indicated that their source of electricity is from personal generators that use fossil fuel for electricity generation as shown in Fig 1. This shows the level electricity access in Nigeria, as literature shows that only about 50% of Nigerians have access to electricity [2]. Hence, creating supply deficiencies for 92,000,000 Nigerians resulting in an overreliance on fossil fuels that contributes to greenhouse gas emissions (GHG). Despite the percentage of respondents indicating electricity as their main source of energy, 32.55% indicated using a combination of sources, implying that their main source of electricity contains a mix of grid-based electricity and personal generators. While 1.81%

indicate the use of renewable energy sources as their main source of electricity, which supports the renewable energy potentials of Nigeria. However, the use of renewable energy resources in many Nigerian household is slow and termed as expensive.

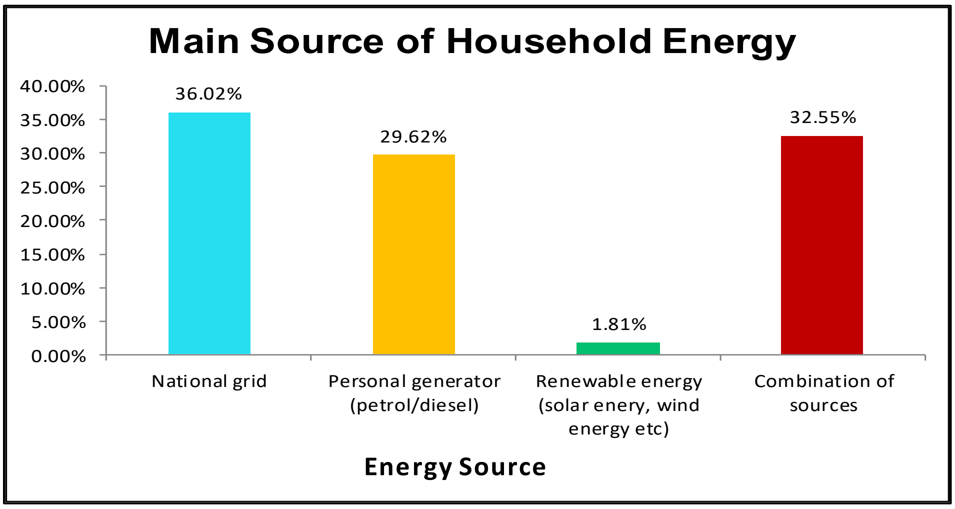

Figure 1: Household Main Source of Energy

4.2. Composition of Household Energy Consumption for Basic Household Activities

Majority of respondents indicated the use of a mix of fuel types for cooking, heating, lighting and air-conditioning purposes. The survey revealed that firewood, charcoal, grid-based electricity, LPG, kerosene, petrol, diesel, biogas, and solar are used in most households for various household activities. Analysis of the survey shows a general trend involving the use of electricity for most household activities as 78.75% of respondents indicate the use of electricity for lighting, while 55.07% and 87.37% use electricity for cooking/heating and air conditioning respectively. However, due to supply shortages and inaccessibility of electricity in Nigeria, the use of diesel or petrol generators is prevalent in most households. The survey shows that majority of respondents use generators for electricity generation for cooking (20.96%), lighting (75.20%) and air-conditioning (43.76%).

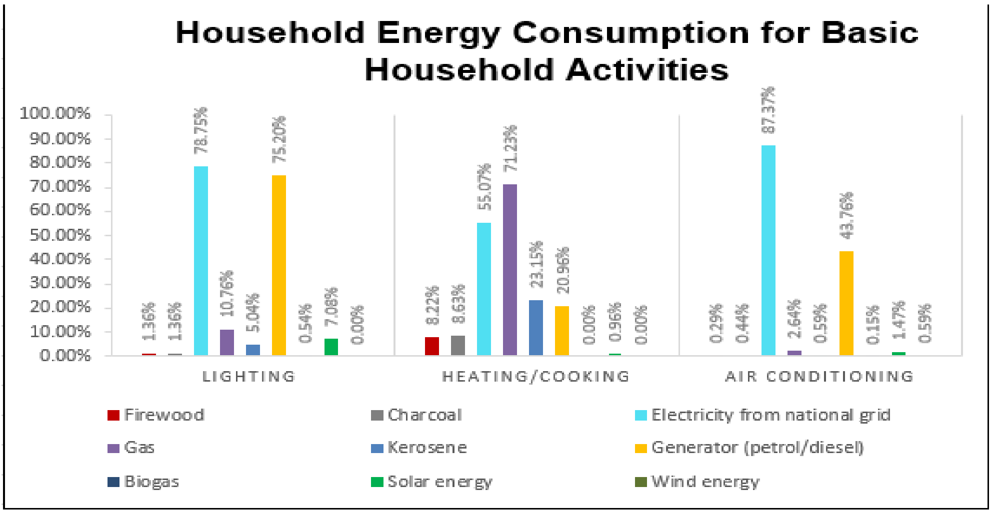

Figure 2: Energy Use for Basic Household Activities

Trends from the survey reveals that household fuel choice in most Nigerian households conforms to ‘Fuel Stacking’ energy model, since most households use a combination of fuel types. The fuel stacking model suggests that households may combine the use of different types of fuels (firewood – electricity – solar energy) depending on certain socio-economic factors such as their household income, household size, affordability or availability of fuels. From Fig 2, it can be observed that the use of firewood is minimal as compared to other fuels which is due to majority of the respondents being urban habitats. However, the use of renewable energy sources such as solar and wind energy for various household activities is low especially the use of wind energy. Based on the energy fuel stacking model, it can be observed that there exist certain factors that act as influencers as regards household choice of fuel.

4.3. Influencers of Household Choice of Fuel

Results from the survey indicates that there are certain factors which influence household choice of fuel source. The survey showed that factors such as; availability, accessibility, fuel cost, size of household, environmental concerns, convenience and culture constitute major factors that influence household choice of fuel. However, availability ranked as the highest influencer of household fuel choice as 60.50% of respondents indicated that the availability of a certain type of fuel determines the likelihood of using that fuel. Other factors the influences household fuel choice includes fuel cost (50.21%), accessibility (41.45%), convenience (41.03%), environmental concern (12.60%). While culture (5.84%) and household size (9.60%) are the least factors that influences household fuel choice.

5. Conclusion

Results from this study show that there has been an appreciable increase as regards household access to modern energy especially electricity attributable to governmental efforts to increase access to modern fuels. However, with electricity supply deficiencies, most households are still likely to use non-renewable forms of energy to meet the energy demands. For a population of 192,000,000 citizens, this poses a huge sustainability concern and strain on Nigeria’s forestlands and increases the likelihood of ARI from exposure to smoke while cooking with firewood. From this study it is apparent that the introduction renewable energy resources such as solar and biogas would reduce household dependence on fossil fuel and aid towards reduction infections from the use of solid fuels. An awareness of the health and environmental impacts of dependence on fossil fuel and solid biomass should be done via policy formation and creating a level playing for renewable energy market entry into the Nigerian energy sector.

6. References

1. Akuru, U.B., Onukwube, I.E., Okoro, O.I. and Obe, E.S., (2017). Towards 100% renewable energy in Nigeria. *Renewable and Sustainable Energy Reviews,* 71, 943-953.
2. Gungah, A., Emodi, N.V. and Dioha, M.O., (2019). Improving Nigeria's renewable energy policy design: A case study approach. *Energy Policy,* 130, 89-100.
3. International Monetary Fund, (2018). *NIGERIA: SELECTED ISSUES, IMF Country Report No. 18/64.* International Monetary Fund Publication Services PO Box 92780 Washington, D.C. 20090: International Monetary Fund Washington, D.C.

4. Le, T., and Nguyen, C.P., (2019). Is energy security a driver for economic growth? Evidence from a global sample. *Energy Policy,* 129, 436-451.
5. Lin, B., and Ankrah, I., (2019). On Nigeria's renewable energy program: Examining the effectiveness, substitution potential, and the impact on national output. *Energy,* 167, 1181-1193.
6. Mensah, J.T., and Adu, G., (2015). An empirical analysis of household energy choice in Ghana. *Renewable and Sustainable Energy Reviews,* 51, 1402-1411.
7. Mohammed, Y.S., Mustafa, M.W., Bashir, N. and Ibrahem, I.S., (2017). *Existing and recommended renewable and sustainable energy development in Nigeria based on autonomous energy and microgrid technologies.*
8. Ogunleye, E.K., (2008). Natural resource abundance in Nigeria: From dependence to development. *Resources Policy,* 33 (3), 168-174.
9. Oseni, M.O., (2012). *Households' access to electricity and energy consumption pattern in Nigeria.*
10. Oyedepo, S.O., (2014). Towards achieving energy for sustainable development in Nigeria. *Renewable and Sustainable Energy Reviews,* 34, 255-272.
11. Oyefusi, A., (2007). *Oil-dependence and Civil conflict in Nigeria.* Oxford University Research Archives.
12. Shaaban, M., and Petinrin, J.O., (2014). Renewable energy potentials in Nigeria: Meeting rural energy needs. *Renewable and Sustainable Energy Reviews,* 29, 72-84.
13. Wang, Q., Kwan, M., Zhou, K., Fan, J., Wang, Y. and Zhan, D., (2019). Impacts of residential energy consumption on the health burden of household air pollution: Evidence from 135 countries. *Energy Policy,* 128, 284-295.
14. Zoë A Chafe, Michael Brauer, Zbigniew Klimont, Rita Van Dingenen, Sumi Mehta, Shilpa Rao, Keywan Riahi, Frank Dentener and Kirk R Smith, (2014). Household cooking with solid fuels contributes to ambient PM2.5 air pollution and the burden of disease. *Environmental Health Perspectives,* 122 (12), 1314-1320.

ICESF
Nottingham | UK | 9–11 September 2019

Role of Renewable Energy Methods for the Development of Structural Health Monitoring System

F. Siddiqui, P. Sargent, N. Dawood, S. Rodriguez

*School of Science, Engineering and Design, Teesside University, Stephenson Building,
Stephenson Street, Middlesbrough, Tees Valley, TS1 3BA, UK*

f.siddiqui@tees.ac.uk

Abstract

Structural health monitoring (SHM) is a process of monitoring the performance of civil engineering infrastructure (CEI). Static and dynamic responses of structures are monitored by the deployment of sensors to determine their condition. Over the past few decades, many studies have been done to improve SHM systems, including power sources for sensors by using renewable energy methods to maximise sustainability. The exposure of CEI to a wide range of environmental conditions such as solar radiation, extreme weather and external loadings such as vehicular trafficking impose temperature gradients and additional vibrations, respectively. These phenomena can also be utilised to detect structural damage within CEI by measuring changes in the amount of energy harnessed from damaged and undamaged surfaces. This paper reviews current research on the application of renewable energy methods, such as piezoelectric and electromechanical methods, in SHM systems for providing energy to sensors and detecting structural damage. In addition, this paper also explores the types of CEI or structural members used in current studies and methodologies for detecting different types of damage. The scope and limitations of renewable energy methods are discussed in the context of SHM systems.

Keywords: Structural Health Monitoring, Sensors, Renewable Energy, Civil Infrastructure

1. Introduction

SHM of large CEIs require robust sensing devices capable of diagnosing their condition under operational and environmental conditions [1]. For uninterrupted long-term monitoring, the power supply to the sensors can be one of the determining factors for their selection and deployment in an SHM system [2]. Recently, this issue has been addressed by focussing on utilising ambient and renewable energy sources to improve the SHM system. This paper reviews different types of renewable energy methods feasible to power sensors and to develop self-powered sensors capable of detecting damage in critical components of infrastructure.

2. Renewable energy sources

Davidson and Mo [3] presented a brief review of various renewable energy sources studied in terms of SHM system application in civil, aeronautical and mechanical engineering. The review depicted that vibrations, wind and solar energy sources have been utilised for powering wireless sensors in CEI SHM systems. Recently, Cao and Li [4] identified that solar and wind energy have been the most widely used sources to date; with vibration, thermal and radio frequency considered as promising power sources for SHM application.

3. Renewable energy methods for SHM

While focussing on CEI, Wang et al. [5] provided a comparative study of renewable energy technologies, including their maturity from research level to practical implementation. Piezoelectric, electromagnetic and thermoelectric have been identified as emerging methods for harnessing energy from vibration and thermal, respectively. Their potentials for powering wireless sensors and detecting damages in the structure have been realised by numerous researchers [6], [7], [8], [9]. Figure 1 shows different energy harnessing methods available for SHM system.

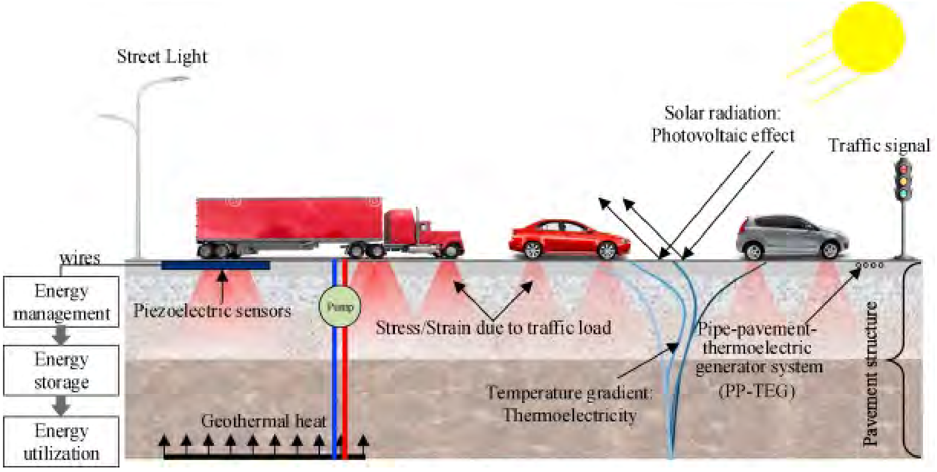

Figure 1: Renewable energy methods for sensors and SHM system (Source: [5]*)*

3.1.Energy for sensors

Sensing devices for SHM systems such as fibre optic, piezoelectric and wireless sensors are low power devices, which can be efficiently powered by energy harvesting methods [10], [11], [12]. Table 1 lists different renewable energy methods utilised in recent studies to demonstrate the capability of harvesting methods to power sensors. Most of these studies used bridges as structural case studies. While most of the studies on piezoelectric and electromagnetic harvesting methods are experimental, solar panels and micro wind turbines were applied to real bridges [13], [14].

3.2.Detection of structural damage

Power generation and energy harvesting capabilities of piezoelectric and electromagnetic devices are affected by the amount of damage incurred by a structure, and therefore, its overall stiffness [15]. Stiffness has been used to detect damages by comparing the amount of energy produced by the undamaged and damaged state. Table 2 lists different types of damage detected using renewable energy devices. One of the most effective energy-based damage detection techniques is the utilisation of smart aggregate made from piezo-ceramic material such as lead zirconate titanate (PZT) [16], [17]. The other prominent experimental study has determined electrical resistivity (ER) in porous materials (e.g. concrete), through electromagnetic induction. ER in concrete is associated with the probability of steel reinforcement corrosion and can be used in highway decks and bridges for long term monitoring [18].

Table 1: Current application of renewable energy for powering sensors

Renewable energy methods	**Structural application**	**Reference**
Piezoelectric Polyvinylideneflouride (PVDF)/Lead Zirconate Titanate (PZT)/Micro-fibre Composite (MFC)	Bridge (Concrete, Steel, Composite), Pavement, Steel Frame	[15], [19]–[28]
Electromagnetic	Bridge, Concrete and soil	[18], [29], [30]
Thermoelectric Generator (TEG)	Asphalt Pavements	[8], [31]
Wind: Micro-wind Turbines	Cable-stayed Bridge	[14]
Solar: Solar Panel, Photovoltaic Standalone System (PVSS)	Roads, Bridge	[13], [32]
Triboelectric Nanogenerator	Railway Track	[33]

Table 2: Current application of renewable energy for detecting structural damage

Structural damage	**Methodology**	**Structural application**	**Reference**
Cracks	Guided stress wave measurement generated using PZT transducer	Piles, Concrete Beams	[16], [17]
Loosening of Bolts, Bottom-up Cracking	Change in voltage generated by PVDF/PZT piezoelectric film	Steel Frame, Asphalt Concrete Pavements	[20], [21]
Cracks	Amount of energy harvested by cantilever piezoelectric harvester	Bridge (Concrete, Composite)	[15], [24]

Fatigue Cracks, Early-age Concrete Strength	Electromechanical impedance based	RC Beam	[34], [35]

4. Discussion and Conclusion

Recent studies suggest that renewable energy methods could be used for efficient SHM systems. Harvesting energy from vibrations caused by external loadings on structures is of increasing research interest. This is due to piezoelectric devices possessing vibration energy harvesting and damage detection capabilities [36]. As most of the studies to date have been performed in laboratory environments, their implementation in full-scale CEI structures under different environmental condition would produce further insights regarding environmental effects and optimal location of sensors and harvesters for efficient SHM system. In addition, traffic flow may also affect harvesting energy production and should be considered while detecting anomalies in structure.

Acknowledgements

Thanks go to the DTA3/COFUND for funding this PhD research and to my supervisory team at Teesside University (Dr Paul Sargent, Prof Nashwan Dawood and Dr Sergio Rodriguez) for helping prepare this paper.

References

1. Brownjohn JM (2007) Structural health monitoring of civil infrastructure. Philos. Trans. R. Soc. A Math. Phys. Eng. Sci. 365(1851):589–622
2. Lynch JP and Loh KJ (2006) A Summary Review of Wireless Sensors and Sensor Networks for Structural Health Monitoring. The shock and vibration digest 38(2):91-128
3. Davidson J and Mo C (2014) Recent Advances in Energy Harvesting Technologies for Structural Health Monitoring Applications. Smart Mater. Res. 2014:1–14
4. Cao S and Li J (2017) A survey on ambient energy sources and harvesting methods for structural health monitoring applications. Adv. Mech. Eng. 9(4):1-14
5. Wang H, Jasim A, and Chen X (2018) Energy harvesting technologies in roadway and bridge for different applications – A comprehensive review. Appl. Energy 212:1083–1094
6. Siang J, Lim MH, and Leong MS (2018) Review of vibration-based energy harvesting technology: Mechanism and architectural approach. Int. J. Energy Res. 42(5):1866–1893
7. Guo L and Lu Q (2017) Potentials of piezoelectric and thermoelectric technologies for harvesting energy from pavements. Renew. Sustain. Energy Rev. 72:761–773
8. Jiang W et al. (2017) Energy harvesting from asphalt pavement using thermoelectric

technology. Appl. Energy 205:941–950

9. Ali SF, Friswell MI, and Adhikari S (2011) Analysis of energy harvesters for highway bridges. J. Intell. Mater. Syst. Struct. 22(16):1929–1938

10. Yun CB and Min J (2011) Smart sensing, monitoring, and damage detection for civil infrastructures. KSCE J. Civ. Eng. 15(1):1–14
11. Chong KP and Zhu S (2018) Innovative technologies in manufacturing, mechanics and smart civil infrastructure. Int. J. Smart Nano Mater. 9(4):261–278
12. Han B et al. (2015) Smart concretes and structures: A review. J. Intell. Mater. Syst. Struct. 26(11):1303–1345
13. Hoult N et al. (2009) Wireless sensor networks: creating 'smart infrastructure'. Proc. Inst. Civ. Eng. - Civ. Eng. 162(3):136–143
14. Park JW, Jung HJ, Jo H, and Spencer Jr BF (2012) Feasibility study of micro-wind turbines for powering wireless sensors on a cable-stayed bridge. Energies 5(9):3450–3464
15. Cahill P et al. (2016) Effect of Road Surface, Vehicle, and Device Characteristics on Energy Harvesting from Bridge-Vehicle Interactions. Comput. Civ. Infrastruct. 31(12):921–935
16. Feng Q, Kong Q, and Song G (2016) Damage detection of concrete piles subject to typical damage types based on stress wave measurement using embedded smart aggregates transducers. Measurement 88:345–352
17. Feng Q, Cui J, Wang Q, Fan S, and Kong Q (2018) A feasibility study on real-time evaluation of concrete surface crack repairing using embedded piezoceramic transducers. Measurement 122:591–596
18. Steinberg MD, Tkalčec B, and Steinberg IM (2016) Towards a passive contactless sensor for monitoring resistivity in porous materials. Sensors Actuators B Chem. 234:294–299
19. Cahill P, Hazra B, Karoumi R, Mathewson A, and Pakrashi V (2018) Vibration energy harvesting based monitoring of an operational bridge undergoing forced vibration and train passage. Mech. Syst. Signal Process. 106:265–283
20. Hasni H, Jiao P, Alavi AH, Lajnef N, and Masri SF (2018) Structural health monitoring of steel frames using a network of self-powered strain and acceleration sensors: A numerical study. Autom. Constr. 85:344–357
21. Hasni H et al. (2017) A new approach for damage detection in asphalt concrete pavements using battery-free wireless sensors with non-constant injection rates. Measurement 110:217–229
22. Park S, Lee C, Kim H, Yun HS, and Kwon S (2013) Development of piezoelectric energy harvesting modules for impedance-based wireless structural health monitoring system. KSCE J. Civ. Eng. 17(4):746–752
23. Kaur N and Bhalla S (2014) Feasibility of energy harvesting from thin piezo patches via axial

strain (d_{31}) actuation mode. J. Civ. Struct. Heal. Monit. 4(1):1–15

24. Cahill P, Nuallain NAN, Jackson N, Mathewson A, Karoumi R, and Pakrashi V (2014) Energy Harvesting from Train-Induced Response in Bridges. J. Bridg. Eng. 19(9):04014034

25. Alavi AH, Hasni H, Jiao P, Borchani W, and Lajnef N (2017) Fatigue cracking detection in steel bridge girders through a self-powered sensing concept. J. Constr. Steel Res. 128:19–38
26. Hasni H, Alavi AH, Lajnef N, Abdelbarr M, Masri SF, and Chakrabartty S (2017) Self-powered piezo-floating-gate sensors for health monitoring of steel plates. Eng. Struct. 148:584–601
27. Aono K, Hasni H, Pochettino O, Lajnef N, and Chakrabartty S (2019) Quasi-self-powered piezo-floating-gate sensing technology for continuous monitoring of large-scale bridges. Front. Built Environ. 5(29):1-14
28. Hou Y et al. (2017) A Preliminary Study on the IoT-Based Pavement Monitoring Platform Based on the Piezoelectric-Cantilever-Beam Powered Sensor. Adv. Mater. Sci. Eng. 2017:1–6
29. Sazonov E, Pillay P, Li H, and Curry D (2009) Self-Powered Sensors for Monitoring of Highway Bridges. IEEE Sens. J. 9(11):1422–1429
30. Han B et al. (2013) Harvesting energy from vibrations of the underlying structure. JVC/Journal Vib. Control 19(15):2255–2269
31. Lee J, Lim C, Lim J, Yang S and Im J (2018) Application of solar thermoelectric generation system for health monitoring system of civil infrastructures. KSCE J. Civ. Eng. 22(1):110–116
32. Fedele R, Merenda M, Praticò FG, Carotenuto R, and Della Corte FG (2018) Energy harvesting for IoT road monitoring systems. Instrum. Mes. Metrol. 17(4):605–623
33. Zhao X et al. (2017) Self-powered triboelectric nano vibration accelerometer based wireless sensor system for railway state health monitoring. Nano Energy 34:549–555
34. Bhalla S and Kaur N (2018) Prognosis of low-strain fatigue induced damage in reinforced concrete structures using embedded piezo-transducers. Int. J. Fatigue 113:98–112
35. Priya CB, Saravanan TJ, Balamonica K, Gopalakrishnan N, and Rao ARM (2018) EMI based monitoring of early-age characteristics of concrete and comparison of serial/parallel multi-sensing technique. Constr. Build. Mater. 191:1268–1284
36. Kaur N, Bhalla S, Naveet K, Suresh B, Kaur N, and Bhalla S (2015) Combined Energy Harvesting and Structural Health Monitoring Potential of Embedded Piezo-Concrete Vibration Sensors," J. Energy Eng. 141(4):D4014001

Nottingham | UK | 9–11 September 2019

A low-error calibration model for an electrostatic gas-solid flow sensor fusion obtained via machine learning techniques with experimental data

Andrew J. Kidd *MSc BEng* Jianyong Zhang *PhD* Ruixue Cheng *PhD*

Teesside University, Middlesbrough, United Kingdom

a.kidd@tees.ac.uk

Abstract

Sensor fusion is the use of software that intelligently combines data from multiple sensors in order to improve overall system performance. This technique can be applied to measurement of mass flow rate of solids in a pipeline with non-intrusive electrostatic techniques. Data fusion from multiple heterogeneous/homogenous sensors can overcome limitations of an individual sensor and measured variable. It is shown that the output voltage of a ring-shaped electrode is predominantly a function of solids mass flow rate, air-solids ratio and particle velocity. By additionally incorporating measured flow velocity in a proposed mathematical model (obtained via machine learning), meter output voltage could be predicted/calculated with superior accuracy, for a range of different flow parameters from numerous experiments with a pneumatic conveying system. A transposed model utilised in software enables accurate mass flow measurement with velocity compensation. Accurate mass flow measurement facilitates enhanced monitoring and controllability of blast furnaces, power stations, chemical reactors etc. where there is a flow of solid fuel/reactant in pipelines. Optimisation of highly materially consumptive and energy intensive processes can yield significant reductions in waste and emissions (CO_2, NOx) and increased efficiencies in global production of energyand materials.

Keywords: sensor fusion, machine learning, electrostatic flow measurement, gas-solid flow, pneumatic conveying, non-linear regression

1. Introduction

Gas-solid flows as pneumatic conveying processes are commonplace in industry. They are utilised in coal-fired power stations, blast furnaces and cement, chemical, pharmaceutical and food production processes as a method to transport bulk solids - being a fuel, reactant or food or pharmaceutical constituent. Often, but not always, the gas phase is air. In order to optimise these processes, reduce waste and emissions or increase combustion efficiencies, it is desirable to be able to accurately measure the mass flow of bulk solids. There are various meters that are commercially available that do enable mass flow measurement of bulk solids [1]. Some are intrusive in nature, and are unable to conduct measurement without disturbing the flow stream.

This is undesirable and wastes energy which has been already invested in the transfer of material. Also, some intrusive sensor designs may be damaged over time by constant abrasion. Some commercially available non-intrusive meters based on electrostatic techniques have been deployed in power stations and blast furnaces. However, current systems do not perform as well as single phase systems, having a notable issue with regards to spatial sensitivity [2] and whilst they can offer flow assurance, they lack the accuracy to be utilised in reactor/furnace control loops – which limits the potential for process optimisation.

A main issue is that, unlike simpler measurement systems, the voltage induced in the electrode is related to not only the mass flow rate of solids, but also air-solids ratio, particle velocity, flow profile, humidity, particle size [3] and electrostatic properties of the bulk material itself. It is a complex relationship with many interacting variables resulting in the measured voltage signal. However we can assume that some of the latter variables remain sufficiently constant for a given system. Variables could be controlled/fixed under experimental conditions and from subsequent observation it was found for a system using the same bulk material, same grade or particle size, same humidity and temperature, the output (rms) voltage of a ring-shaped electrode around a conveying pipeline can said to be primarily a function of the mass flow rate Q_m, air-solids ratio R_{as} and particle velocity v_p. The meter function to be found is therefore;

$$V_{rms}(mV) \cong f(Q_m, R_{as}, \mathrm{v}_p) \tag{1}$$

Solids mass flow rate has proven difficult to measure directly. Therefore, this measurement challenge is still of research interest in a time when we have single phase gas/liquid flow meters (e.g. Coriolis) with accuracies of 0.05%. Current multiphase gas-solid flow meters are somewhat behind (±10%), but accuracy can be improved by utilisation of multiple homogenous/heterogeneous sensors and combining data in software to improve system performance in a method termed ‘sensor fusion’. With electrostatic gas-solid flow measurement, this can be through the use of multiple ring-shaped electrodes at different positions on the pipeline. This can reduce the issue of sensitivity to flow profile and enable simultaneous determination of particle velocity using the cross-correlation technique, which is a well-understood technique described and demonstrated in the literature [4-6].

By obtaining an accurate model, when meter voltage and remaining variables are known/measured, a transposed model utilised in measurement system software, continuously updated with sufficient sensor data should then enable online measurement of mass flow rate. System performance, i.e. measurement accuracy should exceed that of current/existing designs.

2. Experimentation

The Teesside University pneumatic conveying rig shown in Figure 1 was used to collect data. A 40mm pipeline containing conveyed solids consists of a vertical and horizontal section with 4 electrostatic meters. The configuration enables simultaneous measurement of particle velocity using the cross-correlation technique. An inverter-controlled fan takes in air, which is mixed with solids (Fillite) introduced to conveying line via a screw feeder. The reference solids mass flow rate is obtained by mass differentiation. An additional inverter controls the speed of the screw feeder. Air flow rate is measured downstream and air exits the system via an exhaust.

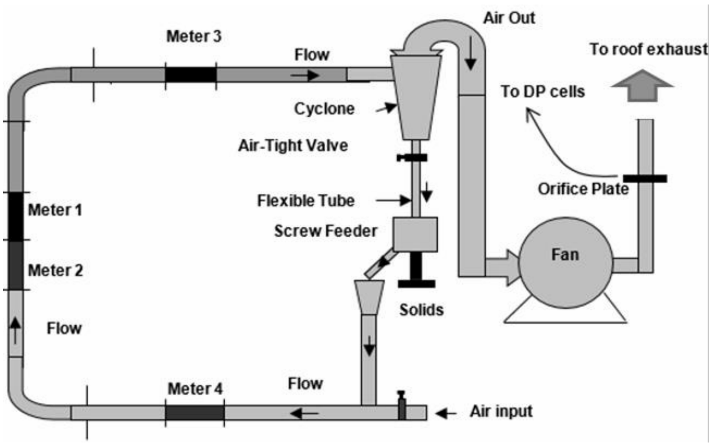

Figure 1 – Diagram of pneumatic conveying rig

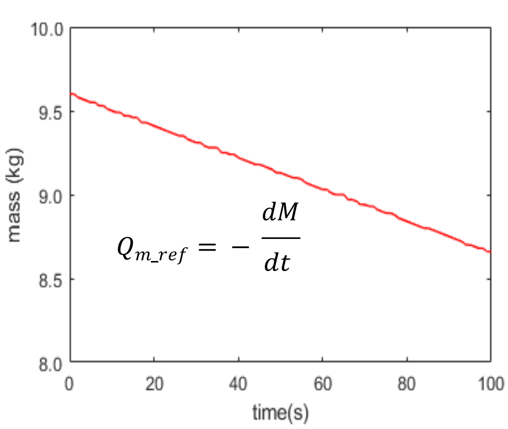

Figure 2 – Reference mass flow rate

The instantaneous root-mean square voltage from each meter, the mass of solids in the hopper, the air flow rate and solids velocity are all logged in software (Labview) every second during an experiment. Over 30 different experiments were conducted, all with different (controllable) mass-flow rates, solids velocity and air-solids ratio. These values were then used to form a split train/test data-set, to enable acquisition of system model via machine learning techniques.

3. Preliminary Model derivation with Machine Learning

Using the Regression Learner app in MATLAB, a variety of machine learning algorithms were deployed with the train data set (70% of overall data) and are ranked below in order of their respective model performance metrics; R^2 value and (root) mean (squared/absolute) error.

Table 1 – Machine learning techniques with model performance metrics (ranked)

Method	R^2	RMSE (mV)	MAE (mV)
Linear Regression	0.93	11.37	9.07
Linear State Vector Machine	0.93	11.48	9.10
Boosted Regression Tree Ensemble	0.89	14.69	10.86
Fine Regression Tree	0.87	15.86	12.46
Bagged Regression Tree Ensemble	0.84	17.30	13.15
Fine Gaussian State Vector Machine	0.74	22.39	15.00

As can be seen, the best-fitting model/technique of those tried is linear regression. This enables the derivation of a linear equation for meter output voltage;

$$V_{rms}(mV) \cong 3.3Q_m + 2.1\mathrm{v}_p + 8.3R_{as} - 48.2 \tag{2}$$

As well as having the best fit to test data, with this type of model there is less concern with regards to overfitting a because the data conforms well to a simple model rather than requiring say a complex regression tree, or state vector machine.

4. Model Refinement

An improved model should also encapsulate the slightly non-linear/curved nature of meter voltage with increased mass flow rate. This is seen in the data set when experiments with similar flows parameters are grouped in terms of air solids ratio and velocity to see the effect of altering each parameter and also mass flow rate in isolation. A higher order model which predicts zero output voltage for zero flow is preferable, because it corresponds to the reality of the system intended to be modelled. Although the initial linear regression model was deemed insufficient, it facilitated the derivation of the unknown coefficients for a second order polynomial model. A model with a structure similar to this this has been presented previously by Zhang [7]. This model expressed meter output voltage as a function of air-solids ratio and mass-flow rate, but did not incorporate particle velocity, and was of the form;

$$V_{rms} = (ARas + B)\, Q_m^2 + (CRas + D)Q_m + ERas + F \tag{3}$$

Where A, B, C, D, E and F are constants to be determined. This model was found to have a maximum relative error of around 7%. The newly proposed model has zero intercept and also incorporates particle velocity and has the form;

$$V_{rms}(mV) \cong \{a + bR_{as} + c\mathrm{v}_p\}Q_m^2 + \{d + eR_{as} + f\mathrm{v}_p\}Q_m \tag{4}$$

Where a, b, c, d, e and f are coefficients which have been determined as;

$$a = 0.047,\ b = -0.008,\ c = -\ 0.002,\ d = 0.111,\ e = 0.546,\ f = 0.136$$

This refined non-linear model was found to be more accurate at predicting meter output voltage than the linear model and also significantly more accurate than the model of equation 3 in the range shown. If then, for a given system, the meter voltage(s) and remaining predictor variables are known/measured, then the mass flow rate can be determined in measurement system software using the available data with the following transposed mathematical model;

$$Q_m = \frac{2V_{rms}}{\sqrt{4V_{rms}(a + bR_{as} + cv_p) + (d + eR_{as} + fv_p)^2} + d + eR_{as} + fv_p} \quad (5)$$

5. Results and Discussion

The following table shows the root mean square meter voltage for a range of experiments conducted with particle velocity varying from 15 to 30 m/s, air-solids ratio ranging from 1.5 to 3.5 (which is typical of power station concentrations) and mass flow rate ranging from 10 to 40 kg/hr. The meter voltage is predicted using the aforementioned non-linear regression model and the relative error (%) of the prediction is also calculated. The model fit to steady state test data from numerous experiments is then shown graphically in Figures 3 and 4.

Table 2: Model fit to experimental data

v_p	R_{as}	Q_m	V_{rms}	V_{fcn}	$e_r\%$
15.59	3.29	10.96	41.18	42.85	-4.06
15.56	2.83	12.64	45.47	46.64	-2.57
15.53	2.46	14.51	51.68	50.95	1.40
19.41	3.15	14.72	59.26	62.09	-4.79
19.38	2.84	16.18	63.91	65.77	-2.91
15.46	2.05	17.34	57.59	57.67	-0.14
23.14	3.27	17.40	81.65	80.06	1.95
19.27	2.46	18.57	74.50	71.84	3.57
23.07	2.85	19.86	86.66	86.75	-0.11
26.73	3.23	20.98	103.4	101.3	1.96
15.31	1.58	22.17	66.40	69.59	-4.81
19.23	2.00	22.67	82.02	82.74	-0.88
23.07	2.45	22.99	97.24	95.51	1.78
26.69	2.86	23.56	107.0	108.6	-1.53
22.95	2.03	27.46	111.2	107.8	3.06
26.69	2.43	27.56	119.3	120.0	-0.59
19.01	1.60	28.03	95.79	97.10	-1.37
30.00	2.48	31.43	136.0	141.8	-4.27
26.34	2.03	32.76	129.8	133.7	-3.04
22.50	1.62	34.04	124.3	125.3	-0.80
18.77	1.19	37.29	118.8	123.4	-3.90
29.78	2.03	38.17	159.5	159.1	0.21
25.91	1.62	40.45	153.9	153.7	0.10

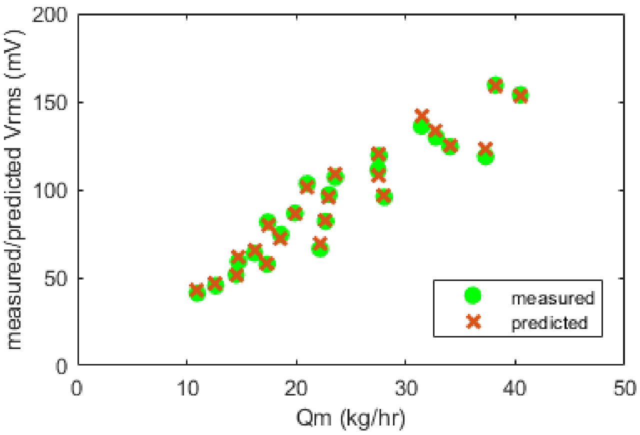

Figure 3: Model fit to Vrms with Qm

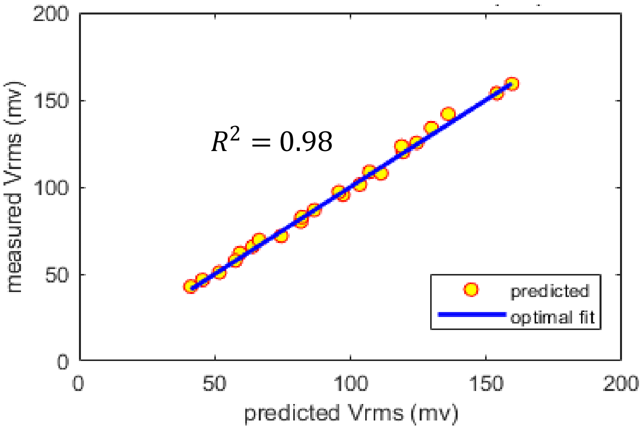

Figure 4: Predicted vs measured Vrms

As expected, the model shows an improved fit to steady state (moving) averaged meter voltage, as opposed to instantaneous values from the original sampled data. As can be seen, the mean relative error is less than 1% and the maximum relative error is less than 5%. This is more than acceptable for a multiphase flow meter and is constitutes a significant improvement to that of the previous model (eq. 3) from the literature, which did not incorporate particle velocity.

6. Conclusions and Future Work

With such a low mean relative error (less than 1%) when compared to test data, this well-fitting model provides the foundation for an accurate solids mass flow meter, capable of utilisation in furnace/reactor control loops. This could then enable process optimisation and reductions in waste and emissions for some of the most energy intensive and polluting industrial processes. Therefore, if widely adopted, even relatively slight resulting optimisations could globally constitute millions of tonnes of carbon prevented from being released into the atmosphere.

As in practice it is difficult to measure air-solids ratio, it is desirable to eliminate it from the model if possible. As both mass flow rate and velocity are both flow variables relating to air solid ratio, and it is thought that a model incorporating only V_{rms}, Q_m and v_p can exhibit sufficient accuracy to constitute a useful multiphase meter. Such a model would have the form;

$$Vrms(mV) = (\alpha + \beta v_p)\, Q_m^2 + (\gamma + \delta v_p) Q_m \tag{6}$$

Preliminary results with such a model indicate a mean relative error of 1.4% and maximum relative error of less than 8.5% - this is acceptable for a multi-phase flow meter (though improvable) and can be achieved without need for new hardware, utilising multiple ring-shaped electrostatic meters as in Figure 1. Subsequent work will ascertain both a theoretical basis for the model and its potential practical performance and results will demonstrate non-intrusive online measurement of mass flow rate of bulk solids in a pipeline, with first-rate accuracy.

References

1. Wuqiang Y, Zhang J, Wang H, (2017). In-Line Sensors for Real-Time Measurement and Analysis of Bulk Dry Powder, International Fine Particle Research Institute Review
2. Zhang J., Cheng R, Yan B, & Abdalla M. (2016). Further Investigation into Spatial Sensitivity of Electrostatic sensors. ICAMEME 2016, Beijing, China.
3. Zhang J, Cheng R, & Zhou B. (2013). Effect of particle size on output signal of electrostatic sensors. ICBMH 2013, Newcastle, Australia
4. Wang S, Li J, Xu C, et al (2015). Local particle mean velocity measurement in pneumatic conveying pipelines using electrostatic sensor arrays. Particulate Science and Technology, vol. 33, no. 1, pp. 81–90
5. Ma J, Yan Y. (2000). Design and evaluation of electrostatic sensors for the measurement of velocity of pneumatically conveyed solids. Flow Measurement and Instrumentation, vol. 11, no. 3, pp.195-204
6. Bentley J. (2005). Principles of Measurement Systems. 4th ed. Essex: Pearson. p344-347.
7. Zhang, J. (2012).Air-solids flow measurement using electrostatic techniques. Canbolat, H. (ed.) Electrostatics, Intech, pp. 61-80

Nottingham | UK | 9–11 September 2019

Decomposing the drivers of residential space cooling consumption in EU-28 countries using a panel data approach

Andreas Andreou [1], Peter Taylor [1, 2], Paul Brockway [1],
Zia Wadud [2,3], John Barrett (Corresponding Auth.) [1]

[1] *Sustainability Research Institute, School of Earth and Environment; University of Leeds, Leeds, LS2 9JT, UK*

[2] *Low Carbon Energy Research Group, School of Chemical and Process Engineering; University of Leeds, Leeds LS2 9JT, UK*

[3] *Spatial Modelling and Dynamics Research Group, Institute for Transport Studies; University of Leeds, Leeds LS2 9JT, UK*

eeaan@leeds.ac.uk

Abstract

While space cooling forms less than 1% of residential energy consumption in the EU-28 region, it is the fastest growing end-use. Still little is known about factors which drove air-conditioning (AC) use over time, since literature is limited to cross-sectional studies which fail to distinguish between climatic and non-climatic influences. Expansion plans of EU's power sector therefore neglect potential implications of booming AC demand. We develop a novel decomposition framework which measures the effect of components on cooling consumption between 2000 and 2015. Panel data models then identify drivers of cooling's climate-sensitive components. Finally, we explore scenarios of AC use up to 2050 and evaluate their impact on peak capacity. AC diffusion was the key driver of cooling, whose effect was partly counterbalanced by efficiency gains. While weather influences households' AC purchasing behaviours, income has larger marginal effect. In baseline scenarios, diffusion saturates by 2050, yet modestly increasing sectoral energy use. Still, IEA's projections underestimate future cooling size, even if compared to the strong efficiency scenario. Security risks emerge from a scenario of fast AC up-take in new buildings, especially for cold regions where peak demand outgrows expansion of solar capacity. Findings have implications for Union's strategy to decarbonise housing stock.

Keywords: Space cooling, AC diffusion, Decomposition, Panel regression, Peak demand

1. Introduction

Global demand for space cooling has increased threefold between 1990 and 2016, showing the strongest average annual growth rate amongst all building end uses [1]. Spread and use of air-conditioning (AC) has been linked to changing climatic and economic conditions. In the

European Union (EU-28), while residential cooling forms a minor share of sectoral final energy consumption (0.5% in 2012 [2]), it has an enormous growth potential as less than 10% of floor area is cooled [3]. The expected rise in cooling demand will intensify pressure on power sectors, through requiring additional generation capacity and calling for more effective management of summertime peak loads, which have already emerged in Mediterranean EU-28 countries [4].

Studies analysing EU's current cooling demand involve estimates obtained through bottom-up modelling which in turn depends on technical parameter values gathered over tiny time frames [3, 5, 6]. These are mixed with crude assumptions about the evolution of involved parameters to define ceiling values for cooling demand, thus limiting understanding about future demand trends and hindering progress towards resilient cooling networks. This paper develops a multi-method modelling framework (Figure 1) to examine the following research questions:

(i) What was the main driving force of EU's residential cooling demand during the time period 2000-15? This question is tackled with an index decomposition analysis (IDA).
(ii) Which are the specific drivers of climate-sensitive components of cooling energy use? This objective is achieved by extending decomposition to a set of panel data econometric models.
(iii) What are the impacts of AC trajectories on sectoral energy use and peak demand capacity up to 2050? Employed scenarios account for (a) projections of socio-economic and climatic data, (b) unit efficiency improvements, and (c) penetration rates in new and renovated buildings.

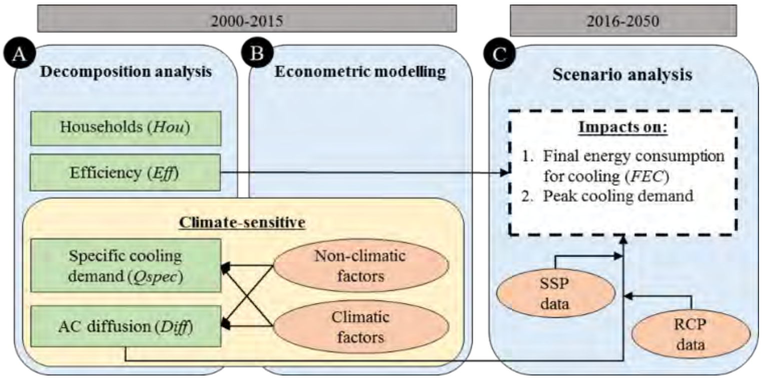

Figure 1: General modelling framework

2. Methodology

2.1 Decomposition analysis of *FEC* (2000-15)

$$FEC = Hou \times Diff \times Qspec \div Eff \tag{1}$$

Final energy consumption for cooling (*FEC*) between 2000 and 2015 is expressed as:

Housing stock (*Hou*) and AC diffusion (*Diff*) is ascribed to the activity and structural parameter, respectively [7]. The intensity indicator is energy used per air-conditioned household, which equals the ratio of "useful" specific demand (*Qspec*) to system's efficiency indicator (*Eff*). The main source of data is the newly-published JRC-IDEES database [8].

2.2 Econometric modelling of *Diff* and *Qspec* (2000-15)

$$\ln\left(\frac{Sat_c}{Diff_{c,y}} - 1\right) = \ln(\alpha_c) + \beta_1 t + \beta_2 INC_{c,y} + \sum_{r=0}^{N} \beta_{3y-r} TMP_{c,y-r} + \varepsilon_{c,y} \tag{2}$$

AC diffusion (2000-15) is studied in a panel data setting through an "s-shaped" logistic curve:

$INC_{c,y}$ denotes personal income for country, c, and year, y, approximated by per capita GDP which is PPP-adjusted to represent between-country price-level differences. $TMP_{c,y}$ stands for mean, population-weighted, summer temperature, whereas a *TMP* lag (N=1) aims as to capture the delayed effect of weather shocks. We implicitly control for evolving efficiency standards and AC prices through a time trend, *t*. Saturation (*Sat*) is maximum attainable diffusion level and can vary across space between 0 and 1. The EU-28 region is first split in *warm* and *cold* countries based on the long-term (1995-2015) cooling degree days (CDDs). Model performance is tested for various group-level saturation points until the R^2 statistic is maximised. A fixed-effects (FE) estimator controls for time-invariant, country-specific characteristics, α_c,

$$Qspec_{c,y} = \gamma_c + \gamma_1 AREA_{c,y} + \gamma_2 AREA^2{}_{c,y} + \gamma_3 CDD_{c,y} + \varepsilon_{c,y} \tag{3}$$

Demand for cooling (2000-15) per unit of activity (households) is modelled through:

Larger-sized (*AREA*) dwellings need more energy to maintain desired indoor temperature [9]. *CDDs* characterize the weather-sensitive part of *Qspec*, as they quantify the annual sum of daily deviations of mean outdoor temperature from a common threshold [10].

2.3 Scenario analysis (2016-55)

In the baseline case, country-level AC diffusion is estimated via (2) and for various income and temperature trajectories, derived from all Shared Socio-economic Pathways (SSPs) ([11]) and Representative Concentration Pathway (RCP) 8.5; an extreme climate change scenario ([12]). Sensitivity of *FEC* to AC up-take is assessed through adjusting *Diff* in (1) to match scenario's value, while keeping *Hou*, *Qspec* and *Eff* at 2015's levels. Estimation of summer-time peak demand is based on rated capacity (*Cap*), conversion efficiency (*SEER*) and respective share (*w*) of space cooling technologies (split, multi-split, single-duct and packed systems):

Policy case 1 – Unit Efficiency Improvement: The general 20% and 30% efficiency targets endorsed in mid-term EU's strategy are adopted, while we assume that super-efficient units swarming the market late in the mid-21st century increase *Eff* by 40% relative to 2015. Policy case 2 – New Buildings AC Rates: Developments in the construction industry could facilitate easier installation of AC in new and renovated buildings [13]. This behaviour could be mimicked by more households causing an abrupt transformation of the AC market. The new *Diff'* parameter is corrected to account for the growing share of new units, AC'_{new}, in total stock. AC'_{new} is set to increase in 10-year steps from 80% in 2020 to full saturation (100%) by 2050.

3. Results

3.1 Retrospective analysis (2000-2015)

EU-28 aggregate *FEC* rose from 6.37 TWh to 15.83 TWh between 2000 and 2015 (6.3%/year). Based on decomposition analysis, AC diffusion had the largest impact on cooling consumption with an average effect (+1.02 TWh/year) being two times as large as that of efficiency gains. This agrees with past evidence that 'extensive margins', namely residents' growing inclination towards AC purchases, are extremely important in electricity demand impact assessments [14].

$$Peak_{c,y} = AC\ Stock_{c,y} \times \frac{\sum_{tech=1}^{4} w_{tech} \times Cap_{tech} \div SEER_{tech}}{\sum_{tech=1}^{4} w_{tech}} \tag{4}$$

As for AC diffusion, optimal model fit is achieved ($R^2 \sim 0.75$) when *Sat* is fixed at 60% for warm and 30% for cold countries. Personal income and summer temperature (contemporaneous and lagged) had a significant positive effect on *Diff*, while a strong trend is also present. To compare the size of partial effects on AC diffusion, a standardization procedure is followed which puts both predictors on similar scales. The new *INC'* estimate is about 5 times bigger than *TMP'* one, implying that household wealth has relatively larger influence on AC purchasing decisions.

With respect to *Qspec, AREA* appears to be a key determinant as both the linear and quadratic term were highly significant. Although the *CDD* coefficient is positive, it is only marginally significant ($p \approx 0.097$) and has small impact on model's performance. Nevertheless, the soft link between *Qspec* and *CDD* supports the argument presented in potential peak demand assessment that simultaneous AC use would more likely occur during the hottest day of the year.

3.3 Future scenarios (2016-2050)

In the baseline case, AC in warm and cold countries reach saturation, which increases EU-28 aggregate diffusion from 9.2% in 2015 to 37.6% in 2050. Saturation is reached under all SSP and RCP combinations, albeit at varying paces. Penetration levels deviate significantly from baseline in the extreme diffusion case, especially in cold countries where new buildings show low installation rates. EU-28 diffusion reaches 85.1% in 2050, without any signs of stagnation.

Baseline *FEC* in the EU-28 region increases by a factor of 3.4 in 2050 (53.7 TWh) relative to 2015 (Figure 2). Despite accounting for a modest share of residential final energy (1.9%) and electricity use (6.0%) in 2050, cooling displays a much greater growth than the one projected by the International Energy Agency (IEA) (21.8 TWh) [15]. IEA's projection is lower than this paper's values even when compared to our efficiency scenario. The sharpest *FEC* increase in 2050 is estimated for the "New Buildings AC rates" case (104.1 TWh). Due to major changes in regional AC markets, cold countries become responsible for the lion's share of *FEC* (60.1%).

Baseline AC peak demand increases from 41.5 GW in 2015 to 170.3 GW in 2050, thereof 99.3 GW in cold countries. In agreement with *FEC* results, potential peak demand is affected the most in the extreme diffusion case, reaching a 9-fold increase in 2050 (385 GW, thereof 292.1 GW in cold countries). Given the growing size of cooling and ambitious plans in the EU to decarbonise electricity grid by 2050, adequate provision of renewable capacity is needed to manage summertime AC loads. Solar, which has higher seasonal output potential than wind and hydro, is the most suitable energy form for serving excess demand. Peak demand in cold countries is shown however to outgrow expansion of solar-based capacity during the analysis period, pointing potential risks of system failure if alternative cooling options are not provided.

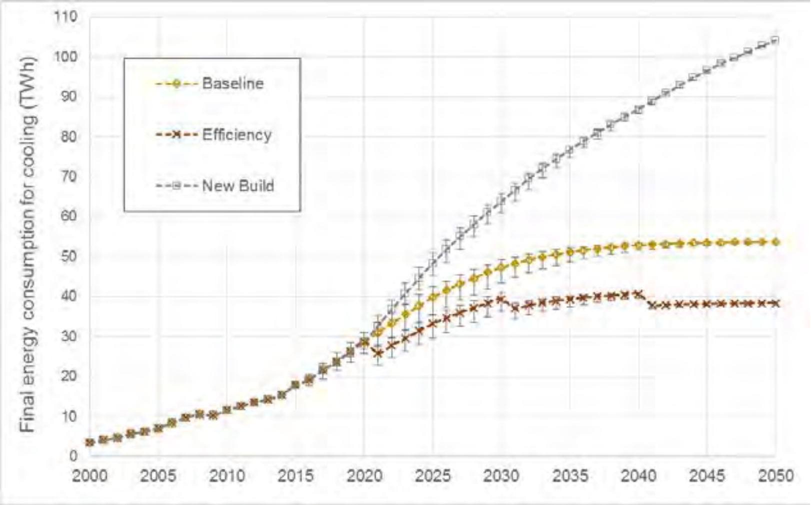

Figure 2: Residential cooling consumption at the EU-28 level based on different scenarios. Note: Error bars represent the range of uncertainty in climatic and economic projections.

4. Policy recommendations

(a) Effective promotion of passive cooling designs: Passive cooling (e.g., natural ventilation, heat sinks and shading systems) needs to receive more support in the Energy Performance of Buildings Directive, as it can reduce the chance of AC mass adoption in buildings.

(b) Amendment of renovation strategies: The growing importance of cooling is overlooked by many cold countries in their long-term renovation strategies. National plans should deal with predicted changes in local climate and address other risk factors, including economic growth.

(c) Diversifying cooling supply: Decentralised production sites, such as district cooling (DC), increase flexibility of cooling supply; however their capacity is currently limited [2]. Local authorities need to design a combination of fiscal incentives for DC suppliers to overcome market obstacles. Building engineering innovations could ease access to nearby DC systems.

5. Conclusion

This paper made initial steps in deciphering trends of cooling energy consumption in EU's residential sector, through a multi-method modelling framework. Findings showed that AC penetration rates and efficiency gains to a lesser extent, will shape future trajectories of cooling consumption, which are underlined by high degree of uncertainty. Future work could focus on developing a framework which models the interactions between cooling and electricity national sectors, effectively assessing the mismatch between AC demand and in-feed renewable energy.

Acknowledgments

This research is funded by the Priestley International Centre for Climate (PICC).

References

1. IEA (2018) The Future of Cooling Opportunities for energy-efficient air conditioning. Paris
2. DG ENER (2016) Mapping and analyses of the current and future (2020 - 2030) heating/ cooling fuel deployment (fossil/renewables) WP1.
3. RESCUE (2014) EU DISTRICT COOLING MARKET AND TRENDS WP2. Brussels
4. Izquierdo M, Moreno-Rodríguez A, González-Gil A, García-Hernando N (2011) Air conditioning in the region of Madrid, Spain: An approach to electricity consumption, economics and CO2 emissions. Energy 36:1630–1639
5. Werner S (2016) European space cooling demands. Energy 110:148–156
6. Jakubcionis M, Carlsson J (2017) Estimation of European Union residential sector space cooling potential. Energy Policy 101:225–235
7. Isaac M, van Vuuren DP (2009) Modeling global residential sector energy demand for heating and air conditioning in the context of climate change. Energy Policy 37:507–521
8. JRC (2017) JRC-IDEES: Integrated Database of the European Energy Sector: Methodological note. doi: 10.2760/182725
9. Yun GY, Steemers K (2011) Behavioural, physical and socio-economic factors in household cooling energy consumption. Appl Energy 88:2191–2200
10. Fazeli R, Ruth M, Davidsdottir B (2016) Temperature response functions for residential energy demand - A review of models. Urban Clim 15:45–59
11. Riahi K, van Vuuren DP, Kriegler E, et al (2017) The Shared Socioeconomic Pathways and their energy, land use, and greenhouse gas emissions implications: An overview. Glob Environ Chang 42:153–168
12. Riahi K, Rao S, Krey V, Cho C, Chirkov V, Fischer G, Kindermann G, Nakicenovic N, Rafaj P (2011) RCP 8.5-A scenario of comparatively high greenhouse gas emissions. Clim Change 109:33–57
13. Biddle J (2008) Explaining the spread of residential air conditioning, 1955-1980. Explor Econ Hist 45:402–423
14. Davis LW, Gertler PJ (2015) Contribution of air conditioning adoption to future energy use under global warming. Proc Natl Acad Sci 112:5962–5967
15. IEA (2017) Energy Technology Perspectives 2017. doi: 10.1787/energy_tech-2017-en

Nottingham | UK | 9–11 September 2019

What is energy security doing to green energy development in Great Britain?

Angelica Rutherford [1]
[1]School of Law and Social Justice, University of Liverpool, Mulberry Court, Mulberry Street, Liverpool L7 7EZ
Angelica.Rutherford@liverpool.ac.uk

Abstract

This paper delves into energy security and green energy in Great Britain (GB). Based on semi-structured interviews with 24 leading energy experts, it focuses on the implications of the discursive links between energy security and law and policies promoting green energy. First, this paper shows that energy security in GB is first and foremost a political issue, particularly as a result of risks associated with governments toppling in cases of energy interruption in the country. Second, this work demonstrates that energy politicisation in GB was framed by participants as having negative impacts on green energy development due to vested interests, unequal lobbying power and association of green energy with left-wing politics. Third, the analysis also reveals a discursive struggle over energy security and green energy links with positive and negative frames identified. In particular, the analysis shows the emergence of two novel themes in relation to energy security and green energy: (i) the potential shift in the debate surrounding green energy intermittency as a result of large-scale commercial energy storage; and (ii) the emergence of 'prosumers', a new actor in the energy market which challenges the current energy system.

Keywords: energy security, green energy, prosumers, energy storage, Great Britain, energy law

1. Introduction

This paper explores the interplay between energy security and green energy in Great Britain (GB) in the context of a transition to a more sustainable, affordable, secure and inclusive energy system. Based on semi-structured interviews with 24 leading energy experts, this work focuses on the implications of the discursive links between energy security and law and policies promoting green energy. The overarching objective is to reveal some of the on-the-ground perceptions of key energy experts in GB on this interplay that so far have remained unseen in scholarly analysis.

Guided by discourse analysis, which is based on the assumption that discourses not only represent reality, but also help shape it in consequential ways, the aim is to present the discursive realities according to interviewees themselves by letting them set out their accounts in their own words and in their own terms. Understanding how participants discursively frame energy security and its links with law and policy on green energy development is crucial because when one frame is selected from amongst a range of competing frames it can be incorporated into law and policies and it has consequences for how green energy development is subsequently seen and acted on.

Based on participants' discursive constructions, this paper will highlight the challenges posed to the transition to a green energy system in GB. First, this work will show that energy security in GB is first and foremost a political issue, particularly as a result of risks associated with governments toppling in cases of energy interruption in the country. Second, this paper will demonstrate that energy politicisation in GB was framed as having negative impacts on green energy development due to vested interests, unequal lobbying power and association of green energy with left-wing politics. Third, the analysis also reveals a discursive struggle over energy security and green energy links with positive and negative frames identified. In particular, the analysis shows the emergence of two novel themes in relation to green energy and energy security: (i) the potential shift in the debate surrounding green energy intermittency as a result of large-scale commercial energy storage; and (ii) the emergence of 'prosumers', a new actor in the energy market which challenges the current energy system.

2. Method

Semi-structured interviews were conducted by the author with 24 participants from June 2016 to November 2016 (appendix A). Participants were placed into three categories according to who they worked for: (i) government/governmental organisations, (ii) private sector and (iii) not-for-profit organisations.

Interviews were face-to-face and took place in London, Leeds, Liverpool, Peterborough, Chester and Kings Langley. Interviewing time ranged from 15 minutes to 90 minutes. 90% of the interviews lasted between 45-60 minutes. Responses from 23 participants were captured with a digital audio recorder and transcribed verbatim by the author. One participant from the private sector did not wish to have the interview recorded, but note-taking was allowed and, therefore, notes were taken. The transcripts were analysed thematically. A data-driven inductive or 'bottom up' approach focused on the lines of similarity and difference emerging from the interviews was followed and the 6-phase guide to performing thematic analysis of Braun and Clarke [1] provided recursive and iterative tools for the analysis of the data.

3. Results and Discussion

3.1. Energy politicisation in GB and barriers for the transition to a green energy system

Energy politicisation, where there is public and political interest in the matter which is subject to contestation and political deliberation [2], was a remarkably dominant frame in the empirical data.

As explained by participants, "governments fall if they don't provide people with electricity, so there is an important political reason why people and Ministers take it seriously"[3], "if you are in government, you would never like to be the government that stands over a bunch of blackouts in the country, would you? It's pretty terminal from a political perspective" [4] or "for democratically elected governments it [energy supply interruption] means that those who are in power are likely to be out of power very quickly." [5] Energy security in GB, therefore, was recurrently construed as a matter of priority because of its direct consequences of governments toppling and its negative impact on the chances of a political party getting re-elected in cases of energy interruption in the country.

In connection with this debate, the analysis of the empirical data showed that, according to participants' accounts, energy politicisation in GB is hindering green energy development as a result of three factors: vested interests, unequal lobbying power and association of green energy with left-wing politics.

3.1.1. Vested interests

Vested interests were constructed as connected to the close personal relationships between the government and the nuclear, oil and gas industries and their unwillingness to see the energy system changed. The rationale provided for this reluctance towards changes to a green energy system was not only due to their familiarity with conventional energy sources but also because the conventional energy industries do not want to lose revenue streams or have their business models negatively affected. Aspects of this are perhaps unsurprising as a fully-fledged policy drive to a green energy system will certainly have important consequences for future revenues of conventional energy industries.

3.1.2. Unequal lobbying power

Unequal lobbying power was advanced by participants as a key issue. A participant pointed out that the nuclear, oil and gas industries in GB are made up of large, multinational and multibillion pound organisations and these were seen as having far more lobbying power over the government than wind, solar and biomass, because the renewable energy sector was framed as not wanting to speak with a single voice and not being as large. Valentine agrees with the existence of a fragmented structure of the renewable energy technology sector and argues that it places the sector at a financial disadvantage when compared to fossil fuels, a sector which does unite to engage in collective lobbying.

3.1.3. Green energy as tied to left-wing politics

Participants also advanced a construction of public perception based on people associating "wind turbines or solar energy as hippy"[6], "totemic for the left" [7] or that "green energy equals left wing" [8]. This equation of green energy with left-wing politics then makes it difficult for a right wing government to support green energy development as a strategic energy policy choice. However, a participant mentioned that attempts have been made to move on from that discussion and associate green energy with business opportunity [9].

In summary, vested interests, unequal lobbying power and association of green energy with left-wing politics were issues advanced by participants which need to be managed to increase the deployment of green energy in the energy system in GB. Law and policies in this area may, therefore, be useful in tackling these issues if the goal is to increase the share of green energy deployment in the energy system.

3.2. Analysing the links between energy security and law and policies on green energy development

The investigation on how participants discursively constructed the links between energy security and law and policies on green energy development in GB shows, in summary, that the construction of energy security and green energy links involves three competing ways of framing how energy security impacts on green energy development. These frames are not entirely clear cut and uniform amongst participants: (i) the positive frame, (ii) the negative frame and (iii) the emerging frame.

3.2.1 Analysing the positive frame

Data analysis produced four themes associated with the interplay between energy security and law and policies on green energy development in a positive way: energy availability, energy diversification, energy independence and energy decentralisation. Participants deployed this positive frame to point out the importance of developing green energy to ensure energy security. In the analysis which follows, there has been no attempt to rank these themes in order of importance.

First, participants praised green energy for its wide availability, for not being subject to depletion like fossil fuel resources, and for delivering energy security as a result of its contribution to meeting energy demands and contribution, second, to the diversification of the energy matrix. Third, energy independence, in the sense of green energy being a domestic source and in the sense of less or no imported fossil fuels, was also mentioned in a positive way in relation to green energy, albeit raising some controversy. Participants pointed out that the emphasis on energy independence does not favour green energy exclusively as this argument has also been used extensively for fracking in the UK.

Moreover, the debate about energy independence was criticised from two different perspectives: (i) less imported fossil fuel was seen as not completely shielding the energy sector from the price effects of a global constraint on oil and gas, and it was recognised that reducing high priced imports would not mean that everybody would be better off because of the way that energy markets work and because of customers contractual structures in place; and (ii) energy independence was constructed as an outdated debate in the context of the current energy interdependence in GB, particularly as a result of installation of interconnectors with neighbouring European countries which allows for energy exportation when there is over-supply or energy importation when there is under-supply, providing, of course, that the continental energy producers themselves are not under stress to produce more for their own local markets. Nevertheless, Brexit and the future uncertainty over the internal energy market was constructed as being capable of influencing the rhetoric around energy independence and energy security as Brexit could potentially make it harder to secure energy supplies from the Continent.

Fourth, energy decentralisation – where a generation plant can be connected to the distribution network or off grid, at a location close to the point of use – as a characteristic of green energy deployment was constructed as contributing to energy security. By being able to supply energy in a decentralised manner, green energy was framed as contributing to the flexibility of the energy system and its resistance to central shocks or system-level failures.

3.2.2 "Energy security is being used as a stick to beat green energy with"[10]: Analysing the negative frame

Data analysis produced two themes associated with energy security and green energy development when framed negatively: grid upgrading issues and unreliability due to intermittency. This negative frame in the discourse had the implication of hindering green energy development. The allegation that some green energy projects in GB could generate energy but could not have the energy gridded due to grid upgrading issues was constructed within the negative frame.

Green energy's intermittent nature was also recurrently presented as negatively affecting the energy security element of reliability. An acknowledged issue with green energy sources, such as solar and wind energy, is the variability in its output. This, therefore, created a general indisposition among some participants to associate green energy sources with energy security in a positive way.

This negative frame was mainly constructed in connection with green energy's impact on the security of the electricity system, particularly the transmission system, due to challenges for the energy system operator to keep the system stable as a result of the intermittent character of green energy. As a result of the negative impact on the functionality of current electricity systems, green energy was framed as causing "genuine risks to energy security in the sense literally of the lights going out" [11].

Those who contested this negative framing sought to refocus the debate on the role of technological advancement. In an attempt to reverse key aspects of the negative frame, these short-term energy security challenges, particularly grid balancing, were framed positively as stimulating innovation via the development of new energy technologies, such as energy storage. Large scale commercial energy storage was also advanced as one of the answers to the short-term energy security challenges that come with green energy deployment in the system, where energy storage would constitute a "game changer" [12] or, as Winfield, Shokrzadeh and Jones have put it, a "technology which may disrupt conventional utility models" [13].

It is acknowledged that low-cost, reliable, and efficient methods to store energy would constitute a valuable addition to a network with a high penetration of green energy generation[14]. Nevertheless, energy storage is not yet a technology that has been commercially proven at large scale and readily available at low cost. An analysis of participants' narratives shows large-scale commercial energy storage to be an essential factor to shift the negative frame to a positive frame surrounding the interplay between energy security and law and policies on green energy development.

3.2.3 Analysing the emerging frame: 'Prosumers' and energy security

Adding green energy to the power sector has given rise to a new actor in the energy debate called the "prosumer", defined as "an energy user who generates renewable energy in his/her domestic environment and either stores the surplus energy for future use or trades to interested energy customers in smart grid [15].

The installation of photovoltaic (PV) panels in properties, for example, along with storage technologies is changing the roles played by the participants in the energy system in GB. For instance, solar energy is directly transmitted to the property via installed solar panels and can be stored via the use of domestic energy storage. As a result, consumers can generate, store and consume energy independently from the grid, reducing, as such, revenues for the utilities sector, and replacing the traditional role of an energy supplier. This transformation in the energy system structure has recently been acknowledged by the Secretary of State for Business, Energy and Industrial Strategy in his statement that '[t]he distinction between [energy] supplier and distributor may no longer hold in this new world'[16].

The appearance of prosumers has been claimed to have both positive and negative implications for energy security. According to Staffell, prosumers add to energy security by, for instance, reducing the need for new generation and infrastructures by generating energy where it is used and by adding to the diversity of the energy supply [17]. However, in an opposite vein, one participant pointed out how prosumers can have a negative impact on energy security. This participant advanced issues related to undermining the integrity of the national energy networks, ownership of the assets and consumer law issues as prosumers impact the perceived fairness of who pays for the physical maintenance and operation of the energy network infrastructure [18].

Those engaged in producing and consuming their own energy do not want to pay for the maintenance of the energy infrastructure, but if the energy network costs are shifted onto a smaller group of energy consumers, their electricity costs can become very high. This means that prosumers have important consequences for future revenues related to the energy infrastructure. Diesendorf and Elliston also add that the increase in local energy self-reliance may reduce the political power of the large energy utilities and the fossil and nuclear power industries [19]. This, therefore, may also cause resistance to further deployment of green energy via prosumers.

One can observe that technological advances, such as energy storage, and the appearance of prosumers are bringing a shift in the frame of the debate. Where green energy was presented as being an energy security concern mainly as a result of supply interruption in the electricity system due to its intermittent nature, as new technologies come on-stream now it is increasingly being presented as a concern because it undermines the integrity of national energy networks, disrupting the traditional way of doing things, disturbing the 'business as usual' scenario, driving changes in old monopoly industries and "forcing big monopoly industries to start thinking differently" [20]. How monopolies, such as the electricity transmission system operator, adapt to these changes has been raised as a current challenge. As a participant put it, "how do you transform a massive business like the National Grid to go from being quite rules based, loving the process and doing the same old thing, quite stagnant, quite stale and not very agile to start being more like a Google or a Tesla?" [21].

Indeed, policies favouring more distributed or decentralised electricity generation have led to concerns in some circles about a 'death spiral' for traditional monopoly electric utilities [22]. This demonstrates the need for energy players to learn how to effectively manage the uncertainties associated with the technological advancements which play a critical role in offsetting the inherently variable nature of green energy sources and can fundamentally change electricity market dynamics. As pointed out by a participant, "any business that has tried to be defensive has just died, it is just death by a thousand cuts" [23]. It cannot be denied that changes to adapt and improve the energy system in GB are greatly needed in the energy transition. The solution then may be to embrace the changes rather than fight them.

In light of the above, then, it becomes clear that the relationship between energy security and green energy is being constructed as a dilemma. On the one hand, green energy is constructed as offering solutions to many energy supply challenges by being able to provide environmentally-friendly availability of energy, energy independence and diversification. On the other, it is constructed as a threat to the current energy system in two different ways: (i) as a threat to short-term energy security as a result of grid balancing and intermittency issues; and (ii) as a threat to the maintenance of the current energy infrastructure as well as to the current electricity market dynamics and its dominant players as a result of technological development and challenges associated with consumers seeking independence from utilities through energy self-sufficiency. One can observe, therefore, that green energy is framed as tackling energy security issues, but also being the cause for the upsurge of emerging energy security problems.

4 Conclusion

This work delved into the interplay between energy security and law and policies on green energy in the context of Great Britain. It sought to examine empirical perceptions of leading energy experts in GB, by presenting the discursive realities according to participants.

A principal finding in this paper was that energy security in GB is first and foremost a political issue and governments will be held responsible and accountable for energy supply interruption in the country. The analysis of the empirical data showed that, according to participants' narratives, energy politicisation in GB is hindering green energy development as a result of three factors: vested interests, unequal lobbying power and association of green energy with left-wing politics. Therefore, these issues need to be managed to increase the deployment of green energy in the energy system in GB, and law and policies in this area may be useful to tackle these issues.

The analysis also found that the construction of energy security and green energy links have been characterised by competing perspectives on how energy security construction is impacting green energy development. Three frames were found which were not entirely clear cut and uniform amongst participants: (i) the positive frame, where energy availability, energy diversification, energy independence and energy decentralisation were generally advanced by participants as a positive frame which pushed forward the promotion of green energy development in the discourse; (ii) the negative frame, where grid upgrading issues and unreliability of green energy due to grid balancing challenges and its intermittent nature were construed as hindering green energy development. However, there is the potential shift in the debate surrounding the negative frame as a result of large-scale commercial energy storage; and (iii) the emerging frame, focused on 'prosumer' as a new actor in the energy market which is challenging the current energy system and threatening the maintenance of the current energy infrastructure.

The interplay between energy security and law and policies on green energy development is, therefore, far from being straightforward. On the one hand, green energy was constructed as offering solutions to core energy security challenges by being able to provide environmentally-friendly availability of energy, energy independence, decentralisation and diversification. On the other, it was constructed as a threat to the current energy system in two different ways: (i) as a threat to short-term energy security as a result of grid upgrading issues, grid balancing and intermittency issues; and (ii) as a threat to the maintenance of the energy infrastructure as well as to the current electricity market dynamics and its dominant players as a result of technological development and challenges associated with consumers seeking independence from utilities and desiring energy self-sufficiency. One can observe, therefore, that green energy was framed as a means to tackle energy security issues, but also a cause for the upsurge of emerging energy security problems.

These findings reveal how existing discursive constructions are broadening, deepening and transforming the relationship between energy security and law and policies on green energy as well as showing its complexity, particularly as a result of technological innovation and the emergence of new challenges to energy infrastructure and market operators following the increasing integration of green energy sources into the system.

Acknowledgments

This work was supported by the Economic and Social Research Council [grant number ES/J500094/1].

References

1. Braun V and Clarke V (2006) Using Thematic Analysis in Psychology. Qualitative Research in Psychology 3: 77-101.
2. Hay C (2013) Why We Hate Politics. Polity Press.
3. Interview with participant from the government sector on 19 October 2016.

4. Interview with participant from the government sector on 11 October 2016.
5. Interview with participant from the private sector on 17 August 2016(a).
6. Interview with a participant from the private sector on 27 July 2016.
7. Interview with a participant from the private sector on 28 September 2016.
8. Interview with participant from the government sector on 22 July 2016.
9. Interview with participant from the government sector on 22 July 2016.
10. Interview with participant from the private sector on 17 August 2016.
11. Interview with participant from the government sector on 20 October 2016.
12. Interview with participants from the private sector on 25 August 2016 and from the government sector on 20 October 2016.
13. Winfield M, Shokrzadeh S and Jones A (2018) Energy Policy Regime Change and Advanced Energy Storage: A Comparative Analysis. Energy Policy 115:572-583.
14. Price A (2014) In Garche J and Moseley PT (eds) Electrochemical Energy Storage for Renewable Sources and Grid Balancing, 1st edn. Elsevier.
15. Rathnayaka AD et al (2015) Framework to Manage Multiple Goals in Community-based Energy Sharing Network in Smart Grid. International Journal of Electrical Power & Energy Systems 73:615-624.
16. The Rt Hon Greg Clark MP (2018) After the Trilemma - 4 Principles for the Power Sector. Speech on the future of the energy market on 15 November 2018 <https://www.gov.uk/government/speeches/after-the-trilemma-4-principles-for-the-power-sector>
17. Staffell I et al (2015) Domestic Microgeneration: Renewable and Distributed Energy Technologies, Policies and Economics. Routledge.
18. Interview with participants from the government sector on 20 October 2016.
19. Diesendorf M and Elliston B (2018) The Feasibility of 100% Renewable Electricity Systems: A Response to Critics. Renewable and Sustainable Energy Reviews 93:318-330.
20. Interview with participant from the private sector on 11 August 2016.
21. Interview with participant from the private sector on 11 August 2016.
22. Armstrong RC et al (2016) The Frontiers of Energy. Nature Energy <https://www.nature.com/articles/nenergy201520>
23. Interview with participant from the private sector on 11 August 2016.

APPENDIX A

Summary of interviews (sector/position/dates)

Sector	Position	Date
Government/Governmental organisation	Managing Director	22 July 2016
Private	Head of Department	27 July 2016
Private	Engineer	3 August 2016
Not-for-profit sector	Policy Analyst	8 August 2016(a)
Not-for-profit sector	Senior Policy Analyst	8 August 2016(b)
Private	Energy Analyst	9 August 2016
Government/Governmental organisation	Head of Department	9 August 2016
Private	Director	11 August 2016
Private	Head of Department	17 August 2016(a)
Private	Solicitor	17 August 2016(b)
Private	Head of Department	18 August 2016
Not-for-profit organisation	Researcher	19 August 2016
Not-for-profit organisation	Chairman	23 August 2016
Private	Head of Department	24 August 2016
Private	Energy Analyst	25 August 2016
Not-for-profit organisation	Chairman	14 September 2016
Government/Governmental organisation	Director	14 September 2016
Private	Managing Director	28 September 2016
Not-for-profit organisation	Head of Department	29 September 2016
Private	Senior Policy Analyst	7 October 2016
Government/Governmental organisation	Director	11 October 2016
Private	Manager	17 October 2016
Government/Governmental organisation	Chairman	19 October 2016
Government/Governmental organisation	Chairman	20 October 2016

ICESF
Nottingham | UK | 9–11 September 2019

Would High Level of Insulation in Buildings Improve Energy Savings ?

Sherna Salim, Amin Al-Habaibeh* and Ahmad Lotfi
Innovative and Sustainable Built Environment Technologies Research Group (iSBET)
Nottingham Trent University, UK

sherna.salim2017@my.ntu.ac.uk; *Amin.Al-Habaibeh@ntu.ac.uk; Ahmad.Lotfi@ntu.ac.uk
*Corresponding Author

Abstract

The UK government is committed to reduce 80% of its carbon footprint by the year 2050. With today's increase in oil prices and the significant growth in energy demand, energy savings in heating and cooling of buildings is becoming an important area to address to reduce energy consumption. This paper reviews literature on energy consumption patterns and investigates the energy consumption in residential buildings based on people's consumption behaviour. Infrared thermography has been used to identify areas in the building where heat is significantly lost. The case studies presented in this paper show that no matter how insulated a building is, significant heat can be lost due to the opening of windows by occupants. This is to improve the ventilation and temperature's comfort level. It can be concluded that proper energy efficient ventilation is necessary to improve the energy efficiency. And the occupant's behaviour plays an important role in controlling the energy savings regardless of the level of insulation of the building.

1. Introduction

Although there is progress on UK's clean energy policy, so far the issue of fuel poverty has not been dealt with effectively. According to Dr Joanne Wade, the CEO of the Association of Conservation of Energy, "The Energy Company Obligation alone will not solve the problem of fuel poverty. To close the investment gap, the Government needs to take robust action to ensure that Minimum Energy Efficiency Standards for the Private Rented Sector are enforced, strengthened, and complemented by strong incentives for action in other housing sectors" [1]. UK has to invest in a nationwide upgrade in energy efficiency of the UK housing stock in order to meet the country's 2050 climate commitments [2]. Such a retrofit might increase the relative impact of the occupant's behaviour on energy use, thereby defining success more and more as the way a building is being used by its occupants [3]. Recent years has seen a rapid increase in urbanisation, a substantial rise from 30% in 1050 to 55% in 2018 [4]. In fact, by 2050, 68% of the world population is projected to live in urban areas [4]. The UK government has committed to reduce 80% of its carbon footprint by the year 2050 [5]. The UK is currently on track with the carbon reduction targets within the second and third budgets (2013 – 2022). But more challenging measures are required in addition to the existing progress, to reach the fourth budget target (2023 – 2027) [6]. Policies such as feed-in-tariffs (FIT) or renewable portfolio standards support the attainment of these tariffs [7]. The effectiveness of this approach is questionable since they rely on the conventional building energy management systems (BEMS). It was found that smart BEMS produce better results when combined with policy measures than conventional BEMS [8]. Although commercial buildings have the high energy consumption, it does not vary significantly with changes in occupancy levels. Consumption patterns depend highly on the way the building is managed [9]. In 2017, the total CO_2 emissions in the UK, from the residential sector was 17% of the overall CO_2 emissions. This was after a drop of 4.3% from the previous year [10]. In contrast, there has been an increase of 3% in CO_2 emissions in 2018, when compared to 2017 [11]. In the past decade the energy used in residential space heating, which accounts for 69% of the total energy consumption, in the UK has only dropped from 1187.55 Petajoule (PJ) to 1107.41 PJ [13]. These numbers make domestic energy use a prominent target for greenhouse gas reduction. There has been a steady increase in the number of households in the UK, since 1991, contributed by factors such as increase in birth rate, net immigration and the long-term trend of single adult households [14]. According to Mintel statistics, the number of households has reached 27.2 million in 2017 and it is projected outreach 32.1 million by 2034 [14]. This means an increase in overall energy consumption. There has been an increasing evaluation of energy use in buildings in the past 15 years, and it has been widely acclaimed that there is a considerable gap between the predicted and actual energy consumption in buildings. Extensive research has been done using energy simulation tools analysing climatic data and properties of buildings, but the impact of occupant behaviour in energy performance analysis has hugely been overlooked. Nevertheless, several studies have been undertaken to analyse post occupancy energy use such as [15, 16, 17, 18]. However, occupant behaviour is one of the most overlooked parameter during energy efficiency design of buildings [17].

In his paper, the occupants' behaviour will be examined with significant focus on windows the relationship between people's behaviour.

2. **Methodology**

In this paper two approaches have been utilised. The first one is to monitor windows open/close status over significant period of time during warm and clod seasons. The other approach is infrared thermography surveys to look at the status of buildings in cold weather and to develop qualitative and quantitative understanding of people's behaviour. In the first part of the study, Nottingham Trent University (NTU), with collaboration from Nottingham City Homes (NCH), have conducted a study to analyse energy efficiency in social housing. This paper focuses on 17 residential buildings based in Nottingham with a diverse construction design, constructed over a period ranging from 1902 to 2012. Houses were equipped with Wireless Sensor networks (WSN) to record opening and closing of windows, in addition to other temperature and energy variables. The experiment was conducted from May 2012 to March 2014. Moreover, to better understand and evaluate occupant behaviour with respect to thermal comfort, a survey was done in different areas of Nottingham in the United Kingdom, during the night, in winter with environmental temperature between 3^{o}C and 5^{o}C. By using infrared technology, areas of heat-loss in the building can be specified accurately, with the temperature values. Thermal images of buildings were taken on two cold winter nights and were studied based on their temperature range and the building features. The images collected were of buildings built in different decades, with different types of insulations.

3. Results

3.1 Longitudinal study of windows status

Figure 1 presents the windows status (open/closed) in 17 of the monitored buildings. Figure -a shows the bedroom window status of the houses, when the outside ambient temperature is 5^{o}C or less. It has been found that 70% of the houses open their windows at least once even when the outside ambient temperature is less than or equal to 5^{o}C. Figure 1-b shows the frequency of opening the bedroom window in each house. Even at a temperature of 5^{o}C or below, 43% of the houses keep the windows open more than 5% of the time, of which 29% keep it open more than 30% of the time.

The highest frequency of opening windows is by house 11, which opens the bedroom window 59% of the time, when outside ambient temperature is 5°C or below. House 11 has good insulation. House 3 is also well insulated and the occupants keep the bedroom window open 37.8% of the time at low temperatures.

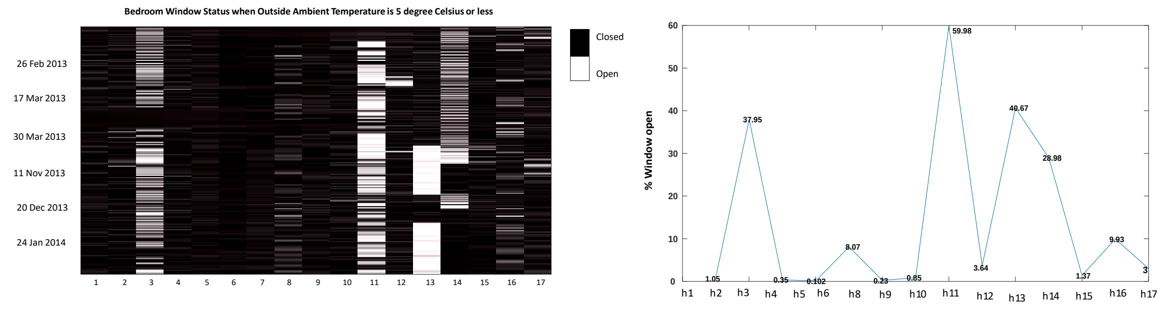

(a) (b)

Figure 1: Window opening frequency

3.2 Infrared Survey

For this part, infrared thermography survey was done in Nottingham city to examine the open windows in cold weather.

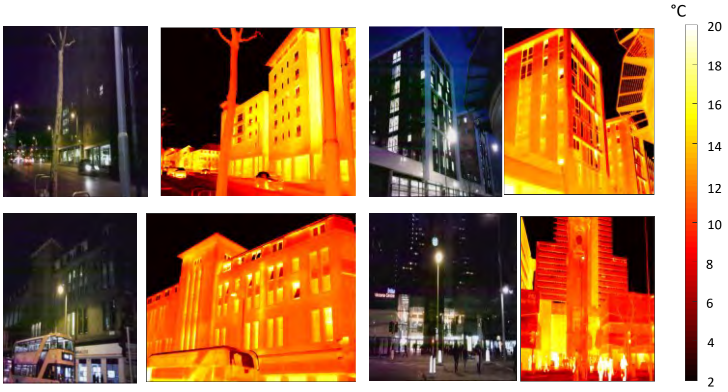

Figure 2:Thermal images of buildings in Nottingham City

Thermal images of buildings in Nottingham city centre are examined including offices, multi-story student accommodation buildings and residential houses. Figure 2 presents examples of surveyed buildings.

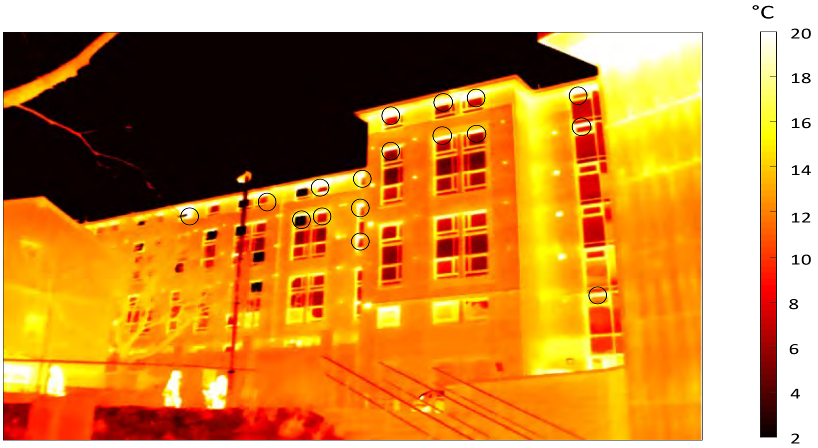

Figure 3: Infrared images of students accommodation

Figure 3 presents a student accommodation. Two windows on the top floor are wide open and 14 other windows can be seen partially open, making a total of 16 windows open, out of 45 observed windows, which makes the total number of opened windows are about 35.5%

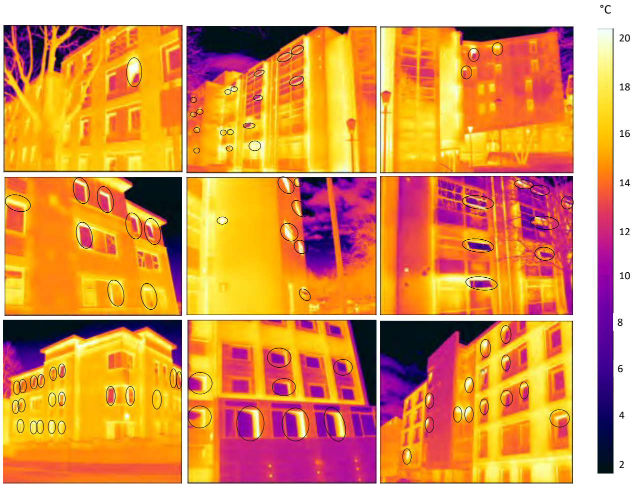

Figure 4: Infrared images of students accommodation buildings

Figure 4 presents more examples of new student accommodation buildings. Although the ambient temperature outside is about 3°C, many of the windows are found open. In the nine buildings shown in Figure 4, out of 152 windows seen, 75 are found open. This implies that even when the temperature outside is cold, 49.3% of the windows are found open in buildings that are well insulated.

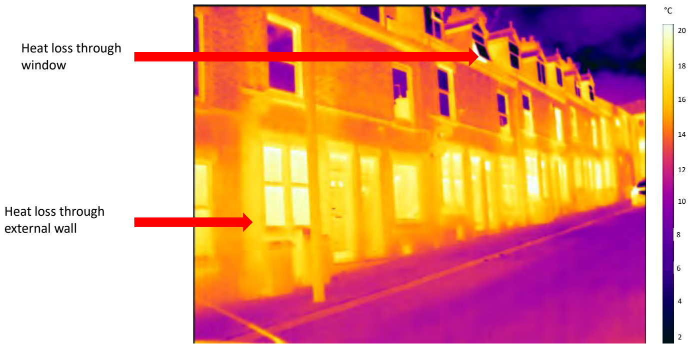

Figure 5: Infrared images of old terraced houses

Figure 5 shows poorly insulated Victorian terrace houses built in the late 19th century. There is heat-loss through windows due to absence of double glazing and through external walls due to absence of insulation. Despite these heat losses the upper floor window can be seen to wide open.

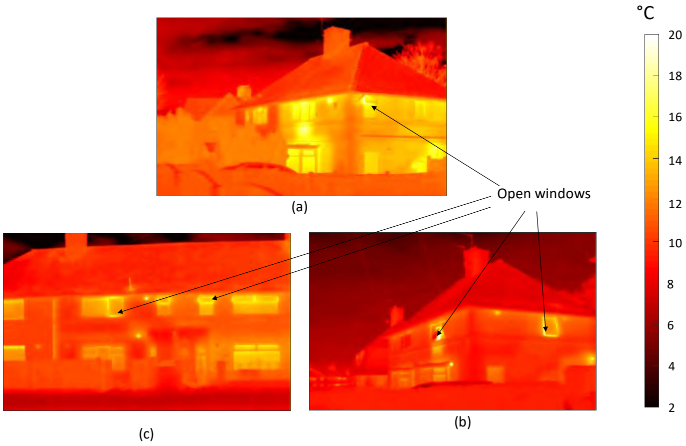

Figure 6: Infrared images of semidetached houses

Figure 6 shows Gregorian houses built in the early 20th century, taken when outside ambient temperature is about 5°C. House (a) has a very poor insulation and single glazed windows, with heat losses through walls. House (b) has wall insulation and double-glazed windows and (c) shows two houses, one with external insulation and one without external wall insulation. Windows can be seen open in the houses, regardless of the insulation properties of the house.

4. Discussion

This paper has explored the relationship between the occupant's behaviour in cold weather in buildings with a wide range of age and characteristics. It can be observed that thermal comfort as well as getting the necessary fresh air is a stronger driver when compared to energy efficiency. A significant variability has been found between different households, irrespective of the insulation, built year or the heating systems used. It has been found that, of the total number of thermal images, 54.8% of the windows in the images were open, when the outside ambient temperature was 3°C.

The American Society of Heating and Air Conditioning Engineers define thermal comfort as "that condition of mind which expresses satisfaction with the thermal environment and is assessed by subjective evaluation" [20]. Well insulated buildings are normally assumed to be more energy efficient, since they have less heat losses through the building's envelope. However, the findings show that people in well insulated buildings tend to open windows even, during very cold winter nights, for managing the thermal comfort of the house. For people to feel comfortable, a balanced thermal environment with the right air temperature, surface temperatures, humidity and absence of draughts is essential [21]. The most effective way to increase energy efficiency of a buildings is by providing proper ventilation systems, along with good insulation and improving occupant's behaviour.

5. Conclusion

The lengthy monitoring process of the status of windows in 17 houses clearly show the tendency of people to open windows even in winter times regardless of the age of the house. Researchers have not found no clear correlation between the age of the house and type with the tendency to open the windows. In relation to the infrared survey, the thermal images are captured during two winter nights, when outside ambient temperature is at 3 and 5°C respectively. It has been found that 54.8% of the windows are found open in the multi-storey buildings and 64.7% of the Gregorian houses had at least one window open. Although factors such as an airtight ventilation or good insulation affect temperature of a building, it can be argued that proper ventilation of building plays a major role in maintaining a well-balanced thermal comfort for the occupant. It can be concluded that regardless of the age and the insulation of buildings, people's behaviour such as opening and closing of windows play an important role in energy savings and buildings efficiency.

References

[1] Energy Institute, "Energy Barometer 2018," London, 2018.

[2] J. Timperley, "UK homes need 'deep efficiency retrofit' to meet climate goals - Energy Post," *energypost*, 2018. [Online]. Available: https://energypost.eu/retrofitting-energy-efficiency-in-uk-homes/. [Accessed: 25-Apr-2019].

[3] M. Schweiker, "Understanding Occupants' Behaviour for Energy Efficiency in Buildings," 2017.

[4] United Nations, "Press Release," 2018.

[5] "Climate Change Act 2008," 2008. [Online]. Available: http://www.legislation.gov.uk/ukpga/2008/27/pdfs/ukpga_20080027_en.pdf. [Accessed: 05-Mar-2018].

[6] "How the UK is progressing - Committee on Climate Change," 2017. [Online]. Available: https://www.theccc.org.uk/tackling-climate-change/reducing-carbon-emissions/how-the-uk-is-progressing/. [Accessed: 08-Mar-2018].

[7] European Union, "DIRECTIVE 2009/28/EC OF THE EUROPEAN PARLIAMENT AND OF THE COUNCIL," *Off. J. Eur. Union* , vol. 140, no. 16, pp. 16–62, 2009.

[8] P. Rocha, A. Siddiqui, and M. Stadler, "Improving energy efficiency via smart building energy management systems: A comparison with policy measures," *Energy Build.*, vol. 88, pp. 203–213, 2015.

[9] M. S. Gul and S. Patidar, “Understanding the energy consumption and occupancy of a multi-purpose academic building,” *Energy Build.*, vol. 87, pp. 155–165, 2015.

[10] Department of Energy and Climate Change, “2017 UK Greenhouse Gas emissions,Provisional Figures,” 2018.

[11] E. & I. S. Department for Business, “2018 UK Provisional Greenhouse Gas Emissions,” 2019.

[12] Committee on Climate Change, “Reducing UK Emissions:2018 Progress Report to Parliament,” London, 2018.

[13] International Energy Agency, “Energy Efficiency Indicators 2018: Highlights,” 2018.

[14] Mintel, “Thermal Insulation - UK - August 2018,” 2019.

[15] E. Delzendeh, S. Wu, A. Lee, and Y. Zhou, “The impact of occupants’ behaviours on building energy analysis: A research review,” *Renew. Sustain. Energy Rev.*, vol. 80, pp. 1061–1071, 2017.

[16] Zero Carbon HUb, “POST-OCCUPANCY EVALUATION,” Gosport, 2015.

[17] K. Schakib-Ekbatan, F. Z. Çakıcı, M. Schweiker, and A. Wagner, “Does the occupant behavior match the energy concept of the building? – Analysis of a German naturally ventilated office building,” *Build. Environ.*, vol. 84, pp. 142–150, Jan. 2015.

[18] T. Hong, S. D’Oca, W. J. N. Turner, and S. C. Taylor-Lange, “An ontology to represent energy-related occupant behavior in buildings. Part I: Introduction to the DNAs framework,” *Build. Environ.*, vol. 92, pp. 764–777, Oct. 2015.

[19] “National Insulation Association.” [Online]. Available: https://www.nia-uk.org/. [Accessed: 17-Jan-2019].

[20] ANSI/ASHRAE Standard 55-2004, “Thermal Environmental Conditions for Human Occupancy,” Atlanta, 2004.

[21] “Thermal comfort in buildings | Multi Comfort - Saint-Gobain.” [Online]. Available: https://multicomfort.saint-gobain.com/comforts-and-solutions/thermal-comfort. [Accessed: 30-May-2019].

Nottingham | UK | 9–11 September 2019

Promoting Sustainable Development Through Privatized Renewable Energy Plant: A case study on Teknaf solar power plant

Zafrin Ahmed Liza[1], Korima Begum[2], Moni Paul[3]

1. 2. 3. Assistant Professor, Dept. of Anthropology, Shahjalal University of Science and Technology

liza-anp@sust.edu

Abstract

Bangladesh is moving rapidly toward development and the country's economy is also growing fast. The Government is giving emphasis on reliable and quality supply of electricity for sustainable and economic development. State's policy on private sector involvement and releasing of marginal lands for energy plantations is intended to enhance access to energy through diversifying energy supply. The country's first solar park with a capacity of 28 MW has established on 116 acres of land in Knila, Teknaf of Cox's Bazar and has started producing electricity from September 2018, which is being added to the national grid. Solar power is one of the cleanest sources of energy, but it doesn't guarantee that it will be sustainable for all society. Sustainability is determined by three different parameters: environmental sustainability, social sustainability and economic sustainability. This paper will critically discuss the impact of the project on the socio-economic and agro-ecological condition of the local people. Using the empirical research method, the effects have been understood and analyzed from the perspective of political economy.

Key wards: Sustainable development, Privatization, Solar Park

1. Introduction

Crisis of power is one of the major problems in Bangladesh. Day by day the gap between demand and production is increasing. With the current population of 167.65 million, Bangladesh is facing an imminent energy crisis [1].Electricity plays a great role wherever people lives and works in industry, agriculture, and transportation etc. With the rapid advancement of technology consumption of power is also rising. Available and reliable source of electricity is considered as a major prerequisite for a sustained and successful economic development effort and poverty reduction [2]. To attain sustainable GDP growth of 6% and above till 2030 and beyond in Bangladesh, it deems necessary to meet the essential energy needs. Government has taken many initiatives to enhance the reliable and quality supply of electricity for sustainable and economic development. Government's policy on private sector involvement and releasing of marginal lands for energy plantations is intended to improve access to energy through diversifying energy supply. With an intention to reduce dependency on fossil fuel electricity generation Government has initiated the plan to set grid tied solar based power generation projects in the non-agricultural lands. Power generated from the solar park will be directly feed into the grid on commercial basis. According to the Renewable Energy Master Database, the total renewable energy capacity including all categories is 2,273.09 MW. Among these, solar park projects are the main contributors in terms of capacity which is 1,905.36 MW. As our Government is under process of establishing more solar parks in the country as a part of the sustainable development, it is the high time to understand the impact of the project on the local community, because sustainability at the macro level might not have the same impact at the micro level [3]. A specific technology can't be appropriate or sustainable for all because the concept of sustainability is ambiguous and situational [ibid].

In a country like Bangladesh, where population density is high and land is highly productive and demandable, is the solar plant project socially sustainable? There is no doubt it will boost up our economy, but we need to understand socio-cultural and agro-ecological challenges. Country's first Solar Park with a capacity of 20 MW has been established on 116 acres of land in Teknaf of Cox's azar district and has started producing electricity which is being added to the national grid.

The power plant has been installed by private organization Joules Power Limited (JPL) with the help of England-based firm Proinsoor. Some 87,500 (total installed capacity 27.69 MW) solar panels have been installed on the bank of the Naf river in the border area of Bangladesh and Myanmar, where rotationally salt and shrimp was cultivated earlier. Now solar power is being generated in that field and it should be benefiting the electricity users in Teknaf and Ukhiyaupazila of Cox's Bazar. It is expected that, up to 80% of the total electricity demand of the two upazila will be fulfilled by the power plant. Bangladesh has a long legacy in the field of Renewable energy, which started back in 1957 with the start of construction of Country's first hydroelectric project on Karnaphully river at Kaptai, Chittagong. Due to negligence to the project effect on local community, the earlier energy project of the Kaptai had to pay high social cost. One of the major goals of the Government is to bring sustainable development in the country and for this it is important to understand social impact of any related project among local people. The solar park is a new intervention in Bangladesh and this paper critically discusses socio-economic impact of the project from the anthropological perspective.

2. Methodology

This qualitative research study aims to understand the impact of socio-economic and agro-ecological condition of local people through Privatized Renewable Energy Plant. The qualitative study was carried out in Knila, Teknaf. Four focus group discussion and seven in-depth interviews were held with local people. Key informant interviews were also carried out with two community leaders and three land lost people. Collected data has been sorted and analysed to understand the situation. Secondary data sources were also used.

3. Discussions and analysis

Every coin has two sides. We know many advantages of the solar park, but we need to look at the other side of it. Our argument is not against the solar energy, but we want to recall what E. F. Schumacher warned us long time before that technology can't solve all our problems, especially in the domain of profit-based economy and advocates for the use of "appropriate Technology"[4]. When we will think about the appropriate technology we must think locally and to consider its impact on local community.

The requisition of huge amount of land is the major drawback of implanting large-scale solar plant in overpopulated country like Bangladesh. Bangladesh has the one of the highest population density in the world. The country has a population density of 1,115.62 people per square kilometer, which ranks 10th in the world [5]. Dependency of that large number of population on a limited area results problem of food, shelter, health. This type of energy production definitely a serious concern for the land-scarce country like Bangladesh which will create extra pressure on the land as the technology is land intensive. Moreover, 910,000 Rohingya refugees took shelter in Coxbazar, Teknaf and surrounding areas from the bordering country Myanmar.[6]

Though the Government policy stated that the solar power plant should be establish in unproductive land, but due to geographical location the land is highly productive and valuable. This value is not necessarily linked to the market but with the environment. This project has been set up on 116 acres of land which was used by rotation, for salt cultivation during the dry season and for the shrimp during the rainy season. Both the salt and shrimp cultivation are labour intensive production and the major source of income for the local inhabitant. The study shows, every year the country is losing 1% of it's farmland for the non-agricultural use and it is specially affecting poor people and, hence, they are becoming more vulnerable to food insecurity [7]. The private company leased the land from the owners without consulting with the farmers. Even local people were not informed about the park. The news papers reports said, in Mymensingh people protest land acquiring for the solar park establishment and after that without consulting the local people it was established at Teknaf.

The local economy is mainly based on the salt productions and fishing. Around one hundred salt cultivators were directly dependent on that land rented for the project and almost hundred and fifty people were indirectly involved as land labourer, transporter, trader, and input supplier. Due to this solar project almost 250 people were lost their job, which economically affected a larger group when we will count their family members. This unemployment also affected the business of other small local vendors. Only a very small number had re-established in local small business and service sectors, but the large number remains unemployed. There wasn't any alternative arrangement neither any compensation provided. Beside this problem, man although with much hardship can manage something to the adjacent area for making their livelihood, but women, as a special vulnerable group got marginalized abruptly. This unemployment has much extensive affect on their family. Our investigation found among the respondents four families withdraw their children from the school and send them for begging and small jobs, six families informed they can provide one-time meal to the family members, especially younger and aged members are suffering from the malnutrition.

Even the project itself doesn't create much job opportunity for the local inhabitants. Depending on the daily demand fifteen to thirty people get hired at the project as casual worker. Our respondents informed that Rohingya refugees get preference for daily labour as they work illegally in cheaper wage. Due to language barrier and community cohesion they are unwilling to migrate and admitted that many of the community members get involved in illegal (Yaba) drug smuggling from the Myanmar, hefting, robbing and begging. The availability of Yaba became one of the major threats for the young generation throughout the country, who get addicted with it. One of the aged man said, "We know drug peddling is bad, but we don't have other choice for earning. It is not us but the Government policy which is forcing us to do bad thing." During our focus group discussion respondents mentioned drug peddling and consumption increased even after Government declared war against Yaba and expressed their concern about increasing offence.

It was assumed that the park will supply 80% of the local energy demand but the situation is different. During our field work we have noticed community people are facing long hours of load shading everyday even after the full production of the plant. The produced electricity transmits to the national grid to support the economic growth of other area remaining local community in the marginal situation. Government had planned to establish economic zone in Teknaf which will create employment opportunity for the local people. Thus country's economic growth is depending on the sacrifice of poor farmer's cultivable land and financial hardship.

The park area is separated by the boundary wall and restricted for the people. This boundary segmented the place and created disturbance to the harmony of the previous cultivation. Our respondents also mentioned that there was a public road within the project area before which has been blocked and restricted for the community people. That road closure has a complex impact on their agro-ecological and economic life. The road was important to the people as it gives the inhabitant and their livestock access to the Naf river. Water source is important for their cultivation. Fishing at the Naf river was an alternative source of earning too.

The government is trying to solve country's electricity problem involving private sectors which was one of their election mandate. Production of solar panels requires capital-intensive manufacturing facilities that are highly automated. At present Bangladesh is unable to manufacture the required PV modules and these are thus imported from outside countries [8]. The government is paying 17 US Cents for per unit which is much higher than its retail price. If we compare the price with the neighbouring India, we can see the state-run Solar Energy Corporation of India (SECI) managed to produce solar energy for 0.036 US Cents (Rs2.44) per kilowatt-hour (kWh)[9]. The situation raised the question why government is buying electricity in such a higher price, specially when the cost of the producing solar power rapidly declining? We need to consider who is selling this technology, who is managing and who is getting advantage of it. As Schmidt (1993) stated, "State activity is derived from the interests of social classes, their organizations, and the institutional condition for government the distribution of conflicts as well as the strategic manoeuvring of the governing elite."Because of this high price the advantage of the energy will enjoy by a special group of people. At the same time, the study observed discrimination in the distribution of the power.

4. Conclusion

Starting from the 1980s, privatization has become a unique characteristic of global political, economic and social transformations. Our Government also, has surrendered grater part of their material wealth and responsibilities on the private actors. State's policy on private sector involvement and releasing of marginal lands for energy plantations is intended to enhance access to clean energy for sustainable development. But the situation raised question on whose development has been considered? Sustainable development is not only economic or environmental sustainability but also social sustainability of the marginal poor people. This solar plant will accelerate country's economic growth, but it has failed to create opportunities for the poor landless farmer, rather unstable their social consistency. As Bangladesh government is going to establish few more solar energy parks, this is the high time to think about its appropriateness. Should we go for such land intensive and costly energy production or we need to search for a better alternative.

References

[1] Worldometers, April 2019, http://www.worldometers.info/world-population/#top20

[2] Haque, M., & Rahman, J, "Power Crisis and Solution in Bangladesh" Bangladesh Journal of Scientific and Industrial Research, vol. 45(2), pp. 155-162, 2010. https://doi.org/10.3329/bjsir.v45i2.5714

[3]Kattel, Shambhu Prasad (2005), Sustainability or sustainable development: An anthropological perspective. DOI: https://doi.org/10.3126/opsa.v9i0.1143.

[4]Schumacher, E. F. (1973). *Small is beautiful: Economics as if people mattered*. New York: Harper & Row.

[5]World Population Review 2019, retrieved from, http://worldpopulationreview.com/countries/bangladesh-population/

[6] UNICEF 2018, Rohingya Crisis, https://www.unicef.org/emergencies/rohingya-crisis

[7]QUASEM, MD ABUL, (2011) Conversion of Agricultural Land to Non-agricultural Uses in Ban00-gladesh: Extent and Determinants , Bangladesh Development Studies Vol. XXXIV, No. 1

[8] Mondal, Md. Alam Hossain & Islam, A.K.M. Sadrul,(2011), Potential and viability of grid-connected solar PV system in Bangladesh, Science direct, https://doi.org/10.1016/j.renene.2010.11.033

[9] Berkey, Jeremy,(2018) One simple chart shows why an energy revolution is coming and who is likely to come out on top, Business Insider, retrieved from, https://www.businessinsider.com/solar-power-cost-decrease-2018-5

Nottingham | UK | 9–11 September 2019

The impact of data segmentation on modelling building energy usage

William Mounter [1], Nashwan Dawood [2], Huda Dawood[3]

[123]Teesside University, Stephenson St, Tees Valley, Middlesbrough TS1 3BA, United Kingdom

W.Mounter@tees.ac.uk

Abstract

Energy is the lifeblood of modern civilisation, with buildings and building construction contributing to roughly 40% of the global energy usage and CO2 pollution. Predicting building energy consumption is essential for energy management and conservation; data driven models offer a practical approach to predicting building energy usage. The aim of this paper is to improve the data driven models available to aid facility managers in planning building energy consumption.

In this case study the 'Clarendon building' of Teesside University was selected for use in using it's BMS data (Building Management System) to predict the building's energy usage. With a particular focus on how data segmentation impacts a model's accuracy and computational time, in predicting temperature related building energy use. Specifically, the effect of segmenting data to accommodate seasonality. With each data segment to be used to train an ANN model (Artificial Neural Network), using ensemble models where data segmentation overlapped.

The potential of these models was compared on the grounds of accuracy and computational speed to each other, then discussed to identify the situational advantages and disadvantages of data segmentation. This study was performed as part of a larger study, in improving building energy use predictions during the operational period in the fields of incorporating user behaviour and accuracy over time.

***Key Words**: Buildings, Deep learning, Data segmentation, Energy, Prediction.*

1. Introduction

The aim of this conference paper is to investigate the impact of data segmentation on the accuracy of building energy use predictions. Data segmentation being the process of dividing and grouping data based on chosen parameters, in this case timeframes, so that it can be used more effectively; (as opposed to data splitting, in which data is randomly split for cross validation usage).

To use an analogy, in cars, winter and summer tyres tend to perform better in their respective seasons than each other and all-season tyres, but poorer than each other and all-season tyres outside of their respective seasons. Would, in the case of machine learning, a model trained with only a season's recorded building data be more accurate at predicting said season's building energy use than a model trained with the variety of data from multiple seasons?

To investigate aim the Clarendon Building, part of Teesside University Campus, was selected for use in this study- due to the data rich environment it's BMS (Building Management system) provided. Previous studies into this building utilising square regression analysis typically had a baseline of "5% Mean Absolute Prediction Error (MAPE)" for the demands of each assets in one day ahead forecasts (Boisson et al.2019). However, the predictions lost accuracy as the rolling horizon increased.

Figure 1: The Clarendon Building, Teesside university (Preston, 2019)

2. Research Method

From the Clarendon building, two main datasets were available: October 2017 to May 2018 and October 2018 to May 2019. These datasets contained 15-minute averages of building elements energy usage, as well as sensory data of the internal and external environmental temperatures, containing approximately 23,000 data events each. Of these building elements, the building chiller system was selected for use in modelling due to the impact seasonality would have on the overall usage of the chillers.

Whilst square regression analysis was used in the previous study into the Clarendon's energy usage patterns, ANN (Artificial Neural Networks) were selected for use for modelling within this study. This was due to ANNs ability to interpret non-liner data (as shown in figure 2) compared to other machine learning methods such as multiple linear regression (Which interprets non-linear data poorly) (Zeyu, W & Ravi, S. 2015). Or in the case of Support vector regression, which is also capable of interpreting non-linear data in irregular energy usage environments, due to the size of the datasets available. SVR possessing greater accuracy in smaller datasets than ANN, but being out performed by ANNs in larger datasets (Grolinger, K, Et al, 2016).

Figure 2

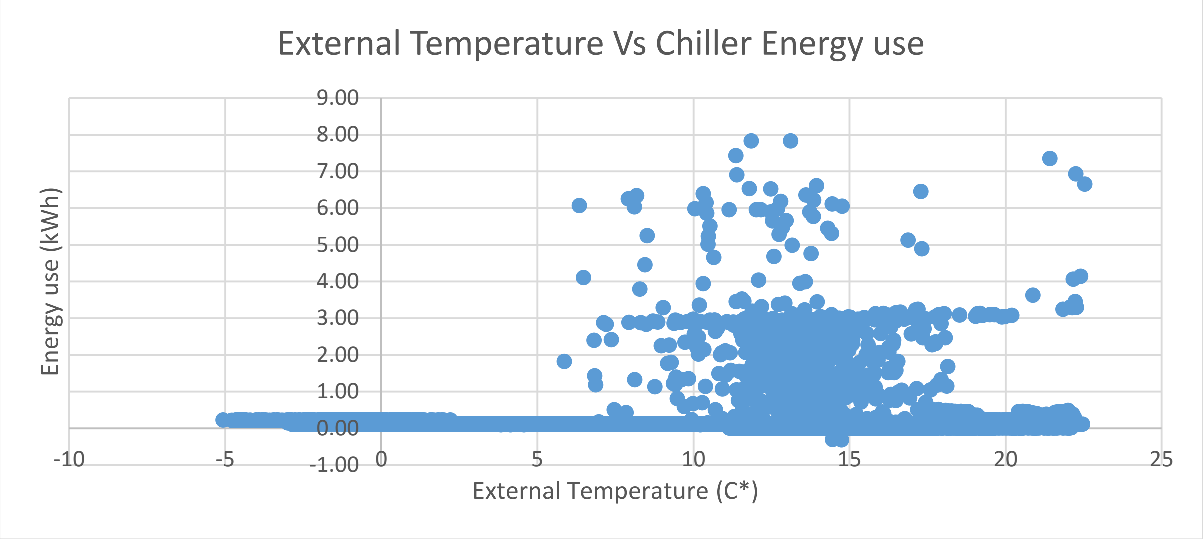

ANNs are based upon the concept of establishing a relationship between independent and dependent variables, though the use of training algorithms (Abbas et al, 2019). In this case study, establishing a relationship between the independent variables of the external and average internal temperature to the dependent variable of the chiller's energy usage in a feedforward neural network. The impact of data segmentation on this process would be observed through changing the size of the training data between: yearly, seasonally, monthly, weekly and daily. Creating an ANN for each dataset and comparing them on the grounds of the percentage error and computation relative to the size of the timeframes being predicted and the time between the training data and predicted events.

2.1. Method limitations

As the external temperature training data used the temperature at the time of each event, opposed to what the external temperature was predicted to be before the event, this would represent an absolute ideal situation. Where in predicting true future events, the difference between the accuracy of the predicted temperature would impact the overall prediction of the building's energy usage and predicting one year into the future in this manner would be significantly inaccurate.

3. Results and Discussion

3.1. Computational time

Whilst choosing the optimum number of hidden layers for the ANN, too few and the ANN would be too linear to predict the outputs, too many and the ANN would overfit the model. It was observed that the computation time did not exceed 1 second until the number of hidden layers approximately exceeded 1000 regardless of size of the dataset used. As changing the size of the dataset did not visibly affect the computational time of the process up until 1000 hidden layers, it can be assumed that the number of times the data is processed has a more significant impact on the computational time than the size of the dataset itself. For all following data 10 hidden layers were used, due to the comparably less percent error observed.

Figure 3

Number of hidden layers	10^0	10^1	10^2	10^3	10^4
Percent Error	4.46E-01	4.09E-01	4.22E-01	4.93E-01	2.87E+01
Computation time (Hour, Min, sec)	0.00.01	0.00.01	0.00.01	0.03.20	00:33:38

3.2. Prediction accuracy

The following is a selection of the percentage errors observed:

Figure 4

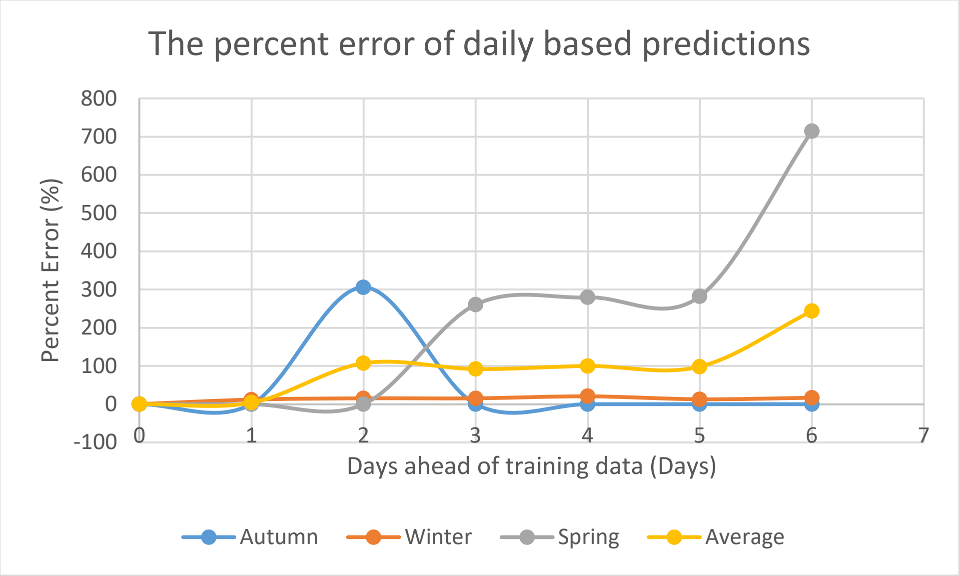

The above is a graphical representation of three days randomly selected from each season and used to model the following week. It was observed that the smaller the training dataset, the more accurate on average it's predictions would be, assuming the areas being predicted did not exceed the parameters of the original training data. Varying from as low as 0.005% error to 715% in a single week of predictions.

Conversely, it was observed that the larger the training dataset, the higher the mean percent error, but the less negative impact anomalies and the time from the training data would have on the predictions. Accuracy would decrease the further the predictions from the training data's relative point in the year, though accuracy would increase as the predictions approached the training data's relative point in the following year.

Figure 5

Percent error	Day 1	Day 1 vs 2	Day 1 vs 3	Day 1 vs 4	Day 1 vs 5	Day 1 vs 6	Day 1 vs 7
Autumn	0.005	0.007	305.738	0.016	0.017	0.016	0.011
Winter	0.223	12.077	15.416	15.417	20.594	12.883	16.810
Spring	0.003	0.003	0.003	260.504	279.331	282.110	714.127
Average	0.077	4.029	107.052	91.979	99.981	98.336	243.649

Figure 6

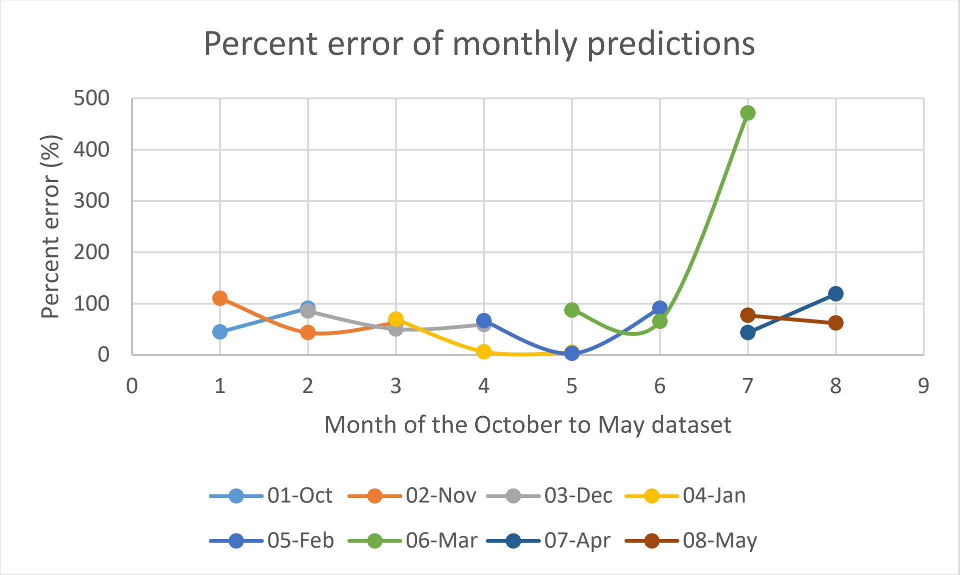

Figure 7

Percent error	2017/2018	2018/2019	1-year predictions	Increase in Error
Autumn	71.41	60.23	73.13	12.90
Winter	23.95	54.37	75.41	21.04
Spring	62.35	61.30	67.83	6.52
Year	64.38	55.17	71.99	16.82

In figure 7 the accuracy of models developed in the 2017/2018 period are compared with models developed in 2018/2019 as well as used to predict the 2018/2018 based upon its independent variables. Of which it can be observed that in predicting in the short term, greater data segmentation produced greater accuracy, but the further the prediction is away from the greater the error caused by data segmentation.

4. **Conclusion**

In conclusion, data segmentation can have both a negative and positive impact upon the accuracy of predicted building energy usage dependent upon the duration of the predicted period and the time between the training data and the predicted events. The smaller the predicted period and the time between the predicted event and training data, the more positive the effect of segmenting the data. The greater the size of the predicted period and time between the predicted event and training data the more negative the impact of data segmentation will have on prediction accuracy. This is likely due to the to larger the period and further away the prediction, the increasing likely there will be anomies outside of the range of the training data.

Under the ideal conditions of predicting one day into the future, using a one-day segment to train the ANN, with completely accurate temperature data, an average mean percent error of 4% could be achieved. It can be expected that this error would increase, in the case of predicting future energy usage based upon predicted weather data for the external temperatures and the building temperate comfort zone for the internal.

Based upon these results, four main areas of future work were identified:

- Investigating alternative forms of data segmentation, such as building active and dormancy periods.
- Investigating the accuracy of smaller data segments such as hours in predicting shorter periods into the future
- Using predicted weather data to investigate its impact on prediction accuracy.
- Investigating the accuracy of other machine learning techniques, such as SVR for use in smaller data segments, or other types of ANN and training algorithms.

5. References

Preston.(2019). *Tessideuniversity.* Available:http://prestonvsteesside.emonsite.com/album/teesside-university/. Last accessed 2019.

Pierre BOISSON, Simon THEBAULT, Sergio RODRIGUEZ, Sylvia BREUKERS, Richard CHARLESWORTH, Sarah BULL, Igor PEREVOZCHIKOV, Mario SISINNI, Federico NORIS, Mihai-Tiberiu TARCO, Andrei CECLAN, Tom NEWHOLM,. (2017). *DR Bob D5.1.*Available: https://www.dr-bob.eu/wpcontent/uploads/2018/10/DRBOB_D5.1_CSTB_Update_2018-10-19.pdf. Last accessed 2019.

Husain Abbas, Yousef A. Al-Salloum, Hussein M. Elsanadedy, Tarek H. Almusallam,

ANN models for prediction of residual strength of HSC after exposure to elevated temperature, Fire Safety Journal, Volume 106, 2019, Pages 13-28.

Wang, Zeyu & Srinivasan, Ravi. (2015). A review of artificial intelligence based building energy prediction with a focus on ensemble prediction models.

Mauro Ribeiro, Katarina Grolinger, Hany F. El Yamany, Wilson A. Higashino, Miriam A.M. Capretz, Transfer learning with seasonal and trend adjustment for cross-building energy forecasting, Energy and Buildings, Volume 165, 2018, Pages 352-363.

Nottingham | UK | 9–11 September 2019

The role of the electrode conductivity on the rate capability of LiFePO4

Michael Castle [1], Rahifa Ranom [2], Giles Richardson [3], Jamie Foster [1]

[1] *University of Portsmouth, Lion Gate Building, Lion Terrace, Hampshire, PO1 3HF*

[2] *Universiti Teknikal Malaysia Melaka, 76100 Durian Tunggal, Malacca, Malaysia*

[3] *University of Southampton, Building 54 Mathematical Sciences, University of Southampton*

michael.castle@port.ac.uk

Abstract

We present a model for the discharge of a Li-ion battery cathode comprised of LiFePO4 particles, based on porous electrode theory introduced by Newman and co-workers in the mid 90's. This modelling approach describes the electrochemical processes inside a Li-ion electrode via a system of partial differential equations for the Li concentrations, electric potentials, and current densities inside the device. Through numerically solving this model, we show that for LiFePO4 electrodes there exists a regime in which increasing the electronic conductivity of the electrode can be detrimental to cell discharge. An explanation for this counterintuitive result is provided, and allows for a way to improve battery design in order to facilitate higher discharge rates.

Keywords: Lithium-ion, Electrode, Conductivity, Lithium-iron-phosphate

1. Introduction

The lithium-ion cell design is a marquee for battery development, having applications from portable electronics such as laptops and mobile phones, to becoming the focus for hybrid electronic vehicles. It is easy to see the economic importance of the battery, and therefore the relevance to formulating accurate mathematical models in order to optimise its design.

In this work we take a single LiFePO4 cathode, as shown in Figure 1. During discharge, lithium-rich electrolyte travels in the form of ionic current from the separator, and traverses across the cathode. The electrode particles, which make up for the capacity of the cell, react with the electrolyte, absorbing the lithium and filling up as the cell discharges, converting ionic current into electronic current which is required to feed an external load on a circuit connected to the current collector.

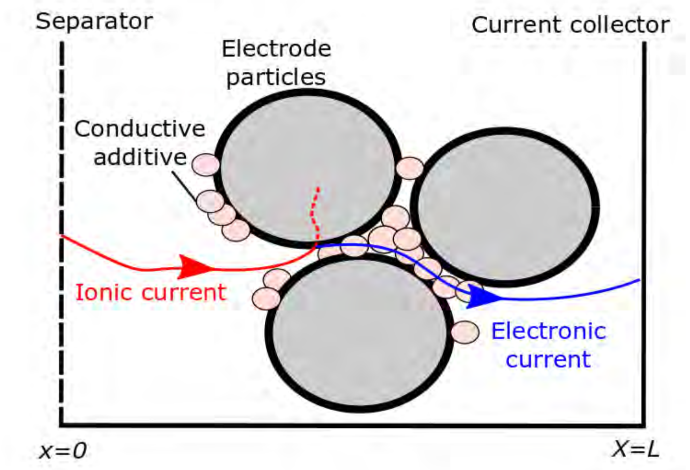

Figure 1: Figure showing diagram of lithium ion cathode. The separator is positioned at the left, separating the cathode from an anode or reference electrode, whilst the current collector on the right transfers the electronic current between the electrode and a connected circuit. Ionic current travels through the electrolyte, and reacts at the surface of the electrode particles, whilst electronic current flows through conductive material coating the electrode particles.

The amount of conductive additive controls how easily electronic current can flow across the cathode. If there is little additive, meaning that the electrical conductivity across the cathode is low, the reaction between the electrode particles and the electrolyte will preferentially occur close to the separator until the electrode particles are fully lithiated there, creating a reaction layer from the current collector to the separator.

2. Model formulation

The equations governing ionic transport through the electrolyte, those governing electronic transport through the porous binder matrix, the lithium content in the electrode particles assuming infinitely fast diffusion, and the Butler-Volmer reaction rate are [1-3][7-9]

$$\varepsilon_V \frac{\partial c}{\partial t} = \frac{\partial}{\partial x}\left(BD(c)\frac{\partial c}{\partial x} + \frac{1-t^+}{F}j\right), \quad j =- Bk(c)\left(\frac{\partial \phi}{\partial x} - \frac{2RT}{F}\frac{1-t^+}{c}\frac{\partial c}{\partial x}\right), \quad \frac{\partial j}{\partial x} = FbG, \quad J =- \sigma\frac{\partial \psi}{\partial x}, \tag{1}$$

$$\frac{\partial J}{\partial x} =- FbG, \quad \frac{dC}{dt} =- \frac{3}{a}G, \quad G =- k_0\sqrt{c(1-C)C}\sinh\left(\phi - \psi + U(c_s)\right). \tag{2}$$

Here, x and t denote position through the electrode and time respectively, c is the molar concentration of lithium ions in the electrolyte, C is the molar concentration of lithium ions in the representative electrode particles, D is the ionic diffusivity of electrolyte, j and J are the ionic and electronic current densities respectively, G is the Butler-Volmer (BV) reaction rate (i.e., the flux (per unit area) of Li through the surface of the particle), k is the ionic conductivity of the electrolyte, ϕ and ψ are the electric potentials in the electrolyte and electrode respectively, U is the equilibrium potential of LiFePO4, σ the electronic conductivity of the electrode, and I is the current demanded from the electrode.

The model equations (1)-(2) are supplemented by the following boundary conditions [7-9]

$$c|_{x=0} = 0, \quad j|_{x=0} = I/A, \quad \psi|_{x=0} = 0, \quad \frac{\partial c}{\partial x}\Big|_{x=L} = 0, \quad j|_{x=L} = 0, \quad J|_{x=L} = I/A, \tag{3}$$

whilst the initial conditions, as well as the parameter values and definitions, are provided in Table 1. The cell voltage is described by [7]

$$V = \psi|_{x=L}, \tag{4}$$

where V is the cell voltage, taken to be the potential difference between the electrode at the current collector and separator. Discharge is terminated when $V = 2.9$ volts, which is typical in order to prevent unwanted side reactions and maintain a safe operating voltage. The proportion of capacity utilised can then be calculated by,

$$Q = (C_{average} - C_0)/C_{max}, \tag{5}$$

where $C_{average}$ is the total average of concentration of lithium inside the electrode particles. The ionic conductivity and diffusivity are respectively given by [3]

$$k(c) = 2.78 \times 10^{-10}c^3 - 1.36 \times 10^{-6}c^2 + 1.87 \times 10^{-3}c + 0.180, \qquad D(c) = 2.66 \times 10^{-7}\frac{k(c)}{c}, \tag{6}$$

and the equilibrium potential of LiFePO4 is given by [9]

$$U(C) = (3.11 + 4.44\arctan(-71.7X + 70.9) - 4.24\arctan(-68.6X + 67.7)), \tag{7}$$

where $X = C/C_{max}$. The remaining undefined terms are provided in Table 1.

Table 1: Table providing the definitions and values of the model parameter. [3][7]

Parameter	**Symbol**	**Value**	**Unit**
Volume fraction of electrolyte	ε_v	0.05	Dimensionless
Brunauer-Emmett-Teller surface area	b	2.7×10^5	m^{-1}

Butler-Volmer reaction constant	k_0	3×10^{-12}	$mol^{-0.5} m^{2.5} s^{-1}$
Permeability factor of electrolyte in electrode	B	0.01118	Dimensionless
Initial concentration of lithium in electrode particle	C_0	18805	$mol\ m^{-3}$
Maximum concentration of lithium in electrode particle	C_{max}	489	$mol\ m^{-3}$
Radius of electrode particle	a	1	μm
Cross-sectional area of electrode	A	1×10^{-4}	m^2
Length of electrode	L	60	μm
Initial concentration of lithium in electrolyte	c_0	1000	$mol\ m^{-3}$
Temperature	T	298.15	K
Ideal gas constant	R	8.3144	$J\ mol^{-1}\ K^{-1}$
Faraday's constant	F	96487	$C\ mol^{-1}$
Transference number	t^+	0.3	Dimensionless

3. Results and Discussion

Numerical simulations to the model equations (1)-(2) were performed using the boundary conditions (3), functions (6)-(7), and parameter values given in Table 1. The solutions were performed for a variety of different currents, namely a low current $I = 0.0014$, an intermediate current $I = 0.0029$, and a higher current $I = 0.0057$. The equations were discretised in space using finite difference method, and a MATLAB ode solver was used to integrate the system through time. An event function was used to track the value of the cell potential described by equation (4) and terminate cell discharge once the stopping voltage was reached.

From Figure 2, it is seen that values of electrical conductivity which are too small almost no capacity was utilized. This is explained by the fact that a large electronic potential gradient is required to push an electrical current through a non-conductive material, and will therefore rapidly increase the cell potential as described by equation (4), hence terminating discharge quickly.

For the lower current and high current scenarios it is seen that once a sufficient conductivity is surpassed, the utilised capacity is unchanged from increasing the conductivity further. For the former case, this can be explained by the fact that the electrode particles cannot reach the theoretical maximum (or minimum) of concentration, C_{max}, otherwise the Butler-Volmer reaction, G, would be zero. Instead, it is true that the capacity has been fully utilised. The high current scenario however quickly drains the electrolyte of lithium, a phenomenon referred to as electrolyte depletion, allowing only the initial concentration of lithium to react with the electrode particles as there is not enough time for lithium to be transported across the electrode.

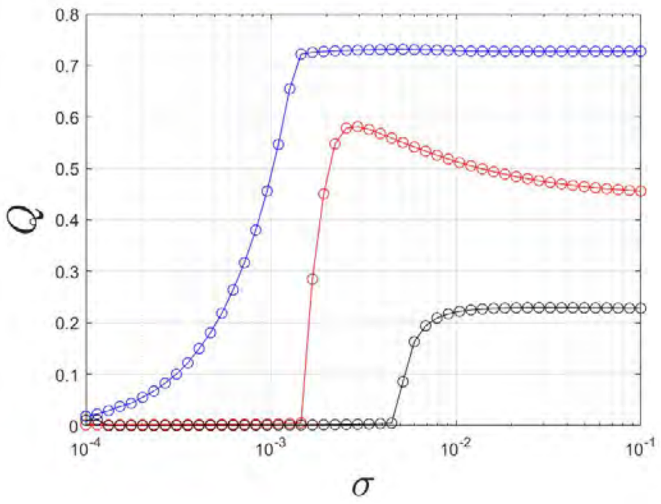

Figure 1: Figure showing numerical simulations to the model described in Section 1. The figure shows how the utilised capacity, as described by equation (5), is influenced by the solid electronic conductivity for a range of current demands. The blue, red, and black curves show the relationship for currents I=0.0014, 0.0029, and 0.0057 amps respectively.

For the intermediate current however, electrolyte depletion occurs but at a significantly slower rate than the high current scenario. This allows for a significant amount of lithium to be transported from the separator and across the electrode before termination occurs. The lithium content in the electrolyte depletes closest to the current collector first, as lithium is supplied from the opposite end of the electrode. Hence, a smaller electrical conductivity will force the electrode particles near the current collector to fill up first, whilst there is still lithium there, allowing the reaction to occur at the separator later. This allows for significantly more capacity to be utilised.

4. Conclusion

A mathematical model describing the lithium-ion cell discharge is provided. An implemented numerical scheme is then used to simulate the model and discern the relationship between the solid electric conductivity and the accessible capacity of the electrode for a range of current demands. It is shown that the electric conductivity both too large and too small can be disadvantageous to cell design, and instead a unique optimal value exists.

References

1. Dargaville S., Farrell T.W., Troy W. (2010) Predicting active material utilisation in LiFePO4 electrodes using a multi-scale mathematical model. J. Electrochem. Soc., 157(7), A830-A840
2. Doyle M, Fuller T.F., Newman J. (1993) Modelling of galvanostatic charge and discharge of the lithium-polymer-insertion cell. J. Electrochem. Soc., 140(6), 1526-1533
3. Ecker M., Tran T.K.D., Dechent P., Kabitz S., Warnecke A., Sauer D.U., (2015) Parameterization of a Physio-Chemical Model of a Lithium-Ion Battery. J. Electrochem. Soc. 162(9), A1836-A1857
4. Johns P.A., Roberts M.R., Wakizaka Y., Sanders J.H., Owen J.R. (2010) How the electrolyte limits fast discharge in nanostructured batteries and supercapacitors. Electrochem. Comm., 11(11), 2089-2092
5. M. Wang, J. Li, X. He, H. Wu, C. Wan (2012) The effect of local current density of electrode design for lithium-ion batteries. J. Power Sources, 207, 127-133
6. M Park, X Zhang, M Chung, GB Less, Sastry A.M. (2010) A review of conduction phenomena in Li-ion batteries. J. Power Sources., 2010.06.060
7. Ranom, Rahifa (2014) Mathematical Modelling of Lithium Ion Batteries. PhD. University of Southampton
8. Richardson G., Dennault G., Please C.P., (2012) Multiscale modelling and analysis of lithium-ion battery charge and discharge. J. Eng. Math. 72(1), 41-72
9. Srinivasan V., Newman J. (2004) Discharge model for the lithium iron-phosphate electrode. J. Electrochem. Soc., 151(10) A1517-A1529

Nottingham | UK | 9–11 September 2019

Guidelines for Large Photovoltaic System Integration

Prof. Silviu Darie, PhD

Technical University of Cluj Napoca, Cluj Napoca, Romania
Former Vice President Power Analytics Corporation, USA

Silviu.darie@gmail.com

Abstract

The paper summarizes the result of a research project funded by the Department of Energy (DOE) in collaboration with the University of California at San Diego (UCSD). One presents a planning guideline and establishes interconnection criteria for integrating Photo Voltaic Generation (PVG) into the power systems (transmission and distribution). Some of the experiences/guidelines in the field of wind farm integration are used here since wind generation and PVG generation share many common power electronics devices used in their control schemes and both generation types are intermittent resources with similar degree of predictability and forecast methodology. Recommendations are given on the best practice promising standards for interconnecting large PV generation to power system.

Keywords: Photovoltaic, photovoltaic generation, planning guideline, system integration**.**

1. Introduction

The intent of this paper is to objectively discuss the issues and concerns related to the integration of PV generation into the utility power system. The outcome is a series of recommendations, all technically feasible and viable, for possible incorporation into broader standards for interconnecting PV plants to the utility system. The goal of any such standard will be to establish minimum technical requirements for connecting PV plants to the power systems at transmission and/or distribution levels. Such a standard will make no distinction as to the preferred technologies or types of PV generation equipment, but rather rely on the ingenuity of the PV plant developers, PV plant manufacturers and other power equipment manufacturers to come up with the most cost effective means of meeting and/or exceeding the technical established standards.

Based on several studies, the salient points of interest are outlined below:

- Interest in PV generation has been growing rapidly in the past few years; one can say that PV is growing at approximately the same rate as Wind Power and is just 6 years behind; by the end of 2009 the cumulative PV power reached 22.8 GW, [2] and the PV forecast worldwide by the year 2014 is 30 GW, [2];
- Power converters have become the major players for renewable energy generation, energy storage, smart grid technologies;

- There has not been any mature planning and interconnection guidelines or standards related to PV generation;
- Major concerns of large scale PV generation integration into power systems are related to variations in the PV active power output due to intermittency of solar irradiance and their impact on system reserve. Even though storage such as Battery Energy Storage Systems (BESS) are being considered for PV applications, this solution is still not economical for large scale PV plant implementations
- With large-scale PVG being connected to the transmission systems, there is no longer an acceptable response. Many utilities in the US and Europe, have made the requirement for a low voltage ride through (ZVRT/LVRT) capability mandatory. This requirement is similar to wind farm interconnection standards;
- Power quality requirements including voltage flicker, harmonics, as well as coordination of controls and protection are important part of the interconnection guideline. The power quality, control and protection requirements for PV should be adopted from the existing guidelines and standards such as IEEE Standard 1547, IEEE Standard 1547.5, IEEE 519, IEC 555, IEC 61000, and IEEE Std. 929-2000;
- The maximum size of PV plant that can be accommodated in a power system, in general, should be limited by the available short circuit capability at the point of interconnection (POI) of the PV plant to the power system. Ratio of available short circuit at POI to the PV plant size of less than five (5) will likely introduce voltage control problems;
- The maximum level of PV penetration into a power system (i.e., percentage of PV generation e.g. 10, 20, 30%, etc. versus total system generation mix) cannot be determined from a simple set of rules. This question has been asked by many of the power system planning/operation engineers in regard to wind farm penetration.
- The only successful solution could be to perform on-line (and near real-time) power system analysis to determine the real impact to the power system.

North American utilities evaluate interconnection requests including a PV plant proposal through a “Feasibility and System Impact Study”. In these studies, system performance is compared with and without the proposed PV plant under various system load/generation dispatches and considering a number of N-1, N-2 creditable contingencies. Generally a typical system interconnection study consists of, [1]:

- Transmission facilities over-load determination (thermal evaluation);
- Impact on transfer capability over the critical tie-lines/interfaces;
- Transient and voltage stability analysis;
- Impact on increased fault levels.

This paper is primarily qualitative providing an overview of existing planning and interconnection criteria established by US utilities. The paper addresses PV integration study, planning guideline, and acceptable level of penetration issues.

A. Interconnection Guideline/Standards and Criteria (PVG less than 10 MVA)

A1. Voltage Control (Automatic Voltage Regulation)

There is a requirement and need for automatic voltage regulation for PV plants. For PV plant technologies that use voltage source inverters, automatic regulators may be applied to regulate the reactive output, to maintain a certain voltage e.g. at the point of interconnection between the PV plant and power system. In other cases voltage regulation can come from a supervisory control system regulating the reactive resources throughout the PV plant. For larger PV installations, SVC or STATCOM coordinated together with a number of mechanically switched capacitors can provide the required voltage regulation. For smaller PV plants in distribution systems, DVAR or DSTATCOM can be utilized.

A2. Frequency Control

Frequency control for PVG is possible but not to the same degree as frequency control with a governor on a classical generator. PV plants should not actively participate in primary frequency control during under-frequency. Having a "governor like" control for a PV plant control scheme is a technical possibility and even desirable. However, it is reasonable to recommend that a PV plant meet an off-nominal frequency operating condition similar to the appropriate operation standards (that is used by many utilities for wind farms and classical generating plants) – Table 1.

Table 1: Frequency range versus time

Frequency Range	Time (seconds)
>61.7	0
61.6 to 61.7	30
60.6 to <61.6	180
>59.4 to <60.6	Continuous Operation
>58.4 to 59.4	180
>57.8 to 58.4	30

A3. Low Voltage Ride-Through

Typically PV plants operate continuously between (90-110) % of nominal voltage at the point of connection to power system. PV plants should be able to stay connected to the power system for voltage dips or voltage rises. Typically PVG will be required to ride-through voltages for the duration required to achieve fault clearing times of a normally cleared fault. The cost of achieving ride-through down to zero voltage (using a combination of battery storage system and voltage source inverter) can be significant and may only be reasonable for larger PV plants installations (greater than 10 MW), [1].

A4. Reactive Power Capability

Reactive power capability is measured at the low voltage side of the PV substation. A PV plant at its full load, should be capable of 0.90 PF lagging and 0.95 PF leading. Automatic voltage regulation that is able to regulate the voltage at this point to a "desired" set-point to within +/-0.5%. The voltage regulation system should have adjustable gain, droop and a reference set-point. Voltage regulation should be provided to adequately control voltage at the point of interconnection throughout the range of power delivery of the PV plant and coordinated with other voltage regulating devices on the transmission system.

In general we recommend adoption of the IEEE Std. 1547 Standard for Interconnection Distributed Resources with Electric Power Systems, and its applicable guides, for PV plants with an aggregated combined power output of 10 MVA or less. This standard was developed for distributed generation facilities of 10 MVA or less. The IEEE Std. 1547.5 under development for facilities with a combined capacity of more than 10 MVA.

B. Interconnection Guideline/Standards and Criteria (PVG greater than 10 MVA)

B1. Active Power Generation

All PV modules in a single PV plant must not start or stop simultaneously. This can be achieved through sequencing of the start-up and shutdown controls of the PV modules in a plant.

- The 15 minutes average megawatt output of a PV plant must not at any time exceed the specified maximum output of each PV plant, [4, 5, 9];
- The system control center, through telemetry or other means of contact with the PV plant operator, must have a means of issuing a directive to reduce the megawatt output of the PV plant, or curtail the PV plant in the event of an emergency condition where the PV plant output is to be reduced to respect thermal limits on nearby transmission corridors or when otherwise generation far exceeds demand. Alternatively, the PV plant operator may intentionally disconnect blocks of PV modules in the plant to effect a reduction in generation. In any case, this should be done in a controlled fashion and at the specified rate by the operator (e.g. certain number of MW/minute);

B2. Zero/Low Voltage Ride Through

PV plants should be able to ride through faults taking place at the high side (transmission voltage level) of the substation transformer. This requirement does not apply to a radial PV plant connection. In such cases, the PV plant should be able to ride through any normally cleared faults external to the radial line feeding the plant, [9, 10].

In the future as the technology improves (and PV penetration increases) then a fault ride-through strategy may be adopted. The recommendation here is to slowly transition to requiring that the PV plant be able to ride-through fault external to the plant for the normal fault clearing durations. For system disturbances with longer durations, where the system voltage does not recover for an extended period of time, the PV plant must be tripped by under voltage protection. Also, any shunt capacitors that are used for power factor correction must disconnect from the system to prevent overvoltage conditions when the system recovers after fault is cleared.

B3. Voltage/Frequency Operating Limits

For steady state, transient voltage conditions, and for off-nominal frequency operation, PV plants should be expected to meet the existing criteria of the respective utilities. Clearly, all PV plants must operate continuously at and between ± 10% of nominal system voltage and ± 0.5 HZ of nominal system frequency.

B4. Power Quality

PV plants owners should be responsible for performing studies where necessary to ensure that they avoid low-order harmonic resonance phenomenon on their system due to shunt capacitors (or cable charging) and power electronics. PV voltage/power variation due to variation in the solar irradiance may also cause voltage flicker. The PV plants owners should take steps to minimize flicker problems from their generation. The standards for voltage fluctuations at the point of connection of the PV plant facility to the power system should be applied.

B5. Reactive Power Requirements

Based on standard industry practice it is recommended that PV plant facilities be able to operate with 0.90 PF lagging and 0.95 PF leading power factor (when generating its peak megawatt output) at the point of interconnection.

B6. Protection Requirements

The PV plant operator:

- Is responsible to implement adequate protection to safeguard all PV generation equipment within the PV plant. The system protection, however, must properly be coordinated with other controls and the protection of the utility power system in its vicinity;
- Should design and implement the appropriate protection;
- In special cases, the plant developer may be required to perform specialized analysis such as:

Electromagnetic transient/harmonic analysis such as switching including the energizing of transformer, capacitor banks, etc.;
Controls interaction studies, if the PV plant is being placed in-service in close vicinity to an existing power plant or HVDC system, etc.

B7. Modeling Requirements and Field/Simulation Verification

The PV plant developer should be responsible to provide adequate steady state and dynamics models of the PV plant to utility where PV plant will be interconnected; The models should be updated when commissioning the PV plant if any model structures or parameters are substantially changed between the planning and commissioning phase of the plant; Based on the author’s experience, Power Flow should be run; the convergence of the Power Flow will demonstrate the system is feasible. One highlights that the Power Flow of the PV farms are not a steady state regime; it is a quasi-steady state due to the sun irradiance variation over time.

Field verification tests or studies should be performed to demonstrate that the PV plant meets all of the requirements set forth by interconnection policy of the utility.

B8. Automatic Voltage Regulators

The concept of automatic voltage regulators (AVR) is not necessarily directly applicable to PV generation technologies. However, it is important to note that the voltage at the point of interconnection (POI) between the PV plant and the transmission network should be automatically controlled/regulated. The manner in which this requirement is achieved can be left at the discretion of the PV plant operator/developer.

B9. Disturbance Monitoring System

For the purpose of continued understanding of PV plant operation and control, utility may consider requiring that each PV plant be equipped with a disturbance monitor. As a minimum (monitor the interconnection point):

- Voltage and current;
- Active power transfer;
- Reactive power transfer;
- System frequency.

B10. Telemetry

A PV plant should make the following information available:

- Active and reactive power output at the PV plant;
- Status of circuit breakers on substation transformer and all shunt compensation devices located at the PV plant substation;
- Meteorological data including average solar irradiance at the site, as required to facilitate the use of the forecasting models;
- Tap position of the PV plant substation transformer if it is equipped with on-load tap-changers;
- Telemetry between PV plant (or PV plant operator) and the system control center to allow for curtailment;
- Telemetry between PV plant and the system control center operator to facilitate specifying voltage regulation set-points for the point of interconnection between the PV plant and the network.

Some of the above data may be used for forecasting purposes and so the data format and quality should be in a format that is suitable for such use.

Conclusions

Photovoltaic (PV) generation is an attractive source of renewable energy due to their relatively small size and operation. Major advantages of the photovoltaic power are:

- Static structure with no moving parts;
- High power density per unit of weight;
- Short lead time to design, install, and start up;
- Highly modular structure, so plant economics are not just a function of size;
- Power output matches well with peak load;
- Expected longer life with low maintenance;
- Highly mobile.

The paper presents a summary of the experience with PV generation in North America and Europe. In addition, one uses the existing surveys on interconnection standards adopted by utilities for integrating classical generators, alternate sources of power generation including wind and PV into the power system to provide guidelines for PV plants. Based on background information obtained and the project team's experience with PV studies, recommendations are given on the best practices and emerging standards for interconnecting large PV plants to power system, [1].

The intent of this summery paper is to objectively discuss the issues and concerns related to the integration of PV generation into the utility power system. The outcome is a series of recommendations, all technically feasible and viable, for possible incorporation into broader standards for interconnecting PV plants to the utility system.

Acknowledgments

This work was supported by the DOE/UCSD, High Solar PV Penetration. FOA-0000085 grant, 2010.
S. Darie was the team leader of the work and has been with Power Analytics Corporation, San Diego, USA

References

1. Darie, S., Zhang, W., Pan, J "Improved Modeling Tools Development for High Penetration Solar", Power Analytics Corporation, San Diego, CA, Tech. Rep. TR-DE-FOA-0000085, 2010.
2. Teodorescu, R., Liserre, M., Rodriguez, P., Grid Converters for Photovoltaic and Wind Power Systems. John Willey & Sons, Ltd., 2011, p.31
3. EPIA "Global market Outlook for Photovoltaic, May 2010. Available: http://www.epia.org/fileadmin/EPIA-
4. WECC "Minimum Operating Reliability Criteria", April 6, 2005, WECC
5. WECC "Coordinated Off-Nominal Frequency Load Shedding and Restoration Requirements", WECC.
6. WECC "Under Voltage Load Shedding Guidelines", Western Systems Coordinating Council, July 1999
7. IEEE Recommended Practices and Requirements for Harmonic Control in Electrical Power Systems, IEEE Standard 519, Aug. 1992.
8. IEEE Standard Definition, Specification and Analysis of Systems Used for Supervisory Control, Data Acquisition and Automatic Control, IEEE Std. C37.1, 2005
9. American Wind Energy Association "Standardizing Generator Interconnection Agreements and procedures", AWEA, No. RM02-1-001. Available at www.ferc.gov
10. WECC "Generator Electrical grid fault Ride through Capability", WECC October, 2004.

Nottingham | UK | 9–11 September 2019

How can statistical data analysis reduce the cost of energy production in the oil and gas industry?

Mahdi Sadri*, Seyed M. Shariatipour, Masoud Ahmadinia

Fluid and Complex Systems Research Centre, Coventry University, UK

*sadrim@uni.coventry.ac.uk

Abstract:

Although our energy supply is not longed purely wedded to fossil fuels but produced from a wider range of sources such as solar or wind these days, there remains a considerable challenge in providing affordable and reliable energy to all households around the world. The economic efficiency of energy producing systems is currently greater than in the past, but there are still many people around the world who live with energy poverty. Data analysis can be a powerful means to increase energy production efficiency further, as a consequence reduce the cost. In this study, hydrocarbon production data from the oil and gas industry has statistically been analysed in order to reduce the total cost of operations and increase the economic recovery of wells. The study has focused on mitigating the uncertainty in well production data caused by discontinuous flow measurement of hydrocarbon production streams of individual wells. Our results show that for oil wells with large flow rate fluctuations, undertaking just one flow test per month can create unacceptable uncertainties in estimating the production of the well. The analysis suggests that increasing the number of flow tests per month from one to four can significantly decrease the estimation uncertainty and eventually increase the economic recovery of oil and gas for an individual field.

Keywords: Energy affordability, data analysis, oil and gas, flow measurement, production data

1. Introduction

There are many people around the world who are unable to afford to keep their homes sufficiently heated. This condition is usually referred to as fuel poverty. Over 11% of the households in England are living in fuel poverty according to the Office of Gas and Electricity Markets [1] and the Department for Business, Energy, and Industrial Strategy of the United Kingdom [2]. This is equivalent to 2.55 million households across England. The situation in many other countries is even worse as a result of a poor economy and the occasional high price of oil and gas or other sources of energy. Under these circumstances, any techniques that can reduce the cost of oil and gas production can have an important role in providing more affordable energy to the market and decreasing fuel poverty.

One way to reduce costs in the oil and gas industry is to mitigate the uncertainties in the available production data. These uncertainties can affect reservoir management [3-5] or hydrocarbon accounting calculations [6, 7]. One of the main sources of uncertainties in the production data of many oil and gas fields is that the production streams of different wells in that field are first commingled and then measured by flow meters. Although flow rates of individual wells are measured during occasional (in many cases monthly) flow tests, their continuous flow rates are just estimated by allocation calculations.

In this research, the production data of oil wells has statistically been analysed to investigate the effect of increasing the frequency of flow tests on the uncertainty in the estimated oil production of individual wells in a field. The associated reductions in the cost of allocation uncertainties have subsequently been estimated and reported.

2. Methodology, Results, and Discussion

The fluctuations in the production data of three oil wells have been statistically analysed in this research. The Relative Standard Deviation (RSD) of the available production data has been calculated to quantify the magnitude of the fluctuation for each well. The obtained RSD values have subsequently been used to generate similar fluctuations in the production data of a simulated oil field with 36 wells, and therefore three data sets have been created (Case A, B, and C). The data sets have subsequently been used in allocation calculations [8, 9] to investigate the effect of increasing the number of flow tests per month (TPM) on reducing the uncertainty of estimated production data of individual wells in each case. Reducing the aforementioned uncertainty is important since it can create extra costs for the operating oil and gas companies. The effect of the uncertainty is clearer when different wells in the same field are owned by different companies. In such a case, any error in allocation calculations may result in allocating the produced oil of a company (and therefore its equivalent revenue) to another one. Hydrocarbon accounting calculations have therefore been undertaken to show the effect of increasing the number of TPMs on reducing the total cost of allocation uncertainty for the investigated cases.

Figure 1 shows the average absolute allocation errors for individual wells in three cases as a function of their RSDs when just one flow test per month is performed.

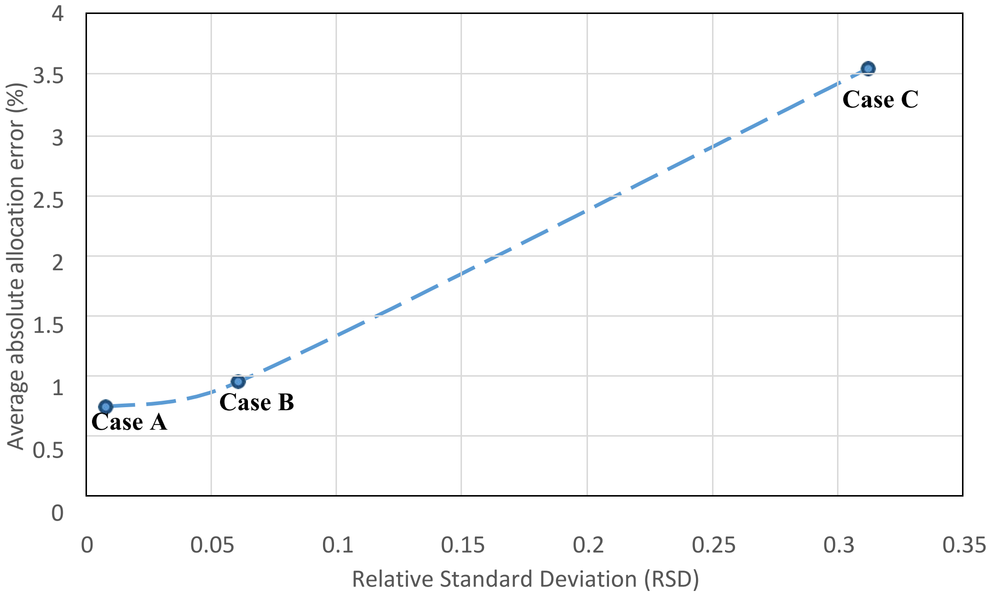

Figure 1: Average absolute allocation error as a function of relative standard deviation for Cases A, B, and C when just one flow test per month is performed: larger fluctuations (or equivalently larger RSDs) result in larger allocation errors

Case A has the smallest RSD (smallest fluctuations) and Case C has the largest (largest fluctuations). Larger fluctuations (or equivalently greater RSDs) have created larger allocation errors as shown in Figure 1. While the error is seen to be less than 1% for Case A, it has risen to more than 3.5% in Case C. Such an error can potentially cause companies to lose a considerable percentage of their revenue. Table 1 shows the equivalent amount of oil which has been allocated to a wrong well in all three cases when just one flow test per month has been performed. The total cost of the wrong allocation has also been calculated and reported considering the value of 60 US dollars per oil barrel.

Table 1: Allocation error and its yearly cost for Cases A, B, and C when one flow test per month is performed

Case	Length of production (days)	Total oil production (million STB)	Average total oil allocated to wrong wells (thousand STB)	The yearly cost of the wrong allocation (million US$)	Allocation error (%)
Case A	365	70.40	598.37	35.90	0.85%
Case B	365	70.07	735.73	44.14	1.05%
Case C	365	69.63	2492.58	149.55	3.58%

The total yearly cost of allocation varies from 36 million US dollars for Case A to 150 million US dollars for Case C. The results, therefore, show that yearly financial cost of allocation errors can be considerable, even for small allocation error values.

In the next step of the research, the number of tests per month was increased to 2, 3, and then 4, respectively. Allocation calculations were undertaken for each number of tests per month in each case and the average errors obtained. Figure 2 shows the average absolute error for all the cases as a function of the number of flow tests per month.

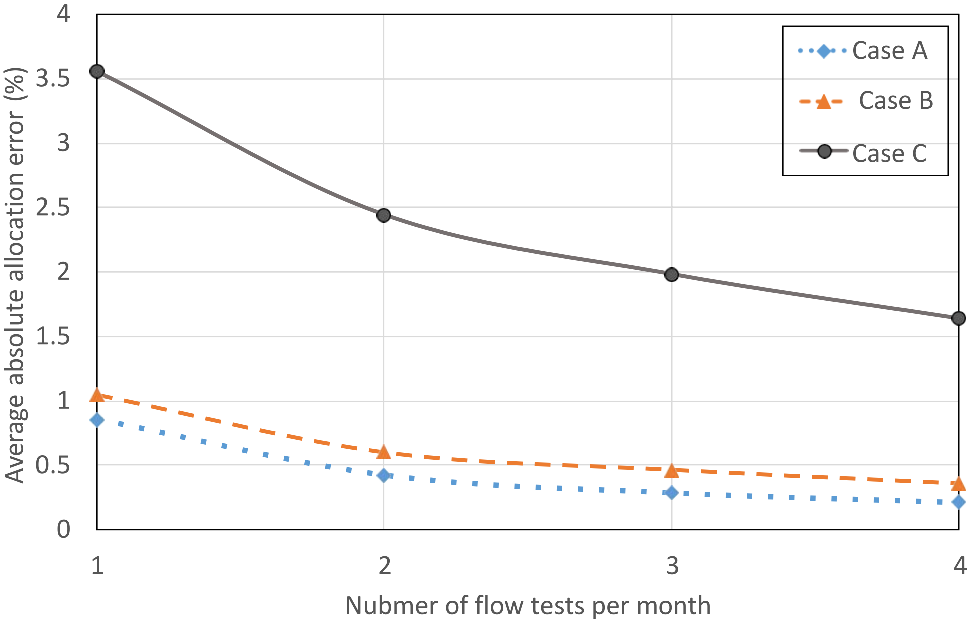

Figure 2: Average absolute errors as a function of the number of flow tests per month for Cases A, B, and C

The average allocation error is seen to decrease in all cases when the number of flow tests per month increases. Therefore, as Figure 2 suggests, increasing the regularity of flow tests can mitigate the uncertainty in the estimated production data of individual wells. The results of hydrocarbon accounting calculations for increasing the number of flow tests per month have been presented in Table 2.

Table 2: Hydrocarbon accounting results

Case	Reduction in the total yearly cost of allocation error as a function of increasing the number of flow tests per month (million dollars)		
	1TPM to 2TPMs	1TPM to 3TPMs	1TPM to 4TPMs
Case A	18.2	24.0	27.1
Case B	18.9	24.5	29.0
Case C	46.5	65.7	80.1

Table 2 shows that the cost of allocation errors can considerably be reduced by increasing the regularity of performing flow tests. The largest cost reductions occur when regularity of the tests increases from monthly to weekly (1 TPM to 4 TPM). In such a case the reductions in the yearly costs of allocation error for Cases A, B, and C are 27M, 29M, and 80M US dollars, respectively.

The results of the research are sensitive to different characteristics of the defined cases since this research has been a case study. However, the research shows how data analysis can be used as a powerful means of reducing the cost of oil production and play an important role in providing more affordable energy to the end users. The key is to undertake the same statistical data analysis for any specific oil field and decide on the optimum number of flow tests per month which is practically possible and at the same time minimises the cost of production.

3. Conclusion

The effect of increasing the regularity of flow tests on allocation errors and decreasing oil production costs was studied in this research using a statistical data analysis technique. The results show that increasing the number of flow tests per month can mitigate allocation uncertainties and significantly reduce their associated production costs. For the three investigated cases, the reduction in allocation errors caused a 27M, 28M, and 80M US dollars reduction in the yearly cost of production when the regularity of undertaking the flow tests changed from monthly to weekly (four times per month). The reduction in the cost of oil production can eventually lead to providing more affordable energy to the market and can play an important role in decreasing fuel poverty.

References

[1] State of the energy market, 2018, Office of Gas and Electricity Markets (OFGEM), UK.
[2] Annual fuel poverty statistics report, 2018, Department for Business, Energy, and Industrial Strategy, UK.
[3] Sadri, M., Shariatipour, S., and Hunt, A., 2017, "Effects of flow measurement errors on oil and gas production forecasts," Computational & Experimental Methods in Multiphase & Complex Flow IX, 115, p. 133.
[4] Sadri, M., Shariatipour, S., Hunt, A., and Ahmadinia, M., 2019, "Effect of Systematic and Random Flow Measurement Errors on History Matching: A Case Study on Oil and Wet Gas Reservoirs," Journal of Petroleum Exploration and Production Technology (in press).
[5] Marshall, C. D., Sadri, M., Hamdi, H., Shariatipour, S. M., Lee, W. K., Thomas, A., and Shaw-Stewart, J., 2019, "The role of flow measurement in hydrocarbon recovery forecasting in the UKCS," Journal of Porous Media. In press.
[6] Cramer, R., Schotanus, D., Ibrahim, K., and Colbeck, N., 2011, "Improving allocation and hydrocarbon accounting accuracy using new techniques," SPE Economics & Management, 3(04), pp. 235-240.
[7] Cramer, R., "Multiphase flow meter on all wells-an operator's perspective," Proc. North Sea Flow Measurement Workshop.
[8] Energy Institute, 2012, HM 96: Guidelines for the allocation of fluid streams in oil and gas production, London.
[9] Stockton, P., and Allan, W., "Allocation Uncertainty: Tips, Tricks and Pitfalls," Proc. 30th International North Sea Flow Measurement Workshop.

Nottingham | UK | 9–11 September 2019

IF CHEAP, EASY OIL IS OVER, WHAT NOW?

Y. Arellano [1], O. Haas [2], H. Ahmed[2], A. Hunt[3] and Lu Ma[3]
[1] *Fluid and Complex Systems Research Centre, Coventry University, UK,*
[2]*Research Institute for Future Transport and Cities, Coventry University, UK*
[3]*iPhase Limited, 7 Intec Business Park, Basingstoke, UK*
prietoy@uni.coventry.ac.uk

Abstract

As oil gets harder to find and produce, the world witnesses a steep shift towards alternative energy sources. This challenges fossil fuel producers to realise advanced, yet financially viable, production techniques under unstable market prices. The oil industry faces previously unseen challenges. In this context, multiphase flow measurement has found a niche application to help decrease production and development costs and enhance production optimization processes. Industrial Computational Tomography (ICT) has the potential to provide the oil industry advantageous metering capacities. The present study comprises a review on the tomography techniques that have attracted interests the recent years in the energy sectors.

Keywords: Petroleum, Multiphase, Measurement, Tomography

1. Panorama of the petroleum industry

The oil industry faces previously unseen challenges imposed by the global market and the finiteness of the resources. Currently, the discoveries of reservoirs and the world oil consumption show opposite trends, as illustrated in Figure (1). This yields the general consensus in the energy community that, at the present rate, oil production will peak before 2050 [1]. After a production peak, the world production would unavoidably decline, leading to an increase in prices of fossil fuels and adding to the already volatile oil price market.

Since the early seventies, the oil price has largely fluctuated, with the largest historic fluctuation registered during the year 2008, see Figure (1). In July of 2008, the oil price peaked at nearly 135 $/bbl, the highest ever registered before dropping by 69% by the end of the same year, following turmoil in the Middle East. The volatility of oil prices is not only by the market forces of supply and demand but by non-technical related aspects. In this regards, economic and political stability, climate station changes, and geopolitical strategies are key in the establishment of the price of the oil [2] [3].

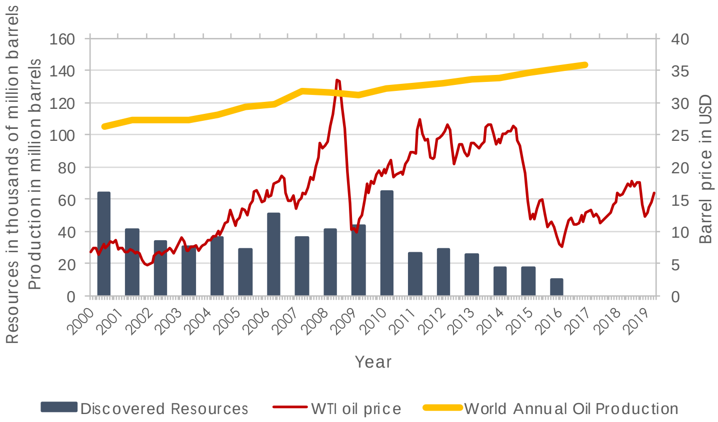

Figure 1: Historic figures of world annual oil production, rate of discovery of resources and oil prices
Source: EIA (2019, pg.1), IEA (2017, pg.1), Rodrigue, J. (2016, pg. 1.), & BP (2018, pg.14.)

2. Flow measurement in the petroleum industry

Production depletion rates from marginal fields and geopolitics are difficult to predict, yet technology development can play a mitigating role. The overall use of technologies in the petroleum industry is fuelled by the need to make marginal fields more cost-effective, to exploit reservoirs in difficult physical environments, e.g. in deep water offshore, to reduce development costs and to improve the energy efficiency and sustainability of fields [8]. Furthermore, production from mature fields unavoidably results in increasing gas and water fractions that creates unstable flow conditions and require more flexible multiphase solutions.

As easy oil becomes scarcer the oil industry has been forced to manoeuvre to meet the world demand and maintain profitability. The development of new technologies has aided petroleum companies to shift their traditional production schemes. Oil companies have been able to make significant savings in exploration and production activities through the use of innovative technologies [9]. The developments of subsea resources and co-mingled production requirements means that there is no longer the possibility to separate oil, gas, and water before metering for production allocation or fiscal purposes. Multiphase flow measurement (MFM) provides a solutions to the offshore oil and gas industry, including the UK sector of the North Sea. MFM ability to continuously measure volume fraction and mixture velocity can replace bulky well-test separators and reduce the development footprint, of great significance in offshore facilities [10] [11]. MFM ability to provide continuous well monitoring permits optimisation of the overall cost-revenue of oil production and enables alternative production scheme and strategies to be developed. MFM enables expedite production allocation, yielding an increasing number of company alliances to share transport and production facilities in order to continue producing from depleting marginal fields or to economically exploit fields in increasingly deeper waters.

Ever since the implementation or early generations of multiphase flow meters (MFM) in oil fields, the trend has exponentially increased as evidenced in Figure (2). The size of the global market for MFM reached 7,500 MMUSD in 2018 and is expected to grow at a 5.9% compound annual growth rate in the following five years [12]. This is partly due to MFM being essential within the petroleum industry for many field developments thanks to its ability to measure production in real-time, to continuously monitor well performance, to correctly allocate production figures, and to survey reservoir life [9].

Within MFM technologies, we find two main groups, namely those that separate the phases and use traditional single-phase flowmeters and those that directly measure the volume fraction and velocity of the multiphase mixture [10]. Available MFM systems are intrinsically complex leading to existing commercial devices with uncertainties that vary from 5% up to over 20% on each of the flowing phases. Industrial Process Tomography (IPT), and more particular soft-field tomography, is one of the possible new technologies to measure multiphase flows, based on systems that are non-intrusive, non-nuclear and with no moving parts. Soft tomography offers an opportunity to achieve similar metering accuracy as existing systems but with substantially less environmental impact and greater ease of deployment and maintenance, resulting in lower costs.

Soft-field tomography technologies have advantageous intrinsic characteristics that make them highly attractive for MFM measurement in the petroleum industry. These characteristics answer to the requirements of the industry and address the challenges that commercial MFM solution face in terms of process invasiveness, costs, speed, capabilities to be adapted to vessels of various sizes, and the use of nuclear sources. The increasing amount of research in the area is evidenced in Figure (2b), where the investigation of soft tomography systems applied to MFM is contrasted to the total number of investigations in medical and industrial tomography. The following section focuses on soft tomography techniques for MFM.

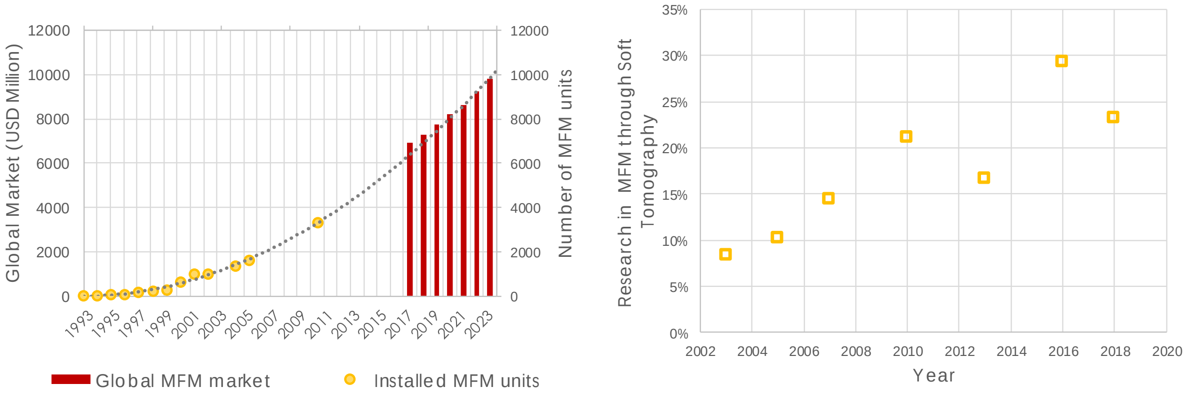

(a) (b)

Figure 2: Worldwide MFM trends showing (a) installed multiphase flow meters, the MFM market size, and (b) the ratio of research on soft-field-based MFM to overall tomography studies

(a) Adapted from Falcone, G and Harrison, B 2011:4 and bv research [online: https://www.kbvresearch.com/flow-meters-market] (b) Source: International Society for Industrial Process Tomography [online: https://www.isipt.org/]

3. Industrial applications of multiphase measurement using Tomography techniques

Soft tomography is based on the measurement of the electric properties of the fluids. The principles of operations rely on the measurement of electrical properties of the materials in the imaging region, where the transmitting signal is significantly affected by the position of the sensors and the distribution of electrical parameters in the surrounding area. Measuring the temporal evolution of phase fractions of multiphase flows in a pipe can be achieved via different techniques, which rely on capacitive, conductivity, impedance, or induction measurements [13]. The choice of the sensing system largely depends on the nature of the multiphase mixture, the operation conditions, the maintenance requirements, and the safety regulations framework.

Tomography technologies provide a wide range of applications within the oil and gas industry that encompasses not only flow transport through pipelines but other plant processes. There are various tomography techniques for multiphase fluid assessment, each one has a specific application niche. Electrical Capacitance Tomography (ECT) is, for instance, the best-developed flow metering technology based on measurements of the dielectric properties of the fluids. Among the most relevant examples of pertinent industrial application, we find flow pattern identification and volumetric rates [14], hydrocarbon phase separation [15], [16], tankers loading [17], and the collapse of oil foams [18].

On the opposite side of the spectrum, we find Magnetic induction Tomography (MIT), the most novel and least developed soft-field technology to date, whose development is still confined to the academic research field. The measurement principle of MIT is based on measurement of the eddy-currents induced in the conductive phase, as illustrated in Figure (3). MIT has been proven to have a good capability in obtaining the image of bubble flow along with various conductive backgrounds such as water formation [19].

The principles of operation of ECT and MIT limit their applicability to the presence, or lack thereof, of a conductive phase. Hence, more research must be done before three-phase measurements can be achieved. To address similar issues and broaden the applicability of the technologies, current research trends benefit multi-modal and multi-spectral imaging methods that address the synchronisation of various process monitoring. Amongst the most novel techniques are the combination of dual-modality tomography to reconstruct the geometric configuration of the inclusions inside the observation domain and to improve the typically low spatial resolution [21][22][23][24][25].

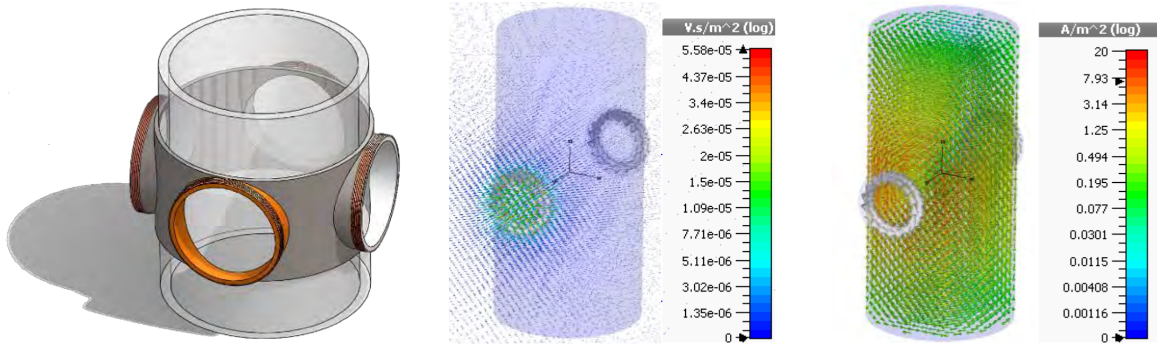

(a) (b) (c)

Figure 3: Magnetic Induction Tomography system showing (a) prototype of an array of coils located on the perimeter of the pipeline, (b) induced magnetic field produced by the excitation coil, and (c) eddy currents induced in a conductive medium which perturbs the primary magnetic field allowing the electric property distribution within the pipe to be inferred. Images (b) and (c) illustrate the intensity of the induced fields according to the adjoined colour bar, showing a higher intensity of the induced physical quantity in the proximity of the excitation coil.

(b)(c) Source: Arellano et al. [online: https://www.isipt.org/world-congress/9/29244.html]

4. Conclusions

The continuous increase in the use of fossil fuels combined with the decreasing rate of discoveries has encouraged the oil industry to venture into hostile physical environments in the search for new field developments and joint efforts to continue producing from mature fields at profitable rates. The challenges that the petroleum industry faces involve making marginal fields more cost-effective, developing production facilities for hostile physical environments and improving energy efficiency. In this context, multiphase flow measurement (MFM) has had an increasing presence in the oil fields to optimise decision-making processes aiming to reduce production and development costs.

Current MFM systems are usually based on intrusive pressure drop techniques associated with nucleonic density measurements in addition to an array of electromagnetic measurements. The commercial solutions available in the market fail to address all the industry requirements in terms of non-intrusiveness, accuracy, costs and environmental impact. This study has summarised a series of technologies that support the use of soft-field tomography as non-invasive and low-cost technologies to acquire information in the volumetric fractions of multiphase flow in pipes.

The intrinsic features of the electrical tomography systems, e.g. ECT or MIT, such as direct measurement of the electrical properties of the flow phases without previous separation and avoiding nuclear sources make them attractive to the researchers aiming to provide metering solutions to the Oil industry. Nonetheless, more research must be done before three-phase measurement from ICT-based technologies meet the industry standards for flow imaging and reach the oil fields.

References

[1] U.S. Energy Information Administration, “Annual Energy Outlook 2019 with projections to 2050,” 2019.

[2] A. Michael, “Economic Implications Of The Current Geopolitical Forces Vis-à-vis Hydrocarbons On Global Energy Markets,” 2014.

[3] R. Priddle, “The development of world energy markets,” in *World Petroleum Congress*, 1997, pp. 77–84.

[4] U.S. Energy Information Administration, “WTI Spot Price FOB (dollars per Barrel),” 2019. [Online]. Available: https://www.eia.gov/dnav/pet/hist/LeafHandler.ashx?n=pet&s=rwtc&f=m. [Accessed: 17-May-2019].

[5] International Energy Agency, “Global oil discoveries and new projects fell to historic lows in 2016,” 2017. [Online]. Available: https://www.iea.org/newsroom/news/2017/april/global-oil-discoveries-and-new-projects-fell-to-historic-lows-in-2016.html. [Accessed: 15-May-2019].

[6] J.-P. Rodrigue, “World annueal oil production (1900-2016) and peak oil (2005-2020),” *The Geography of Transport Systems*, 2019. [Online]. Available: https://transportgeography.org/?page_id=5944. [Accessed: 15-May-2019].

[7] BP, “BP Statistical Review of World Energy 2018,” 2018.

[8] Ministry of Petroleum and Energy of Norway, “OG21 - Oil and Gas in the 21st Century,” 2016. [Online]. Available: www.og21.no. [Accessed: 17-May-2019].

[9] G. Falcone and B. Harrison, “Forecast expects continued multiphase flowmeter growth,” *Oil Gas J.*, vol. 109, no. 10, pp. 68–73, 2011.

[10] R. Thorn, G. A. Johansen, and B. T. Hjertaker, “Three-phase flow measurement in the petroleum industry,” *Meas. Sci. Technol.*, vol. 24, no. 1, 2013.

[11] Quest offshore, “Quest Deepwater Market Insight,” Sugar Land, 2015.

[12] kbv research, “Global Flow Meters Market By Product Type (Magnetic, Positive Displacement, Differential Pressure, Ultrasonic, Coriolis, Turbine, Vortex), Application (Water & Wastewater, Power Generation, Pulp & Paper, Chemicals, Oil & Gas, Food & Beverages),” 2018.

[13] R. A. Williams and M. S. Beck, “Process Tomography: Principles, Techniques and Applications,” p. 565, 1995.

[14] A. Hunt, “Industrial Applications of High-speed Electrical Capacitance Tomography,” in *9th World Congress on Industrial Process Tomography*, 2018, pp. 857–864.

[15] W. Yanga *et al.*, “Imaging wet gas separation process by capacitance tomography,” in *SPIE*, 2002, vol. 4665, pp. 347–358.

[16] S. F. A. Bukhari, I. Ismail, and W. Q. Yang, “Visualising Oil Separator Vessel and Decision-Making for Control,” in *4th World Congress on Industrial Process Tomography*, 2004, pp. 855–860.

[17] R. Deloughry, M. Young, E. Pickup, and L. Barratt, “Cost Effective Loading of Road Tankers Using Process Tomography,” in *2nd World Congress on Industrial Process Tomography*, 2001, no. August, pp. 565–572.

[18] D. Pacho and G. Davies, “Application of Electrical Capacitance Measurements to Study the Collapse of Oil Foams,” in *2nd World Congress on Industrial Process Tomography*, 2001, no. August, pp. 618–627.

[19] L. Ma, A. Hunt, and M. Soleimani, “Experimental evaluation of conductive flow imaging using magnetic induction tomography,” *Int. J. Multiph. Flow*, vol. 72, pp. 198–209, 2015.

[20] Y. Arellano, L. Ma, A. Hunt, and O. Haas, “Characterisation of the Effects of Sensor Geometry on the Performance of Magnetic Induction Tomography Systems,” in *9th World Congress on Industrial Process Tomography*, 2018, pp. 373–381.

[21] L. Ma, D. Mccann, and A. Hunt, “Combining Magnetic Induction Tomography and Electromagnetic Velocity Tomography for Water Continuous Multiphase Flows,” *IEEE Sens. J.*, vol. 17, no. 24, pp. 8271–8281, 2017.

[22] G. Liang, S. Ren, and F. Dong, “An Inclusion Boundary Reconstruction Method Using Electrical Impedance and Ultrasound Reflection Dual-Modality Tomography,” in *9th World Congress on Industrial Process Tomography*, 2018, pp. 11–19.

[23] Y. D. Jiang and M. Soleimani, “Capacitively Coupled Impedance Imaging Based on Wideband Phase Measurement,” in *9th World Congress on Industrial Process Tomography*, 2018, pp. 3–9.

[24] Q. Wang and M. Wang, “Thresholding Values and Fuzzy Logic Fusion in Visualisation of Gas-Oil-Water Horizontal Flow using Dual-Modality Electrical Tomography,” in *9th World Congress on Industrial Process Tomography*, 2018, pp. 749–758.

[25] M. Wagner *et al.*, “Non-Invasive Multimodal Monitoring of Transport and Storage Containers for Spent Fuel,” in *9th World Congress on Industrial Process Tomography*, 2018, vol. 19, pp. 61–66.

Nottingham | UK | 9–11 September 2019

Development of Land Resources Inventory for a watershed in Bundelkhand Region, India

A. Tejasi Shah[1] , B. Jyoti P Patil[2] , C. V C Goyal[3]
[1]Presenting author and M Sc Student, TERI School Of Advanced Studies, India
[2]Scientist C, National Institute of Hydrology, Delhi, India
[3]Scientist G, National Institute of Hydrology, Roorkee, India
tejasishah2@gmail.com

Abstract

Land Resources Inventory (LRI) is a compilation and description of the existing natural resources data, and indicates potentials and constraints for developing a site-specific resource conservation plan. A study was carried out for Kathan river watershed in Madhya Pradesh, Bundelkhand region, India to characterize the natural resources like soil, water, and land. The study involved assessment of the suitability of land for major crops and delineation of homogenous areas in form of land management units based on soil-site characteristics. The analysis included interpretation of climatic data, soil data, assessment of crop water requirements, number of irrigations, depth of irrigation, and establishment of watershed level digital land resources database in a GIS framework. The suitability and limitations of land for selected kharif and rabi crops were presented in the form of thematic layers. Further, land management units of the watershed were suggested for the identified crops covering aspects such as crop rotation, intercrops, and suitable interventions for improving the land productivity. The study concluded that LRI provides detailed analysis of natural resources, which is important for watershed planning process. Further, LRI can be a scientific tool to educate people and stakeholders on the watershed conditions and to identify specific actions needed to improve water management in the study area.

Keywords: Watershed, Land Resources Inventory, Kathan River, Land Suitability, Land Management Unit, LULC

1. INTRODUCTION

Land Resources Inventory (LRI) is a mapping process along with the compilation and description of existing natural resources data. Land Resources Inventory maps show the location and the presence of existing land resources, such as soil and forest. It also includes agricultural area (farmlands), waterbodies and built-up area. These maps are useful in many applications, for example, it can be useful in land use planning, local land conservation programs, and development proposal.

The various studies have reported for land resources inventory in India and outside India too. The Town of Rosendale Natural Resource Inventory includes 21 maps, which help to demonstrate how its resources and topography have shaped the town’s history and development. The LRI comprehensive plan helped in conserving the town’s natural and historical resources and recommended a strategic plan for open space preservation in Rosendale, New York [1]. Similar work was done by Town of Berne, New York, Environmental Commission. Their goal was to develop a natural resource overlay map and provide data to support land use decisions and wetland protection. The report discusses habitat composition and wildlife values. A separate inventory of regulatory freshwater wetlands greater than 12.4 acres was carried out, including fairly detailed wetland classification and assessment. The natural resources inventories and biodiversity assessment training have helped conservation board members to identify wetland and other sensitive habitats during site plan review and to negotiate design modifications with applicants that preserve intact habitats and the benefits they provide the community [2]**.** In Taranaki, New Zealand a Land Resource Inventory was developed to assist in the planning for future land use, particularly agriculture, because it assesses the land resource and its potential for sustainable agricultural production [3].

In India, The National Bureau of Soil Survey and Land Use Planning (NBSS&LUP), Nagpur has been engaged in carrying out soil resource survey, agro-ecological and soil degradation mapping at the country, state and district levels for qualitative assessment and monitoring the soil health towards viable land use planning.

In Karnataka, a Land Resource Inventory of Yelishirur-1 micro-watershed (Gadag taluk in Gadag district) was prepared for Watershed Planning. It was undertaken to provide comprehensive site specific cadastral level information useful for farm level planning and integrated development of the area under Sujala – III, Karnataka Watershed Development Project- II. The research activities have resulted in identifying the soil potentials and problems, and the various applications of the soil surveys with the ultimate objective of sustainable agricultural development [4].It also contains database collected at land parcel/ survey number level on soils, climate, water, vegetation, crops and cropping patterns which helps to develop site-specific plans as well as the need to conserve and manage this increasingly threatened natural resource through sustainable land use management. In Dehradun, a study was conducted in the watershed of Tons river to ascertain crop suitability assessment for mango and wheat using land capability classification through appropriate GIS techniques. Physiography of this region consists of Himalayan Mountains (higher and lower), Shiwalik hills, Piedmont plains, terraces and Flood plains. Various landforms were identified based on physiographic variations. Based on the slope map, land characteristics of each physiographic unit and land capability criteria for land qualities, land capability classes and sub-classes were assigned. These assignments were translated into a land capability map. Further from the slope map, a slope suitability map was generated, which was combined with land characteristics and crop suitability criteria to generate crop suitability maps for mango and wheat. These landforms were further subdivided based on colour, tone, texture, pattern, association and land use [5].

In Bundelkhand, agriculture is the predominant occupation. Land available and the land that is used for cultivation in the region is considerably lower than in other agriculture zones of the country. Due to large area of wasteland in the Bundelkhand Intermediate Region and Bundelkhand Upland sub-regions, the percentage of land used for cultivation falls drastically, to around 50% in Chitrakoot and Lalitpur districts, and less than that in Chhatarpur, Tikamgarh and Damoh districts. Apart from size of land cultivated, agriculture production is primarily determined by availability of water. Considering this, objective of this study was set to develop an inventory of land resources for Kathan River watershed, Bundelkhand region, India, which can aid in the planning for potential future land use, particularly in agriculture.

2. STUDY AREA

The area selected for this study is Kathan river watershed situated in Chhatarpur and Sagar districts of Madhya Pradesh, India. Both districts forms part of Bundelkhand region. The total geographical area of Kathan watershed is 1341 sq km. The mainland watershed area extends between latitudes 24°05’0” N to 25°45’0” N and between 78°55’0” E to 79°30’0” E. The climate of the watershed is characterized by extremely hot summers and general dryness except during the monsoon season. The normal annual rainfall of watershed is 1068.3 mm.

The watershed receives maximum rainfall during south west monsoon period i.e. June to September. About 90.2% of the annual rainfall received during monsoon season. The maximum temperature is observed during the month of May and is recorded as 42°C and minimum temperature during the month of January is 9°C.Land use and land cover of Kathan watershed was prepared by LISS IV data. The major landuse of the watershed is agriculture which covers about 40.57% area. Forest is dominant in southwest and southeast part (Figure-1).

The spatial database related to soil like average depth, texture, maximum depth and soil reaction (pH) were prepared for the study watershed. The maximum depth observed in this watershed is about 115 cm. Such soil covers about 276.9 km^2 of the watershed. About, 293.8 $km^2$is under the soil depth of 60 cm. Another about 480.6 km^2 is under soils of 25-50cm. About 188.9 is under soil depth of 10-25 cm.

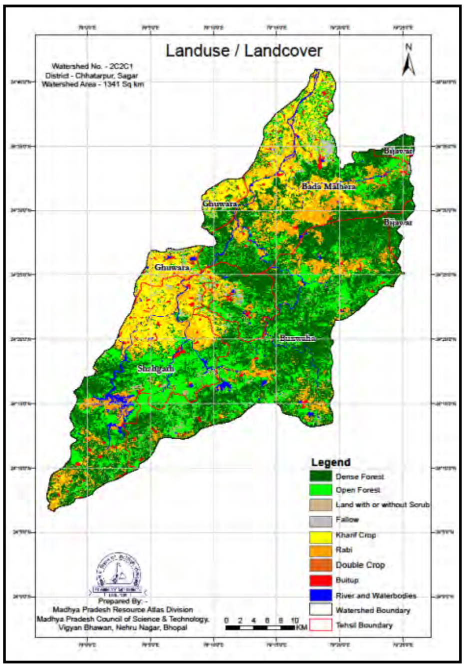

Figure 1: Land use land cover

The soils in this watershed area have fine clay to sandy texture. Nearly 276.9 $km^2$of the area is covered with clay and another 293.8 $km^2$of the area is covered with clay-loam soil. The soil texture characterization is consistent with evolution of the soils of the Chhatarpur district through the slow erosion of hard massive granites. The majority of soil present in Kathan river watershed is slightly alkaline, which covers 897.4 sq.km of the total watershed area.

3. METHODOLOGY

This section provides a description of the methods that were used in this study.

CROPWAT model: In this study, CROPWAT model was used for the computation of crop water requirement and irrigation requirement of the crop that are grown in Kathan watershed. After putting all the input climatic parameters, CROPWAT calculates reference evapotranspiration by FAO Penman-Monteith method, effective rainfall and after putting input values of crop data and soil data, we get the results for evapotranspiration and irrigation requirement for the region [6].

Land Suitability Classification: The FAO land suitability classification system was used in this study, which has four different categories: Orders, Classes, Subclasses and Units. The process of land suitability classification is the appraisal and grouping of specific areas of land in terms of their suitability for defined uses. There are two orders(S and N) which reflect the kind of suitability (S for suitable and N for unsuitable land).

Land Suitability Classes: The framework at its origin permits complete freedom in determining the number of classes within each order. However, it has been recommended to use only 3 classes within order S and 2 classes within order N [8].The class will be indicated by an Arabic number in sequence of decreasing suitability within the order and therefore reflects degrees of suitability within the orders. (Examples: S1: Highly Suitable; S2 : Moderately suitable; S3 : Marginally suitable; N1 : Actually unsuitable but potentially suitable; N2 : Actually and potentially unsuitable).

Land Suitability Subclasses: The sub classes reflect kinds of limitations or main kinds of improvement measures required within classes. They are indicated in the symbol using lower case letters (c: Climatic conditions; t: Topographic limitations; w: Wetness limitations; n: Salinity (and/or alkalinity) limitations; f : Soil fertility limitations not readily to be corrected; s: Physical soil limitations (influencing soil/water relationship and management)).

Land suitability units: This grouping is used to identify land development units having minor differences in management requirements. This can indicate the relative importance of land development works. It is indicated by Arabic numerals, enclosed in parenthesis, following the subclass symbol. (Example of total unit: The whole unit is indicated by a symbol; for example: S2w(2). Here "S" represents Order (Suitable); the number 2 after the letter S represents Class 2(moderately suitable); "w" represents Subclass w (wetness limitation); and (2) represents Unit 2).

Land Management Unit (LMU): There are a number of management practices that could address some or most of the land and water degradation issues in this watershed. However, because of the wide variation in physical characteristics across the Kathan watershed, not all practices will suit, or are applicable to, every part of the landscape. Consequently, the watershed has been divided up into more homogeneous parcels of land, which have similar management requirements. These are referred to as Land Management Units (LMUs). So, a land management unit (LMU) can be defined as a homogeneous block of land that responds in a similar way under similar management.

4. RESULTS AND DISCUSSIONS

The land resource inventory of Kathan watershed was done in terms of land suitability for major crops grown in the area. The analysis included interpretation of climatic data, soil data, assessment of crop water requirements, number of irrigations, depth of irrigation, and establishment of watershed level digital land resources database in a GIS framework. The suitability and limitations of land for selected kharif and rabi crops were presented in the form of thematic layers. Land suitability is evaluated in five major soils that are present in this watershed, which are clay, clay-loam, loam, sandy-loam and sandy-clay-loam soil. The results of the study are discussed in the following section:

As per agriculture data of the watershed; Soybean, Blackgram, Sesame, Barley and Sorghum are major kharif crops, whereas, Wheat, Chickpea, Mustard, Barley and Peas are major rabi crops being practiced in the watershed. For this study, these ten major crops were selected on the basis of the area under the crop that is, crops which are grown in more than 10,000 hectares of the area. The input data pertaining to these crops was fed to the CROPWAT software for estimating crop water requirements, number of irrigations, and depth of irrigation.

Land Suitability for selected crops

The winter wheat is a Rabi crop which can be grown in wide range of soils. Soils with loamy texture or clay loam and have moderate holding capacity, are best for wheat cultivation. Wheat is sensitive to water logging, so heavy soils with good drainage are best suited for wheat cultivation. Keeping this in mind, land suitability for wheat is evaluated on the basis of net irrigation value and number of irrigation required for this crop.

Since the lowest net irrigation value was coming out for the clay and number of irrigation required is 2, S1 class is designated to clay followed by S2 class to clay loam, S3 to sandy-clay-loam. Further, subclasses were designated; loam soil was designated as S3r class, ‘r’ representing rooting condition as limitation and sandy-loam was given S3t, where‘t’ represents texture as limitation.

Likewise, database of net irrigation amount and number of irrigations for five major soil types was prepared for all selected crops using outputs of CROPWAT software. Then database was used for preparing the spatial layers for each crop. The land suitability of Wheat, Mustard, Barley and Soybean are presented in maps shown in Figure- 2.

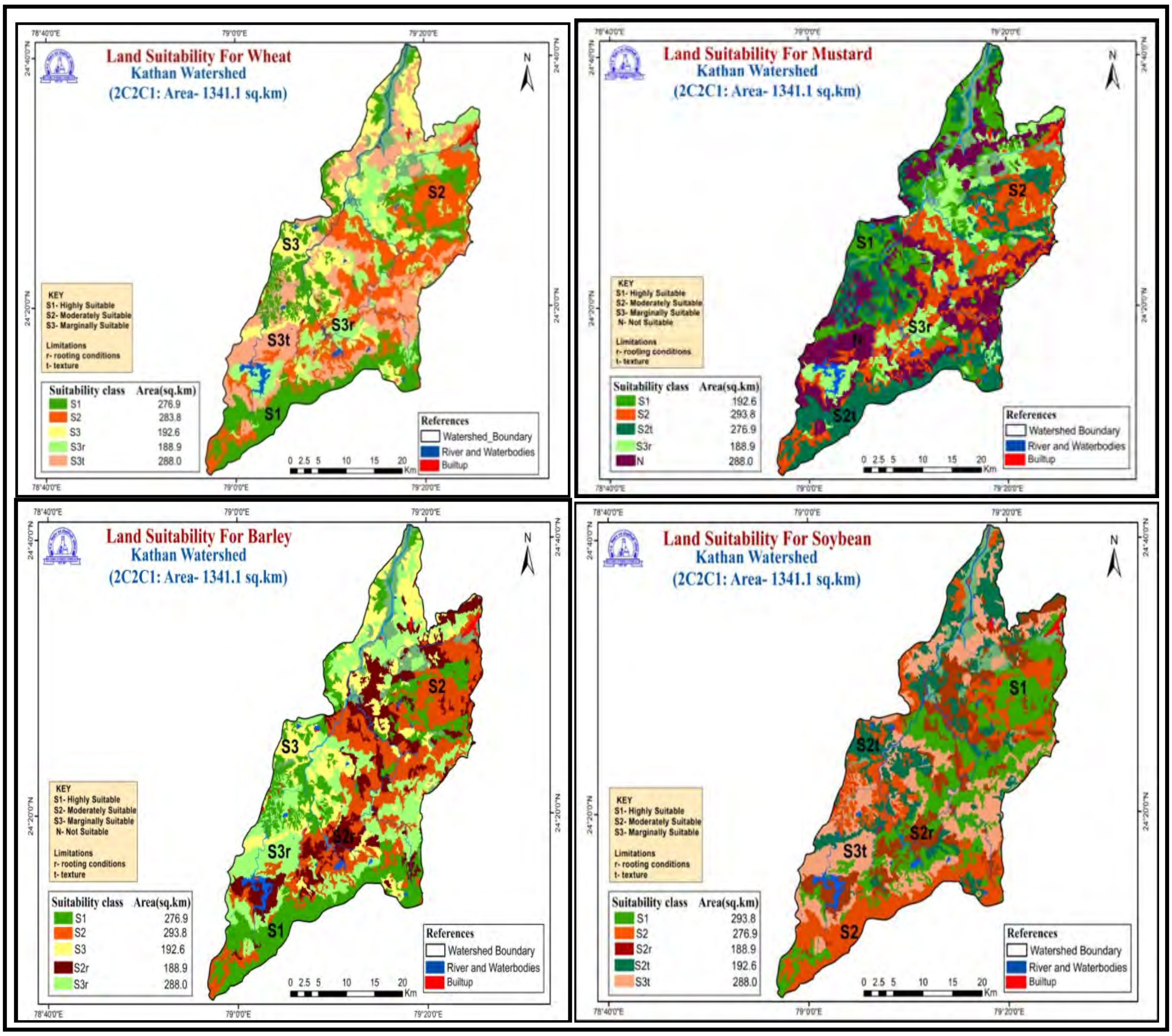

Figure 2: Map showing land suitability for selected crops

Land Management Unit

There are five significantly different Soil type within the Kathan river watershed. These soil types are assigned into different Land Management Units. The LMUs are described in the table 1. They are named in numerological order e.g LMU-1 and LMUs are always written with capital letters. There is variation within the LMUs, so it is important that land managers can recognize the different soils types and be familiar with their characteristics and limitations. This will help them to select and implement the most appropriate land use and management options.

Soil types vary widely across the watershed and a number of different soil types with different soil depth are seen within a property. The soil types and soil depth are described for each LMU, which can help in recognizing properties and problems for that unit of land, and can be used as a general guide to land management.

A proposed crop plan is also given in the LMU table; it is a soil-site–crop suitability assessment. It includes suitable agriculture interventions like crop rotation and intercropping along with suitable soil and water conservation interventions.

Many crops may have positive effects on succeeding crops in the rotation, leading to greater production overall. Rotations are used to reduce pests and diseases in the cropping system and to control weeds . Rotations may also give benefits in terms of improved soil quality, better distribution of nutrients in the soil profile (deep rooted crops bring up nutrients from below) and to increases biological activity where as intercropping is growing of two or more crops simultaneously on the same piece of land which helps in crop intensification in both time and space dimensions.

Table 1: Proposed Crop Plan for LMU's

LMU No.	Soil Depth	Soil type	Field Crops	Crop Rotation	Intercrop	Suitable Intervention
LMU 1	Deep soil (100-150cm)	Clay, Siltyclay, Siltyloam	Wheat, Sesamum, Barley, Peas & beans	Wheat-Soybean, Sorghum-Wheat, Peas- Blackgram	Barley+Peas, Sesamum+Maize Wheat+Chickpea	Mulching, Tillage practices, Drip Irrigation
LMU 2	Moderately Shallow Soil (50-75cm)	Clayloam, Clay	Chickpea, Wheat, Blackgram, Groundnut, Soybean, Sorghum, Mustard, Sesamum	Chickpea-Soybean, Sorghum-Wheat, Soybean- Wheat, Groundnut-Wheat, Blackgram-Peas	Groundnut+ Sorghum, Blackgram+ Sorghum Wheat+Chickpea	Mulching, Tillage practices, Drip Irrigation
LMU 3	Shallow Soil (25-50 cm)	Sandyloam, Sandyclayloam, Clay,	Mustard, Chickpea, Groudnut, Soybean, Barley	Blackgram-Mustard, Soybean- Mustard Groundnut-Wheat	Mustard+ChickpeaGroundnut+Sorghum	Mulching, Tillage practices, Drip Irrigation
LMU 4	Very Shallow Soil (10-25 cm)	Loam, Sandyloam, Sandyclayloam	Groundnut, Soybean, Chickpea, Barley, Peas & beans	Chickpea-Soybean Peas- Blackgram	Mustard+Chickpea, Barley+Peas,	Mulching, Tillage practices, Drip Irrigation

5. CONCLUSION

The information present in LRI maps and their description can be used to educate partners and stakeholders on watershed conditions, generate local support, and identify specific actions needed to improve water management. Land Resources Inventory (LRI) can contribute to a watershed assessment or characterization report, which can become part of a watershed plan. Comprehensive LRI can help in land conservation planning, and allows natural resources information to be included in local planning and zoning.

Furthermore, LMU can help in determining number of management practices that could address some or most of the land and water degradation issues in a watershed.

REFERENCES

[1] Commission Rosendale Environmental, 2010.Town of Rosendale Natural Resources Inventory, Rosendale : Ulster County Department of the Environment, New York Rural Water Association, and Cornell Cooperative Extension of Dutchess County.

[2] Design, Landscape , 2011. Town of Berne Inventories of Forests, Wildlife and wetland, Berne: Town of Berne Environmental Commission.

[3] Trc.govt.nz. (2019). [online] Available at: https://www.trc.govt.nz/assets/Documents/Guidelines/Land-infosheets/LM07landresourceinventorymapping2.pdf [Accessed 30 May 2017].

[4] Rajendra Hegde, NiranjanaK.V, Srinivas S, Nair K.M,Dhanorkar B.A, Reddy R.S and Singh S.K, 2016.Land Resource Inventory of Yelishirur-1 Micro-watershed for Watershed Planning and Development, Gadag Taluk and District, Karnataka, Bangalore: Sujala LRI Atlas No.14, ICAR – NBSS & LUP, RC, Bangalore, p.58.

[5] Bhandari S, Santosh T, Jhadav, 2013. Land Capability Classification and Crop Suitability Assessment in a Watershed Using RS and GIS – a Case Study of Watershed in Dehradun, Uttarakhand,ESRI India, Esri India User Conference.

[6] Banik. P, Tiwari N.K. and Ranjan S, 2014.Comparative Crop Water Assessment, International Journal of Sustainable Materials, Processes & ECO-Efficient, Vol. 3: pp. 11-19.

[7] Environment Department, Natural Resources Management,2004.FAO.org. http://www.fao.org/docrep/x5310e/x5310e04.htm (accessed march 16, 2017).

[8] Odisha.gov, 2013. Orissareview. http://odisha.gov.in/e-magazine/Orissareview/nov-2007/engpdf/Pages65-68.pdf (accessed march 15, 2017).

Nottingham | UK | 9–11 September 2019

Energy Conservation in Old People homes and Excess Winter Deaths in the UK

Ali Mohamed Abdi[1,a], *Dr Andrew Arewa*[1,b] ,*Mark Tyrer*[1,c]

[1]*Coventry University, Faculty of Engineering, Environment & Computing*
Priory Streeet, Coventry, CV15FB

[a] abdia7@uni.coventry.ac.uk
[b] ab6887@coventry.ac.uk

[c] ac5015@coventry.ac.uk

Abstract

Recent research reveal that the UK has the "sixth-highest rate of excess winter death (EWD) in Europe. Yet, common contributor to EWDs remain poor energy efficiency in buildings and high costs of heating homes which exacerbate risks of respiratory, circulatory and mental health problems. Evidence show that certain vulnerable groups in households such as older people and children are most at risk of health detriments associated with cold homes. Yet, there is little research regarding condition of elderly homes, energy conversation and excessive winter deaths in the UK. The study aim to investigate conditions of old people's homes, energy conservation and associated impact on excessive winter death in the UK. Research questions asked are: How robust are energy conservation features in old people's homes? What is the relationship between energy conservation in old people homes and excessive winter deaths? The study adopted mixed research methods with participants drawn from low/average income households in specific regions where excess winters deaths were recorded between 2015/16 to 2017/18. The study used open ended questionnaire to collect data from industry experts such as government health officials, medical doctors, careers, social workers and elderly people. Archive data concerning excess winter mortality rates between 1991/92 and 2017/18 were also obtained and analysed for better understanding of the research problem. Initial findings show that there is significant relationship between energy efficient buildings and excessive winter deaths. Other findings reveal that old people's home are in deplorable conditions in terms of energy conservation and adaptation of energy efficiency. This study is part of ongoing PhD study that seek to investigate "Predictive Analytics of Energy Efficiency in Buildings and Health Vulnerabilities of Elderly People".

Key words: old people's homes, energy efficient buildings and excessive winter death

1. Introduction

There are numerous factors that contributes to excess winter deaths; and other diseases common among elderly people such as respiratory, circulatory, influenza, hypothermia and depression. However, cold weather in particular cold homes are believed to be a main contributor to respiratory and circulatory diseases in the UK [1]. Recent study by the 3rd Environmental Generation (2018) reveal that the UK has the "sixth-highest rate of excess winter death in Europe". In 2017 to 2018 there were estimated 50,100 excess winter deaths (EWDs) in England and Wales. This exceeded the number of EWDs recorded since winter of 1975 to 1976[2]. Moreover, old people were most vulnerable to EWDs during winter of 2017/2018 period, with males and females aged 85 years and over accounting 36.1% and 43.3% respectively. Similarly, the number of deaths per day increased in 2017/18 period compared to all other winter periods in the UK. Though winter mortality rates are higher in other countries with extreme cold conditions, recent research show that most UK buildings (particularly old people's homes) have poor energy conservation system3. Yet, there is scarce research that investigate conditions of old people's homes, energy conservation associated impact on excessive winter death in the UK. Therefore, the study seek to investigate relationship between conditions of old people's homes, vis-à-vis energy efficient buildings and attendant effects on EWDs.

2.0 Energy Efficiency Building and Fuel Poverty in the UK

According to Energy Technology Institute (2016) energy efficiency can be best described as using less energy such as electricity, heat and transport fuel to produce the same output or service. There are different methods and measures that are mainly used to improve energy efficiency, for instance; home insulation, motor insulation, Infrastructure, business processes and facilities. Energy efficiency benefit include; reduction of cost, waste, fuel poverty and Greenhouse Gas emissions (GHG) and improve household's wellbeing. Conversely, the concept of energy conservation is similar to energy efficiency because it entails deliberate effort made to reduce consumption of energy by using less of energy. However, the impact of energy efficiency or energy conservation on EWDs is rarely investigated.

Perhaps, affordability of building quality, energy efficient buildings, property size, and number of occupants are mostly linked to income of building occupants [1]. Besides, there are scarce research that examine conditions of old people's home *vis-à-vis* energy conservation. Moreover, technical details; behavioural mind-set, and regulations behind the use of energy efficiency are often not clear to old people. The 3rd Environmental Generation (2017) opine that old people are more prone to health issues due to inability to heat their homes; these category of people are often cut between the "choice of eating decent meal and heating their homes". Recent, UK government literature described the condition of forging warm home for food as fuel poverty.

Indeed, fuel poverty is caused by low-income, high energy prices and energy inefficient houses [**Error! Bookmark not defined.**]. On the other hand, an empirical definition of "fuel poverty is having to spend 10% or more of a household's net income to heat their homes to adequate standard of warmness" [1]. In 2016, the number of households across England with fuel poverty was estimated at 2.55 million that is 11.1% of all English households [**Error! Bookmark not defined.**]. Similarly, fuel poverty statistics in other nations of the UK are: Scotland 649,000, Wales 291,000 and Northern Ireland 159,530. Perhaps, these figures are lower compared to England due to population of each nation.

1.1. Health Vulnerability of Elderly people

Older people are more likely to be vulnerable to cold weather as they may have an underlying medical condition. Additionally, their temperature control is weaker than younger people, hence making them vulnerable to hypothermia [4]. Other issues that result to hypothermia and cold among the elderly are: chronic illness and multiple medications; Poor nutrition and tendency drinking less water; Inactivity at home and inappropriate dressing during winter; Less heating of home to save heating cost.

Moreover, the main health condition associated with cold housing are circulatory disease, respiratory problems and mental ill-health. Circulatory diseases are believed to cause around 40% of excess winter deaths, whilst respiratory disease are responsible for about a third. Hence, there is close relationship between mental health and financial stress associated with fuel poverty[5]. Other conditions influenced by cold housing include common flu, cold, arthritis and rheumatism. It has also been suggested that exposure to cold temperatures triggers the above conditions, therefore affecting the most vulnerable people. Similarly, cold can cause physiological effects leading to death to elderly people; it can also lower the immune system resistance to respiratory infections [6].

Excess winter deaths

In England and Wales, more deaths occur in winter period than in summer where the mortality level is low and stable [7]. Excess winter deaths (EWDs) and health conditions are attributable to cold housing according to survey conducted by E3G and NEA (2018). The survey suggest one common contributors of EWDs is poor efficiency homes that are hard or expensive to heat thereby exacerbating the risks of respiratory, circulatory problems and poor mental health. Table 1 below shows the number excess winter deaths in UK since 2011.

Table 1: Excess winter deaths across UK [8]

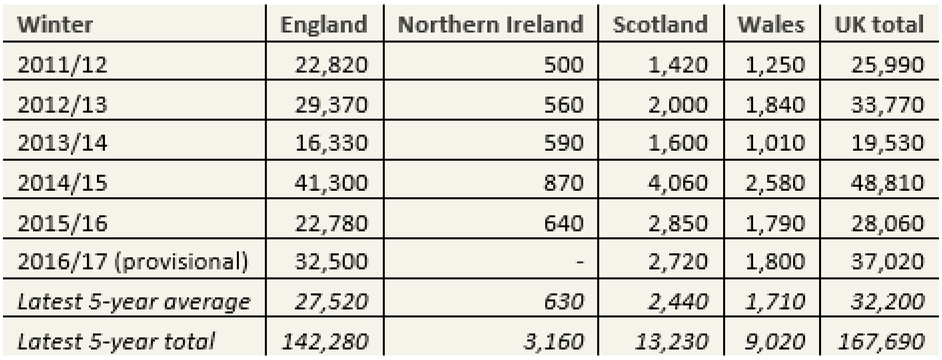

Winter	England	Northern Ireland	Scotland	Wales	UK total
2011/12	22,820	500	1,420	1,250	25,990
2012/13	29,370	560	2,000	1,840	33,770
2013/14	16,330	590	1,600	1,010	19,530
2014/15	41,300	870	4,060	2,580	48,810
2015/16	22,780	640	2,850	1,790	28,060
2016/17 (provisional)	32,500	-	2,720	1,800	37,020
Latest 5-year average	*27,520*	*630*	*2,440*	*1,710*	*32,200*
Latest 5-year total	*142,280*	*3,160*	*13,230*	*9,020*	*167,690*

Studies reporting on mortality deaths show that frequency of deaths is higher in winter months than other months of the year. For instance Johnson and Griffiths (2003)[9] investigated seasonal mortality and reported that historically in UK, the mortality rate is seen between December and March. Moreover, the standard method used to calculate looks at deaths in December to March and the average deaths occurring from August to November and the following April to July. The ONS standard method for measuring excess winter deaths is calculated as; **EWD = winter deaths – Average non-winter deaths**

3.0 Research Method

The research design adopted sequential explanatory type of mixed methods with QUAN-QUAL concept meaning quantitative method is the lead data collection instrument (Creswell 2015). While, qualitative data are used to support and validate the quantitative findings. The data collection tools for the study includes semi-structured interview and questionnaires. The study questionnaire and interview questions were designed based on existing literature. Pilot studies were conducted to ensure that the data collection tools were designed correctly. Ethnical approval was sought from Coventry University Research Ethics Committee and it was granted, see attached ethics certificate in appendix A.

Study Location, Population sample and Data Collection Method

Data collected for the study were obtained from difference location in England. The main data collection instruments were designed to answer the study research questions. Stratified random sampling was used to select the study participants for both quantitative and qualitative data. The population sample consist of, Building and health care industries experts such as government health officials, medical doctors, careers, social workers, energy efficient building specialists and elderly people. For reliability and validity, the study data collection (both questionnaire and interview data) were conducted on one-to-one basis. This method allowed the researchers to conduct deep probe regarding the study aim and research question. On the other hand, the study participants had opportunity to ask questions that were not clear.

Quantitative Data Analysis

Total of 41 questionnaires were administered, 36 were returned and five were considered invalid because they were not completed correctly. 31 questionnaires were used for statistical analyses; performed using SPSS version 25. Cronbach's alpha sigma value of 0.79 was obtained meaning that internal reliability of the quantitative data is very good. Exploratory Factor Analysis (EFA) was used to determine underlying relationship between combinations of factors that influences poor condition of old people's home and excess winter deaths in England. The factor loading was run for both Principal Axis (PA) and Principal Component Analysis (PCA). The communality factor was calculated to be C2 = 0.6112 + 0.5072 = 0.794. Therefore, because the communality factor is close to 1; it indicate that conditions of old people's homes measured by the study were better explained by the factors identified by the study. Table 1 illustrate identified building conditions associated with old people's home involved in excessive winter deaths in the UK between 2012 to 2017.

Poor indoor temperature scored 23% (n = 31%); Poor energy efficiency in buildings 19% (31) and significant deterioration in building 16% (31) recorded the highest marks. Undeniably, conditions are directly related to lack of robust energy efficiency facilities in buildings.

Table 1: Percentage of building conditions associated with old people's home involved in EWDs

Percentage of poor building conditions associated old people involved in EWDs		
Conditions associated 2 in 5 old people's home involved in EWD between 2012 to 2018	**n**	**%**
Poor energy efficiency in buildings	6	19%
Poor gladded doors and windows	2	7%
Damp in floor and walls	2	7%
Draughty rooms	2	7%
Poor ventilation	1	3%
Poor Indoor temperature	7	23%
Significant deterioration in building	5	16%
Peeling paint	2	6%
Carpets worn out	1	3%
Broken windows	1	3%
Overgrown garden	2	6%
	31	100%

Subsequently, Pearson correlation analysis test was conducted. The correlation coefficient between temperatures in old people homes and EWDs produced a value of 0.64. The mean there significant relationship between temperature in old people's homes and EWDs. Figure 1 show a scatter diagram of temperatures in old people homes and EWDs. The chart reveal that the lower the temperature in old people's homes the higher EWDs.

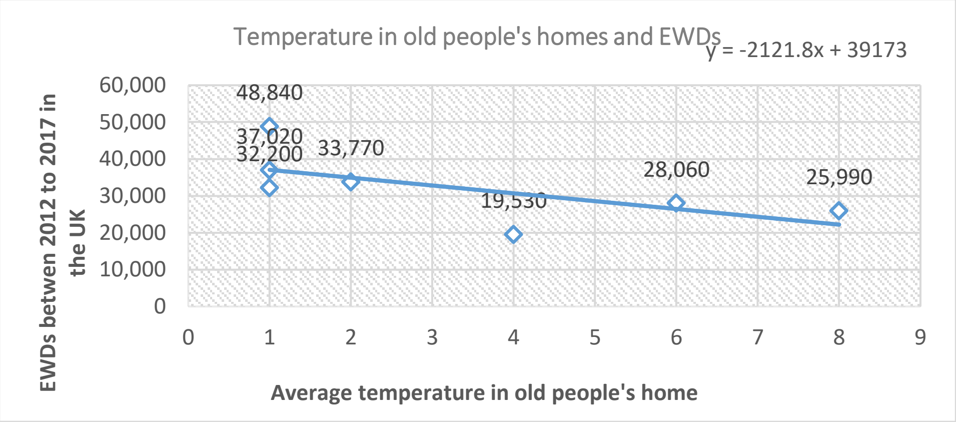

Figure 1: Industry and business specific factors that influence unfair payment practices

4.0 **Interviews data analysis**

Validity of the study qualitative data was upheld in three main areas: selection of participant profile, design of interview questions, and processing/presentation of interview data. Overall, a total of 11 semi-structured interviews were conducted with industry clients and construction contractors. The study targeted interviewees with seasoned construction experience. All interviews were recorded using a digital recorder and personal information linked to study participants was removed because of data protection regulation.

Textual contents of the interview data were transcribed into manuscript, inputted into Nvivo 12 software. Codes were assigned to key themes to facilitate filtering and sorting of data. The themes emerged from the transcribed data with the help of codes and sub-codes created during the analysis process. Content analysis was used to analyse the data for easy inferences to antecedents of discussions between interviewees and interviewer. For example, when interviewees were asked to express their view concerning conditions of old people's homes, energy efficient buildings and excessive winter deaths host of issues were raised about the subject matter. Subsequently, key contents were trimmed for better understanding and spontaneity of interaction between the researcher and study participants. Some textual excerpts are expressed verbatim; as illustrated below for confirmability and better understanding of participants' views.

> *"... building conditions of older people that prefer* care at home *... are often appalling ... usually characterised with damp and draughty ... on average old people in care or nursing homes have better warm and cosy indoor experience compared to those that wishes to continue living in their private houses"* – (Senior Social Health workers for Local Government authority UK).

> *".... we have countless cases of old people admitted to hospital regularly ... in some cases when they are discharged from hospital they are reluctant to go back to their houses ... the pattern is consistent with older people that want to retain independence by living in their private houses ... sadly, EWDs are common with these categories of older people"* (Senior Medical Consultant - NHS).

> *"…. most elderly in their private homes have huge challenges ranging from poor energy efficiency in buildings, adaptation to modern energy technology, old houses with draughty conditions, and so on … these categories of older people are more vulnerable to EWDs"* (Building Services Engineer - Birmingham).

5.0 Findings, Discussion and Conculsion

The study literature provided clear understanding that on average the UK has poor record of energy conservation or efficiency in old people homes compared to colder climates. Generically, the UK have better insulated homes compared to other countries in the continent. More importantly, both quantitative and qualitative findings reveal that there is significant relationship between energy conservation in old people homes and excessive winter deaths. Older people that want to retain independence in their private homes are more vulnerable to EWDs compared to those that are in care or nursing home. Possible reason for the study deduction is that 62% of older people buildings that prefer care at home were discovered to be in appalling condition. The study identified that 1.2 million older people are living in fuel poverty; and it is estimated that 9 out of 10 winter deaths related to cold are among older people. Moreover, 48% of older people that live above fuel poverty threshold claim that they find it difficult to adapt to modern energy efficiency technology. Findings from the study infer that improving energy efficiency in the UK housing stock is the most effective way of reducing fuel poverty for current and future generation. Thus, there is need for innovating housing option for older people with better energy for healthy lifestyle. The study recommends prompt development of housing strategy with specific energy efficiency adaptive features, cost effective and universally available to meets the need of older people.

References

---

[1] *The Health Impacts Of Cold Homes And Fuel Poverty* (2011) London: Friends of the Earth & the Marmot Review Team. available from <https://friendsoftheearth.uk/sites/default/files/downloads/cold_homes_health.pdf> [13 November 2018]

[2] *Excess Winter Mortality In England And Wales - Office For National Statistics* (2019) available from <https://www.ons.gov.uk/peoplepopulationandcommunity/birthsdeathsandmarriages/deaths/bulletins/excesswintermortalityinenglandandwales/2017to2018provisionaland2016to2017final> [21 April 2019]

[3] Age UK (2017) [online] available from <https://www.ageuk.org.uk/Documents/EN-GB/For-professionals/Research/Living_on_a_low_income_full_report.pdf?dtrk=true> [4 May 2019]

[4] El-Ansari W and El-Silimy S (2008) Are fuel poverty reduction schemes associated with decreased excess winter mortality in elders? A case study from London, UK. Chronic Illness, 4(4), pp.289–294.

[5]

[6] Hajat S, Kovats RS and Lachowycz K (2007) Heat-related and cold-related deaths in England and Wales: who is at risk? Occupational and Environmental Medicine, 64(2), pp.93–100

[8] GUERTLER, P. and SMITH, P. (2018) *COLD HOMES AND EXCESS WINTER DEATHS*[online] available from

---

<https://www.e3g.org/docs/E3G_NEA_Cold_homes_and_excess_winter_deaths_2018.02.pdf > [10 April 2019]

[9]

Nottingham | UK | 9–11 September 2019

India’s clean energy transition while meeting the growing consumption

Radhika Sharma

Shakti Sustainable Energy Foundation, The Capital Court,104 B, 4th Floor
Munirka Phase III
New Delhi 110067, India

dutt.radhika1988@gmail.com

Abstract

India stands at the critical juncture of becoming one of the leading nations in transitioning towards cleaner use of energy sources while dealing with the ever-increasing population and its demand. This transition is a resultant of both static (fundamental) as well as dynamic adoption of clean energy policies (at both Central and State level), market creation and evolution of businesses and jobs, emergence and adoption of new and clean technologies and efficient fuels. This adoption has resulted from the International momentum for climate change along with India’s commitment to the Nationally Determined Contributions (NDCs). Consequently, India’s National policies, programs and schemes such as National Solar Mission, Saubhagya, Ujjwala, National Wind Solar Hybrid Policy, etc., and the state-level policies such as mini-grid policy in Uttar Pradesh, have further paved the way. Also, a wide network of civil society organizations, think-tanks, power sector consultants, engineering procurement construction companies, have emerged and evolved. This review discusses the conducive ecosystem which has been created over the years, challenges and future aspects of India’s clean energy sector. It also includes emerging technologies and enablers such as electric mobility, grid-interconnected decentralised renewable energy systems, energy/electricity storage, use of thermoelectric generators, smart grid and meters, energy and system efficiency, for advancing RE in the future.

Keywords: Renewable energy, emerging technologies, clean energy transition

1. Introduction

India is one of the fastest growing economies with an additional challenge of exponential population growth, leading to increasing energy demand. The country continues to grapple with the issues of access to energy, energy security and supporting cleaner sources of energy [1]. India has observed a significant increase in renewable energy (RE) generation in the last decade. The RE component in the energy generation mix has augmented from *6* per cent in 2007 to approximately *21* per cent in 2019 [2] [3] [4]. One reason for this low-carbon energy transition is India's commitment to its Nationally Determined Contributions (NDCs) and alignment with the international community on climate change mitigation plans and strategies [5]. But the challenge has always been the exponential increase in the energy demand and the concurrent nature of the subject of electricity in India. The states must put in equal efforts to expedite the deployment of RE. Hence, the culmination of efforts at both Central and state governments along with the building of a conducive ecosystem of developers, manufacturers, distribution companies, regulators, civil society organisations have led the country to this advancement in clean energy.

The high penetration of RE has supported the country's need to meet the growing energy demand. It has also reinforced the Government's commitment to providing electricity to all the households by 2019, under the Saubhagya Scheme and an opportunity for the electricity distribution companies to connect with households through grid connection and through stand-alone solar power packs in distant rural hamlets [6]. RE stands at the centre of India's transition story towards a clean energy future. But in order to expand it further, there is a necessity to identify certain critical enablers which will reinforce the sector and provide the basis for expansion in the future. This review paper provides an overview of the clean energy transition in India, key drivers and suggests key enablers to advance the clean energy momentum in the country.

2. Approach

The approach followed by this review paper included extensive secondary research through research papers, reports published by departments such as NITI Aayog, Central Electricity Authority, Ministry of Statistics and Programme Implementation, Ministry of New and Renewable Energy, etc. Various policy and regulations on RE and electricity were referred for understanding the technical and commercial arrangements. This was followed by aligning and building a chronological order of the developments in the energy sector in the country. The observations were then captured, and the discussion points reinstated through policy briefs, technical papers and opinion pieces, published during the last decade.

3. Discussion

Advancing India's clean energy: Key developments

India's journey in exploring RE came into the fore after the announcement of the Jawaharlal Nehru National Solar Mission (JNNSM) [7]. Prior to that, the wind projects were being implemented and the main driver was the incentive of Accelerated Depreciation [8]. Over the last decade, this momentum could thrive due to two main reasons- (i) India's commitment to international climate mitigation targets and (ii) India's aim to provide reliable and quality electricity to all. The JNNSM also included targets to promote off-grid applications through both solar thermal and solar PV technologies. But solar thermal applications did not get deployed at the same pace owing to various reasons such as expensive technology, the requirement of space, etc. The other sources of RE such as biomass and small hydro also observed limited success, unlike solar PV. The exponential advancement in solar PV was majorly due to the large-scale deployment goals and the drastic reduction of the cost of solar power generation. There were significant policy and regulatory developments at the state level to promote solar PV. The distribution companies were made responsible for the penetration of RE in their electricity mix through mechanisms such as renewable purchase obligation (RPO) and Renewable Energy Certificates (RECs) [9]. The solar energy technology deployment was further reinforced through solar generation based mini-grids projects and mass uptake of stand-alone solar home systems by rural households, especially the ones which were distant and still disconnected with the main electricity grid. With the promotion of solar charging stations for electric vehicles, solar-powered agriculture pump sets, electric storage and other renewable energy applications, there is a thrust to identify potential opportunities for public-private partnerships and techno-commercially viable projects. The financial viability and techno-commercial feasibility will allow the sustainability of these projects. Additionally, there are solutions being developed for the advent of the grid and the issue of integrating variable renewable energy into the electricity grid.

Linking RE and modern energy services

Now, with the electricity connection reaching all the households, the existing, as well as upcoming decentralized renewable energy projects, can connect with the existing grid. The advent of grid and interconnection with RE-based projects would fulfil the key requirements of clean, reliable and quality supply of power. And, this modern energy system must enable better health, education for all and a sustainable livelihood generation opportunity for all. For this, the clean energy sector will require subsequent efforts in research, development and demonstration of the RE technology, creation of a robust power market, development of a conducive policy and regulatory regime as well as development of effective demand and supply side business models leading to enhanced energy efficiency, low-carbon intensive and cost-effective solutions. There are certain impediments towards meeting these RE targets, some crucial ones include intermittent nature of the RE source, absence of comprehensive market strategies, changing policy and regulatory regime, lack of subsidizing mechanisms and high capital investments. One of the major impediments in the process of such a transition is to secure the necessary finance to achieve the transformative goal of producing *175* gigawatts of renewables by 2022 [10].

Supporting the development of RE through critical enablers

Further development of RE in India could lead to increase in energy productivity, increase in electrification rate, enhancing carbon mitigation by limiting the use of fossil fuels, supporting job creation and providing a quality and healthy life to the country's population. There are certain enablers that could strengthen the role of RE in India.

Technical

There is certain advancement required at the technical front to strengthen the reach and capacity of RE. As variable renewable energy (VRE) would grow to critical levels, electricity systems will require greater flexibility [11]. Electricity storage can drive electricity decarbonisation and aid-in the transformation of the sector. The range of services provided by electricity storage includes bulk energy services, ancillary services, transmission and distribution infrastructure services, energy management services, apart from the storage requirements in the transport sector and the decentralised renewable energy (DRE) applications. Other enablers include the integration of energy efficiency for optimising and integrating cost and energy use and effective demand-side management and deployment of smart meters for undertaking effective monitoring and evaluation.

Innovations and development

There are emerging technologies to enhance the use of cleaner sources of generation as well as improve the conversion efficiency. Thermoelectric generators (TEGs) are a clean and efficient means to convert the thermal energy into electrical energy and the technology can be used in both air-conditioning and electrical energy generation [12]. Another such practical innovation is the interoperability of AC and DC systems. This convergence would help reduce conversion losses, improve efficiency and adaptability to the grid. Introduction of induction cooking to the fore would also require certain innovations to promote mass adoption of the application. In terms of fostering other sources of RE such as biomass and bagasse cogeneration, small hydro, offshore wind, there is a prerequisite to identify the impediments and their nature of use.

Policy and Regulatory

The policy and regulatory landscape in India, especially for the RE sector has been ever-changing and evolving. But there is a critical want for a robust and a conducive policy ecosystem to provide confidence among the developers and investors. It is critical to facilitate coordination among the state and central government over the policy directives. Apart from notifying policies and regulations, it is of significance to formulate operational and technical guidebooks to direct the relevant stakeholders.

Socio-economic and sustainable development

The provision of clean, reliable and affordable electricity and modern energy services to all are critical to the socio-economic development of a nation. It is essential to explore the potential of the impact on health, livelihood generation, education, women empowerment and rural development, with energy being an enabler. It can be reflected by the per capita energy consumption which is still very low (*849* kWh), as compared to the other developed economies [13]. There is a facilitation required among different sectors and government ministry of rural development, women empowerment, skill development, power, renewable energy, health, education, etc. to carve a roadmap for an integrated socio-economic development.

Business models and opportunities

In order to meet the growing energy demand and creating sustenance for RE, there is a need to develop techno-commercially feasible business models. These business models, if demonstrated, could lead to creating a market opportunity as well as will open the market for public-private partnerships. There are opportunities especially in the rural energy access space, with households being connected, there is an expected surge in the rural electricity demand and a rise in the requirement of operational and services ecosystem. There is a huge opportunity to integrate clean energy generation, distribution and energy efficiency components and deliver quality services. Other business opportunities would emerge under the KUSUM Scheme such as deployment of individual pumps, pumping and drinking as-a-service model, grid-connected solar pumps, solarization of feeders and community irrigation [14].

Finance for renewable energy

There are many incentives in place to promote RE. Some of them are National Clean Energy Fund, soft loans from Indian Renewable Energy Development Agency Limited (IREDA), tax-free bond issuance, etc. [15] But there are certain measures which are fundamental in nature such as addressing institutional and policy-level complexities and uncertainties. As an overall solution, it is important that the government should act as a facilitator and should devise innovative policy mechanisms to not just introduce innovative financing instruments, but to create a conducive environment which minimizes the associated risk factor [16].

4.Conclusion

India's transition to a clean energy future will be a result of multiple approaches to be undertaken by various actors at the Central Government and state government levels, collaboration among implementors and research institutions, strengthening the civil society network, building capacity of distribution and generation companies and financing institutions, among others. It is substantial to create awareness among these stakeholders which would in turn aid building and strengthening of a conducive ecosystem of technical, commercial, operational and socio-economically feasible opportunities for the sector to thrive upon. These opportunities would lead to building and deepening of the market, hence would further the sustainable and clean future for India.

References

1. M. M. a. G. Bhattacharya, "Energy Transitions in India," *Georgetown Journal of Asian Affairs,* 2019.
2. M. o. S. a. P. Implementation, "New and Renewable Energy," 2007. [Online]. Available: http://mospi.nic.in/sites/default/files/reports_and_publication/statistical_publication/economic_statistics_2007/es07_section7.pdf.
3. M. o. S. a. P. Implementation, "Electricity in India," 2007. [Online]. Available: http://mospi.nic.in/sites/default/files/reports_and_publication/statistical_publication/economic_statistics_2007/es07_section5.pdf.
4. "Executive Summary on Power Sector," Central Electricity Authority, New Delhi, 2019.
5. K. Mangotra, "Discussion Paper: India's NDCs," November 2018. [Online]. Available: https://www.teriin.org/sites/default/files/2018-12/India%27s%20NDCs%20Key%20Messages.pdf. [Accessed May 2019].
6. "Saubhagya Dashboard," Ministry of Power, Government of India, [Online]. Available: https://saubhagya.gov.in/.

7. M. o. N. a. R. Energy, “Annual Report,” 2009. [Online]. Available: https://mnre.gov.in/file-manager/annual-report/2009-2010/EN/Chapter%203/chapter%203_1.htm.

8. T. Sud, “Case Study:India's Accelerated Depreciation Policy for India,” International Institute of Sustainable Development, 2015.

9. REC, “About REC,” [Online]. Available: https://recregistryindia.nic.in/index.php/publics/AboutREC.

10. G. K. Sarangi, “Green Energy FInance in India: Challenges and Solutions,” August 2018. [Online]. Available: https://www.adb.org/sites/default/files/publication/446536/adbi-wp863.pdf. [Accessed 20 May 2019].

11 IRENA, “Electricity Storage and Renewables:Costs and Markets to 2030,” [Online]. Available: https://www.irena.org/-/media/Files/IRENA/Agency/Publication/2017/Oct/IRENA_Electricity_Storage_Costs_2017.pdf

12 R. A. Hayati Mamur, “A Review: Thermoelectric Generators in Renewable Energy,” *International Journal of Renewable Energy Research-IJRER,* vol. 4, 2014.

13 WorldData, “Energy Consumption in India,” 2015. [Online]. Available: https://www.worlddata.info/asia/india/energy-consumption.php.

14 G. o. I. Press Information Bureau, “KUSUM Scheme,” February 2019. [Online]. Available: http://pib.nic.in/newsite/PrintRelease.aspx?relid=188499.

15 CRISIL, “Enabling Low-cost Financing for Renewable Energy in India,” 2014. [Online]. Available: https://shaktifoundation.in/wp-content/uploads/2014/02/RE-Financing-Final-report.pdf.

Nottingham | UK | 9–11 September 2019

CFD performance analysis of finned-tube CO_2 gas coolers with various inlet air flow patterns

Xinyu Zhang[1], Yunting Ge*[1], Jining Sun[2]

[1]Sustainable Environment Research Centre, Faculty of Computing, Engineering and Science, University of South Wales, Pontypridd, CF37 1DL, UK

[2]RCUK National Centre for sustainable Energy Use in Food Chains (CSEF), Institute of Energy Future, Brunel University London, Uxbridge, Middlesex, UB8 3PH, UK.

xinyu.zhang@southwales.ac.uk; yunting.ge@southwales.ac.uk

Abstract

A detailed model of three-dimensional computational fluid dynamics (CFD) on a finned-tube CO_2 gas cooler has been developed and demonstrated in this paper. The model is applied to predict airside heat transfer coefficients and performance of the coil under the conditions of uniform and maldistribution airflow inlet profiles. The simulation results reveal that different types of inlet airflow patterns have significant effects on the gas cooler performance. Air-side average heat transfer coefficients vary from 47.1 W/m^2-k to 73.37 W/m^2-k when uniform air inlet velocities vary in the range of 1-3 m/s. Compared with linear-up air velocity profile, the uniform and linear-down velocity patterns can appreciably influence more on the coil heat transfer performance. The model also enables to predict the CO_2 temperature profile along the coil pipes from refrigerant inlet to outlet at different operation conditions. It is found from the simulation results that higher airflow velocity can lead to less coil approach temperature and thus better gas cooler performance under uniform airflow pattern. The research method and outcomes presented in this paper can have great potentials to optimize the performance of CO_2 gas cooler and its associated refrigeration system.

Keywords: CO_2 finned-tube gas cooler, maldistribution airflow inlet, heat transfer coefficient, refrigeration system, Computational Fluid Dynamics (CFD) modelling

1. Introduction

Finned-tube coil is a competent heat exchanger owning to its simplicity, durability and cost-effectiveness characteristics, which has been widely used in various engineering applications, including air conditioning, refrigeration and heat pump systems. The performance of such a heat exchanger plays an important role in its associated system and is necessarily to be further improved.

Subsequently, during the past decades, a great deal of experimental and theoretical analyses on such heat exchangers have been carried out by researchers in order to understand the characteristics of fluid heat transfer and friction involved and thus optimise their performances. Once validated with experimental measurements, the theoretical model for the heat exchanger can be utilised as an efficient tool for the heat exchanger optimisation. For the theoretical analyses, most of the early researchers developed conventional numerical simulation models with in house software such as Fortran to investigate the performances of the heat exchangers by means of modelling methods of ε-NTU or LMTD i.e. lumped, tube-in-tube or distributed. Ge and Cropper [1] used a distributed method to calculate CO_2 temperature profile along refrigerant pipe flow direction of a CO2 finned-tube gas cooler. Due to the complicated performance of airflow side and abrupt property changes of supper critical CO_2 flow side in the CO_2 gas cooler, Computational Fluid Dynamics (CFD) modelling tends to be more favourable method and an efficient tool to predict fluid heat transfer characteristics associated. Sheik et al. [2] used CFD to study the effects of airflow misdistributions on the performance of three different types of finned-tube heat exchangers but the hot fluid was not CO_2. Even so, most of the researches on heat exchanger CFD modelling were based on uniform airflow velocity. There is a lack of research investigation and data for the analyses of airflow misdistribution effect on the CO2 gas cooler performance. This paper aims to address this and investigate the effects of different airflow patterns on the thermal performance of CO_2 gas cooler in a refrigerant system.

2. Numerical Methodology

Physical model

The geometry and dimension details of the studied finned-tube CO_2 gas cooler are demonstrated in Figure 1 and Table 1. Air flows through the passages between outer tubes and fins and CO_2 refrigerant flows in tubes from the top pipe numbered ‘0’ to the bottom one numbered ‘54’ in counter flow.

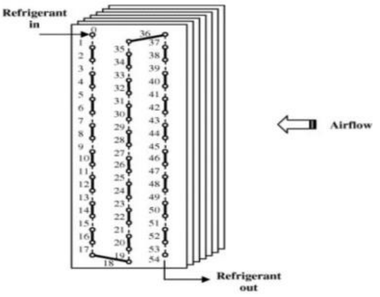

Figure 1: Modelled gas cooler of numbered tube pipes.

Table 1: Specification of gas cooler.

Dimensions	
W × H × D (m)	0.61 × 0.46 × 0.05
Front area (m^2)	0.281
Fin shape	Raised lance
Fin pitch (mm)	1.5
Fin thickness (mm)	0.13
Number of tubes row	3
Tube outside diameter (mm)	7.9
Tube inside diameter (mm)	7.5
Tube shape	smooth

CFD approach

Due to the complicated fluid flow characteristics, a three-dimension CFD model on the CO_2 finned-tube gas cooler has been developed and analysed numerically in this paper. The CFD model development is based on the following assumptions:

(a) The models is developed under steady state condition;

(b) The actual raised lance fins are simplified as plain fins;

(c) An individual coil consists of two consecutive fins and associated air domain and is used to calculate airside heat transfer coefficient;

(d) Heat transfer characteristic of airside between each individual coil is assumed the same under the consideration of symmetrical geometry;

(e) Assuming the temperature of refrigerant does not change when it flows a short distance

The entire CFD modelling development consists of two phases. In phase I, according to assumption (d), an individual coil which contains two consecutive fins and air domain was created to calculate airside heat transfer coefficient. Figure 2(a) shows the geometry of phase I model. In phase II, the gas cooler is divided into 10 segments along the pipe length direction. Each segment contains approximately 37 consecutive individual coils. According to the assumptions of (d) and (e), the entire gas cooler model is developed based on 10 consecutive elements to simplify the model development and simulation processes as shown in figure 2(b). The airside heat transfer coefficient calculated in phase I will be applied in the model of phase II. In addition , to predict the performance of gas cooler precisely, transverse heat conduction is considered in the CFD model.

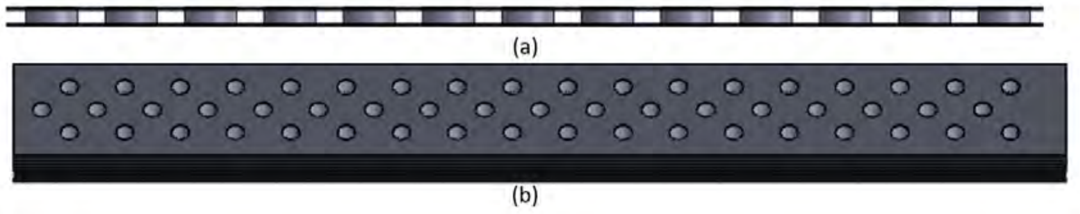

Figure 2: (a) phase I model; (b) phase II model.

The modelling development routine starts firstly from phase I. The governing equations are based on the conservations of mass, momentum and energy to capture the characteristics of air side heat transfer and fluid flow. Since transverse heat conduction could affect the gas cooler performance, more detailed model is created to include the effect of the transverse heat conduction. In the second phase, the calculated airside heat transfer coefficient from phase I is used to predict refrigerant temperature profile along the pipe from inlet to outlet. Two 3D geometry models are built in SolidWorks software and then imported to ANSYS ICEM CFD 18.2 to complete the step of meshing. A code has been developed by Visual Studio 2017 to assign the calculated airside heat transfer coefficient to the coil surfaces and calculate refrigerant temperature profile along pipe flow direction in FLUENT 19.2.

The boundaries conditions for the phase I model are listed as below:

(a) Aluminium and copper are selected as materials of fins and tubes respectively;

(b) The coil top and bottom surfaces are assigned as adiabatic walls;

(c) Air is considerded as compressible fluid;

(d) The air thermo-physical properties of density, viscosity, specific heat capacity and thermal conductivity are all functions of temperature and pressure, which are obtained from REFPROP software;

(e) The 'velocity inlet' and 'pressure outlet' are respectively used at the coil inlet and outlet;

(f) Refrigerant flows through tubes is assigned by variable wall temperatures and heat transfer coefficeints. The airside heat transfer coefficient profile developed and calculated from phase I analysis is used in phase II model as the boundary condition of coil fin and tube surfaces.

Airside heat transfer

Two evaluation planes are assumed and formed an indevidual coil to determine the average air temperature and thus heat transfer coefficient , as shown in Figure 3. Airside heat transfer coefficient is calcualted by following equation:

$$h_{a,i} = \frac{Q_i}{A_i\left(T_{w,i} - T_{air,average}\right)} \tag{1}$$

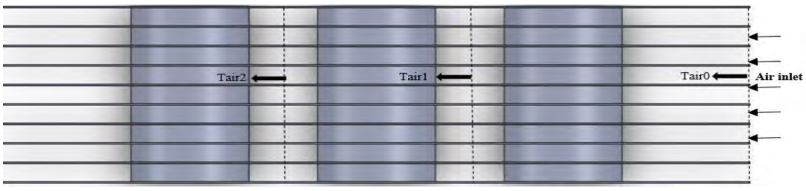

Figure 3: Evaluation planes between tube rows for obatining average air temperarture.

Refrigerant heat trasnfer

Gnielinski correlation [3] is used in the calculation of CO2 heat transfer coefficient as listed in equation(2).

$$Nu = \frac{\xi/8(Re-1000)Pr}{12.7\sqrt{\frac{\xi}{8}}\left(Pr^{\frac{2}{3}}-1\right)+1.07} \tag{2}$$

Where, Filonenko's correlation is used to predict the friction coefficient,

$$\xi = (0.79\, ln(Re) - 1.64)^{-2} \tag{3}$$

Airflow maldistributions

In order to investigate the effect of airflow velocity maldistribution on the performance of CO2 finned-tube heat exchanger, four inlet air velocity profiles are studied in the CFD simulation: (a) uniform velocity profile; (b) linear-up velocity profile; (c) linear-down velocity profile; (d) parabolic velocity profile. The four velocity profiles have the same average face velocity. The uniform airflow parttern is used as baseline model. From the simulation results, air temperature contours under different air velocity profiles can be seen in Figure 4.

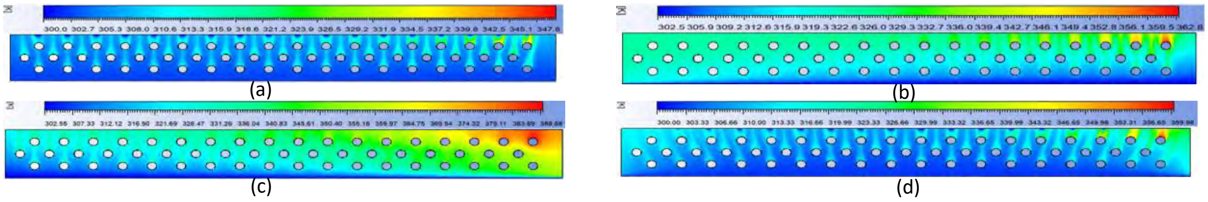

(a) (b)

(c) (d)

Figure 4: Air temperature contours under the condition of different airflow patterns: (a) unifrom air velocity;(b) linear-up air velocity; (c) linear-down air velocity; (d) parabolic air velocity.

3. Results and Discussion

The CFD simulation results are validated with empirical corrleations of airside heat transfer carried out by Wang et al.[4] and are also compared with experimental results from published literature of Ge and Cropper [1] for refrigerant side temperature profiles, as shown in Figure 5 and Figure 6 respectively. The results show good agreements in these comparsions. As seen from the results, airside average heat transfer coefficients vary from 47.1 W/m^2-k to 73.37 W/m^2-k when uniform air inlet velocities change in the range of 1-3 m/s , as shown in Figure 5(a).

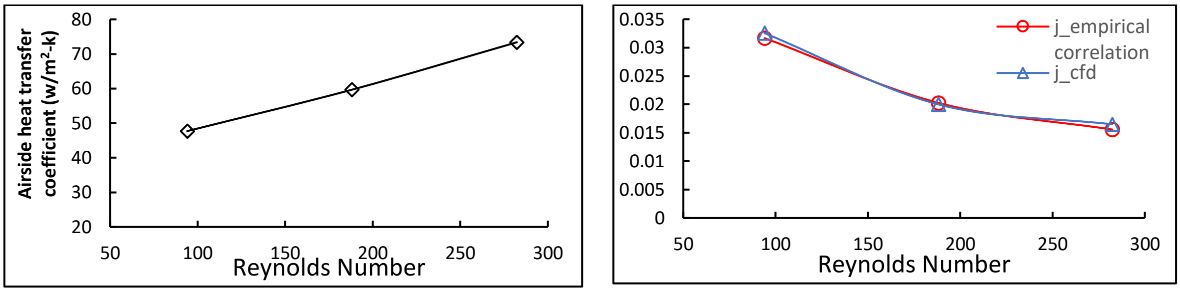

Figure 5 : Uniform airflow pattern: (a) Average airside heat transfer coefficient of CFD results; (b) Comparasion of Colburn-j factor of varying reynolds number.

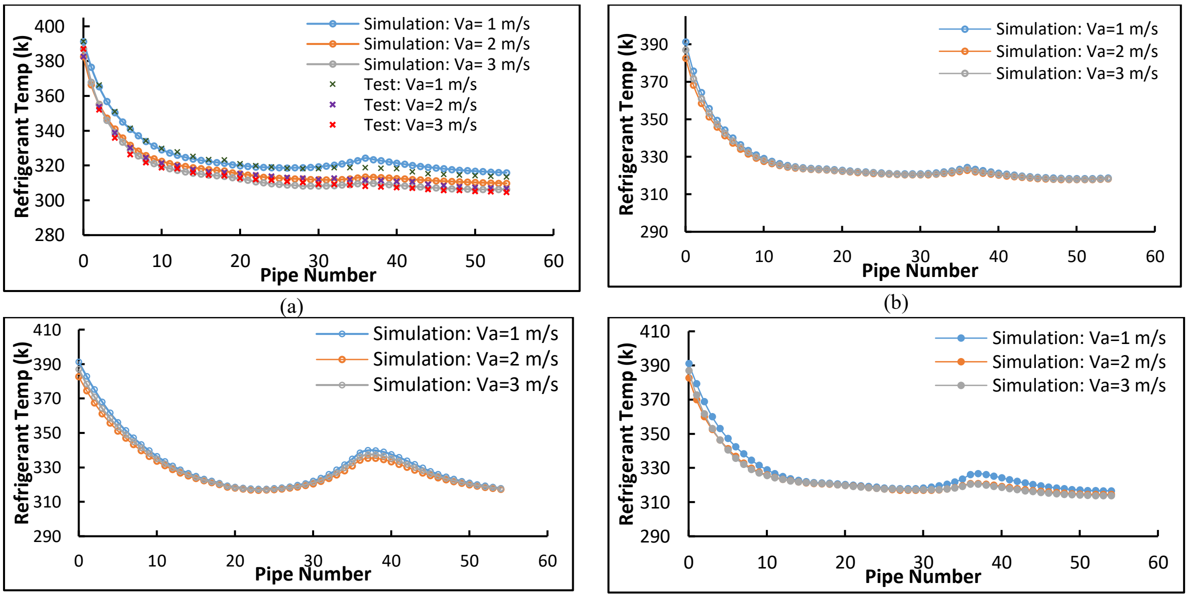

(a) (b)

(c) (d)

Figure 6: Temperature profile of refrigerant along flow direction of different conditions (CO2 mass flow rate=0.038kg/s, pressure=9Mpa): (a) Uniform airflow; (b) Linear-up airflow; (c) Linear-down airflow; (d) Parabolic airflow.

It can be seen from both simulation and experimental results of uniform airflow pattern that most of refrigerant temperature drops occur in the first-row tubes from numbered ‘0’ to ‘18’. In the second row, refrigerant temperature decreases slightly from pipe ‘19’ to ‘26’. However, there is an upward trend when refrigerant flows from pipe ‘34’ to ‘36’. This is due to transverse heat conduction involved which is an important factor to affect the coil heat transfer performance. The thermal conductivity of a specified material is affected by temperature, material properties and path length. It can be observed from figure 6(c) that there is a clear upward trend of refrigerant temperature from pipe ‘32’ to ‘36’ since higher temperature causes higher heat transfer rate through material. As figures demonstrate, linear-down air velocity profile can cause more impact on the performance of heat exchanger compared with linear-up and parabolic velocity distribution. Uniform airflow velocity profile has the best thermal performance on heat exchanger since it can lead to the lowest approach temperature. It is noted that to improve the CO_2 gas cooler performance, the coil approach temperature at the CO_2 fluid exit needs to be minimized.

4. Conclusion

A three-dimensional CFD model has been developed for a CO2 finned-tube gas cooler. The model development consists of two phases in which phase I is used to calculate heat transfer coefficient profile and used into phase II model. Subsequently, the phase II model can be used to calculate the refrigerant side heat transfer and temperature profiles at different operating conditions. The developed CFD model is used to evaluate and compare the heat exchanger performance at various inlet airflow patterns including uniform, linear-up, linear-down and parabolic. From the model simulation results, maldistribution of airflow in the CO_2 finned-tube gas cooler could cause dramatic impact on the coil performance particularly CO2 temperature profile and coil approach temperature. The results of CFD simulation can contribute better understanding the influence of airflow maldistributions and subsequent design optimisation of the heat exchanger.

Acknowledgments

The authors would like to acknowledge the support received from GEA Searle and Research Councils UK (RCUK) for this project.

Reference

1. Ge, Y.T., Cropper, R., 2009. Simulation and performance evaluation of finned-tube CO2 gas coolers for refrigeration systems. Applied Thermal Engineering 29(5-6),957-965.

2. Sheik Ismail, L., Ranganayakulu, C. and Shah, R. (2009). Numerical study of flow patterns of compact plate-fin heat exchangers and generation of design data for offset and wavy fins. International Journal of Heat and Mass Transfer, 52(17-18), pp.3972-3983.

3. Pitla, S., Groll, E., Ramadhyani, S., 2002. New correlation to predict the heat transfer coefficient during in-tube cooling of turbulent supercritical CO2. Int. J. Refrigeration 25(7),887-895.

4. Wang, C., Chi, K. and Chang, C. (2000). Heat transfer and friction characteristics of plain fin-and-tube heat exchangers, part II: Correlation. International Journal of Heat and Mass Transfer, 43(15), pp.2693-2700.

Nottingham | UK | 9–11 September 2019

Using frequency-weighted sums to project data into future scenarios: the case study of heating systems

Miquel Banchs-Piqué[1], Dr David J Hutchinson[2], Prof Victor Becerra[3], Prof Mark Gaterell[1]
[1] *School of Civil Engineering and Surveying, University of Portsmouth, Portsmouth, UK. ORCID: 0000-0002-9022-2453 - ORCID: 0000-0002-0504-4841*
[2] *Faculty of Technology, University of Portsmouth, Portsmouth, UK.*
ORCID: 0000-0002-0023-4689
[3] *School of Engineering, University of Portsmouth, Portsmouth, UK.*
ORCID: 0000-0002-3790-4236

miquel.banchs-pique@port.ac.uk

Abstract

Carefully planning the future of the building sector is key to mitigate greenhouse gas (GHG) emissions. The largest contributor of the building sector to GHG emissions is the energy used for space and water heating. Therefore, information on its possible future evolutions can be very valuable. Future scenarios can be used to investigate the behaviour of existing data into the future. Here, electricity demand data are projected to four distinct futures of the household's use of electric heating systems. The projection method used involves breaking the data into groups with similar characteristics which are then weighted according to their frequency in each scenario. These projections offer, however, only partial information about the possible evolutions of the residential energy demand, as they account only for changes in the type of heating systems used. This information could, together with a range of other projections, be used to improve the planning of the future residential sector.

Keywords: Future scenarios, foresight, data projection, frequency-weighted sum, household energy demand, heating systems.

1. Introduction

There exists consensus in the scientific community on the fact that climate change is human-made and driven by greenhouse gases (GHG) [1]. The UK has recently committed to net zero carbon emissions by 2050 [2] and it recognises that the built environment plays a crucial role in achieving this target [3]. The International Energy Agency estimates that the building sector needs to reduce its carbon dioxide emissions by 77 % compared to the 2013 baseline in order to achieve the goal to limit the temperature rise to 2 ºC [4]. Therefore, carefully planning the future of the building sector is key to mitigate greenhouse gas emissions.

However, development does not follow a linear path, which renders it impossible to predict the future [5]. If uncertainty is not taken into account in its design phase, a seemingly appropriate solution may stop delivering its advantages within its life-time if the future is different than anticipated. Scenario analysis can help avoid assets growing stranded and resources being lost by portraying a range of possible futures [6-8]. If a solution delivers its intended benefits in a wide range of sufficiently distinct future scenarios which extend to the extremes of plausibility, one can be confident that the solution is resilient [8].

One tool which is especially suited to study the future performance of interventions in the urban environment and, therefore, in the building sector, is 'Designing Resilient Cities' (DRC) [8]. DRC use the 'Urban Futures Method' [9] on integrated scenarios —considering major economic, social, cultural, institutional, technological and environmental questions at the same time— adapted to urban UK in 2050 [8,10]. These scenarios are based on those developed by the Global Scenarios Group, which are explorative scenarios covering a broad range of distinct futures [11]. They are logical and plausible evolutions from the world today and are internally consistent [12].

The projection of micro-data into scenarios is not common. A method to do this has been developed by Banchs-Piqué et al. in [13]. The core of this method are frequency-weighted sums of the average energy demand (or the value conveyed by the data in the general case) of different groups of households (or agents in the general case) to obtain the total average energy demand. With this method, by evaluating the frequency of each group in the data set and their evolution in each future scenario, one can obtain an approximation to the average energy demand in the different scenarios. These groups sort agents with similar features based on one variable; for example, for the variable *income*, households can be grouped by social class, or for the variable *household size*, households would be grouped according to the number of people forming the household.

This method can be used with scenarios described by a set of indicators of which at least some are related to the data intended to be projected. The data must include enough relevant metadata related to these indicators and the scenarios cannot be too disruptive to be able to obtain a projection. These projections simulate the behaviour of the data in the different scenarios one variable at a time. This paper provides a case study of the use of this method. The evolution of dwelling heating systems is chosen as a case study because the energy used for space and water heating is the largest contributor of the building sector to GHG emissions [14]. Therefore, information on its future evolutions can be very valuable and could be used to improve the planning of the future residential sector. The projections obtained with this method do not take into account any technological progress or any other future feature which is not conveyed by the scenarios. Additionally, the projection of dwelling heating systems is partial, as residential energy demand depends on many other variables other than the heating system used by the dwellings.

2. Data, scenarios and projections method

The data used for this case study are the household data obtained for the CER Smart Metering Project - Electricity Customer Behaviour Trial [15]. This trial took place between July 14 2009 and Dec 31 2010, and contains the power consumption data (in 30-minute intervals) and the answers to a pre- and a post-trial survey for around 3500 households in Ireland. The surveys convey information on the demographics of the households, which includes information about the heating systems they use.

The scenarios where these data are projected are the ones developed by DRC [8] and adapted by Banchs-Piqué et al. [7]. Their names, which give a good idea of their characteristics, are *New Sustainability Paradigm* (NSP), *Policy Reform* (PR), *Market Forces* (MF), and *Fortress World* (FW). Find a brief description of these scenarios in Table 1 and a complete one in [8]. The characteristics which the projections have to follow are these of the indicator *Use of electric space (and water) heating* from the extension of the DRC provided by Banchs-Piqué et al. [7] and found in Table 2.

Table 1: Brief description of the scenarios from Designing Resilient Cities (DRC) [8].

NSP	**PR**	**MF**	**FW** (rich 35:65 poor)
An ethos of 'one planet living' facilitates a shared vision for more sustainable living and much improved quality of life. New socio-economic arrangements result in changes to the character of urban industrial civilisation. Local is valued but global links also play a role. A sustainable and more equitable future is emerging from new values, a revised model of development and the active engagement of civil society. *Key driver: Equity and sustainability*	Policy Reform depends on comprehensive and coordinated government action for poverty reduction and environmental sustainability, negating trends toward high inequity. The values of consumerism and individualism persist, creating a tension with policies that prioritise sustainability. *Key driver: Economic growth with greater equity*	Market Forces relies on the self-correcting logic of competitive markets. Current demographic, economic, environmental, and technological trends unfold without major surprise. Competitive, open and integrated markets drive world development. Social and environmental concerns are secondary. *Key driver: Competitive, open global markets*	Powerful individuals, groups and organisations develop an authoritarian response to the threads of resource scarcity and social breakdown by forming alliances to protect their own interests. Security and defensibility of resources are paramount for these privileged rich elites. An impoverished majority exists outside the fortress. Policy and regulations exist but enforcement may be limited. Armed forces act to impose order, protect the environment and prevent societal collapse. *Key driver: Protection and control of resources.*

The projections follow the method presented in Banchs-Piqué et al. [13]. The expression used to find the projections derives from expression (20) in [13] considering all corrections equal to 1 (the scenarios' characteristics indicate the magnitude of data values is constant):

$$\boxed{E^{Sc} = E_1 \cdot f_1^{Sc} + \cdots + E_i \cdot f_i^{Sc}} \tag{1}$$

Where E are average electricity demand per household, f frequency of the household group, Sc indicate scenario, and i indicate household group.

Table 2: Characteristics of indicator Use of electric (and water) heating from Banchs-Piqué et al. [7].

Metric Base (UK 2012)	NSP	PR	MF	FW
% of households using electric heating 8.5 % (2.2m households) gas: >80% other: ~10 %	⇑ There is a moderate increase in use of electric space heating.	⇑ There is an important growth in the use of electric heating, mainly incentivised by the government. Probably the increase is slightly smaller in electric water heating as technologies as solar thermal are normally not used for space heating.	⇑ There is a slow increase in the use of electric space and water heating systems.	⇑ | ⇓ The general trend is a decrease in the use of electric and space heating. However, it increases within the rich.

The heating systems used by the households in the data set are very mixed, including a large percentage of households using oil and solid heating systems besides electric and gas systems. This is not ideal since the scenarios assume only one heating system per household, and electric and gas heating systems to be the norm in the base scenario, with the rest being mainly district heating which is not represented in the data. As the data projected are electricity demand data, and in order to follow the assumptions of the scenarios, the groups used for the projection sort households using electric central heating which do not also have gas, oil or solid heating systems (78 households, 7.03 % of the sub-sample), and households using gas heating which do not also have electric central or plug-in (1053 households, 92.97 %). The frequencies obtained for each future scenario are shown in Table 3.

Table 3: Household group frequencies for the projections.

Group	NSP	PR	MF	FW (rich | poor)
Electrical heating	0.432	0.355	0.202	0.228 | 0.039
Other heating	0.568	0.645	0.798	0.772 | 0.961

3. Projections

The projections of daily and total household electricity demand averaged for the period August 2009 – June 2010 for the sub-sample of the data set are shown in Table 4. And the daily electricity profiles for the same period, and for the summer and winter in the period, for both groups as in the sample, and the projections in the future scenarios are shown in Figure 1

Table 4: Daily and total household average electricity demand in a one-year period (August 2009 – July 2010) for the 'Electric heating' and 'Other' groups, the sub-sample of data, and the projections for all scenarios.

(kWh)	Electric	Other	Total data	NSP	PR	MF	FW
Daily average	12.58	10.96	11.08	11.66	11.54	11.29	11.13
Total average	4591	4001	4043	4256	4210	4120	4063

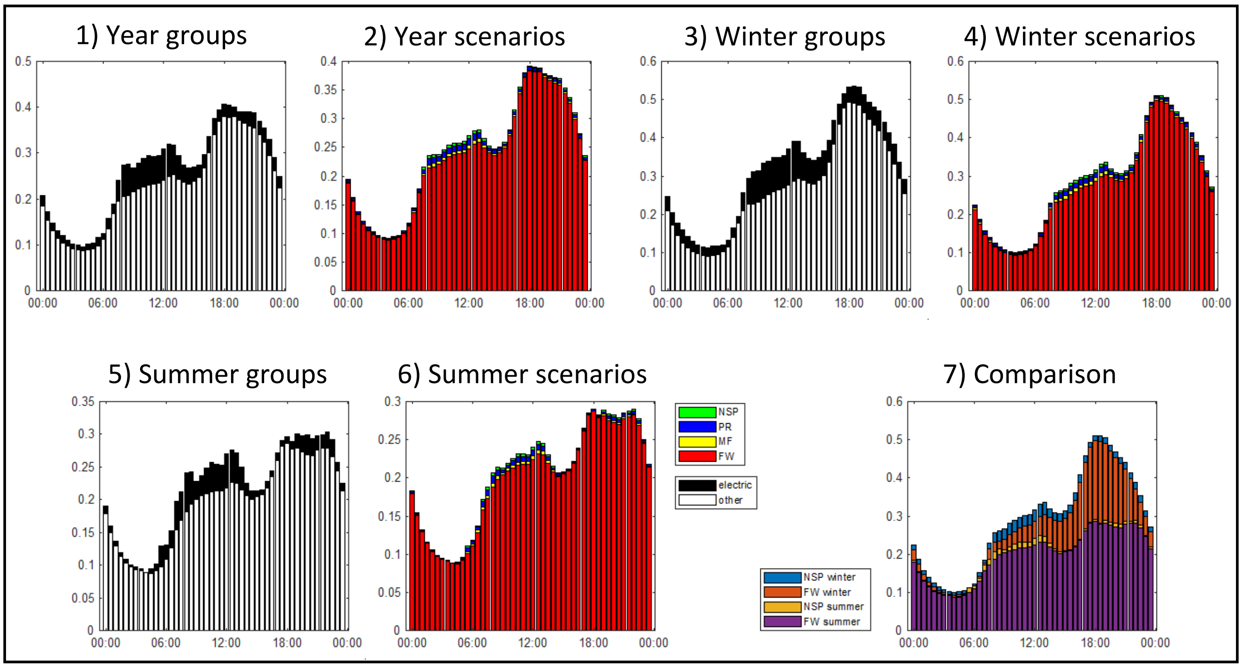

Figure 1: Average household electricity demand profile for different periods of time (year, winter and summer) for the data groups (black/white), the projections to the different scenarios (colours), and comparison between NSP and FW for winter and summer. Demand in kWh.

This figure also shows a comparison between the projections for NSP and FW (the two most different scenarios) in winter and in summer.

4. Discussion

As seen in parts 1), 5) and especially 3) from Figure 1, the difference in electricity demand between the group using exclusively electric heating systems and the group using gas (and no electric) heating systems is very small. Space heating is the largest contributor to household energy demand by far [14]. Therefore, the difference between these groups was expected to be much larger. This small difference translates in small differences between scenarios. The metadata used to sort the groups was obtained via very long telephone surveys. It is likely that a number of respondents were unsure of the heating systems their household use, giving unreliable information. Something similar happens with other not-straightforward questions from the survey, *i.e.* number of bedrooms has been used as proxy for dwelling size in [16] because the answers from the survey question about dwelling size are not reliable.

Even though the differences between scenarios are small one can see interesting outcomes: there is an increase in electricity demand in all scenarios, and the increase is larger the more sustainable the scenario is. This is because in NSP and PF energy use is heavily electrified (with electricity produced by no GHG generating means) in order to cut carbon emissions. The differences between scenarios are, as expected, larger in winter than in summer.

Although the data do not contain households using district heating, which appears in the (extended) characteristics of the indicator *Use of electric space (and water) heating*, this does not make the scenarios be too disruptive. This is because the data projected is electricity demand and, therefore, the relevant groups for these projections are those sorting households which use electric heating systems, and those which do not. The scenario FW can be seen as too disruptive because the data do not contain households in extreme poverty or in informal developments. However, these effects would be taken into account with the projection of a variable related to income. This, however, shows a disadvantage of this projection method: when a scenario is heavily shaped by one specific (group of) variable(s), the projections of other variables portray effects of very secondary order in comparison. This should be taken in consideration when combining a set of projections to obtain a meaningful picture of the scenario.

5. Conclusions

The projection method can effectively be used to project data in future scenarios. A single projection is, however, partial and should be combined with a range of projections representative of the properties of the scenarios. Yet, a single projection can convey interesting or counterintuitive information about the scenarios as seen with the increase of electricity demand the more sustainable a scenario is. This method relies highly in the quality of the data and metadata,

Acknowledgments

CER Smart Metering Project - Electricity Customer Behaviour Trial, 2009-2010 accessed via the Irish Social Science Data Archive - www.ucd.ie/issda.

References

1. Cook, J. et al. (2016). Consensus on consensus: a synthesis of consensus estimates on human-caused global warming. Environmental Research Letters, 11(4). https://doi.org/10.1088/1748-9326/11/4/048002
2. HM UK Parliament. (2008). Climate Change Act 2008 (2050 Target Amendment). HM Government.
3. Department of Energy and Climate Change. (2009). The UK Low Carbon Transition Plan: National strategy for climate and energy.
4. IEA (International Energy Agency). (2013). Transition to sustainable buildings: Strategies and opportunities to 2050. In Iea.Org. https://doi.org/10.1787/9789264202955-en
5. Schwartz, P. (1991). The Art of the Long View: planning for the future in an uncertain world. New York: Currency Doubleday.
6. Hunt, D. et al. (2012a) Scenario archetypes: Converging rather than diverging themes, Sustainability, 4(4), pp. 740–772. doi: 10.3390/su4040740.
7. Banchs-Piqué, M et al. (2019) Adapting futures scenarios to study household energy demand. Manuscript submitted for publication.
8. Lombardi, R. et al. (2012). Designing Resilient Cities: a guide to good practice. Bracknell: IHS BRE Press.
9. Rogers, C. et al. (2012) The urban futures methodology applied to urban regeneration, Proceedings of the Institution of Civil Engineers - Engineering Sustainability, 165(1), pp. 5–20. doi: 10.1680/ensu.2012.165.1.5.
10. Boyko, C. et al. (2012) Benchmarking sustainability in cities: The role of indicators and future scenarios, Global Environmental Change. Elsevier Ltd, 22(1), pp. 245–254. doi:
11. Raskin, P., Electris, C. and Rosen, R. (2010) The century ahead: Searching for sustainability, Sustainability, 2(8), pp. 2626–2651. doi: 10.3390/su2082626.
12. Gallopin, G. et al. (1997) Branch Points: Global scenarios and human choice, Stockholm Environment Institute.
13. Banchs-Piqué, M et al. (2019) Novel methodology to project data into scenarios. Manuscript in preparation.
14. Palmer, J. and Cooper, I. (2013) United Kingdom housing energy fact file, Department of Energy & Climate Change. doi: URN: 13D/276.
15. Commission for Energy Regulation (CER). (2012). CER Smart Metering Project - Electricity Customer Behaviour Trial, 2009-2010 [dataset]. 1st Edition. Irish Social Science Data Archive. SN: 0012-00. www.ucd.ie/issda/CER-electricity
16. McLoughlin, F., Duffy, A., & Conlon, M. (2012). Characterising domestic electricity consumption patterns by dwelling and occupant socio-economic variables: An Irish case study. *Energy and Buildings*. https://doi.org/10.1016/j.enbuild.2012.01.037

Nottingham | UK | 9–11 September 2019

Robust Controller Design for a Solar Powered Sustainable Energy System

Kary Thanapalan [*], Ewen Constant, Mark Bowkett

[*] *School of Engineering, Faculty of Computing, Engineering & Science, University of South Wales, Pontypridd CF37 1DL, United Kingdom*

E-mail: kary.thanapalan@southwales.ac.uk

Abstract

A self-sustainable energy system configuration is of interest to many groups and users, and as the supply of fossil fuels runs down they will have to become more widely used and accepted methods for energy capture, storage and use. This work intends to prove a more cost effective system other than grid connected systems that are available and provide cost effective solutions to consumers. This research investigates typical self-sustainable energy system configuration and looks to develop a performance optimisation model with robust controller design. The potential benefits of such a system design is investigated using data collected at three specific location and the performance of the system under variable conditions are determined. The work goes onto describe a robust controller design and implementation of an efficient self-sustainable energy system. The combination of solar PV cells combined with a battery energy storage system (BESS) carries great promise for cleaner, more efficient energy future. It allows domestic users the opportunities to significantly reduce their bills, carbon footprint and the payback periods for standalone solar PV systems and finally avoid the high costs of dynamic electricity pricing.

A photovoltaic array is considered as the main power source to the system. Solar PV systems are common and widely accepted in the UK, they provide the only realistic home energy generating possibilities for the majority of homeowners. A self-managed highly sustainable and environmentally sound approach for consumers to manage their energy will have a fundamental role to play in addressing issues of reducing cost and maximising self-sufficiency. It is important to note that the very long payback rates for solar PV systems, which is a hurdle to implementation. But, with the addition of BESS and the design of robust controller with optimal power management capability will reduce the payback period significantly.

Keywords: Energy storage, Energy Management, Sustainable energy system, Robust Controller, Energy consumption.

1. Introduction

Rapid growth in global energy demand coupled with limited supply of fossil fuels, calls for development of new self-sustainable renewable energy system. Renewable energy can be part of the solution to provide clean and sustainable energy supply. Furthermore, solar energy is a very promising renewable energy source to moderate the growth of energy demand. However, the inherent intermittency in most of the renewable sources causes problems for energy – on demand requirements. The combination of solar PV cells combined with a battery energy storage system (BESS) carries great promise for cleaner, more efficient energy future to compensate this problem. Renewable energy systems can be either standalone or grid connected. Recently, the development and application of such systems has increased significantly. A large body of research work addressed various topics for such systems, including modelling, simulation, optimisation, control and performance evaluation [1 – 2].

A typical system will have the following structure, which are PV modules, battery pack, energy management system and load [3]. This work is intends to prove a more cost effective system other than grid connected systems that are available and provide cost effective solutions to consumers. This research investigates typical self-sustainable energy system configuration and looks to develop a performance optimisation model with energy management controller. The potential benefits of such a system design is investigated using data collected at three specific location and the performance of the system under variable conditions are determined.

2. System Configuration

A structural block diagram for the solar energy system is shown in Fig.1. The system will have the following elements; PV modules, battery pack, energy management system and load [4].

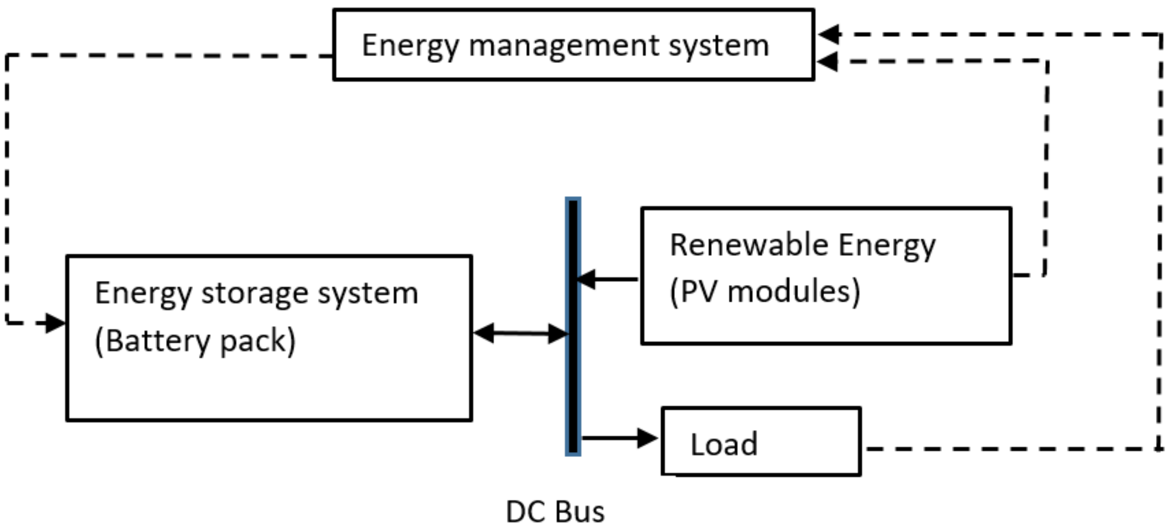

Fig.1. Solar powered sustainable energy and storage system

The solid arrows represent the electricity flow and the dotted arrow represent the control/sensor signals. A photovoltaic array is considered as the main power source to the system, which enables it to meet the load demand. Due to the inherent intermittency of solar irradiation, BEES is included, not only to smooth the fluctuation of the solar energy generated, when such smoothing is necessary, but when excess energy is available it will be stored in BEES. However, when there is a shortage of direct solar energy, the stored energy will be used.

The load characteristics selected for the energy management system (EMS) applied to a solar based renewable energy system were based on data collected from three distinct areas, Plymouth on the South West Coast of England, St Athan in the Vale of Glamorgan in South Wales and Nottingham in the North Midlands of England. The choice of location was to give a broad geographic spread to the sizing algorithms whilst validating the calculations. Authors, previous work [4] shows that, if the consumer stores the excess energy, and bills are calculated over a 12 month period, the cost of domestic energy bill can be reduced. It has been shown that in the South of England there is a break even point very close to 16 panels under idealised conditions. In the South Wales region, the bills can be reduced around £48/year and in the North Midlands of England, the annual bill may be reduced to around £115/year (see Fig.2). It should be noted that adding more panels to the system, may continue to reduce the overall cost to the consumer. It also highlights regional variations in the UK, primarily due to geographic changes in irradiance. It can be seen that with a 16 panel system, almost break-even on an annual basis in the South West of England, saving the consumer over £500/year in electricity. Whilst in Nottingham a 16 panel system has an annual cost of around £150, but only produces around £35 from FIT. However, this is still a significant saving over the approximate £630 of energy consumed every year. The overall payback periods can be constructed by considering the initial investment of the BEES. It is interesting to note that due to the regional variations in both solar irradiance, the amount of daylight per region and the electricity demand due to climate conditions, the payback period for the three regions chosen is similar (See Fig.3).

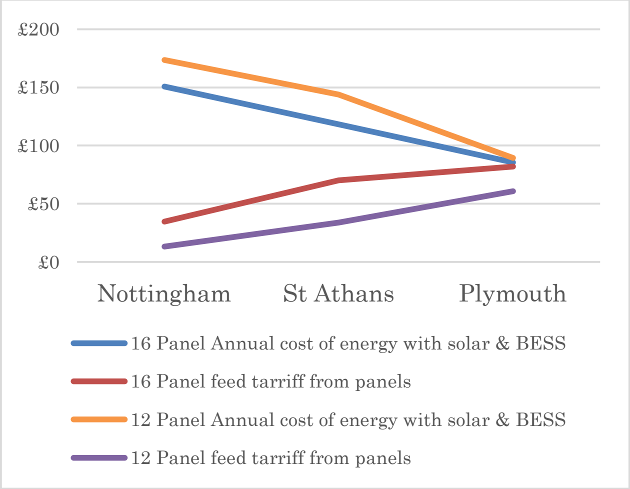

Fig.2. Cost analysis and break even indicator

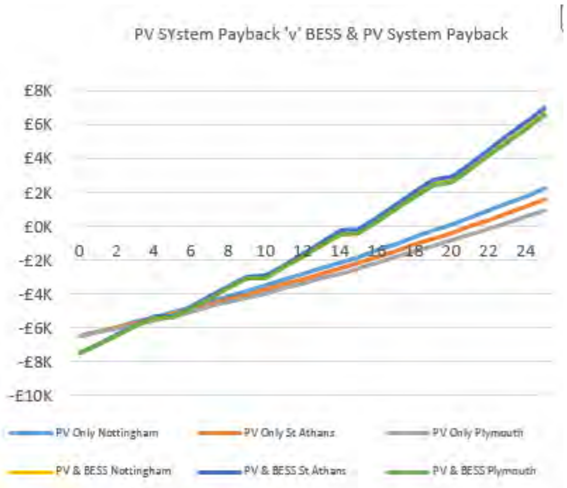

Fig.3. Payback periods

The payback period of a current solar powered system alone can be shown to be in the region of 21 years, this is primarily due to over production being fed in the grid, but with a BEES and Solar PV system, this can be reduced to 15 years. However, the key issue is that the development of a demand side management system (DSMS), that will be form a crucial part of the energy management control system. It will ensure the optimal energy management of the system.

3. Robust Controller Design

In this section, the design of controllers for renewable energy systems will be described, in particular for home energy system based on PV-BEES components. There are three major control subsystem loops in the system that regulates the energy demand / supply, the energy management and the energy storage. Several researchers have addressed EMS and the design and applications of renewable energy systems [5 - 8]. In this study, the target of the control strategy is to use the solar energy to meet the energy demand, then utilise any additional energy to maximise the storage and minimise the usage of battery at the same time. Therefore, the overall system's efficiency will be increased and lifetime of the battery pack will be extended. The operating strategies for energy management system are as follows; firstly, on the basis of the efficiency, the highest priority is to utilise solar power to satisfy the energy demand. If excess solar energy is available, it will be sent to BEES, which will be compressed and stored for future use in electrical energy generation. If there is still additional energy generated by the PV array, when the load demand is satisfied, the extra solar energy will be utilised to charge the battery, if the battery SOC is sufficiently low. If the energy generated by the PV array is insufficient to support the electrical energy demand, the different is to be supplied by the BESS, hence provide a short-term compensation. It should be noted that with carefully selected system components, all the energy generated by solar PV array will be used either to support the load demand, or to charge the battery pack. The required control objects are governed by two-input-one-output fuzzy logic controller. The two inputs to the fuzzy logic controller are the differential energy flow (dE) and the battery's SOC. The differential energy flow represents the difference between available solar energy and the energy demand. The controller will use this information to decide whether excess solar energy is available for storage. The SOC input is used to maintain the battery's SOC at a desired level in order to prevent overcharging or overly deep discharge of the battery pack. The fuzzy mechanism consists of triangular membership functions for the two inputs and for the one output. The reason for choosing a triangular membership function is simplicity and ease of computation. The dE flow is divided into eight variables. A negative energy supply means that the battery is required to supply the difference and positive energy means additional solar energy can be used to charge the battery. The battery SOC is also described by three variables. It is desirable that the SOC be maintained within a region of between 50 ~55%. The rules of the fuzzy logic controller are presented in Table 1 and the definitions of the linguistic variables are elaborated in Table 2.

Table 1: Basic rules table of the fuzzy inference.

dE

		NL	NM	NS	Z	PS	PM	PL	PEL
SOC	L	NL	NL	NM	NS	Z	PS	PM	PL
	C	NL	NM	NS	Z	PS	PM	PL	PEL
	H	NM	NS	Z	PS	PM	PL	PEL	PEL

In Table 1, the top row of the table shows the differential of energy flow (dE) and the left column is the battery's SOC. The cells of the table at the intersection of rows and columns contain the linguistic value for the output corresponding to the first input written at the beginning of the row and to the value of the second input written on the top of the column. The rule output was defuzzified using a centroid computation.

Table 2: Linguistic variables in the fuzzy inference system

Linguistic	Linguistic meanings
NL	Negative Large
NM	Negative Medium
NS	Negative Small
Z	Zero
PS	Positive Small
PM	Positive Medium
PL	Positive Large
PEL	Positive extreme Large
L	Low
C	Correct
H	High

The results based on real data indicates that the proposed controller can direct the energy flow wisely between different elements such as load and battery, it is capable of meeting the daily energy demand and using the excess solar energy to store it while maintaining the battery’s health and stage of charge in a desired region in order to extend the lifespan of the BEES.

4. Concluding Remarks

This paper presented a solar powered self-sustainable energy system designed for domestic users. System sizing and cost analysis are carried out with reference to specific locations and the best configuration for the case has been identified. The system uses solar energy as a main energy source to meet the energy demand, and utilises the BESS to store excess solar energy. When required the stored solar energy will be used. The proposed robust (FL) controller determine the time to use the stored energy from BESS. The purpose of the controller is to maximise the usage of the solar energy and minimise the stored energy in BESS to increase the system’s efficiency and to extend the lifetime of the system. The analysis indicated that the controller was able to satisfy the energy demand and to store the excess energy when possible, while maintain the battery’s SOC/SOH at desired level.

5. References

[1]. Eroglu M, Dursun, E, Sevencan S, Song J, Yazici, S, and Kilic, O. A mobile renewable house using PV/wind/fuel cell hybrid power system. International Journal of Hydrogen Energy 2011; 32: 7985 – 7992.

[2]. Ziogou C, Ipsakis D, Elmasides C, Stergiopoulos F, Papadopoulou S, Seferlis P, and Voutetakis S. Automation infrastructure and operation control strategy in a stand-alone power system based on renewable energy sources. Journal of Power Sources 2011; 196:9488 – 9499.

[3]. Constant E, Thanapalan K, and Bowkett M. Optimal energy storage evaluation of a solar powered sustainable energy system. SICE-ISCS 2018 IEEE International Conference: 193 – 198; 2018.

[4]. Constant E, Thanapalan K, and Bowkett M. System sizing for solar powered sustainable energy system designed for domestic users Renewable Energy and Power Quality Journal 2019; 17: 254.

[5]. Cervin, A., Henriksson, D., Lincoln, B. and Arzen, K. Jitterbug and true time: analysis tools for real-time control systems. 2nd Workshop on Real-Time Tools, Copenhagen, Denmark, 2002.

[6]. Driankov, D. Fuzzy gain scheduling, in C. Bonivento, C. Fantuzzi and R. Rovatti (Eds.): Fuzzy Logic Control: Advances in Methodology, World Scientific, Singapore, 1998.

[7]. Astrom, K.J. and Wittenmark, B. Adaptive Control, 2nd ed., Addison-Wesley, Reading, MA., 1995

[8]. Zhao, Z., Xie, W.F. and Hong, H. A fuzzy optimal controller for the mechatronic system with non-smooth non-linearities’, Int. Journal of Advanced Mechatronic Systems, Vol. 1, No. 2, pp.90–99, 2008.

Nottingham | UK | 9–11 September 2019

Destressing yeast for higher biofuel yields

David J Timson[1] and Joshua Eardley[1],

[1]*School of Pharmacy and Biomolecular Sciences, University of Brighton, Huxley Building, Lewes Road, Brighton, BN2 4GJ. UK.*

d.timson@brighton.ac.uk

Abstract

Biofuels have the capacity to contribute to carbon dioxide emission reduction and to energy security as oil reserves diminish and/or become concentrated in politically unstable regions. However, challenges exist in obtaining the maximum yield from industrial fermentations. One challenge arises from the nature of alcohols. These compounds are chaotropic (i.e. causes disorder in the system) which causes stress in the microbes producing the biofuel. Brewer's yeast (*Saccharomyces cerevisiae*) typically cannot grow at ethanol concentration much above 15%(v/v). Mitigation of these properties has the potential to increase yield. Previously, we have explored the effects of chaotropes on model enzyme systems and attempted (largely unsuccessfully) to offset these effects by kosmotropes (compounds which increase the order of the system, i.e. the "opposite" of chaotropes). Here we present some theoretical results which suggest that high molecular mass polyethylene glycols may be the most effective kosmotropic additives in terms of both efficacy and cost. The assumptions and limitations of these calculations are also presented. A deeper understanding of the effects of chaotropes on biofuel-producing microbes is likely to inform improvements in bioethanol yields and enable more rational approaches to the "neutralisation" of chaotropicity.

Keywords: Bioethanol; kosmotropicity; chaotropicity; fermentation; biofuel yield; bioenergy

1. Introduction

Biofuels have the potential to replace fossil fuels in many applications. They offer considerable environmental advantages over fossil fuels since they are truly renewable and have lower overall net carbon dioxide emissions. Since the normal precursors are either crop plants or organic waste, these can be produced locally reducing the need to transport fuels over long distances. This has consequent benefits for the environment, the cost of the fuel and for energy security [1]. However, there are a number of problems with biofuels which may prevent their more widespread adoption. The reliance on crop plants means that there is the potential for competition between food and fuel uses of crops and the land used to produce them [1]. There are also several challenges in achieving high yields. These relate in part to difficulties in digesting some plant matter, notably celluloses and lignins [1]. This means that a substantial fraction of the carbon in the plants is not readily converted to fuel. The fuels themselves often inhibit their own production, by "poisoning" the microbes which are producing them. This "toxic" effect has a variety of causes, but a key issue is the chaotropicity of compounds typically used as biofuels, e.g. ethanol and butanol. This is recognised as a significant, limiting factor in maximising biofuel yields [2]. However, to improve the environmental and economic attractiveness of biofuels, yields need to rise. This paper focusses on some theoretical considerations in the mitigation of chaotropicity in the fermentation of ethanol by the baker's or brewer's yeast, *Saccharomyces cerevisiae*. Many of the issues considered will also apply to other biofuel fermentation processes.

2. Chaotropes and kosmotropes of relevance to biofuel fermentations

Chaotropes are compounds which increase the overall entropy of a solution [3]. This has particular relevance in biology since this tends to result in the disordering and unfolding of macromolecules and the disruption of biological membranes. Since cells rely on membranes to define their various compartments and biological macromolecules depend on their three-dimensional conformations for their correct activities and functions, chaotropes often cause generalised, non-specific toxicity to living systems. The molecular basis of chaotropicity remains uncertain, somewhat controversial and may vary with the chaotrope and the system being disrupted. It is clear that chaotropes cause disruption of the hydrophobic interactions which stabilise proteins, DNA and membranes. This is likely to be due partly to the increased system entropy reducing the entropic penalty for exposing hydrophobic residues to the bulk water and may also result from specific interactions between the chaotropic molecule and functional groups within the macromolecule [3,4]. Kosmotropes have the opposite effects. They reduce solution entropy and promote the ordering and rigidification of biological macromolecules.

The quantification of chaotropicity has not been straightforward. Given the links to entropic changes, entropies of solvation often correlate with the effects observed on phenomena such as protein stability [3]. However, the most extensive quantitative scale of chaotropicity available to date is based on an empirical measure, changes to the gelling temperature of agar. This scale can be used with almost any water soluble compound and has been applied to salts, small organic molecules and macromolecules such as (poly)ethylene glycol (PEG). It spans a wide range of values of chaotropicity (positive) and kosmotropicity (negative). Values around zero are considered to be “neutral” [3].

The products of biofuel fermentations are typically chaotropic, for example ethanol (molar chaotropicity 5.93 kJ kg^{-1}) and butanol (37.4 kJ kg^{-1}). Microbial cells naturally mitigate the effects of chaotropicity by producing compatible solutes, many of which are kosmotropes. These include trehalose (-10.6 kJ kg^{-1}), betaine (-25.5 kJ kg^{-1}), proline (-5.8 kJ kg^{-1}) and glycerol (1.1 kJ kg^{-1}) [3]. This raises the interesting hypothesis that it may be possible to regulate the chaotropicity of biofuel fermentations by the addition of kosmotropic solutes. This would be analogous to the regulation of the pH of fermentations by the addition of acids and bases. Ideally it would be possible to predict the effects of kosmotrope addition (just as it is with acid/base addition). To do this, it is necessary to understand how to calculate the net chaotropicity of a mixture of chaotropic and kosmotropic compounds.

3. The problem with glycerol

Although glycerol is commonly produced by microbes as a compatible solute, it is not a kosmotrope. On the agar gel point scale, it is mildly chaotropic at moderate concentrations (<5 M) and more chaotropic at higher concentrations [3]. This suggests that its mode of action is not through the direct “neutralisation” of chaotropicity, but perhaps through more direct interactions which stabilise biological macromolecules. It also suggests that its chaotropicity is not a linear function of its concentration. While this effect has not been observed with other compounds, the limited state of our knowledge means that this possibility cannot be ruled out. Non-linear relationships between concentration and chaotropicity would considerably complicate any calculations of net chaotropicity and thus the practicalities and economics of using this in commercial biofuel fermentations.

4. Quantification of chaotropicity – some assumptions and conclusions of relevance to biofuels

In calculating net chaotropicities, we make two assumptions. First, we assume that there is a linear relationship between chaotropicity and concentration. This means that the chaotropicity of any concentration of a compound can be readily calculated from the molar chaotropicity. We also assume that chaotropicities (and kosmotropicities) are additive. In other words, if we have two compounds in solution, with one compound contributing a chaotropicity of X kJ kg^{-1} and the other Y kJ kg^{-1}, the net solution chaotropicity should be

X+Y kJ kg^{-1}. This follows from the assumption of linearity of the relationship between chaotropicity and concentration. It is based on an underlying assumption that the molecular mechanism of chaotropicity is essentially the same for all compounds. It also assumes no significant interactions between the two types of molecule in solution which might affect their chaotropic effects.

Bioethanol fermentations rarely proceed beyond around 15%(v/v) ethanol. This represents the concentration at which yeast cells cease to function. (Note, that yeast cells are remarkably well adapted to functioning in relatively high ethanol concentrations compared to most microbes. This is one feature which has led them to be considered “microbial weeds” [5]). A concentration of ethanol of 15%(v/v) is equal to a molar concentration of 2.6 M and, therefore, to a solution chaotropicity of 15.2 kJ kg^{-1}. To return this value to “neutral” would, assuming that chaotropicities are additive, require the addition of a kosmotropic compound at a concentration which has a chaotropicity of -15.2 kJ kg^{-1}. This could be achieved by adding 0.23 M ammonium sulphate, 0.60 M betaine, 2.6 M proline, 1.0 M PEG 200, 0.12 M PEG 1000 or 0.02 M PEG 6000. However, experimental investigations suggest that the situation is more complex. Attempts to offset the chaotropic effects of alcohols on the enzyme β-galactosidase were largely unsuccessful. Indeed, when used on their own, all of the kosmotropes tested also inhibited the enzyme to similar extents to the chaotropic alcohols [6]. Similar results have been obtained in a yeast model in which the effects of chaotropes, kosmotropes and mixtures thereof on growth were tested (JE and DJT, manuscript in preparation).

5. The economics of kosmotrope addition

If kosmotropes are to be added to biofuel fermentations, it will need to make sense economically as well as scientifically. There would be little point in adding expensive, additional reagents for a marginal increase in yield. This means that we need to consider the cost per unit kosmotropicity (Table 1). This calculation suggests that ammonium sulphate or PEG 6000 would be the best additives to consider in commercial fermentations. However, it should be noted that this calculation is based on current prices (with no allowance for commercial pricing or deals for large orders) and further assumes (unrealistically) that prices would be unchanged in the event of considerably increased demand for a compound from the biofuel industry. Nevertheless, the rankings presented here are likely to be broadly correct.

Table 1: Some costs per unit kosmotropicty *of compounds of relevance to the biofuel industry*

Compound	**Molar chaotropicty**[a] **kJ kg^{-1} mol^{-1}**	**Cost per unit kosmotropicity**[b] **(£ per kJ kg^{-1} mol^{-1})**
Betaine	-25.5	0.58
Proline	-5.8	11.35
Trehalose	-10.6	46.89
Ammonium sulphate	-66.9	0.14
PEG 200	-15.0	0.84
PEG 1000	-126	0.29
PEG 6000	-659	0.16

Notes: [a] *Values from ref [3]; a negative value for chaotropicity represents a kosmotropic compound.* [b] *Prices from the current Sigma-Aldrich price list (www.sigmaaldrich.com/catalog/) as of 28th April 2019.*

6. (Currently) unanswered questions

In addition to the problems noted above with the quantification of mixtures of chaotropes and kosmotropes, there are some other areas which require further elucidation. A greater understanding of the molecular basis of chaotropicity and kosmotropicity is required from experimental and *in silico* studies. The mode of action of glycerol also requires greater understanding. How ethanol’s chaotropic properties interact with its mildly hydrophobic properties also need to be explained. A method to measure experimentally the net solution chaotropicity would circumvent the need for calculating this value. This would require the invention of a chaotropicity meter, similar to instruments which measure pH or ionic strength.

7. Conclusion

There is scope to use kosmotropes as additives to mitigate the chaotropic effects observed in biofuel fermentation. However, much greater understanding of the mechanism of chaotropicity and the quantification of this phenomenon is required before this can be done rationally. Until then, it may be possible to develop empirical, “trail and error” methods which are specific to particular fermentation conditions.

Acknowledgments

JE thanks the University of Brighton and the Universities Alliance Doctoral Training Alliance for a PhD studentship. DJT acknowledges his long-standing collaboration with Dr John E

Hallsworth (Queen’s University, Belfast) who first encouraged him to think about problems of chaotropicity in cellular systems.

References

1. das Neves MA, Kimura T, Shimizu N, Nakajima M (2007) State of the Art and Future Trends of Bioethanol Production. Dyn Biochem Process Biotechnol Mol Biol 1:1-14
2. Cray JA, Stevenson A, Ball P, Bankar SB, Eleutherio EC, Ezeji TC, Singhal RS, Thevelein JM, Timson DJ, Hallsworth JE (2015) Chaotropicity: a key factor in product tolerance of biofuel-producing microorganisms. Curr Opin Biotechnol 33:228-259
3. Cray JA, Russell JT, Timson DJ, Singhal RS, Hallsworth JE (2013) A universal measure of chaotropicity and kosmotropicity. Environ Microbiol 15:287-296
4. Salvi G, De Los Rios P, Vendruscolo M (2005) Effective interactions between chaotropic agents and proteins. Proteins 61:492-499
5. Cray JA, Bell AN, Bhaganna P, Mswaka AY, Timson DJ, Hallsworth JE (2013) The biology of habitat dominance; can microbes behave as weeds? Microbiol Biotechnol 6:453-492
6. Bell AN, Magill E, Hallsworth JE, Timson DJ (2013) Effects of alcohols and compatible solutes on the activity of β-galactosidase. Appl Biochem Biotechnol 169:786-94

Nottingham | UK | 9–11 September 2019

Supervisory Optimisation of HVAC Control Systems for Demand Response

A. Akinkunmi Adegbenro [1], B. Michael Short [2]

[1&2] *Teesside University, School of Science, Engineering and Design*

Teesside University, TS1 3BX, UK

a.adegbenro@tees.ac.uk, m.short@tees.ac.uk

Abstract

Heating, ventilating and air-conditioning (HVAC) systems account for large proportion of energy consumption in buildings. Implementation of efficient optimization and control mechanisms has been identified as one crucial way to help reduce and shift HVAC systems energy consumption to both save economic costs and foster improved integration with renewables. This has led to the development of various control techniques, some of which have produced promising results. However, very few of these control mechanisms have fully considered important factors such as electricity time of use (TOU) price information, as well as occupant thermal comfort to effect cost savings in the operations of non-linear HVAC systems. In this paper, the use of a model predictive control (MPC) based optimizer for supervisory setpoint control in a demand response environment is investigated. The optimizer is designed to shift heating load (and hence electrical load) to off-peak periods and with sufficient regards for electricity costs, and generates a set-point trajectory for an inner loop HVAC controller. By combining the proposed mechanism with a previously proposed adaptive digital controller, it is found that significant energy saving and cost reduction can be achieved in comparison to a traditional on/off controller based HVAC system with a fixed setpoint temperature.

Keywords: HVAC; Optimisation; MPC; Energy; Demand Response

1. Introduction

Increase in the cost of energy as well as concerns about the environment have driven up interests in demand-based HVAC control. On average, heating ventilating and air-conditioning systems account for up to 40% of energy consumed in buildings [1], and in colder climates such as Canada, this can rise to as high as 60%. This significant share demonstrates the importance of implementing an effective control strategy for reducing cost and energy consumption of HVAC systems in buildings.

There are certain characteristics that render HVAC system control different and uniquely challenging in comparison to other processes. These include: nonlinear and time-varying dynamics, time-varying disturbances, and interacting and sometimes conflicting loops. Also, many processes in HVAC systems are slow moving with time delays. There are also constraints on the actuator rates and range limits [2].

Several methods have been developed or proposed for HVAC control, however traditional techniques such as thermostatic on/off and PID controllers are still the most widely used [3]. Other more sophisticated approaches have been found in literature, including nonlinear controller [4], robust controller [5] and soft control techniques such as those based on fuzzy logic [6] as well as artificial neural network (ANN).

Another control algorithm which has gained popularity in recent years for HVAC control is model predictive controller (MPC). This is because it offers solutions to some of the aforementioned challenges of HVAC control and can be deployed for multivariable control as well as handle time delays and actuator constraints. It also uses cost function and optimisation techniques to achieve multiple objectives. However, more importantly for the purpose of this study, MPC can be used in both local and supervisory level of HVAC control.

In this paper, we implemented a MPC-based supervisory setpoint control in conjunction with a previously proposed digital adaptive controller. Unlike classical controllers, the adaptive controller developed in [7] eliminates the need to retune controller parameters because of changes to operating conditions, whilst producing faster response with smaller overshoot than regular adaptive PI/PID controllers do. The controlled process is initially assumed to be a first-order system with no delay. The motivation for this is that we were able to initially simplify the process of developing the optimizer and verify its operation, before extending its application towards more complex building HVAC systems in a future work.

The rest of the paper is structured as follows. Section 2 provides a brief description of the system and the mathematical models used. It also provides necessary details of the cost function and weightings. Results of simulations are presented and analysed in section 3, while in section 4, the paper is concluded with recommendations for future work.

2. System description and mathematical modelling

The supervisory control architecture uses a hierarchical structure, with a supervisory optimiser at the upper level and a local digital adaptive controller. A schematic diagram of the supervisory architecture is shown in figure 1.

The supervisory MPC is fed with (known or estimated) energy costs and measured temperature as inputs (incorporation of weather forecast information is possible and forms future work). These form part of the objective function that is used to minimise overall energy and thermal costs over a finite future time horizon. A temperature setpoint is generated during optimisation and sent to the localised adaptive controller. The MPC optimiser continues iterating until a setpoint trajectory that produces the least cost is found.

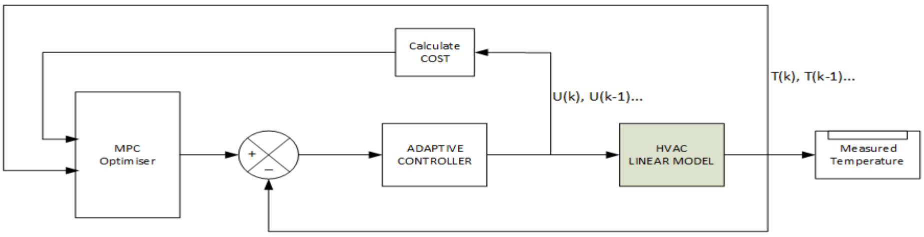

Figure 1: Supervisory MPC plan

2.1. Digital Adaptive controller

The digital adaptive controller was previously described in [9], and referring to figure 2, specifies a digital feedback control law given by:

$$D(z) = \frac{K_p A(z)}{P(z) - K_p B(z)} \tag{1}$$

Where z is the shift operator, $P(z)$ is a monic polynomial which specifies the closed-loop poles to meet the designer's requirements, with $B(z)$ and $A(z)$ being the numerator and denominator polynomials of the process model G(z), estimated online using the recursive least squares (RLS) method. The scalar $K_p = P(1)/B(1)$ to ensure on offset-free control in the closed-loop.

2.2. HVAC process models

If measured temperature, T is the output of the closed loop system, then we can describe the HVAC process around a local operating point by the simple first-order transfer function below:

$$G_{cl} = \frac{T(s)}{R(s)} = \frac{K_s}{s\tau+1} \tag{2}$$

If sampling time is set to T_s, the z-transform of the above transfer function can be expressed as:

$$G_{cl}(z) = \frac{T(z)}{R(z)} = z\left(\frac{1-e^{Ts}}{s} \cdot \frac{K_s}{s\tau+1}\right) = \frac{b}{1-az^{-1}} \tag{3}$$

Where $a = e^{-T_s/\tau}$ and $b = K_s\left(1 - e^{-T_s/\tau}\right) = K_s(1-a)$. If control law (1) is applied to this process, with $(z) = 1\ pz^{-1}$ to give a controllable closed-loop lag response, then the closed loop becomes:

$$G_{cl}(z) = \frac{T(z)}{R(z)} = \frac{1-p}{1-pz^{-1}} \tag{4}$$

Then we can write a difference equation relating temperature to setpoint changes as:

$$T(k) = pT(k-1) + R(k)(1-p) \tag{5}$$

With $R(k)$ the reference setpoint. Energy consumed can be estimated as the product of the controller output, $u(k)$, heater power rating, W_{heater} and the electricity time of use cost, E_{TOU}. The controller output can be estimated as described below. From figure 2, we can deduce that:

$$\frac{U(z)}{R(z)} = \frac{D(z)}{1+D(z)G(z)} \tag{6}$$

As $G(z) = \frac{B(z)}{A(z)}$ and the digital controller $D(z)$ is as described in (1), then (6) can be rewritten as below.

$$\frac{U(z)}{R(z)} = \frac{K_p A(z)}{P(z)} \tag{7}$$

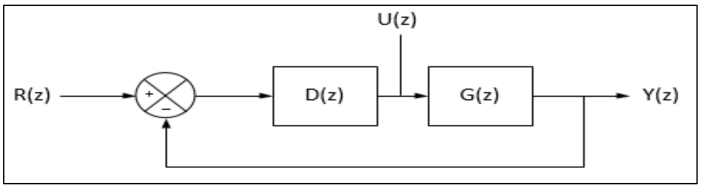

Figure 2: Closed loop block diagram

Also, as $P(z)$ is specified as above, and we extend the parameters of $A(z)$ from (3), (7) becomes:

$$\frac{U(z)}{R(z)} = \frac{K_p[1-az^{-1}]}{1-pz^{-1}} \tag{8}$$

Then we can write a difference equation relating control signal to setpoint changes as:

$$U(z)(1-pz^{-1}) = R(z)K_p[1-az^{-1}]$$

$$U(k) = pU(k-1) + K_p[R(k)-(1-a)R(k-1)] \tag{9}$$

2.3. Objective function

The objective function can be derived as follows. Cost of energy consumed between the current time step *k* over a horizon of *m* steps:

$$E_c = \sum_k^{k-m}(U(k) \cdot W_{heater} \cdot E_{TOU}) \tag{10}$$

From a thermal comfort point of view, the nominal temperature is set at 22°C, while thermal cost is defined across an m-step horizon as:

$$T_c = \sum_k^{k-m}|T(k)-22| \tag{11}$$

Equations (5) and (9) are employed to predict temperature and applied controls across the prediction horizon. The objective function to be minimised by MPC optimiser can therefore be stated as (12). Weightings are added to determine relative importance between energy cost and thermal cost.

$$J = \sum(\lambda \cdot E_c + \gamma \cdot T_c) \tag{12}$$

Since the optimisation problem is linear in the decision variables $R(k)$, $R(k+1)$, … , $R(k+m)$, linear programming was applied for solving the optimisation problem. Representative hourly times of electricity price were obtained from the Nord Pool Spot Market – a leading online electricity trading platform. The prices were then interpolated at 15 minutes intervals over a 24-hour period. In our experiments, we varied the energy and thermal cost weightings in order to explore the capabilities of our supervisory optimiser. We first specified the energy cost weighting, λ as 50 and thermal cost weighting, γ as 1. Then λ was set to 5 and γ to 1. Both results were then compared to the characteristics of the system when operated in on/off mode with a fixed setpoint temperature. To simulate a traditional on/off fixed setpoint control scheme, a constant reference input of 22°C was passed to the inner loop throughout the 24-hour period

3. Results and Analysis

From figure 3a & 3b, it can be observed that the electricity price plot (black broken lines) had two peaks over the 24-hour period, with the peak price (£0.064/KWh) occurring at the 20:00 mark.

From figure 3a, we noticed that at weightings ratio 50:1 (blue plot), the optimiser quickly increased the inner loop setpoint around the 06:30 mark in anticipation of a peak price period, resulting in a noticeable spike in energy cost. However, this was compensated for later when energy consumption was kept fairly low during peak price period. Likewise at the 17:15 mark, another spike was seen just as price trend headed for another peak. Again, this was compensated for by a near-zero energy consumption immediately after. A close look at the optimiser's performance at weightings ratio 5:1 (green plot) and the fixed setpoint plot (red) shows a fairly moderate energy consumption rate throughout.

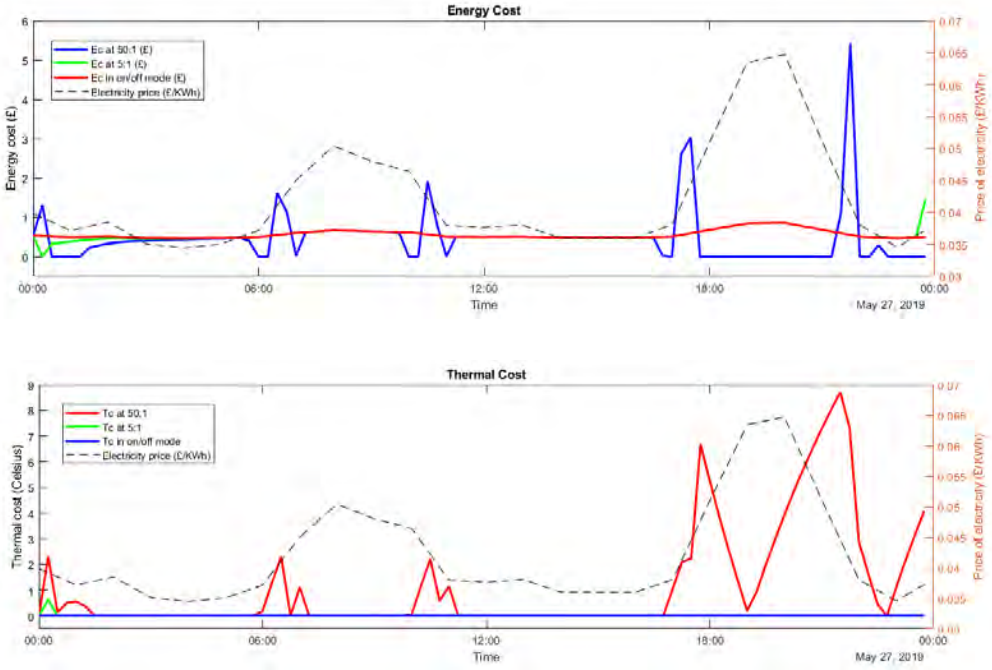

Figures 3a & 3b: Energy and thermal cost comparison of all three optimisation strategies

Overall in terms of the energy cost saving, the 50:1 weighted strategy clearly performed better than the other two. It costs 12% less to operate than the traditional on/off controller and approximately 7% less than 5:1 optimised strategy. On the other hand when comparing the thermal cost performances of all three optimisation strategies in figure 3b, it is no surprise that the fixed setpoint strategy performed the best. The 5:1 weighted strategy also did a good job keeping thermal cost as close to zero as possible. However due to the high cost saving emphasis placed on the 50:1 strategy, thermal comfort was significantly sacrificed especially around peak price periods.

4. Conclusion

In this paper, we presented a supervisory model predictive controller for a simplified HVAC system. For this purpose we incorporated factors such as thermal comfort and energy cost into a linear objective function and tested the performance of the supervisory MPC by varying energy and thermal costs weightings against a traditional on/off controller with fixed setpoint temperature. Trends observed suggested that by increasing the energy cost weighting and keeping the thermal cost weighting constant, we are able to save more money (even though this is achieved at the expense of the occupant thermal comfort). The MPC optimiser pre-empts periods of peak electricity prices and shifts heating load in order to minimise the total cost of energy used. This is particularly useful in demand response context, in that we are able to pre-arm our algorithm to respond to future DR events by taking actions such as preheating, precooling or storing heat energy for future use.

We made some assumptions and simplification in order to facilitate the development of our supervisory MPC; demonstrating our algorithm without these simplifications is part of our goals for future works. We would also like to incorporate weather data into our controller design in the future.

References

[1] A. Costa, M. M. Keane, J. I. Torrens, and E. Corry, “Building operation and energy performance: Monitoring, analysis and optimisation toolkit,” *Appl. Energy*, vol. 101, pp. 310–316, Jan. 2013.

[2] A. Afram and F. Janabi-Sharifi, “Theory and applications of HVAC control systems - A review of model predictive control (MPC),” *Building and Environment*. 2014.

[3] C. . Underwood, *HVAC control systems: modelling, analysis and design*. London: Taylor & Francis/Spon, 1999.

[4] H. Moradi, M. Saffar-Avval, and F. Bakhtiari-Nejad, “Nonlinear multivariable control and performance analysis of an air-handling unit,” *Energy Build.*, 2011.

[5] S. A. K. Al-Assadi, R. V. Patel, M. Zaheer-uddin, M. S. Verma, and J. Breitinger, “Robust decentralized control of HVAC systems using -performance measures,” *J. Franklin Inst.*, 2004.

[6] S. Soyguder, M. Karakose, and H. Alli, “Design and simulation of self-tuning PID-type fuzzy adaptive control for an expert HVAC system,” *Expert Syst. Appl.*, vol. 36, no. 3, pp. 4566–4573, Apr. 2009.

[7] A. Adegbenro, M. Short, and S. Williams, “Development of a Digital PID-like Adaptive Controller and its Application in HVAC systems,” in *Proceedings of the International Conference on Innovative Applied Energy*, 2019.

ICESF
Nottingham | UK | 9–11 September 2019

The Role of BIM Level 3 and Data Analytics in carbon emissions assessments for railway systems

Anderson Akponeware [1], Nashwan Dawood [1], Sergio Rodriguez [1], Huda Dawood [1]

[1] *Teesside University, School of Science, Engineering & Design, United Kingdom*

a.akponeware@tees.ac.uk

Abstract

Central to the UK government's carbon agenda is the drive to achieve an 80% greenhouse gas (GHG) emissions reduction target by 2050 through decarbonisation of constructed assets. Most studies in the construction management 'buildings' domain have focused on measuring the embodied, operational or life cycle carbon footprints of buildings using Building Information Modelling (BIM) integrated with emerging technologies. However, limited studies in the rail sector explore how energy efficiency assessments can be achieved through collection of carbon-based data in BIM or non BIM-based solutions thus hindering the efficient application of digital and integrative technologies by rail construction professionals to meet zero carbon targets. A systematic literature review (SLR) of the main areas of research interest in the energy efficiency domain for rail transport will identify research themes, methodologies and gaps that can be explored further to promote an energy-efficient rail infrastructure. The study therefore seeks to investigate current energy efficiency strategies in the rail industry to promote the development of a novel approach and platform, for the potential analytics of rail carbon data within open BIM. The findings will supplement current academic and industry efforts aimed at promoting energy efficiencies in rail assets through harnessing ubiquitous technologies that promote synchronous carbon data sharing in open BIM.

Keywords: energy efficiency, carbon footprint, LCA, low carbon, BIM, rail infrastructure

1. Introduction

The transport sector is a major contributor to GHG emissions with the industry's carbon emissions estimated to be 20% of global energy utilisation [1], making it the second most significant emitter of GHG emissions within the EU [2]. In particular, the annual GHG emissions from maintenance and renewal of UK's rail track is estimated to be between

430,000 – 934,000 tCO^2 [3]. Crucial policy changes are needed to decouple CO2 emissions to achieve the 1.5^0C and 2.0^0C pathways (Pan et al., 2018), which explains while the UK government's infrastructure agenda aims at achieving an 80% GHG emissions reduction target by 2050 [4]. It has been suggested that estimating carbon-related emissions is crucial to understanding GHG impacts in rail projects [5]. This therefore necessitates the incorporation of a systematic carbon emissions assessment method for the rail industry.

2. Methodology and research methods

This paper adopts the SLR approach and the method is summarised and described below.

2.1 Summary of the Systematic Literature Review: stages and implementation

The SLR was done across five stages as shown in figure 1 below.

Figure 1: SLR stages of the study

2.2 Extraction of papers and search strategy (planning and searching)

A review protocol was designed for the SLR which informed the search strategy used for the study. The adopted search strategy is shown in figure 2 below. The main inclusion criteria were: i) studies within 2012 – 2019; ii) studies in English, iii) papers addressing the research objectives, and iv) journals, conferences and reports. The main exclusion criteria were: i) books, ii) papers outside the transportation domain and iii) papers that exclude emissions assessments. The study's objectives and the selected SLR papers are shown in appendix 1 and 2 respectively.

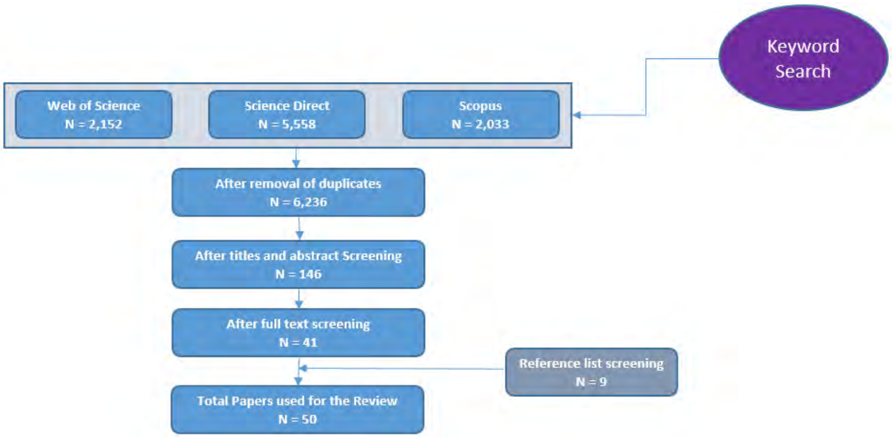

Figure 2: SLR stages of the study

3. Results and Discussion (data evaluation and reporting)

Descriptive and content analysis were employed in systematically analysing the papers.

3.1 Descriptive Analysis

In terms of the location of the studies, 22% were UK-based while 14% were from the U.S. The remaining 64% of the papers are fairly distributed in about 16 other countries. Further analysis shows that the two major journals from which the selected papers were based are Transportation Research (18%) and Journal of Cleaner Production (22%). In addition, the 50 SLR papers consisted of 43 journal articles, 5 conference papers and 2 reports.

3.2 Content Analysis

3.2.1 Application areas and phases

A detailed analysis of the SLR papers revealed that 26% of the papers are integrated-based studies (vehicle and infrastructure footprints). The remaining 74% of the papers are a mix of tailpipe emission studies (50%) and infrastructure-focused studies (24%). Analysing the latter papers further reveal the following proportions: entire infrastructure, 4%; sleeper pads, 2%; track beds, 8%; tunnels, 2%; railway bridges, 2%; railway turnout systems, 2%; station buildings, 2% and railway – bridge transition zones, 2%. In terms of the application phases, the energy efficiency assessment methods were distributed as follows: 50% on whole of life; 10% on construction and operations; 4% on maintenance; 32% on operations and 2% on the design phase. 2% of the papers did not state the application phase of their studies.

3.2.2 Current approaches of carbon emissions assessment

To address the first objective of the SLR, (see appendix 1), the different approaches of carbon emissions assessments were reviewed and analysed. Assessment methods applied across the studies were further categorised into LCA and non-LCA approaches. The three LCA variants alongside their proportions identified across the studies were bottom-up LCA (38%), top-down LCA (18%) and hybrid LCA (18%). The non-LCA approaches identified were statistical modelling (12%) and system analysis (14%). To assess the trend of carbon assessment methods over time, the assessment approaches were then time-analysed. The results reveal a steady trend in the use of bottom up approaches over time. Interestingly, statistical modelling based studies were seen to have grown in popularity especially from 2018. In contrast, hybrid-based methods were only found within 2015 to 2017 in the papers analysed. A categorisation of the research methodologies, emissions assessment methods and validation techniques employed in the SLR is shown in table 1 below. The table shows the popularity of validation techniques employing comparative and sensitivity analysis.

Table 1: Methodologies, assessment techniques and validation methods across studies

Categorisation of methodologies, emissions assessment techniques and validation methods used across studies			REFERENCES																																																	
			Vandanjon et al.(2012)	Westin and Kågeson (2012)	Chan et al.(2013)	Du and Karoumi (2013)	HM Treasury (2013)	Chester et al. (2013)	Kimball et al.(2013)	Pietzcker et al. (2014)	Bhandari et al.(2014)	González-Gil et al. (2014)	Esters and Marinov (2014)	Nahlik and Chester (2014)	Duan et al. (2015)	Pero et al. (2015)	Banar and Özdemir (2015)	Douglas et al. (2015)	DiDomenico and Dick (2015)	Yue et al. (2015)	Andrade and D'Agosto (2016)	Andrade and D'Agosto (2016b)	Cuenot (2016)	Fernández et al (2016)	Barrientos et al. (2016)	Saxe et al. (2016)	Powell et al. (2016)	Chester and Cano (2016)	Menezes et al. (2017)	Meynerts et al. (2017)	Dimoula et al. (2017)	Bizjak et al.(2017)	Bueno et al. (2017)	Dalkic et al. (2017)	Miah et al. (2017)	Krezo et al (2018)	Pan et al. (2018)	Fan et al. (2018)	Siskos et al. (2018)	Shinde et al.(2018)	Bressi et al. (2018)	Alfieri et al. (2018)	Bressi et al. (2018b)	Rocha et al. (2018)	De Martinis and Corman (2018)	Ortega et al. (2018)	Pritchard and Preston (2018)	Kaewunruen and Xu (2018)	Ghofrani et al. (2018)	Zhu et al. (2019)	Martínez Fernández et al. (2019)	Kaewunruen and Lian (2019)
Research Methodologies		Case Studies			X	X	X		X					X					X	X	X			X			X	X		X		X										X		X	X	X	X			X		
		Literature / Doc Survey					X					X	X					X							X		X		X		X									X									X		X	
		Content Analysis																					X				X																						X			
		Field data collection	X					X					X									X														X		X														
		Interviews					X				X											X												X		X		X														
		Computational Modelling		X				X		X			X		X	X	X			X	X	X		X	X				X				X	X		X	X	X	X		X	X	X	X	X	X	X	X			X	X
		Exploratory																								X									X																	
Emissions Assessment Methods	LCA BASED	Bottom up / LCA	X	X	X	X	X		X						X	X															X		X							X	X		X			X		X				X
		Top-down / Input-Output						X		X	X		X	X							X								X					X		X	X										X					
		Hybrid LCA															X			X		X	X		X	X		X		X					X																	
	NON LCA	System Analysis method	X									X						X	X								X											X	X			X										
		Statistical Modelling																						X																				X	X				X	X	X	
Validation Methods in Studies		Comparative Analysis				X		X			X		X	X			X		X				X				X					X		X		X	X			X	X	X										
		Case study Validation			X																			X																				X	X	X		X				
		Sensitivity Analysis		X					X						X	X				X	X	X			X				X				X										X									
		Expert Judgement					X																																													
		Methodology Implementation																																																X		
		Experimental Validation	X																																																	

3.2.3 Use of BIM in emissions assessment

BIM use in carbon emissions assessment was analysed across the studies to address the second research objective. The results show that non-BIM based assessment methods were predominant in the studies analysed. Only 4% of the studies adopted BIM as a sustainability assessment in carbon footprinting for rail infrastructure. In these studies, carbon emissions assessment was applied as the 6D maturity level. In addition, only 2% of the studies suggested the use of open BIM via co-creation as a carbon assessment strategy. However, the results suggesting BIM use in LCA analysis were basic and did not describe an actual BIM-enabled carbon assessment technique.

3.2.3 Use of data analytic technique in emissions assessment studies

To address the third research objective, a detailed analysis was conducted to assess the use of data analytics in carbon emission studies. The studies reviewed showed a direct correlation between studies employing statistics and those using data analytics. Nevertheless, the use of analytics was still limited as only 10% of the studies reported the use of analytics. Of this proportion, deep learning, meta-heuristics and neural networks were adopted in 2%, 3% and 5% of the studies respectively. The analytics software used in these studies included MapReduce, Tashi cloud middleware, MATLAB, Apache Hadoop and MongoDB amongst others. Data collection were facilitated with the use of video, GPS, autonomous vehicles, road-side sensors, smart cards and drones.

4. Conclusion and recommendations

Research findings to date from the study reveal little agreement among researchers on the appropriate energy efficiency quantification methodology in the rail sector. Although, as shown in table 1, bottom up LCA approaches are more popular (38%), the use of statistical modelling is gaining popularity among researchers in recent times. This has been facilitated with innovations in infrastructure-based technological solutions with important implications for carbon emissions measurement. Although, BIM is often viewed as a game changer for the construction industry, it was found that the capability of BIM is under-explored in carbon emission studies. Despite BIM’s capability to improve decision-making in the design phase of infrastructure projects, only 2% of the papers focused on the design phase.

Also, there is a notable paucity of scientific literature focusing on implementing the capital carbon (CapCarbon) and operational carbon (OpCarbon) methodology which can be integrated in BIM-based carbon emission assessments. Already, several decision points between the briefing and the design phases are available in [4] which are viable points to feed carbon data within BIM to facilitate the selection of low carbon infrastructure solutions. This explains the trend in the recent popularity of statistical modelling techniques as larger amounts of data can now be collected in rail sites by sensors, smart cards and drones. Howbeit, data analytics have been applied in accident analysis, traffic flow prediction, services planning and asset maintenance in the selected SLR papers, its suitability in carbon footprinting remain unexplored in literature. Therefore, the required data points or data robustness needed for data analytics of carbon emissions data is unconfirmed. This lack of academic-led inquiries into how the industry can achieve low carbon footprints through collection, analysis and use of BIM-integrated carbon data could have negative implications and potentially derail its focus towards achieving the 2050 carbon targets. The following recommendations are therefore provided:

I) LCA estimation process need to be holistically applied simultaneously with the planning and design process so that the carbon estimation process is part of decision-making.

II) It is suggested that data analytics be explored further in carbon emission studies to facilitate the integration of ubiquitous technologies in the infrastructure domain.

III) There is urgent need for the scientific community to promote BIM-based studies on carbon footprinting.

References

1. Ceylan H, Haldenbilen S, Baskan O (2008) Transport energy modeling with meta-heuristic harmony search algorithm, an application to Turkey. Energy Policy 36 (7):2527-2535
2. Pero FD, Delogu M, Pierini M and Bonaffini D (2015) Life Cycle Assessment of a heavy metro train. Journal of Cleaner Production 87:787–799
3. Milford R, Allwood J (2010) Assessing the CO_2 impact of current and future rail track in the UK. Transportation Research Part D 15(2):61-72
4. BSI (2016) PAS 2080:2016 Carbon Management in Infrastructure. BSI Standards Limited, London
5. Saxe S, Casey G, Guthrie P, Soga K and Cruickshank H (2016) Greenhouse gas considerations in rail infrastructure in the UK. Proceedings of the Institution of Civil Engineers - Engineering Sustainability 169(5):171-180.

Appendix 1 - Research objectives refined through the SLR review planning

I). To classify current approaches of measuring energy efficiency of rail systems

II). To assess the use of BIM level 3 in carbon emissions assessment

III). To assess the use of data analytics in carbon emissions assessment

IV). To provide recommendations aimed at promoting efficient carbon assessment techniques for the rail industry

Appendix 2 – The SLR papers used for the review

Author(s)	Title	Year	Type
Vandanjon, P.O., Coiret, A., Muresan-Paslaru, B., Fargier, A., Bosquet, R., Dauvergne, M., Jullien, A., François, D., Labarthe, F.	Practical guidelines for Life Cycle Assessment applied to railways project	2012	Conference
Westin, J. and Kågeson, P.	Can high speed rail offset its embedded emissions?	2012	Journal
Du, G., and Karoumi, R.	Life cycle assessment of a railway bridge: comparison of two superstructure designs	2013	Journal
Kimball, M., Chester, M., Gino, C. and Reyna, J.	Assessing the Potential for Reducing Life-Cycle Environmental Impacts through Transit-Oriented Development Infill along Existing Light Rail in Phoenix	2013	Journal
Chan, S., Miranda-Moreno, L. and Patterson, Z.	Analysis of GHG Emissions for City Passenger Trains: Is Electricity an Obvious Option for Montreal Commuter Trains?	2013	Journal
Chester, M., Pincetl, S., Elizabeth, Z., Eisenstein, W. and Matute, J.	Infrastructure and automobile shifts: positioning transit to reduce life-cycle environmental impacts for urban sustainability goals	2013	Journal
HM Treasury	Infrastructure Carbon Review	2013	Report
Nahlik, M. and Chester, M.	Transit-oriented smart growth can reduce life-cycle environmental impacts and household costs in Los Angeles	2014	Journal
González-Gil, A., Palacin, R., Batty, P. and Powell, J.P.	A systems approach to reduce urban rail energy consumption	2014	Journal
Esters, T. and Marinov, M.	An analysis of the methods used to calculate the emissions of rolling stock in the UK	2014	Journal
Pietzcker, R., Longden, T., Chen, W., Fu, S., Kriegler, E., Kyle, P. and Luderer, G.	Long-term transport energy demand and climate policy: Alternative visions on transport decarbonization in energy-economy models	2014	Journal
Bhandari, K., Advani, M., Parida, P. and Gangopadhyay, S.	Consideration of access and egress trips in carbon footprint estimation of public transport trips: case study of Delhi	2014	Journal
Pero, F. Del, Delogu, M., Pierini, M. and Bonaffini, D.	Life Cycle Assessment of a heavy metro train	2015	Journal
Duan, H., Hu, M., Zhang, Y., Wang, J., Jiang, W., Huang, Q. and Li, J.	Quantification of carbon emissions of the transport service sector in China by using streamlined life cycle assessment	2015	Journal
Banar, M. and Özdemir, A.	An evaluation of railway passenger transport in Turkey using life cycle assessment and life cycle cost methods	2015	Journal
Yue, Y., Wang, T., Liang, S., Yang, J., Hou, P., Qu, S., Zhou, J., Jia, X., Wang, H. and Xu, M.	Life cycle assessment of High Speed Rail in China	2015	Journal
DiDomenico, G. and Dick, C.	Methods of Analyzing and Comparing Energy Efficiency of Passenger Rail Systems	2015	Journal
Douglas, H., Roberts, C., Hillmansen, S. and Schmid, F.	An assessment of available measures to reduce traction energy use in railway networks	2015	Journal
Barrientos, F., Moral, A., Rodríguez, J., Martínez, C., Campo, F., Carnerero, R., Parra, M., et al.	Knowledge-based Minimization of Railway Infrastructures Environmental Impact	2016	Conference
Saxe, S., Casey, G., Guthrie, P., Soga, K. and Cruickshank, H.	Greenhouse gas considerations in rail infrastructure in the UK	2016	Conference
Powell, J., Batty, P., González-Gil, A. and Palacín, R.	Determining system-wide energy use in an established metro network	2016	Conference
Andrade, C. and D'Agosto, M.	Energy use and carbon dioxide emissions assessment in the lifecycle of passenger rail systems: the case of the Rio de Janeiro Metro	2016	Journal
Chester, M. and Cano, A.	Time-based life-cycle assessment for environmental policymaking: Greenhouse gas reduction goals and public transit	2016	Journal
Andrade, C. and D'Agosto, M.	The Role of Rail Transit Systems in Reducing Energy and Carbon Dioxide Emissions: The Case of The City of Rio de Janeiro	2016	Journal

Cuenot, F.	Carbon Footprint of Railway Infrastructure: Comparing existing methodologies on typical corridors. Recommendations for harmonized approach	2016	Report
Fernández, P., Román, C. and Franco, R.	Modelling Electric Trains Energy Consumption Using Neural Networks	2016	Journal
Meynerts, L., Götze, U., Claus, S., Peças, P. and Ribeiro, I.	Concept of Integrated Life Cycle Assessment and Costing – Application to the Case of Designing a Hybrid Train	2017	Conference
Bizjak, K.F., Knez, F., Lenart, S. & Slanc, K.	Life-cycle assessment and repair of the railway transition zones of an existing bridge using geocomposite materials	2017	Journal
Dimoula, V., Kehagia, F. and Tsakalidis, A.	A Holistic Approach for Estimating Carbon Emissions of Road and Rail Transport Systems	2017	Journal
Bueno, G., Hoyos, D. and Capellán-Pérez, I.	Evaluating the environmental performance of the high speed rail project in the Basque Country, Spain	2017	Journal
Miah, J., Koh, S. and Stone, D.	A hybridised framework combining integrated methods for environmental Life Cycle Assessment and Life Cycle Costing	2017	Journal
Dalkic, G., Balaban, O., Tuydes-Yaman, H. and Celikkol-Kocak, T.	An assessment of the CO2 emissions reduction in high speed rail lines: Two case studies from Turkey	2017	Journal
Menezes, E., Maia, A. and de Carvalho, C.	Effectiveness of low-carbon development strategies: Evaluation of policy scenarios for the urban transport sector in a Brazilian megacity	2017	Journal
Shinde, A.M., Dikshit, A.K., Singh, R.K. and Campana, P.E.	Life cycle analysis based comprehensive environmental performance evaluation of Mumbai Suburban Railway, India	2018	Journal
Ortega, A., Blainey, S. and Preston, J.	Assessing Whole-Life Carbon Footprint of Under Sleeper Pad Installation for Ballasted Track	2018	Journal
Kaewunruen, S. and Xu, N.	Digital Twin for Sustainability Evaluation of Railway Station Buildings	2018	Journal
Bressi, S., Santos, J., Giunta, M., Pistonesi, L. and Lo Presti, D.	A comparative life-cycle assessment of asphalt mixtures for railway sub-ballast containing alternative materials	2018	Journal
Bressi, S., D'Angelo, G., Santos, J. and Giunta, M.	Environmental performance analysis of bitumen stabilized ballast for railway track-bed using life-cycle assessment	2018	Journal
Krezo, S., Mirza, O., Kaewunruen, S. and Sussman, J.	Evaluation of CO2 emissions from railway resurfacing maintenance activities	2018	Journal
Alfieri, L., Battistelli, L. and Pagano, M.	Energy efficiency strategies for railway application: alternative solutions applied to a real case study	2018	Journal
Fan, Y. Van, Perry, S., Klemeš, J.J. and Lee, C.T.	A review on air emissions assessment: Transportation	2018	Journal
Siskos, P., Zazias, G., Petropoulos, A., Evangelopoulou, S. and Capros, P.	Implications of delaying transport decarbonisation in the EU: A systems analysis using the PRIMES model	2018	Journal
Pritchard, J. and Preston, J.	Understanding the contribution of tunnels to the overall energy consumption of and carbon emissions from a railway	2018	Journal
Pan, X., Wang, H., Wang, L. and Chen, W.	Decarbonization of China's transportation sector: In light of national mitigation toward the Paris Agreement goals	2018	Journal
Ghofrani, F., He, Q., Goverde, R.M.P. and Liu, X.	Recent applications of big data analytics in railway transportation systems : A survey	2018	Journal
De Martinis, V. and Corman, F.	Data-driven perspectives for energy efficient operations in railway systems: Current practices and future opportunities	2018	Journal
Rocha, A., Araújo, A., Carvalho, A. and Sepulveda, J.	A New Approach for Real Time Train Energy Efficiency Optimization	2018	Journal
Kaewunruen, S. and Lian, Q.	Digital Twin aided Sustainability-based Lifecycle Management for Railway Turnout Systems	2019	Journal
Zhu, L., Yu, F., Wang, Y., Ning, B. and Tang, T.	Big Data Analytics in Intelligent Transportation Systems: A Survey	2019	Journal
Martínez Fernández, P., Villalba Sanchís, I., Yepes, V. and Insa Franco, R.	A review of modelling and optimisation methods applied to railways energy consumption	2019	Journal

Nottingham | UK | 9–11 September 2019

Electricity Demand Forecasting in Decentralised Demand Side Response for Blocks of Buildings

A. Sean Williams [1], B. Michael Short [2]

[1-2] *School of Science, Engineering and Design,*

Teesside University, TS1 3BX, UK

sean.williams@tees.ac.uk

Abstract

A downturn of centralised conventional fossil fuel fired power plants and increased proportion of distributed power generation adds to the already troublesome outlook for operators of low-inertia energy systems. The role of an emerging decentralised energy sector allows separation of local energy needs from major power networks. However, the diversion of energy generation means diminishing levels of system inertia on the network needs to be better monitored and controlled. Reducing the overall energy consumption at times of peak demand through demand-side response (DSR) is conducive to intelligent use of electrical power. However, in the absence of reliable demand forecasting measures, effective decentralised demand-side energy planning is often problematic. In this work we formulate a simple yet highly effective approach for forecasting univariate quantitative time series by utilising electricity demand in a decentralised demand-side optimisation model. The forecasting session is constructed initially through analysis of a chronological sequence of discrete observations. Interpretations concerning the generalisation of demand data shows behaviour that allows symbolic representation of the time series. Calculation of short-term forecasting problems have been obtained. Results for medium-term forecasts that extend beyond 12-months are also very promising. In addition to motivating the construction of a forecasting method, the main intention of this article is to derive a practical solution that will evolve a novel proactive approach to existing demand response mechanisms.

Keywords: Demand Response, Decentralised, Time Series Forecasting.

1 Introduction

An energy transition is needed to address environmental challenges of greenhouse gas-induced warming and increased carbon emissions, which are largely driven by a rapid growth in global population [1]. Constructing energy systems into more sustainable forms means electricity demand forecasting is necessary. As a broad guideline, research has shown that energy consumption in buildings accounts for approximately 40% of the world's energy resources and emits circa one-third of greenhouse gases [2,3]. Considering the long lifespans and complex challenges associated with regeneration of old building stock [4], more accessible energy retrofit initiatives to achieve energy saving targets are needed. Tangible measures that improve energy efficiency include lifestyle changes, e.g. use of smart meters [5], and distribution system planning as well as improving load and resource forecasting methods and approaches [6].

Analysis of temporal data and development of prediction forecasting models are often presented as multivariate time series prediction problems [7–10]. However, multivariate time series considers simultaneous time-dependant variables where each variable depends not only on its past values but also has some dependency on other variables. Thus, multivariate prediction may prove difficult to extract enough meaningful information that is useful for predicting future states. In contrast, a univariate time series with a single time dependent variable, may offer an improved alternative when prediction time horizons are small [11].

In this paper, we propose a univariate time series electricity demand prediction forecasting methodology. This work has uniqueness by using techniques that are in part long established in data mining processes that aim to extract useable patterns in huge data sets [12]. Furthermore, the approach is developed on the premise that a forecasting session is dependent on a look up table derived solely from a univariate quantitative time series. Thus, making the opportunity to deploy the prediction algorithm on low software complexity platforms a viable option.

The rest of the paper is structured as follows. Section 2 provides a brief description of related work. Section 3 introduces the proposed methodology for demand prediction forecasting. Results and discussions are provided in Section 4. Finally, in Section 5, the conclusions are provided with recommendations for future work.

2 Related Work

A conceptual framework that places an energy optimisation system (EOS), designed to optimise energy consumption in blocks of buildings, makes use of decentralised grid frequency [13]. The conceptual framework promotes using a univariate quantitative time series to help in the restoration of frequency equilibrium during network stress events. As a prelude to using grid frequency, this paper details a demand prediction methodology developed to influence the EOS optimisation cost function. Using pattern sequence similarity to derive a series of demand prediction look up tables, setting a demand prediction model forecast horizon to 4-hours offers consumers an opportunity to participate in a decentralised proactive demand response mechanism. A generalised block diagram that shows the contribution of demand prediction is shown at Figure 1.

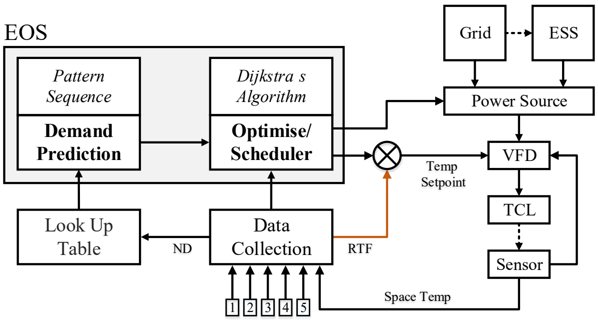

Figure 1 Information flow block diagram

3 Electricity Demand Time Series Forecasting Methodology

The proposed methodology is divided into two distinct parts. Analysis of a chronological sequence of discrete observations is first performed and the composition of the univariate one-dimensional time series is determined. In the second step, a dimensionality reduction technique is applied. The subsequent look up table allows the predictive forecast algorithm (PFA) to be deployed on inexpensive and low software complexity microcontrollers. The objective is to maintain an accurate 4-hour prediction horizon. However, results show this can be changed to much longer periods while maintaining competitive results.

3.1 Composition of Time Series

The Electricity System Operator (ESO) in Great Britain publishes historic national demand data [14]. The data represents the generation requirement and is the sum of metered generation recorded at 30-minute intervals. In this paper analysis is based on national demand data from 2005 to 2019; comprising 246,288 data items. The first task is to extract meaningful characteristics. Computing the autocorrelation of the time series identifies the periodicity of the signal. Figure 2 shows the time period between each peak is consistent with a typical weekly pattern consisting 5 similar weekday oscillations followed by 2 weekend day oscillations, also of similar form.

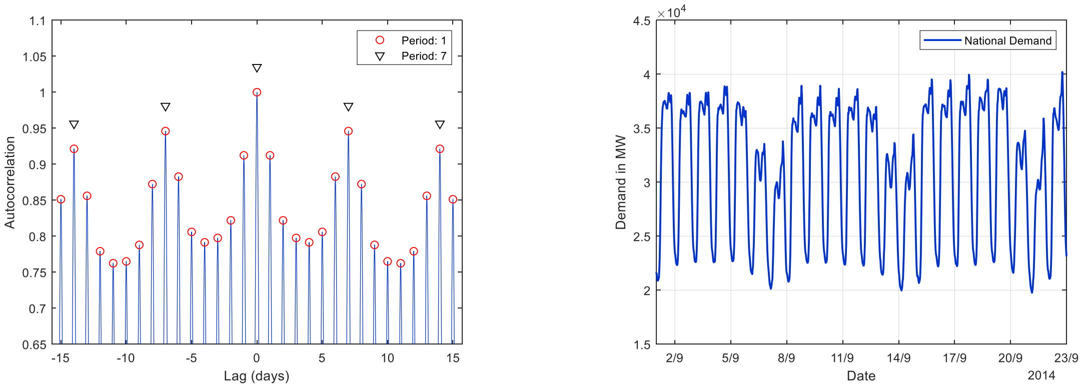

(a) (b)

Figure 2 (a) Autocorrelation shows weekly pattern, (b) UK National Demand profile

Regression is used to remove fluctuations in the time series and to identify potential seasonal and cyclic behaviour, that is regularly repeating patterns of highs and lows related to calendar time such as seasons, quarters, months and so on. The approach used to removing the trend from the time series first calculates the least squares regression line, then subtracts the deviations from the least squares fit line from the time series. Given the equation for a straight line is $y = bx + a$ where b is the slope of the line and a is the y-intercept, the best fit line for points $(x_1, y_1), \cdots, (x_n, y_n)$ is given by $y - \bar{y} = b(x - \bar{x})$ where

$$b = \sum_{i=1}^{n} (x_i - \bar{x})(y_i - \bar{y}) \,/\, \sum_{i=1}^{n} (x_i - \bar{x})^2 \tag{1}$$

and $a = \bar{y} - b\bar{x}$. In the absence of outliers, Eq. (2) is used to apply the min-max feature scaling which normalises the time series. Where the lower input range $l = 0$ and maximum of input range $u = 100$.

$$x' = l + [(x - x\text{min})(u - l)]/(x\text{max} - x\text{min}) \tag{2}$$

A set made up of 14 distinct weeks, where each week identified commences on the Monday immediately following the lowest recorded demand data in each year (2005 to 2019), is identified. A 3-dimensional array (9×48×14) that characterises the set, where each page represents 1 week, is subsequently created. Measurements recorded at 30-minute intervals for each day are assigned to columns 1 to 48; the mean value of rows 1-5 (weekdays) and rows 6 and 7 (weekend days) are assigned to rows 8 and 9 respectively. A mean value of rows 8 and 9 are then computed to enumerate a generalised demand profile shape for any weekday and weekend day respectively.

A simple moving average of order n process given at Eq. (3) smooths the original demand data; where n represents a set number of observations for one month and year respectively.

$$y_t = \frac{1}{n}\sum\nolimits_{i=t-n+1}^{t} y_i \tag{3}$$

Analysis reveals in addition to daily/weekly characteristics, the time series also displays seasonality and negative secular trend with constant variability. The general idea is to define a model from historical time series that enumerates the daily/weekly, seasonality and negative secular trend that can be used as part of the forecasting prediction algorithm. For seasonality, the basic route is to calculate the mean of each moving average 12-month period before applying a dimensionality reduction technique. Furthermore, in this strategy the negative secular trend is expressed in mathematical terms by using Eq. (1). Here, the coefficients for a polynomial that is a best fit (least squares method) of the given set of data are calculated.

The composition of the time series observed is characterised by 3 predominant features: (1) Day (weekday and weekend day), (2) Month and (3) Year. In the following subsections we first present a method to reduce time series feature dimensionality and then formulate the forecast prediction algorithm.

3.2 Dimensionality Reduction

Piecewise aggregate approximation (PAA), proposed by Keogh et al. [15], is a technique that reduces the dimensionality of a time series and for data representation. We choose to approximate the data with a piecewise coefficient such that the period between each change point is 2-hours. In this method, the normalised demand time series window of size n is first divided into k segments of equal length, and the average value of the data of the segments is then used as the representative value of each segment. Therefore, the demand time series PAA representation will be a k-dimensional vector $\bar{X}_i = \bar{x}_1, \dots, \bar{x}_n$ of the mean values of each segment. The dimensionality reduction calculation is computed by Eq. (4).

$$\bar{x}_i = \frac{k}{n}\sum\nolimits_{j=\frac{n}{k}(i-1)+1}^{\frac{n}{k}i} x_j \tag{4}$$

The equation provides the mean of the elements in the equi-sized frames which makes up the vector of the reduced dimensional time series. The method is applied to the *day* and *month* features. A numerical investigation comparing different piecewise coefficients confirms reduced dimensionality while preserving enough information about the original data.

3.3 Symbolisation of each PAA Segment

Having transformed the time series into segments using PAA technique, the data is discretized; grouping the continuous input into a finite number of discrete bins. The translation means the data dimensionality can be reduced further and converted into a symbol string using symbolic aggregate approximation (SAX), i.e. each region is assigned a symbol according to the determined change points. In the context of data mining, SAX is comparable to other techniques including discrete Fourier transform and discrete wavelet transform, while requiring less storage [16]. This strategy ensures the forecasting algorithm is more transferrable to low software complexity microcontrollers. In this work the SAX symbol string is a 4-bit binary representation of the discrete bin the continuous input was assigned after discretization.

3.4 Predictive Algorithm Look Up Table

As an alternative to making use of techniques based on pattern sequence similarity, the proposed methodology instead extracts singularities of bin data to create a series of look up tables (LUT). Given the length of each piecewise segment, the process of creating look up tables for weekday, weekend day and month PAX or SAX representations is straightforward. In this paper we present a LUT based on piecewise coefficient only. Assuming each PAA segment is 2-hours, a key observation is that the time series original 246,288 data items is reduced to 12 elements for each *day* and *month* feature (Table 1). To perform forecasting up to 1 calendar month requires weekday and weekend day LUT. Extending the time horizon further up to 12-months requires the month LUT, and beyond 12-months, a seasonal adjustment is required. The mathematical representation of seasonal adjustment is derived using a straight-line approximation of the 12-month moving average, i.e. $y = bx + a$ where $b = 0.000442$ and the y-intercept a, is set to the initial calculated weekday value.

Table 1 Piecewise Coefficient Look Up Table

Weekday	Weekend Day	Month
[15.34, 10.47, 24.00, 77.11, 95.94, 98.02, 93.98, 94.64, 96.79, 84.46, 73.32, 36.16]	[11.87, 3.80, 3.29, 29.24, 55.42, 60.76, 53.30, 51.31, 59.67, 58.02, 55.84, 28.58]	[40.11, 32.81, 30.23, 29.39, 29.00 34.97, 44.18, 57.63, 61.01, 65.00, 63.33, 53.23]

4 Results and Discussion

The above methodology has been applied to the UK electricity demand data (2005 to 2019). Figure 3 shows demand data after dimensionality reduction using PAA has been applied and where each region has been subsequently assigned a 4-bit binary representation of the discrete bin the continuous input was assigned after discretization. A visual representation of generalised weekday and weekend days are shown. The effect of SAX encoding reduces the weekday and weekend day LUT further from 12 elements to 7. Although discretization and SAX encoding offers the potential to reduce PAA dimensionality further, in the context of an EOS where a balance between accuracy and how easily the algorithm can be deployed to low software complexity microcontrollers, a prediction forecast based on PAA and discretization has the potential to offer greater benefit. In this instance encoding PAA bin categories to binary string format should be a straightforward task. Furthermore, applying a first-order edge-preserving filter to PAA data (Figure 3 (a)) provides a competitive smoother during transition from one frame to another.

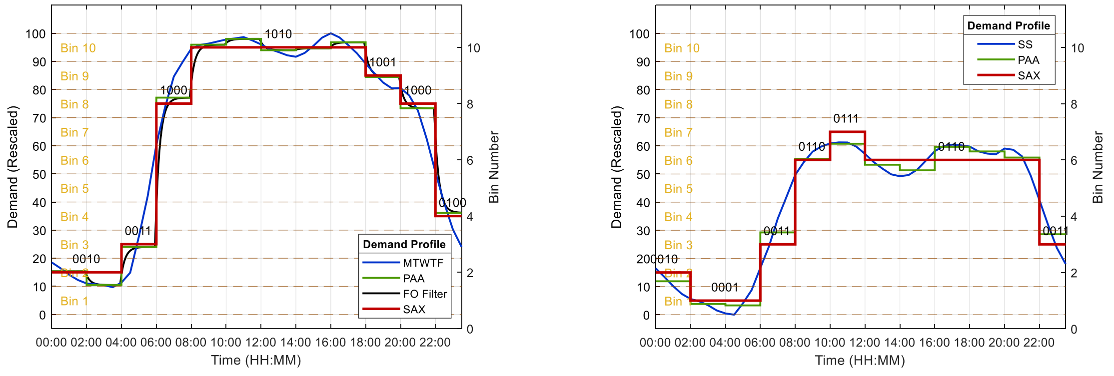

(a) (b)

Figure 3 24-hour period PAA (2-hour) & SAX representations (a) weekday, (b) weekend day

Experimental results of reconstructing prediction forecasts by limiting the input to piecewise coefficient only, over a 24-hour period (weekday) where the PAA segment is set to 2-hours, is shown in Figure 4 (a). The plot compares the reconstructed PAA representation with mean values of selected weekday demand profiles extracted from the 3-dimensional array introduced earlier. Figure 4 (b) shows a 12-month predicted demand data profile calculated using weekday PAA LUT; *month* and *year* trend features are also shown.

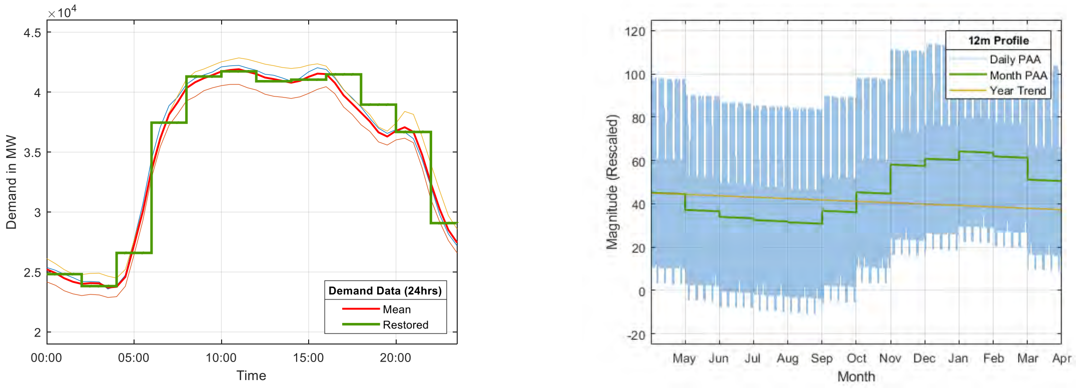

(a) (b)

Figure 4 Restored Demand Data (a) 24-hour PAA (2 hour) format, (b) 12-month period

5 Conclusion

The main contribution of this paper is to show that a series of simple data transformations provide an effective representation of demand time series. More sophisticated models are available, however in the context of a decentralised Energy Optimisation System (EOS) we have demonstrated the features offer distinct advantages when considering deployment to low software complexity platforms. This finding suggests that the behaviour of exiting energy optimisation technologies may benefit from similar approaches. For example support for energy planning of isolated islands or domestic households. In future work we intend to explore the feasibility of substituting LUT where assigned values originate from historical data, with real-time grid frequency data measured locally (decentralised).

Acknowledgments

The first author wishes to acknowledge the financial support provided by Teesside University and the Doctoral Training Alliance (DTA) scheme in Energy. The authors also acknowledge elements of the work was carried out as part of the DR-BOB project (01/03/16–28/02/19) which is co-funded by the EU's Horizon 2020 framework programme for research and innovation under grant agreement no. 696114.

References

[1] C.P. Chang, M. Dong, B. Sui, Y. Chu, Driving forces of global carbon emissions: From time- and spatial-dynamic perspectives, Econ. Model. (2019). doi:10.1016/j.econmod.2019.01.021.

[2] L. Pérez-Lombard, J. Ortiz, C. Pout, A review on buildings energy consumption information, (n.d.). doi:10.1016/j.enbuild.2007.03.007.

[3] Y.L. Li, M.Y. Han, S.Y. Liu, G.Q. Chen, Energy consumption and greenhouse gas emissions by buildings: A multi-scale perspective, Build. Environ. 151 (2019) 240–250. doi:10.1016/j.buildenv.2018.11.003.

[4] M.C.P. Sing, P.E.D. Love, H.J. Liu, Rehabilitation of existing building stock: A system dynamics model to support policy development, (2019). doi:10.1016/j.cities.2018.09.018.

[5] D.B. Avancini, J.J.P.C. Rodrigues, S.G.B. Martins, R.A.L. Rabêlo, J. Al-Muhtadi, P. Solic,

Energy meters evolution in smart grids: A review, J. Clean. Prod. (2019). doi:10.1016/j.jclepro.2019.01.229.

[6] J. Malinauskaite, H. Jouhara, L. Ahmad, M. Milani, L. Montorsi, M. Venturelli, Energy efficiency in industry: EU and national policies in Italy and the UK, Energy. (2019). doi:10.1016/j.energy.2019.01.130.

[7] S. Muzaffar, A. Afshari, Short-Term Load Forecasts Using LSTM Networks, Energy Procedia. 158 (2019) 2922–2927. doi:10.1016/j.egypro.2019.01.952.

[8] C. Robinson, B. Dilkina, J. Hubbs, W. Zhang, S. Guhathakurta, M.A. Brown, R.M. Pendyala, Machine learning approaches for estimating commercial building energy consumption, Appl. Energy. 208 (2017) 889–904. doi:10.1016/j.apenergy.2017.09.060.

[9] A. González-Vidal, F. Jiménez, A.F. Gómez-Skarmeta, A methodology for energy multivariate time series forecasting in smart buildings based on feature selection, Energy Build. 196 (2019) 71–82. doi:10.1016/j.enbuild.2019.05.021.

[10] R. Nepal, N. Paija, A multivariate time series analysis of energy consumption, real output and pollutant emissions in a developing economy: New evidence from Nepal, Econ. Model. (2019). doi:10.1016/j.econmod.2018.05.023.

[11] M. Chayama, Y. Hirata, When univariate model-free time series prediction is better than multivariate, Phys. Lett. A. 380 (2016) 2359–2365. doi:10.1016/j.physleta.2016.05.027.

[12] N. Bokde, M.W. Beck, F. Martínez Álvarez, K. Kulat, A novel imputation methodology for time series based on pattern sequence forecasting, Pattern Recognit. Lett. 116 (2018) 88–96. doi:10.1016/j.patrec.2018.09.020.

[13] S. Williams, M. Short, T. Crosbie, Decentralised Energy Optimisation For Blocks of Buildings, in: Int. Conf. Innov. Appl. Energy 2019, 2018.

[14] National Grid, Balancing Data, Natl. Grid ESO. (2019). https://www.nationalgrideso.com/balancing-data/data-finder-and-explorer (accessed May 5, 2019).

[15] E. Keogh, K. Chakrabarti, M. Pazzani, S. Mehrotra, Dimensionality Reduction for Fast Similarity Search in Large Time Series Databases, Knowl. Inf. Syst. (2006). doi:10.1007/pl00011669.

[16] J. Lin, E. Keogh, S. Lonardi, Experiencing SAX: a Novel Symbolic Representation of Time Series, n.d. https://cs.gmu.edu/~jessica/SAX_DAMI_preprint.pdf (accessed June 7, 2019).

Nottingham | UK | 9–11 September 2019

Virtual design based on CFD of high efficiency and zero emission systems

F. Gerbino, R. Morgan, P. Atkins, K. Vogiatzaki

University of Brighton, Mithras House - Lewes Road - Brighton - BN2 4AT, UK

F.Gerbino@brighton.ac.uk

Abstract

As the concern for the environment is increasing and the regulations around harmful emissions are becoming more strict, novel Internal Combustion Engine (ICE) concepts are becoming an absolute necessity in order to keep high thermal efficiencies while reducing the pollutant emissions. Moving towards more radical engine designs based on novel thermodynamic cycles comes also with the lack of knowledge and understanding of the physical phenomena involved in the combustion process. As experimental activities have time and cost implication, Computational Fluid Dynamics (CFD) is becoming a promising tool for virtual design of future energy systems. In this paper we demonstrate the role CFD can play in future engine design, using as a basis the Split Cycle engine, a novel ICE concept based on separating the compression and the combustion stages. A prototype, under development by Ricardo Innovation, offers a potential breakthrough reducing both CO_2 emissions and the fuel consumption. The CFD analysis presented here focuses on the injection strategy of such engine, as it differs from conventional Diesel engines and potentially holds the key of the performances of this device.

Keywords: CFD, Split Cycle Engine, Impinging Jet, Crossflow

1. Introduction

During the last two decades, there is an increasing concern in power and transportation sector regarding environmental and energy issues. ICEs are still the main devices used in land transportation, however they are slowly being replaced by batteries in small vehicles. Though, low power densities typical of batteries are not suitable for long range mobile applications, as trucking industry. Due to this, engine manufacturers are focusing on new strategies and design, in order to reduce the pollutant emissions to near zero levels, keeping high thermal efficiency [1]. Concerning the energy balance of ICE, more than half of the input energy is lost as waste heat. Hence, recovering such heat and converting it to useful work would improve the overall engine efficiency up to $45 - 50\%$ [2]. Further improvements to efficiencies require a fundamental change to the ICE cycle. The Recuperated Split Cycle Engine (RSCE) is a concept developed initially at Ricardo in 1908 and the subject of active R&D by Ricardo Innovation for approximately ten years. Thanks to its entirely new approach to combustion, it is a potentially game-changing engine technology, offering significant reductions in engine-out emissions without compromising efficiency . The prototype currently under development by Ricardo Innovation offers a potential breakthrough, reducing CO_2 emissions by approximately 30% and saving 20% in operating fuel costs[3]. Figure 1 shows the split cycle schematic and its stages of operation.

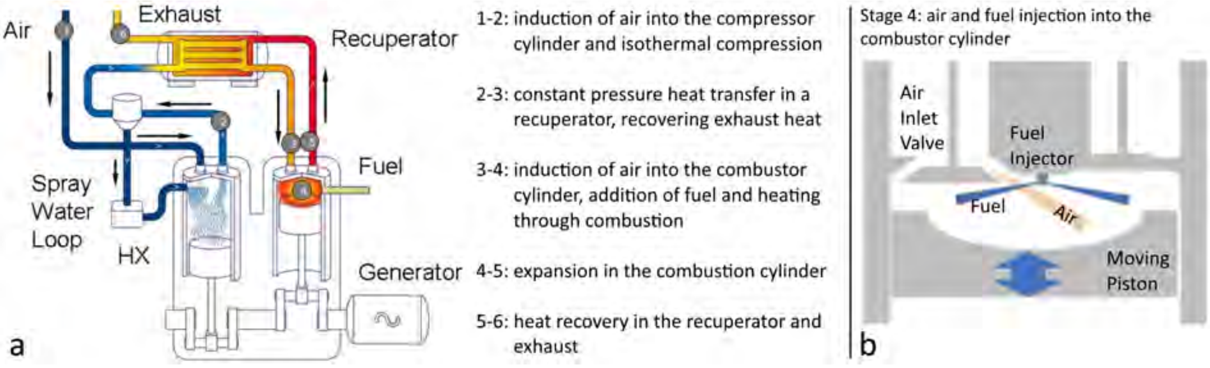

Figure 1: Schematic of the split cycle engine and its stages (a); conceptual representation of the air and fuel injection into the cylinder (b) (adapted from[3]).

Experimental tests for RSCEs are in their early stages. Hence, the actual physical phenomena involved within the combustor, affecting the fuel injection and mixing, have not been widely investigated and understood. Moreover, because of the harsh and extreme environment within the combustion chamber, experimental tests and direct observations are not always feasible. Thanks to the increasing computing capabilities, numerical simulations are the most promising way to study the flows within ICEs, being more cost and time-effective than experimental facilities.

The challenge is that the simulation accuracy depends on the reliability of the virtual tools, requiring rigorous validation over a wide range of operating conditions. The currently available quantitative data are based on lab-scale experiments representing isolated operating conditions, at fixed pressures and temperatures. In a real engine, where the piston is moving, a range of these conditions is present simultaneously. As regards novel ICE concepts, further levels of complexity are present. In fact, within RSCE, an air jet is injected in the combustion cylinder at high pressure and velocity (up to $100-200m/s$ [3]) causing shock waves and impinging the fuel jet. Injecting the fuel against a high velocity air jet causes unusual fuel-air interactions, since in conventional ICEs the fuel is injected in a "static" environment (with very low air velocities). It is expected that the presence of shock waves affects both the mixing and the spray atomization. In the current work we use numerical simulations to provide insight on the physical phenomena involved in these condition. In the next sections we will briefly discuss the numerical set up and the CFD models used, then we will present the numerical results that show how the impinging jet dynamics affect the mixing process.

2. Numerical setup and validation

To keep an acceptable compromise in terms of computational time and accuracy (resembling industrial purpose CFD), the Reynolds Averaged Navier Stokes (RANS)/Eulerian-Lagrangian approach is used here. In such method, the liquid phase is treated using the Lagrangian particle tracking, while the gas phase is modelled using the Eulerian framework. Initially the code has been validated in a simpler configuration against the experimental cases documented by the Engine Combustion Network (ECN)[4] for Spray A in inert conditions. The input conditions are reported in table 1 and they correspond to conditions close to standard Diesel engine conditions. Figure 2a shows the setup for Spray A.

Table 1: Operating condition of spray A

Ambient properties		Spray properties	
Pressure:	$p_{amb} = 6MPa$	Single hole Injector:	$d_{inj} = 90\mu m$
Temperature:	$T_{amb} = 900K$	Fuel:	N-dodecane
Density:	$\rho_{amb} = 22.8kg/m^3$	Injection pressure:	$p_{inj} = 150MPa$
Inert condition:	$0\%O_2$	Inj. temperature:	$T_{inj} = 363K$

After a thorough sensitivity analysis, the optimum mesh cell size for RANS simulations is found to be $0.25mm$ [5]. As regards the spray droplets atomization, the Reitz-KHRT break-up model is used, as it is the most commonly used for diesel-like fuels as N-dodecane [6]. Both the optimum mesh size and the break-up model coefficients, have been selected, validating

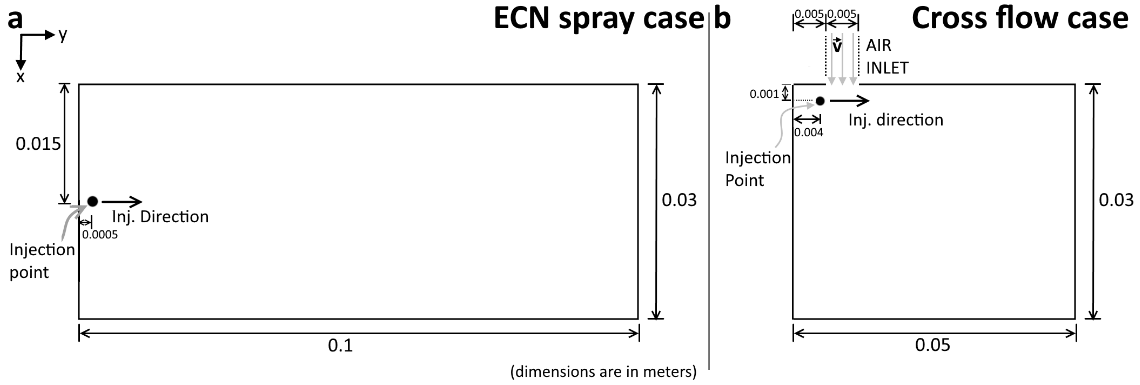

Figure 2: Schematics for the simulations of: ECN spray A case (a) and the crossflow case (b).

the results against the ECN experimental data. Such numerical set up is used here for the investigations on the impinging jet, as no experimental data are available for such case. The air inlet is represented by a square hole of $5x5mm$ and three different cases are compared varying the air inlet velocity, setting $\mathbf{v} = 0$ (no cross-flow, similar to ECN Spray A), 30 and $100m/s$. The injection point is moved closer to the air inlet. Figure 2b shows the schematics of the crossflow case. Notice that $\mathbf{v} = 10 - 30m/s$ are typical velocities observed in conventional ICEs, while in RSCE velocities in the range of 100 to $200m/s$ are predicted [3].

3. Results and Discussion

Comparison between the three cases, varying the air inlet velocity, shows that although there aren't major differences between the case with 0 and $30m/s$, the effects of the crossflow became much more important as $\mathbf{v} = 100m/s$. Figure 3a demonstrates the fuel vapour distributions for $t = 0.0005s$ (i.e. as the liquid jet reach its stationary length). As $\mathbf{v} = 100m/s$ the vapour mass fraction gets more dispersed, and it is possible to observe some oscillations on the vapour front facing the air jet. These oscillations can be better explained observing the pressure field.

Looking at the pressure field in Fig. 3b, the first two cases are similar and pressure oscillations (potentially shock waves) appear around the injection point. On the other hand for $\mathbf{v} = 100m/s$ a noticeable pressure rise occurs along the entire leading edge of the liquid jet, followed by a much lower pressure region. Such a behaviour indicates that as the crossflow contacts the liquid jet a shock wave occurs in that region. Pressure waves can be observed as well further up the liquid jet tip, explaining the oscillations in the vapour mass fraction field. Another parameter shown here, relevant for the fuel-air mixing, is the vorticity. Once again, there aren't major differences between the case without crossflow and with $\mathbf{v} = 30m/s$. In fact, looking

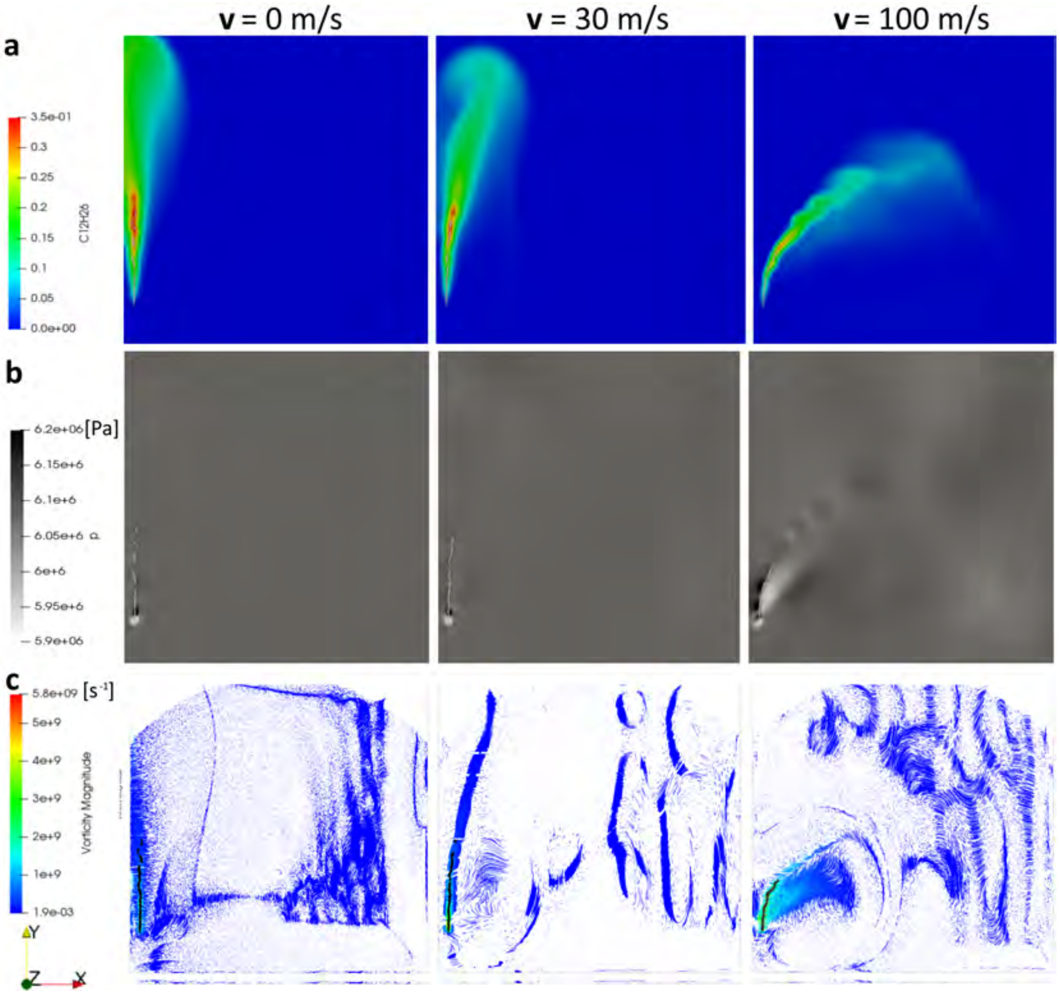

Figure 3: Simulations outcomes for different air inlet velocity at $t = 0.0005s$*: fuel vapour mass fraction (a); pressure field (b); vorticity streamlines (c)*

at Fig.3c which reports the vorticity streamline, it can be seen that as the crossflow velocity is 0 and $30m/s$ the vorticity is kept confined around the liquid jet (the black particles), while as $\mathbf{v} = 100m/s$ it extends downstream the jet, indicating a higher mixing occurring in that region.

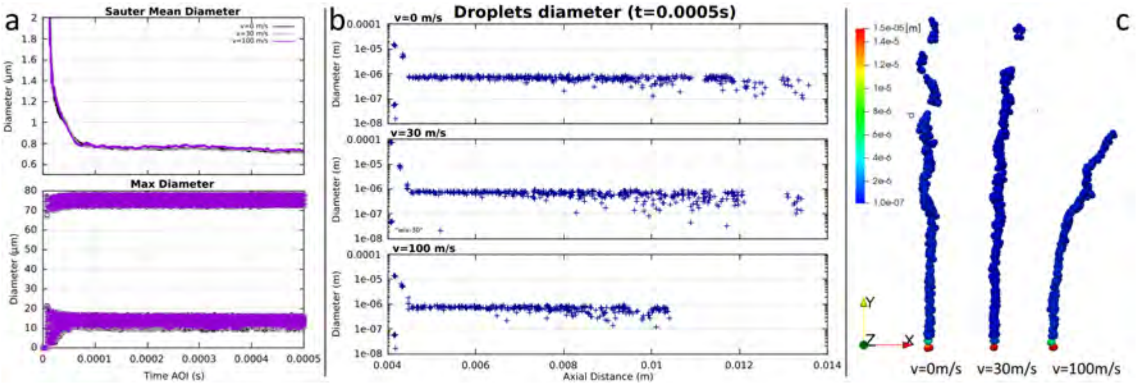

Figure 4: Simulations outcomes for the Lagrangian particle: Sauter mean diameter and maximum diameter as a function of time (a); droplets diameter distribution at $t = 0.0005s$ *for different* $\mathbf{v}$ *(b); liquid jet morphology at* $t = 0.0005s$ *for different* $\mathbf{v}$*(c).*

Notice that these effects are observed on the Eulerian field as the crossflow velocity gets higher, but there aren't major effect on the the liquid parcels, with the exception of their trajectory deviation, as shown in Fig.4. Analysing the spray droplets diameter, the droplets size distribution remain the same for all the cases (Fig.4a and b). Moreover Fig.4c shows there aren't ligaments or smaller droplets on the trail of the liquid jet, downstream the crossflow (as proposed in [7]). This indicates a certain inadequacy of the Lagrangian approach used here for the liquid jet characterization, in particular as regards the spray break-up model. In fact, the Lagrangian particle behave, to some extent, independently from the surrounding Eulerian field.

4. Conclusion

In this paper we demonstrate how a virtual design tools can support the development of future engine concepts, also when experimental data are not available, using a case relevant to industrial interest (a novel ICE concept). Numerical simulation performed here prove that, in conditions relevant to the RSCE, unusual physical phenomena may affect the fuel-air mixing and the spray atomisation process, with respect to conventional injection conditions. The presence of a high velocity impinging jet implies the occurrence of shock waves, as well as a more distributed viscosity field, which extends further downstream the jet region. The numerical coupling between the Lagrangian and the Eulerian framework has to be improved.

References

1 . Stanton DW (2013) Systematic Development of Highly Efficient and Clean Engines to Meet Future Commercial Vehicle Greenhouse Gas Regulations. SAE Int. J. Engines 6(3):1395-1480

2 . Sprouse C, Depcik (2013) Review of organic Rankine cycles for internal combustion engine exhaust waste heat recovery. Appl Therm Eng 51(1–2):711–22

3 . Morgan R et al. (2019) The Ultra Low Emissions Potential of the Recuperated Split Cycle Combustion System, Submitted to SAE ICE Conference, Capri

4 . Engine Combustion Network, http://www.sandia.gov/ecn/

5 . Gerbino F, Morgan R, Atkins P, Vogiatzaki K (2019) Quantifying the effect of the turbulence and break up modelling for spray simulations through a dimensionless number analysis, Submitted to International Journal of Engine Research, IJER-19-0097

6 . Baumgarten C, Mewes D, Maxinger F (2006) Mixture Formation in Internal Combustion Engines, Lehrbuch, Springer Verlag, Heidelberg

7 . Lia X, Gao H, Soteriou M C (2017) Investigation of the impact of high liquid viscosity on jet atomization in crossflow via high-fidelity simulations, Physics of Fluids 29, 082103

Nottingham | UK | 9–11 September 2019

The Future of Clean Coal in India

A. Madhu Madhavi [1], B. William J Nuttall[2]
[1]*PhD Research Student, The Open University, UK*
[2] *Professor of Energy, Faculty of Science, Technology, Engineering & Mathematics*
School of Engineering & Innovation, The Open University, UK
madhu.madhavi@open.ac.uk

Abstract: India's energy demand is expected to grow many times as its population base grows and its economy expands. While renewable energy costs are falling and further reductions in them are predicted, there are formidable challenges around its storage and intermittency. On the other hand, India has sizeable coal reserves mined in many Indian states. Until such time solutions to the challenges posed by renewable technologies are clearly worked out, India will have to consider a mix of large and small, central and distributed technologies. Coal can be expected to play a major role in India's energy mix for decades to come.

As international efforts to decarbonise energy systems intensify, the role of technological intervention, which can effectively reduce energy intensity and help India with its Nationally Determined Contributions (NDCs), will increase in importance. A future Indian energy system is likely to be a combination of various technologies deployed with an intention to deliver against various energy policy objectives including, but not restricted to, reduced emissions. In this context, one technology of potential importance is Coal to Hydrogen Technology, which can present interesting prospects for India's ambitions to minimise greenhouse gas emissions while maintaining some of the economic benefits arising from the utilisation of local coal.

This paper presents the status of clean coal technology in India, while briefly outlining some of the issues relating to the integration of coal to hydrogen technology in India. This paper is a part of an ongoing study that takes a whole systems approach and seeks to explore the balance of a possible future portfolio of energy technologies in India assessed against multiple desirable attributes.

Keywords: *Energy policy in India; coal; clean coal technology; coal to hydrogen technology in India; coal gasification; sustainability; energy security*

1. Introduction

India's energy system is expected to undergo significant transformation. Already the third-largest economy in the world, and with a predicted robust growth outlook, India's economic growth is likely to remain strong in the future according to various outlooks and reports (World Bank, 2015;

International Energy Agency (IEA), 2015). India is already home to over one-sixth of global population and is predicted to leave China behind as the most populous country of the world by 2022 according to a UN report (2017). With policies in place to bolster country's modernisation and support the expansion of its manufacturing sector, it is hardly surprising that India's energy demand growth is likely to double over the next two decades (International Energy Agency, 2015). It is also notable that with a Human Development Index of 0.586 and a global rank of 135, there are significant progresses that need to be made to improve the standard of living of its expanding population base and eradicating energy poverty. In the meantime, in its nationally determined contribution (NDCs) India has pledged to improve its emission intensity of its Gross Domestic Product (GDP) by 33 to 35 percent below 2005 levels and increase the share of renewable resources to 40 percent by 2030 (Ministry of Environment, Forest and Climate Change (MoEF), 2015). India is heavily reliant on fossil fuels for meeting its energy demand, with coal accounting for over 70 percent of power sector generation. Coal's share in India's primary energy mix has grown due to expansion of India's power generation fleet and increased use of coking coal for India's industrial growth at the back of policies like 'Universal Electrification (*Saubhagya*)' and 'Make in India'(IEA, 2015). India has sizeable coal reserves mined in many Indian states. A cumulative total of 319.02 Billion tonnes of Geological Resources of Coal have so far been estimated in the country by the Geological Survey of India (Ministry of Coal, 2018). Coal mining, also, continues to remain the main source of economic activity of these Indian states, employing close to a million people and supporting their families and making it important to the social-economic-political construct of the region. Given India's development agenda, its infrastructure deficit and its NDC targets, India faces significant challenges while balancing its various energy policy objectives.

With a justifiably high dependence on coal to meet increased energy demand growth while aiding a reliable and affordable provision of electricity in India, at a time of intensifying global pressure to transit to cleaner energy pathways, the role of technological intervention in helping India balance its various energy policy objectives becomes invaluable. Given coal's contribution to India's GHG emission growth and its importance to India's energy systems, any reduction in India's emissions necessitates a special focus on coal-based power plants in the country. Furthermore the inherent technical, financial and political complexities mandate a non-intuitive and systems study of various aspects associated with future policy options to avoid policy failure and associated social, environmental and financial costs. It is in this context that this paper examines the viability of Coal to Hydrogen Technology, and underlines options and recommendations for future. Given the ongoing nature of the work, more concrete conclusions will follow as the research progresses to its final stages.

2. Coal Power Sector in India : A Status Update

Coal is the most abundant fossil fuel in India, accounting for more than half of country's energy needs. Indian hard coal reserves are spread over 27 major coalfields, scattered across many Indian states mostly in the eastern and south central parts of the country. India also has sizeable lignite reserves, which stand at around 36 billion tonnes, deposited mainly in the southern Indian state of Tamil Nadu. A table showing India's state-wise distribution of coal has been presented in Appendix A.

For reasons alluded to earlier, coal dominates India's energy matrix, accounting for 56 percent of country's total primary energy consumption, presented in Figure 1 (BP, 2018).

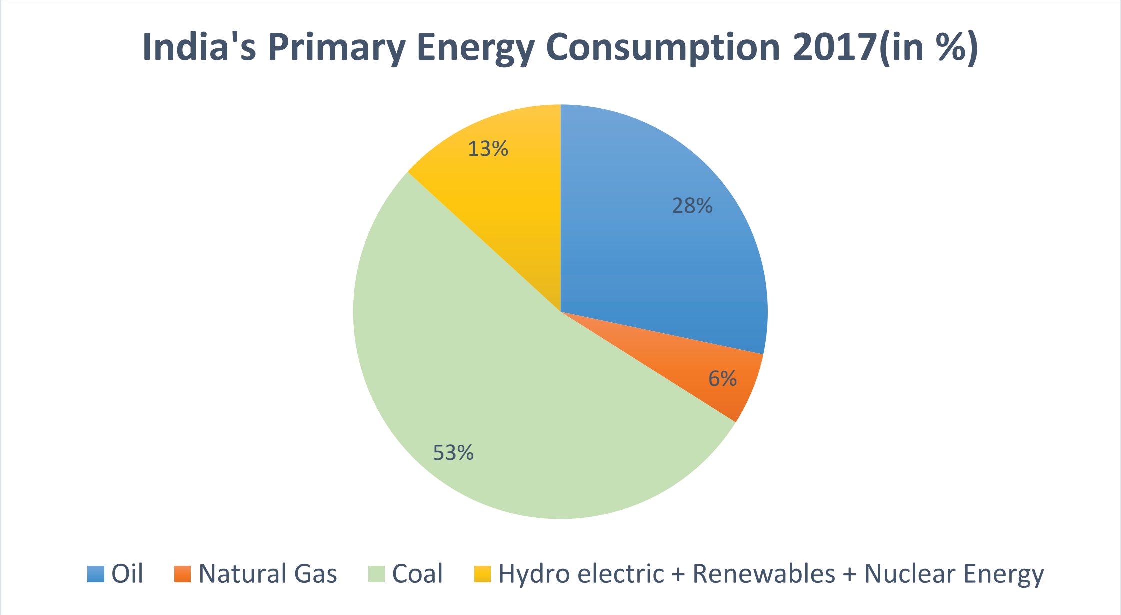

Figure 1: Primary Energy Consumption Matrix in India in 2017,

Source: Data from BP, 2018

During the year 2016-17, about 82% of total coal and lignite was despatched to the power sector (Indian Minerals Yearbook, 2017). Coal is also used as a raw material by industries like cement, fertiliser, chemical, papers etc. For details on coal classification, uses and other basic coal facts, see Madhavi and Nuttall (2019). Ranked third in 2015, India has since increased the production of both coal and lignite to keep pace with projected increase in demand growth. A number of reforms have been introduced in the coal sector by the government over the years to increase the productive efficiency of various units associated with coal supply chain, including the landmark intervention by the Supreme Court of India declaring all coal allocations since 1993 as illegal and paving way for allocation through reverse bidding under Coal Mines Special Provision Act 2015(Indian Chambers of Commerce).

India's total installed capacity was reported at 350,162 Megawatts (MW) in 2019, of which coal's share stands at 56.4 percent at 197,353 MW (Ministry of Power). Figure 2 presents India's electricity generation profile in 2017 (BP, 2018). The power sector is likely to remain one of the biggest consumers of coal as the expected growth in electricity projected in the immediate future will be based on coal. According to India's Niti Yog scenarios, coal-based capacity is likely to be in the range of 200-400 GW in 2030, from 77GW in 2008; while IEA scenarios predict a two-and-a-half-times increase in India's coal fleet, reaching almost 440 GW in 2040 (IEA,2015).

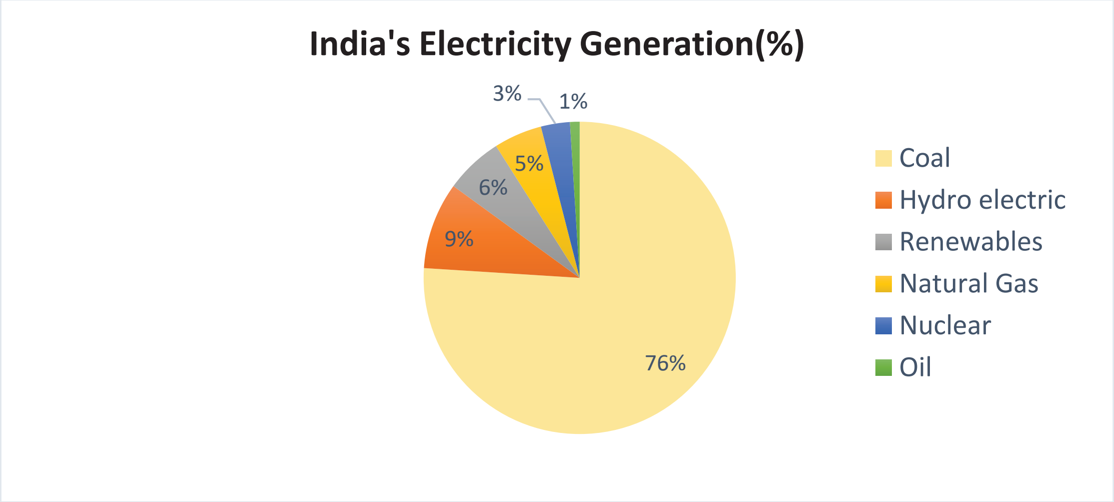

Figure 2: Electricity generation from various sources in India 2017

Source: Data from BP, 2018

While other resources will remain prevalent in the mix, coal is predicted to score better due to its economic advantage and abundance. Given the rising energy demand driven by the rising population, expanding economy and a quest for better living standards, and the limited reserve potentiality, geo-political restrictions and infrastructure shortfall associated with other resources, coal is poised to remain centre-stage in India's energy mix and energise the power sector in India .

3. Clean coal technology in India

According to a report by IEA, currently 85 percent of Indian coal plants are based on subcritical boiler technology, which have been adapted to be used with Indian coal and in general terms perform poorly given their low conversion efficiency (IEA, 2015). Efficiency is an important performance parameter in coal-fired power plants, as it can determine emission reductions as well as higher output from relatively smaller amounts of coal (IEA, 2011). Pulverised coal combustion (PC), which was, not long ago, the most widely used technology in coal-fired power plants globally, can be categorised into subcritical, supercritical(SC) and ultra-supercritical (USC) technologies based on the differences in temperature and pressure. A detailed overview of various clean coal technologies has been presented in Madhavi and Nuttall (2019). Replacing the existing subcritical technologies with SC and USC technologies can potentially achieve higher efficiencies resulting in, according to IEA's Clean Coal Centre, around 23 percent reduction in CO_2 emission per unit of electricity generated (Nalbandian, 2008). This presents exciting prospects for a country like India, scrambling to balance policy priorities between attaining economic growth, energy security and prosperity for its citizens in the least environmentally damaging manner possible. High efficiency low emission (HELE) clean coal technologies will therefore be of vital importance to policy makers in the immediate future, given the net efficiency of India's entire fleet of coal power plants stands at 29 percent, leaving much room for improvement.

In India, the standard for coal-power technologies have traditionally been the Bharat Heavy Electricals Limited (BHEL) 500 MW sub-critical pulverised coal units, supported by assisted boilers with a main steam-pressure of 170 kg/cm^2, the best of these units operating at a higher than average efficiency of 33 percent (Central Electricity Authority, 2003). Despite steady improvements in unit-sizes and efficiencies, these BHEL-manufactured units lag behind the range of advanced, more efficient and cleaner technologies now available internationally. Efficiency-improvements are critical considerations for future coal-based generation in India. According to an estimate by India's Ministry of Power, introduction of new ultra-supercritical (USC) technology can improve efficiency of coal-based power generation in India by 1.5 percent over supercritical units(CEA, 2018). In recent years, Indian's Ministry of Power has reported that some 660/ 800MW Units are operational in the country and many more supercritical units of 660/800 MW are under construction for likely commissioning in the years ahead. Initially supercritical units were designed with steam parameters of 247 kg/cm^2, 537/565 ℃(CEA, 2018: 77). The ministry also reports that the USC technology with steam-pressure of 280 kg/cm^2 and temperature of 600℃ is currently being considered for recently awarded plants of Khargone Super Thermal Power Station (TPP) and National Thermal Power Corporation Limited (NTPC) in

Madhya Pradesh(CEA, 2018:32). According to IEA, the supercritical plants have been commissioned in the recent years account for roughly around 15 percent of India's total coal-powered fleet; and forecasts it to increase to almost half of the total including some USC and integrated gasification combined-cycle (IGCCs), significantly improving the country's coal plant efficiency to close to 38% by 2040, a notably significant achievement given high ash-content of Indian coal (2015).

In this context, one such technology of potential interest to India is Coal to Hydrogen Technology, which can present interesting prospects for India's ambitions to minimise greenhouse gas emissions while maintaining some of the economic benefits arising from the utilisation of local coal. Hydrogen is a key raw material for various industries (chemical, fertilizer and petrochemical), used in the form of high purity oxygen or a mixture of hydrogen and carbon monoxide also known as HyCO gas. The gasification of coal is one method that can produce power, liquid fuels, chemicals, and hydrogen. The feasibility of setting up commercial scale demonstration plant based on IGCC with Indian coal is currently underway and needs to be carefully analysed as they will significantly impact the technology trajectory over a longer-time horizon. In India's rapidly-evolving policy landscape, policy choices cannot be made blithely; it could be a costly mistake to make *a priori* policy choices. A systems study, one that takes into account various delays, emerging dynamics, fluctuations etc. all characteristic of complicated system like India's energy sector, is needed to consider the long-term implication of various policy choices. Effective policy choices should be considered after carefully analysing various possible assumptions and scenarios. System dynamics, a computer-aided simulation technique, has the ability to take into account feedback loops, delays and interactions between various sub-systems and therefore serves as a powerful tool for energy-policy analysis relevant to this study. More details on System Dynamics methodology are presented in the following section together with a mental model that will guide the further stages of this study.

4. A System Dynamics based analysis of Coal to Hydrogen Technology in India

System Dynamics, developed by Jay W. Forrester during the mid-1950s at Massachusetts Institute of Technology, has been widely used as a tool to investigate, analyse and forecast a system's behavior (Hosseini and Shakouri, 2005). System dynamics modelling represents the system structure in terms of stocks, flows, and the causal mechanisms that control their rates of change, with feedback loops formulating various causalities represented in these models. The behaviour of energy systems can be analysed by evaluating and understanding the interaction between various feedback loops, which also helps to understand the long-term impact of existing policies (Madnick and Siegel, 2008). It has been used for designing policies through computer-aided modelling and simulation of complex situations and has proved particularly significant in studies that include cross-cutting implications from socio-economic, political, management, market and environmental domains (Choucri et al., 2007:3-4); analyse dynamic relationship of energy and the economy (Sterman, 1982; 1987); map the future of resource development under different price scenarios (Hosseini and Shakouri, 2005; Samii & Teekasap:2009); or study the regional and global market impacts on policy dynamics (Kiani & Pourfakhraei, 2010). The relevance and application of system dynamics method for analysing the long-term impact of policy choices and gaining insight into emerging dynamics has been established through various studies. However, literature on the specific application of system dynamics to the context of clean-coal-technology in India could not be found. This study contributes to the body of work by pioneering the application of system dynamics in analysing the viability of clean-coal-technology in India. It also, therefore, help in analysing the wider impact of coal-aided energy demand expansion in India. A simple mental block to guide the modelling approach is provided in Figure 3.

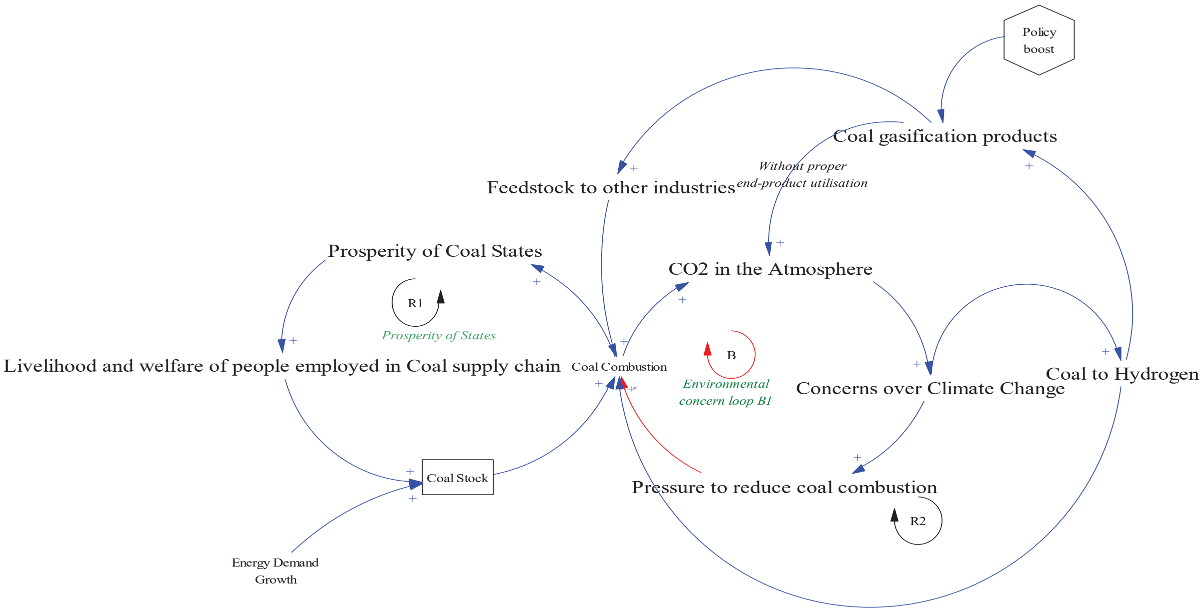

Figure 3: Mental model feedback loop diagram of exchanges in India’s coal-to-hydrogen system

Some of the Policy Scenarios that will be explored through the modelling method are:

1. Efficiency Improvement
2. Advanced Carbon-capture and storage
3. Long-term impact and feasibility assessment

5. Conclusion

There are a number of challenges like the need to provide affordable electricity to India's growing population, provide secure supplies to fuel economic expansion and transit to sustainable and low carbon-intensive pathways that the coal-power sector in India will have to consider for India to successfully deliver on its energy policy objectives. Financing provisions and linkages for a successful adoption of available technologies emerging from a fair international climate regime in the form of actions, commitments and support from industrialised countries will be critical not only for catalysing new research and but making them affordable for a country like India. Wider systemic interaction between various feedbacks will need to be closely studied to consider the best suited set of policy options and minimise the risks and costs associated with policy failure.

Appendix A

Table 1: State-wise distribution of India's Coal Reserves in Million Tonnes

State	Proved	Total
Jharkhand	45563	83152
Odisha	37391	79295
Chhattisgarh	20428	57206
West Bengal	14156	31667
Madhya Pradesh	11958	27987
Telangana	10475	21702
Maharashtra	7178	12299
Andhra Pradesh	0	1581
Bihar	161	1367
Uttar Pradesh	884	1062
Meghalaya	89	576
Assam	465	525
Nagaland	9	410
Sikkim	0	101
Arunachal Pradesh	31	90
Total	**148788**	**319020**

Source: Geological Survey of India

Acknowledgments

Burnard, K. and Bhattacharya, S., 2011. Power generation from coal.

Central Electricity Agency, 2003, Report of the committee to recommend next higher size of coal fired thermal power stations; Available at: http://www.cea.nic.in/reports/others/thermal/tetd/committee_recommend_thermal.pdf

Choucri, Nazli, Daniel Goldsmith, Stuart Madnick, Dinsha Mistree, J. Bradley Morrison, and Michael Siegel. "Using system dynamics to model and better understand state stability." (2007).

Coal Reserves, Ministry of Coal, Government of India, Available at: https://coal.nic.in/content/coal-reserves

Data from BP 2018

High Efficiency Low Emissions Coal, Available at: https://www.worldcoal.org/file_validate.php?file=Hele%20Factsheet.pdf

Hosseini, S.H. and Shakouri, H., 2016. A study on the future of unconventional oil development under different oil price scenarios: A system dynamics approach. Energy Policy, 91, pp.64-74.

India Energy Outlook, International Energy Agency, Available at: https://www.iea.org/publications/freepublications/publication/IndiaEnergyOutlook_WEO2015.pdf

Indian Chambers of Commerce; Coal Sector Reforms in India: Analysing from the Lens of Competition & Regulatory Architecture Available at: http://www.cuts-ccier.org/pdf/Presentation_on-Coal_Sector_Reforms_in_India.pdf

Kiani, B. and Pourfakhraei, M.A., 2010. A system dynamic model for production and consumption policy in Iran oil and gas sector. Energy Policy, 38(12), pp.7764-7774.

Madhavi, M. and Nuttall, W.J., 2019. Coal in the twenty-first century: a climate of change and uncertainty. *Proceedings of the Institution of Civil Engineers-Energy*, pp.1-34.

Madnick, S. and Siegel, M., 2008. A system dynamics (SD) approach to modeling and understanding terrorist networks. D&B DUNS Number 00-142-5594 Commercial and Government Entity (CAGE) code, 80230.

Ministry of Environment, Forest and Climate Change, Government of India, 2015, India's Intended Nationally Determined Contribution: Working Towards Climate Justice, Available at: https://nmhs.org.in/pdf/INDIA%20INDC%20TO%20UNFCCC.pdf

Ministry of Power, 2018; Committee On Optimal Energy Mix In Power Generation On Medium And Long Term Basis, Available at: https://powermin.nic.in/sites/default/files/webform/notices/Report_of_the_Committee_on_optimal_energy_mix_in_power_generation_on_medium_and%20long_term_basis.pdf

Nalbandian, H., 2008. *Performance and risks of advanced pulverised coal plant*. IEA Clean Coal Centre.

Power Sector at a Glance, Ministry of Power, Government of India, Available at: https://powermin.nic.in/en/content/power-sector-glance-all-india

Samii, M. and Teekasap, P., 2010. Energy policy and oil prices: system dynamics approach to modeling oil market. Global Commerce Forum.

Sterman JD. 1987. The energy transition and the economy: a system dynamics approach. PhD thesis, MIT Sloan School of Management, Cambridge MA.

Sterman, J., 1982. The energy transition and the economy: A system dynamics approach (Doctoral dissertation, Massachusetts Institute of Technology).

UN Population Revision Citation, United Nations, Department of Economic and Social Affairs, Population Division (2017). World Population Prospects: The 2017 Revision, Available at: https://esa.un.org/unpd/wpp/Download/Standard/Population/

Nottingham | UK | 9–11 September 2019

A review of Semantic Web Technologies and Linked Data, in facilitating the Whole Life Cycle (WLC) of information flow in the construction industry

Yasir Alani[1], Nashwan Dawood[2], Sergio Rodriguez[3], Huda Dawood[4]

[1,2,3,4] *Teesside University, Southfield Road, Middlesbrough, TS1 3BX, UK*

y.alani@tees.ac.uk

Abstract

One of the main problems facing Building Information Modelling (BIM) application is the complexity of domain data exchange among stakeholders. The Whole Life Cycle (WLC) approach is the seamless integration of the product or asset information from outline design, and up to decommissioning. This needs to be underpinned by digital technologies, well-defined interoperable standards, and Linked Data approaches, to improve efficiency and reduce carbon footprint across all project domains.

The IFC EXPRESS schema was developed in an attempt to facilitate the exchange of information among project domains. This data schema requires extensive mapping when including attributes of infrastructure domains other than buildings, and hence, these domains are prone to interoperability discrepancies or inconsistencies. Semantic Web Technologies (SWT) are not only expected to tackle the interoperability barrier that is currently affecting the progression of BIM, but to facilitate the application of rule checking and compliance checking through their logical inferences. Henceforth, SWT are expected to improve the modelling process.

Through a structured literature study, this paper explores the research on applying SWT in the Architecture, Engineering, and Construction (AEC) industry. Results suggest that research on WLC of information flow is minimal in the literature. Also, SWT are promising in enhancing the modelling philosophy (representing data) across all industries. However, SWT are immature and face few challenges, mainly the creation of links between data sets, and large file sizes.

Keywords: BIM, Ontology, RDF, SWT, WLC

1. Introduction

The concepts behind Semantic Web Technologies were introduced in the late 1990s and early 2000s. However, the literature on utilising these concepts in the Architecture, Engineering and Construction (AEC) industry started cumulating in the early 2010s (Zhong *et al.*, 2019). The Semantic Web allows a smarter querying and data inferencing, through a rather simple, yet elegant way of representing data, called the Resource Description Framework (RDF). The RDF is a data modelling framework that forms the basis for the Semantic Web (Allemang & Hendler, 2011). In a relational database, datasets are represented in tables, and therefore, establishing relationships between datasets in different cells of the table is a tedious and restricted process, which results in limited querying and inferencing capabilities. Thus, when representing a relational database in RDF, the row, the column, and the cell each receive a global reference, resulting in the RDF *triple* in a graph-like structure. Furthermore, there exist few languages that can be used to model data in RDF, such as RDF Schema (RDFS), RDFS-Plus, and Web Ontology Language (OWL). The degrees of complexity and inferencing capabilities vary among these languages. The concept of creating semantic data repositories is what is known as ontology construction. An ontology as defined by Gruber (1993) as an "explicit specification of a shared conceptualisation". One of the issues SWT are ought to tackle is the interoperability among distinct domains which, as described by Pauwels et al. (2017), is loading the same content in multiple applications. Thus, due to the capabilities of the SWT, it is possible to connect or *link* data available in different domains/repositories rather than *mapping* it. In addition to interoperability, Pauwels et al. (2017) also identified two other areas that SWT are expected to improve; linking across domains—which is combining different content in multiple domains, and logical inference and proofs. They argue that with linked sets of data, the problem of interoperability exists on a different level; the data level, as the creation and management of links needs human interference. Zhong et al. (2019) conducted a scientometric analysis on ontology research in construction between 2007 and 2017. They concluded that the focus of researchers was initially on applying ontology in several areas of construction management. However, around 2016 the focus shifted towards solving interoperability across the building life cycle. Moreover, they concluded that SWT and linked data are not part of the "hot topics" in ontology research, which suggests that the technical aspects of ontology research is not the main concern of researchers. In addition, Pauwels et al. (2015) stated that research is needed on the technical issues that are preventing/slowing the implementation and deployment of semantic web technologies in the construction industry. Niknam and Karshenas (2017) presented an ontology approach to semantically represent building information. They suggest that every domain in AEC industry should develop their own ontology by extending a foundation (common) ontology.

In this paper a literature review is conducted to quantify the amount of research that has been done on SWT in AEC for each domain. Consequently, the least researched area/domain is discussed alongside future research aspirations.

2. Methodology

A structured literature review has been conducted to identify some of the current gaps in knowledge in terms of leveraging Semantic Web Technologies in the AEC industry. Few papers have been published in the past on reviewing Semantic Web Technologies in AEC such as Abanda et al. (2013); Pauwels et al. (2017); Zhong et al. (2019). However, these papers typically focus on the general application of these technologies in the AEC. This research identifies all the researched domains in the highly technical papers exclusively. The used databases in this research were ScienceDirect and Scopus, in which, specific search terms were used; “ontology” AND “RDF” AND “OWL” AND “BIM”. These terms were used in querying for journal articles only. Also, no time frame was set, up to May 2019. These terms were selected to exclude non-technical and review articles. A total of 82 articles were retrieved, and quantitatively categorised based on their research domain in the AEC industry. Then, a qualitative assessment of the least researched domain has been conducted, which will form the basis for future work.

3. Semantic Web Technologies

The essence of SWT is data modelling, and thus, it facilitates tackling issues at the finite data level, which can be utilised across a broad range of domains. Figure 1 depicts the nine categories that resulted from reviewing 82 relevant articles. One can go into more detail and further divide these categories to subcategories. However, ontology research in AEC has not reached this level of saturation yet. It is worth noting that these categories overlap, and other researchers might have slightly different categorisation criteria. This is because SWT deal with the data itself, whether this data was consisting of numbers, rules, or classifications. Thus, harnessing data modelling introduces more flexibility in constructing various ontologies. For instance, most of the overlapping was between the “BIM-FM ontology” and the “Energy ontology”, as energy management is an important aspect of facility management.

Results show that the Product Life cycle Management (PLM) is the least topic, see figure 1. However, one can argue that technical research on applying SWT in AEC industry is far from being intensively saturated and, in general, all domains need further research efforts.

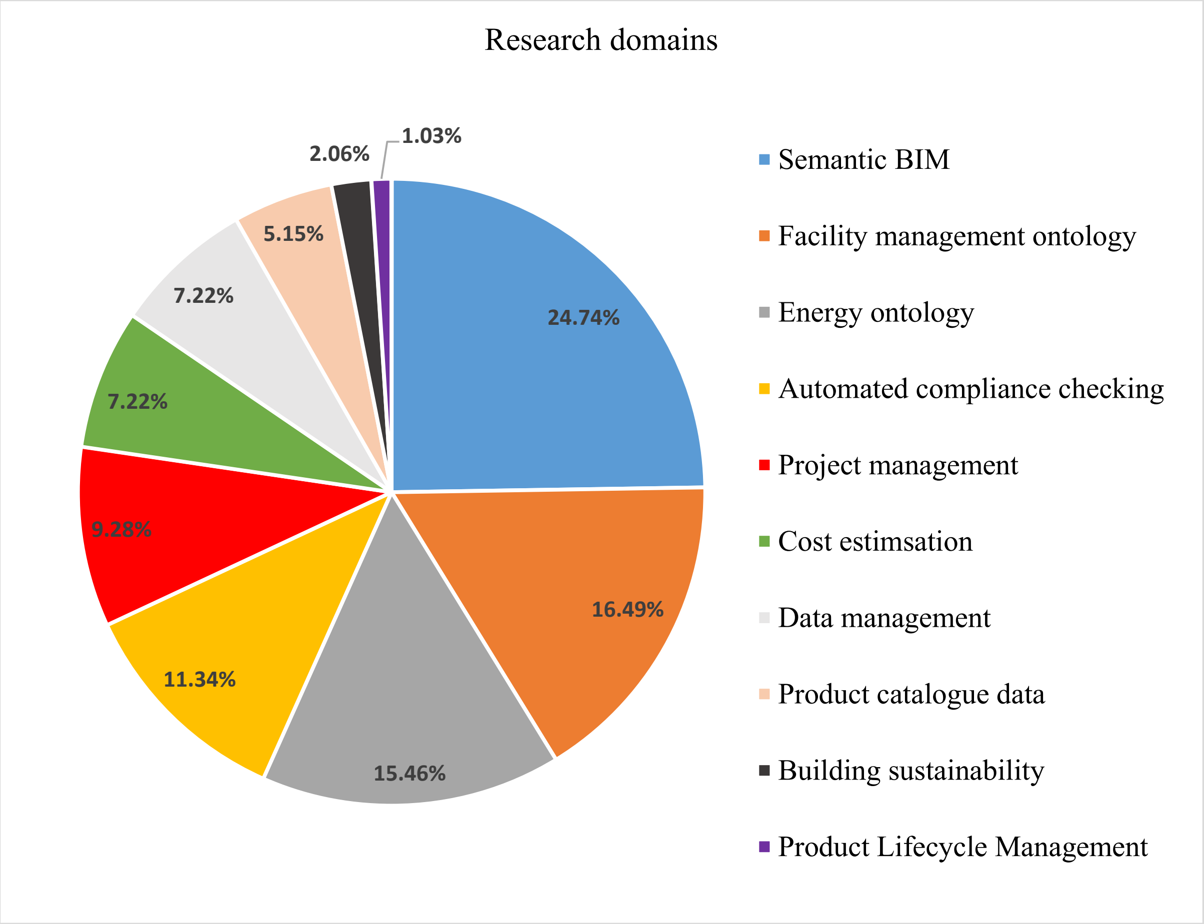

Figure 1: Research domains for applying SWT in AEC

Furthermore, it was noticed during this review that researchers generally improvise in terms of ontology construction and data management process. This indicates the lack of standardised procedures and guidelines to support the application of SWT in the AEC sector. Another important aspect most researchers seem to omit is the large file size generated from the RDF format. Barbau et al. (2012) stated that the larger the ontology is, the poorer is its performance time, resulting in a trade-off between the ontology's quality and the computing power required. On these grounds, the advancement of SWT is restrained by computers performance.

4. Whole Life Cycle (WLC) of information flow

Within the context of this study, Fortineau et al. (2019) were the only researchers that tackled the Product Life cycle Management (PLM). However, PLM focuses on the system engineering and rule validation processes rather than on the information flow. Consequently, their study mainly focused on utilising business rules using the Semantic Web Rule Language (SWRL). In this review, research on WLC of information flow was not observed in the literature. However, it was derived from the literature, that for such an approach to be valid, three important aspects must be satisfied, namely data creation, data validation, and data management.

4.1. Product manufacturer data

Obtaining the product data is the creation point of data and the first step in the data management chain. The process starts by enhancing data querying and allowing users to search for the most suitable BIM models for their design. In an ideal scenario, product manufacturers would publish their data online using the RDF format, which would facilitate a relatively intelligent querying. However, it would take some time into the future for RDF formats to become widely adopted by product manufacturers. An alternative would be to construct an ontology consisting of classification clusters of all the related terms and use this ontology in producing meaningful search terms as executed by Gao et al. (2015). Furthermore, Gao et al. (2017) have expanded and used such ontology in annotating BIM documents, and hence, retrieving the most relevant documents. As the desired product model is selected, it is then imported into the BIM model. Nevertheless, in addition to the technological limitations facing this process, identifying the required attributes of an asset to be entered into the BIM model or asset management system is a current problem. It is worth noting that searching for product data through the thresholds identified in the BIM model, embodies the "linking across domains" principles as identified by Pauwels et al. (2017). Similarly, integrating the chosen design product into the BIM model alongside its attributes manifests the "interoperability" principles.

4.2. Regulation compliance checking

The second step in WLC would be the logical data inference. Models are governed by rules, and when these rules are semantically modelled—using RDF, then less processing layers are required (Allemang & Hendler, 2011). Predictions can be made using these rules, which in semantic models, is called *inference*. From figure 1, the results suggest that researchers mostly use the SWT inferencing capabilities for automated compliance checking, which is the fourth most researched domain. However, a current problem to applying SWT in compliance checking is the fact that Open World Assumptions (OWA), on which SWT are based, do not indicate missing information as a "fault" when making inferences.

4.3. Data management

Data management include different subcategories such as integrating static and dynamic data, data archiving, and Internet of Things (IoT) ontologies. For a purposeful data management model, attention must be given to constructing a precise and comprehensive ontology at the point of data creation—subsection 4.2—to ensure that the adopted classification system and standards support data management requirements. The RDF relationships are not a direct solution to the problem of naming and classifying objects. Yet, they enhance the process through the ability to *construct* property relationships between classes in separate ontologies. These ontologies can then be used to complement the original ones.

5. Conclusions and future work

A structured literature review has been conducted on SWT in AEC to identify the current research domains. Results showed that research on SWT in AEC varies considerably across domains, as semantic BIM modelling, facility management, and energy management form more than 50% of the entire research spectrum. Yet, Research on SWT in the AEC is far from being intensively saturated in any domain. Also, the SWT field lacks the standards and guidelines to facilitate their deployment in the AEC industry. The WLC of information flow, alongside PLM, are the least intensively researched domains. This may be due to the fact that it encompasses all of the three research areas identified by Pauwels et al. (2017), namely interoperability, linking across domains, and logical inference.

A case study is currently being developed with a water utility company, in which, a framework is ought to enable the WLC approach through SWT, see figure 2. The process will start by querying assets/products data during the design stage. Then, product data will be imported into the asset management model to be integrated with the dynamic data from the operational phase.

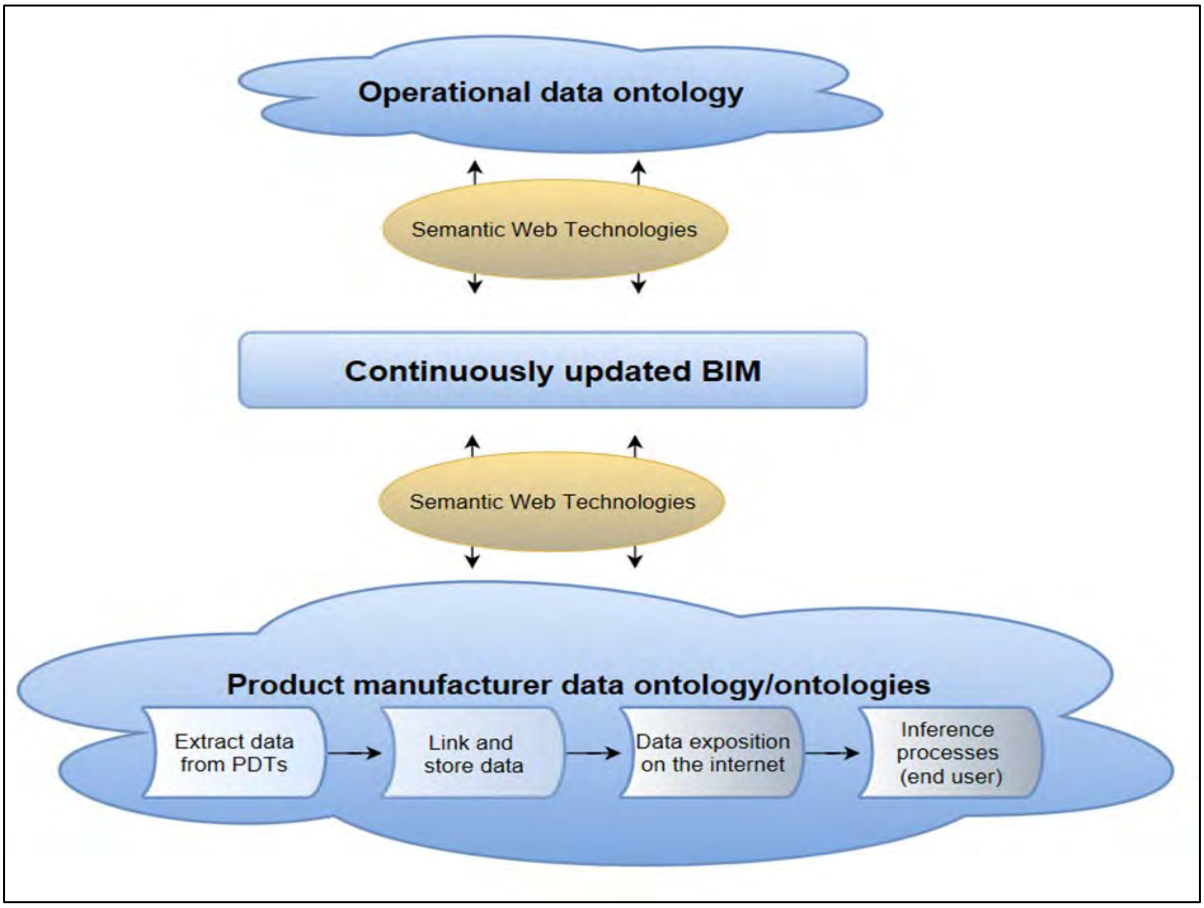

Figure 2: A simplified process flow diagram of the suggested framework. PDTs refer to Product Data Templates

References

- Abanda, F.H., Tah, J.H.M. and Keivani, R. (2013), “Trends in built environment Semantic Web applications: Where are we today?”, *Expert Systems with Applications*, Elsevier Ltd, Vol. 40 No. 14, pp. 5563–5577.
- Allemang, D. and Hendler, J. (2011). Semantic web for the working ontologist. 2nd ed. Morgan Kaufmann.
- Barbau, R. et al. (2012) ‘OntoSTEP: Enriching product model data using ontologies’, CAD Computer Aided Design. Elsevier Ltd, 44(6), pp. 575–590.
- Fortineau, V., Paviot, T. and Lamouri, S. (2019), “Automated business rules and requirements to enrich product-centric information”, *Computers in Industry*, Elsevier B.V., Vol. 104, pp. 22–33.
- Gao, G., Liu, Y.S., Lin, P., Wang, M., Gu, M. and Yong, J.H. (2017), “BIMTag: Concept-based automatic semantic annotation of online BIM product resources”, *Advanced Engineering Informatics*, Elsevier Ltd, Vol. 31, pp. 48–61.
- Gao, G., Liu, Y.S., Wang, M., Gu, M. and Yong, J.H. (2015), “A query expansion method for retrieving online BIM resources based on Industry Foundation Classes”, *Automation in Construction*, Elsevier B.V., Vol. 56, pp. 14–25.
- Gruber, T. (1993). A translation approach to portable ontology specifications. Knowledge Acquisition, 5(2), pp.199-220.

- Niknam, M. and Karshenas, S. (2017), “A shared ontology approach to semantic representation of BIM data”, *Automation in Construction*, Elsevier B.V., Vol. 80, pp. 22–36.
- Pauwels, P., Törmä, S., Beetz, J., Weise, M. and Liebich, T. (2015), “Linked Data in Architecture and Construction”, Automation in Construction, Vol. 57, pp. 175–177.
- Pauwels, P., Zhang, S. and Lee, Y.C. (2017), “Semantic web technologies in AEC industry: A literature overview”, *Automation in Construction*, Elsevier B.V., Vol. 73, pp. 145–165.
- Zhong, B., Wu, H., Li, H., Sepasgozar, S., Luo, H. and He, L. (2019), “A scientometric analysis and critical review of construction related ontology research”, *Automation in Construction*, Elsevier, Vol. 101 No. November 2018, pp. 17–31.

Nottingham | UK | 9–11 September 2019

On-Site Development in Food Industry for Sustainable Utilisation of Food Waste

Nimra Shahab [1], Dr. Martin Howarth [1], Dr. Bipro Dubey[1]

[1] *National Centre of Excellence for Food Engineering, Material & Engineering Research Institute, Sheffield Hallam University, United Kingdom*

Nimra.Shahab@student.shu.ac.uk

Abstract

The discovery of biohydrogen and the possibility of its utilisation to produce renewable electricity has open door to innovate the food industries. Biohydrogen is renewable as it is derived from biological process using natural waste as a substrate. It is highly efficient fuel with energy value of 120-142 MJ which is three times higher than conventional fuel derive from fossils. It is environmental friendly and sustainable at the same time as it doesn't release greenhouse gases (GHG) emission and produce water on combustion. Discharged effluent from food industries and discarded fruit and vegetable peeling are carbohydrate rich substrate. The possibility of its on-site utilisation and conversion to biohydrogen is economical and smart solution as it eliminates the cost to transport the waste and to recover energy from waste. This study comprises of testing the feasibility of biohydrogen production from the waste starch water from potatoes based on primary experiments without adding nutrient and heavy pre-treatment methods.

Keywords: Dark fermentation, Renewable energy, Bio-hydrogen, Energy conversion

1. Background

Increase in demand of various products and services has altered the way of production by amendments in different sector of food industries not only this, food industries require optimum plant infrastructure to store, produce variety of products (non-vegetarian, vegetarian and vegan) and valorise the waste from the by-product [1]. Based on the amount of waste generation food industry have a room for improvement to utilise the by-product on site and make renewable energy from it which can be consumed at the same time[2]. Waste generated by food industries varies and destined to different waste management authorities by adding a cost into it depending on the complexity and nature of waste[3]. Figure 1 below shows waste generated in general food industries at different stages and the way it is managed so far. Waste like packaging can be recycled and final product which does not meet the quality standards cannot be further utilised and must be transported to other routes for utilisation[4]. At the same time the waste which generates as a result of cleaning and prior to the final product is rich in carbohydrates and proteins in order to recover the value from this waste it is transported and processed to derive useful products from it for e.g. oil extract, anti-oxidant, flavonoids and whey powder. Apart from food application the waste is used in the paper making, concrete, pharmaceutical industries, cosmetics and furniture making [5].

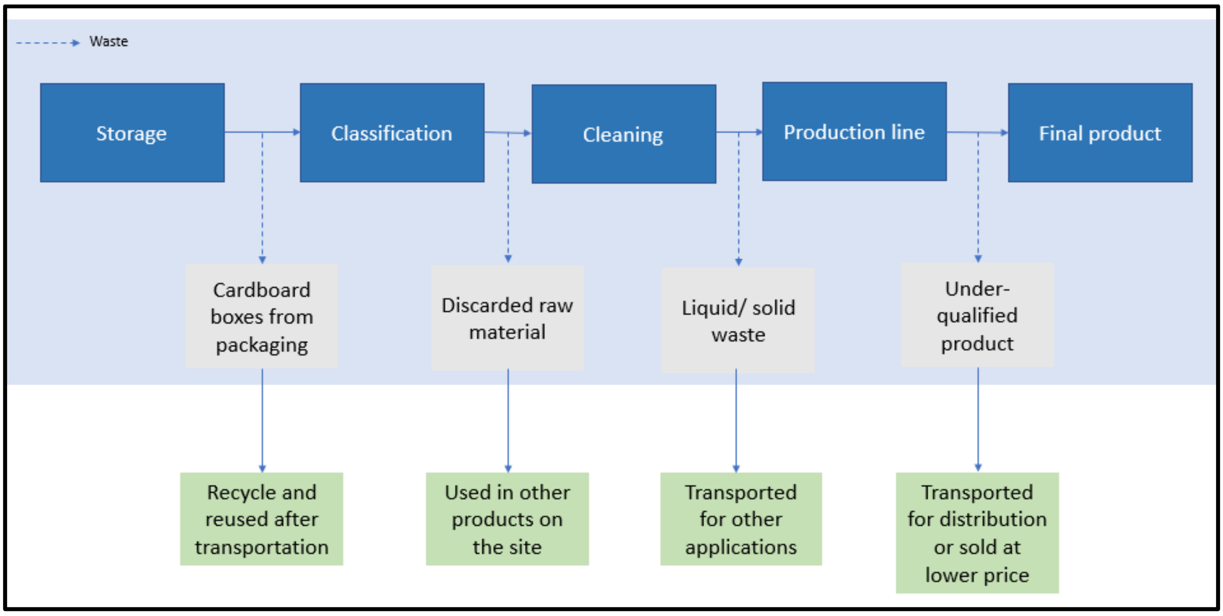

Figure 1 Waste in food industries

2. Introduction

According to the food waste prevention hierarchy it is the best practice to direct the waste towards incineration and landfill after the extraction of all the valuable products from it [6]. In order to achieve this there is a need to modify the design of the present process on site in a way which can help to recover the value from the waste. There are several biological methods which are used to process the wastewater and solid waste for biogas production [7]. Biogas composition depends upon the nature of raw material supplied in the reactor; general composition of bio-gas has 48-65% methane, 36-41% carbon dioxide, 0.8% carbon dioxide, 0-

2% hydrogen gas, 1-17 % nitrogen and <1%oxygen along with traces of ammonia and siloxanes [8]. Based on the energy content bio-hydrogen is three times more energy intensive (120-140 MJ/kg) as compared to bio-methane (50-55.5 MJ/kg) therefore conversion of waste into bio-hydrogen and then bio-methane is another approach to recover energy from waste[9]. Adding value to the waste requires economical and efficient process, dark fermentation is a biological process in which organic waste in converted into bio-hydrogen in absence of light the reasons to choose this procedure are 1) It can be integrated with light fermentation to improve the yield 2) It doesn't require external source of energy 3) it can be carried out in the absence of oxygen 4) it can be carried out using simple design reactor [9]. Potato is one of the major crop productions in the UK and it produce more than 250000 ton starch/year [10]. Using it in the industry for the generation of electricity or store the fuel in tank is the only feasible way to utilise the waste at initial scale, As in 2015 2 sisters food group installed a plant to valorise the mash potato waste and installation of the plant claim to produce 3500 MW hour electricity per year [11]. There are industries which produce uniform nature of food waste, the idea of bio-hydrogen production is practical because of steady supply of raw material, and the process doesn't need major modification because of even composition of the waste throughout[12]. Microbes are important for the improve production of bio-hydrogen because it provides nutrients and nitrogen which favours the degradation of carbohydrate contents easily [13].

3. Experimental Setup

Two types of potato waste were used in this study raw potato waste water and boiled potato waste water. Nitrogen gas at a flowrate of 0.2L/min was sparged to create anaerobic environment. The temperature was kept constant at 35˚C and a stirring speed of 350 rpm with reactor volume of 1.5L. Bio-hydrogen production was monitored by sensors and the result is plotted as a function of concentration. Experimental setup is shown in figure 2. In order to compare the production by waste experiment was conducted using pure starch source at concentration of 10g/L at same operational parameters. The concentration of bio-hydrogen was monitored at uncontrolled pH for all set of experiments. C.butyricum was injected as an inoculum source and the substrate to inoculum ratio was 0.2.

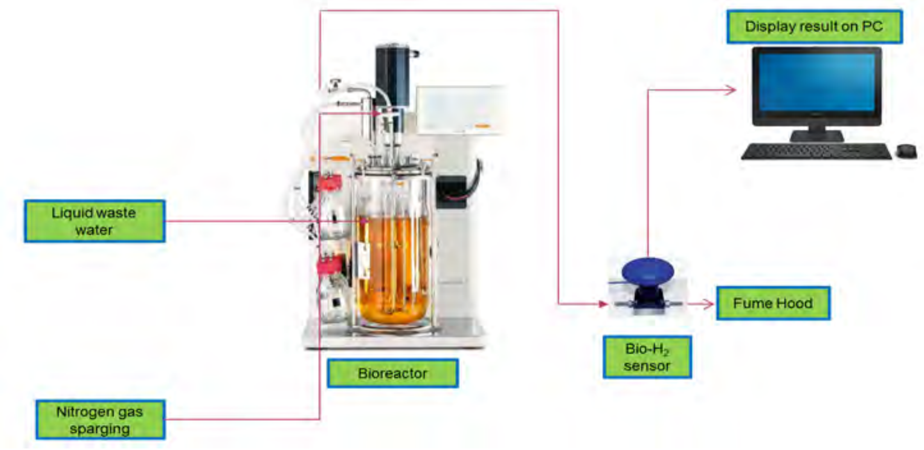

Figure 2 Experimental setup

4. Results and Discussion

The results obtained are shown in figure 3-6 below. The concentration of bio-hydrogen is more as compared to the original waste. Treatment has the effect on concentration of hydrogen produced as the boil potato waste was able to produce more concentration of hydrogen.

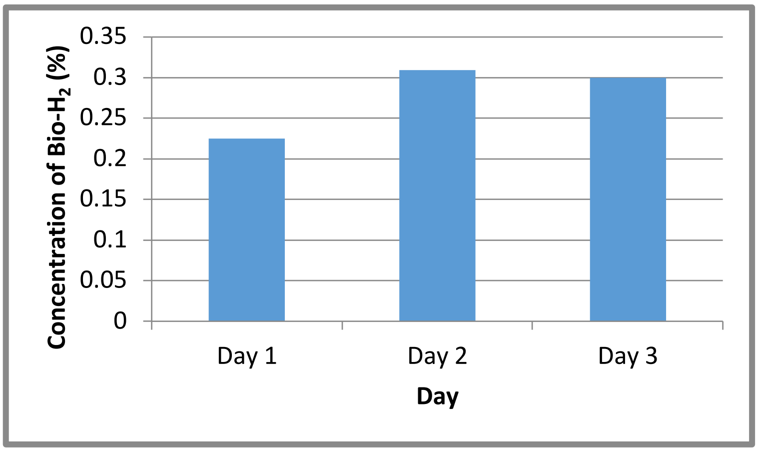

Figure 3 Bio-hydrogen production using pure starch

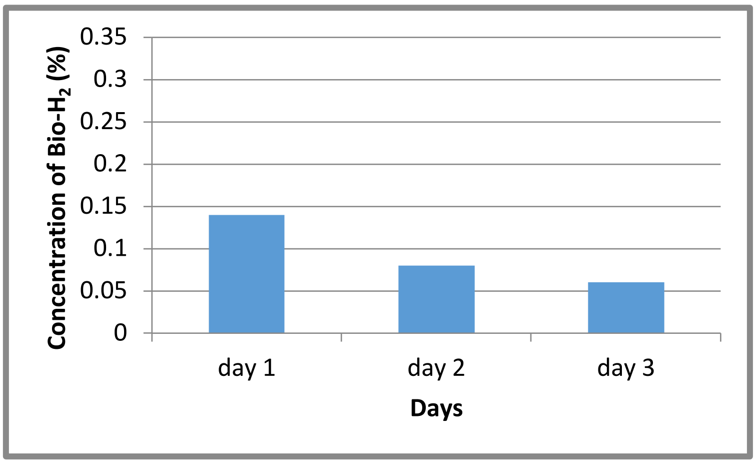

Figure 4 Bio-hydrogen production using boil potato waste water

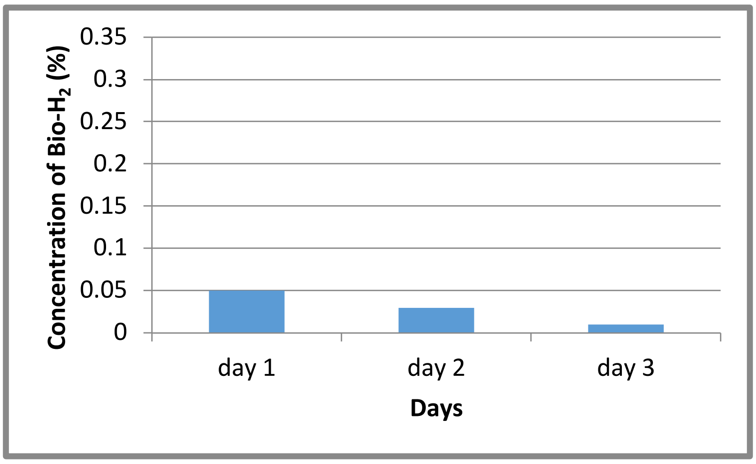

Figure 5 Bio-hydrogen production using raw potato waste water

5. Conclusion

Industries have to evolve in order to overcome their waste. This experiment was carried out to find the possibility of driving hydrogen from liquid waste. Biohydrogen is considered as a fuel of future. Integration of dark fermentation with fuel cell technology has capability to meet minor electricity requirement. Although Bio-hydrogen production is less as compared to the hydrogen driven from conventional methods but the energy produced from it is renewable, environmental friendly and sustainable.

References

[1] B. Notarnicola, K. Hayashi, M. A. Curran, and D. Huisingh, “Progress in working towards a more sustainable agri-food industry,” J. Clean. Prod., vol. 28, pp. 1–8, 2012.

[2] T. P. T. Pham, R. Kaushik, G. K. Parshetti, R. Mahmood, and R. Balasubramanian, “Food waste-to-energy conversion technologies: Current status and future directions,” Waste Manag.,

vol. 38, no. 1, pp. 399–408, 2015.

[3] A. Cerda, A. Artola, X. Font, R. Barrena, T. Gea, and A. Sánchez, “Composting of food wastes: Status and challenges,” Bioresour. Technol., vol. 248, pp. 57–67, 2018.

[4] J. Parfitt, M. Barthel, and S. MacNaughton, “Food waste within food supply chains: Quantification and potential for change to 2050,” Philos. Trans. R. Soc. B Biol. Sci., vol. 365, no. 1554, pp. 3065–3081, 2010.

[5] L. D. Stearns, T. A. Petry, and M. A. Krause, “Potential Food and Nonfood Utilization of Potatoes and Related Byproducts in North Dakota,” J. Food Sci., vol. 3, no. 322, pp. 1–5, 1994.

[6] E. Papargyropoulou, R. Lozano, J. K. Steinberger, N. Wright, and Z. Bin Ujang, “The food waste hierarchy as a framework for the management of food surplus and food waste,” J. Clean. Prod., vol. 76, pp. 106–115, 2014.

[7] S. Manish and R. Banerjee, “Comparison of biohydrogen production processes,” Int. J. Hydrogen Energy, vol. 33, no. 1, pp. 279–286, 2008.

[8] S. Rasi, A. Veijanen, and J. Rintala, “Trace compounds of biogas from different biogas production plants,” Energy, vol. 32, no. 8, pp. 1375–1380, 2007.

[9] F. R. Hawkes, I. Hussy, G. Kyazze, R. Dinsdale, and D. L. Hawkes, “Continuous dark fermentative hydrogen production by mesophilic microflora: Principles and progress,” Int. J. Hydrogen Energy, vol. 32, no. 2, pp. 172–184, 2007.

[10] R. Messias de Braganca and P. Fowler, “Industrial markets for starch,” … Centre, Univ. …, no. June, pp. 1–63, 2004.

[11] F. Times, “Food company cashes in chips with potato power,” 2015. [Online]. Available: https://www.ft.com/content/fdd8883e-62cd-11e5-9846-de406ccb37f2.

[12] “Sewage sludge addition to food waste synergistically enhances hydrogen fermentation performance,” Bioresour. Technol., vol. 102, no. 18, pp. 8501–8506, Sep. 2011.

[13] S. H. Kim, S. K. Han, and H. S. Shin, “Feasibility of biohydrogen production by anaerobic co-digestion of food waste and sewage sludge,” Int. J. Hydrogen Energy, vol. 29, no. 15, pp. 1607–1616, 2004.

Nottingham | UK | 9–11 September 2019

Evaluation of Power Consumption Signal Features in Non-Intrusive Load Monitoring

Pascal A. Schirmer and Iosif Mporas
Communications and Intelligent Systems Group
School of Engineering and Computer Science, University of Hertfordshire
Hatfield AL10 9AB, UK
{p.schirmer,i.mporas}@herts.ac.uk

Abstract

In this article we investigate the effect of feature selection on the energy disaggregation accuracy in a non-intrusive load monitoring setup. The effectiveness of 15 different statistical features was evaluated using the ReliefF feature ranking algorithm and seven subsets of features were formed based on their feature ranking scores. The evaluation was performed on five datasets out of the publicly available REDD database using a Deep Neural Network (DNN) for classification. The experimental results demonstrate the contribution of subsets of features in energy disaggregation with performance increase of up-to 16.3%.

Keywords: Non-Intrusive Load Monitoring (NILM), energy disaggregation, feature selection

1. Introduction

With the development of technology and the increasing usage of electrical appliances and automated services, the electric energy needs have been growing steadily for the last century with an annual growth of approximately 3.4% per year in the last decade [1]. Nowadays residential and commercial buildings account already for roughly 36% of the total electrical demand in the USA and 25% in the EU [2, 3]. Furthermore, studies indicate that detailed analysis and real-time feedback of energy consumption can lead up-to 20% savings in energy consumption through detection of faulty devices and poor operational strategies [4, 5]. Therefore in the last few decades extensive research in the area of smart grids, smart systems and demand management was carried out and different techniques have been developed to reduce residential energy consumption [6].

To make use of those techniques accurate and fine-grained monitoring of electrical energy consumption is needed [7], since the energy consumption of most households is monitored via monthly aggregated measurements and therefore cannot provide real-time feedback. Moreover, according to [8] the largest improvements in terms of energy savings can be made when monitoring energy consumption on device level. The term Non-Intrusive Load Monitoring (*NILM*) is used to describe the estimation of the power consumption of individual appliances, based on a single measurement on the inlet of a household or building [9]. In contrast to NILM, the term Intrusive Load Monitoring (*ILM*) is used when multiple sensors are used, usually one per device. *ILM* compared to *NILM* has the drawback of higher cost through wiring and data acquisition making it unsuitable for monitoring households where appliances can change, while *NILM* has the goal of finding the inverse of the aggregation function through a disaggregation algorithm using as input only the aggregated power consumption which makes it a highly underdetermined problem and thus impossible to solve analytically [10].

Considering the wide range of appliances in nowadays households accurate modelling of appliances is essential to solve the *NILM* problem with sufficient accuracy. Furthermore low cost algorithms are preferred and thus electrical appliances are modelled according to their steady state behaviour using low sampling frequencies [9]. To capture the steady state behaviour as well as the transitions between the steady states with low sampling frequencies for different electrical appliances (e.g. one/multi-state, non-linear or continuous [11, 12]), investigation of the effect of different features is essential. In this paper we evaluate the performance of various features on the energy disaggregation task for the *NILM* approach. The remainder of this paper is organized as follows: In Section 2 the baseline *NILM* system is presented. In Section 3 the experimental setup is described and in Section 4 the evaluation results are presented. Finally the paper is concluded in Section 5.

2. NILM Architecture

NILM energy disaggregation can be formulated as the task of determining the power consumption on device level based on the measurements of one sensor, within a time window (frame or epoch). Specifically, for a set of $M-1$ known devices each consuming power p_m with $1 \leq m \leq M$, the aggregated power P_{agg} measured by the sensor will be

$$P_{agg} = f(p_1, p_2, \dots, p_{M-1}, g) = \sum_{m=1}^{M-1} p_m + g = \sum_{m=1}^{M} p_m \tag{1}$$

where $g = p_M$ is a ‘ghost’ power consumption usually consumed by one or more unknown devices. In NILM the goal is to find estimations $\hat{p}_m$, $\hat{g}$ of the power consumption of each device m using an estimation method f^{-1} with minimal estimation error, i.e.

$$\begin{gathered}\hat{P} = \{\hat{p}_1, \hat{p}_2, \dots, \hat{p}_{M-1}, \hat{g}\} \leftarrow f^{-1}(P_{agg}) \\ \text{s.t. } \underset{f^{-1}}{\operatorname{argmin}} \{ \left(P_{agg} - \sum_1^M \hat{p}_m - \hat{g}\right)^2 \}\end{gathered} \tag{2}$$

The block diagram of the NILM architecture adopted in the present evaluation is illustrated in Figure 1 and consists of three stages, namely the pre-processing, feature extraction and appliance detection. In detail, the aggregated power consumption signal calculated from a smart meter is initially pre-processed i.e. passed through a median filter [13] and then frame blocked in time frames. After pre-processing feature vectors, v of dimensionality $||v||$, one for each frame are calculated. In the appliance detection stage the feature vectors are processed by a regression algorithm using a set of pre-trained appliance models to estimate the power consumption of each device. The output of the regression algorithm estimates the corresponding device consumption and a set of thresholds T_m with $1 \leq m \leq M$ with $T_g = T_M$ for the each device including the ghost device ($m = M$) is used to decide whether a device is switched on or off.

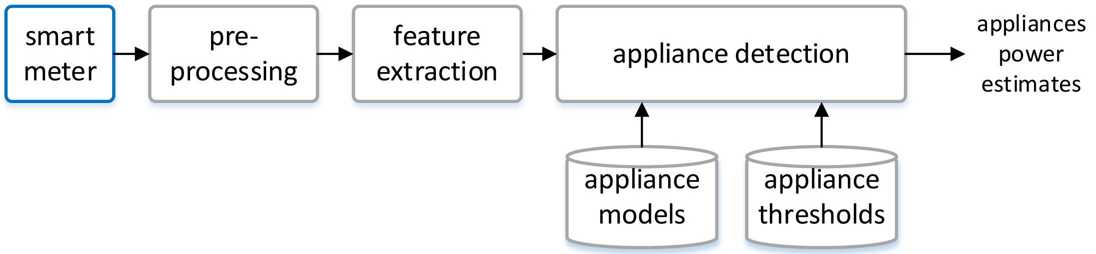

Figure 1: Block diagram of the NILM architecture used.

3. Experimental Setup

The NLIM architecture presented in Section 2 was evaluated using a number of publicly available datasets and a deep neural network for regression.

3.1. Datasets

To evaluate performance five different datasets of the *REDD* [14] database were used. The *REDD* database was chosen as it contains power consumption measurements per device as well as the aggregated consumption. The *REDD*-5 dataset was excluded as its measurement duration is significantly shorter than of the rest datasets in the *REDD* database [15]. The evaluated datasets and their characteristics are tabulated in Table I with the number of appliances denoted in the column #App. In the same column, the number of appliances in brackets is the number of appliances after excluding devices with power consumption below 25W, which were added to the power of the ghost device, similarly to the experimental setup followed in [16, 17]. The next three columns in Table I are listing the sampling period T_s, the duration T of the aggregated signal used and the appliance type for each evaluated dataset. The appliances type categorization is based on their operation as described in [18, 19].

TABLE I. List of the evaluated datasets and their corresponding properties.

Dataset	**Properties**			
	# App.	T_s	T	***Appliance Type***
REDD-1	18 (17)	3s	7d	One state/ multi state/ non-linear
REDD-2	9 (10)	3s	11d	One state/ multi state
REDD-3	20 (18)	3s	14d	One state/ multi state/ non-linear
REDD-4	18 (16)	3s	14d	One state/ multi state/ continuous / non-linear
REDD-5	24 (17)	3s	3d	One state/ multi state / non-linear
REDD-6	15 (14)	3s	12d	One state/ multi state / continuous / non-linear

3.2. Pre-processing and Feature Ranking

During pre-processing the aggregated signal was processed by a median filter of 5 samples as proposed in [13] and then was frame blocked in frames of 10 samples with overlap between successive frames equal to 50% (i.e. 5 samples). For every frame a feature vector consisting of 15 statistical features (mean value, minimum and maximum values, Root-Mean-Square (*RMS*) value, median value, percentiles 25% and 75%, variance, standard deviation (*Std*), skewness, kurtosis, range, energy and Zero Crossings (*ZC*)) was calculated resulting to a feature vector of dimensionality equal to 15. In order to calculate the statistical importance of the 15 features the *ReliefF* feature ranking algorithm [20] was used and the results are shown in Figure 2.

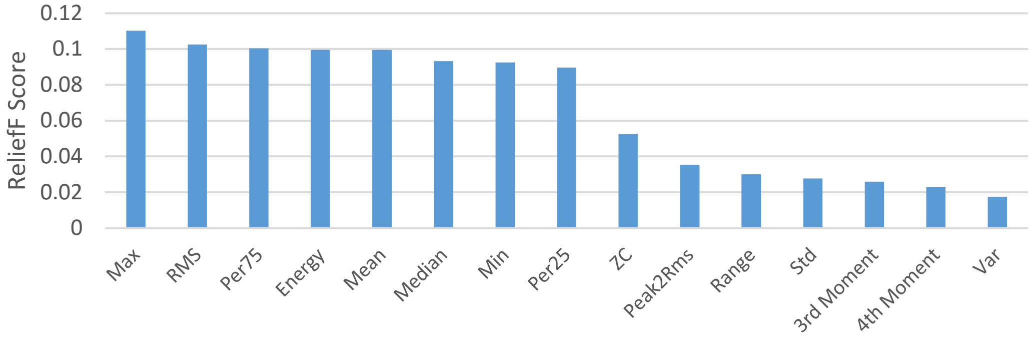

Figure 2: Feature ranking for 15 statistical features

As can be seen in Figure 2 features can be divided into two groups based on their *ReliefF* scores. The first group includes eight features with high ranking score (>0.05) while the second group includes features with lower ranking score (<0.05). The outcome of the feature ranking was used to design a set of seven experimental protocols, with the first five including statistical features with higher ranking score and two additional experiments also including those with lower ranking score. The chosen features for each experiment are tabulated in Table II where the first experiment is only considering the mean value of the active power and is considered here as baseline system.

TABLE II. Definition for seven different experimental protocols including different numbers of features determined from the feature ranking

Protocol	**Features**	**Categories**
1	Mean	Statistical Features (>0.05)
2	Mean, Max, Min	Statistical Features (>0.05)
3	Mean, Max, Min, RMS	Statistical Features (>0.05)
4	Mean, Max, Min, RMS, Median, Per25, Per75	Statistical Features (>0.05)
5	Mean, Max, Min, RMS, Median, Per25, Per75, Energy	Statistical Features (>0.05)
6	Mean, Max, Min, RMS, Median, Per25, Per75, Energy, ZC	Statistical Features (≥0.05)
7	Mean, Max, Min, RMS, Median, Per25, Per75, Energy, ZC, Peak2Rms, Range, Std, Skewness, Kourtessis, Variance	Statistical Features

For the regression stage a feed-forward Deep Neural Network (*DNN*) has been employed. The free parameters of the *DNN* were empirically optimized after grid search on a bootstrap training subset with ideal aggregated data (without ghost power) resulting to a regression model with a feed-forward architecture of 3-hidden layers and 32 sigmoid nodes per layer.

4. Results and Discussion

The NILM architecture presented in Section 2 was evaluated according to the experimental setup described in Section 3. The performance was evaluated in terms of appliance power estimation accuracy (E_{ACC}), as proposed in [14] and defined in Eq. 3. The accuracy estimation is taking into account the estimated power p_m for each device m, where T is the number of frames and M is the number of disaggregated devices.

$$E_{ACC} = 1 - \frac{\sum_{t=1}^{T}\sum_{m=1}^{M}|\hat{p}_m^t - p_m^t|}{2\sum_{t=1}^{T}\sum_{m=1}^{M}|p_m^t|} \tag{3}$$

The evaluation results for different experimental protocols and different regression models are tabulated in Table III. As can be seen in Table III including additional statistical features results to improvement of the energy disaggregation performance across all datasets.

TABLE III. Disaggregation results (%) for five different datasets across the seven experimental protocols using different numbers of features.

Protocol	1	2	3	4	5	6	7
REDD-1	67.63%	69.52%	**73.37%**	71.08%	72.11%	68.21%	69.80%
REDD-2	63.62%	78.79%	79.63%	78.39%	**79.92%**	79.44%	77.37%
REDD-3	63.67%	69.16%	66.31%	68.23%	67.44%	**69.87%**	68.96%
REDD-4	73.00%	**73.36%**	72.45%	73.06%	73.35%	72.67%	73.26%
REDD-6	75.25%	77.05%	76.25%	76.79%	**77.05%**	77.03%	76.06%
AVG	68.63%	73.58%	73.60%	73.51%	**73.97%**	73.44%	73.09%

As can be seen in Table III all datasets reach their highest performance within protocols 2-6. In detail all datasets benefit by adding features with high ranking score in the features space (≥ 0.05) while the addition of features with low ranking score (<0.05) lead to a decrease in performance while having a significant increase in the number of dimensions. Specifically the increase in performance varies between 0.4% and 16.3% with an average increase of 5.3%. The highest performance increase was observed for the *REDD*-2 dataset (16.3%), followed by the *REDD*-1/3 datasets (5.7% and 6.2%) while the performance increase for the *REDD*-4/6 datasets is significantly lower (0.4% and 1.8% respectively). Comparing the performance increase with the properties of datasets shown in Table I no significant influence of the number of appliances in performance was observed. However considering the appliance types, datasets without continuous appliances (*REDD*-1/2/3) had significant performance increase while those with continuous appliances (*REDD*-4/6) had smaller improvements. This is due to the fact that the continuous appliances which do not have a set of specific power states cannot be learnt by employing a higher number of features. On the contrary, increasing the number of features improves the performance of appliances with well-defined states namely the one/multi-state and non-linear appliances.

5. Conclusion

In this paper the performance of different sets of features for energy disaggregation in non-intrusive load monitoring was investigated. The evaluation results showed the importance of the selection of features in combination with different appliance types, with performance increase varying between 0.4% and 16.3%, while datasets without continuous appliances improving significantly more than datasets with continuous appliances. After evaluating energy disaggregation across several datasets protocol five was found as the best performing protocol with an average energy disaggregation accuracy of 73.97% and 5.3% performance increase respectively.

Acknowledgment

This work was supported by the UA Doctoral Training Alliance (https://www.unialliance.ac.uk/) for Energy in the United Kingdom.

References

[1] B. Yu, Y. Tian, and J. Zhang, “A dynamic active energy demand management system for evaluating the effect of policy scheme on household energy consumption behavior,” *Energy*, vol. 91, pp. 491–506, 2015.

[2] O. Elma and U. S. Selamogullar, “A survey of a residential load profile for demand side management systems,” in *2017 the 5th IEEE International Conference on Smart Energy Grid Engineering (SEGE): 2017, UOIT,* Canada, 2017, pp. 85–89.

[3] Eurostat, *Energy statistics - an overview.* [Online] Available: https://ec.europa.eu/eurostat/statistics-explained/index.php?title=Energy_statistics_-_an_overview#Final_energy_consumption. Accessed on: Mar. 27 2018.

[4] D. Lee and C.-C. Cheng, "Energy savings by energy management systems: A review," *Renewable and Sustainable Energy Reviews*, vol. 56, pp. 760–777, 2016.

[5] M. Zeifman and K. Roth, "Viterbi algorithm with sparse transitions (VAST) for nonintrusive load monitoring," in *2011 IEEE Symposium on Computational Intelligence Applications in Smart Grid*, 2011, pp. 1–8.

[6] I. V. *et al.,* "Multi-objective optimization and energy management in renewable based AC/DC microgrid," *Computers & Electrical Engineering*, vol. 70, pp. 179–198, 2018.

[7] A. Chis, J. Rajasekharan, J. Lunden, and V. Koivunen, "Demand response for renewable energy integration and load balancing in smart grid communities," in *24th European Signal Processing Conference (EUSIPCO)*, Budapest, Hungary, 2016, pp. 1423–1427.

[8] M. N. Meziane and K. Abed-Meraim, "Modeling and estimation of transient current signals," in *23rd European Signal Proc. Conf. (EUSIPCO)*, 2015, pp. 1960–1964.

[9] G. W. Hart, "Nonintrusive appliance load monitoring," *Proc. of IEEE*, vol. 80 (12), pp. 1870–1891, 1992.

[10] M. Gaur and A. Majumdar, "Disaggregating Transform Learning for Non-Intrusive Load Monitoring," *IEEE Access*, vol. 6, pp. 46256–46265, 2018.

[11] Y. Zhu and S. Lu, "Load profile disaggregation by Blind source separation: A wavelets-assisted independent component analysis approach," in *2014 IEEE PES general meeting: Conference & exposition ; 27 - 31 July 2014, National Harbor, MD*, 2014, pp. 1–5.

[12] H.-H. Chang, K.-L. Lian, Y.-C. Su, and W.-J. Lee, "Power-Spectrum-Based Wavelet Transform for Nonintrusive Demand Monitoring and Load Identification," *IEEE Transactions on Industry Applications*, vol. 50, no. 3, pp. 2081–2089, 2014.

[13] C. Beckel, W. Kleiminger, R. Cicchetti, T. Staake, and S. Santini, "The ECO data set and the performance of non-intrusive load monitoring algorithms," in *BuildSys'14: Proceedings of the 1st ACM Conference on Embedded Systems for Energy-Efficient Buildings*, 2014, pp. 80–89.

[14] J. Z. Kolter and M. J. Johnson, Eds., *REDD: A Public Data Set for Energy Disaggregation Research*, 2011.

[15] V. Andrean, X.-H. Zhao, D. F. Teshome, T.-D. Huang, and K.-L. Lian, "A Hybrid Method of Cascade-Filtering and Committee Decision Mechanism for Non-Intrusive Load Monitoring," *IEEE Access*, vol. 6, pp. 41212–41223, 2018.

[16] H. Wang and W. Yang, "An Iterative Load Disaggregation Approach Based on Appliance Consumption Pattern," *Applied Sciences*, vol. 8, no. 4, p. 542, 2018.

[17] S. M. Tabatabaei, S. Dick, and W. Xu, "Toward Non-Intrusive Load Monitoring via Multi-Label Classification," *IEEE Trans. on Smart Grid*, vol. 8 (1), pp. 26–40, 2017.

[18] S. R. Shaw, S. B. Leeb, L. K. Norford, and R. W. Cox, "Nonintrusive Load Monitoring and Diagnostics in Power Systems," *IEEE Transactions on Instrumentation and Measurement*, vol. 57, no. 7, pp. 1445–1454, 2008.

[19] A. Zoha, A. Gluhak, M. A. Imran, and S. Rajasegarar, "Non-intrusive load monitoring approaches for disaggregated energy sensing: A survey," *Sensors (Basel, Switzerland)*, vol. 12, no. 12, pp. 16838–16866, 2012.

[20] R. J. Urbanowicz, M. Meeker, W. LaCava, R. S. Olson, and J. H. Moore, "Relief-Based Feature Selection: Introduction and Review," [Online] Available: http://arxiv.org/pdf/1711.08421v2.

Nottingham | UK | 9–11 September 2019

Building thermal output determination using visible spectrum and infrared inputs

G.Sfikas[1,2], A.Noula[1], J.Patacas[3], D.Ioannidis[1], D.Tzovaras[1]

[1] *Centre for Research & Technology, Information Technologies Institute, Thessaloniki, Greece*

[2] *Computer Science & Engineering Dpt., University of Ioannina, Ioannina, Greece*

[3] *School of Science, Engineering and Design, Teesside University, Middlesbrough, UK*

{sfikas,antigoni,djoannid,Dimitrios.Tzovaras}@iti.gr, J.Patacas@tees.ac.uk

Abstract

Accurate building thermal output determination is key for the development of energy use optimisation strategies, including demand response strategies. The analysis of thermal images of buildings presents the opportunity to estimate energy demand based on the actual as-built buildings, as opposed to the current assessment procedures used in the industry which are based on design values.

In this work, we present an image processing pipeline for calculating the thermal output of buildings, by identifying regions of interest given a dual modality (visible spectrum/RGB, infrared) input. The region of interest is assumed to be a building found approximately at the centre of the image field of view ('target building'). The visible spectrum/RGB input is first used to determine the position and outline of the target building in the field of view, and create a pixel-level binary mask with non-zero mask elements corresponding to the target. Subsequently, the produced mask is used to binarize the thermal imaging input and produce an intensity matrix containing only values that correspond only to the building / region of interest. With the proposed method, we are able to take into account only the thermal output of the region of interest, leaving out other image objects and other elements that act as 'noise' in this context. Once computed, the thermal signature of the target building can be subsequently used as input to an energy auditing process or as a component of urban energy planning. The proposed pipeline is evaluated on dual RGB/synthetic thermal image pairs captured on various buildings.

Keywords: Thermal imaging, thermal output determination, object detection, energy demand, Demand Response

1. Introduction

Accurate building thermal output determination presents a series of challenges, due to the difficulty in accounting for differences between the building design values that are used for estimation of energy consumption, and the actual performance of buildings, which is largely influenced by uncertainties associated with the quality of building materials, and the quality of the construction and installation process. Accurate methods for the estimation of energy demand in buildings are a key input for the optimisation of building energy use, including effective demand response (DR) programs that can be leveraged both by smaller energy consumers and energy providers in order to increase the amount of flexibility in DR. The analysis of thermal images for the estimation of energy demand in buildings has been proposed as an alternative to the current energy demand assessment methods, such as the Standard Assessment Procedure (SAP) in the UK [1], however there are still uncertainty issues regarding the proposed methods [2,3,4].

This research investigates how the use of combined thermal and visible-spectrum (RGB) digital images can be used to identify the demand response potential of building assets. In this paper, we propose a method for the identification of potential DR building assets through the application of a novel image processing pipeline for calculating the thermal output of a region of interest given a dual modality (visible spectrum/RGB, infrared) input. Our motivation of using a visible-spectrum input to detect the region of interest is that the infrared input in itself is not appropriate to be used to semantically differentiate objects; the infrared signature may be useful to determine areas of low or high thermal output, but in itself is insufficient to delineate a region of interest efficiently.

The proposed image processing pipeline will be used to identify and provide a range of temperature values for individual building features such as walls, windows, roofs and HVAC assets. Using the proposed image processing pipeline it is possible to isolate features from the building envelope such as the external walls and roof of the building and estimate their U values (i.e. overall heat transfer coefficient (W/m2K)), as well as the transmission heat losses [2,3]. The estimated transmission heat losses will be considered as an input to the estimation of energy demand, and will be used to estimate demand-side improvement potential, which will inform the DR potential estimation process.

Results from the proposed method are expected to provide improved baseline estimation and improved DR flexibility estimation to increase exploitation potential of building assets in DR programs. In particular, the resulting thermal imagery data can be analysed to provide more detailed information about users/customers behaviour.

2. **Experimental**

The proposed method involves correctly estimating the thermal signature of a target structure, given a thermal imaging camera input, along with an aligned visible spectrum / RGB input. In what follows, thermal signature is understood as the per-pixel statistics of the infrared image input, though the discussed pipeline is applicable to virtually any processing performed over an infrared input. The proposed processing pipeline involves the following steps: a) Use the RGB input to localise the region of interest / target building. This step provides a per-pixel mask that is used to b) determine the thermal output of the target building, using the IR input. The proposed processing pipeline can be examined at figure 1. We have performed our experiments at the 'smart home' site, situated at Pylaia-Thessaloniki, Greece and part of the facilities of the Centre for Research and Technology Hellas (CERTH). We have captured 5 visible-spectrum (i.e. colour) images of the target building taken from different poses. As hardware that would include an IR camera aligned with the visible-spectrum was unavailable, we have taken advantage of an available fixed-position IR camera to create synthetic IR images that are aligned pixel-to-pixel with the available RGB shots. Below, we discuss the aforementioned components in further detail.

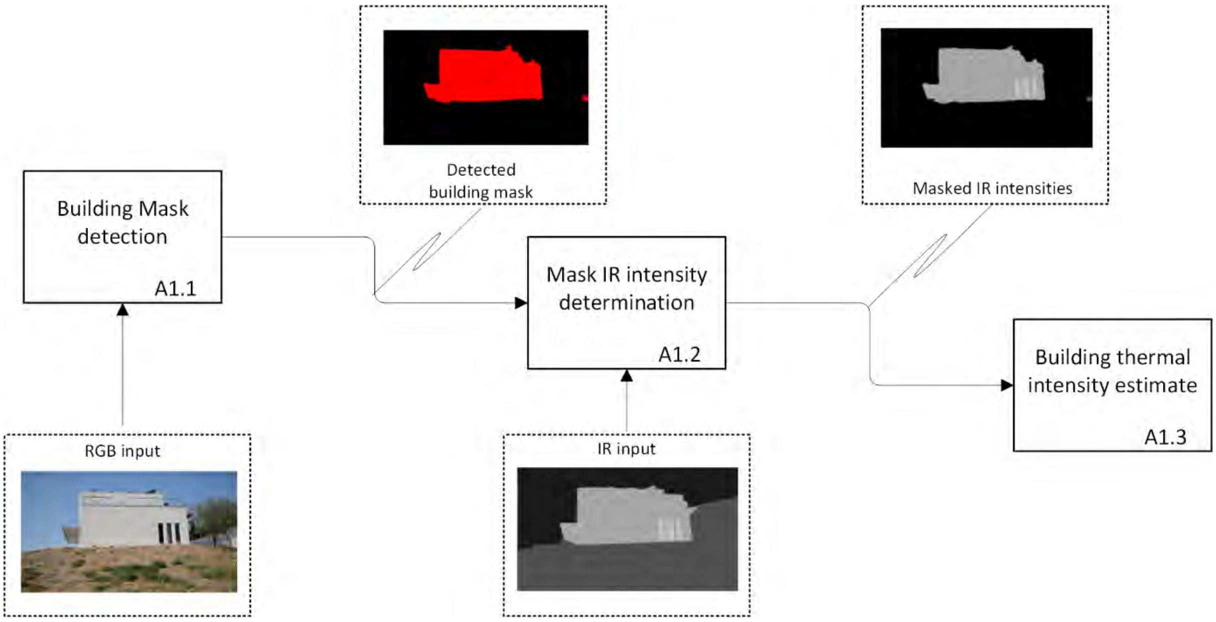

Figure 1: IDEF0 process diagram for the proposed image processing pipeline. The RGB image is used to detect the Region of Interest (target building). The IR image is then masked accordingly and thermal intensity statistics are computed over relevant IR pixels. Without the

proposed RGB-based detection component, statistics over the IR image take into account irrelevant pixels, thereby leading to an erroneous thermal signature estimate.

2.1 Region of interest detection

Detection of the region of interest, or in other words localisation of the target building is performed solely over the visible-spectrum/RGB input. Our motivation in using an assumed RGB input for this task is that the latter is semantically much richer than the corresponding IR input; detection of an object is a task related to semantics, as opposed to thermal determination which does not involve image understanding at all, but low-level processing of the IR channel. To the end of target localization, we have used DeepLab v3+ [5], a state-of-the-art neural network-based model for semantic image segmentation. Instead of using this model to directly segment the RGB input, we have used it as a feature extractor, providing so-called Deep Features [6,7]. In this work, we use the activations of the last convolutional layer as our 'deep' features. This is performed without any further training over a pre-trained model[1], by a simple feed-forward pass of the network. We then perform k-means [8] over the extracted deep features, after having reduced the set of the 256-dimensional deep features to 8-dimensional vectors with Principal Component Analysis (PCA, [8]). We use 3 clusters for k-means, which we have found to roughly correspond to the target building, the sky, and other areas/objects (ground, etc.). Clusters are initialised with k-means++. The advantage of using DeepLab directly over this approach, is that the learning task 'becomes' unsupervised, despite that the base model (the neural network) had been pre-trained with a supervised learning process. Consequently, no annotated data is necessary to perform ROI localisation. The cluster with the least average per-pixel distance to the centre image pixel is chosen as the cluster that is related to the target building. The rest are classified as background.

2.2 Thermal output determination

Once the area corresponding to the target structure is localized in the previous step, we simply compute mean and standard deviation of the recorded IR intensities. Note that if the previous step was missing, we can expect that IR statistics should be a bad estimate of the target building thermal signature, since it would include pixels not corresponding to the region of interest. This is indeed corroborated by our experiments (cf. following section).

---

[1] The model backbone we used is Xception, pre-trained on the ADE20K dataset [5].

(1) (2) (3) (4) (5)

Figure 2: Visible-spectrum/RGB images used to test the proposed pipeline (top row) and corresponding synthetic thermal IR images (bottom row), created using real IR image statistics (see text for details).

Figure 3: IR image used to obtain pixel-level intensity statistics, used to create the synthetic IR images in fig. 2.

2.3 Infrared image synthesis

While this is not part of the main proposed pipeline per se, this step is necessary to evaluate the algorithm, in order to create aligned RGB/IR pairs where the IR image is as close as possible to a real IR image, w.r.t. to thermal output statistics. We have used a real IR image of the target building (fig. 3) to obtain statistics of IR intensities. In particular, we have computed mean and standard deviation values for pixels in four semantic groups: sky, walls, windows and ground/other. To this end, the real IR image has been manually annotated w.r.t. to the aforementioned semantic classes, and intensity statistics were computed per class. Subsequently, we performed manual annotations on our RGB images w.r.t. to the same classes. For each of the semantic classes and manually delineated areas per image, we drew normally distributed intensity samples that follow the statistics of the real IR image corresponding class statistics. In the context of the current problem, reassuring that the synthesized images follow real image statistics is important, as thermal intensity statistics is what we want to measure.

Table 1: Quantitative comparison of proposed pipeline versus baseline method that does not incorporate visible-spectrum based salient building detection and an Otsu-based localizer. Average absolute values over test images are presented. Lower absolute values are better.

	Percentage offset from ground truth					
	Image 1	Image 2	Image 3	Image 4	Image 5	Mean +- St.dev.
Baseline method	25.7%	29.8%	17.4%	25.1%	24.8%	24.5 +- 4
Otsu-based method	0.9%	38.3%	50.1%	69.6%	46.1%	40.9 +- 22.5
Deep feature-based method (Proposed)	0.3%	2.9%	0.7%	21.9%	21.4%	9.4 +- 10.0

3. Results and Discussion

In order to test the proposed thermal determination method, we have evaluated it quantitatively versus a ‘baseline’ method and another method where an alternative ROI detection scheme is used (‘Otsu-based’). The baseline method involves simply computing statistics of IR image raw intensity values over the whole IR image, as if the full image were of interest. The Otsu-based method employs Otsu [8], a standard binarization algorithm to segment into building and background. Again, the class that is closest to the centre is tagged as building. The proposed method gives the lowest divergence w.r.t. to the true IR mean thermal intensity, i.e. the best result. For 3 out of 5 images, this divergence is minimal, corresponding to an extremely accurate delineation of the target structure boundary. On the other hand, the other methods are consistently far from the real thermal signature; perhaps surprisingly, Otsu results in a worse estimate compared to the baseline, i.e. versus not using ROI localisation at all. This should be attributed to the low quality of ROI localisation attained by Otsu. Results can be examined in table 1, where quantitative results over each shot individually (following the numbering of figure 1), and average offset values are reported.

4. Conclusion

We have shown how to use a neural network-based system to compute a significantly improved estimate of the thermal signature of a target structure. This estimate is useful to applications using heat loss estimates as input, such as Demand Response programs. While our result is to be understood on the premise that we use only synthetic infrared data in this work, we believe that our conclusion can be in all probability extended to real-world data, as we have taken care to use statistics of real IR footage to construct our dataset. Hence, we look forward to testing the proposed pipeline on data that fully include real RGB+infrared image pairs. Future experiments on non-artificial IR data will also determine whether a combination of IR+RGB is useful towards salient object detect, and compare versus using the IR input only for the full processing pipeline.

Acknowledgments

The work presented was carried out as part of the eDREAM project which is co-funded by the EU's Horizon 2020 framework programme for research and innovation under grant agreement No 774478. The authors wish to acknowledge the European Commission for their support, the efforts of the project partners, and the contributions of all those involved in eDREAM.

References

1. BEIS (2014) Standard Assessment Procedure Guidance on how buildings will be SAP energy assessed under the Green Deal and on recent changes to incentivise low carbon developments. Available at: https://www.gov.uk/guidance/standard-assessment-procedure Accessed on: 16th May 2019
2. Paris A. Fokaides, Soteris A. Kalogirou (2011), Application of infrared thermography for the determination of the overall heat transfer coefficient (U-Value) in building envelopes, Applied Energy, Volume 88, Issue 12, 2011, Pages 4358-4365, ISSN 0306-2619, https://doi.org/10.1016/j.apenergy.2011.05.014.
3. D. González-Aguilera, S. Lagüela, P. Rodríguez-Gonzálvez, D. Hernández-López (2013), Image-based thermographic modeling for assessing energy efficiency of buildings façades, Energy and Buildings, Volume 65, 2013, Pages 29-36, ISSN 0378-7788, https://doi.org/10.1016/j.enbuild.2013.05.040.
4. Y. Ham & M. Golparvar-Fard (2012) Rapid 3D Energy Modeling for Retrofit Analysis of Existing Buildings Using Thermal and Digital Imagery. LiDAR Magazine, Vol. 2, No. 4
5. L.C. Chen, Y.Zhu, G.Papandreou, F. Schroff, A. Hartwig (2018), Encoder-Decoder with Atrous Separable convolution for semantic image segmentation, the European Conference on Computer Vision (ECCV), pp. 801-818

6. G.Sfikas, G.Retsinas, B.Gatos, Zoning Aggregated Hypercolumns for Keyword Spotting (2016), International Conference on Frontiers in Handwriting Recognition (ICFHR), Shenzhen, China
7. G.Retsinas, G.Louloudis, N.Stamatopoulos, G.Sfikas, B.Gatos, An Alternative Deep Feature Approach to Line Level Keyword Spotting (2019), IEEE Computer Vision and Pattern recognition (CVPR), Long Beach (CA), USA
8. C.M.Bishop (2006), Pattern Recognition and Machine Learning, Springer.

Nottingham | UK | 9–11 September 2019

Computational Fluid Dynamics (CFD) fire modelling in mechanically ventilated nuclear compartments

Okorie Ukairo[1*], Siaka Dembele[1], Ali Heidari[1], Konstantin Volkov[1] and Jennifer Wen[2]
[1]*Department of Mechanical Engineering, Kingston University, London SW15 3DW, UK*

[2]*School of Engineering, University of Warwick, Coventry CV4 9YP, UK*

* O.Ukairo@kingston.ac.uk

Abstract

The outbreak of fires in nuclear power plants is a major risk due to the potential leak of radioactive materials. The use of traditional prescriptive fire safety regulations has shown its limitations and there is now a shift towards performance based fire safety engineering, which requires well validated fire models. Nuclear power plants require the use of mechanical ventilation which provides confinement for the nuclear material by maintaining the required pressure. During a fire there is the possibility of pressure variations within the power plant which modify the confinement level leading to the escape of nuclear materials.

The current project study aims to build on existing research by making use of an emerging open source fire CFD simulation tool known as FireFOAM to predict the fire and pressure behaviours in a mechanically ventilated room. A ventilation model has been developed and implemented into FireFOAM and coupled with a conjugate heat transfer solver to account for the heat transfer between combustion gases and solid boundaries. Preliminary results are presented for the validation of the ventilation model and velocity of the ventilation duct in the nuclear compartment. Overall, there are good agreements between the results and some benchmark data

Keywords:

Fire; CFD; Mechanical Ventilation Model; FireFOAM; Validation; Heat Transfer

1. Introduction

Nuclear facilities consist of rooms that are equipped with mechanical ventilation that ensures dynamic confinement and control any possible emission of radioactive materials during a fire outbreak. During fires, pressure variations occur within the nuclear plants because of the high confinement level. The consequences of these pressure variations in a highly confined nuclear room is the loss of dynamic confinement because of the internal pressure exceeding the outside pressure the nuclear plants.

Several theoretical and experimental studies have been conducted that dealt with specific areas of fire modelling in nuclear compartments. Among them, the experimental projects PRISME 1 & 2' [1] conducted at the French "Institut de Radioprotection et de Sûreté Nucléaire" (IRSN) between 2007 and 2011. The data from PRISME would be used in the present study to validate the numerical simulation. Suard et al. [2] performed a study showing the predictive simulations of fires in mechanically ventilated nuclear plants by coupling boundary conditions of the ventilation mass flow rate and the pressure within the compartment. Le et al. [3] investigated the capabilities of FireFOAM applied to PRISME Integral 4.There was acceptable agreement between the simulated results and experimental values in these previous studies for pressure and velocity and the need to improve the models was highlighted.

The simulation of nuclear compartments fires and ventilation networks is very time consuming leading to the decomposition into 1D and 3D models. In the present study, a ventilation model was developed and implemented in the fires CFD code FireFOAM. The predictions are compared to some benchmark numerical data and PRISME Source experimental data consisting of a single mechanically ventilated, fire room.

2. Mathematical and numerical approaches

The majority of 1D ventilation models are based on a generalized Bernoulli formulation [4]. The 1D steady state ventilation model used in the present study is based on the momentum equation and its governing equation is given as [5]:

$$(P_i - P_{i-1}) + \Delta P_{FAN,j} - \frac{1}{2}K\rho_j u_j^2 + (\rho g \Delta z)_j = 0 \qquad (1)$$

Where ρ_j represents the average density, u_j is the average velocity, of the ventilation duct, $P_i - P_{i-1}$ represent the pressure difference in a duct. $\Delta P_{FAN,j}$, $\frac{1}{2}K\rho_j u_j^2$ and $(\rho g \Delta z)_j$

represent the source term due to fan, friction and buoyancy term respectively**.** The term K is the total flow loss in the duct. Subscript i represents the node and j represents the branch. The node contains state properties such as temperature, pressure, molar fractions etc. and the branch contains geometrical and flow properties like length, area, roughness, wall temperature etc.

FireFOAM-2.2.x is used in combination with OpenFOAM-2.2.x as the open-source fire simulation package. FireFOAM uses a Favre-filtered fully compressible flow formulation and solves for the Navier-Stokes Equations and transport equations for species mass fractions alongside sensible enthalpy. FireFOAM solver was coupled with the conjugate heat transfer solver, chtMultiRegionFoam located in OpenFOAM. The coupling allowed for combustion to be taken into account alongside heat transfer between the solid and fluid. Combustion is modelled using the eddy dissipation concept (EDC) extended by Chen [6] in which the author extended EDC to the Large eddy simulation (LES) framework. Turbulence is modelled using the one equation eddy viscosity model for sub-grid scale (SGS) closure. Radiation is modelled using a modified finite volume implementation of discrete ordinate method (fvDOM) developed by Sikic [7]. The modified fvDOM allows for banded or non-grey solutions of the radiative transfer equation (RTE).

3. Experimental configuration for model validation

The single room from PRISME 1experiments has a volume of 120m^3 (5m x 6m x 4m) and a 30cm thick reinforced concrete [1]. The doors are leak tight and made of steel. The room is mechanically ventilated and closed. The ceiling is insulated with 5cm panels of thick rock wool. All materials' properties are provided in [1].

The mechanical ventilation consists of rectangular ducts with cross-section of 0.18m^2 (0.3m x 0.6m) entering the rooms. The ventilation system has an air-renewal rate of 180m^3/h. The density of air is assumed to be 1.18 kg/m^3. The pool fire consists of 14.6kg of circular hydrogenated tetra-propylene (TPH). The heat of combustion of fuel is $4.2 \times 10^7 J/kg$ and the boiling point is 461K. The fuel tank is placed on a scale located 0.4m above the floor. The area of the pool surface is 0.4m^2.

At the inlet and outlet, the mechanical ventilation model is coupled with FireFOAM where pressure and velocity variables would be exchanged. The ventilation model is set as a boundary condition using the momentum equation that allows the velocity at the outlet and inlet to be determined using the pressure difference. The turbulent kinetic energy is set at the outlet and inlet using the branch velocity, turbulent intensity and dissipation rate. The pressure is set to 98384Pa. The heat transfer between the concrete walls and Rock wool ceiling are calculated using the mixed boundary condition for temperature and radiation. At the pool surface, the fuel velocity and temperature is set using the experimental profiles of mass loss rate and heat release rate. Boundary conditions with the exterior is assumed to be adiabatic including the ventilation inlet and outlet.

4. Results and discussion

As a first stage of the validation process, the ventilation model is verified without fire by comparing its predictions to some numerical results using another CFD code, FDS (Fire Dynamics Simulator) [8]. Figure 1 shows the comparative results for a duct split into a tee joint with one inlet and two outlets. The inlet duct is assigned a flow of 3m/s. The ducts have the same area and density. The outlet ducts are assigned a loss coefficient of 4 and 16 at the same height. The pressure is also the same at both the outlets. The simplified momentum (1) shows that the difference in pressure is given by the loss coefficient, density and velocity. Solving for the velocities using the known pressure values, the velocities in the ducts are expected to be 3m/s, 2m/s and 1m/s. The results from Figure 1 therefore show some good agreements between the predictions from the ventilation model and the benchmark numerical data obtained from [8].

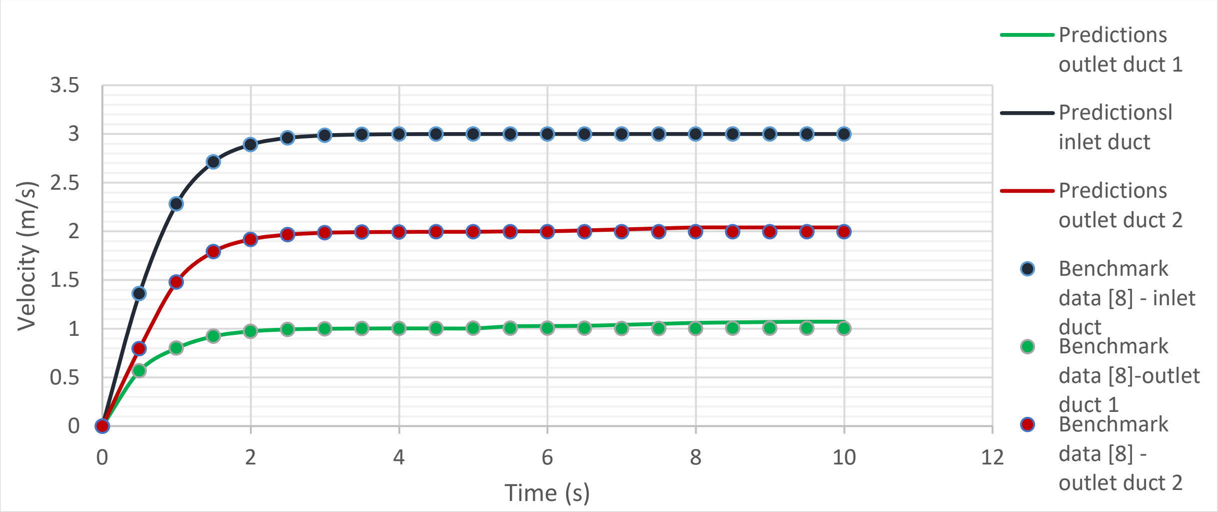

Figure 1: Comparisons of velocities

Figure 2 and 3 show the validation of the ventilation model using the PRISME Source experimental results. The ventilation model contained the pressure at the inlet or outlet ducts coupled with the pressure in the nuclear compartment which was used to predict the inlet and outlet velocities. Overall, the predictions from the ventilation model capture relatively well the variations in volume flow rates, when compared to the experimental data. The peaks are slightly over-predicted with the model. The first peaks after 60 sec are overestimated by 17% in Figures 2 and 3. Overall, the behaviour of the flows is captured accurately by the ventilation model. The reasons for the over-prediction of the flow are the experimental errors, loss coefficient used to predict the flow or a change in the compartment during experiments which would be further investigated.

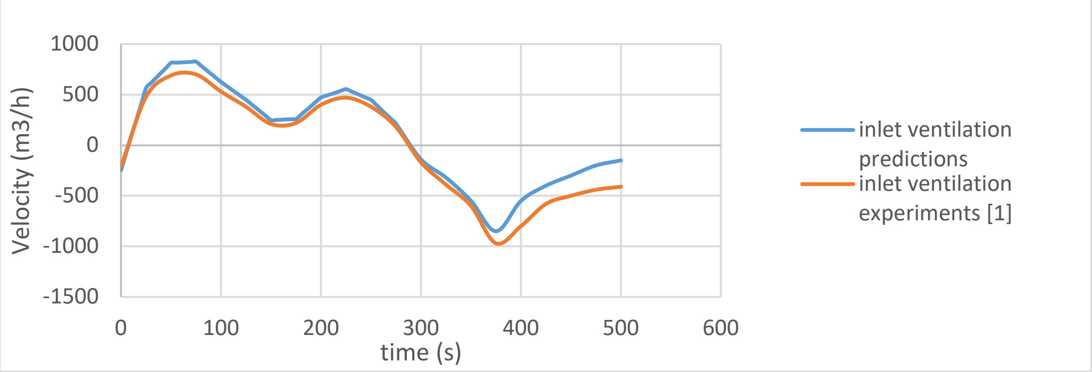

Figure 2: Volume flow rate at intake of ventilation branch – Predictions vs experimental data [1].

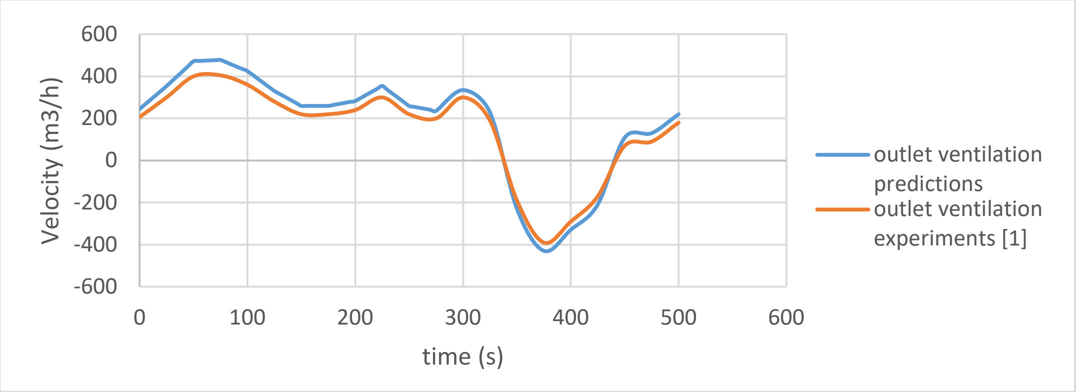

Figure 3: Volume flow rate at exhaust of ventilation branch – Predictions vs experimental data [1].

5. Conclusion

Overall, the FireFOAM solver coupled with the conjugate heat transfer solver was able to predict the flow rates the inlet and outlet ventilation branches. This was possible using the mechanical ventilation model as a boundary condition. The ventilation model was verified and also validated as seen from the results provided. The errors present are as a result of the loss coefficients and errors in the experiment. Resolving the issue of loss coefficients by changing the values would improve the existing results. Further analysis will be carried out on other variables such as the oxygen concentration, heat release rate, mass loss rate, pressure in the compartment and temperature. Studying this variables would give a better insight into the various processes and stages of the fire in the compartment and would assist in further improving the sub-models in the coupled solver.

Acknowledgments

The authors would like to thank the Doctorial Training Alliance (DTA) for its financial support during the project. They are also grateful to Dr Hugues Pretrel from Institut de Radioprotection et de Sûreté Nucléaire (IRSN) for useful discussion on the work.

References

1. Audouin L, et al (2013) OECD PRISME project: Fires in confined and ventilated nuclear-type multi-compartments – Overview and main experimental results. Fire Safety Journal 62: 80-101
2. Suard S, Forestier M, Vaux S (2013) Toward predictive simulations of pool fires in mechanically ventilated compartments. Fire Safety Journal 61: 54-64
3. Le D, Labahn J, Beji T, Devauld C, Weckman E, Bounagui A (2017) Assessment of the capabilities of FireFOAM to model large-scale fires in a well-confined and mechanically ventilated multi-compartment structure. Journal of Fire Sciences 36: 100-115
4. Fox RW, McDonald AT (1995) Introduction to fluid mechanics 4th edition. John Wiley and Sons, Singapore
5. Colella F (2010) Multiscale Modelling of Tunnel Ventilation Flows and Fires. PhD. Politecnico di Torino.
6. Chen Z, Wen J, Xu B, Dembele S (2014) Extension of the eddy dissipation concept and smoke point soot model to the LES framework for fire simulations. Fire Safety Journal 64: 12-26
7. Sikic I (2018) Radiative Heat Transfer for Modelling Fire and Fire Suppression. PhD. Kingston University.
8. McGrattan K, Hostikka S, McDermott R, Floyd J, Vanella M (2019) Fire Dynamics Simulator Technical Reference Guide Volume 1: Mathematical Model. NIST 6: 1 - 195

Nottingham | UK | 9–11 September 2019

Prediction of Thermal Performance of Glass Roof Atriums using CFD Modelling

Abhishek Asthana, Ramamoorthy Sethuramalingam, Peter Weston, Mukesh Goel, Sarvanakumar Kandasamy

Hallam Energy, Sheffield Hallam University, United Kingdom

r.sethuramalingam@shu.ac.uk

Abstract

Glass covered or glazed atriums are becoming increasingly popular in public spaces for their aesthetics, quick installation and building energy reduction by taking advantage of natural daylight and heating by greenhouse effect. The estimation of the building load of atrium buildings is complicated due to the various thermal phenomena involved. The study aims to estimate the cooling loads or heat gain of glazed atriums, using computational fluid dynamics (CFD) modelling using an actual semi-open pedestrian walkway between two building blocks. Steady Reynolds Averaged Navier Stokes modelling approach with the RNG K-epsilon turbulence model, and the Discrete Ordinates (DO) Radiation models were used in the simulation. The temperature and air flow patterns predicted by the CFD simulations are discussed in this paper under various weather conditions. Results predict temperature gains inside the atrium, identify hot and cold spots and predict thermal comfort.

Keywords: Glazed Buildings, Building Thermal Performance, Computational fluid dynamics (CFD), Solar load

1. Introduction

High-glazed atrium-type spaces are becoming increasingly popular in public areas and buildings due to their architectural aesthetics as well as daylighting and solar heating advantages. The complex solar, airflow and thermal phenomena occurring in atrium spaces makes conventional load calculations difficult since they rely on assumptions of thoroughly mixed air and are thus inadequate to predict the thermal behaviour and energy performance in these spaces [1]. The well-stirred zone model is well applied to typical forced air system where relatively good air mixing is the design intent, but might cause unacceptable calculation errors for such system designs or operating modes as displacement ventilation, underfloor air distribution, chilled ceiling, natural ventilation, mix-mode ventilation, large spaces e.g., atria, auditoria, and so on, where nonuniformity of zone air temperature is designed intently to improve energy efficiency and indoor air quality [2]. It is of importance to consider the impact of nonuniform indoor air temperature on building load and energy use, which create a need for a different load calculation and system design method. Several researchers made efforts to find out a relatively accurate method for these particular spaces and systems. Beausoleil-Morrison [3] developed an adaptive controller to manage the interactions between the thermal and CFD modelling domains and implemented it within the ESP-r simulation program to support the conflation of CFD with dynamic whole building thermal simulation. Zhai et al [4] described several different approaches to integrating energy simulation and CFD and proposed a staged coupling strategy for different programs. Djunaedy et al [5] studied the implementation of external coupling between building energy simulation and CFD rather than a traditional internal coupling between the two different domains. Recently CFD strategies have been employed to investigate the natural ventilation air flow patterns and temperature gradient due to solar radiation [6]. Previous studies have confirmed that the temperature distribution and airflow velocity patterns predicted by the ANSYS Fluent turbulence models and solar radiation models were reasonably agreed with the experimental and analytical flow field data [6, 7]. The studies also discovered that as the solar intensity increases, the temperature inside the walkway increases too. In the same way, Ijaz et al. [8] evaluated the thermal comfort of the room using the ANSYS solver to support the natural ventilation for a school building in Singapore. Shafqat et al. [9] also investigated the CFD performance over the experimental work in natural convection with solar radiation exchange in an inclined solar plate heat exchanger using ANSYS DO irradiation model. The authors found agreement between numerical CFD results and experimental data in temperature and air flow velocity. A similar approach has been carried out in this present study but using the solar radiation as a heat source. The present study evaluates the thermal comfort in various weather conditions for the proposed walkway design using the validated CFD model procedures as referred by Halford [6] and Hunt, Shafqat Hussain [9].

2. CFD Methodology

The walkway temperature gradient and airflow pattern are governed by the conservation laws of mass, momentum, and energy equations in the CFD solver. These equations are standard and can be found in many textbooks and papers. Decomposing the Navier-Stokes equations (1) into RANS equations makes it easy to simulate realistic engineering problems in less computational time. A comprehensive description of these equations is provided in the papers by Hussain S et al., and Zhiyin Y [7, 10]. For example, the steady state equation is expressed below, [7] (1)

$$\frac{\partial(\rho u_i \phi)}{\partial x_i} = \frac{\partial}{x_i}(\Gamma_\phi \frac{\partial \phi}{\partial x_i}) + S_\phi \tag{1}$$

The mathematical model in the CFD includes numerical techniques to solve Reynolds Averaged Naiver Stokes equations (RANS) for incompressible three-dimensional turbulent flows. The commercial CFD code of ANSYS Fluent 18.0 solver for 3D double precision, pressure-based and the steady RANS equations have been used to solve the solution in combination with standard k–epsilon turbulence model. The governing equations of the solver include momentum, continuity and energy equations.

CAD model and Meshing

The 3-D model of the walkway has been constructed using the ANSYS design modeller. The CAD model, including brick works, granite slab works on the ground and the glass works of shops inside the walkway, has been constructed in the ANSYS software. Figure 3 illustrates the named surface materials in the 3D domain walls. Heights of the glass and bricks used in the walkway are depicted in figure 3: a); the glass wall is from 0 to 4.2 meters height from the ground, above 4.2 meters it is brick wall. In Figure 3: b), the brick wall is from 0 to 4.2 meters height from the ground and above 4.2 meters a combination of glass wall and brick wall is used. The westward (X) and northward (Z) lengths of the walkway are 101.4 meters and 84 meters respectively. The height of the canopy is 10 meters from the ground as shown in Figure 2. Prior to the CFD simulations, a mesh independence study was conducted over four mesh resolutions. Among four resolutions, results of 4.0 million mesh elements were proved to be sufficiently grid independent (Y+ = 1). A coarse structured mesh was used as shown in Fig.4.

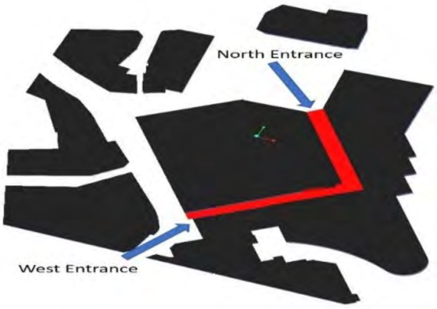

Figure 1: L-shaped walkway with nearby building

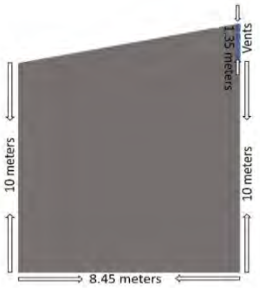

Figure 2: Cross section of the walkway

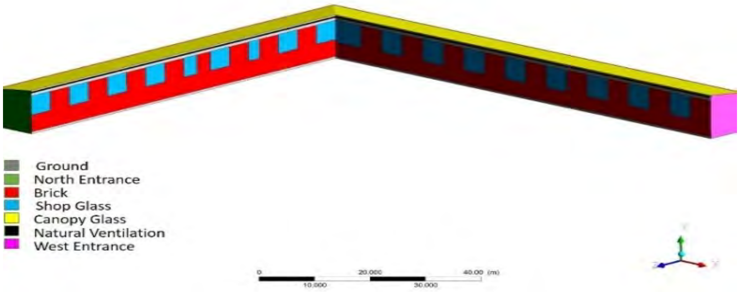

Figure 3: a) 3D view of the walkway with surface materials

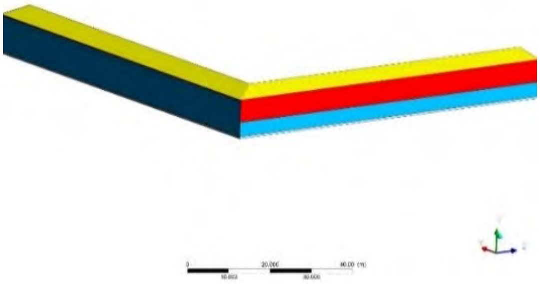

Figure 3: b) 3D view of the walkway

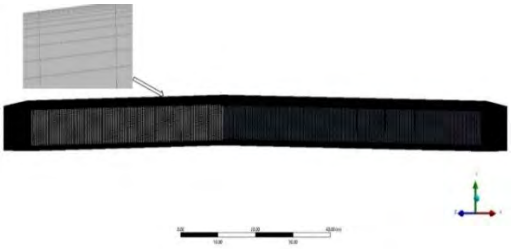

Figure 4: Structured mesh for the CFD model

Boundary Conditions:

Heat transfer through solar radiation is extremely important to consider in a naturally ventilated building. ANSYS Fluent Solver solves the radiation intensity transport equation which is derived from the solar radiation model. The outdoor wind speed and air through walkway entrances change the air flow pattern inside the walkway which affects the thermal sensation experienced by pedestrians inside the walkway. In this present study, the focus was to evaluate the thermal performance and thermal comfort of the building walkway during different weather conditions and at various wind speeds. Therefore, to determine the local wind speed and temperature data, government-supplied meteorological data is required. The Met Office's actual climatic data, such as temperature and sunshine factor, is collected from the nearest weather station (Ryhill, Met Office) and wind data from Emley Moor Met Office weather station for the proposed building. The conditions for various scenarios were selected according to the requirements of standards: ASHRAE 55 [11] and BS EN ISO 13792:2012 [12]. The conditions considered include average and peak day temperatures, normal direct solar irradiation and diffused horizontal irradiation, wind direction and speed at proposed location (Barnsley, UK). The ANSYS Fluent DO irradiation model was considered for this present study. The north entrance and ventilation in the walkway were considered as pressure outlets and the west entrance of the walkway was considered as a velocity inlet for windy conditions. The west entrance of the walkway was considered as a pressure outlet during the no wind condition. The level of comfort is often characterised using the ASHRAE thermal sensation scale. ASHRAE Index of PMV (predicted mean vote) is used to predict the sensation of pedestrians (+3 hot, +2 warm, +1 slightly warm, 0 neutral, -1 slightly cool, -2 cool, -3 cold) [13]. The material properties of bricks, glass and granite slabs are taken from the Heat Transfer Fundamentals book [14]. The transmissivity and absorptivity properties for the canopy's double-glazed glass are considered to be 0.70% and 0.35% respectively as per ASHRAE standards.

Table 1: Solar radiation and outside weather conditions as per fluent solar load calculator

Sun direction vector	**x- 0.7335 y- 0.3832**	**z- -0.56123**
Month	June	October
Sunshine Factor	1	1
Direct normal solar irradiation (W/m^2)	1219.6	1257
Diffuse Solar irradiation – horizontal surface (W/m^2)	163.429	91.8

Table 1: Scenarios as per the standards suggested [11, 12]

Cases	**Month**	**Ambient Temp(°C)**	**Day**	**Wind Speed(mph)**	**Weather Condition**
1	Jun	31	D	0	Peak
2	Jun	31	D	0.2	Peak
3	Jun	31	D	5	Peak
4	Jun	20	D	1	Average
5	Oct	10	D	1	Average

3. Results and Discussion

A series of Computational Fluid Dynamics simulations were considered to investigate the temperature distributions inside the walkway. No wind condition and a series of windy conditions were studied in this paper. The comparative results reveal that in the critical scenarios, such as case 1, extra ventilation strategies are needed to reach neutral human comfort (-0.5 <PMV>+0.5). Increasing the solar intensity does increase the temperature inside the walkway. Figure 5 a) indicates that the stack pressure has been built up between the inside and outside of the building due to hot air generated inside the walkway. Similar phenomena were noticed in the study conducted by Hussain S et al. [7].

The overall results of the CFD simulations show that the natural convection process is not enough to reduce the heat built up inside the walkway to achieve the human comfort zone. Figure 5: a) illustrates the no wind scenario during peak summer weather conditions; there is a 4^{o}C increase inside the walkway above the ambient temperature of 31^{o}C. The buoyancy-driven steady state simulation was carried out in case 1 by utilizing the DO irradiation model in Fluent. Air is drawn from both opening entrances of the walkway and passes through the pedestrian walking space. Then the air is drawn out through the ventilation which is at the top of the walkway canopy. The driving force of the ventilation flow is assumed to be the temperature difference between the inside and outside of the walkway. A similar approach has been carried out to simulate the no wind scenario in a previous study [7]. The resultant PMV value of the walkway is thermally 'hot' in case 1. In the rest of the cases, the wind velocity was applied from the west side of the entrance.

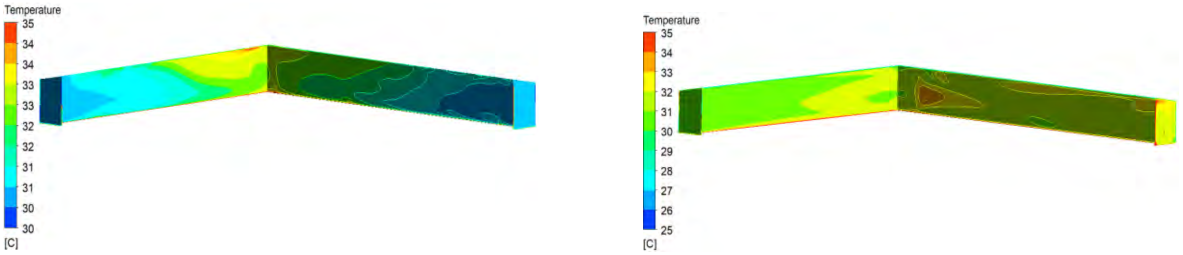

Figure 5:a) Case 1: Buoyancy driven flow (31,0mph) b) Case 2: Peak average summer weather (June)

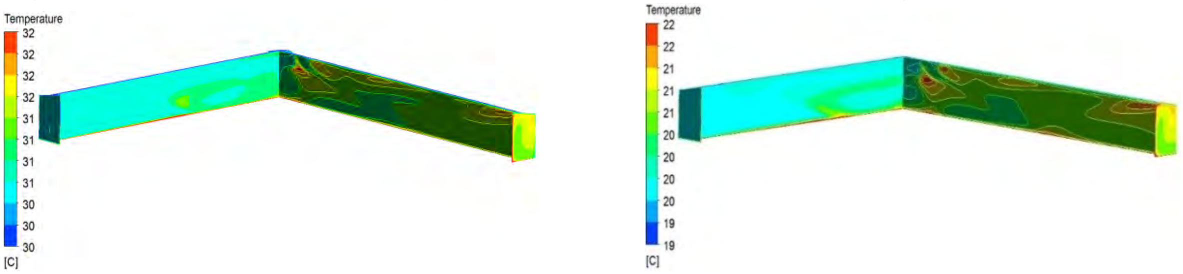

c) Case 3: Peak average weather (June, 5mph) *d) Case 4: Average summer weather (June)*

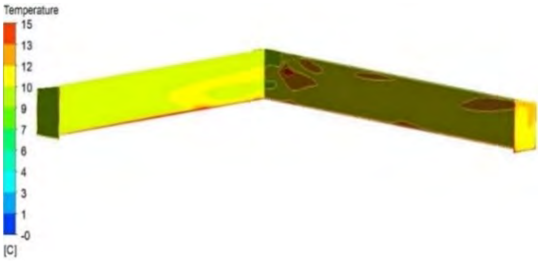

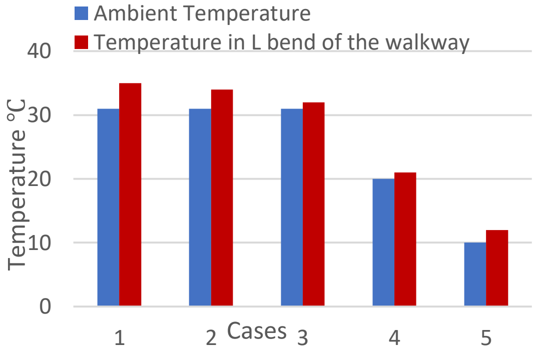

e) Case 5: Autumn average weather (October) *Figure 6: Summary of temperature rises in all 5 cases*

In Figures 5: b) and c) the maximum temperature rise seen near the L-bend of the walkway is 3°C and 1°C when there is wind velocity of 0.2 mph and 5 mph respectively. As in case 1, the resultant PMV value is thermally 'hot' in case 2. Alternatively, the resultant PMV value of the walkway in case 3 is thermally 'natural' which indicates the key role of wind velocity in thermal comfort. Similar behaviour was also detected in the study by Ijaz Fazil S et al. [8]. Figure 5: d) illustrates the average temperature in June at a wind speed of 1 mph. It can be noted that the temperature inside the walkway increases by 1°C above the ambient temperature (20°C) due to solar intensity. The resultant PMV value of the walkway is thermally 'slightly cold'. Figure 5: e) represents the temperatures at 10°C during the spring and autumn months with a wind speed of 1 mph. It is seen that the temperature inside the walkway increased by about 2°C above the ambient temperature of 10°C. The resultant PMV value of the walkway is thermally 'cold'. Like the study by Hussain S eta al., [7] the solar intensity and wind speed played key roles in the temperature rise and decrease in the present study. A summary of temperature rises in all 5 cases are presented in Figure 6. Figure 6 illustrates all temperature data collected from the probe located in the centre of the L–bend at 1.75 meters height from the ground. In cases 1 to 3, as the wind velocity increases, the temperature inside the walkway decreases. Similar behaviour was shown in the study conducted by Ijaz Fazil S et al. [8].

4. Conclusion

The study results recognized that the ambient temperature and wind speed have a greater influence in the temperature distribution inside the walkway. In hot weather, wind will play a key role in removing heat from the walkway. Similarly, inclined solar radiation plays a key role in determining the temperature distributions inside the walkway. CFD techniques developed in this study can be employed in the initial design stage of naturally ventilated buildings to promote human thermal comfort and its energy efficiency. The future work of this research will include the experimental validation against the numerical work. Overall, the methodology developed in this study can be used as a procedure for construction firms to evaluate energy-efficient building designs.

Acknowledgements

This work is supported by Barnsley Council and Hendry Boot Construction Ltd.

References

1. Griffith B., Chen Q (2004) Framework for coupling room air models to Heat Balance Model Load and Energy Calculations. HVAC&R RESEARCH, Vol 10, No 2.

2. Yiqun Pan, Yuming Li, Zhizhong Huang (2009), Study on Energy Modelling Methods of Atrium Buildings, 11th International IBPSA Conference, Glasgow, July 27-30.
3. Beausoleil-Morrison I (2001) The adaptive coupling of computational fluid dynamics with whole-building thermal simulation. Building Simulation. Brazil.
4. Zhai Z., Chen Q., Klems J. H., Haves P (2001) Strategies for coupling energy simulation and computational fluid dynamics programs. Building Simulation. Brazil.
5. Djunaedy E., Hensen J.L.M., Loomans M.G.L.C (2005) External coupling between CFD and Energy Simulation: implementation and validation. ASHRAE Transactions, Vol. 111, Part 1.
6. Holford, Hunt et al (2003) Fundamental atrium design for natural ventilation. Building and Environment 38: 409-426
7. Hussain S, Patrick H (2013) Numerical study of buoyancy- driven natural ventilation in a simple three storey atrium building. International Journal of Sustainable Built Environment 1:141-157
8. Ijaz Fazil S A K and Sivamoorthy K et al (2017) Performance evaluation of airflow and thermal comfort in the room with wind catcher using different CFD techniques under natural atmosphere boundary layer. Applied Energy Symposium & Forum: Low Carbon Cities & Urban Energy Joint Conference 143: 199-203
9. Shafqat H (2017) Natural ventilation of natural convection and radiation exchange in an asymmetrically heated inclined channel. Imam Journal of Applied Science Volume -1
10. Zhiyin Y (2014) Assessment of unsteady RANS approach against steady RANS approach for predicting twin impinging jets in a cross flow. Cogent Engineering 1: 936995
11. ASHRAE 55 (2017) Thermal environmental conditions for human occupancy. American National Standard Institute ISSN 1041: 2336
12. BS EN ISO 13792 (2012) Thermal performance of the building – calculation of internal temperatures of a room in summer without mechanical cooling – simplified methods. BSI Standard Publication ICS 91.120.10
13. Juyoun K, Ken P (2008) Evaluation of the PMV thermal comfort index in outdoor weather conditions. Environmental Ergonomics Research Centre, Loughborough University.
14. Yildiz B, Necati O (2012) A Textbook for Heat Transfer Fundamentals. Begell, Danbury.

Nottingham | UK | 9–11 September 2019

Methane Yields from Anaerobic Digestion of *Sargassum muticum* Following Ethanol and Water Extractions

Supattra Maneein[1], Dr. John Milledge[1], Dr. Birthe Nielsen[1]

[1]*Algae Biotechnology, University of Greenwich, Chatham Maritime, ME4 4TB, UK*

sm8149w@gre.ac.uk

Abstract

Biofuel in the form of biogas from seaweed could aid in achieving EU targets of reducing greenhouse gas emissions. Biogas production from seaweed is limited partly by low methane (CH_4) yields. This research aims to enhance CH_4 yields by extracting potential inhibitors, such as polyphenolic compounds, of anaerobic digestion (AD) from *Sargassum muticum* (SM) using 70% ethanol (EtOH) and only water as extracting solvents. 70% EtOH and water were shown to be unsuitable solvents for extraction of potential inhibitors from spring harvested SM as CH_4 yields were not statistically different from the control SM. Water extraction of SM reduced CH_4 potential by 34.9% indicating that compounds beneficial for CH_4 production during AD were extracted. Extractions using other solvents may be beneficial in determining the presence of potential AD inhibitors in SM. Alternatively, AD inhibitors may be absent in spring SM, and durable seaweed cell architecture may be the cause of low CH_4 yields.

Keywords: Biogas; Biofuel; Seaweed; Polyphenols.

1. Introduction

Sargassum muticum (SM) is an invasive brown seaweed species that can pose economic and environmental issues [1]. Anaerobic digestion (AD) of SM for biofuel production would be a beneficial method for its elimination and valorisation. Furthermore, biofuel in the form of biogas from seaweed could aid in achieving EU targets of reducing greenhouse gas emissions.

Use of SM, however, is partly limited by low methane (CH_4) yields, 17% of the theoretical CH_4 yields [1]. This could be due to the recalcitrance of seaweed to hydrolysis during AD. Several authors have also associated high polyphenolic content in seaweed to low CH_4 yields, showing an increase in CH_4 yields by fixing polyphenols with formaldehyde [2,3].

Polyphenolic compounds encompass a wide range of compounds, with those found in brown seaweeds mainly being phlorotannins composed of polymers of phloroglucinol [4]. Polyphenolic compounds that can limit CH_4 production have not yet been elucidated. Aqueous ethanol (EtOH) and water are solvents shown to extract polyphenols from brown seaweed [5,6]. This work aims to understand the influence of EtOH and water extraction of SM on CH_4 yields. This would elucidate the presence of any potential inhibitors present within these extracts, provided the extraction enhances CH_4 yields.

2. Experimental Method

Seaweed Collection and Treatment

SM was collected in April 2018 from Ramsgate, UK. It was washed with distilled water to remove sand and other attached seaweeds and organisms. The thallus of SM was stored at -18℃ before freeze-drying at -55℃ for 48 hours. Freeze dried (FD) SM was ground using a coffee grinder until a fine powder was formed.

Two different extractions were carried out in duplicates. 5 g of the processed seaweed was stirred using a magnetic stirrer in deionised water (dH_2O) (50 mL, room temperature, 6 hours) and was centrifuged (3,900 rpm, 20 minutes). The pellet was incubated in dH_2O (50 mL, room temperature, 1 hour) and centrifuged as above. It was further incubated for 24 hours (50 mL dH_2O, room temperature) and centrifuged as above. The procedure was repeated with 70% (*v/v*) EtOH/water on FD SM.

The two replicates were pooled and mixed with approximately 100 mL of dH_2O. It was centrifuged (3,900 rpm, 20 minutes) and was repeated 5 times to ensure removal of any remaining EtOH which may impact the AD process. This washing procedure was repeated on water-extracted residues and the control SM using 10 g of FD SM.

Biochemical methane potential determination

BMP tests are used to calculate CH_4 production potential of different substrates [3]. The inoculum used for AD was collected from an anaerobic digester treating paper-making waste at Smurfit Kappa Townsend Hook Paper Makers, Kent, United Kingdom. It was ‘degassed’ at 37 ℃ for three days. The inoculum was homogenised using a handheld blender prior to use.

The Automatic Methane Potential Test System II (AMPTS II) was used to measure CH_4 production. This system contains 500 mL reactors in a temperature controlled water bath with a CO_2 capturing unit and a gas measuring device. 3 replicates were made with each reactor containing approximately 1 g volatile solids (VS) content of each extracted residue, inoculum to make an inoculum-to-substrate (I/S) ratio of 5, and made up with water to 400 g. A blank was also made with only inoculum and water to calculate net CH_4 production from extracted residues. Reactors were mixed continuously at 75% power and incubated at 37 ℃. CH_4 volumes were recorded daily over 28 days, and corrected to water vapour content at 0 ℃, 101.325 kPa. CH_4 yields were corrected to 1 g VS at the end of the BMP test.

Phenol extraction and analysis

Phenol extraction was performed on all residues at a solid/liquid ratio of 1:200 using 60% (v/v) acetone/water, incubated in a shaking incubator (250 rpm, 1 hour, 40 ℃), then centrifuged (21,000×*g*, 20 minutes). The supernatant was collected and the process was repeated on the pellet three times. This was done in triplicates for EtOH-extracted residue and the control SM, and duplicate for water-extracted residue due to insufficient quantities.

Phenol concentration was determined according to a modified protocol of the Folin–Ciocalteu (FC) method performed at room temperature, using 2 minutes incubation of FC reagent rather than 1 minute [7]. The absorbance was measured at 750 nm in a UV-visible spectrophotometer (Jenway 6305). Phloroglucinol was used to generate a calibration curve to determine the polyphenolic concentration, reporting total polyphenolic content (PC) values as phloroglucinol equivalent (PGE) per gram dry weight (DW) of residues.

Statistical Analysis

Excel (2016) was used for student’s t-test and IBM SPSS version 25 was used for one-way and two-way ANOVA analysis. Dependent variable: cumulative CH_4 yield; daily CH_4 production. Independent variables: treatment (Control SM, EtOH- or water-extracted SM), day (time after incubation).

3. Results and Discussion

Initial CH_4 production

The slope of CH_4 production in the first three days indicates a more than two-fold higher CH_4 production rate from residues of EtOH-extracted SM compared to water-extracted SM, with the control SM showing a similar trend (Figure 1A). Furthermore, the peak daily CH_4 production is delayed by two days in water-extracted residues compared to the control SM and EtOH-extracted SM (Figure 1B).

Results of a two-way ANOVA analysis showed that the treatment of SM and the time the residues are digested in the reactor, as well as the interaction between the two, have a statistically significant impact on the daily CH_4 production volume ($p < 0.05$). This type of delay was also evident during washing of SM [8]. As 70% EtOH/H_2O is often used in antiseptic techniques, this would have eliminated the majority of hydrolytic bacteria present on SM surfaces, indicating that dH_2O is likely to extract readily digestible substrates, leaving more complex compounds. These complex substrates would require a higher degree of

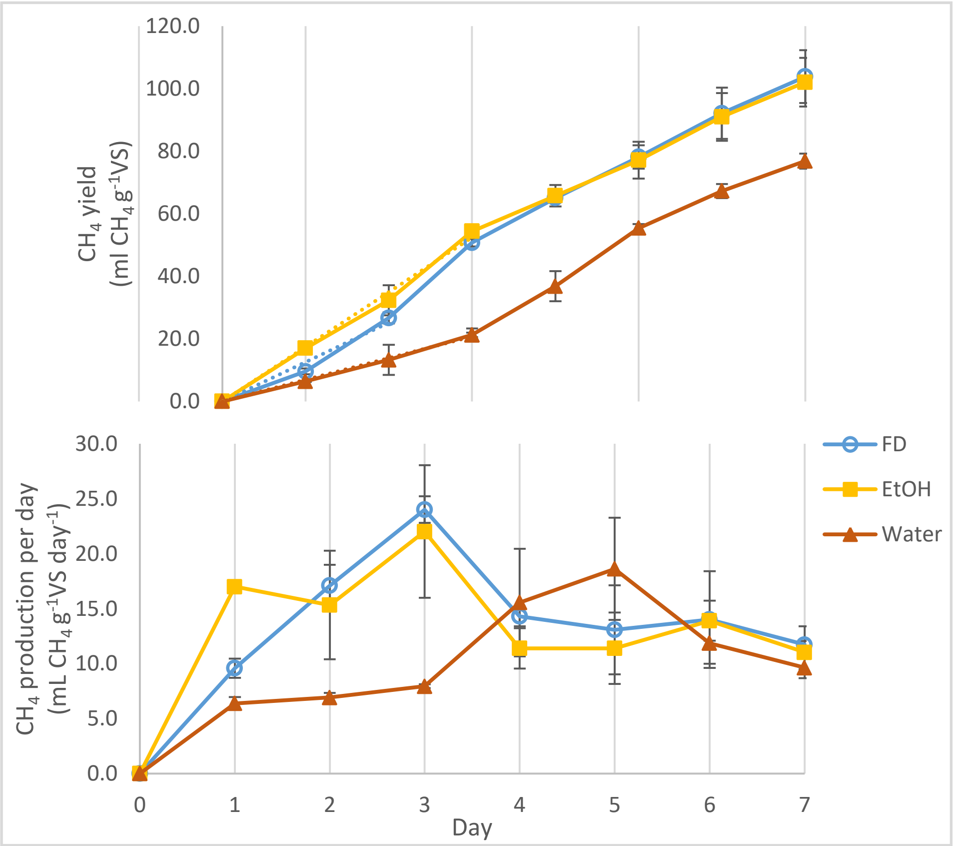

Figure 1A: Cumulative CH_4 production in the first 7 days using the control SM, EtOH-extracted SM and water-extracted SM (n=3). Trendlines (dotted): rate of CH_4 production of EtOH-extracted SM (y = 17.5x) and water-extracted SM (y = 6.9x) for the first three days, and the control SM for the first 2 days (y = 12.6x). B: CH_4 production per hydrolysis to produce CH_4, delaying initial CH_4 production [9].

CH_4 yield

The net average cumulative CH_4 yield produced by each type of residue after 28 days is shown in Figure 2. Student's t-test indicates that CH_4 potential of the control SM at the end of the BMP test is not statistically higher than EtOH-extracted SM, suggesting that EtOH extraction had no effect on CH_4 potential. However, the two-way ANOVA analysis shows that EtOH-extracted SM has a statistically lower CH_4 production compared to the control SM from day 25 – day 28 when comparing the effect of the interaction between time and treatment of SM on CH_4 yields ($p < 0.05$). This suggests that 70% EtOH could be extracting compounds that would otherwise enable microbes in the digester to maintain CH_4 production towards the end of the BMP test.

The net cumulative CH_4 yields produced by the control SM and EtOH-extracted SM are statistically higher than water-extracted SM when comparing the effect of the interaction between time and treatment of SM on CH_4 yields ($p <0.05$). CH_4 potential was also reduced by 34.9% relative to the control SM, indicating that water can extract compounds useful for CH_4 production during AD. These water-soluble compounds may include laminarin (up to 35% DW in brown seaweed) and mannitol (up to 34% DW in *Sargassum*); low concentrations of these in *Laminaria digitata* were associated with lower CH_4 yields [4,9,10].

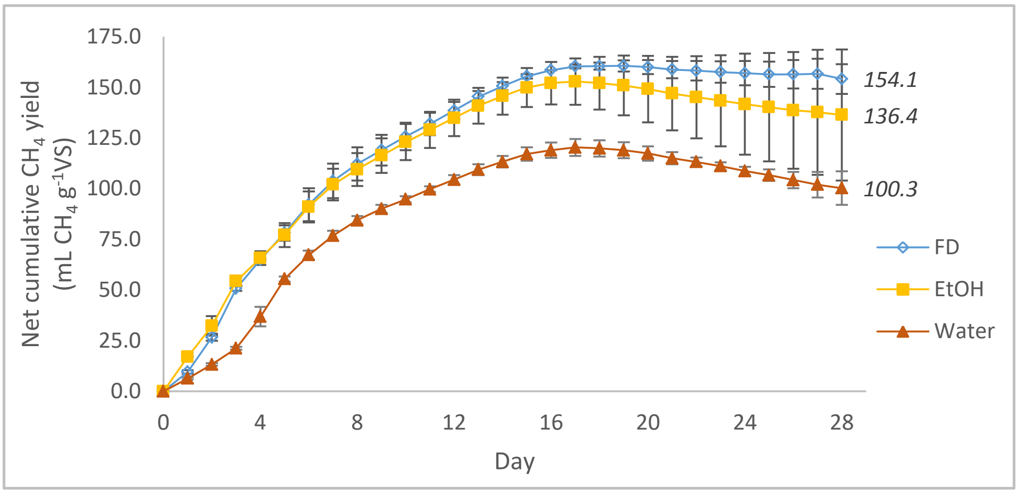

Figure 2: Net cumulative average CH_4 production over 28 days with three different SM residues (n=3). CH_4 potential for each residue is labelled in

Polyphenolic content

Total PC was measured to elucidate the possible effects of total PC on CH_4 yields (Table 1). EtOH-extracted residues showed that 70% EtOH was successful in extracting polyphenolic compounds, indicated by statistically lower PC compared to the control SM (student's t-test, $p < 0.05$). The control SM showed similar PC to water-extracted residues. These results indicate that low CH_4 potentials of EtOH-extracted and water-extracted residues cannot be directly attributed to total PC.

Table 1: Total polyphenolic content of the control SM and extracted residues

	Phenolic content (mg PGE g^{-1} DW)
Control SM	6.7 ± 0.3
EtOH-extracted	4.9 ± 1.1
Water-extracted	6.2 ± 0.2

4. Conclusion

31 hours of 70% EtOH extraction successfully reduced polyphenolic content in SM residues. However, EtOH-extracted residues could not enhance CH_4 yields of spring harvested SM relative to the control SM. Polyphenolic content in water-extracted residues were similar to the control SM. Water may also extract easily hydrolysable substrates used for CH_4 production. Hence, 70% (v/v) EtOH/water and water are unsuitable solvents for extraction of potential inhibitors from spring SM. Treatments using other solvents of different polarities (e.g. dichloromethane) may be beneficial in determining the presence of potential AD inhibitors in SM. Alternatively, AD inhibitors may be absent in spring SM, and durable seaweed cell architecture may be the cause of low CH_4 yields.

Acknowledgements

The author would like to acknowledge the financial support of the University of Greenwich and the Doctoral Training Alliance.

References

1. Milledge, J. J.; Harvey, P. J. Ensilage and anaerobic digestion of Sargassum muticum. *J. Appl. Phycol.* 2016, *28*, 3021–3030.
2. Moen, E.; Horn, S.; Østgaard, K. Alginate degradation during anaerobic digestion of Laminaria hyperborea stipes. *J. Appl. Phycol.* 1997, *9*, 157–166.
3. Tabassum, M. R.; Xia, A.; Murphy, J. D. Seasonal variation of chemical composition and biomethane production from the brown seaweed Ascophyllum nodosum. *Bioresour. Technol.* 2016, *216*, 219–226.
4. Zubia, M.; Payri, C.; Deslandes, E. Alginate, mannitol, phenolic compounds and biological activities of two range-extending brown algae, Sargassum mangarevense and Turbinaria ornata (Phaeophyta: Fucales), from Tahiti (French Polynesia). *J. Appl. Phycol.* 2008, *20*, 1033–1043.
5. Ye, H.; Zhou, C.; Sun, Y.; Zhang, X.; Liu, J.; Hu, Q.; Zeng, X. Antioxidant activities in vitro of

ethanol extract from brown seaweed Sargassum pallidum. *Eur. Food Res. Technol.* 2009, *230*, 101–109.

6. Rastian, Z.; Mehranian, M.; Vahabzadeh, F.; Sartavi, K. Antioxidant Activity of Brown Algae Sargassum vulgar and Sargassum angustrifolum. *J. Aquat. Food Prod. Technol.* 2007, *16*, 17–26.
7. Matanjun, P.; Mohamed, S.; Mustapha, N. M.; Muhammad, K.; Ming, C. H. Antioxidant activities and phenolics content of eight species of seaweeds from north Borneo. *J. Appl. Phycol.* 2008, *20*, 367–373.
8. Milledge, J. J.; Nielsen, B. V; Sadek, M. S.; Harvey, P. J. Effect of Freshwater Washing Pretreatment on Sargassum muticum as a Feedstock for Biogas Production. *Energies* 2018, *11*, 1771.
9. Adams, J. M. M.; Toop, T. A.; Donnison, I. S.; Gallagher, J. A. Seasonal variation in Laminaria digitata and its impact on biochemical conversion routes to biofuels. *Bioresour. Technol.* 2011, *102*, 9976–9984.
10. Vera, J.; Castro, J.; Gonzalez, A.; Moenne, A. Seaweed Polysaccharides and Derived Oligosaccharides Stimulate Defense Responses and Protection Against Pathogens in Plants. *Mar. Drugs* 2011, *9*, 2514–2525.

Nottingham | UK | 9–11 September 2019

Design, development, testing and evaluation of an innovative floating hydro-generator

Abhishek Asthana [1] and Sanjay Mukherjee [2]

[1]*Hallam Energy, MERI, Sheffield Hallam University, Sheffield, S1 1WB, United Kingdom*

[2]*SWEE, Cranfield University, Cranfield, MK43 0AL, United Kingdom*

asthana@shu.ac.uk

Abstract

Undershot waterwheels have existed for centuries with most designs using radially extending paddles. This work involves developing and testing prototype of a newly designed floating undershot waterwheel with a unique paddle-shaft linkage mechanism that increases the power transmission and efficiency. The prototype was tested in two different field trials: (i) a swimming pool with jets of water to replicate low-flow conditions and (ii) a millstream to replicate normal flow conditions to experimentally measure the mechanical power outputs. The experiments proved that the device was functioning with an efficiency of 55-69%, which is close to the best performances for undershot water wheels recorded in literature. The floating design of the water wheel also allows aquatics to move freely under the wheel and does not require disruptive construction of barrages or other permanent structures. The findings from this study will be useful to further optimise the current design and target even higher efficiencies.

Keywords: Hydropower, water wheels, power generation

1.Introduction

Waterwheels have been a lucrative technology used to harness the kinetic energy of the flowing water (such as small rivers, pluvial drainage systems, wastewater treatment plants, water supply systems and irrigation channels) into mechanical work and electrical power [1, 2, 3]. Until the 20th Century, wood was the most common material for making the blades of waterwheels, which made the fabrication difficult, and the durability poor. Consequently, waterwheels had a very simple design with low efficiency and apparently, little scope for improvement [2]. Thereafter, due to developments in hydraulic engineering, progress in material science, advancement of sophisticated computerised numerical control (CNC) production machines and the availability of computer aided design CAD and computer aided manufacturing CAM tools, the size, shape, design, efficiency and output power generation of waterwheels have considerably improved [4]. Several numerical and experimental methods were developed by many researchers to estimate the optimal design parameters, which can enhance the power generation using a micro hydropower [4, 5, 6]. Khan et al. [4] suggested that the undershot floating waterwheels are advantageous over the fixed undershot wheels and can be further used to develop power in the Pico range. Later, Emanuele and Roberto [7] examined that by changing the blade's shape of existing wheels to circular profile, the performance could be improved by approximately 4 %. In most of the studies and designs, the paddles are radially attached to the wheel.

In this work, a prototype of an undershot water-wheel floating generator (F-Gen) was developed using an innovative linkage mechanism to maximise power transmission and efficiency. The prototype was tested in two different field trials, namely, in a swimming pool with jets of water in order to test the device in low flow conditions and in a millstream under normal flow conditions. The performance of the F-Gen was evaluated through experiments and computational models for generating power from a small irrigation millstream.

2.Methodology

Design of the F-Gen

Figures 1 shows the F-Gen with four paddles, each 1.75 m wide and 3 m in diameter with an area of 0.9616 m^2. The paddles are circular-arc shaped and made of aluminium. The angular distance between the paddles is $2\pi/n$ where n is the total number of paddles. In the design, the position of the paddles is always normal to the water flow while entering, leaving or any time in between, thereby extracting maximum kinetic energy from the water flow. Due to its floating design, the F-Gen's installation, operation and maintenance are not disruptive to the environment as fish can pass under it. The F-Gen could be placed in a water stream requiring almost no other facilities such as training walls and penstock. It can be installed in any place with a water current without requiring construction of weirs or other large structures. The floating generator does not require a diversion of the water. Instead, there is only a temporary slowing down of the water flow under the impeller. In the case of flooding or abnormally high flow conditions, actuators can be used to alter the paddle angle to minimise the drag from the paddles. Also, the generator does not require scaling-up in case of water streams. Especially in case of wider but shallow streams, a bigger generator would be impossible to use as its wheels may strike the bed of the millstream. Instead, a number of these generators could be used in a parallel arrangement, fastened to each other and floating on the water surface (Figure 2).

	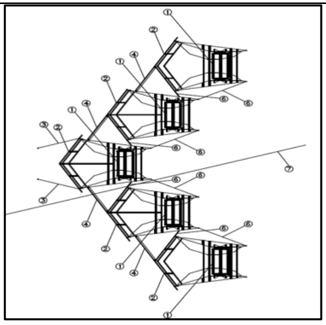
Figure 1: F-Gen hydro generator with vertical paddles.	*Figure 2: Top view of a parallel arrangement of the F-Gen generator for wide waterways.*

Swimming pool experiments

An indoor swimming pool with two symmetrical water jets positioned under the water surface, shown in Figure 3, was selected for the trials. These two water jets were the only source of input power for driving the F-Gen paddles. The power available to the paddles (input power) was estimated by measuring the flow velocity and the volumetric flow rate of water at the outlet of the jets. Since the paddles were situated some distance away from the underwater jets, the power available to the F-Gen paddles would consequentially decrease as the jets diffuse into the water.

Figure 3: Jets of water in the pool for driving the hydro generator.

The accurate measurement of the input power available to the paddles was not possible experimentally and therefore computational fluid dynamics (CFD) simulations were used to estimate it at fixed distances from the jets. The output power from the F-Gen was measured using a pulley and weight mechanism, shown in Figure 4a. To estimate the power output, the time to lift the bucket of known weight over a height of 1 m was recorded. This process was repeated by positioning the F-Gen at different distances from the jets. A schematic of the distances of the paddle's positions from the water jets is shown in the Figure 4b. The x1 and x2 represent the positions of the paddles when they begin to enter water and when they are fully inside the water respectively. The following equation was used to estimate the output power generated by F-Gen.

$$P_o = w\frac{\Delta h}{\Delta t} \qquad \text{Eq 1}$$

Where w is gross weight of the load lifted, Δh is height through which the weight is lifted and Δt is time for lifting the load.

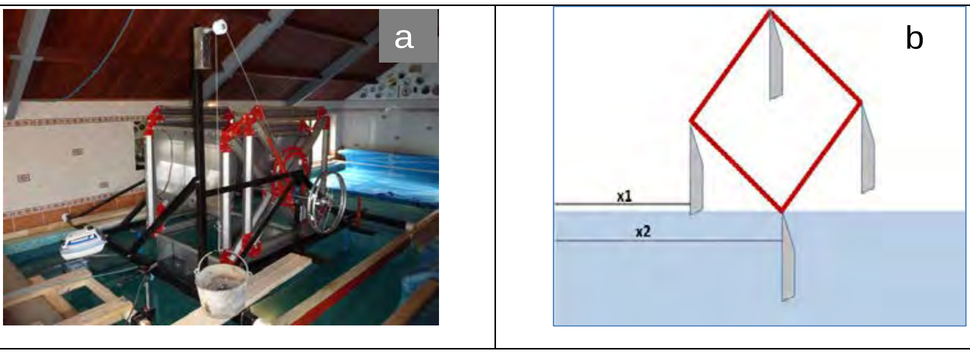

Figure 4: (a) The pulley mechanism with bucket; (b) Schematic of the distances of the paddle positions from the jets.

Millstream

In millstream trials (Figure 5), the F-Gen was subjected to a steady water velocity of 0.63 m/s.

Figure 5: Millstream setup with constant water flow and longer string to lift weights.

Hence, the power input to the F-Gen was determined experimentally by measuring the area swept by the generator and the velocity of the stream as follows:

$$P_i = \frac{\rho A u^3}{2} \qquad \text{Eq 2}$$

Where ρ is density of water, A is Area of the paddle normal to water flow and u is speed of water. The pulley mechanism described in section 2.3.1 was used to assess the output power.

3.Results and discussions

Swimming pool experiments

The output power of the F-Gen model was estimated by the pulley mechanism explained in section 2.2. The observations indicate that an average of 4.47±0.21 s was required to lift the load of 7 kg by a height of 0.25 m. The average speed of lifting is thus 0.0572 m/s. The observations and findings from the swimming pool experiments are given in Table 1. The maximum power produced by the F-Gen was found to be 3.7 W. A maximum efficiency of 69.7 % was observed, which was an encouraging sign. The aim of this experiment was solely to determine the efficiency of the F-Gen at lower flow velocities. The experiment indicates that a full-scale model of the F-Gen can produce higher power suitable for practical applications. It was observed that the efficiency of F-Gen increased as the paddles were pushed away from the jets. This increase in the efficiency was not the expected result but it can be explained as follows. The entire flux of the jets was covered by the paddles as they move away from the jets. When they were too close, some of the flow escaped without engaging the paddles.

Table 5: Power and efficiency results from Swimming pool experiments.

Parameters	**Unit**	**Test A**	**Test B**	**Test C**
x1	m	0.605	1.105	1.605
x2	m	1.450	1.950	2.450
Average lifting speed	ms^{-1}	0.0536	0.0541	0.0605
Water speed	ms^{-1}	0.270	0.251	0.224
Area of paddles	m^2	0.713	0.713	0.713
Output Power	W	3.680	3.714	3.365
Water Power available	W	7.037	5.653	4.836
Efficiency	%	52.3	65.7	69.7

Millstream experiments

The power and efficiencies observed in the millstream experiments are summarised in Table 7. The maximum power obtained in the millstream experiments is 55 W with an efficiency of 62.1%, which is 7.6 % lower as compared to the swimming pool experiments. For validation purpose, efficiencies of the F-Gen from both the experiments were compared with results reported by Ikeda et al. [8] for undershot water wheels. A close agreement with the existing literature has been achieved for the efficiencies; hence, the experimental and calculation methods were reliable. The experiments in the millstream prove that the device was functioning well with efficiencies between 55.7 and 62.1%, which was comparable to the best performance recorded in literature for undershot water wheels (65%) [8, 9].

Table 7: Power and efficiency results from millstream experiments.

Parameters	Unit	Test 1	Test 2	Test 3
Average lifting speed	ms^{-1}	0.0679	0.0609	0.0613
Water speed	ms^{-1}	0.63	0.63	0.63
Water Density	$kg\ m^{-3}$	998	998	998
Area of paddles	m^2	0.713	0.713	0.713
Output Power	W	55	49	50
Water (input) Power	W	88.41	88.41	88.41
Efficiency	%	62.1	55.7	56.1

4.Conclusions

Waterwheels are eco-friendly and effective technology to harness energy from low flow water streams and therefore, may constitute an appropriate technology particularly in small city streams and rural irrigation canals. In this study, an undershot waterwheel (F-Gen) was designed, built and tested in swimming pool and millstream. Efficiencies of up to 69.7% and 62% were observed in the swimming pool and millstream experiments, respectively, which was an encouraging sign.

References

1. Reynolds, T.S., Stronger than a hundred men: a history of the vertical water wheel. 1983: Johns Hopkins University.
2. Müller, G. and K. Kauppert, Performance characteristics of water wheels. Journal of Hydraulic Research, 2004. **42**(5): p. 451-460.
3. Rao, J.S., Water Wheels, in History of Rotating Machinery Dynamics. 2011, Springer Netherlands: Dordrecht. p. 9-12.
4. Khan, F., et al., Modeling, simulation and fabrication of an undershot floating waterwheel. Journal of Engieering and Apllied Science, 2015. 34.
5. Quaranta, E. and R. Revelli, Performance characteristics, power losses and mechanical power estimation for a breastshot water wheel. Energy, 2015. 87(Supplement C): p. 315-325.
6. Yah, N.F., M.S. Idris, and A.N. Oumer, Numerical Investigation on Effect of Immersed Blade Depth on the Performance of Undershot Water Turbines. MATEC Web Conf., 2016. 74: p. 00035.
7. Quaranta, E. and R. Revelli, CFD simulations to optimize the blades design of water wheels. 2017. 1-8.
8. Ikeda, T., S. Iio, and K. Tatsuno, Performance of nano-hydraulic turbine utilizing waterfalls. Renewable Energy, 2010. 35(1): p. 293-300.
9. Singh, D., Micro Hydro Power: Resource Assessment Handbook 2009: Asia Pacific Center for Technology Transfer.

Nottingham | UK | 9–11 September 2019

Computational Fluid Dynamics Modelling to design and optimise Power Kites for Renewable Power Generation

Yatin Suri [1], Christopher Pegg [1], Sheikh Zahidul Islam [1], Abhishek Asthana [2]

[1] *The Robert Gordon University, School of Engineering, Aberdeen, U.K.*

[2] *Sheffield Hallam University, Hallam Energy, Sheffield, U.K*

y.suri@rgu.ac.uk

Abstract

Power kites provide the potential rewards of obtaining the disused energy supply from high altitude wind. This paper aims to provide a design of Power kite and optimise the potential for renewable power generation. The Power kite was modelled using Computational Fluid Dynamics (CFD) to study its characteristics. The numerical modelling results were compared against the wind tunnel experimental study and two 3D printed Power kites. The design was optimised using several variables, including aerofoil choice, surface roughness, wind speed and operating parameters. Attempts at optimising the kite design were implemented. The results suggest that operating the kites at minimum 15 m horizontal separation is favourable, with the trailing kite operating below the leading, removing the potential for this kite to operate in the wake turbulence of the first. As the wind speed is generally very low at low altitudes, it is recommended to use a symmetrical aerofoil for the kite design, as these tend to produce greater lift with low Reynolds airflow. This paper presents relevant, applicable data which can be used for predicting the performance, and potentially optimising further Power kite designs.

Keywords: Power kites, CFD, Wind energy, Renewable power generation

1.Introduction

Wind energy is the world's fastest growing renewable resource sector, and in many countries, is the largest provider of renewable power [1]. Unfortunately, wind turbines have inherent limitations when harnessing the power of the wind. It is well recognised that with increased altitude come increased wind power densities; this is reflected in the continual rise in wind turbine heights [2]. The current wind turbine technology possesses limitation to harness the abundant natural resource of high altitude wind [3]. Power kites are more effective at high altitudes due to both aerofoil design and location of components [4], the generator of a power kite is left on the ground; connected by a tether. This allows the kite to spin the generator, as the available power at high altitudes is significantly greater [2].

Being a somewhat novel approach, there exist few readily available resources to predict kite performance accurately [2,3]. Without accurate performance prediction and the ability to optimise kite design at an early stage, these power generation systems will struggle to reach their full potential [5]. Thus, it is important to maximise the lift produced to optimise the efficiency. Previous research [2,3,5] has targeted aerofoil shape which is undoubtedly a significant factor in efficiency but surface roughness was ignored in these studies. An aerofoil with a high surface roughness will produce turbulent airflow over the body, which, in turn, will increase the resistance due to drag on the kite [3]. Drag also occurs on the tether over its length; over 500 metres it is possible to develop significant drag, enough to have a large impact on the overall efficiency of the system. It is, therefore, necessary to study aerodynamic drag over the kite, while also optimising the aerofoil shape to produce maximum lift [2,3]. This paper uses computational fluid dynamics to solve Navier-Stokes equations and model the wind flow in design and optimisation of power kites, under varying input parameters, namely horizontal and vertical separation distances and surface roughness. The role of the change in lift and drag coefficients has been investigated in detail.

Computational domain and Boundary Conditions

In the present study, NACA 0018 Aerofoil is used [4]. The kite dimensions can be found in Table 1. The computational domain used in the present study is in the form of a cuboid with dimensions 1.22 m×0.46 m×0.46 m based on the wind tunnel experiment performed shown in Figure 1. The kite is located at 0.6 m from the inlet. The experiment and the validation are performed with a single kite. Following that two kites are located and analysis was carried out to understand the horizontal and vertical separation distance between them. The Power kite was modelled using Computational Fluid Dynamics (CFD) by solving the Navier-Stokes equation (continuity and momentum conservation equations) assuming isothermal, steady state, and incompressible flow. A velocity inlet boundary condition was used with 10 m/s at inlet and pressure outlet was used at the outlet with 0 Pa pressure. All the other boundaries were configured as no slip wall. A mesh independence study was performed by progressively refining the mesh whilst monitoring the lift (C_L) and drag (C_D) coefficients. Convergence was deemed to have been reached when refining the mesh began to have little to no effect on both these coefficients. The number of cells used in the present study are 8×10^5.

Table 1: Kite dimensions

Component	Length (m)	Angle (°)
Wingspan	11.128	N/A
Centre Chord	2.903	N/A
End Chord	1.7418	N/A
Kite Arc	N/A	180

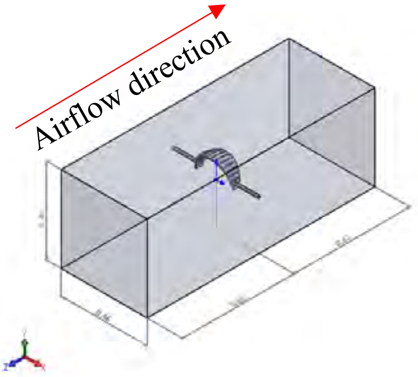

Figure 1: Computational domain, in meters

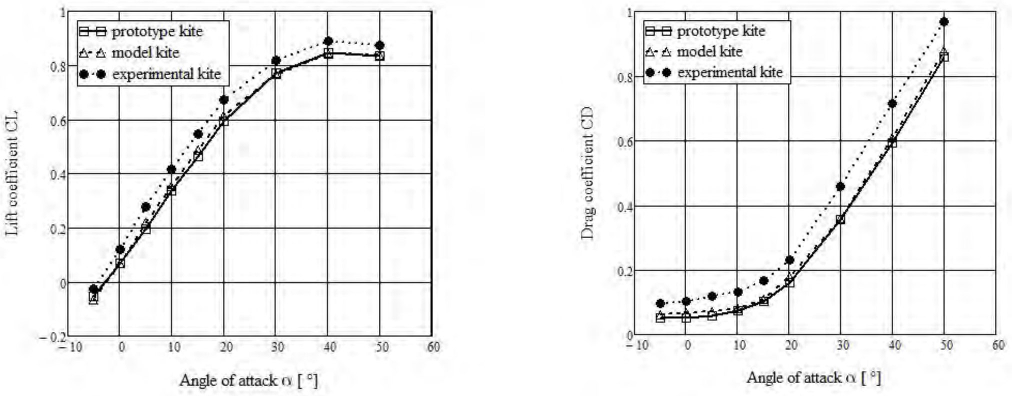

Figure 2: Comparison of Experimental and CFD results

2.Experimental Validation

In order to provide validation of the CFD simulation, a direct comparison was made between the simulated results, dimensionless analysis and the experimental results obtained via low-speed wind tunnel testing (Figure 2). It can be seen from Figure 2 that the experimental lift and drag results obtained via the low-speed wind tunnel, are slightly increased compared to the simulated CFD results. The deviation in the CFD results from the experimental results can be explained by CFD model is based on the assumption of the air entering the boundary is uniform, with constant air density and perfectly smooth kite surface. However, in the experimental setup, the air density is not uniform, and the 3D models have minor roughness. Although the experimental lift and drag coefficient curve shows slightly higher values than the CFD results, the curve is still a close match i.e. stall occurs at an equivalent angle of attack of 40° with a percentage error of 10% suggesting the CFD model can be used for further analysis.

3.Results and discussion

While in operation for power generation, it is likely that the power kites will be operating in close proximity. A single kite can create a large area of turbulent flow, which can impact the efficiency of a kite operating nearby. To find the ideal distance that the kites can operate safely, two kites were simulated by varying horizontal separation distances from 200 mm, 400 mm to 550 mm and vertical separation distance from 150 mm, 0 mm to -150 mm. It is to be noted that the simulation is scaled using a 1:35.5 model; the distance separating the models can be scaled to appropriate the actual position when in industrial use.

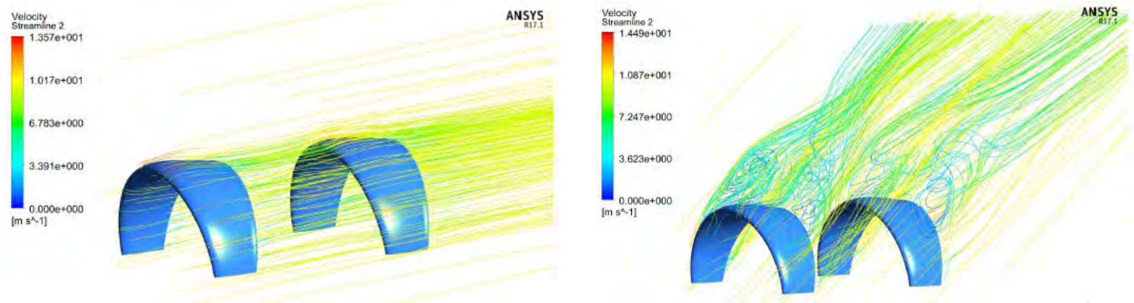

Figure 3: Comparison of velocity streamline plot for horizontal separation distance 400 mm and 200 mm

Figure 3 shows the comparison of velocity streamline contour plots with horizontal distance 400 mm and 200 mm respectively, and Figure 4(a) shows both the comparison of the Lift and Drag Coefficients of the three different horizontal kite separation distance simulations. When comparing the Drag Coefficients, it can be concluded that the drag is not a significant factor in the choice of arrangement to be carried forward, the coefficient of lift, however, does vary, meaning a setup can be chosen from this. In comparison, the Lift produced by each wing is very similar throughout each simulation, with the greatest variation occurring at an AoA of both 15° and 25°. At these deviations, the lowest Lift Coefficient, and therefore the lowest efficiency, is seen to be at a horizontal displacement of 400 mm, in this setup, the leading kite produces the lowest lift coefficient out of the three simulations, with the rear producing the 2nd lowest. From these results, it can be concluded that the horizontal displacement of 400 mm creates the least efficient setup.

Figure 4(b) shows both the comparison of the Lift and Drag Coefficients of the three different vertical kite separation distance simulations. From this figure, the drag coefficient is almost identical for each setup, the only variation being at 15° AoA for the trailing kite located above the leading. The lift coefficient for each kite working close together is greater than that of the single for most AoA. The greatest lift coefficient, produced at 40°, is created by the leading kites in both setups, the trailing kite located 150 mm below generally produces a more significant lift over a wider AoA, and therefore this setup will be able to obtain more energy out of the wind, thus obtaining a more efficient setup for power generation.

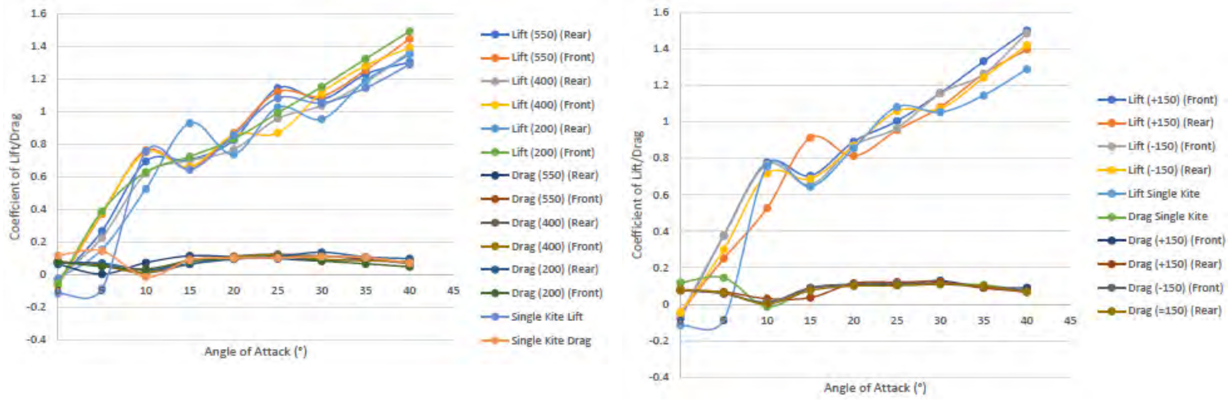

(a) *(b)*

Figure 4: Comparison of lift and drag coefficients for different (a) horizontal separation distances (b) vertical separation distances

From the results above, it can be concluded that the leading kite will always produce a lift coefficient greater than that of the trailing kite, this lift coefficient, however, can vary. The rear kite at a horizontal displacement of 200 mm only generally produces the lowest lift coefficient out of the four kites, with the rear kite for the vertical setup producing a greater lift for a majority AoA. For the front kite, the efficiency of the two setups is very close for several AoA, with generally the same lift coefficient produced. To conclude, at these specific conditions, the most energy efficient setup produced by the power kites is at a horizontal displacement of 400 mm (14.2 m), with a vertical displacement of -150 mm (5.325 m).

4. Effect of Surface Roughness

All previous CFD results assume the kites surface to be perfectly smooth. In reality, the surface roughness is present and play an essential role. Therefore simulating a surface roughness on the kite is an essential factor. The roughness height and roughness constant used in the present student is 0.001 m and 0.5. The results obtained are shown in Figure 5. Figure 5 compares the drag of a smooth kite with that of the rough; it is shown that the rough kite has a larger drag coefficient and a lower lift. A larger drag is expected, as the kite surface imposes a larger resistive force to the air flowing over it, which in turn reduces the wind speed over the kite surface and reduces the lift.

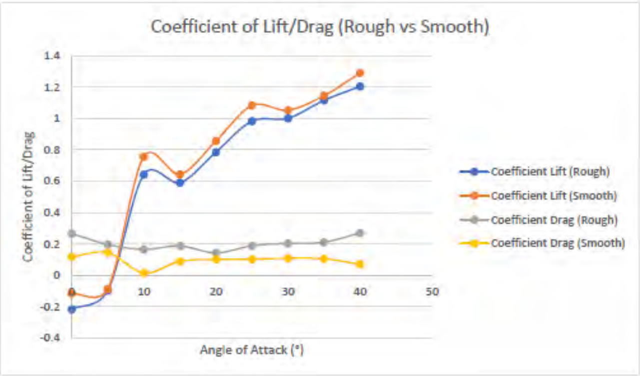

Figure 5: Comparison of lift and drag coefficients for smooth and rough aerofoil

Conclusion

This paper aimed to optimise a power kite suitable for renewable power generation; one of the main topics discussed was the operating distance between kites and how it impacts the efficiency of each kite. Generally, the leading kite is not impacted when working in close vicinity to other kites, the trailing one, however, was subject to significant variations in lift and drag coefficient. These results suggested that the optimal positions for the rear kite are either to be directly behind the leading kite, a large distance between the two (at least 15 m) or for the trailing kite to operate below the leading. Due to the risk of kite tethers wrapping around each other if operating in close proximity, the ideal choice is operating the kites at minimum 15 m horizontal separation, with the trailing kite operating below the leading, removing the potential for this kite to operate in the wake turbulence of the first. As the wind speed is generally very low at low altitudes, it is recommended to use a symmetrical aerofoil for the kite design, as these tend to produce greater lift with low Reynolds airflow.

References

1. Blanco MI (2009) The economics of wind energy. Renewable and sustainable energy reviews, 13(6-7), pp.1372-1382
2. Zhang H (2013) Kite modelling for higher altitude wind energy. Energy and Power Engineering, 5(07), p.481.
3. Canale M, Fagiano L, Milanese M (2009) High altitude wind energy generation using controlled power kites. IEEE Transactions on Control Systems Technology. 18(2), pp. 279-93
4. Gerakopulos R, Boutilier M and Yarusevych S (2010) Aerodynamic characterization of a NACA 0018 airfoil at low Reynolds numbers. In 40th Fluid dynamics conference and Exhibit (p. 4629)
5. Bauer F, Kennel RM, Hackl CM, Campagnolo F, Patt M and Schmehl R (2018) Drag power kite with very high lift coefficient. Renewable energy, 118, pp.290-305

Nottingham | UK | 9–11 September 2019

Coupled Capacity Fade Modelling of Lithium Ion Battery for Prognostics

Nneka C. Daniel, Chris Bailey, Chunyan Yin and Stoyan Stoyanov
University of Greenwich, Old Royal Naval College, Park Row, London SE10 9LS
n.c.daniel@gre.ac.uk

Abstract: Lithium-ion batteries (LIBs) experience capacity loss due to unwanted side reactions that occur during battery's cycling at high charge and discharge rates (C-rates). In this work, a coupling multi-physics model approach for the electrochemical and capacity fade phenomena of LIB is developed and demonstrated. The effects of the SEI layer formation, film resistance, solvent reduction reaction, and graphite expansion due to particle cracking causing capacity loss at different charge and discharge rates under cycling condition are investigated and reported. The simulation results show that charge-discharge cycling at faster rates of a Lithium-Ion (Li-ion) battery accelerates the capacity fade of the battery. A major finding is that with increasing values of the C-rates, SEI formation is most pronounced in the anode region near the separator. This leads to a reduction in the electrolyte volume and to a higher potential drop. The loss of lithium during discharge cycling is found to be the major cause of capacity fade associated with Li-ion batteries.

Keywords: Lithium-ion battery, capacity fade, solid electrolyte interface, C-rates.

1. Introduction

Lithium-ion battery (LIB) is gaining greater interests in application areas over other batteries due to its lead in energy storage and supply. LIBs are light in weight, have high energy/power density, low self-discharge rate when not in use, exhibit no memory effect, high operating voltage, and long cycle life [1, 2]. However, LIBs experience capacity fade and electrochemical degradation due to side reactions happening during cycling. Other major ageing phenomena that lead to capacity fade in LIBs include; diffusion stress, electrolyte decomposition, active material degradation, surface film formation, over-charging, phase change, and ageing mechanisms due to Solid-Electrolyte Interface (SEI) layer growth [3, 4]. LIBs suffer an irreversible capacity loss during the first few charge/discharge cycles due to the formation of a passive film over the anode (the solid electrolyte interface, SEI). This formation is intentional designed to serve as a passivating layer isolating the electrolyte from the negative electrode. However, as the battery is being cycled continuously, the SEI continues to form and grow, thus, trapping more lithium and causing an increase of film resistance and solvent reduction. All these hinder the charging/discharging processes of the battery for which lithium is required. In addition, the negative electrode particles become more susceptible to cracking and stress. Stress as lithium diffuses into the active materials and cracking due to formation of SEI layer on the material. These cause a volume change and local deformation of the solid materials in the battery [5]. The formation of SEI layer at the surface of the negative electrode is considered as the dominant aging mechanism triggering the irreversible capacity loss [6].

Also, cycling LIBs at high charge and discharge rates is a factor promoting the battery degradation [8]. Discharging/charging the battery at a high rate can cause changes in the morphology of the electrode crystals resulting to cracking and crystal growth that can affect the internal impedance of the cell. There is a chemical limitation to the rate at which Li ions intercalate/de-intercalate into the anode particles. Thus, forcing them to move at faster rate will amount to higher current being forced through the battery during discharge/charge process.

Depositing more Li-ions on the anode surface in the form of Li metal results in an irreversible capacity loss. The battery may also experience electrolyte decomposition since higher voltage is required to maintain the fast charging process, also leading to capacity loss.

The effect of solvent reduction reaction and film formation has been studied by different authors [4, 9–12] discounting the effect of graphite expansion during intercalation due to diffusion-induced stress. The effect of SEI growth at different C-rates under constant-current constant-voltage (CC-CV) charging scenarios has also been researched [13–17] also discounting the graphite expansion during intercalation as a result of diffusion-induced stress. Nonetheless, some authors [18, 19] have studied the effect of graphite expansion due to cracking during intercalation with SEI layer side reaction but did not considered the effect of C-rates. Hence, in order to realistically simulate and fully understand the charge-discharge performance and degradation of an LIB, a coupled effects of SEI layer growth, film resistance, solvent reduction reaction, and graphite expansion during intercalation due to diffusion-induced stress with the electrochemical model at different charge/discharge rates during cycling is required.

To accurately predict the capacity fade and the electrochemical degradations of the battery under specified test or operating conditions (charge and discharge rates, voltage, current, temperature, etc.), physics-of-failure (PoF) approach that captures the battery dynamics with high precision is very crucial [20]. PoF approach has been grouped into four different models that support capturing battery behaviour and predicting its performance. These include: empirical, molecular/atomistic, multi-physics, and electrochemical models [21]. Among these approaches, a multi-physics approach that couples the side reactions models (causing the capacity fade) and electrochemical battery level models is desirable [16]. This approach comprises of coupling and decoupling of various physical phenomena such as mechanical stress, electric, thermal, side reactions, and electrochemical occurring at different levels in the battery system [22]. This has the ability to predict accurately and under varied operating conditions and aging cycles; the internal dynamics and external characteristics of the battery system with no substantial experimental support for model calibration [23]. It helps to understand the physics of failure mechanisms associated with the complex multi-physics interaction within the batteries, and how batteries degrade overtime.

In this paper, a multi-physics approach that couples an electrochemical model with a capacity fade model is developed and demonstrated. The aim is to simulate, study, and better understand the interactions and the effect of SEI layer formation, film resistance, solvent reduction reaction, and graphite expansion during intercalation as a result of diffusion-induced stress that cause capacity loss under different charge/discharge rates (C-rates). The work provides a building block of a higher-level computational framework for a novel fusion prognostic approach that aims to integrate multi-physics models with data-driven models for key degradation parameters. Thus, enabling more accurate reliability and remaining useful life predictions.

2. Simulation Model

LIB is a dynamic and nonlinear electrochemical system and hence a coupled multi-physics approach is best suited to capture the complexity in such analysis. A pseudo two dimensional (P2D) model describing the electrochemical phenomena in a battery cell is adopted for the physics simulation [24, 25]. This model solves the battery phenomena such as lithium transport and diffusion in solid and liquid phases, and electrochemical kinetics in great details using a set of partial differential equations (PDEs). A parasitic kinetic expression is coupled with the P2D model for SEI formation reaction model [18], and for the graphite electrode particles expansion which leads to particle cracking due to SEI film formation. In addition, models for solvent reduction reaction comprising of the film resistance and dissolving depositing species was also integrated [9]. Further details on equations and appropriate boundary conditions on respective models can be found in previously published work [9, 18, 25].

The battery cell investigated in this study comprises of a graphite negative/Lithium Nickel Cobalt Aluminium Oxide (NCA) positive electrodes in liquid electrolyte of LiPF6 in mixture of Ethylene Carbonate (EC): Ethyl Methyl Carbonate (EMC) (3:7). A finite element analysis software (COMSOL Multiphysics 5.4v) is used to undertake the respective simulation. In this case, a two-dimensional (2D) representation of the geometry of the LIB cell is realised, hence all calculations are performed on a 2D model. Fig.1 shows the 2D battery geometry with the three battery domains: negative electrode, positive electrode, and separator, and two current collectors surrounding the electrodes. The battery is simulated under constant current-constant voltage (CC-CV) charge and constant current discharge cycle with end of charge voltage of 4.1 V, cut-off current of 50mA, and minimum voltage of 2.5V. Different charge and discharge rates of 1C, 0.75C, 0.6C, 0.5C-rates have been analysed assuming LIB at 45^0C. The battery cell data and parameters used in this simulation are obtained from [15, 18, 26, 27]. To demonstrate the simulation of the multi-physics ability, a 2D simulation showing the maximum concentration of lithium on particle surface for different C-rates at the end of each cycle is shown in Fig. 1b. Decrease in lithium concentration was more on 1C (3.29×10^4 mol/m^3) when compared with 4.16×10^4 mol/m^3 for 0.5C against its initial maximum concentration of 4.77×10^4 mol/m^3. This suggests loss of cyclable lithium in the electrode.

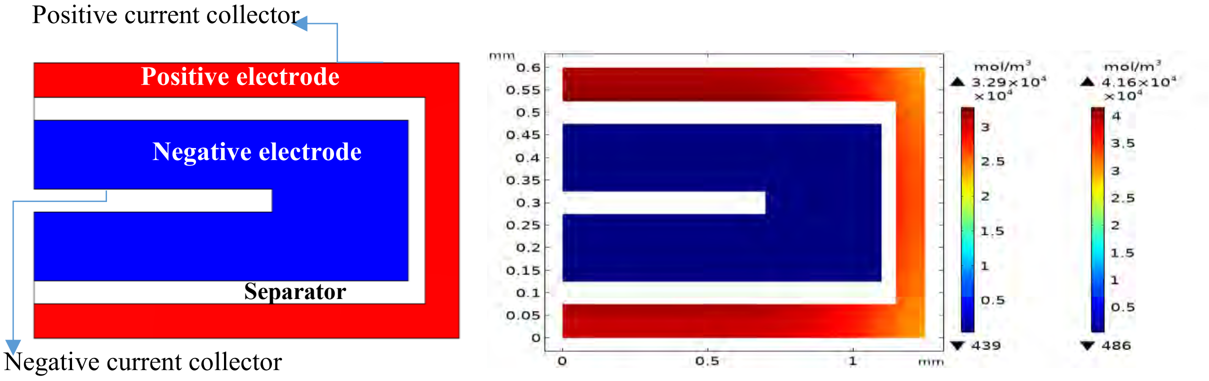

Figure 1:(a) Geometric domain of the LIB cell (2D model representation), and (b) Li concentration on particle surface.

3. Modelling Results and Discussions

3.1 Capacity Fade During Cycling

Fig. 2a shows the cycling performance comparison of NCA/graphite cell at different C- rates. The solid lines represent the cell capacity based on the total amount of cyclable lithium as a result of film formation at the negative electrode, while the dotted lines represent the discharge capacity at varied C-rates. Looking at the total amount of cyclable lithium available after 2000 cycles, a sharp decrease in capacity due to the SEI formation occurs at the first few cycles of the battery. The decrease in the capacity tends to accelerate when the C-rates increase - that is 0.5C, 0.6C, 0.75C, and 1C, leading to capacity fade of 9.33%, 10%, 11%, and 12.24% respectively. The charge/discharge capacity fade during cycling decreases by 17.16%, 24.29%, 30.02%, and 34.34% for 0.5C, 0.6C, 0.75C, and 1C respectively. However, it is observed that the capacity loss based on discharge cycle is much higher, indicating that Li-ion loss during cycling is the main contributor of capacity loss. This comes from the fact that the number of moles of lithium transferred between the positive and the negative electrode during battery charge or discharge is directly related to cell Amp-hour capacity. The more the cell is being cycled, the more the trapping of Li into the freshly formed SEI layer. Also, Fig. 2b shows the discharge capacity at different discharge rates as it varies with the cell voltage. The solid lines represent the first discharge cycle while the dashed lines represent the last discharge cycle. This also shows that the higher the C-rate, the more the capacity fades. This suggests that the discharge rates influence the rate at which the cell degrades over time. Similar conclusion related to this problem was drawn from earlier experimental work [26].

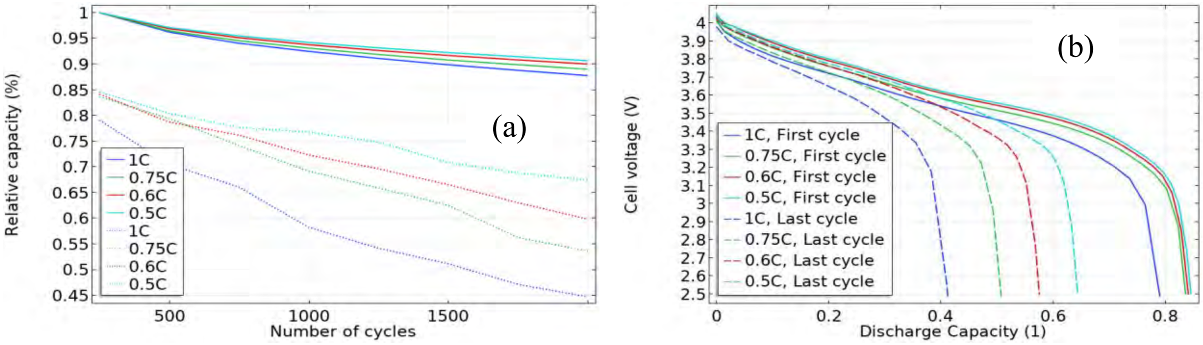

Figure 2:Cycle performance of graphite/NCA-based cell at different discharge rate. (a) Relative capacity over 2000 cycles; (b) Discharge curve

3.2 Parasitic Reaction at Negative Electrode Interfaces

Another problem which has been addressed in this work is how the parasitic reactions on the negative electrode interfaces associated with the SEI formation occur. The modelling results from this analysis are shown in Fig. 3. Point 10 and 13 are chosen to be the points nearest to the current collector/negative electrode interface and the separator/negative electrode interface respectively. Fig.3a illustrates the change in film thickness as it increases during cycling at higher C-rates. The increase in thickness of SEI is more pronounced near the separator/negative electrode interface. Fig.3b illustrates the reduction in the electrolyte volume fraction due to the formation of the SEI layer. The initial process of SEI film formation serves the role of passivating film which provides isolation between the interface of the electrolyte and the negative electrode. However, this SEI film continues to grow on the surface of the electrode, thereby causing the volume fraction of the electrolyte to decrease. This reduction is particularly notable in the region near the separator, and in the case of higher C-rates.

Dissolving-depositing species concentration due to SEI formation is observed to grow as the battery is being cycled at higher C-rates nearer to the separator, as shown Fig.3c. Fig.3d illustrates the increase in the potential drop over the SEI layer across the battery cycle. These modelling results suggest that the SEI layer growth occurs closer to the interface of the separator and the negative electrode and is the main factor for the capacity loss because of the solvent reduction, film resistance, and the drop in the potential.

3.3 Lithium Concentration at Different C-Rates

The concentration of Li-ion at different C-rates as a function of the particles' radius is shown in Fig.4. The concentration of Li-ion near the current collector (CC), middle of the negative electrode, and near the separator at different C-rates rates are represented with solid, solid diamond, and dashed lines respectively. The ions distribution increases as the C-rates increase. This is due to the chemical-mechanical degradation at particle level, with higher stresses induced in the region near the separator. Based on these results, particles nearer to the separator are most likely to experience mechanical degradation due to cracking and fracture of the active material in the anode.

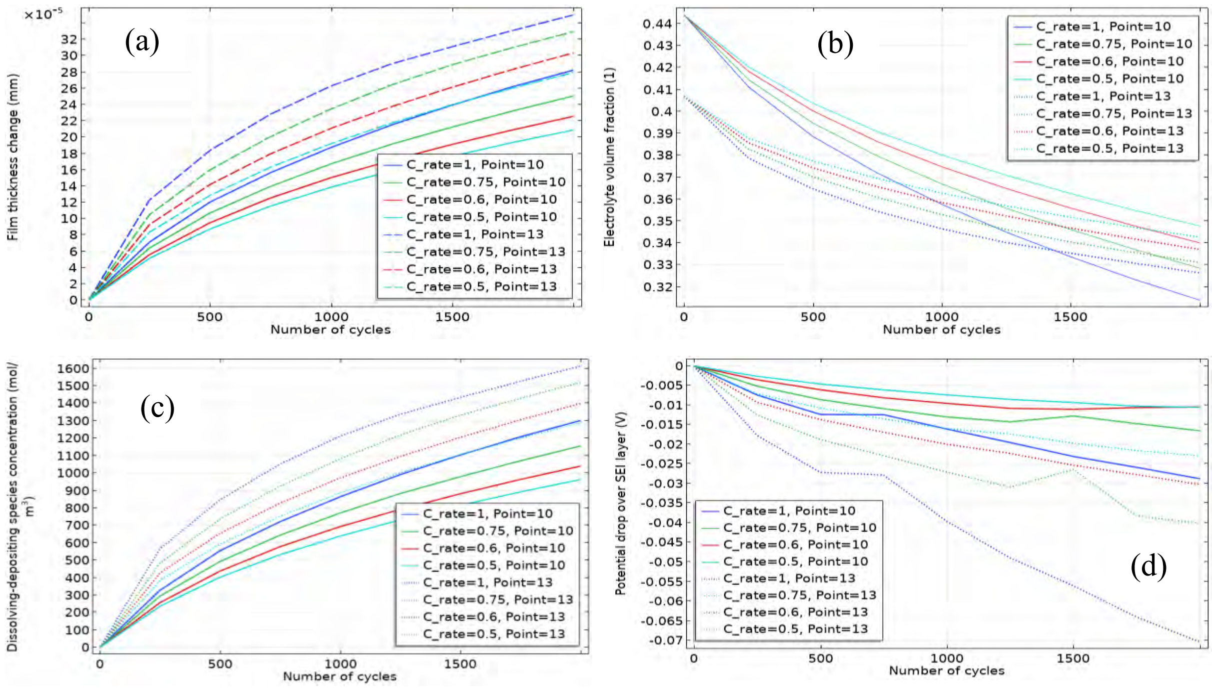

Figure 3:SEI parasitic reactions at the negative electrode current collector and separator interfaces. (a) SEI film thickness change; (b) Electrolyte volume fraction; (c) Dissolving-depositing species concentration; (d) Potential drop over SEI layer.

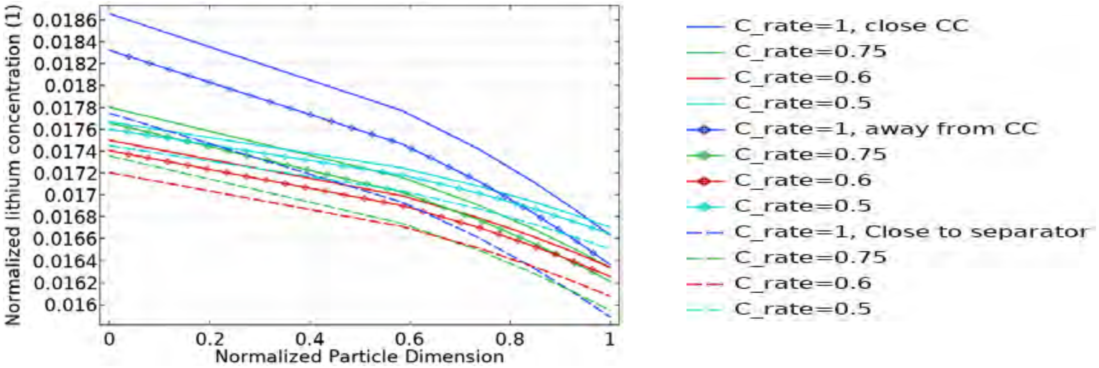

Figure 4:Lithium concentration in anode particle

4. Conclusion

Accurate predictions for the degradation of LIBs require a multi-physics approach, and the integration of both physics (electro-chemical) and capacity fade models. Such modelling capability has been shown to support studying the effect of SEI layer formation, film resistance, solvent reduction at the graphite negative electrode material. It also supports understanding the effect of diffusion-induced stress that cause capacity loss at varied charge/discharge rates (C-rates) under cycling condition. The modelling results obtained in this work show that charge/discharge cycling of lithium ion battery cells at faster rates will accelerate the capacity fade of the batteries. There is a reduction in the electrolyte volume and high increase in the potential drop near the separator as formation of a SEI takes place. The SEI growth rate is higher in increase C-rates of the charge-discharge cycle. Loss of cyclable lithium is also predicted and identified as the major factor for capacity fade during the discharge cycles. Further work will include exploring the prediction of capacity fade and remaining useful life of battery while applying a fusion based model that integrates multi-physics and data-driven aspects for better accuracy and implementation.

Acknowledgement: This work has been supported through Vice Chancellor's scholarship fund from the University of Greenwich and Doctorial Training Alliance (DTA).

References

1. Hannan MA, Lipu MSH, Hussain A, Mohamed A (2017) A review of lithium-ion battery state of charge estimation and management system in electric vehicle applications: Challenges and recommendations. Renew Sustain Energy Rev 78:834–854
2. Oh K-Y, Samad NA, Kim Y, Siegel JB, Stefanopoulou AG, Epureanu BI (2016) A novel phenomenological multi-physics model of Li-ion battery cells. J Power Sources 326:447–458
3. Arora P, White RE, Doyle M (1998) Capacity Fade Mechanisms and Side Reactions in Lithium-Ion Batteries. J Electrochem Soc 145:3647–3667
4. Ploehn HJ, Ramadass P, White RE (2004) Solvent Diffusion Model for Aging of Lithium-Ion Battery Cells. J Electrochem Soc 151:A456–A462
5. Zhao Y, Stein P, Bai Y, Al-Siraj M, Yang Y, Xu B-X (2019) A review on modeling of electro-chemo-mechanics in lithium-ion batteries. J Power Sources 413:259–283
6. Zhao P, Li M, Kang J, Rizzoni G (2017) Analysis of fading characteristics of a lithium ion battery based on an integration model. Int J Heat Mass Transf 104:1317–1324
7. Chattopadhyay S, Lipson AL, Karmel HJ, Emery JD, Fister TT, Fenter PA, Hersam MC, Bedzyk MJ (2012) In Situ X-ray Study of the Solid Electrolyte Interphase (SEI) Formation on Graphene as a Model Li-ion Battery Anode. Chem Mater 24:3038–3043
8. Rejovitzky E, Di Leo C V., Anand L (2015) A theory and a simulation capability for the growth of a solid electrolyte interphase layer at an anode particle in a Li-ion battery. J Mech Phys Solids 78:210–230
9. Ramadass P, Haran B, Gomadam PM, White R, Popov BN (2004) Development of First Principles Capacity Fade Model for Li-Ion Cells. J Electrochem Soc 151:A196–A203
10. Ning G, Popov BN (2004) Cycle Life Modeling of Lithium-Ion Batteries. J Electrochem Soc 151:A1584–A1591
11. Ning G, White RE, Popov BN (2006) A generalized cycle life model of rechargeable Li-ion batteries. Electrochim Acta 51:2012–2022
12. Sankarasubramanian S, Krishnamurthy B (2012) A capacity fade model for lithium-ion batteries including diffusion and kinetics. Electrochim Acta 70:248–254
13. Spotnitz R (2003) Simulation of capacity fade in lithium-ion batteries. J Power Sources 113:72–80
14. Safari M, Morcrette M, Teyssot A, Delacourt C (2009) Multimodal Physics-Based Aging Model for Life Prediction of Li-Ion Batteries. J Electrochem Soc 156:A145
15. Delacourt C, Safari M (2012) Life Simulation of a Graphite/LiFePO4 Cell under Cycling and Storage. J Electrochem Soc 159:A1283–A1291
16. Xie Y, Li J, Yuan C (2014) Multiphysics modeling of lithium ion battery capacity fading process with solid-electrolyte interphase growth by elementary reaction kinetics. J Power Sources 248:172–179
17. Lawder MT, Northrop PWC, Subramanian VR (2014) Model-Based SEI Layer Growth and Capacity Fade Analysis for EV and PHEV Batteries and Drive Cycles. J Electrochem Soc 161:A2099–A2108
18. Ekstrom H, Lindbergh G (2015) A Model for Predicting Capacity Fade due to SEI Formation in a Commercial Graphite/LiFePO4 Cell. J Electrochem Soc 162:A1003–A1007
19. Kindermann FM, Keil J, Frank A, Jossen A (2017) A SEI Modeling Approach Distinguishing between Capacity and Power Fade. J Electrochem Soc 164:E287–E294
20. Narayan A (2017) State and Parametric Estimation of Li-Ion Batteries in Electrified Vehicles. KTH Royal Institute of Technology
21. Daigle M, Kulkarni C (2013) Electrochemistry-based Battery Modeling for Prognostics. In: Annu. Conf. Progn. Heal. Manag. Soc. pp 1–13
22. Abada S, Marlair G, Lecocq A, Petit M, Sauvant-Moynot V, Huet F (2016) Safety focused modeling of lithium-ion batteries: A review. J Power Sources 306:178–192
23. Li X, Pan K, Fan G, Lu R, Zhu C, Rizzoni G, Canova M (2017) A physics-based fractional order model and state of energy estimation for lithium ion batteries. Part II: Parameter identification and state of energy estimation for LiFePO4battery. J Power Sources 367:202–213
24. Doyle M, Fuller T., Newman J (1993) Modelling the Galvanostatic Charge and Discharge of the Lithium/Polymer/Insertion Cell. J Electrochem Soc 140:1526–1533
25. Fuller TF, Doyle M, Newman J (1994) Simulation and Optimization of the Dual Lithium Ion Insertion Cell. J Electrochem Soc 141:1–10
26. Ning G, Haran B, Popov BN (2003) Capacity fade study of lithium-ion batteries cycled at high discharge rates. J Power Sources 117:160–169
27. Safari M, Delacourt C (2011) Simulation-Based Analysis of Aging Phenomena in a Commercial Graphite/LiFePO4 Cell. J Electrochem Soc 158:A1436

Nottingham | UK | 9–11 September 2019

A Novel Approach for the Evaluation of the Dynamic Thermal Behaviour of a Building by Continuous Monitoring using Autonomous Infrared Thermography

Amin Al-Habaibeh, Latifimran Jalil, Ahmed Lotfi, and Bubaker Shakmak

Nottingham Trent University, NG1 4FQ, UK

Amin.al-habaibeh@ntu.ac.uk

Abstract

In this paper, a novel approach is utilised for longitudinal study to evaluate the dynamic behaviour of a building using autonomous infrared thermography. This unique test has been conducted to investigate the dynamic performance of a building continuously over several days. This paper presents the monitoring process to investigate the behaviour of a poorly insulated building using infrared thermography. The experimental work is conducted over 13 days and an image is captured every hour for analysis. The results show that poorly insulated walls significantly contribute to heat losses and the most significant location and time for such losses have been identified. Based on which, the paper suggests some simple measures to improve insulation. This suggested approach has been found beneficial to understand the dynamic thermal behaviour of buildings over significant period of time.

1. Introduction:

The 2008 Climate Change Act has committed the UK government to reduce 80% of its 1990 carbon footprint by the year 2050 [1]. Statistics have shown that about 40% of carbon emission is emitted from buildings. Approximately 90% of homes are heated with a gas-fired central heating system and it is estimated that the domestic space heating alone accounts for approximately 11% of the country's carbon emissions [2]. The United Kingdom's housing stock is older than that of most European countries. Numerous houses date back to the Victorian era (1837–1901 AD) [3] and it is also predicted that by the year 2050 over 70% of the current stock of buildings will still be occupied. According to [4] as at 1990, 22% of houses were built before 1919, which were constructed without wall cavities and are of solid wall build, having poor heat retaining abilities. Moreover, based on the same reference, 39% of homes in England were built before the Second World War and 59% were built before 1965. It is understood that houses built after the 1920s, are likely to have cavity walls but were not filled with any insulations. It was not until 1965 that building regulations were introduced. Research show that “buildings don’t consume energy but people do” [5]. In an average UK home, over 60% of the used energy consumption is for space heating, 24% for hot water and the remaining 16% usage is for electrical appliances and lighting [6]. Around 4 million UK householders spend more than 10% of their income on energy bills. On average, they spend between 2.7 and 8.4 per cent on gas and electricity and 0.5 to 3 per cent on water. To enhance the understanding of energy efficiency in UK homes, seven main factors have been identified by [7] which are: building fabric; heating system; occupancy behaviour; comfort; health, life style; fuel poverty and government policies.

The UK government has introduced many measures to reduce the carbon footprint produced from its housing sector which include the loft insulations of domestic housing as well the replacements of inefficient boilers. This is in addition to the introduction of the Green Deal to insulate internal and external walls of solid brick homes. Between March 2014 and March 2015, 410,000 homes had cavity wall insulation installed. 320,000 and 49,000 houses also had loft and solid wall insulation respectively within the same period. [8]. As an outcome of such additions, the percentage of homes with insulation has reached 70%, 73% and 4% for loft, cavity walls, and solid wall insulation respectively [9]. These insulation measures have resulted in an estimated annual savings of over one billion pounds on national heating bills in the UK [8].

There are many factors that could influence energy consumption in homes including occupants’ behavior, household characteristics, energy price and how much the householders can afford to spend on energy. End use energy efficiency and fuel poverty is one of the major issues in the UK social housing sector. It is estimated that about 10% of households in England live in fuel poverty [8]. A good understanding of how occupants use a building can provide a possibility of promoting the building's energy efficiency through changing occupant behavior [10-15]. Another innovative method for understanding building energy related issues is the use of infrared thermography which has been successfully applied in various sectors. The use of infrared thermography to measure thermal performance of buildings has seen an increase in recent years where references [16-20] have all concluded its benefits. This paper presents approach where a longitudinal study is performed to evaluate the dynamic thermal behaviour of a building using infrared thermography. This unique test has been conducted to investigate the dynamic performance of a building over several days. This research is utilised to monitor the behaviour of a poorly insulated building using infrared thermography to explore its performance and identify the most critical areas in the building and the nature of heat losses.

2. Methodology

For this work, a unique test has been done to investigate the dynamic performance of a building over several days. This test is an attempt look at the behaviour of poorly insulated house with solid walls to understand the behaviour of the building in Nottingham between 26th of February and 8th of April 2013 for over 320 hours. An ethical approval process was put in place to ensure the exact location of the building is anonymous. An image was captured every hour for comparison. Figure 1 presents the setup where Flir A310 was installed externally looking at the building to measure its performance. Infrared data was captures and transferred digitally to Matlab for analysis.

Figure 1: The installation process of the autonomous infrared camera

3. Results and Discussion

Figure 2 presents an example of the infrared image obtained and a visual image of the monitored building.

Figure 2 : An Example of the infrared results obtained for the group of buildings.

The images are captured and calibrated to a different colour-map, see for Figure 3, where several animated videos of the behaviour of the building are developed and presented.

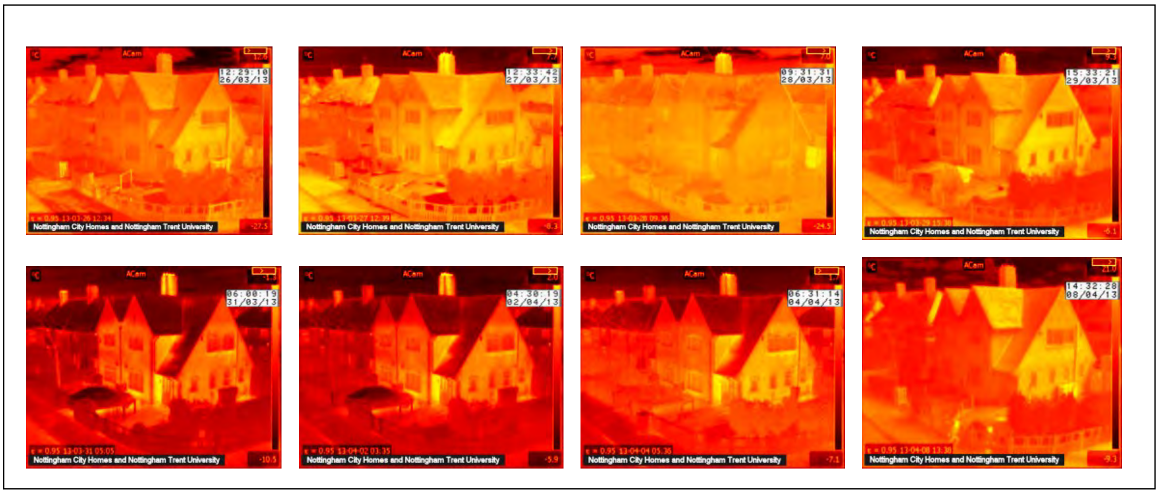

Figure 3: Infrared thermal behaviour of the building which was monitored for 13 days continuously for energy performance.

For quantitative analysis of the infrared data, consider Figure 4 which includes several points of interests on the infrared image: Point 1 presents the infrared radiation of the sky, this could also be used to evaluate the clarity of the sky. Point 2 is the temperature of the chimney; this could also indicate heat losses as well as the functionality of the heating system. Point 3 presents the wall of the loft. Point 4 presents first floor wall under the window (opposite to the radiator). Point 5 presents first floor wall. Point 6 shows the south facing wall. Point 7 presents ground floor wall under the window (opposite to the radiator). Point 8 presented ground floor wall and point 9 presents the ground temperature.

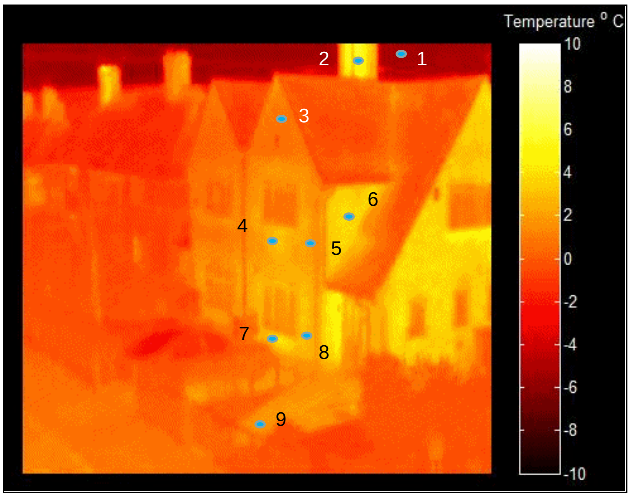

Figure 4: Comparison between the points monitored for analysis from the infrared images.

Figure 5 presents a comparison between the relative temperature of the loft wall (point 3) and the first floor wall (point 4). Notice that there is about 3°C difference on average. This is due to loft insulation and the effect of solid walls.

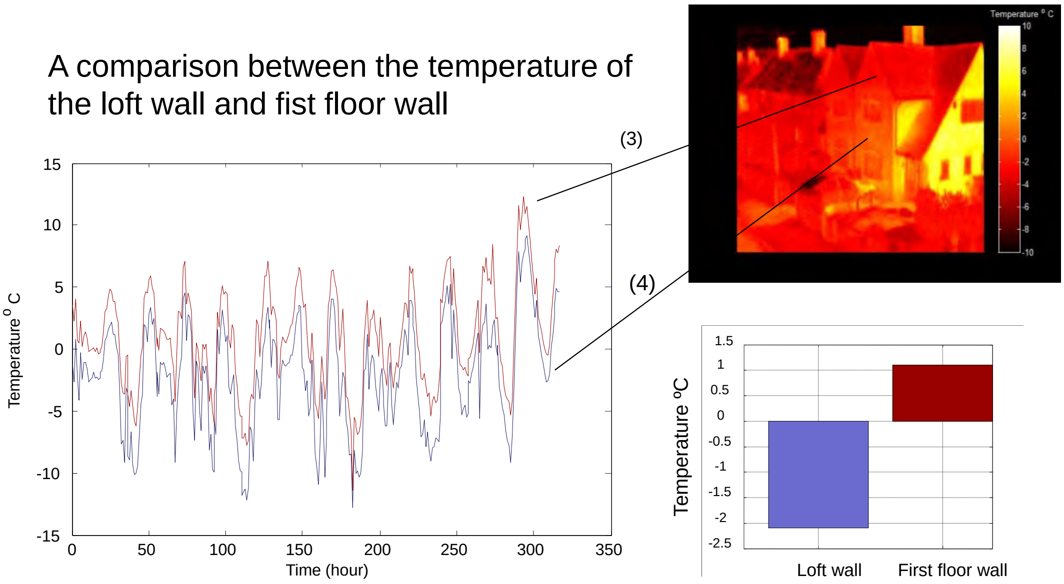

Figure 5: The loft wall is always lower than first floor wall by about average 3 °C due to loft insulation.

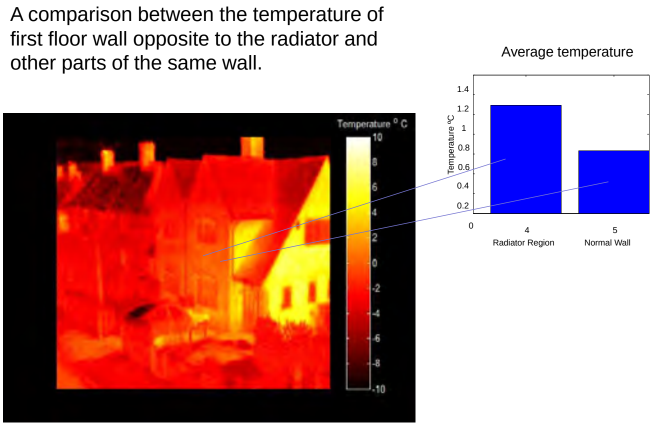

Figure 6: A comparison between different areas of the first floor.

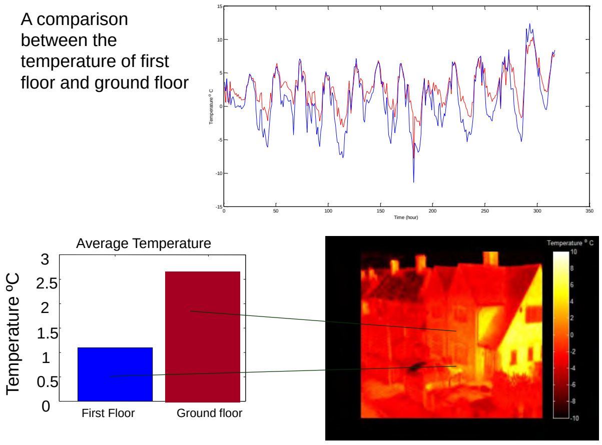

Figure 7: A comparison between first floor and ground floor.

Figure 6 indicate that the temperature of the wall behind the radiator is much warmer than other parts of the wall. Figure 7 indicates that that ground floor is always warmer than first floor wall, particularly during the colder periods. The average difference is found to be about 2 ^{o}C.

4. Conclusion

Old buildings are expected to lose significant heat through solid walls, single glazing, poorly insulated loft and chimney structure with the use of inefficient boilers. This paper has presented part of the results for monitoring an old and poorly insulated building using infrared thermography over significant number of days. The building has loft insulation and solid walls. The introduction of loft insulation has been found significant to reduce the loft temperature and hence heat losses via the roof and loft's walls. The dynamic analysis of infrared thermography has confirmed the performance of poorly insulated buildings. Infrared thermography result has shown the significant heat transfer via the walls. Further work is needed to quantify the payback period of each energy saving measure taking into consideration post occupancy behaviour.

Acknowledgment

This project is in collaboration with Nottingham City Homes, UK through a Knowledge Transfer Partnership. The authors would like to thank them for their support.

References

1. Climate Change Act 2008. In Wikipedia, The Free Encyclopedia. Retrieved 25/05/2019,ttp://en.wikipedia.org/w/index.php?title=Climate_Change_Act_2008&oldid=534636005
2. Adorkor Bruce-Konuah, Rory V. Jones, Alba Fuertes, Pieter de Wilde Central heating settings and heating energy demand in low energy social housing in the United Kingdom Energy Procedia, Volume 158, February 2019, Pages 3658-3663.
3. DBEIS 2017a 2015 UK Greenhouse Gas Emissions, Final Figures. London: Department for Business, Energy & Industrial Strategy.
4. DECC 2012 The Energy Efficiency Strategy: The Energy Efficiency Opportunity in the UK. London: Department of Energy and Climate Change.
5. Kathryn. B. Janda Buildings Don't Use Energy: People Do, 26th Conference on Passive and Low Energy Architecture, Quebec City, Canada, 22-24 June 2009.
6. J. Palmer, I. Cooper, "Great Britain's housing energy fact file", 2011.
7. Ahmad Lotfi, Latif Imran Jalil, Amin Al-Habaibeh, Investigating Occupant Behaviour to Improve Energy Efficiency in Social Housing Case Study, The 9th International Conference on Intelligent Environments (IE'13) At: Athens, Greece. 2013.
8. Shuli Liu, Obiajulu Iweka, Ashish Shukla, Georgina Wernham, Atif Hussain, Rosie Day, Mark Gaterell, Panagiotis Petridis and Dan Van Der Horst. Impact of Emerging Interaction Techniques on Energy Use in the UK Social Housing, Future Cities and Environment, 4(1): 8, 1–11, DOI: https://doi.org/10.5334/fce.36
9. DECC 2015 Domestic Green Deal, Energy Company Obligation and Insulation Levels in Great Britain, Detailed report. London: Department of Energy and Climate Change
10. Stone, B 2008 Human Factors Guidelines for interactive 3D and Games-based training Systems. [Online] Available at: http://www.birmingham.ac.uk/Documents/college-eps/eece/research/bob-stone/human-factors-guidance.pdf [Accessed 2019 April 25].
11. Bainsbridge, W S 2007 The scientific research potential of virtual worlds. Science, 317: 472–476. DOI: https://doi.org/10.1126/science.1146930
12. Mayo, M J 2009 Video games: A route to large-scale STEM education? Science, 323: 79–82. DOI: https://doi.org/10.1126/science.1166900
13. Subrahmanian, V S and Dickerson, J 2009 What Can Virtual Worlds and Games Do for National Security? Science, 326(5957): 1201–1202. DOI: https://doi.org/10.1126/science.1182660
14. James Fisher[1], Imma Farré[2], Anne Dray[3], Nirav Khimashia[4] and Pascal Perez, Serious games to explore uncertainty of future farms, Proceedings of 16th Agronomy Conference 2012, University of New England in Armidale, NSW 14-18th October 2012.
15. Wood, G., van der Horst, D., Day, R., Bakaoukas, A.G., Petridis, P., Liu, S., Jalil, L., Gaterell, M., Smithson, E., Barnham, J., Harvey, D., Yang, B. & Pisithpunth, C. (2014). 'Serious games for energy social science research'. Technology Analysis & Strategic Management.
16. Matthew Fox, DavidColey Steve Goodhewa, Pieterde Wilde: A Thermography methodologies for detecting energy related building defects Renewable and Sustainable Energy Reviews 40(2014) 296–310

17. Kylili, Angeliki; Fokaides, Paris A.; Christou, Petros; Kalogirou, Soteris A. (2014). "Infrared thermography (IRT) applications for building diagnostics: A review". Angeliki Kylili, Paris A. Fokaides, Petros Christou, Soteris A. Kalogirou. 134: 531–549. doi:10.1016/j.apenergy.2014.08.005.
18. Angeliki Kylili , Paris A. Fokaides ,Petros Christou , Soteris A. Kalogirou : Infrared thermography (IRT) applications for building diagnostics: A review Applied Energy 134 (2014) 531–549
19. Alex Marshall 1, Johann Francou , Richard Fitton , William Swan , Jacob Owen, and Moaad Benjaber 1 Variations in the U-Value Measurement of a Whole Dwelling Using Infrared Thermography under Controlled Conditions, Buildings 2018, 8, 46; doi:10.3390/buildings8030046
20. Elena Lucchi⁎ Applications of the infrared thermography in the energy audit of buildings: A review, Renewable and Sustainable Energy Reviews 82 (2018) 3077–3090.

Nottingham | UK | 9–11 September 2019

The Role of Heritage-BIM in the Process of Energy Retrofitting of Heritage Buildings - A Literature Review

Ahmed Khalil [1], Spyridon Stravoravdis [2]

[1]*University of Greenwich, London, UK.*

[2]*University of Liverpool, London, UK.*

a.khalil@greenwich.ac.uk

Abstract

Heritage-BIM is an emerging domain which addresses the potentials and challenges of managing the documentation, retrofitting and operation of heritage buildings through BIM tools. HBIM can play an efficient role in the sustainable retrofitting and the optimisation of the building`s energy performance. This paper will investigate the role of HBIM in the performance documentation, simulation and retrofitting frameworks through current literature in the field.

Keywords: H-BIM; Documentation; Simulation; Retrofit;

1.Introduction

Achieving sustainability and energy efficiency is becoming more and more a hot topic in architecture. While existing buildings are responsible for more than 40% of the world's total primary energy consumption and for 24% of global carbon dioxide emissions [1,2], Considering current energy performance standards, heritage buildings are facing many challenges that, potentially, can be addressed in the retrofitting process. This process is in need of careful consideration to balance listed buildings` protection, energy performance, users` comfort and functionality. In order to achieve these objectives, BIM could be of great benefit in managing the retrofitting process throughout the building`s lifecycle.

Heritage-BIM is an emerging domain which addresses the potentials and challenges of managing the documentation, retrofitting and operation of heritage buildings through BIM tools. HBIM can also represent a contribution towards energy analysis, economic analysis up to multi-thematic analysis within sustainability [3, 4, 5].

A lot of research has already been conducted in the field of HBIM to address its different aspects, especially the documentation and modelling phase with its different implications. However, fewer researches addressed specifically the topic of HBIM's role in the sustainable retrofitting and the energy performance of listed buildings. This paper aims to review the available literature for the energy performance and energy retrofitting of heritage buildings, and the potential application of HBIM within this domain, in order to contribute towards implementing HBIM tools into the process of energy retrofitting of heritage buildings.

The role of Heritage-BIM in the process of energy retrofitting of heritage buildings can be studied in three aspects, which this paper will focus on; the documentation phase, the building performance simulation and the frameworks to manage the retrofitting process.

2. H-BIM Documentation

Heritage documentation is seen as the systematic collection and archiving of tangible and intangible elements of historic structures and environments. Its purpose is to supply accurate information that will enable correct conservation, monitoring and maintenance for the survival of the building [6,7,8]. HBIM offers very versatile solutions for modelling and managing information relating to existing and heritage buildings. It can be used as a documentation and management tool for conservation work, retrofitting, renovations and building analysis. It can also be used as a research tool for documentation that can incorporate both quantitative assets (intelligent objects, performance data) and qualitative assets (historic photographs, oral histories, music) [9]. acquisition of all possible data is the first step to contribute towards fundamental modelling for building recording and documentation [10].

Data Concerning building performance and energy consumption could be crucial for heritage buildings retrofitting and management. Hence, building performance data could be of great importance to be included into the phase of survey and documentation of heritage buildings [11]. Building performance in its broad understanding can represent many aspects such as energy performance, thermal performance, visual performance, acoustic performance, indoor air quality, systems efficiency, as well as functional and structural performance.

Some research has been conducted to achieve the integration of the different performance data into BIM modelling of heritage buildings. An innovative example can be seen in the work of Wang and Cho [12], as they tried to combine laser scanning of an existing building with thermal imaging to help assess the thermal performance of the building`s outer envelope. For this purpose, they proposed a framework by developing a hybrid 3D LIDAR system with an IR camera to measure the temperature of the building`s surface so the temperature data are automatically fused with corresponding points during the data collection process and every point of the point cloud is defined by its x-y-z coordinates and corresponding temperature data (Figure 1) [12].

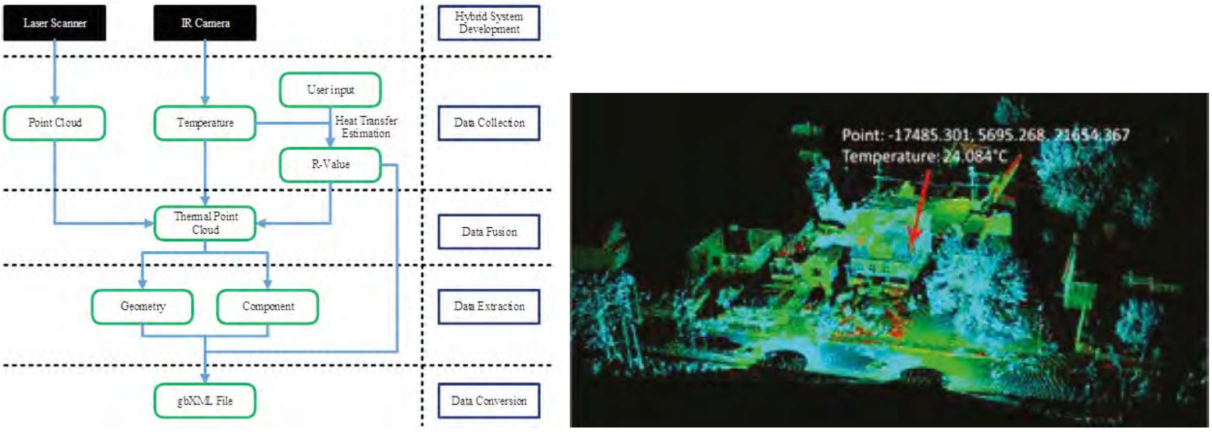

Figure 1: The framework for sustainability assessment proposed by Wang and Cho, and the point cloud of the building including the thermal information.

Another research by Pocobelli et al [13] focused on measuring moisture data of the facades of the Jewel tower in London, dated back to the fourteenth century. They integrated these data into Revit through the "Schedule" command. These reading points had to be modelled as family masses "spheres" because Revit can create schedules only for families. They used Dynamo platform to create an algorithm to depict moisture variation in walls, using the data that are stored in Revit through spreadsheets linked to smart masses (Figure 2).

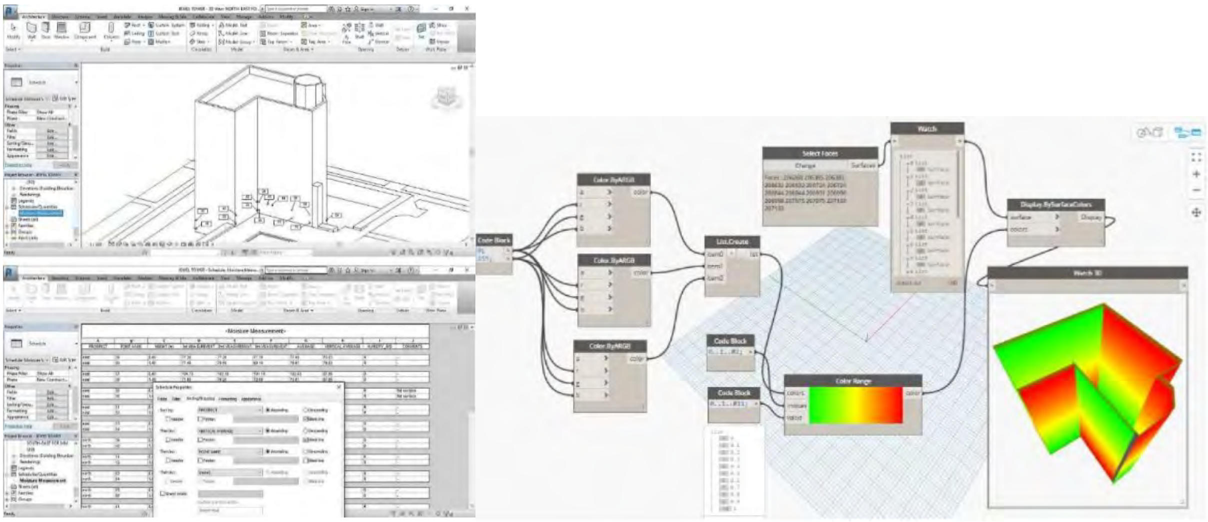

Figure 2: Moisture readings positions on the BIM model and the creation of Dynamo workflow to depict moisture – focus on colour creation and model importation by Pocobelli et al.

3. H-BIM Modelling and Simulation

Building modelling and simulation is a great tool to predict the building performance and can help in the optimisation of retrofitting decisions and design alternatives. BIM helps to integrate building simulation and performance data into heritage building modelling that can facilitate collaboration of different stakeholders and helps in the retrofitting process [3,4,5].

Brumana et al [14] surveyed and modelled the St. Maria church in Scaria d'Intelvi, Italy, they performed a building performance analysis through simulation, using a simplified version of the model. This simulation, however, was based on a lot of parameters taken as assumptions just to start the process (Figure 3).

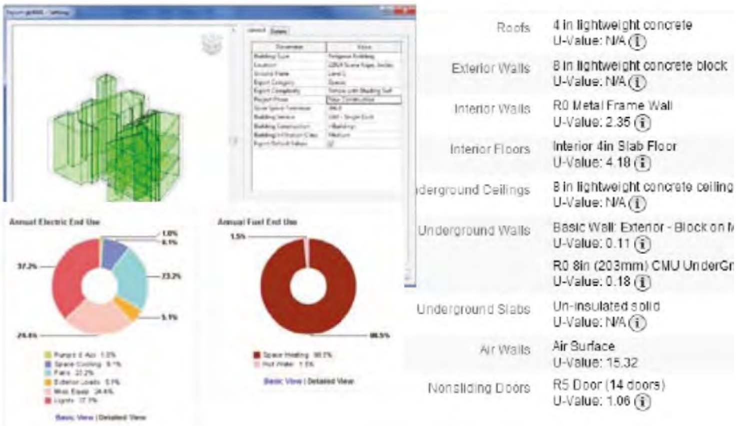

Roofs	4 in lightweight concrete U-Value: N/A ⓘ
Exterior Walls	8 in lightweight concrete block U-Value: N/A ⓘ
Interior Walls	R0 Metal Frame Wall U-Value: 2.35 ⓘ
Interior Floors	Interior 4in Slab Floor U-Value: 4.18 ⓘ
derground Ceilings	8 in lightweight concrete ceiling U-Value: N/A ⓘ
Underground Walls	Basic Wall: Exterior - Block on U-Value: 0.11 ⓘ R0 8in (203mm) CMU UnderGr U-Value: 0.18 ⓘ
Underground Slabs	Un-insulated solid U-Value: N/A ⓘ
Air Walls	Air Surface U-Value: 15.32
Nonsliding Doors	R5 Door (14 doors) U-Value: 1.06 ⓘ

Figure 3: The model spaces and some parameters of the BPA of St. Maria church. By Brumana et al

Several simulation tools can be linked to BIM models of existing and heritage buildings, to achieve dynamic simulation of the performance of the building in several aspects such as Comfort and weather analysis, Thermal performance, Daylight performance, Acoustic performance, Air flow analysis and Energy consumption. A case study of S. Habibi [5] proved the feasibility of conducting several performance simulations within BIM environment of an existing building at University of Ferrara, Italy (Figure 4).

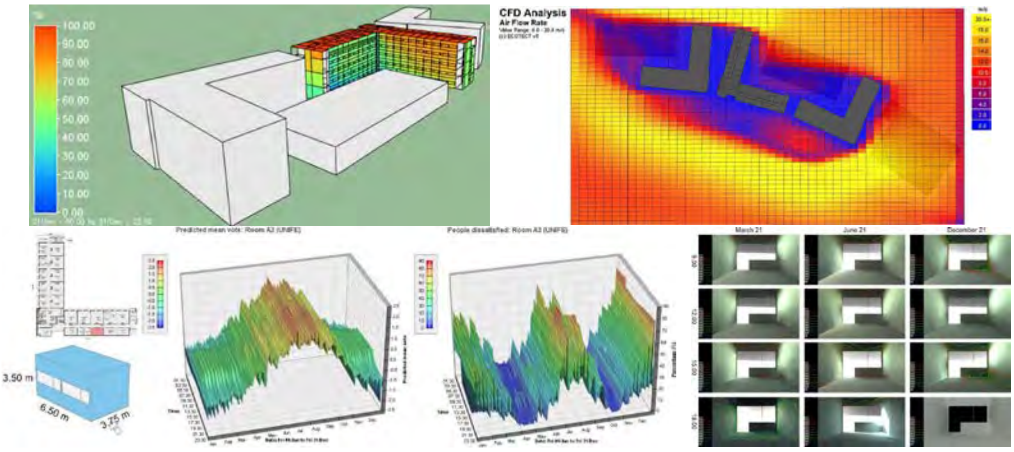

Figure 4: Different building performance simulation performed by S. Habibi, including Solar radiation, CFD, Thermal comfort and Daylighting.

4. H-BIM Management

Many frameworks and protocols were proposed to manage BIM procedures in the heritage environment, but still a few did focus on the sustainable retrofitting and energy performance of Heritage buildings.

Jordan-Palomar et al [15] suggested a protocol they called "BIMlegacy" to manage heritage building interventions using HBIM, in which they addressed the HBIM Energy consumptions 4D simulations within their proposed HBIM phases (Figure 5).

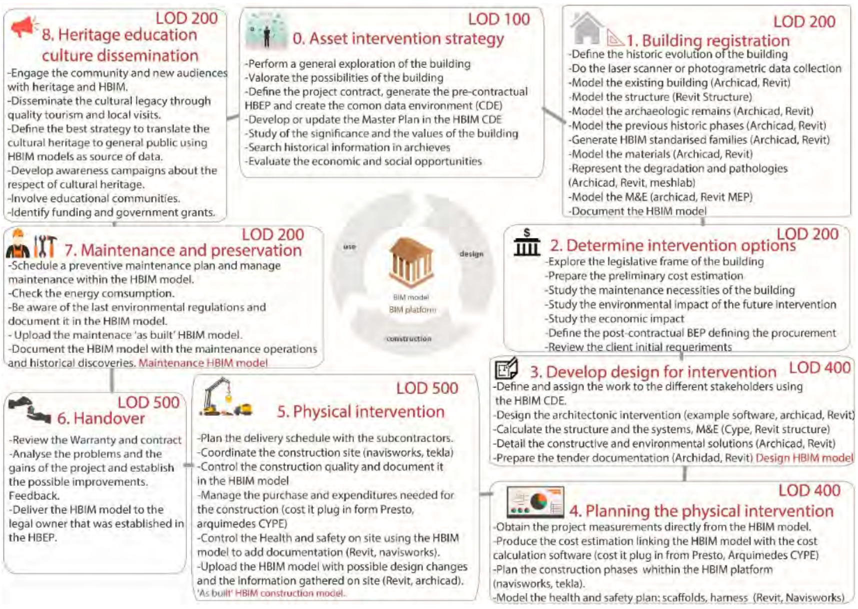

LOD 100
0. Asset intervention strategy
-Perform a general exploration of the building
-Valorate the possibilities of the building
-Define the project contract, generate the pre-contractual HBEP and create the comon data environment (CDE)
-Develop or update the Master Plan in the HBIM CDE
-Study of the significance and the values of the building
-Search historical information in archieves
-Evaluate the economic and social opportunities

LOD 200
1. Building registration
-Define the historic evolution of the building
-Do the laser scanner or photogrametric data collection
-Model the existing building (Archicad, Revit)
-Model the structure (Revit Structure)
-Model the archaeologic remains (Archicad, Revit)
-Model the previous historic phases (Archicad, Revit)
-Generate HBIM standarised families (Archicad, Revit)
-Model the materials (Archicad, Revit)
-Represent the degradation and pathologies (Archicad, Revit, meshlab)
-Model the M&E (archicad, Revit MEP)
-Document the HBIM model

LOD 200
2. Determine intervention options
-Explore the legislative frame of the building
-Prepare the preliminary cost estimation
-Study the maintenance necessities of the building
-Study the environmental impact of the future intervention
-Study the economic impact
-Define the post-contractual BEP defining the procurement
-Review the client initial requeriments

3. Develop design for intervention LOD 400
-Define and assign the work to the different stakeholders using the HBIM CDE.
-Design the architectonic intervention (example software, archicad, Revit)
-Calculate the structure and the systems, M&E (Cype, Revit structure)
-Detail the constructive and environmental solutions (Archicad, Revit)
-Prepare the tender documentation (Archidad, Revit) Design HBIM model

LOD 400
4. Planning the physical intervention
-Obtain the project measurements directly from the HBIM model.
-Produce the cost estimation linking the HBIM model with the cost calculation software (cost it plug in from Presto, Arquimedes CYPE)
-Plan the construction phases whithin the HBIM platform (navisworks, tekla).
-Model the health and safety plan: scaffolds, harness (Revit, Navisworks)

LOD 500
5. Physical intervention
-Plan the delivery schedule with the subcontractors.
-Coordinate the construction site (navisworks, tekla)
-Control the construction quality and document it in the HBIM model
-Manage the purchase and expenditures needed for the construction (cost it plug in form Presto, arquimedes CYPE)
-Control the Health and safety on site using the HBIM model to add documentation (Revit, navisworks).
-Upload the HBIM model with possible design changes and the information gathered on site (Revit, archicad). 'As built' HBIM construction model.

LOD 500
6. Handover
-Review the Warranty and contract
-Analyse the problems and the gains of the project and establish the possible improvements. Feedback.
-Deliver the HBIM model to the legal owner that was established in the HBEP.

LOD 200
7. Maintenance and preservation
-Schedule a preventive maintenance plan and manage maintenance within the HBIM model.
-Check the energy comsumption.
-Be aware of the last environmental regulations and document it in the HBIM model.
- Upload the maintenace 'as built' HBIM model.
-Document the HBIM model with the maintenance operations and historical discoveries. Maintenance HBIM model

LOD 200
8. Heritage education culture dissemination
-Engage the community and new audiences with heritage and HBIM.
-Disseminate the cultural legacy through quality tourism and local visits.
-Define the best strategy to translate the cultural heritage to general public using HBIM models as source of data.
-Develop awareness campaigns about the respect of cultural heritage.
-Involve educational communities.
-Identify funding and government grants.

Figure 5: BIM legacy framework by Jordan-Palomar et al

Another framework suggested by Khodeir et al [16] focused on the sustainable retrofitting of heritage buildings. They addressed the building performance evaluation in the problem formulation step within the visioning phase. Then they suggested within the third phase the evaluation of different alternatives of sustainable retrofit based on simulation tools embedded in HBIM as a testing tool that can help to compare different design options and make decisions about the solutions that will be applied further on the project (Figure 6).

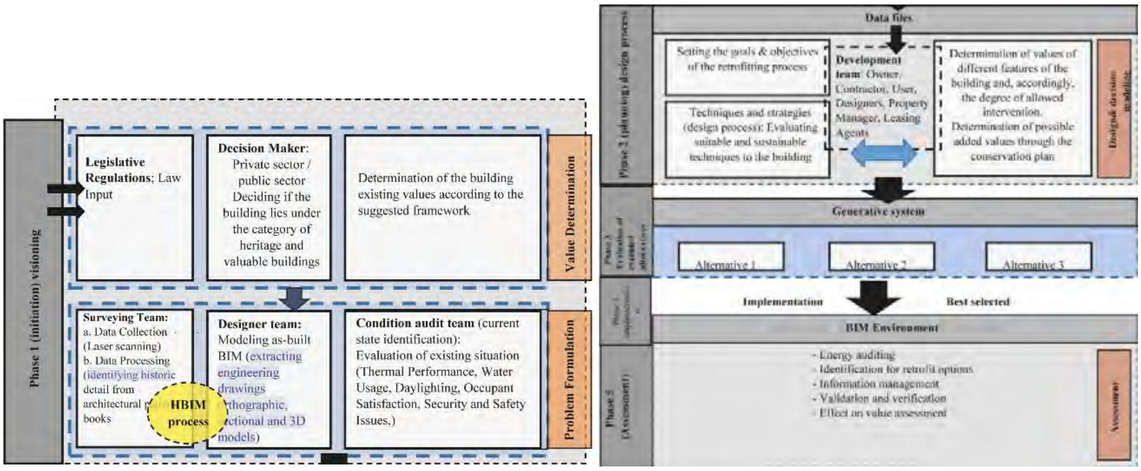

Figure 6: Framework suggested by Khodeir et al.

References

---

1 Howe, J. (2010). Overview of green buildings. National Wetlands Newsletter, 33(1).

2 Abohela, I., Dudek, S. and Hamza, N. (2012) 'Roof Mounted Wind Turbines: The influence of roof shape, building height and urban location on wind speed', PLEA2012 - 28th Conference, Opportunities, Limits & Needs Towards an environmentally responsible architecture, (November), pp. 1–6. Available at: http://www.plea2012.pe/pdfs/T11-20120131-0087.pdf.

3 Azhar, S. et al. (2011) 'Building information modelling for sustainable design and LEED®rating analysis', Automation in Construction. Elsevier B.V., 20(2), pp. 217–224. doi: 10.1016/j.autcon.2010.09.019.

4 Azhar, S. and Brown, J. (2009) 'Bim for sustainability analyses', *International Journal of Construction Education and Research*, 5(4), pp. 276–292. doi: 10.1080/15578770903355657.

5 Habibi, S. (2017) 'The promise of BIM for improving building performance', Energy and Buildings. Elsevier B.V., 153, pp. 525–548. doi: 10.1016/j.enbuild.2017.08.009.

6 Dore, C. and Murphy, M. (2017) 'CURRENT STATE OF THE ART HISTORIC BUILDING INFORMATION MODELLING', The International Archives of the Photogrammetry, Remote Sensing and Spatial Information Sciences, XLII-2/W5(5), pp. 185–192. doi: 10.5194/isprs-archives-XLII-2-W5-185-2017.

7 Letellier, R. (2007) Recording, Documentation, and Information Management for the Conservation of Heritage Places. guiding principles. Los Angeles: The Getty Conservation Institute. doi: 363.6'9 GET.

8 Bryan, P. et al. (2009) Metric Survey Specifications for Cultural Heritage. Edited by D. Andrews. English Heritage. Available at: http://archaeologydataservice.ac.uk/archiveDS/archiveDownload?t=arch-1416-1/dissemination/pdf/9781848021716.pdf.

9 Fai, S. et al. (2011) 'Building Information Modelling and Heritage Documentation', Proceedings of the 23rd International Symposium, International Scientific Committee for Documentation of Cultural Heritage (CIPA), pp. 12–16.

10 Cheng, H. M., Yang, W. Bin and Yen, Y. N. (2015) 'BIM applied in historical building documentation and refurbishing', International Archives of the Photogrammetry, Remote Sensing and Spatial Information Sciences - ISPRS Archives, 40(5W7), pp. 85–90. doi: 10.5194/isprsarchives-XL-5-W7-85-2015.

11 Khalil, A. and Stravoravdis, S.: H-BIM AND THE DOMAINS OF DATA INVESTIGATIONS OF HERITAGE BUILDINGS CURRENT STATE OF THE ART, Int. Arch. Photogramm. Remote Sens.

Spatial Inf. Sci., XLII-2/W11, 661-667, https://doi.org/10.5194/isprs-archives-XLII-2-W11-661-2019, 2019.

12 Wang, C. and Cho, Y. K. (2015) ‘Performance Evaluation of Automatically Generated BIM from Laser Scanner Data for Sustainability Analyses’, Procedia Engineering. Elsevier B.V., 118, pp. 918–925. doi: 10.1016/j.proeng.2015.08.531.

13 Pocobelli, D. P. et al. (2018) ‘Building Information Models for Monitoring and Simulation Data’, ISPRS TC II Mid-term Symposium “Towards Photogrammetry 2020”, XLII(June), pp. 4–7. doi: 10.5194/isprs-archives-XLII-2-909-2018.

14 Brumana, R. et al. (2017) ‘HBIM challenge among the paradigm of complexity, tools and preservation: The basilica Di collemaggio 8 years after the earthquake (L’aquila)’, International Archives of the Photogrammetry, Remote Sensing and Spatial Information Sciences - ISPRS Archives, 42(2W5), pp. 97–104. doi: 10.5194/isprs-archives-XLII-2-W5-97-2017.

15 Jordan-Palomar, I. et al. (2018) ‘Protocol to Manage Heritage-Building Interventions Using Heritage Building Information Modelling (HBIM)’, Sustainability, 10(908). doi: 10.3390/su10030908.

16 Khodeir, L. M., Aly, D. and Tarek, S. (2016) ‘Integrating HBIM (Heritage Building Information Modelling) Tools in the Application of Sustainable Retrofitting of Heritage Buildings in Egypt’, Procedia Environmental Sciences, 34, pp. 258–270. doi: 10.1016/j.proenv.2016.04.024.

Nottingham | UK | 9–11 September 2019

A Small Solar Thermal Power Generation System

Hassan Mahmood

Department of Mechanical and Construction Engineering, University of Northumbria,
Newcastle upon Tyne, United Kingdom

hassan.mahmood@northumbria.ac.uk

Abstract

The paper presents results of simulations of the thermal performance of a small Organic Rankine Cycle (ORC) plant, coupled to the solar collector filed to supply heat input energy. The energy transfer between the collector and ORC take place via a heat exchanger. The thermodynamic modeling is performed for the case in which R134a working fluid is used. The model calculates the heat energy absorbed by the solar collector field, number of transfer units of the heat exchanger and amount of heat input required by the evaporator to generate a certain amount of mechanical work by the turbine. The simulation model is designed to determine the day-long performance of the SORC plant using steady flow conditions. The water is the heat transfer fluid for the solar collector field. The value of the total solar irradiance is determined using the Meteonorm database for the latitude angle of 37.4°, which corresponds to Sevilla. The results show the mechanical power of the Solar Organic Rankine Cycle (SORC) depends upon the area of the solar collector and mass flow rate of the working fluid.

Keywords:

SORC Organic Rankine Cycle plant; ORC Organic Rankine Cycle; R134a tetrafluoroethane.

1. Introduction

Several authors have studied the ORC plants powered by solar energy. Wang et al. showed that the performance of the ORC running on 245fa as the working fluid and powered with solar energy was a feasible way of generating power [1]. Suresh et al. presented the analysis of SORC based on the area of the collector, solar heat input and thermal efficiency by using the R245fa, R123, R114b and ethanol working fluids. The simulation and economic modeling of SORC investigated to produce the power of 1 kW [2]. Emily Spayde et al evaluated the SORC performance, which runs on R218, R227ea, R236ea, R236fa, and Rc318 working fluids [3]. Adweek Odhiambo et al investigated the performance of the SORC with R245fa as the working fluid. The temperature in the exit from the solar filed was 163.5 ^{o}C and the turbine output power was determined as 33.34 kW. The system's thermal efficiency was found to be 14.55 % [4]. Chakkraphan et al presented a solar organic Rankine cycle (ORC) to be coupled with evacuated tube solar collectors and operate under Thailand climate conditions. The ORC generates the power of 280 kW by using the working fluid R245fa and estimated electricity generation cost of the system varies between 0.37 and 0.43 USD/kWh [5].

2. Description of the SORC plant under investigation

The SORC plant contains the solar field, pump, evaporator, turbine, and condenser. Thermal energy is delivered to the ORC from the solar collector via a heat exchanger. A PI controller is used which fixes the temperature of steam at desirable pressure. A liquid tank stores the heat transfer fluid that circulates within the solar collector. The heat exchanger block transfers the heat of collector fluid to the working fluid of the ORC. The second component of the model is the ORC. The R134a is evaporated at 10 bar pressure within the evaporator. The turbine outlet pressure is 1 bar to condensate the working fluid. The pump pushes back the liquid into the evaporator and increases its pressure via a heat exchanger. The SORC model is designed with input signals to visualize the collector temperature, steam temperature, heat energy absorbed by collector and rate of heat added and converted into power. The simulation scheme of the plant is shown in Figure 1 and main parameters of the plant are presented in Table 1.

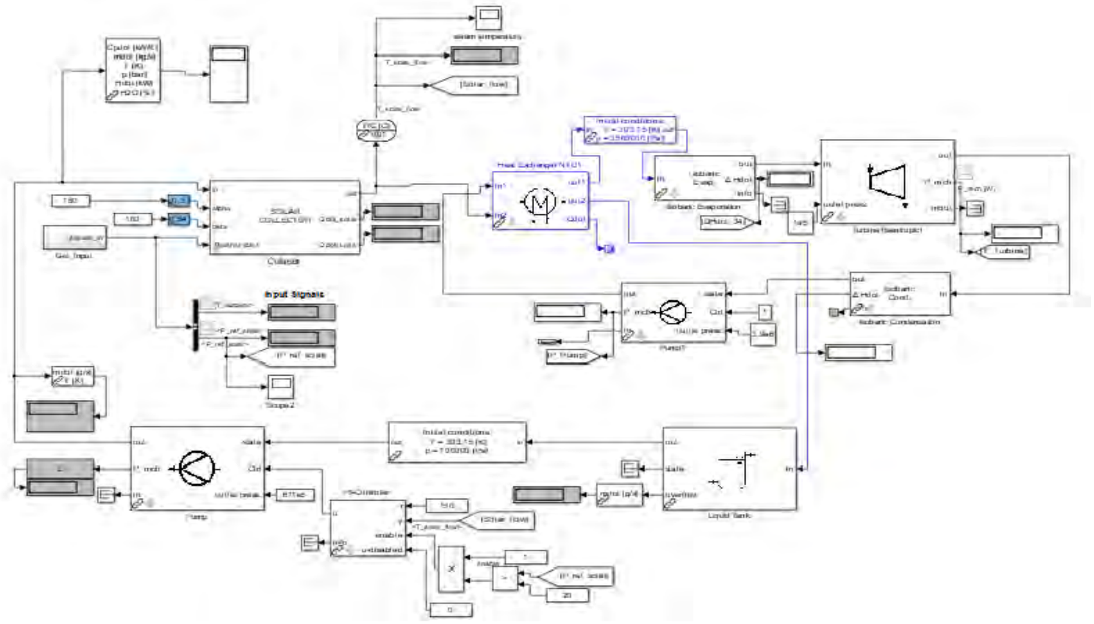

Figure 1: Simulation Scheme for the Solar Power Organic Rankine Cycle

Table 1: The key parameters of the SORC plant

Pump and Turbine Efficiency	80 %
Area of Collector	600 m^2
Collector Inlet Temperature	70 ^oC
Collector Outlet Temperature	150 ^oC
Collector Absorptance and Transmittance	0.96
Evaporation Pressure	10 bar
Condensation Pressure	1 bar
Water Pressure within the collector	8 bar
Mass Flow Rate of Water	0.1 kg/sec
Mass Flow Rate of Working Fluid	0.350 kg/sec

The proposed system is suitable for small power generation applications. For the global horizontal radiation of 238 kWh/m^2 at Sevilla latitude 37.4 N / 6.00 E in July and using R134a as a working fluid, the power output level was about 10 kW.

3. Thermodynamic Modelling of SORC

The set of equations was used for thermodynamic modeling of the operation of the plant.

The amount of solar energy absorbed by the surface of the collector (Q_c) depends on the inlet and outlet temperature, specific heat and steady flow mass flow rate of the fluid circulated within the collector:

$$\mathrm{Q_c} = \dot{\mathrm{m}} c_{\mathrm{p}}(\mathrm{T_2} - \mathrm{T_1}) \qquad (1)$$

The solar collector field efficiency is the ratio of the total energy absorbed by the solar collector field and solar energy available at the collector aperture area:

$$\eta = \frac{\mathrm{Q_C}}{\mathrm{A_{SC}G_h}} \qquad (2)$$

The effectiveness (ϵ) of the intermediate counterflow heat exchanger depends on the ratio of the temperature difference of heat transfer fluids and working fluid and specific heat capacity ratio (c) of these fluids.

$$\epsilon = c\frac{(T_{wf_1} - T_{wf_2})}{(T_{htf_1} - T_{htf_2})} \qquad (3)$$

The number of transfer units (*NTU*) of the counterflow heat exchanger is based on the specific heat capacity ratio of hot and cold fluid streams and the effectiveness of heat exchanger as follow.

$$\mathrm{NTU} = \frac{1}{\mathrm{c}-1}\ln\frac{\epsilon-1}{\epsilon\mathrm{c}-1} \qquad (4)$$

The overall heat transfer coefficient *(U*) of the heat exchanger depends on the number of transfer units (*NTU*) and specific heat capacity ratio and area (*A*).

$$U = \frac{\mathrm{NTU}\times c}{A_{HE}}$$

(5)

The input heat energy is required to vaporize the working fluid in the evaporator. The rate at which this heat (Q_{in}) is added to the working is determined by the enthalpy difference at the inlet and outlet of the evaporator.

$$\frac{Q_{in}}{m} = \dot{m}_{wf}(\mathrm{H_1} - \mathrm{H_4})$$

(6)

The turbine lowers the pressure of the vapors of the working fluid to lower pressure. The rate of the turbine generates mechanical work ($\mathrm{w_t}$) per unit mass is the enthalpy difference between the turbine inlet and outlet.

$$\frac{w_t}{m} = \dot{m}_{wf}(\mathrm{H_1} - \mathrm{H_2})$$

(7)

The condenser converts the liquid back to vapors by eliminating the heat energy (Q_{out}). The rate of heat energy is rejected per unit mass is the enthalpy difference of the working fluid.

$$\frac{Q_{OUT}}{m} = (\mathrm{H}_2 - \mathrm{H}_3)$$

(8)

4. Results and Discussion

The enthalpy values of the model are calculated that corresponds to pressure by using the NIST standard reference database. The thermodynamic results show the amount of solar energy absorbed by a solar collector is 65 kW at the peak hour of the day. The optical efficiency of the solar collector is 73%. Based on heat transfer fluid water and R134a working fluid the effectiveness of heat exchanger is 0.52. The number of transfer units is 0.854 and the overall heat transfer coefficient is 30.97 W/m^{2}k.and assumed area of the heat exchanger is 15 m^2. The solar collector is transferring the heat input to the evaporator. The total amount of heat energy required to vaporize the R134a working fluid at 10 bar pressure is 31.8 kW that produces the total mechanical output power of the turbine is 10 kW. The condenser dissipates the 59.8 kW energy to condense the working fluid at 1 bar pressure. The 0.2 kW power required by the pump to pushes the liquid back to the evaporator at pressure 10 bar.

Figure 2 and 3 show the simulation results of the turbine output work and mass flow rate of the working fluid. It can be seen in the graph that the total output power of the turbine increases with increasing the mass flow rate of the working fluid, as a result, the input energy required to vaporize the working fluid increases. The amount of heat energy absorbed by a solar collector depends on the area of a collector. The results show that the heat energy absorbs by a solar collector increases as an increase in the surface area of the collector.

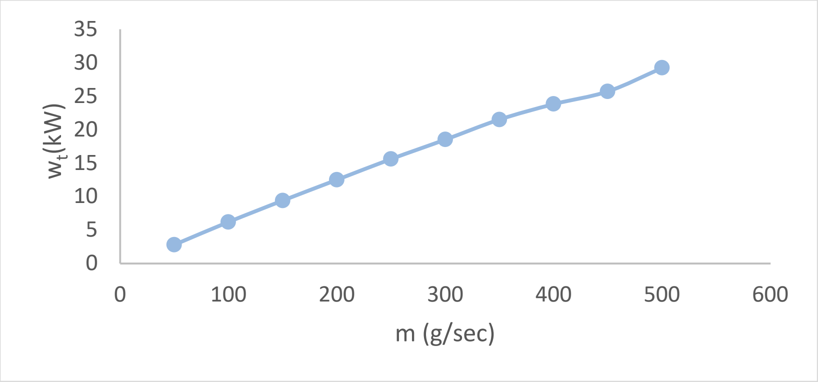

Figure 2: Between Mass Flow Rate & Turbine Work

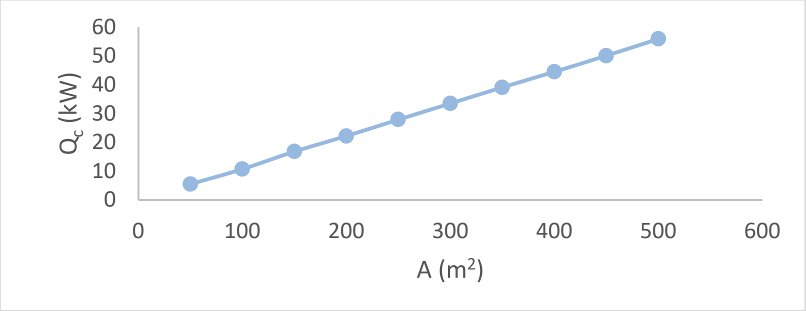

Figure 3: Heat energy absorbed by collector & Turbine Work

The amount of heat energy absorbed by solar collector increases as increase by a global irradiance as shown in table 2. The required amount of heat energy absorbed by the collector to operate power system is 48 kW. It is transferring the 31.7 kW heat input energy to the evaporator via a heat exchanger.

Table 2: Simulation results of collector heat utilize by the evaporator of ORC

Time	Global Irradiance Received W/m^2	Collector Heat (Q_c) kW	Heat Input Supplying to Evaporator (Q_{in}) kW
5:15	85	0	0
7:00	165	3	28.7
8.30	180	15.69	16.01
10:30	205	48	31.7
12:00	230	52.46	31.7
14:00	240	67.5	31.7
17:00	190	64	31.7
18:30	140	55.5	31.7

5. Conclusion

The SORC model based on two different types of heat transfer and working fluid has not been investigated. The present work is presenting the heat transfer of the solar collector to ORC by using a heat exchanger. The amount of heat energy absorbed by the solar collector depends on the area of collector and total solar irradiance. The mechanical power of the system can be increased by increasing the mass flow rate of the working fluid. The model is fully utilizing the collector heat energy to evaporate the R134a working fluid within 10:30 to 7:00 sunlight hours. The model can be further updated with concentrated types of solar collector and low temperature working fluids to generate more feasible results.

References

1. Wang, X.; Zhao, L.; Wang, J.; Zhang, W.; Zhao, X.; Wu, W.2010, ''Performance evaluation of a low-temperature solar Rankine cycle system utilizing R245fa''. Sol. Energy 2010, 84, 353– 364.
2. Suresh Baral and Kyung Chun Kim, January 2015,'' Simulation, Validation and Economic Analysis of Solar Powered Organic Rankine Cycle for Electricity Generation'' Journal of Clean Energy Technologies, Vol. 3, No. 1.
3. Emily Spayde1 and Pedro J. Mago, March 2015 ''Evaluation of a solar-powered organic Rankine cycle using dry organic working fluids''. Department of Mechanical Engineering, Mississippi State University, Mississippi, MS 39759, USA.
4. Adwek Odhiambo George, Imran Ali Shah, Xiang Gou, April 2017, ''Energy analysis of Organic Rankine Cycle for a residential apartment using solar energy based on Aspen Plus''.
5. Chakkraphan Thawonngamyingsakul, Tanongkiat Kiatsiriroat, 2012 ''Potential of a Solar Organic Rankine Cycle with Evacuated-Tube Solar Collectors as Heat Source for Power Generation in Thailand''.
6. P.J. Linstrom and W.G. Mallard, Eds., May 2019 ''NIST Chemistry WebBook, NIST Standard Reference Database Number 69'' National Institute of Standards and Technology, Gaithersburg MD, 20899, https://doi.org/10.18434/T4D303.

Nottingham | UK | 9–11 September 2019

Dynamics of Inverter Droop Control and OLTC using Power Hardware In the Loop (PHIL)

(Ancillary Services Supply in Low Voltage Grid)

Solomon Oyegoke[1], Yehdego Habtay[1], Marios Maniatopoulos[2], Panos Kotsampopoulos[2], Simeon Keates[3].

[1]*Faculty of Engineering and Science, University of Greenwich, Medway, Kent, UK*

[2]*School of Electrical and Computer Engineering, National Technical University of Athens, Athens, Greece*

[3]*School of Engineering and the Built Environment, Edinburgh Napier University, Edinburgh, UK*

o.solomon@greenwich.ac.uk

ABSTRACT

Distributed Energy Resources (DER) sources installed closer to end users serve as local distributed generators, but they are regarded intermittent sources that pose a challenge to grid operators. Moreover, an increase in penetration of DER into the grid network has created problems related to power quality issues such as voltage sags and swells. The obligation of the grid operators to address power quality issues and energy demand has created an opportunity in the energy market due to the need for ancillary services. In resolving these power quality issues, the coupling DER-inverter becomes an effective tool in supplying ancillary services to the grid.

This paper explores the dynamic functionality of a modelled droop-controlled inverter against the conventional OLTC transformers in a Low Voltage grid. The experiment is designed using the Power Hardware in the Loop (PHIL) test setup which combined a hardware DER-inverter, to a simulated low voltage AC distribution network. The test results show that inverter based DERs could enhance ancillary service provision at the distribution level by supporting the operation of the existing OLTC in realizing voltage control.

Keywords— Power Quality; Ancillary Services; DER; PHIL; Inverters; LV grid; Distributed Generation (DG).

1. INTRODUCTION TO LOW VOLTAGE DISTRIBUTION NETWORK

The inclusion of Distributed Generation (DG) units into distribution networks has aided grid capacity over time but also on the other hand affects the network in several manners. Such issues include the change of active and possibly reactive power flow which has an impact on the overall power flow in the network. The network becomes imbalanced, as some nodes in the network could be overloaded in comparison to other nodes and as a result, this can worsen the network voltage and bring about network losses. Furthermore, the issues mentioned above affect the operation of voltage control devices such as the On-Load Tap Changer (OLTC). Therefore, the research and reliability studies become important for DER sizing, optimum penetration, placement and operation in situations where the penetration of DER becomes significant [1-3].

The continuous grid voltage variation as a result of the high penetration of the DER sources could make the OLTC transformer taps work endlessly in bringing the voltage back to the ideal range and this could gradually reduce the lifespan of the OLTC over time [4].

The low voltage distribution network is described as the last part of the network from a substation to the customers where majority of the consumers are residential loads. Small scale DER units such as photovoltaics (PV), mini-scale wind turbines, etc., are now usually integrated into the low voltage distribution networks, which could be negligible to the grid operators until they are of a higher power rating in the region of hundreds of kilowatts which could affect power quality [5]. To maintain power quality in the distribution network, voltage and frequency support, which is the core of ancillary services, becomes significant and hence can be provided using the modern power devices such as the inverter with advanced control functions [5].

Ancillary services are distinct components of electric service required to support the reliable delivery of electricity and operation of transmission systems; it is fundamental for the power system operation to maintain the balance between generation and demand when variation occurs [6-7]. Generally, ancillary services are designed to support frequency stability (frequency control, power regulation, operating reserves); voltage control (tap changer control and reactive power control), power balancing (scheduling and dispatch of power) [6]. Various forms of ancillary service solutions were fully discussed in [7] with their strengths and weaknesses highlighted; the paper also presented a comprehensive solution for ancillary service provision for the smart grid.

Hardware in the Loop (HIL) is regarded as a process of integrating physical hardware and software during testing; it is acceptable as a viable option for power system testing and provides real-time interaction between the physical hardware and the simulated circuit [8]. The most essential part of a HIL simulation is the real-time simulator which computes the simulation model and offers I/O capabilities. This allows the user to alter parameters of either the Hardware under Test (HUT) or the software circuit design that runs via a digital simulator and observe results for the new condition in real time. PHIL integration allows users to see actual behavior of the HUT and supports scalability of the HUT [8-10].

PHIL is now globally accepted as a procedure and standard practice (IEEE P2004) for power systems testing. Using the IEEE P2004 standard practice, the authors of [5] presented the concept of PHIL testing for Power Conditioning System (PCS) to coordinate and improve grid frequency and voltage stabilization.

The application of the droop control concept is explored to resolve voltage instability and is employed in this research work to relieve the recurring tap changes of the OLTC by controlling grid voltage through ancillary service provision.

The rest of this paper covers the notion of OLTC, the reactive power Q(U) supplied by the inverter via droop control, active and reactive power generation concept. The latter part of this paper then presents the power hardware in the loop design; various test case combinations for voltage control, and finally concludes by outlining the benefit of this work and further future work.

2. VOLTAGE CONTROL IN A LOW VOLTAGE (LV) GRID

In this section, the operation and response of the OLTC and the inverter droop control principle are examined as tools to improve grid stability.

A. Voltage Droop Controlled inverter in a LV microgrid

The droop control technique can be extended to inverters that link renewable energy sources to the grid and it is acknowledged as an effective method of inverter control in a multitude of operating scenarios and at different power levels [11-12]. The droop control strategy becomes useful in decentralized systems and is employed to resolve power quality issues with no need for communication kit to coordinate the integrated systems [16]. The inverter can therefore, be placed in the LV grid network as a shunt device to provide ancillary service (reactive power) to the grid, playing a crucial role stabilizing system voltage [17].

Power vs. frequency *P(f)* droop, which is termed frequency control, causes the frequency to decrease as the real power load on the system increases and vice versa. On the other hand, the reactive power vs. voltage *Q(U)* droop control corrects voltage errors in the network by injecting or absorbing reactive power because of changes to the nominal voltage. Using recent standards, the droop curves can be implemented locally in the inverter [16]. The extent of the inverter's response is based on the configured parameters of the droop controller, i.e. the voltage dead-bands, Q_{min} and Q_{max} as shown in Fig. 1 below.

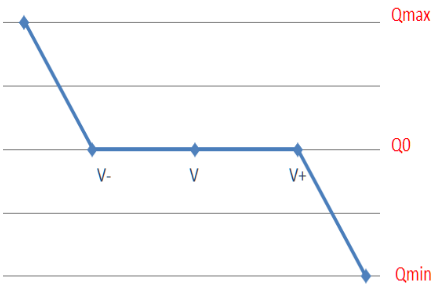

Fig. 1: The inverter's Voltage Droop Control

With the application of the droop, the inverter can positively contribute to feeder voltage control for high DER penetration concerns mention in section 1 above, and yields an improved voltage profile, reliability and reduction of transmission loss [11]. The response of the inverter controllers must be very fast in terms of responding to changes in network conditions and the advantages of using the droop control results in the overall system being more damped; it provides automatic harmonic current sharing via the inverters and phase errors barely affect active power sharing.

B. *OLTC Transformer in an LV microgrid*

The transformer is one of the oldest voltage control devices in power networks. It is used in a High Voltage (HV), Medium Voltage (MV) and LV grid applications. In order to maintain grid stability, it may be necessary to make use of power transformers with on-load tap changers to compensate the voltage drop/gain along the distribution feeders to keep the voltage within the nominal range. Various OLTC topologies have been discussed in [13] based on different configuration of the conventional two-winding transformer. OLTC utilises the conventional voltage control and responds to the change in the measured voltage and current of the secondary side of the transformer through appropraite tap switching.

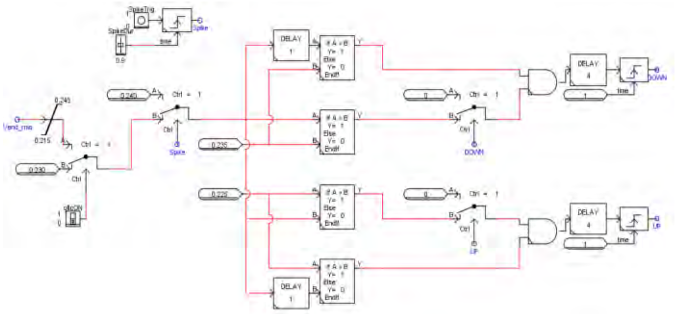

Fig. 2: The transformer's OLTC control

Although the application of OLTC is an effective solution for overvoltage prevention; the effective control of the OLTC is essential to increase the transformer's lifespan and provide efficient voltage control in the grid during high PV generation periods. As a result, the mobile moving part (mechanical switches) of the OLTC transformer is subjected to wear and tear leading to huge maintenance costs. When the voltage falls outside the permitted deadband, the automatic voltage control (AVC) relay of the OLTC then decreases or increases the secondary voltage by altering the OLTC tap position.

The OLTC control, which is shown in Fig. 2, is utilized in this paper where a fixed step voltage change has been implemented in the OLTC controller. From the model in Fig. 2 above, a tap change occurs if the measured voltage is higher than 235 (~1.02pu) or lower than 225 (~0.98pu) for longer than 1 second. The starting tap position corresponds to voltage of 1p.u and the step size of each tap change was set to 0.01pu (1%).

3. ACTIVE AND REACTIVE POWER CONCEPT IN LV GRIDS

When considering a Low Voltage grid, the power flowing into a line at point A towards point B as shown in Fig. 3a below is given as [14-15]:

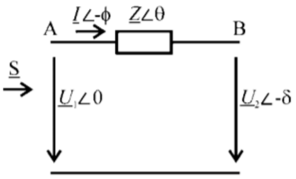

(a)

Fig. 3a: Power flow in line from Point A toward B

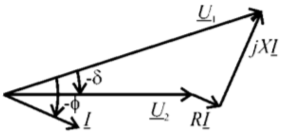

(b)

Fig. 3b: Phasor diagram representation [14-15]

$$P + jQ = \underline{S} = \underline{U_1}\underline{I}^* = \underline{U_1}\left(\frac{\underline{U_1} - \underline{U_2}}{\underline{Z}}\right)^* = U_1\left(\frac{U_1 - U_2\, e^{j\delta}}{Ze^{-j\theta}}\right) \qquad (1)$$

$$= \frac{U_1^2}{Z}e^{j\theta} - \frac{U_1U_2}{Z}e^{j(\theta+\delta)}$$

In the line, the Active and Reactive power flowing can be written as:

$$P = \frac{U_1^2}{Z}\cos\theta - \frac{U_1U_2}{Z}\cos(\theta+\delta) \qquad (2)$$

$$Q = \frac{U_1^2}{Z}\sin\theta - \frac{U_1U_2}{Z}\sin(\theta+\delta) \qquad (3)$$

From $Ze^{j\theta} = R + jX$, we can re-write equation (2) and (3) as:

$$P = \frac{U_1^2}{R^2 + X^2}[R(U_1 - U_2\cos\delta) + XU_2\sin\delta] \qquad (4)$$

$$Q = \frac{U_1^2}{R^2 + X^2}[-RU_2\sin\delta + X(U_1 - U_2\cos\delta)] \qquad (5)$$

Or,

$$U_2\sin\delta = \frac{XP - RQ}{U_1} \qquad (6)$$

$$U_1 - U_2\cos\delta = \frac{RP + XQ}{U_1} \qquad (7)$$

Various elements in a network are characterized by their ability to inject or absorb reactive power; assuming that an inductive load is represented by $R + jX$ and that $\underline{S} = \underline{U_1}\underline{I}^*$ convention is used, then an inductive load absorbs positive VArs and a capacitive load produces VArs [14]. In (6) and (7), the angle δ can be controlled by regulating P, while the inverter voltage $\underline{U_1}$ is controlled via Q [15].

4. POWER HARDWARE IN THE LOOP (PHIL) TEST

For this paper, a Power Hardware in the Loop (PHIL) design was implemented in testing the dynamics of the ancillary service devices in the LV voltage micro grid set up. In the PHIL set up, a Regatron PV Simulator was used to model the characteristics of the photovoltaic panels connected to the inverter (1 kilowatt PV in this design). The PV simulator was controlled using dedicated software via an ethernet connection and this gives the opportunity to load in either preset or an actual day's solar insulation values and can be further varied during the simulation to observe the changes on the LV grid and the response of the connected ancillary service devices, i.e., the PV inverter and the OLTC.

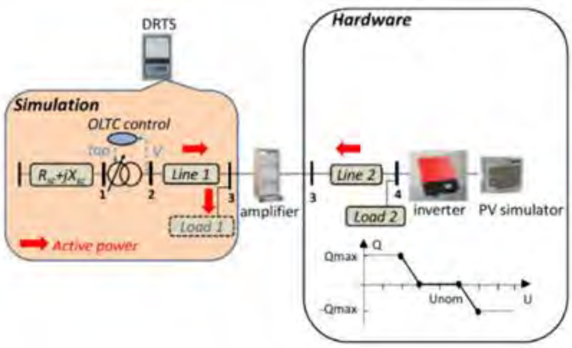

Fig. 3c: PHIL testbed with DG and OLTC Voltage Control [18]

Fig. 3c above is a block diagram of the PHIL test setup combining a physical inverter, PV simulator, line and loads to a simulated low voltage AC grid. The AC side of the LV grid was modelled and simulated using the Real Time Digital Simulator (RTDS) as shown in Fig. 3c above. A linear amplifier (4-Quadrant, 5kVA) was introduced in the PHIL setup to link the physical hardware to the RTDS.

Next, the Sunny boy SMA inverter was coupled to the PV simulator on the DC side and to the amplifier on the AC side. The AC current of the inverter was also measured and sent back to the RTDS to close the loop of the PHIL setup. The inverter droop parameters were set through Ethernet to realize voltage stabilization via Q_{min} and Q_{max}.

A protection control circuit is included in RTDS to protect the laboratory equipment (inverter, amplifier, RTDS) from possible instability of the PHIL setup, since it is a closed-loop system. The AC circuit made up of an 11kv AC power source, active transformer with OLTC tap controls, PHIL instability protection control circuit, distribution lines and loads were designed via the RSCAD software (a Power Simulation software) and simulated in the RTDS.

In this experiment, three test cases were carried out to realize ancillary service contribution via the droop inverter and/or OLTC transformer. The PHIL results were also validated against pure simulation test with no hardware. This is advisable so as to establish ideal parameters for the PHIL test and to avoid damaging the hardware equipment as a result of over current or voltages.

A. *Test Case 1 – OLTC only.*

The test commenced with no load and a fixed active power being supplied from PV inverter into the grid. The voltage at the end of the feeder line initially was unchanged and the OLTC tap position was kept constant untill loads were turned on at 13s time as shown in Fig. 5 (Simulation) and Fig. 6 (PHIL hardware test) below. Due to the voltage drop, there was need for the OLTC to adjust the on tap position in order to stabilise the voltage. The OLTC tap moved 5 steps (position) until 33s and the correction was realised in about 20s.

B. *Test Case 2 – Droop Q(U) inverter only.*

The physical inveter in this experiment functions as a watt-priority inverter and, therefore, the remaining part of the inverter capacity can serve the purpose of reactive power compensation via the droop parameters.

The droop characteristics for the hardware inverter were set via the software gui of the SMA inverter with certain voltage values; the range (0.99 – 1.01 p.u) being the norminal value V_{norm}. Once the voltage rises/falls above/below V_{norm} due changes in load, the inverter supplies/absorbs reactive power up to Q_{min} or Q_{max} . For test case 2, the OLTC tap controller was deactivated so that only the inverter responds to the grid voltage changes. Initailly (before the loads were switched on at time t=7s to realise the grid voltage drop), the PV inverter generated a steady active power which was fed into the grid.

From the result recorded in Fig. 7 (Simulation) and Fig.8 (PHIL hardware test) below for test case 2, it can be seen that as a voltage drop was experienced, the inveter quickly kicks in to stabilise and compensate the grid with reactive power (Qpv) within 4s. In comparison, this is significantly faster response than that achieved by the OLTC in test case 1.

C. *Test case 3 – OLTC and Droop Q(U) inverter.*

In test case 3, the conventional OLTC voltage control and the PV interver droop were to resolve the voltage problems across the feeder. During the initial stage of the simulation and PHIL hardware experiment, the hardware inverter supplied steady active power while the grid voltage is maintained at the nominal value. When the loads were turned on, a voltage drop was experienced across the line; the OLTC tap position changed initially with fixed step changes and stabilization of the voltage was further realized through the inverter's *Q(U)* droop controller by supplying reactive power as shown in Fig. 9 and Fig. 10 below. It can be seen that the OLTC had a lesser OLTC tap position (steps) because of the support from the hardware inverter's droop control in the PHIL experiment compared to the result in test case 1 above.

The number of step changes of the OLTC taps could be further reduced (lesser operation of the OLTC taps in realising voltage control) if the set parameter and the triggering time of the inverter droop controller are further modified. However the aim was to initally allow the conventioanl OLTC voltage control to to provide support before the hardware inverter droop controller was activated.

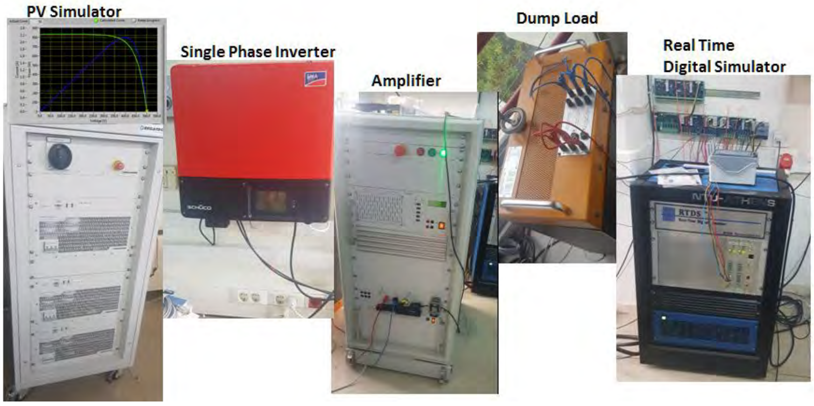

Fig. 4. PHIL Experimental Test Setup Facility

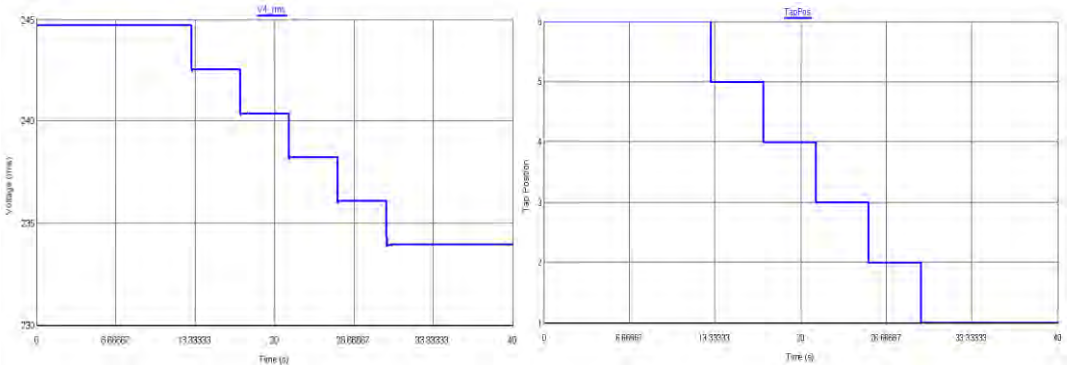

5a). Grid Voltage. 5b). OLTC tap position during voltage control.

Fig. 5. Simulation Case 1 – Voltage Control by OLTC only

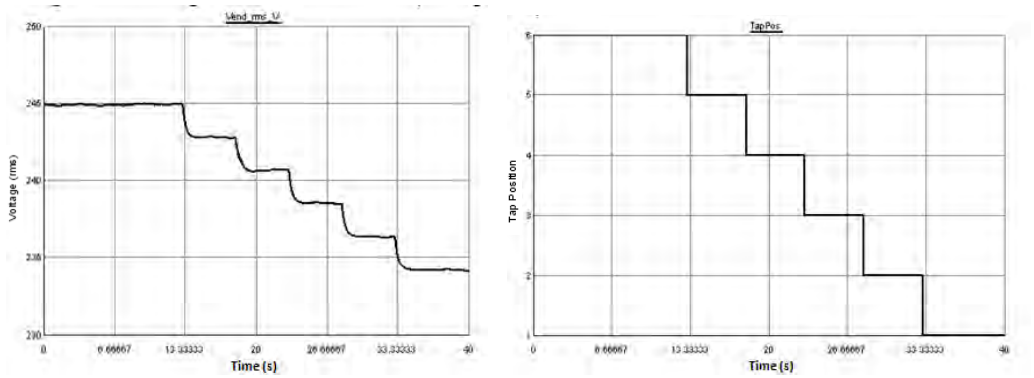

6a). Grid Voltage. 6b). OLTC tap position during voltage control.

Fig. 6 PHIL Test Case 1 – Voltage Control by OLTC only

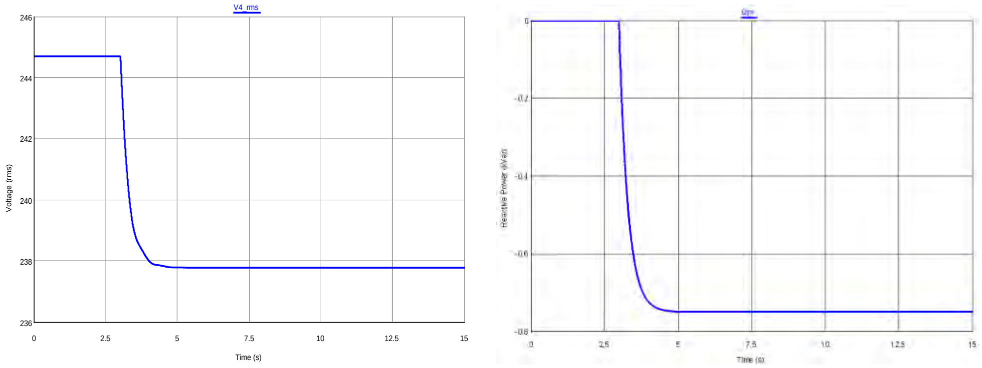

7a). Grid Voltage. 7b). Reactive power Qpv from the inverter.

Fig 7: Simulation Case 2 – Voltage Control by Q(U) droop inverter only

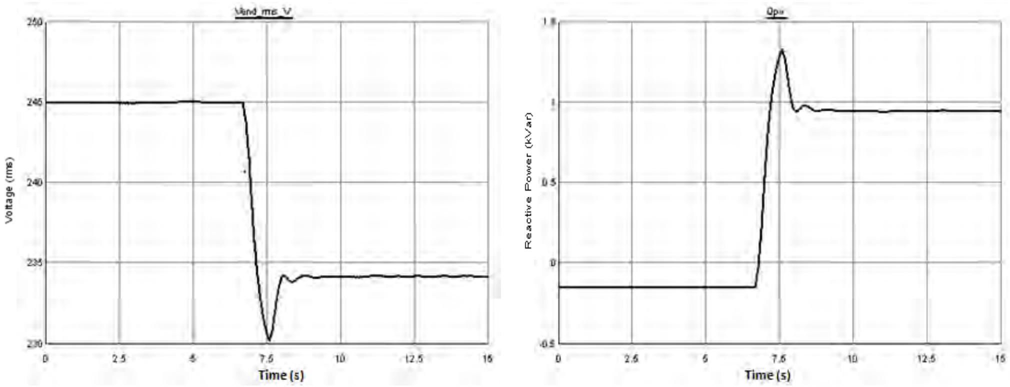

8a). Grid Voltage. 8b). Reactive power Qpv from the inverter.

Fig 8: PHIL Test Case 2 – Voltage Control by Q(U) droop inverter only

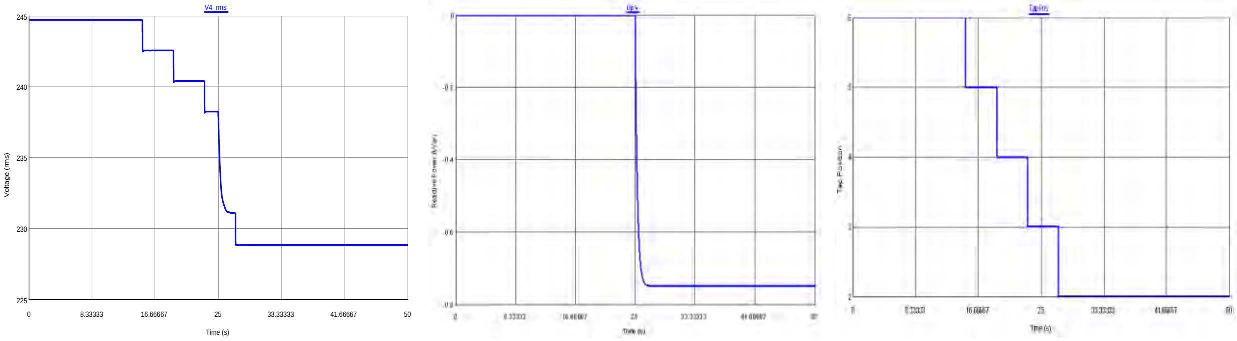

9a). Grid Voltage. 9b). Reactive power Qpv from the inverter. 9c). OLTC tap position during voltage control.

Fig 9: Simulation Case 3 – Voltage Control by OLTC and Q(U) droop inverter.

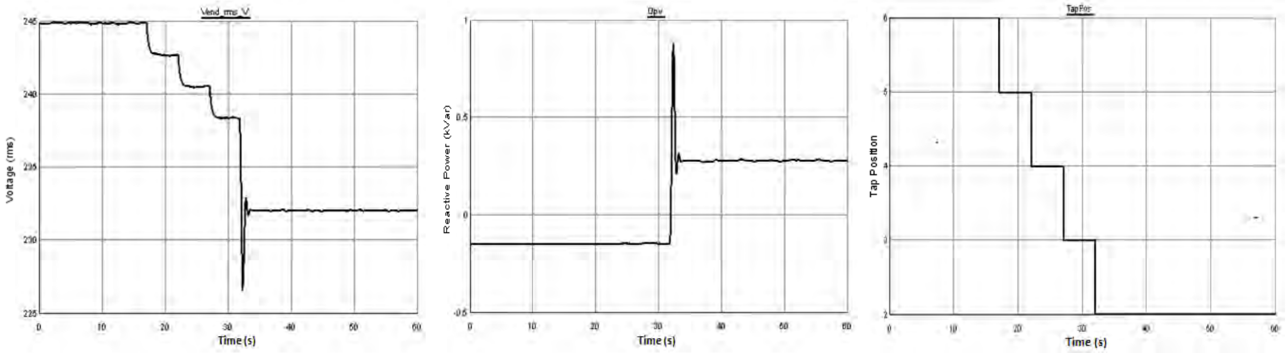

10a). Grid Voltage. 10b). Reactive power Qpv from the inverter. 10c). OLTC tap position during voltage control.

Fig 10: PHIL Test Case 3 – Voltage Control by OLTC and Q(U) droop inverter.

5. CONCLUSION

The above experiment was carried out to showcase the ancillary service supply opportunities from the inclusion of DGs in the LV grid, despite being regarded as intermittent sources by grid operators. Using the PHIL test set up, ancillary services where supplied to the grid using the conventional OLTC, which was further supported with the physical inverter's *Q(U)* Droop control which reduced the number of tap position. By extending the concept further from the results, a higher DG penetration could be considered to be of greater advantage to the grid if properly coordinated. An aggregation of multiple droop inverters could aid and reduce the operation of the OLTC taps when the DGs can compensate the grid a notable amount of reactive power where the DGs could be operated in a decentralized or centralized manner.

ACKNOWLEDGMENT

This research experiment has been performed using the ERIGrid Research Infrastructure and is part of a project that has received funding from the European Union's Horizon 2020 Research and Innovation Programme under the Grant Agreement No. 654113. The Support of the European Research Infrastructure ERIGrid and its partner Smart Grids Research Unit (Smart RUE) - Electric Energy Systems (EES) laboratory at ICCS-NTUA is very much appreciated. The authors acknowledge the support of Prof. Nikos Hatziargyriou.

REFERENCES

[1] J. O Petinrin, M. Shaaban, "Impact of renewable generation on voltage control in distribution systems" 2016, *Sc. Direct Journal on Renewable and Sustainable Energy Reviews*, Vol. 65, pp 770-783

[2] F. Adinolfi, G.M Burt, P. Crolla, F. D'Agostino, M. Saviozzi, F. Silvestro, "Distributed Energy Resources Management in a Low-Voltage Test Facility", 2015 *IEEE Trans on Industrial Electronics,* Vol. 62, No. 4

[3] O. Ansari, N. Safari,C. Y. Chung "Reliability Assessment of Microgrid with Renewable Generation and Prioritized Loads", 2016 *IEEE Green Energy and Systems Conf. (IGSEC),* 10.1109/IGESC.2016.7790067

[4] J. Quevedo, F. Cazakevicius, R. Beltrame , T. Marchesan , L. Michels, C. Rech, L. Schuch, "Analysis and Design of an Electronic On-Load Tap Changer Distribution Transformer for Automatic Voltage Regulation" *IEEE Trans on industrial electr*, Jan 2017 vol. 64, no. 1, pp. 883 -894

[5] T. S. Ustun, H. Konish, J. Hashimoto, K. Otani, "Hardware-in-the-loop simulation based Testing of power conditioning systems", *2018 IEEE International Conference on Industrial Electronics for Sustainable Energy Systems (IESES)*, pp 546 – 551

[6] A. S. Chuang, C. Schwaegerl, "Ancillary Services for Renewable Integration", CIGRE/IEEE PES Joint Symposium on Integration of Wide-Scale Renewable Resources into the Power Delivery System, 2009

[7] G. D. Zotti, S. A. Pourmousavi, H. Madsen, N.K Poulsen, "Ancillary Services 4.0: A Top-to-Bottom Control-Based Approach for Solving Ancillary Services Problems in Smart Grids", *IEEE Access*, 2018, Vol 6, pp 11694 - 11706

[8] P. Kotsampopoulos, F. Lehfuss, G. Lauss, B. Bletterie, N. Hatziargyriou, "The Limitations of Digital Simulation and the advantages of PHIL Testing in Studying Distributed Generation Provision of Ancillary Services," *IEEE Trans on Indus Electronics*, Sept 2015, vol 62, no 9, pp.5502 -5515

[9] Z. Zhang, L. Fickert, "Power Hardware-in-the-Loop testing for the Inverter based Distributed Power Source", 2016, 14th Symposium on Energy Innovation, Vol 10, Issue 1

[10] M. Maniatopoulos, D. Lagos, P. Kotsampopoulos, N. Hatziargyriou, "Combined control and power hardware in-the-loop simulation for testing smart grid control algorithms", *IET Generation, Transmission & Distribution,* 2017, Vol: 11, Iss: 12, pp. 3009 – 3018

[11] D.S Kumara, D. Srinivasana, T. Reindl, "Maximizing DG Penetration using Optimal Placement of Shunt Devices in Distribution Systems", 2016 *IEEE Region 10 Conference (TENCON), pp 1921 -1924*

[12] E. Alegria, T. Brown, E. Minear, and R. H. Lasseter, "CERTS Microgrid Demonstration With Large-Scale Energy Storage and Renewable Generation," *IEEE Transactions on Smart Grid*, vol. 5, no. 2, pp. 937– 943, Mar. 2014.

[13] G. Ram, V. Prasanth, P. Bauer, E. Bärthlein, "Comparative analysis of On-Load Tap Changing (OLTC) transformer topologies", *IEEE 16th Int'l Power Electronics and Motion Control Conf and Exposition*, 2014, pp 918-923

[14] B. M. Weedy, B. J. Cory, N. Jenkins, J.B. Ekanayake, G.Strbac, "Electric Power Systems", *5th edition, John Wiley & Sons,* 2012

[15] K. D. Brabandere, B. Bolsens, J. Van den Keybus, A. Woyte, J. Driesen, R. Belmans, "A Voltage and Frequency Droop Control Method for Parallel Inverters", *IEEE Trans on Power Elect,* Vol 22, No 4, July 2007

[16] P. Kotsampopoulos, N. Hatziargyriou, B. Bletterie, G. Lauss, "Review, analysis and recommendations on recent guidelines for the provision of ancillary services by Distributed Generation", *IEEE Int'l Workshop on Intelligent Energy Systems (IWIES),* Vienna, November 2013

[17] S. Oyegoke, Y.T. Habtay, "Contribution of inverter based photovoltaic generators to power quality at low voltage", *IEEE, 50th Int'l Universities Power Engineering Conf (UPEC)*, 2015, pp 1-6

[18] P. Kotsampopoulos, V. Kleftakis, N. Hatziargyriou, "Laboratory Education of Modern Power Systems using PHIL Simulation",2016, *IEEE Transactions on Power Systems*, Vol. 32, Issue: 5

Nottingham | UK | 9–11 September 2019

Investigating the Effect of Expanding The Use of Electric Cars On The Environment - A Case Study From Scotland

George Milev [1], Astley Hastings [2], Amin Al-Habaibeh [3]

[1] PhD Researcher, Nottingham Trent University, United Kingdom

[2] Senior Research Fellow, University of Aberdeen, United Kingdom

[3] Professor, Nottingham Trent University, United Kingdom

george.milev@ntu.ac.uk

Abstract

This paper investigates that expansion of the use of electric cars on the environment; a situation in which all of the lightweight vehicles that use an internal combustion engine are replaced by electric cars in Scotland. The idea is to estimate whether it would have a positive impact on the environment. The methodology is based on analysing the most common electric and conventional vehicles helped to estimate the amount of additional electricity that would be needed to charge that expansion. The paper has also looked at the running costs. The results show that approximately 4,066 GWh per year of additional electricity will be needed to compensate for such expansion. With that rise in electricity production, the amount of carbon emissions from the electrical grid will increase slightly by 0.47 megatons CO_2 per year. Given that the carbon dioxide generated by the light internal combustion vehicles at the moment is 3.6 megatons of CO_2 per year, it is concluded that the total amount of greenhouse gases will decrease if all electric cars in Scotland are replaced by electric cars. The initial cost of an electric car is found to be higher than the conventional one, but in the long term, recharging an electric vehicle will be much cheaper.

Keywords: Electric, cars, greenhouse, emissions, carbon, vehicles

1. Introduction

The first internal combustion engine (ICE) powered by gasoline was invented in 1870 [1].

But due to its complexity, the cars were expensive to build. Surprisingly, the electric cars were more common at the end of the 19th century and it has been observed in 1899 that 90% of New York City's taxi cabs were electric vehicles [2]. However, Henry Ford has selected the internal combustion engine to be the technology used for his mass production lines which make the internal combustion engine cars affordable to the average person. The rest is history and this what made internal combustion engine the most common technology for the 20th century and beyond.

The internal combustion engine was improved greatly over the years, nevertheless even with the best improvement, internal combustion engines still produce a significant amount of carbon emission and pollution. The world population has increased approximately 7 times since 1870 [3]. With the increasing population and the increasing number of vehicles, the traffic carbon emissions increase as well. Internal Combustion Engine Vehicles (ICEV) discharge gases through their exhaust pipes as a result of the burnt fuel in the engine, directly polluting the environment. Those gases consist mainly of Carbon Dioxide (CO_2), Nitrous Oxides (NO_x) and Particulates. CO_2 and water are emitted from the burning process, Nitrogen (N) and Oxygen (O) also react during the fuel burning process forming NO_x and causing pollution. The increase in concentration in pollutants and carbon dioxide causes global warming and also causing health issues such as asthma. Different brands and models of ICE cars produce different amount of emissions. Approximately 20% of the greenhouse gases are emitted by conventional cars. A big portion of these gases is CO_2, the rest is NO_x. [4]. On the other hand, electric vehicles do not pollute the atmosphere directly, but they do contribute in greenhouse accumulation through their consumption for electricity, which is generated in power plants, who in the process produce greenhouse gases [5]. Different sources and methods for energy generation produce different amounts of greenhouse emission. The carbon factor for each source of electricity is different.

Table 1: Carbon factor of each source of electricity generation [6]

Source	Carbon Factor (gCO2eq/kWh)
Coal CCS	220
Gas CCS	170
Solar	88
Geothermal	34
Nuclear	26
Wave/Tidal	23
Wind	20
Hydro	7
Bioenergy	300

Table 2: Annual average electricity generation in Scotland and the percentage distribution of sources [7]

Source	Average Production GWh	Percentage Distribution
Nuclear	16,820	33.6 %
Coal	12,410	24.8 %
Gas	9,464	19 %
Hydro	5,290	10.5 %
Renewable	6,070	12.1 %
TOTAL	**50,054**	**100 %**

The annual electricity consumption in Scotland is roughly 38,000 GWh per year. It also has to be mentioned that the country is producing approximately 50,000 GWh of electricity a year, of which 14,000 are exported to Northern Ireland and England. The losses of electricity along the grid are estimated to be approximately 17% [8]. The price of electricity in the UK is estimated to be approximately 12 pence [9]. The source distribution of electricity production plays a vital role. If a country is generating electricity mostly from renewable sources or nuclear power, the emissions from the electricity production sector will not be high. The average annual mileage of a car in Scotland in 2015 was approximately 11,362 km and the number of light vehicles in the country for that year was about 2,240,000 [10].

It is important to take into consideration the fact that different brands of electric cars have different battery capacity and electric consumption for a unit of distance.

Table 3: Top 5 electric vehicles in the UK in 2015 and their specifications [11]

Brand	Battery capacity (kWh)	Consumption (kWh/100km)	Registered cars in 2015	Price (£)	Distribution (%)
Nissan Leaf	24	14	11,000	29,000	49
BMW i3	22	13	3,574	38,000	16
Renault Zoe	22	11	3,327	21,000	15
Volkswagen e-UP	18.7	14	2,500	19,000	11
Tesla Model S	85	16.9	2000	75,000	9

It is necessary to mention that the most popular conventional cars for 2015, their carbon factor and their price on the market. The price of fuel in the UK is approximately £1.3 [12].

Table 4: Top 5 conventional cars sold in the UK for 2015, their CO_2 factor, price, Distribution and average fuel consumption [13]

Vehicle model	**CO_2 (g/km)**	**Price (£)**	**Distribution (%)**	**Registered car**	**Consumption (L/100 km)**
Ford Fiesta	147	15,400	30	133,434	4
Vauxhall Corsa	129	10,800	21	92,077	4.7
Ford Focus	159	18,000	19	83,816	3.7
Volkswagen Golf	112	20,600	16	73,409	3.9
Nissan Qashqai	162	19,800	14	60,814	4

2. Methodology

Knowing the required parameters, calculations are made for determining how much the electricity demand would rise if conventional cars to be replaced by electric ones and how that would affect the carbon emission. A comparison between the vehicles' price and cost of maintenance in the long term has also been made. In order to acquire a proper value for the average tank/battery capacity, price and emissions it is important to take into consideration the percentage distribution of different brands since they have different specifications. The formula which represents the average consumption of fuel or electricity from cars can be expressed as

$$\sum_{i=1}^{n}(C_i \times PD_i) \qquad \text{(Eq. 1)},$$

where ***C*** represents the Energy or fuel consumption, ***PD*** is the percentage distribution (value%) and ***n*** represents the number of vehicles that were part of this investigation. This equation is also used to determine the average price for both EV and ICEV and carbon emission for conventional cars.

The average annual distance traveled by cars in Scotland in 2015 was determined and after using Eq1, the average fuel and electricity required by EVs and ICEVs to travel a given distance can be calculated by using the following equation:

$$RFE = (DT \div 100) \times AFEC \qquad \text{(Eq. 2).}$$

RFE is the Required fuel/electricity for the cars to travel the annual distance, *DT* is the Distance traveled divided by 100, and *AFEC* is the Average fuel/electricity consumption.

Eq 2 is used for both conventional and electric cars. Both values are then multiplied by the number of light vehicles in Scotland to determine the total fuel and electricity required for every car in the country. After that, both values are used to compare the annual price for the fuel and electricity needed for that distance. Determining the additional electricity needed for one year to charge the electric cars, the contribution to the production of carbon emission is calculated. The calculations have taken into account the losses through the gird and of course the distribution of the sources of electricity production. Eq 1 is used to determine the average carbon factor for ICEV, and that value is multiplied by the annual distance traveled and then by the number of ICEV in Scotland; this is performed in order to calculate how much carbon emission is produced by all cars in Scotland for a period of one year. The CO_2 emission from the possible additional annual electricity generation, including the addition from the EVs' demand and the grid losses, and from the traffic are compared. First, the amount of electricity generated per source according to the percentage allocation of the total amount of produced electricity is calculated; taken into account the carbon factor gCO_2eq/kWh for each source and the dimensions (kWh) in which the electricity consumption is measured. The amount of energy generated by each source is multiplied by its carbon factor to determine the total carbon emissions generated per source per year. This is done for both current and future possible electricity generation, in order to determine the increase in carbon emissions with the additional energy production.

3. Results

The average price of electric and conventional cars and their maintenance price has been calculated by applying Eq. 1. This has revealed that the average price of electric cars in 2015 is about £ 32,239 while for conventional cars is about 16,376. Hence the cost of electric cars on average is double of the conventional car.

In relation to the required fuel and electricity to cover the annual distance traveled, using Equation (2) has revealed that the required electricity for a single EV to cover the annual mileage of 11,362 km is 1551 kW/h. For a conventional car, this would require approximately 463 liters of fuel to cover the same annual distance. When those values are multiplied by the number of light cars in Scotland (2,240,000), it has been revealed that the total electricity required for EVs would be 3,475 GWh per year, and by including an additional 17% of the grid losses that number would increase to a total of 4,066 GWh of electricity demand. As for the conventional cars, the total fuel required per year by all of the light cars in Scotland to cover the annual distance is approximately 1 billion liters of fuel. Therefore, the price of electricity per year that an EV owner has to pay to run his car is expected to be £ 218. In comparison, the amount of money the owner of ICEV has to pay annually for fuel is approximately £ 602.

Knowing that the electricity generation in Scotland is approximately 50,054 GWh per year, the electricity required by the EVs for a year are added to that amount and it is estimated that the additional annual electricity production would be around 4,066 GWh and the total amount of electricity per year will rise to approximately 54,120 GWh.

Using Equation (1) it has been revealed that the average carbon factor of ICEV is 141.8 gCO_2eq/km. A single conventional car will generate approximately 1.6 tons CO_2eq/km. When multiplying this by the number of cars in Scotland, the traffic emissions from all cars for a period of one year will be estimated to be 3.6 Megatons CO_2eq/km.

Regarding the electricity generation, Carbon emissions depend on the energy source for electricity generation. Table 5 presents the energy type mix within the grid electricity generation

Table 5: Results from comparing the carbon emissions from the current electricity generation per source and total, and the possible future emissions.

Source	**Current carbon emissions (Megatons CO_2eq/kWh)**	**Possible future carbon emissions (Megatons CO_2eq/kWh)**
Nuclear	0.44	0.47
Coal	2.7	2.95
Gas	1.6	1.74
Hydro	0.04	0.04
Renewable	0.25	0.27
TOTAL	**5.03**	**5.47**

As a result of the change from conventional to electric cars, the emissions will increase by 0.47 Megatons. Currently, the traffic of light vehicles in Scotland produce 3.6 Megatons of CO_2 per year, and that is significantly higher than the amount of emissions that would be produced from the additional electricity generation for the EVs per year.

4. Discussion

The current finding could have some limitations. For example, the results in relation to the prices of EVs and ICEVs are based on the market research of new conventional and electric cars in 2015. Through the years, those prices may vary. The paper also did not take into consideration the fact that each person who purchases an EV will be granted a subsidy of about £ 3,500 [14]. There is also a price variance on the electricity (pence/kWh) and the fuel (£/litre) through months and years. With the increase in electricity demand, the price of energy per kWh is expected to increase as well. The calculations do not take into consideration the maintenance of electric and conventional cars, particularly in relation to the life of the battery or the engine. The electricity that would be required for electric cars is based on calculations made using parameters such as the number of cars, registered cars of each brand and average electricity consumption. Such numbers are expected to vary in the future. It is also worth mentioning that the current percentage distribution of both conventional and electric cars is calculated using the current best-sold cars of both types in the UK. This could also change in the future, depending on what brand would be the most looked for.

The reduction in the use of coal in the generation of electricity and the focus on renewable energy makes the Carbon emission figures in reality much better over the coming years in Scotland.

5. Conclusions

EVs are approximately two times more expensive than ICEVs on average, but the amount of money that would be spent annually to recharge an electric car is lower than the one of refueling a conventional car. In the case where all ICEVs are replaced with EVs, the electricity demand would rise slightly and with it the carbon emissions from the grid, but removing conventional cars from the traffic will have a positive impact on the environment, with significantly lowering CO_2 emission. With all the calculations made in this paper, it can be estimated that electric vehicles will have a positive impact regarding the environment, but economically that may bring some challenges. The paper, however, did not include the carbon emission produced during the production of the cars neither did not discuss the effect of battery production on the environment. This should be considered in future papers.

References

1. Eckermann, Erik (2001). World History of the Automobile. SAE Press. p. 14.
2. Hiskey, D. (2011). In 1899 Ninety Percent of New York City's Taxi Cabs Were Electric Vehicles. [online] Today I Found Out. Available at: https://www.todayifoundout.com/index.php/2011/04/in-1899-ninety-percent-of-new-york-citys-taxi-cabs-were-electric-vehicles/ [Accessed 20 May 2019].
3. Aubuchon, Vaughn (2016). World Population Growth History. Vaughn's Summaries
4. Brinson, Linda C. (n.d.). How much air pollution comes from cars?. https://auto.howstuffworks.com/air-pollution-from-cars.htm [Accessed: 25.04.2019]
5. Dotzauer, E. (2010). Greenhouse gas emissions from power generation and consumption in a nordic perspective. Energy Policy, 38(2), pp.701-704.
6. Parliamentary Office of Science & Technology (2011). Carbon Footprint of Electricity Generation. Houses of Parliament
7. Www2.gov.scot. (2016). Energy - Electricity Generation. [online] Available at: https://www2.gov.scot/Topics/Statistics/Browse/Business/TrendElectricity [Accessed 25 Apr. 2019].
8. "Electricity Generation And Supply Figures For Scotland, Wales, Northern Ireland And England, 2010 To 2013". www.gov.uk. N.p., 2016. [Accessed: 25.04.2019]
9. Electricity price in the UK - https://www.ukpower.co.uk/home_energy/tariffs-per-unit-kwh [Accessed: 30.04.2019]
10. Transport Scotland (2014) Table 1: Basic travel statistics – national travel survey: http://www.transport.gov.scot/statistics/j314725-05.htm [Accessed: 30.04.2019].
11. Lane, B. (2016) Quick links. Available at: http://www.nextgreencar.com/electric-cars/statistics/ [Accessed: 30.04.2019].
12. Price of fuel in the UK between 2015 and 2019 https://www.statista.com/statistics/299552/average-price-of-diesel-in-the-united-kingdom/ [Accessed: 30.04.2019]
13. Top 6 conventional cars, their price, and carbon factor: https://www.autoexpress.co.uk/best-cars/90327/best-selling-cars-2015-record-year-for-uk-car-sales [Accessed: 30.04.2019]
14. Government electric car grant: the complete guide https://www.buyacar.co.uk/cars/economical-cars/low-emission-cars/536/government-electric-car-grant-the-complete-guide [Accessed: 01.05.2019]

ICESF
Nottingham | UK | 9–11 September 2019

Heating, Cooling and Desalination with Sustainable Renewable Energy

Muhammad Wakil Shahzad, Muhammad Burhan and Kim Choon Ng
Water Desalination & Reuse Centre,
King Abdullah University of Science and Technology (KAUST),
Saudi Arabia.
Muhammad.shahzad@kaust.edu.sa

Abstract:

The inevitable escalation in economic development have serious implications on energy and environment nexus. The International Energy Outlook 2016 (IEO2016) predicted that the Non Organization for Economic Cooperation and Development (non-OECD) countries will lead with 71% rise in energy demand in contrast with only 18% in developed countries from 2012-2040. Most of energy is consumed to provide basic needs of life such as heating, cooling and fresh water. Traditionally, these sources are produced from conventional fossil fuels operated plants those are not only energy intensive but also environment unfriendly. We proposed highly efficient energy storage syatem based on Magnesium oxide (MgO) to provide these utilities for life cycle. The condensation of Mg(OH)2 dehydrated vapor during day operation with concentrated solar energy and exothermic hydration of MgO at night can produce 24 hour thermal energy for cooling, heating and water production without any interruption. It was showed that, Mg(OH)2 dehydration vapor condensation produce 120C and MgO hydration exothermic reaction produce 140C heat during day and night operation respectively correspond to energy storage of 81kJ/mol and 41kJ/mol. We believe that the proposed energy storage driven cycles are sustainable solutions for future heating, cooling and water supplies.

Keywords: Heating, Cooling, Desalination, Renewable energy, solar energy, energy storage material.

1. Introduction

In UK, heating, cooling and water treatment are the major source of energy consumption and corresponding carbon emissions. All these three basic necessities are important for life cycle and need to be carried out by innovative solutions to save energy and environment. The UK national heat and electricity yearly demand trend is shown in Figure 1. Space heating and hot water accounted for 82% of domestic use of energy, 64% of commercial use of energy and15% of industrial energy.

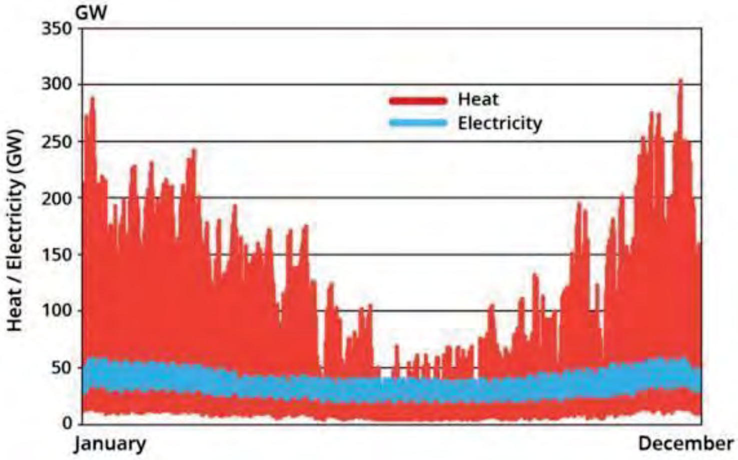

Figure 1. UK national heat and electricity demand in 2010 [1]

On the other hand, the UK population will grow to 73 million by 2037 and the drought and water shortages could therefore become more common, especially in the southeast of the UK. The water demand will increase by 6%, or an extra 800 million liters of water per day, by 2030. This water drought is majorly due to low rainfall in those areas as shown in Figure 2.

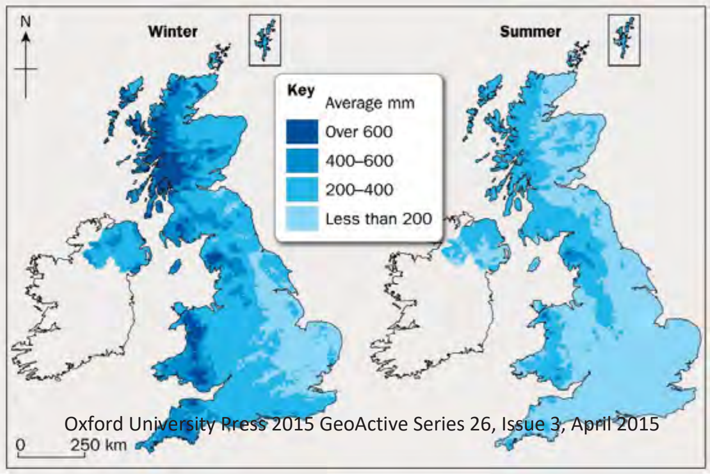

Oxford University Press 2015 GeoActive Series 26, Issue 3, April 2015

Figure 2. UK average rainfall from summer to winter session.

Decarbonising heat, electricity and water is very difficult and expensive. Reducing the dependence on fossil fuel and increasing the uptake of Renewable Energies will lead to an energy system with a diverse energy generation mix and greater electrification of the energy demand sectors, including domestic heating. It will also help to achieve UK CO_2 2030 emission level targets as shown in Figure 3.

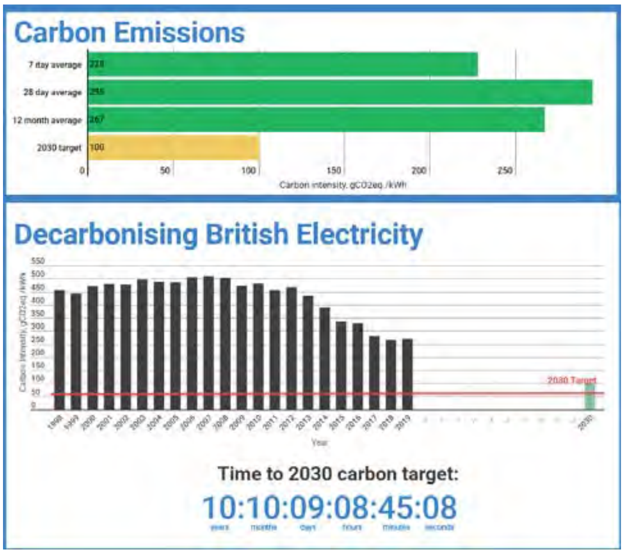

Figure 3. UK 2030 CO_2 emission targets (https://www.mygridgb.co.uk/dashboard/).

2. Proposed Renewable Energy System

The proposed renewable energy system will help to produce heating, cooling, electricity and water for 24 hours with energy storage facility. The concept schematic is shown in Figure 4.

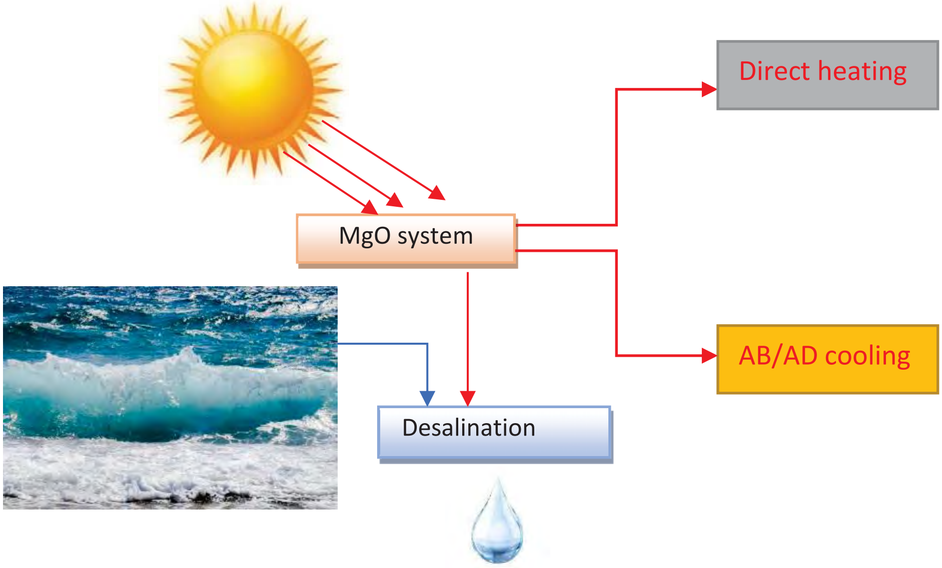

Figure 4: 24 hours process using solar energy storage.

3. Results and Discussion

The principle of energy storage system is shown in Figure 5 (Kato, Takashi, Sekiguchi & Ryu, 2009; Kato, Nakahata, Yoshizawa, 1999; Kato, Yamashita, Kobayashi & Yoshizawa, 1996). It consist of a magnesium oxide reactor and an evaporator. During day operation, ($Mg(OH)_2$) regenrated by solar energy and heat is produced at around 120C. At night, when dehydrated MgO is exposed to an evaporator, it attaract water vapors and produce heat due to exothermic adsorption processes. The heat produced at day and night operation is enough to opetare a system to generate three mentioned useful effects.

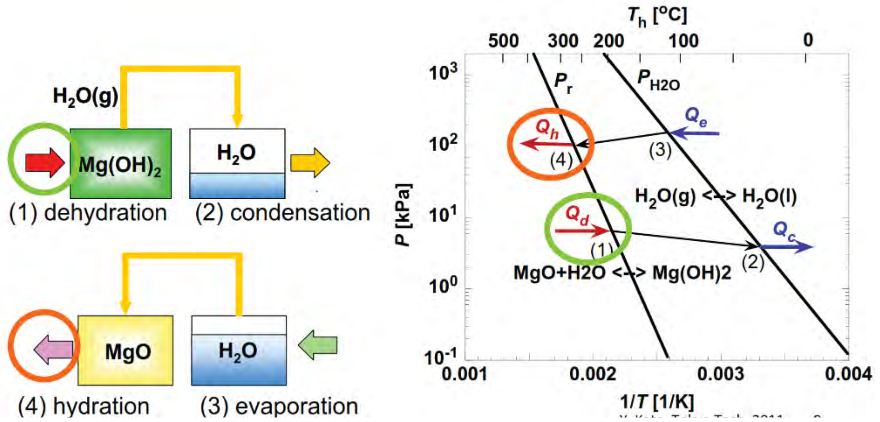

Figure 5: Solar energy storage system.

3.1- Heating for Winter Season

The produce heat at 120C as shown in Figure 5 can be directly used in building heating.

3.2- Cooling for Summer

The adsorption chiller are famous to operate at low grade waste heat at 60-80C to produce cooling. As shown in Figure 6, it are normally consist of adsorbent, typically silicagel, evaporator, condenser and circulation pumps. Figure 7 shows the cooling capacity of an adsorption chiller. It can be clearly seen that it can operate 65C to 85C and can produce chilled water at 10C. These chillers are widely used in the industry due to their easy operation, low maintenance cost and low grade energy utilization.

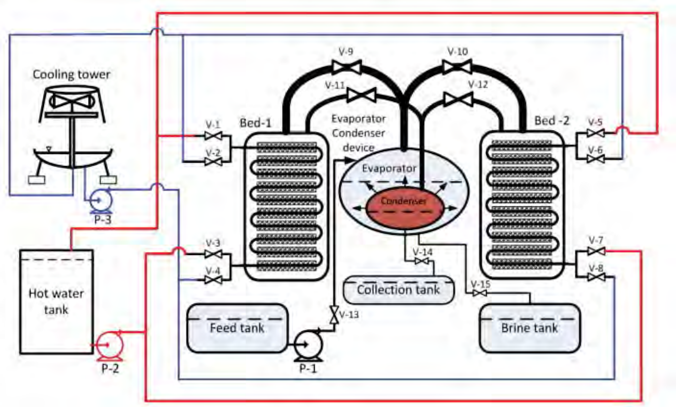

Figure 6: Basic adsorption chiller system (used with author permission [3]).

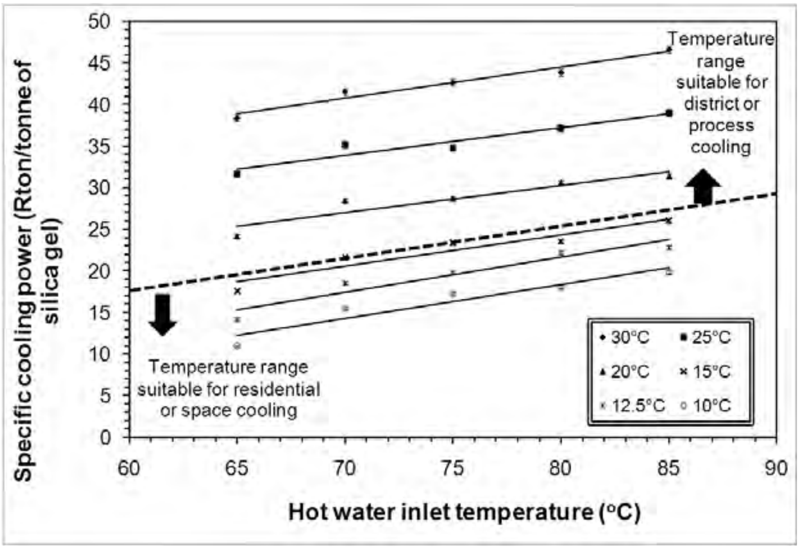

Figure 7. Specific cooling capacity of adsorption chiller (used with author permission [3].

3.3- Water Production

The low grade heat produced by proposed system can also be used to produce fresh water. We tested hybrid multi effect desalination system integrated with adsorption system (MEDAD) at assorted heat source upto 70C and showed successful operation. This system is not only workable at low grade heat but also boost water production to almost two folds due to thermodynamic synergy between two thermodynamic cycles. The water production is shown in Figure 8.

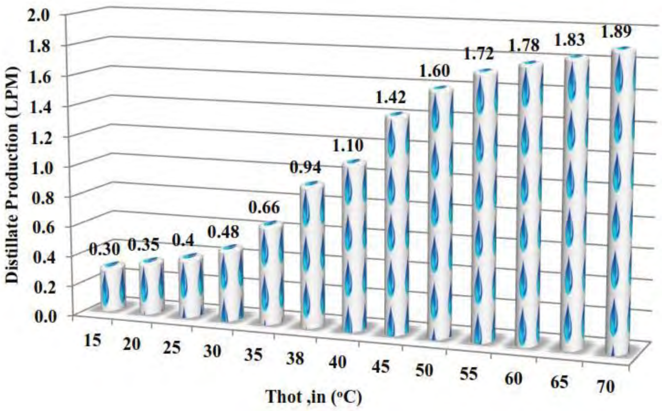

Figure 8. Water production of proposed MEDAD cycle with renewable energy storage (used with author permission [4].

4. Conclusion

To save energy and achieve sustainable development goals, the renewable energy storage system is one of the best solution. It will also help UK to achieve 2030 emission goals.

References

1. Mike Colechin, Creating an affordable low carbon energy system for the UK, Energy Technologies Institute, at the UKCCSRC ECR Winter School 2015.
2. Jason Palmer, Ian Cooper, United Kingdom housing energy fact file, Department and Energy and Climate Change Report 2013.
3. K. C. Ng, K. Thu, M. W. Shahzad and W. Chun, IDA Journal of Desalination and Water Reuse, DOI 10.1179/2051645214Y.0000000020 (2014).
4. Muhammad Wakil Shahzad, The hybrid multi-effect desalination (MED) and the adsorption (AD) cycle for desalination, PhD Thesis, National University of Singapore (2014).

Nottingham | UK | 9–11 September 2019

Dynamic clustering mechanism using forecasted input data

N.Bezas[1], A.Noula[1], D.Ioannidis[1], D.Tzovaras[1], Tommaso Bragatto[2], Francesca Santori[2]

[1]*Centre for Research & Technology, Information Technologies Institute, Thessaloniki, Greece*

[2]*ASM Terni S.p.A.*

{bezas, antigoni, djoannid, Dimitrios Tzovaras}@iti.gr,

{tommaso.bragatto, francesca.santori}@asmterni.it

Abstract

Clustering techniques is a powerful technological component that can be used in handling large volume of data emerging from the increasing use of smart metering devices in the modern power networks. Their outcome can be provided to energy market stakeholders, such as Aggregators for formulating efficient Demand Response (DR) strategies. The analysis achieved with this algorithmic technique produces groups of customers with similar features.

In this work, we present a processing technique for updating the static clusters that were created based on historical prosumers' consumption data from one year. In our approach, a dynamic way of changing the structure of clusters is proposed by using forecasted rather than previous measurements, thus providing an adaptive, near-real time mechanism. The present study concerns the identification of dynamic prosumers' groups with different flexibility on a daily basis (day-ahead time scale) using machine learning techniques. Our motivation to consider the two techniques in combination is that the clustering technique itself cannot provide the correct groups for day-ahead resources scheduling. Therefore, we have used the result of load forecasting for identification of day-ahead consumption pattern, in order to observe the changes in the static clusters.

Keywords: Dynamic clustering, Static clustering, Load forecasting, Demand Response (DR), Day-ahead scheduling

1. Introduction

Background

Nowadays, the utility companies have a large number of customers in their portfolio. The transition of electrical power systems includes the use of Demand Response [1] programs in the scope of increasing profit, adjusting consumption specifically during peak hours and serving flexibility requests from DSO/System Operator. The large number of customers urges their grouping in different clusters [2] taking into account different features, such as the consumption, the geographical location etc. The common grouping is carried out using only historical data of prosumers consumption from smart meters infrastructure. Utilities should identify the groups of prosumers who have similar consumption behavior in terms of consumption characteristics. The aggregator normally informs its customers one day before the DR event. It should be mentioned that there is the possibility that a selected prosumers was wrong classified to a specific group according to the historical data. However, due to unpredictable events, the consumption pattern of a prosumer may be quite different the day ahead when the DR event will take place. Thus, there is a risk of choosing a customer who is not able for the DR program to be applied that entails other risks both for aggregator and prosumer, such as profit reduction, customer discomfort etc. The usual clustering techniques [3] identify groups of prosumers considering bulk historical data without taking into account the consumption pattern over several consecutive days and consecutive hours. Thus, there is a lack of consistency in the static clusters that have been created based on historical data.

The proposed paper presents a dynamic clustering method in order to facilitate demand side management [4] on a daily basis. In the context of this dynamic approach, the clustering algorithm can run every day for the day ahead using as input the forecasted flexibility pattern of consumption for day ahead. The basic idea is the exploitation of clustering tool on real time from the side of aggregator in order to extract useful information of the flexibility capabilities of his portfolio. In the first stage flexibility profiles of all the prosumers are extracted from the forecasted load consumption profiles. The forecasting process was conducted using Artificial Neural Networks and more specifically a Multilayer Perceptron (MLP). At the next stage, a proposed clustering technique is applied on the daily flexibility profiles, thus grouping the prosumers based on their flexibility capacity.

2. Experimental results

Load Forecasting

Predicting day ahead electricity load accurately, enables utility providers to manage power loads more efficiently and to facilitate the scheduling and future capacity with higher precision. Over the last few years the rise of Artificial Neural Networks and especially deep learning made it possible to achieve accurate results regarding predictions based on historical data.

Multilayer Perceptron

Multilayer Perceptron [4] belongs to the category of Neural Networks and is a type of supervised machine learning algorithm [5]. MLP consists of connected hidden layers, where each layer contains units or nodes that are called artificial neurons. The input signals are processed in every neuron and after are transmitted into the other neurons.

Model Framing

There are some time series where multiple time steps must be predicted. Day ahead forecast is such an example, where the next *24* hours must be predicted. Contrasted to the one-step forecast, these are called multi-step or multi-step time series forecasting problems [6]. The most commonly used strategy for making multi-step forecasts is:

Direct Multistep Forecast: The direct method [7] involves developing a separate model for each forecast horizon. For day ahead load forecasting *24* different models are trained for each hour for the day respectively as follows:

$$\begin{aligned} &prediction(t+1) = model_1\big(obs(t-1), obs(t-2), \dots, obs(t-n)\big) \\ &prediction(t+2) = model_2\big(obs(t-1), obs(t-2), \dots, obs(t-n)\big) \qquad (1) \\ &\dots \\ &prediction(t+24) = model_{24}\big(obs(t-1), obs(t-2), \dots, obs(t-n)\big) \end{aligned}$$

Due to the fact models are developed separately no dependencies are occurred between the predictions, such as the prediction of $model_2$ being dependent on the prediction of $model_1$.

As mentioned above, Multilayer Perceptron is the selected algorithm for training the models [8]. The inputs of Multilayer Perceptron algorithm are: *24* previous measurements of load consumption, *24* of previous measurements of weather, *1* index of the day and *1* more index of the month.. In figure 1, an example of a day ahead load forecasting predicted by MLP is presented:

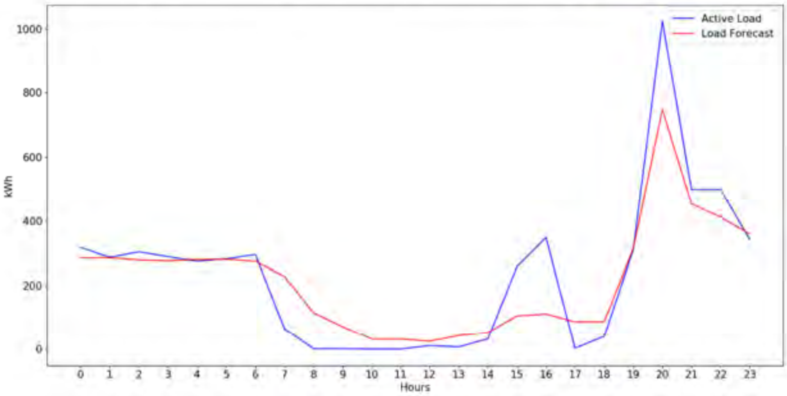

Figure 1: Day Ahead Load Forecasting

For the evaluation of forecasted results, three indices can be used [9]: root mean square error (RMSE), mean absolute percentage error (MAPE), symmetrical mean absolute percentage error (SMAPE).

Clustering Framework

In this paper, DBSCAN [10], is the chosen clustering technique to identify and organize prosumers into groups. DBSCAN [11] belongs to the category of unsupervised data mining techniques. Essentially, the algorithm groups together points that are close to each other (points with many neighbors), marking as outliers points that appear alone in low-density regions. DBSCAN, defines as clusters dense groups of points. In DBSCAN there is no need to predefine the number of clusters. *2* parameters are necessary for the algorithm:

- *eps*: the minimum distance between two points. It means that if the distance of two points is lower or equal to this value (eps), these points are marked as neighbors. The eps neighborhood of a point:

$$N(p) = \{qD|dist(p,q) \leq Eps\} \quad (2)$$

- *minPoints***:** the minimum number of points to form a dense region.

Given eps and minPoints categorize the objects into three exclusive groups:

1. A point is considered as a core point if the corresponded number of points within *eps* is greater than a predefined number of points (*minPoints*)
2. A border point has fewer than *minPoints* within *eps*, but belongs to the neighborhood of a core point.
3. A noise point is any point that is not core point nor a border point.

Considering the parameter *minPoints*, a general rule is that it can be derived from the number of dimensions (*D*) in the dataset [12] as *minPoints* >= *D+1*. Larger values are usually better for datasets with noise and will form more significant clusters.

Flexibility Extraction

In this paper, flexibility is defined as the degree in which it can modify its baseline load profile by either increasing or decreasing its load. Otherwise, flexibility could be defined as the difference between actual consumption and baseline. Baseline refers to the minimum demand to meet the fundamental electrical needs of a prosumer.

Calculation of baseline method was conducted by the average method [13]. Average method combines the hourly loads for a certain time of period and results to the average baseline load. In this paper, the period to estimate the baseline was set to one year to have a complete "view" of the load behavior of prosumers. After the baseline was established, daily flexibility was estimated from the actual consumption and baseline. Daily flexibility was used to extract a generic flexibility profile for each prosumer for one year. In figure 2, an example of flexibility calculation is depicted

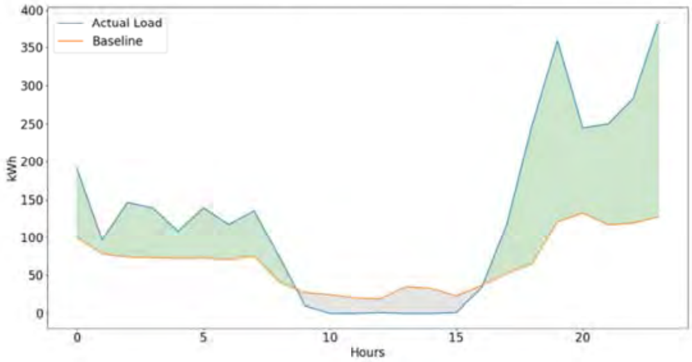

Figure 2: Flexibility Estimation

A crucial task for the aggregators is to have an overall sight of the prosumers of their portfolio that are capable of providing the necessary flexibility for DR programs [14]. In section *III,* flexibility was described as the difference between the actual value and a baseline that was defined by the average method. Averaging the daily flexibilities for each prosumer results to the average flexibility profile. Applying DBSCAN clustering to the flexibility profile of all prosumers as it gives aggregators the ability to be aware of the flexibility capacity of their portfolio. The methodology followed to find the representative prosumer's flexibility profiles is in figure 3.

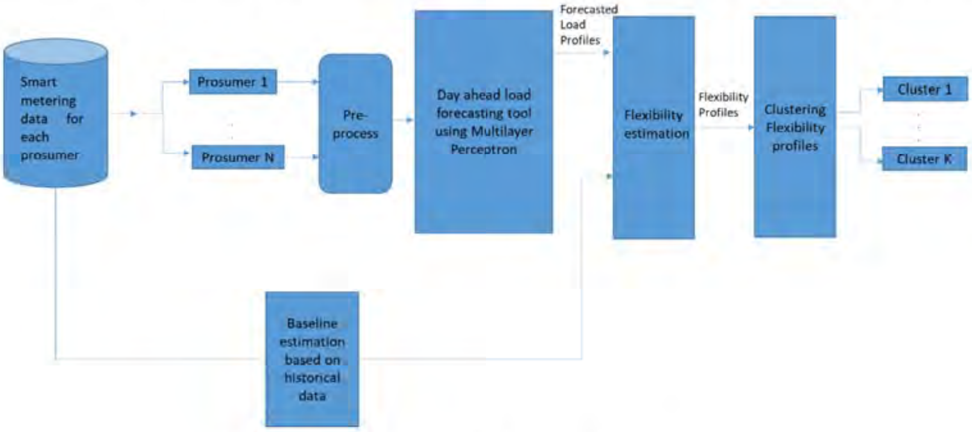

Figure 3: Architectural scheme of the mechanism

3. Results and discussion

Data Description

This section studies the results of clustering process based on the day-ahead forecasted flexibility curves to detect the flexible and non-flexible prosumers. Electricity data is obtained from ASM archive and is consisted of *83* prosumers. The dataset is monitored during the year of *2017* and the data are logged at *15* min intervals. Before proceeding to clustering, filtering the data from outliers is a necessary step. After filtering, the consumption data is aggregated to hourly time intervals in order to reduce the dimensionality and computational effort. The final-preprocessing stage consists of the normalization [15] of the dataset in order the forecasting model to capture the correlations between historical data more precisely.

Evaluation results of static and dynamic clustering

A comparison between the static and day ahead clusters is conducted. After the prediction of day ahead load profiles and extracting the flexibility profiles as it was described above, day ahead clusters are formed. Day ahead clusters could be considered as a dynamic clustering process that provides more accurately information of energy behavior regarding the prosumers. As it shown in table 1, the number of prosumers belonging to a specific class varies from static and day ahead clustering. According to Table 1 in day ahead clustering a *9%* was classified into a different cluster than in static clustering.

Table 1: Results of static and day ahead clusters

Number of Clusters	Labels of Clusters	Number of Prosumers in Static Clusters	Number of Prosumers in Day Ahead Clusters
2	*0*	*77*	*69*
	1	*6*	*14*

An illustration of the resulted labels of both clusters in a small sample of the dataset is shown below.

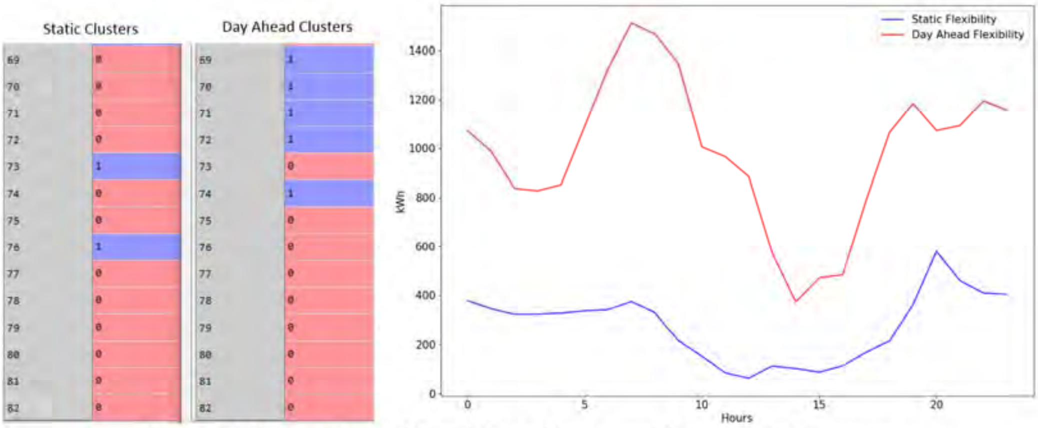

Figure 4: Comparison of Flexibility of Static and Day Ahead Clustering

In figure 4, the left image shows the resulted labels. The first column corresponds to the *ID* of each prosumer and the second column represents the label of the classes in which the prosumers were classified based on the adopted clustering techniques. It is evident that prosumers who have been classified into a particular cluster based on static clustering is possible to move to another cluster by day ahead clustering. The right image gives an example of the change of the cluster label of a user during static and day ahead clustering process is given.

It is important to note that the effectiveness of the clustering technique is based on the reliability of the forecasted results. The more accurate the results are the more accurate will be the classification of the prosumers in the correct clusters.

4. Conclusions and future work

This paper proposes a method to take advantage of real-time clustering based on load forecasted flexibility profiles in order the aggregator to be aware of the energy behavior of his portfolio for next day. The proposed clustering technique is applied on flexibility day ahead profiles and a comparison is made between day ahead and static clustering results. Day ahead clustering can be used with greater precision by the aggregator for mining knowledge for the flexibility capacity of his portfolio for next day. As future work the day ahead forecasting tool could be recalibrated based on short term predictions, such as one hour or intraday ahead predictions.

Acknowledgements

The work presented was carried out as part of the eDREAM project which is co-funded by the EU's Horizon 2020 framework programme for research and innovation under grant agreement No 774478. The authors wish to acknowledge the European Commission for their support, the efforts of the project partners, and the contributions of all those involved in eDREAM.

References

1. Saeed Rahmani Dabbagh et al. (2015), Participation of Demand Response Resources through Virtual Power Plant: A Decision Framework under uncertainty, IEEE 15th International Conference on Environment and Electrical Engineering (EEEIC), DOI: 10.1109/EEEIC.2015.7165490.

2. Yi Wang et al. (2016), Clustering of Electricity Consumption Behavior Dynamics Toward Big Data Applications, IEEE Transactions on Smart Grid, Vol. 7, No. 5, September 2016, pp. 2437 – 2447, DOI: 10.1109/TSG.2016.2548565.
3. Amit Saxena et al. (2017), A Review of Clustering Techniques and Developments, Neurocomputing, doi: 10.1016/j.neucom.2017.06.0.
4. Hassan Ramchoun et al. Multilayer Perceptron: Architecture Optimization and Training, International Journal of Interactive Multimedia and Artificial Intelligence, Vol. 4, Nº1.
5. Danilo Bzdok et al. (2018), Machine learning: Supervised Methods, January 2018.
6. Masum S., Liu Y., Chiverton J. (2018) Multi-step Time Series Forecasting of Electric Load Using Machine Learning Models. In: Rutkowski L., Scherer R., Korytkowski M., Pedrycz W., Tadeusiewicz R., Zurada J. (eds) Artificial Intelligence and Soft Computing. ICAISC 2018. Lecture Notes in Computer Science, vol 10841. Springer, Cham.
7. Souhaib Ben Taieb, Rob J Hyndman (2012), Recursive and direct multi-step forecasting: the best of both worlds.
8. Markos Markou et al., 24-Hour Ahead Short Term Load Forecasting Using Multiple MLP.
9. Nijat Mehdiyev et al. (2016), Evaluating Forecasting Methods by Considering Different Accuracy Measures, Procedia Computer Science 95 (2016), pp. 264 – 271.
10. Martin Ester et al. (1996), A Density-Based Algorithm for Discovering Clusters in Large Spatial Databases with Noise, KDD-96 Proceedings.
11. Ling Jin et al. (2017), Comparison of Clustering Techniques for Residential Energy Behavior using Smart Meter Data, AAAI-17 Workshop on Artificial Intelligence for Smart Grids and Smart Buildings WS-17-05.
12. Jorg Sander et al. (1998), Density-Based Clustering in Spatial Databases: The Algorithm GDBSCAN and Its Applications, Data Mining and Knowledge Discovery, June 1998, Vol. 2, Issue 2, pp. 169–194.
13. Kanping Li et al. (2017), A Baseline Load Estimation Approach for Residential Customer based on Load Pattern Clustering, Energy Procedia, Vol. 142, December 2017, pp. 2042-2049.
14. Mahnoosh Alizadeh et al. (2014), Capturing Aggregate Flexibility in Demand Response, 53rd IEEE Conference on Decision and Control, DOI: 10.1109/CDC.2014.7040399.
15. Gopal Krishna Patro, Kishore Kumar Sahu, Normalization: A Preprocessing Stage.

Nottingham | UK | 9–11 September 2019

Influence of graphite addition on the thermal performance of energy pile

A. Elkezza Omar [1], B. Mohamed Mostafa [2], C. Khan Amir [3]

[1] *Phd student, Civil Engineering, Faculty of Engineering and Informatics, University of Bradford, UK*

[2] *Senior lecturer, Civil Engineering, Faculty of Engineering and Informatics, University of Bradford, UK*

[3] *Lecturer, Civil Engineering, Faculty of Engineering and Informatics, University of Bradford, UK*

o.elkezza@student.bradford.ac.uk

Abstract

The use of geo-energy piles in commercial and residential buildings has increased exponentially in Europe and the UK. The thermal performance of geo-energy piles may directly influence the energy- saving on the buildings. Apart from the geometrical optimization, many other factors influence the thermal efficiency of the energy piles. The aim of this study is to evaluate the effect of the thermal properties of concrete on the performance of geo- energy piles. Firstly; the effect of graphite content on the thermal conductivity and compressive strength of concrete are determined in order for the optimum graphite content to be selected, then a prototype of an energy pile with a normal concrete and graphite concrete were tested to evaluate the effect of using the graphite concrete on the thermal performance of the energy piles. The heat transfer efficiency of the graphite modified concrete has been increased by 55% when is compared with the efficiency of the conventional concrete energy pile under the same conditions.

Keywords: *graphite modified concrete, energy pile efficiency, thermal conductivity of concrete*

1. Introduction

Geo-energy structural is a new form of ground source heat pump systems that include conventional geo-structure (*e.g: tunnel lining, pile foundation, diaphragm wall*) [1]. This system has been considered as a promising source of energy [2]. The enhancement of heat transfer mechanism of geothermal energy piles has been critically analysed. Four different aspect have been suggested to affect the thermal enhancement which are; i. geometrical optimisation, ii. introduction of Nano fluid as circuit fluid, iii. pipe materials, and iv. concrete heat transfer enhancement. Geometrical optimization mainly focuses on the pile dimensions such as pile depth, pile diameter, concrete cover …etc. and the pipe configuration (number of pipes and pipe configurations). Nanoscale particles can be mixed with the fluid to enhance its thermal properties, this topic has been extensively studied and proven to provide significant increase in thermal properties of fluid with very low concentration of nano partials [4] revealed that the thermal conductivity of the fluid increased by 15% for the higher concentration. The pipe is the interface of the heat transfer between the fluid and the concrete. The pipe material for the energy pile should be selected carefully to ensure high thermal conductivity and durability since it embedded in concrete [5] . [6] Suggested the application of graphite to improve the thermal conductivity of concrete and pointed out at the room temperature and with the increase of graphite content the thermal conductivity of concrete rapidly increased. On another study, a series of graphite concretes were mixed using cement, sand, water, water-reducing agent, and different volumetric contents of powdered graphite (0%, 5%, 10%, 15%, and 25%) The results indicate that the addition of graphite clearly enhances the heat transfer co- efficient, especially for concretes with graphite contents higher than 15%. [7]

The aim of this paper is to evaluate the effect of the thermal properties of concrete on the performance of geo-energy piles. Firstly; the effect of graphite content on the thermal conductivity and compressive strength of concrete are determined and the optimum graphite content was selected, then a prototype of an energy pile with a normal concrete and graphite concrete were tested to evaluated the effect of using the graphite concrete on the thermal performance of the energy piles.

2. Experimental

The graphite concretes were prepared by mixing cement, sand, water, aggregate with maximum size of 10mm and different weight contents of **graphTHERM** (0%, 5%, 10%, 20%, 30%, 40% and 50%) to confirm the thermal characteristic enhancement of concrete, Table (1) presented the weight percentage of each mix. Mixer was used to stir the mix for 2-3 min. Then, the concrete poured in special cylindrical moulds with dimension 100 mm diameter and 50mm height to create suitable samples for hotplate testing procedure. Also, 100mm cubic moulds were filled with concrete to assess the effect of graphite on the compressive strength, the both concrete samples were cured for 28 day in water and 2 day afterwards for air dry (and this due to the sensitivity of water on the thermal conductivity measurements), the measurement Three samples were tested for each percentage. The hot plate tests were carried out according to BS 874:1986 to measure the thermal conductivity of the concrete samples.

A Fully instrunmented tank with inner dimensions of 1m×1m×1m was manufucture. Figure (1) shows a graphic diagram of the tank. The tank walls are fully insulated to minimise the effect of the ambient air temperature. A drainage system was installed at the base of the tank to uniformly present the drain groundwater over the whole cross-section of the tank. The drainage system includes: perforated pipes, manifold, gravel bed and filter sheet. The perforated pipes and manifold were surrounded with a gravel bed that was wrapped by a synthetic filter sheet to prevent blockage of the drainage system. The drainage system (manifold) was joined with an external water controlled well so as to regulate and maintain the water level inside the tank at determined levels.

A concrete pile with embedded nylon U shaped heat exchange was located at the centre of the tank and buried with building sand , the pile dimensions 900mm Length ,150 mm in Diameter and the U heat exchange 1800mm total length with 8mm outer diameter and 6mm inner diameter The pipes were installed and separated by tied it into built cage inside the pile to ensuring an even separation of the pipes and a centre to centre spacing between the two legs of the U tube of around 100mm. Degradable glycol and water mix at a ratio of 1 part glycol to 3 parts water was prepared and circulated in the energy pile and its flow rate was controlled using a peristaltic pump. In over-all 21 T-type thermocouples were employed for measurements of the temperature at different locations, e.g. inlet and outlet, running glycol, soil temperature, drainage tank and in the laboratory space.

Table 1: Composition of graphite concrete

graphite content	Cement (g)	Water (g)	Sand (g)	Aggregate (g)	Graphite (g)
0%	124	85	283	433	0
10%	124	85	283	433	13
20%	124	85	283	433	25
30%	124	85	283	433	38
40%	124	85	283	433	50
50%	124	85	283	433	62

Fixed and variable parameters of four tests undertaken in this investigation are illustrated in Table (2). The first two tests were conducted on dry sand with different energy pile material a control test **D-N-1**was carried out with normal concrete energy pile and test **D-G-2** was conducted with graphite concrete .Two more tests were then performed in which a water level was kept at 500 mm. building sand was used to fill the tank and it's thermal conductivity were measured in dry and wet conditions , the thermal conductivity of sand in dry form was measured by kd2 pro and was found to be 0.36 w/m.k .Wet sand samples were compacted with water content of 1%, 3%, 5%, 10%, 20% and 30% under static load and dry density 1.35gm/cm^{3}.The thermal conductivity was taken using a K2D Pro thermal meter device. The kd2 pro was inserted in the surface into the sand sample and readings were taken. Each measurement was repeated three times and the average value was taken.

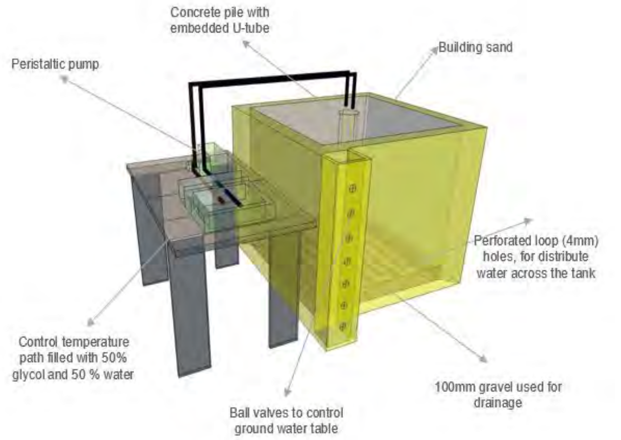

Figure 1: Schematic diagram for the experimental

Table 2: Parameters for different tests

Test	Fixed parameters	Variable parameters	Inlet c^{o}	Outlet c^{o}	ΔT k	Dissipated heat Watts
D-N-1	Dry soil, flow =67l/h	Normal concrete	52.14	50.49	1.65	102.67
D-G-2	Dry soil, flow =67l/h	Graphite concrete	52.41	50.05	2.36	146.13
W-N-3	Wet soil, flow =67l/h, water table 500mm.	Normal concrete	52.01	49.97	2.04	126.31
W-G-4	Wet soil, flow=67l/h, water table 500mm.	Graphite concrete	52.52	48.82	3.7	229.10

3. Results and Discussion

Thermal conductivity of concrete results analysis

The results of thermal conductivity of concrete samples prepared with 0%, 10%, 20%, 30%, 40% and 50% graphite tested under the room temperature are shown in Table (3).It can be observed that the highest thermal conductivity value is 3.10 w/m.k on sample was graphite content of 50%, which considered about 2 times that attained on normal concrete which was 1.44 w/m.k , which is in line with the results reported by [7] . This is mainly attributed to the higher thermal conductivity value of the graphTHERM which normally > 50 w/m.k . The smaller particle size of graphTHERM is contributed in filling the air voids between the concrete components and increase the packing density of the concrete .in other words, replacing the air voids in concrete by higher thermal conductivity partials result increasing the thermal conductivity of concrete. [8]

Table 3: Thermal conductivity test results

graphTHERM Content %	Room Temperature	Thermal Conductivity (W $m^{-1}k^{-1}$)
Zero	24.4c	1.44
10%	24.7c	1.60
20%	25.9c	2.10
30%	24.6c	2.64
40%	24.3c	2.97
50%	24.8c	3.10

Compressive strength test results analysis

Figure 2 shows the influence of graphTHERM on the compressive strength after 28 days of curing in water. From the figure, it can be observed that by adding graphite into concrete, the compressive strength started enhancing until 10% graphite content, reporting almost 22% improvement compared to the conventional concrete, before being gradually decreased. However, it is still higher than conventional concrete until reaching almost 45% graphite, when the strength becomes almost similar, while any further over this ratio, the strength would be lower than conventional concrete.

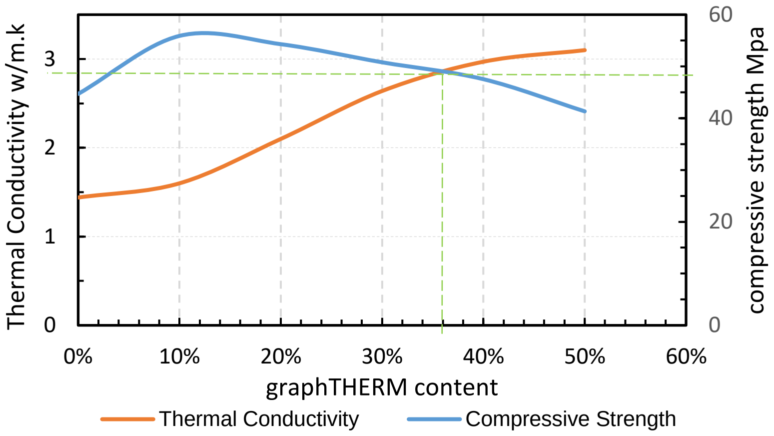

Figure 2:thermal conductivity & compressive strength vs graphTHERM content

Optimum graphTHERM content

In order to determine the optimum graphite content for geo-structural elements applications, two aspects were taken inconsideration which are compressive strength and thermal conductivity. Figure (2) shown the compressive strength variation with different graphite content on the right-hand y-axis. Whereas, the left-hand y-axis presenting the thermal conductivity with different graphite contents. The intersection points between the two curves represent the optimum graphite content for maximise the thermal conductivity and minimize the effect on the compressive strength. The optimum graphite content was found to be around 36% of the cement weight

Temperature difference between outlet and inlet

Throughout all testes, the fluid temperature was recorded at the inlet and outlet points of the circulation tube embedded in the experimental pile. The temperature difference Δ**t** between these two points would indicate the amount of energy the pile was able to dissipate into the soil.

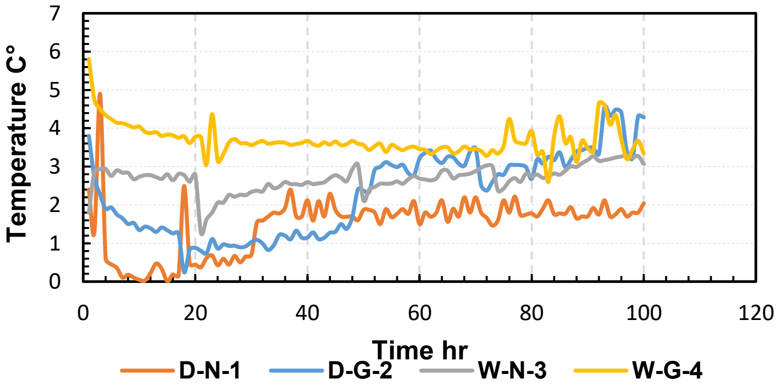

Figure 3: Temperature difference inlet-outlet

Figure (3) presents the temperature difference (inlet-outlet) for the four tests and evidently demonstrates that test w-g-4 gives the higher temperature difference which in average about 3.7C° for the SteadyState behaviour. The measured temperature difference for normal concrete pile in dry building sand is 1.65 C° these values increased by 43% when the graphite concrete used for the energy pile. This shows an increase of 55% when the water table was maintained at 500mm above the tank base. The pile thermal performance increased when the graphite concrete used for the geo-energy pile. According to the obtained results, the heat dissipated into the soil was actually less for the dry soil. This is consistent with [9] as explain this phenomenon due to the difference in specific heat capacity between the dry and saturated sand. Specific heat capacity is defined as the amount of energy to unit increase in temperature of a unit mass of material. Therefore, it takes a larger amount of energy rejected from the geothermal pile to observe an identical change in temperature in the saturated sand.

4. Conclusion

The influences of graphTHERM powder on the heat transfer performance of the concrete geo-energy piles was experimentally investigated and the following conclusions could be drawn:

- The thermal conductivity of graphite-modified concrete materials is significantly increased, in comparison to that obtained from normal concrete under the same environmental temperature.
- The compressive strength significantly improved by adding the graphTHERM to concrete; the highest strength was obtained with 10% graphite, whilst a gradual decrease was observed above this ratio until about 45%, when the compressive strength becomes less than the conventional concrete.
- the thermal performance for the energy pile was extraordinary improved by incorporating graphTHERM in to concrete in both conditions: dry soil and wet soil. While above 40% improvement was obtained in the former case, about 55% improvement was reported with the latter case.

References

1. Dong, S., Li, X., Tang, A. M., Pereira, J. M., Nguyen, V. T., Che, P., & Xiong, Z. (2019). Thermo-mechanical behavior of energy diaphragm wall: Physical and numerical modelling. *Applied Thermal Engineering*, *146*, 243-251.
2. Amis, A., & Loveridge, F. A. (2014). Energy piles and other thermal foundations for GSHP– developments in UK practice and research. *REHVA Journal*, *2014*(1), 32-35.
3. Faizal, M., Bouazza, A., & Singh, R. M. (2016). Heat transfer enhancement of geothermal energy piles. *Renewable and Sustainable Energy Reviews*, *57*, 16-33.

4. Ghozatloo, A., Rashidi, A., & Shariaty-Niassar, M. (2014). Convective heat transfer enhancement of graphene nanofluids in shell and tube heat exchanger. *Experimental Thermal and Fluid Science*, *53*, 136-141.
5. Noorollahi, Y., Saeidi, R., Mohammadi, M., Amiri, A., & Hosseinzadeh, M. (2018). The effects of ground heat exchanger parameters changes on geothermal heat pump performance–a review. *Applied Thermal Engineering*, *129*, 1645-1658.
6. Guo, C., Zhu, J., Zhou, W., & Chen, W. (2010). Fabrication and thermal properties of a new heat storage concrete material. *Journal of Wuhan University of Technology-Mater. Sci. Ed.*, *25*(4), 628-630.
7. Li, Q., Chen, L., Ma, H., & Huang, C. H. (2018). Enhanced Heat Transfer Characteristics of Graphite Concrete and Its Application in Energy Piles. *Advances in Materials Science and Engineering*, *2018*.
8. Arora, A., Almujaddidi, A., Kianmofrad, F., Mobasher, B., & Neithalath, N. (2019). Material design of economical ultra-high performance concrete (UHPC) and evaluation of their properties. *Cement and Concrete Composites*, 103346.
9. Kramer, C. A. (2013). An experimental investigation on performance of a model geothermal pile in sand.

ICESF
Nottingham | UK | 9–11 September 2019

Review of Waste to Energy Projects in Developing Countries

A. Abhishek Asthana, B. Sanjay Mukherjee

Hallam Energy, Sheffield Hallam University, Howard Street, Sheffield, S1 1WB, United Kingdom

asthana@shu.ac.uk

Abstract

Waste to Energy (WTE) projects have been running successfully in many countries but have produced only mixed results in developing and have often been plagued with controversies. This is due to various technical, financial, environmental, political and social factors involved. Hallam Energy at Sheffield Hallam University was commissioned by the Government of India, to conduct a detailed independent investigation into the techno-economic feasibility of such a WTE project in Delhi. The goals of this study were (i) to make an informed decision on whether the proposed WTE facility for Delhi will be technically and financially viable, and (ii) to gain a reasonable understanding of the costs and resources involved in this investment. This work looks at the various challenges associated in setting up WTE plants in developing countries and address key findings including: 1. The capacity of the plant, 2. The capital cost, 3. The electrical power output, 4. Land area requirement, 5. Site selection for the plant, 6. The choice of processes and pre-processing of the feed, 7. Feasibility of trigeneration or CHP, 8. Choice of technologies and equipment, 9. Financial models, 10. Emissions of pollutants, 11. Lessons learnt from past WTE projects in India.

Keywords: Waste to Energy (WTE), Municipal Solid Waste (MSW), Refuse Derived Fuel (RDF), Developing Countries, Trigeneration, Landfill

1. Introduction

India, the second most populated country in the world and one of the fastest growing economies, is experiencing an unprecedented growth in its industrial sector and is undergoing rapid urbanisation (Bhagat 2011, Pradhan 2017). The number of towns in India has increased by 50% from 2001 to 2011. Such growth and lifestyle transformation inevitably bring along a much augmented volume of municipal solid waste (MSW), produced from the country's recently transformed commercial, industrial and residential areas. In 2013-14, India was generating an estimated 143,449 tonnes per day of MSW at 0.11 kg/capita/day, out of which only 32% was treated or processed (MoUD, 2016). The per capita MSW generation rate for Indian cities with population above 1 million varies between 0.4-0.6 kg/day. Any disorder in handling of the

MSW generated can have catastrophic impact on India's booming economy, environment and population in future. One such accident happened on 2 September 2017 at Ghazipur landfill site in Delhi which collapsed, killing 2 people (Hindustan Timesa, 2017). Therefore, the sustainable management of the MSW is a critical concern for municipal authorities throughout the country (Hoornweg and Bhada-Tata 2012).

Most of the MSW collected in India is either burnt in open air without central collection or dumped in landfill sites. The existing landfill sites in mega cities like Delhi, Kolkata and Mumbai have dangerously exceeded their capacity already. Moreover, the traditional waste disposal technique by landfill is considered the most unfavourable route in the waste management hierarchy, as it wastes valuable land and gives rise to Green House Gases (GHG) emissions, primarily methane (Liu et al. 2017). Consequently, policies and regulations in many countries, such as the Landfill Directive in Europe, discourage landfilling and encourage recycling and resource recovery (Lukumon et al. 2013). With the drive towards circular economy gaining momentum, under current proposals, landfilling of all recyclables will be substantially reduced in the European Union (EU) in the near future (Costa et al. 2010). In India, the Ministry of Urban Development (MoUD) is seeing a long-term solution for MSW disposal in a number of large cities under Swachh Bharat Mission (MoUD 2016).

The waste incineration is seen as a conducive technique for scientific disposal of MSW that has the potential to replace landfilling of MSW. Countries such as Denmark, Japan, USA and Sweden have been leaders in using the energy generated from incineration in localised facilities supporting power generation schemes (Nakakubo et al. 2017, Lu et al. 2017). A number of other European countries rely heavily on incineration for handling municipal waste, in particular Luxembourg, Netherlands, Germany, and France. The MoUD plans to build a new state-of-the-art WTE plant in Delhi to set an example for other cities to follow. This paper aims to evaluate the feasibility of the proposed plant. It outlines the specification of the plant including the land area required, the type and quality of fuel, potential electrical outputs and capital cost requirements. Finally, it aims to identify the technical, social, political and economic challenges in the implementation of such projects and suggests solutions to overcome these challenges.

2. Size of the plant

Delhi, with a population of 19 million, currently produces circa 8,500 tonnes per day (TPD) of MSW which is expected to increase to 14,302 TPD by the year 2024 (MCD 2004). According to conservative estimates (GAIA, 2016), Delhi would require 100 km^2 of landfill area or 6.7% of the total land area in Delhi by the year 2050 if scientific methods of disposal of MSW are not implemented on a large scale. For a densely populated metropolitan city like Delhi, it would be extremely challenging to find such large land area for waste disposal. Three of the four existing landfill sites in Delhi have already far exceeded their capacity. While the permissible upper height limit for dumping garbage at a landfill is approximately 15 to 20 metres, the sites at Okhla, Ghazipur and Bhalswa are well past 40 metres (Hindustan Times^b, 2017). The Ghazipur site has now crossed 50 m. it should have been closed in 2002 but continues to receive 3,000 TPD of MSW. Apart from dumping its waste in landfills, Delhi also uses its daily waste generated in three WTE plants that can only treat maximum of 8,000 TPD combined, as compared to 8,500 TPD generated. Based on the forecast increase in MSW generation and capacity of the existing WTE plants, it was estimated that a new WTE plant would need to process at least 4,000 TPD to keep up with the demands by 2020.

3. Quality of MSW in Delhi

The electrical output of any WTE plant depends upon the composition of the MSW that is incinerated. The waste collected in Delhi contains a complex mixture from various sources – kitchen/food waste, road sweeping, drain silt, construction and demolition (C&D), industrial, etc. The composition of MSW varies in India from place to place, depending on the level of urbanisation, living standards and population density. For instance, MSW in metropolitan cities contains more packaging materials and plastics than that in small and semi-urbanised cities. The MSW, regardless of its place of origin, could contain approximately 30-40% moisture in it which is mainly due to the large quantities of kitchen and food wastes that come under biodegradable matter. Due to a lack of segregation practices at source, direct incineration of the waste would not be viable. Using raw or untreated MSW directly in the incinerator can cause incomplete combustion (or no combustion in some cases) which would ultimately result in higher emissions, energy losses and higher operating costs. Thus, the MSW should be pre-processed to separate the non-combustible and compostable or biodegradable parts. Its moisture content must be reduced and the MSW should be converted to Refuse-Derived Fuel (RDF).

In pre-processing, the moisture content is reduced to approximately 20%. The RDF produced after separation stages is rich in combustible matter, low in moisture and accounts for approximately 30-40% of the raw MSW on dry basis. On a typical day, 1,200 to 1,600 TPD of RDF will be produced in the new plant out of a feed of 4,000 tonnes of MSW. Raw MSW has a calorific value of 800-1000 kcal/kg (Lower heating value, LHV) whereas the RDF can have nearly 2,500 – 3,000 kcal/kg (LHV) depending on how efficiently the separation is carried out (Dubey 2013).

4. Electrical output from the WTE plant

The electrical output for the 4,000 TPD capacity WTE plant proposed in this report is estimated using both MSW and RDF fuels. The key outputs of the analysis are shown in Table 1. MSW being very low in calorific value and high in moisture content should not be sent directly to the incinerator. Rather, it should be converted to RDF before it is burned in the furnace. A 4,000 TPD capacity WTE plant would treat approximately 166 tonnes of MSW per hour to produce 49.9 - 66.6 tonnes of RDF per hour (which is 30-40% of MSW by mass) depending on the quality of MSW. The calorific value of the produced RDF is taken as 2,500 kcal/kg, as recommended by the Central Electricity Regulatory Commission (CERC, 2015). Table 1 indicates that processing 166.66 tonnes per hour of raw MSW (or burning 49.9 to 66.6 tonnes of RDF in the incinerator) can produce 36 - 48 MW_e of gross power output. In other words, it can be said that the plant will use 3.4 - 4.5 tonnes of MSW per hour to produce 1 MW_e of power.

Table 1: MSW treated and RDF burned per hour for 1MW_e gross power output

	Raw MSW	***RDF (@ 30% MSW)***	***RDF (@ 40% MSW)***
Fuel used per hour (kg/hr)	*166,666*	*49,998*	*66,664*
Calorific value (kcal/kg)	*800-1,000*	*2,500*	*2,500*
Thermal Energy in fuel used per hour (MW_{th}/hr)	*155.0-193.3*	*145.3*	*193.8*
Gross electricity (MW_e) @ 25% efficiency	-	*36.3*	*48.4*
Fuel processed/burned per hour for producing 1 MW of power ($tMW_e^{-1}hr^{-1}$)	*3.4-4.5 (processed)*	*1.37 (burned)*	*1.37 (burned)*

5. Capital requirements and cost of electricity

The CERC collected data on the existing WTE projects in India to calculate the capital cost requirements for WTE projects. The capital cost of the existing WTE plants ranges between £1 to 2.9 million per MW_e. Some of these costs also include the cost incurred in pre-processing of the MSW to produced RDF. Several other regional authorities such as Madhya Pradesh Electricity Regulatory Commission (MPERC) and Gujarat Electricity Regulatory Commission (GERC) also provided similar capital cost estimates for WTE plants.

In MSW-based WTE projects, the raw MSW used as fuel is supplied free of cost by the local municipalities. Therefore, the operation and maintenance (O&M) expenses mainly involve labour, insurance, consumables, repair and statutory expenses only, and are considered to be 5% of the capital cost with an escalation of approximately 5 to 5.72% per annum. The repair, maintenance and spares cost is 15% of the total O&M cost. On the proposed normative capital cost of £1.7 million/MW_e for MSW based projects, the proposed normative O&M expenses works out to £86,200/MW_e for the year 2015-16. The fixed cost involves O&M cost, Depreciation, Interest on Term Loan, Interest on Working Capital and Return on Equity, and it comes out to be 25 - 26% of the total capital cost. A levelised cost of electricity of £0.078/kWh has been calculated by CERC for MSW-based WTE projects.

In RDF-based WTE plants, the RDF fuel is either purchased from an external supplier or produced by the WTE plant operator at the same or a different site. The RDF, if purchased, currently costs about £20/tonne. The fixed O&M cost for an RDF-based WTE plant is the same as that for MSW-based plant, i.e. 5% with an escalation of 5.72%. On the proposed normative capital cost of £1.03 million/MW_e for RDF based projects, the proposed normative O&M expenses works out to £51,700/MW_e for the year 2015-16. The fixed cost per annum for RDF projects is approximately 27.5 - 28.5% of the total capital cost. A levelised cost of electricity of £0.0106/kWh was estimated by CERC for RDF-based WTE projects.

6. Funding model for the project

BOOT (build, own, operate, transfer) is a public-private partnership (PPP) project model in which a private organisation conducts a large development project under contract to a public-sector partner, such as a government agency. A BOOT project is often seen as a way to develop large public infrastructure projects with private funding. Most of WTE projects in India have been based on this BOOT model and have been running successfully. It is thus the only proven financial model for such WTE projects in developing countries like India.

7. Key issues and mitigating factors

The WTE in India is perceived as "wealth from waste" since such projects had run successfully in many developed countries (The Economic Times, 2018). Articles published in newspapers described WTE as a gold mine (World Economic Forum, 2017). Such statements caused many businesses and investors in India to rush into the WTE business without full knowledge of the reality and key local factors. The first WTE plant in India was setup in 1987 at Timarpur, Delhi which failed primarily because of poor quality of MSW used as fuel in the plant (GAIA 2016, Dhamija 2013). Since then, the WTE projects have produced mixed results in India (Joshi and Ahmed, 2016). There are no proven examples of successful WTE projects in India and the initial plants faced many failures. The critical factors of failure and mitigating factors of WTE projects in India are summarise in Table 2.

Table 2: A summary of the causes of failures/pitfalls for WTE project in India and their possible mitigating factors.

Cause of Failure/Pitfalls	Cause	Possible Mitigating Solutions
Omitting pre-processing MSW before incineration	Technical	• Sorting of waste to remove non-combustible components • Pre-processing to produce RDF as the fuel

Underestimated electrical tariffs by bidders	Economic	• Minimum tariff recommended by the CERC should be agreed to allow for effluent treatment and viability • Tariff for tri-generation can certainly supplement the revenues for the operator • Offer gate-fees for receiving the waste at the plant
Defective tendering system – based on lowest electricity unit price only	Economic	• Careful screening of bids for financial viability • Consider WTE plants as primarily waste management sites and not power plants
Abuse of government grants	Policy	• Revoke up-front government grants • Offer performance/output-based grants to encourage operation and support genuine bidders/operators
Arbitrary and unpredictable one-sided changes from regulators, e.g. stricter emission limits	Policy	• Contract should allow a revision of tariff for electricity if emission limits are changed after the plant is built. • Else, the government should offer a grant or subsidy to support the operator • Plants should be designed from start to comply with the EC Waste Incineration Directive which imposes the strictest emission limits
Fluctuations in carbon credit prices	Economic	• Financial model should not include revenues from volatile streams like carbon credits but on steady and reliable outputs like power, hot water and cooling
NIMBY syndrome and public propaganda	Social	• Early public engagement • Use of an industrial land for the plant site • CSR fund could be used to build a visitor centre and invite public to learn about the MSW processing and its environmental benefits
Conflicts of interests	Social	• Careful planning, dumping legislation and monitoring of the operator and contractors.

Acknowledgments

The authors are grateful to Mr A.K. Gupta, Director (Electrical) and Mr Manuj Singhal, CEE (Planning) of Delhi Metro Rail Corporation (DMRC) and the Ministry of Urban Development, India for funding this work. The authors would like to express their special gratitude to Mr Khandelwal of East Delhi Municipal Corporation for sharing their experience of operating WTE projects in India.

References

1. CERC. (2015). Central Electricity Regulatory Commission of India. Available at http://www.cercind.gov.in/2015/draft_reg/Noti11.pdf. (Accessed on 7 February 2018).
2. Costa I., Massard G., and Agarwal A. (2010). Waste management policies for industrial symbiosis development: case studies in European countries. Journal of Cleaner Production. 18(8): p. 815-822.

3. Dhamija U. (2013). Sustainable municipal solid waste management in a capital city territory and the role of waste to energy: a study of Delhi. WIT Transactions on Ecology and The Environment, (179). Available at https://www.witpress.com/elibrary/wit-transactions-on-ecology-and-the-environment/179/25290.
4. Dube R et al. (2013). Status Paper on Utilisation of Refuse Derived Fuel (RDF) in India. Indo-German Environment Partnership: New Delhi, India
5. GAIA, (2016). The Timarpur-Okhla Waste to Energy Venture. Available at http://www.no-burn.org/wp-content/uploads/Timarpur.pdf. (Accessed on 7 February 2018).
6. Hindustan Times[a]. (2 September 2017). Delhi's Ghazipur landfill collapse: 2 dead as mountain of trash sweeps many into nearby canal. Available at https://www.hindustantimes.com/delhi-news/ghazipur-landfill-site-collapses-in-east-delhi-one-dead-many-fear-trapped/story-oSqDJtp4zqrB0yHOWCER9J.html. (Accessed on 9 February 2018).
7. Hindustan Times[b]. (1 September 2017). Ghazipur landfill collapse in Delhi was a tragedy waiting to happen. Available at https://www.hindustantimes.com/delhi-news/ghazipur-landfill-site-collapse-why-it-was-a-tragedy-waiting-to-happen-in-delhi/story-8sUu69iu1JsHYNzE6OY22N.html. (Accessed on 9 February 2018).
8. Hoornweg D. and Bhada-Tata P. (2012). What a Waste: A Global Review of Solid Waste Management. Urban development series - knowledge papers no. 15. Washington, DC: World Bank.
9. Liu, Y et al. (2017). Greenhouse gas emissions from municipal solid waste with a high organic fraction under different management scenarios. Journal of Cleaner Production. 147 (Supplement C): p. 451-457.
10. Lu, J.-W et al. (2017). Status and perspectives of municipal solid waste incineration in China: A comparison with developed regions. Waste Management, 69(Supplement C): p. 170-186.
11. Lukumon O.O., et al. (2013). Reducing waste to landfill in the UK: identifying impediments and critical solutions. World Journal of Science, Technology and Sustainable Development, 10 (2): p. 131-142.
12. MCD, Municipal Corporation of Delhi. (2004). Feasibility study and master plan for optimal waste treatment and disposal for the entire state of Delhi based on public private partnership solutions. Available at http://www.seas.columbia.edu/earth/wtert/sofos/COWI_Waste_Characterization_Study.pdf (Accessed on 7 February 2018).
13. MoUD, Ministry of Urban Development. (2016). Swachh Bharat Mission, Municipal Solid Waste Management Mannual Part I. Available at: http://indiawashforum.com/wp-content/uploads/2016/06/Book-1.pdf (Accessed on 7 February 2018).
14. Nakakubo T., Yoshida T, and Hattori Y. (2017). Analysis of greenhouse gas emission reductions by collaboratively updating equipment in sewage treatment and municipal solid waste incineration plants. Journal of Cleaner Production, 168(Supplement C): p. 803-813.
15. The Economic Times, (2018), How to make Waste-to-Wealth a reality. Available at https://economictimes.indiatimes.com/industry/energy/power/how-to-make-waste-to-wealth-a-reality/articleshow/62490388.cms (Accessed on 30 January 2018).
16. World Economic Forum, (2017), Landfill mining: is this the next big thing in recycling? Available at https://www.weforum.org/agenda/2017/06/landfill-mining-recycling-eurelco/ (Accessed on 7 February 2018)
17. Joshi R., Ahmed S. (2016). Status and challenges of municipal solid waste management in India: A review, Cogent Environmental Science. 2(1). 1139434 . (DOI: http://dx.doi.org/10.1080/23311843. 2016. 113943)

Nottingham | UK | 9–11 September 2019

Review of Waste Heat Utilisation from Data Centres

Ramamoorthy Sethuramalingam, Abhishek Asthana, Peter Weston

Hallam Energy, Sheffield Hallam University, Department of Engineering and Mathematics, United Kingdom

r.sethuramalingam@shu.ac.uk

Abstract

Rapidly increasing global internet traffic, mobile internet users and the number of Internet of Things (IoT) connections are driving exponential growth in demand for data centre and network services, which in turn is driving their electricity demand. Data centres now account for 3% of global electricity consumption and contribute to 4% of the global greenhouse gas emissions. This study discusses the potential of reusing the waste heat from data centres. An overview of imbedding heat recovery systems into data centres is presented. The implications of economic cost and energy efficient heat recovery systems in data centre buildings are also discussed. The main problems with implementing heat recovery systems in existing data centre designs are (i) high capital costs of investment and (ii) low temperatures of the waste heat. This study suggests alternatives that could allow data centre operators to utilise waste heat with more efficiencies. It also discusses how liquid-cooled data centres can be more efficient in utilising their waste heat than the air-cooled ones. One possible solution suggested here is that data centre operators can decrease their environmental impact by exporting waste heat to the external heat networks. The barriers in connecting datacentres to heat networks are discussed and suggestions to overcome those barriers have been provided.

Keywords: Data centres, District heating, Waste heat recovery, Liquid cooling, Energy efficiency.

1. Introduction

Global internet traffic has tripled since 2015 and is expected to further double by 2022 to 4.2 zettabytes per year (4.2 trillion gigabytes) [1, 2, 3]. The number of mobile internet users is expected to increase from 3.6 billion in 2018 to 5 billion by 2025, while the number of

Internet of Things (IoT) connections is expected to triple from 7.5 billion in 2018 to over 25 billion by 2025 [4].

Most of the world's Internet Protocol (IP) traffic goes through data centres (DCs). Greater connectivity is therefore driving up demand for data centre services and energy use (mostly electricity), with multiplying effects: for every bit of data that travels the network from data centre to end users, another 5 bits of data are transmitted within and among data centres [5]. Global data centre electricity demand in 2018 reached an estimated 198 TWh [6].

Heating and cooling in buildings and industry accounted for 50% of the total energy consumption in the Europe in 2012 [7]. Along with other industries, DCs are producing a reliable and stable waste heat source. As per a study in 2016 by Ascierto et al [8], DCs in Europe generate 56 TWh of waste heat. Thus, there is significant pressure on DC sector to reduce its energy consumption.

DC operators are thus investing heavily in low energy designs such as implementing heat recovery systems [9, 10]. DCs are using various types of cooling solutions such as Computer Room Air Handling (CRAC) and water cooled systems. Another important concern is the cost effectiveness of implementing heat recovery systems into existing DCs. The choice of correct heat recovery system is thus, very important. Using data centre cooling solutions such as air handling unit (CRAC) provide opportunity to recover up to 50% energy from its waste heat [9]. Data centre heat recovery systems have been already used by data centres in Nordic countries. High heat density and efficient heat recovery allowed these countries to remove the waste heat efficiently and utilise it in district heating in Sweden and Finland [11]. Similarly, there is huge demand for data centre heat recovery systems all over Europe. This study analyses the present cooling systems in the data centres and suggests possible approaches to utilise the waste heat in existing DCs.

2. Literature Review

There are many studies have around the energy efficiency of DCs but only a few have discussed the utilisation of waste heat recovery from DCs. Typically, all medium-sized DCs produce low temperature waste heat. The real DCs energy efficiency has evaluated by Lu et al for potential of capturing the waste heat [12]. The study found that, 97 % energy consumption can be recovered as waste heat from the data centre's total energy consumption. It showed that a DC operating at 1 MW waste heat capacity is enough to fulfil the heat demand of 60,000 m2 space. An article by Ebrahimi et al. [13] analysed the thermodynamics of ultra-low temperature waste heat recovery systems. The economic analysis of the study indicated a payback period for ultra-low temperature waste heat recovery system of 4 to 8 years. At present, the biggest barrier is high capital cost investment in low grade heat recovery systems. It is also to be noted that, operating temperature of the data centres also plays key role in energy consumption. A study by Carbo et al. noted that there is a 3% increase in the energy consumption when there is increase in the inlet water temperature for cooling [14]. Similarly, the same phenomenon was reported, where a server's energy consumption increased by around 11 % when using an advanced microchip device. This indicates that there should always be a balance between server operating temperature and energy consumption. The possibility of using the DCs waste heat in London city District Heating (DH) has been discussed by Davies et al. [15]. The study predicted a profit of £875,000/year for 3.5 MW waste heat from a DC. Many studies forecast enormous saving in energy spend along with low payback periods, even though it is difficult to utilise the low-grade waste heat in the commercial market. However, these studies rarely discuss the actual possibilities and practicalities of utilising the data centre waste heat. Implementing the waste heat recovery system in the DCs can be quite complicated due to various logistical and economic factors. This study will discuss a systematic approach to analysis the waste heat recovery from a real DC.

3. Methodology

The potential for waste heat utilisation is evaluated by conducting a literature review on:

- Measuring energy efficiency
- Cooling technologies available for DCs
- Utilisation of waste heat
- Barriers in utilising the waste heat

The potential for waste heat utilization from DCs was analysed by conducting a literature review on cooling technologies and solutions for waste heat utilisation. The methodology behind analysing energy efficiency metrics, the economic and emission analysis, and systematic change process for adapting to waste heat utilisation are presented below. Parssinen (2016) analysed 20 metrics includes six different energy-efficiency domains with consumption, seven technology domains and overlay metrics.

Waste heat utilisation economics in DH are based on the assumption that waste heat will replace both solid fuel CHP and heat-only boiler (HOB) production in the DH network. Variable costs of heat production are determined the increased costs of electricity consumption due to Heat Pumps (HP), reduction in fuel utilisation for CHP and HOB and the capital investment for HPs. Income loss from export of electricity from CHP was also considered.

3.1 Measuring energy efficiency

The ideal objective for a DC is to become a net-zero energy building (NZEB). In NZEB, servers are included in the overall energy plan of the building. DC energy contributes to the energy demand in advanced energy efficient buildings. DC operators should establish project targets for energy reuse effectiveness (ERE). Better ERE reduces the renewable energy requirements of the building [16].

ERE and power usage effectiveness (PUE) by themselves are not sufficient for engineering analysis purposes [17]. Additional metrics required include return temperature index (RTI), power density efficiency (PDE), performance per watt (PPW), workload power efficiency (WPE), network power usage effectiveness (NPUE), data center workload power efficiency (DWPE), fixed to-variable energy ratio (FVER), supply heat index (SHI), return heat index (RHI), system power usage effectiveness (sPUE), and data center energy productivity (DCeP). These metrics provide a more complete view of DCs energy usage and is used for energy efficiency optimisation and equipment selection.

PUE and ERE are most common ways to evaluate the energy usage effectiveness and energy reuse in the DCs. PUE is defined as the total annual energy divided by the total annual energy used in the IT [16]. PUE-based metrics are not useful for DC energy analysis. The PUE variables are difficult to measure and calculate when facilities or primary equipment are shared. With energy reuse, the PUE value could go below 1.0, but this is not allowed, which is contrary to PUE definition [18]. PUE ignores IT load changes, and it does not address the DC utilization level [19].

$$\mathrm{PUE} = \frac{Total\ Energy}{IT\ Energy} \tag{1}$$

$$= \frac{Cooling + PowerDistribution + Misc + IT}{IT}\ ;\ 1.0 \leq \mathrm{PUE} \leq \infty \tag{2}$$

ERE includes the reuse of energy from a DC to PUE which must be reused outside the DC. Energy Reuse Factor (ERF) can be used to calculate ERE from the site PUE [28]. The ERE and ERF equations are;

$$\mathrm{ERE} = \frac{Total\ Energy - Reuse\ Energy}{IT\ Energy}\ ;\ 0 \leq \mathrm{ERE} \leq \infty \qquad (3)$$

3.2 Cooling Technologies in Data centres

DC cooling is an essential part of DC efficiency. For safe functioning of servers, the air temperature in the servers should be maintained at 18 to 27 °C [20]. Traditionally, DC operators have tried to maintain them as cool as possible. However, with the rising costs of cooling, the system needs to optimised for each DC individually.

Servers in DCs are packed in racks that are cooled by cold air entering from the front and hot air leaving from the back. Racks are usually arranged back-to-back to create cold and hot channels to avoiding the mixing of hot and cold airs and thus maximising the cooling efficiency. Fig. 1 shows a schematic of waste heat recovery system for a remote air-cooled DC, where waste heat is utilised in a DH network. The chilled water is pumped to the computer room air conditioner (CRAC). CRACs supply chilled air that is injected into the cold aisle via a perforated and raised floor. Waste heat is recovered from the hot aisles through ventilation or redirected to the CRAC. The collected waste heat can go through different stages, e.g., an evaporator and condenser and subsequently a HP to be able to be used in the reuse application (e.g., the DH network) [21].

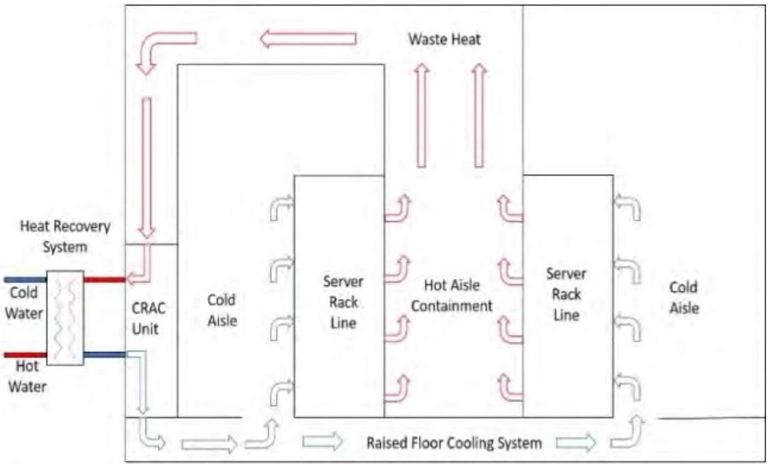

Figure 1: Typical hot aisle air containment system in data centre with heat recovery system.

3.3 Utilisation of waste heat:

Modern cooling technologies such as liquid cooling increase the efficiency of heat recovery although it could equally be utilised from air-cooled DCs. DCs are beginning to capitalise on waste heat, but the scale of utilisation is still rather small considering its economic potential. This section discusses how and where waste heat could be utilised.

The main considerations in waste heat utilisation are the proximity of heat demand and profitability. The amount and quality of waste heat, and the profitability, depend a lot on the choice of cooling technologies.

The best points for heat recovery are summarised in [10] and [15]. The best points in air-cooled servers are at the return of air flow to the CRAC where heat can be captured between 25 and 35°C, whereas liquid cooling can capturing it at 50–60°C due to capturing it closer to the central processing units (CPUs) and other components, which are hotter (up to 85 °C). The higher specific heat capacities of liquids allow circulating water temperature to be set close to 60°C without compromising CPU performance. This eliminates the need for chillers and CRACs [9] and can increase processor performance by 33% compared to air-cooled systems [22, 23]. Waste heat could also be captured in the chilled supply water as cold as 10–20°C [15].

HPs could be used in DCs to upgrade the waste heat temperatures up to 95°C which would make it useful for many other processes (e.g DH networks). HPs in DCs have typical COP values of 2 to 7, depending on the number of cycles and the temperature [15]. Increased electricity consumption in HPs decreases the PUE value of the system but by utilising the waste heat, it decreases the ERE value and improves the energy efficiency of the DC.

Various uses for waste heat exist, e.g. small-scale and location-specific solutions (e.g., heating swimming pools) do not require heavy investments as compared to large-scale installations e.g. connection to a DH network. Different applications for waste heat have been studied comprehensively, for example, in [9] for internal and external uses.

Some DC projects with waste heat utilisation in Nordic countries are summarised in Table 1

Table 1: DC Projects with Waste Heat Utilisation in Nordic Countries [21]

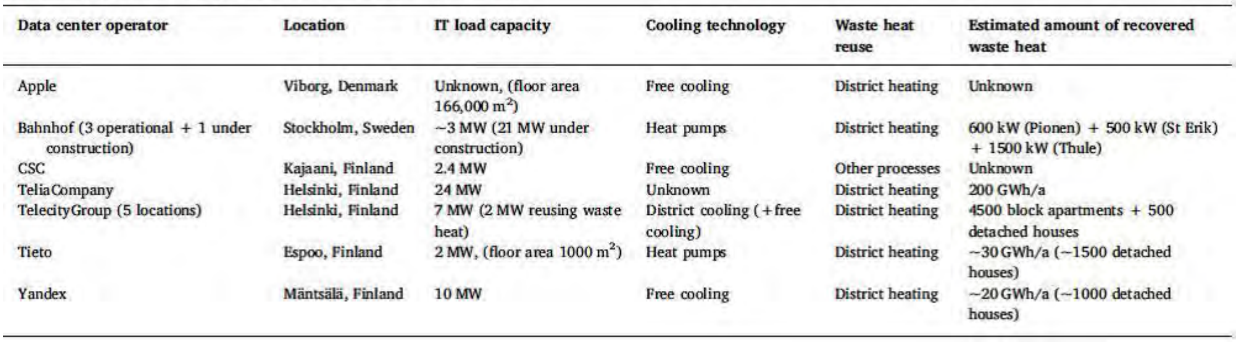

Data center projects considering waste heat utilization in the Nordic countries.

Data center operator	Location	IT load capacity	Cooling technology	Waste heat reuse	Estimated amount of recovered waste heat
Apple	Viborg, Denmark	Unknown, (floor area 166,000 m^2)	Free cooling	District heating	Unknown
Bahnhof (3 operational + 1 under construction)	Stockholm, Sweden	~3 MW (21 MW under construction)	Heat pumps	District heating	600 kW (Pionen) + 500 kW (St Erik) + 1500 kW (Thule)
CSC	Kajaani, Finland	2.4 MW	Free cooling	Other processes	Unknown
TeliaCompany	Helsinki, Finland	24 MW	Unknown	District heating	200 GWh/a
TelecityGroup (5 locations)	Helsinki, Finland	7 MW (2 MW reusing waste heat)	District cooling (+free cooling)	District heating	4500 block apartments + 500 detached houses
Tieto	Espoo, Finland	2 MW, (floor area 1000 m^2)	Heat pumps	District heating	~30 GWh/a (~1500 detached houses)
Yandex	Mäntsälä, Finland	10 MW	Free cooling	District heating	~20 GWh/a (~1000 detached houses)

3.4 Barriers for waste heat utilisation:

The main barriers limiting the utilisation of waste heat are studied in [10] and [24] and can be categorised as follows:

- Low-quality heat and lack of heat demand
- Seasonal variations in demand
- Need for ancillary heat production
- High investment costs and inconvenient infrastructure
- Differing financial outcome expectations of DC and DH operators
- Information security and reliability
- Business models and mutual contracts
- Thermodynamic limitations

5. Conclusions

There is enormous potential for waste heat utilisation from DCs. The barriers for waste heat utilisation are not technical but rather a lack of solutions for DC operators on profitability due to seasonal demand variations and capital costs due to an absence of established and transparent business models of selling waste heat to DH companies. Awareness of energy-related costs must reach decision-makers in the ICT field. A standard way of measuring energy efficiency and waste heat potential needs to be established. In addition, there needs to be sufficient activities from government regulation and legislative enforcement to further enable transformation towards energy efficiency and waste heat utilisation. ERE and PUE values are symptoms of actions. In order to understand the causes and actions required, more detailed energy efficiency metrics, such as those suggested in this article, are required.

Acknowledgments

This work is sponsored by Innovate UK under KTP Programme No KTP011150 and Impetus Enclosure Systems (Orion).

References

1. Cisco (2015) "The History and Future of Internet Traffic", , https://blogs.cisco.com/sp/the-history-and-future-of-internet-traffic.
2. Cisco (2018) Cisco Global Cloud Index: Forecast and Methodology, 2016–2021., , https://www.cisco.com/c/en/us/solutions/collateral/service-provider/global-cloud-index-gci/white-paper-c11-738085.pdf.
3. Cisco (2019) Cisco Visual Networking Index : Global Mobile Data Traffic Forecast Update , 2017 – 2022., , https://www.cisco.com/c/en/us/solutions/collateral/service-provider/visual-networking-index-vni/white-paper-c11-738429.pdf.
4. GSM Association (2019) The Mobile Economy, https://www.gsmaintelligence.com/research/?file=b9a6e6202ee1d5f787cfebb95d3639c5&download.
5. Cisco (2016) "Cisco Global Cloud Index 2015-2020 - Cisco Knowledge Network Session".
6. Masanet, E. R. et al. (2018), Global Data Center Energy Use: Distribution, Composition, and Near-Term Outlook, Evanston, IL.

7. Eurostat Statistics (Accessed August 2019) Online available in http://ec.europa.eu/eurostat/statistics-explained/index.php/Energy.
8. Ascierto R, Donoghue A, Lawrence A, Bizo D (2016) Trends in data centre technology. Research 451.
9. Ebrahimi K, Jones G, Fleisher A (2014) A review of data centre cooling technology, operating conditions and corresponding low-grade waste heat recovery opportunities. Renewable and Sustainable Energy Reviews 31: 622 - 638
10. Ebrahimi K, Jones G, Fleisher A (2015) Thermo-economic analysis of steady state waste heat recovery in data centres using absorption refrigerant. Applied Energy 139:384-397
11. Mikko W, Matti P, Jukka M, Sanna S (2017) Utilizing data centre waste heat in district heating- impacts on energy efficiency and prospects for low-temperature district heating networks. Energy 140:1228-1238.
12. Lt T, Lu X, Remes M, Viljanen M (2011) Investigation of air management and energy performance in a data centre in Finland: case study. Energy Build 43: 3360-72
13. Ebrahimi K, Jones G. Fleischer A (2017) The viability of ultra-low temperature waste heat recovery using organic Rankine cycle in dual loop data centre applications. Applied Thermal Engineering 126: 393-406.
14. Carbó A, Oró E, Salom J, Canuto M, Macías M, & Guitart J (2016) Experimental and numerical analysis for potential heat reuse in liquid cooled data centres. Energy Conversion and Management 112: 135-145.
15. Davies G, Maidment G, Tozer R (2016) Using data centres for combined heating and cooling: an investigation for London. Applied Thermal Engineering 94:296–304.
16. Patterson M, Tschudi W, VanGeet O, Azevedo D (2011) Towards the net-zero data centre: development and application of an energy reuse metric. ASHRAE 117:10–7.
17. Pärssinen M (2016) Analysis and forming of energy efficiency and green it metrics framework for sonera helsinki data centre hdc master's thesis espoo, Aalto University.
18. Uddin M, Alsaqour R, Shah A, Saba T (2014) Power usage effectiveness metrics to measure efficiency and performance of data centers. Applied Mathematics and Information Science 8 :2207–16. http://dx.doi.org/10.12785/amis/080514
19. Fiandrino C, Kliazovich D, Bouvry P, Zomaya A (2015) Performance and energy efficiency metrics for communication systems of cloud computing data centers. IEEE Transactions on Cloud Computing Volume 5: 738.
20. ASHRAE (2011) Thermal Guidelines for Data Processing Environments – Expanded Data Centre Classes and Usage Guidance. [accessed 30 August 2019].
21. Mikko Wahlroos, Matti Pärssine, Samuli Rinne, Sanna Syri, Jukka Manner (2018) Future views on waste heat utilization - Case of data centres in Northern Europe. Renewable and Sustainable Energy Reviews 82:1749 -1764.
22. Finnish Energy Industries (2006) Kaukolämmön käsikirja .In Finnish, District Heating Handbook, Helsinki.
23. Ellsworth M, Iyengar M (2009) Energy efficiency analyses and comparison of air and water cooled high performance servers. Proceeding of ASME Inter Conference San Francisco, USA. 19-23.
24. Linna O (2016) Kansainvälinen katsaus datakeskusten hukkalämmön hyödyntämiseen, In Finnish, Global overview on data center waste heat utilization. Bachelor's thesis Espoo, Finland, Aalto University.

Nottingham | UK | 9–11 September 2019

SMART VISION WALLET

A. Dr.Susan Augustine [1], B. Dr.J.P Ananth [2], C. Dr.S.Balakrishnan[3]

[1]Anna University, Associate Professor/CSE,Sri Krishna College of Engineering and Technology, Coimbatore,Tamil Nadu,India

[2]Anna University, Professor/CSE,Sri Krishna College of Engineering and Technology, Coimbatore,Tamil Nadu,India

[3]Anna University, Professor /IT,Sri Krishna College of Engineering and Technology, Coimbatore,Tamil Nadu,India

rsusanaugustine@gmail.com

Abstract

In a developing country like India around 26.8 million people are differently abled. In this population around 50 percentage of the differently abled people are identified with vision problems which tops the list and following with a 5 percentage of people with hearing disability and 3 percentage of deaf blindness.[1]

There is very less awareness about deaf blindness and so till date their needs were not addressed by any inventions. In a day to day life of visually impaired person, money management is a vital part of living independently. Our work aims at easing the task of money management by concentrating on two major phases concerned with money management task, identifying the denominations of currency notes and detecting counterfeit currency notes. The solution to these addressed problems in money management is a Smart Eye Wallet which is an accurate solution for money management in an efficient and common man approach. This is easily portable and easy to use and which does not reveal people their disability in a common place or in midst of a crowd. This would equip them with the necessary attitude to confront life and be successful.

Keywords: sensors, Currency,Bluetooth,counterfeit,android application

1. Introduction

The Smart-Eye Wallet is a simple and efficient money counter and a counterfeit detector designed to be used by the visually impaired and the hearing impaired community. Most of the machines use an LCD display to notify their users the sum of the counted money or that a fake currency has been detected, which makes it nearly impossible for the visually impaired community to use them. Moreover, such a device is costly and carrying it is difficult and uncomfortable without modification.

1.2 Indian Currency Security Features

(i) Watermark

On the obverse side of Rs.100, Rs.50 and Rs.20 notes, a vertical band on the right side of the Mahatma Gandhi's portrait contains a latent image showing the respective denominational value in numeral. The latent image is visible only when the note is held horizontally at eye level.[5]

Figure 1.2.1: Watermark in a twenty rupee note

(ii) Latent Image

On the obverse side of Rs.100, Rs.50 and Rs.20 notes, a vertical band on the right side of the Mahatma Gandhi's portrait contains a latent image showing the respective denominational value in numeral. The latent image is visible only when the note is held horizontally at eye level.[5]

Figure 1.2.2: Latent image in one hundred rupee note

(iii) Microlettering

This feature appears between the vertical band and Mahatma Gandhi portrait. It contains the word „RBI" in Rs.5 and Rs.10. The notes of Rs.20 and above also contain the denominational value of the notes in microletters. This feature can be seen better under a magnifying glass.[5]

Figure 1.2.3: Microlettering in a ten rupee note

(iv) Intaglio printing

The portrait of Mahatma Gandhi, the Reserve Bank seal, guarantee and promise clause, Ashoka Pillar Emblem on the left, RBI Governor's signature are printed in intaglio i.e. in raised prints, which can be felt by touch.[5]

Figure 1.2.4: Intaglio printing in one hundred rupee

(v) Identification mark

A special feature in intaglio has been introduced on the left of the watermark window on all notes except Rs.10 note. This feature is in different shapes for various denominations and helps the visually impaired to identify the denomination.[5]

(vi) Fluorescence

Number panels of the notes are printed in fluorescent ink. The notes also have optical fibres. Both can be seen when the notes are exposed to ultra-violet lamp.[5]

Figure 1.2.5: Fluorescent ink in a fifty rupee note

(vii) See through register

The small floral design printed both on the front (hollow) and back (filled up) of the note in the middle of the vertical band next to the watermark has an accurate back to back registration. The design will appear as one floral design when seen against the light.[5]

Figure 1.2.6: See through register in one hundred rupee note

2. Purpose of the System

The embedded system known as the smart eye wallet is solely created with the desire to assist the blind community to live along the others in their community with an equal footing. The device is fashioned into the shape of a common wallet. It doesn"t exactly weigh more than any wallet. It works by placing the currency note into the wallet, after pressing a button in the wallet; the devices within the wallet will scan the currency for its denomination. It will also on check if the currency is original or counterfeit. The output will be given via vibration; a vibration pattern is assigned for each currency denomination, or through audio output, as it can be connected to android devices via Bluetooth. An android app is also developed that will work along this system, it will also provide User Interface in scanning the currency or finding the total currency that is scanned previously.

Obviously, this system doesn't exactly require much effort on the user's side. The only effort that the user will have to spend is on placing the currency, pressing the button in the device or pressing the button in the GUI interface of the android app.

Such a device will give the visually impaired independence in finding the money. It will eliminate the need of another person's help in finding the currency denomination for the blind. As the device is designed a discreet fashion and the information for the currency is produced in a subtle manner, the device will provide the user with adequate privacy. Due to the device's portability and ability to differentiate counterfeit noise, the device is also useful for everyone

3. System Requirements

Smart Eye Wallet is a money identification device specifically designed for visually impaired and hearing impaired community. This device can effectively differentiate different denominations available on Indian economy. It also offers Counterfeit detection and have an appropriate signalling mechanism to inform the user.

3.1 Hardware Requirements

The hardware required to implement Smart Eye Wallet are,

1. Arduino Uno development board
2. TCS 3200 Colour sensor
3. UV LEDs
4. HC- 05 Bluetooth Interface
5. Vibration motor
6. Android Mobile

3.2 Software Requirements

The software that are made use for the implementation of the Smart Eye Wallet are

1. Arduino IDE
2. MIT App Inventor

4. System Design

This outlines the design of Smart Eye Wallet. Smart Eye Wallet is a money counter and counterfeit identifier that is designed to be used by the visually impaired and the hearing impaired community.

The purpose of this system design is to provide a detailed description on how the Smart Eye Wallet is constructed. The system design document has been created to ensure that the design of the Smart Eye Wallet meets the specifications mentioned in the requirements phase of this project. This describes the architecture, hardware and software of the system.

The design of Smart Eye Wallet comprises of three modules

1. Currency differentiation
2. Counterfeit detection
3. Notification

4.1 Currency Differentiation

The currency differentiation module identifies the different denominations of the currency. There are numerous technologies and methods that achieve the same. Smart Eye Wallet is a device that has to meet two requirements which are affordability and portability. The device has to be affordable by a common person and it has to be concealed as a wallet, so its size must not exceed that of an ordinary wallet. The primary difference between the denominations of the Indian currency is its colour. And hence, the most effective and simple means to identify the denominations of Indian currency is to detect these unique difference in colour and to do that a colour sensor with great precision is required. There are numerous colour sensors available in the market.

TCS series of colour sensors are precise and detects the colours at a high resolution. TCS 3200 is a programmable clear light sensor that converts light into frequencies of primary colours of red, green and blue. It can be directly interfaced with the Arduino and programmed with relative ease. It converts light to frequency and contains an array of 8 x 8 photo diodes, of which sixteen photodiodes have red filters, sixteen have green filters, sixteen have blue filters and the rest have no filters.[3]

Arduino Uno development board is based on ATmega328P microcontroller. The board is equipped with sets of digital and analog input/output pins that may be interfaced to various expansion boards and circuits. It features serial communications interfaces, including Universal Serial Bus, which is also used for loading programs from personal computers. The ATmega328P microcontroller is programmed using a dialect of features from the programming languages C and C++. Arduino project provides an integrated development environment based on the processing language project.[6]

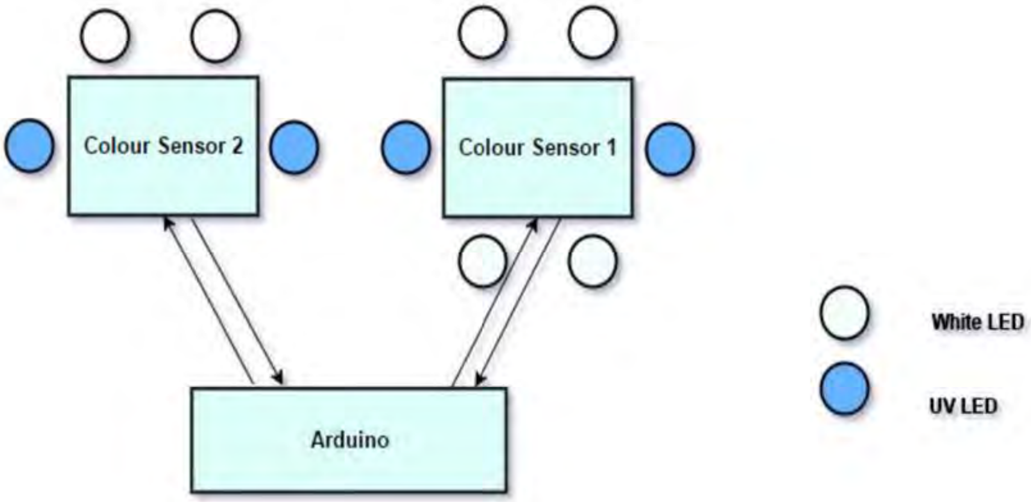

Figure 4.1.1: Design of the currency differentiating module

The design of the currency differentiating module is as shown in Figure 5.1.1. The currency is first illuminated using white LEDs. TCS 3200 will detect the colour of the reflected light, converts them to frequency values and gives them as input to the Arduino.

The currency is illuminated in the presence of UV LEDs and the same procedure is repeated. The programmed ATmega328P microcontroller using these inputs identifies the denomination.

4.2 Counterfeit Detection

This module checks the authenticity of the currency and detects whether the currency is fake or genuine. In order to do so we need to check the validity of one or more security features implemented in the Indian Currency. Smart Eye Wallet makes use of a colour sensor and a programmed ATmega328P microcontroller to identify the denomination of the currency. The addition of any module or component to the system must not jeopardize the primary objectives of the project which are affordability and portability.

Figure 4.2.1: Genuine and fake currency on UV light

In the figure 4.2.1 a genuine currency under UV light and a fake currency under UV light is shown. The genuine currency absorbs UV light and the fake reflects it. This change in the behavior of the currency note is due to the presence of fluorescent ink, optical fibres and the very nature of material used in the currency.

The figure 4.2.2 shows the design of the counterfeit detection module. The colour sensor illuminates the currency and detects the reflected light. The currency is illuminated in the presence of UV light and the colour sensor detects the intensity and composure of the reflected light and converts them to frequency values. These detections are given as the input to the programmed ATmega328P and it verifies whether the currency is authentic or not.

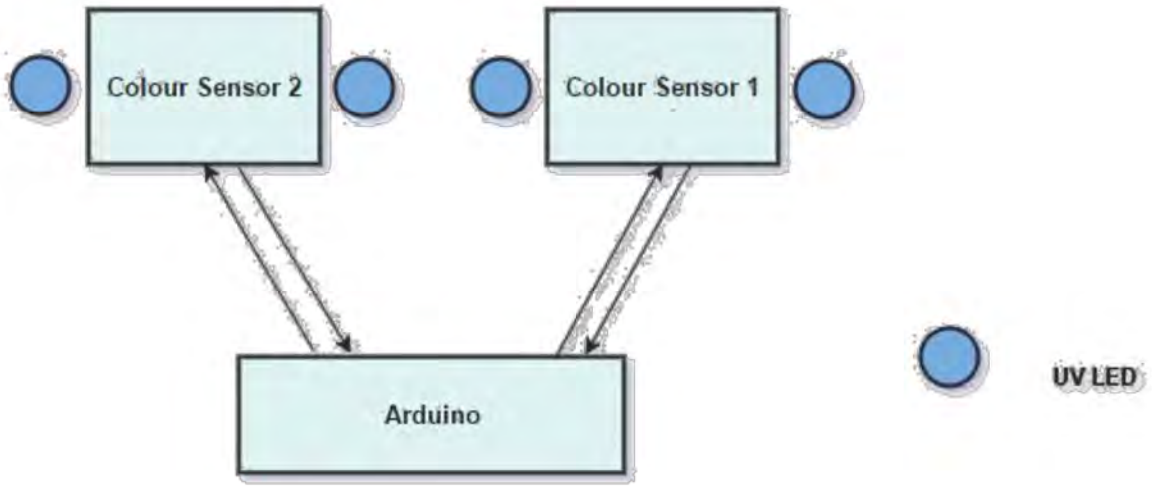

Figure 4.2.2: Counterfeit detection module

As it is seen in this design, we are not making use of any additional hardware or physical unit. The hardware required is exactly the same as the one used in the previous module. This has added advantages. The design of the system is kept simple, the cost of additional hardware is eliminated, the design workload is reduced, and the time is saved. Moreover, this design phase can be seen as another function of the currency differentiating unit. The factors taken into account for counterfeit detection are the presence of fluorescent ink, optical fibres and the very nature of the material used in the currency. These factors altogether are extremely difficult to replicate, making it a robust counterfeit detecting mechanism.

4.3 Notification

The final phase is to design how the user will be informed of the counted sum or the detected counterfeit. The Smart Eye Wallet is designed to be used by the visually impaired and the hearing impaired community. There are two ways in which the users are notified. First the denomination is announced by a pattern of tones and the second generates sequences of vibration. The sequence is different for different denominations.

The voice output is designed for the visually impaired community and the vibration output is designed for the visually and hearing impaired community as well as a privacy measure. The voice output is generated using an android app that is specifically designed for this purpose and to be used by the visually impaired.

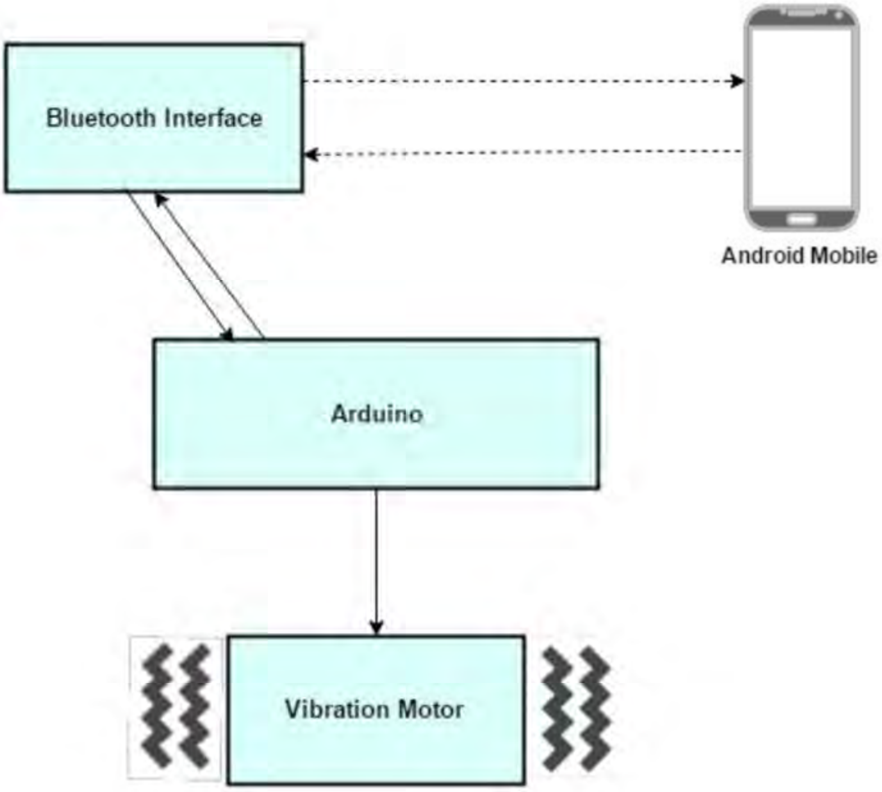

Figure 4.3.1: Design of the notification module

The figure 4.3.1 shows the design of the notification module. Designing the notification module involves the design of the Android app that acts as the interface of the Smart Eye Wallet, and the vibration sequence. The colour sensor detects the filtered and unfiltered frequency of the reflected light from the currency and feeds them to the programmed microcontroller, which identifies the denomination and sends the value to the smartphone connected to the Arduino via the HC05 Bluetooth interface as well as turns the vibration motor on and off in the specified sequence.[7]

There are seven different vibration sequence for the seven denomination of the Indian currency. A dc button type vibration motor is chosen to produce the required sequence of vibration. The vibration motor is interfaced with the Arduino using the N-type MOSFET 2N7000. The Pulse Width Modulation feature of the Arduino is used to reduce the output voltage from 5V to 3V and the 2N700 acts as a switch to turn the motor on or off.[7] The colour sensor detects the frequency of reflected light from the currency and gives the data as input to the programmed microcontroller. The Microcontroller identifies the denomination, turns on and off the dc vibration motor in the specified sequence causing the Smart Eye Wallet to vibrate. The sequence is as shown in figure 4.3.2.

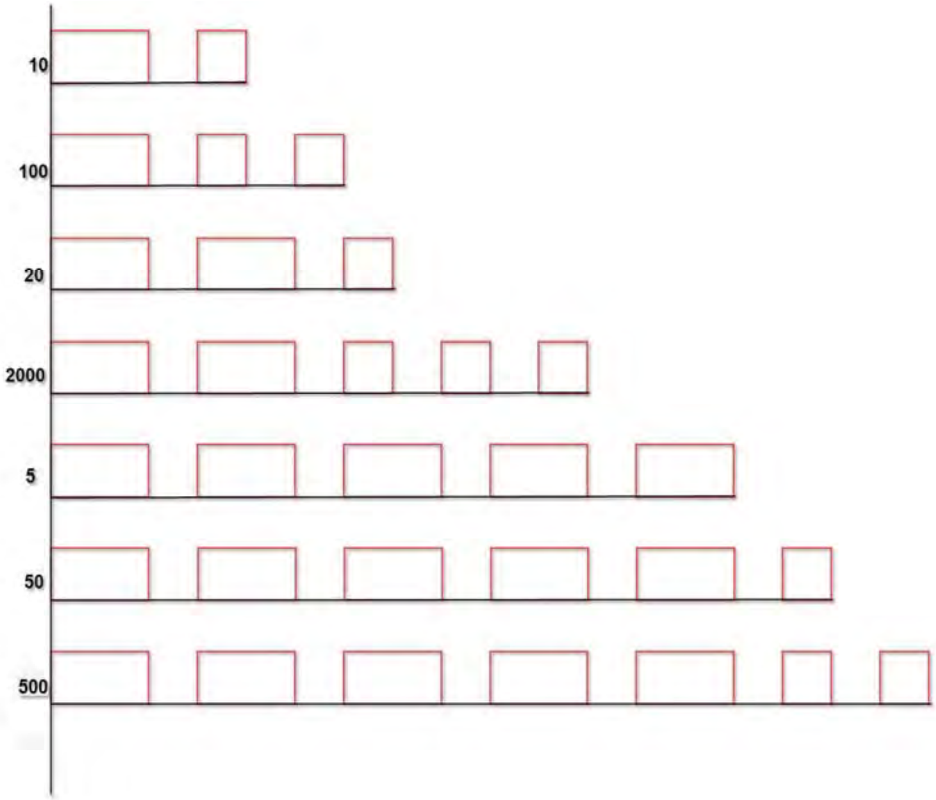

Figure 4.3.2: The different vibration sequence for different denominations

The user interface of the android app used to generate the audio output is designed in such a way that it can be used by the visually impaired community with great ease. The design of the user interface of the app is shown in figure 4.3.3.

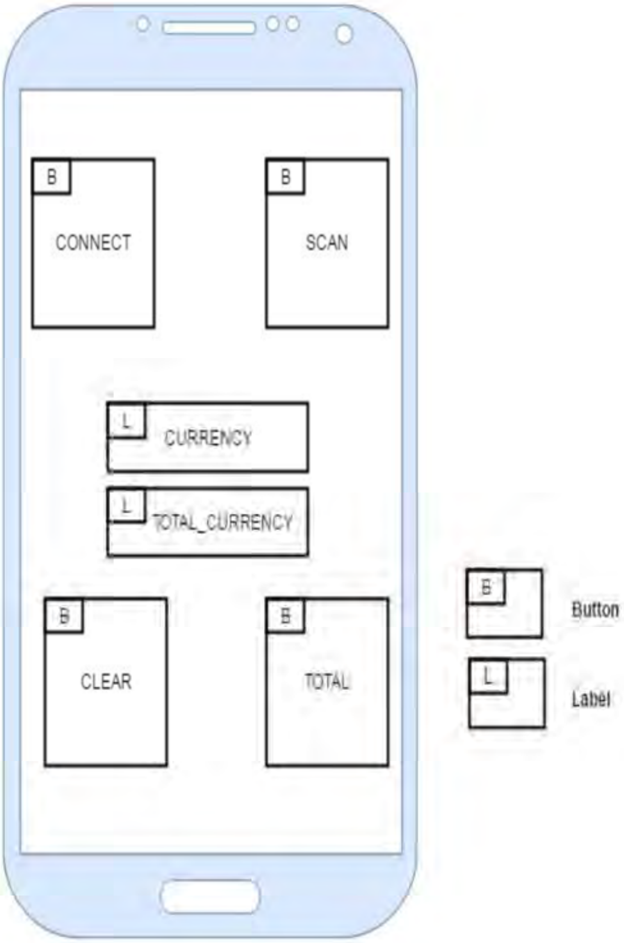

Figure 4.3.3: The user interface of the android app

The app consists of four buttons located at the four corners of the screen, this design of the app guarantees its ease of use by the visually impaired community. The four buttons are CONNECT, SCAN, TOTAL, and CLEAR. The CONNECT button is used to establish a Bluetooth connection to the device, The SCAN button is used to signal the device to begin scanning the currency. And the TOTAL button announces the computed total as a voice output. The CLEAR button clears the computed sum to zero, so that the computation of the sum can start again.[4]

The Android app itself consists of four modules. The modules are connection module, scanning module, computing module and the resetting module. The connection module handles the connection of smartphone with the Arduino, the scanning module sends the scan command to the Smart Eye Wallet, retrieves the denomination and announces it in a voice. The computational module computes the sum of the currency notes and the reset module restores the initial state of the app. [4] The activity diagram is shown in figure 4.3.4

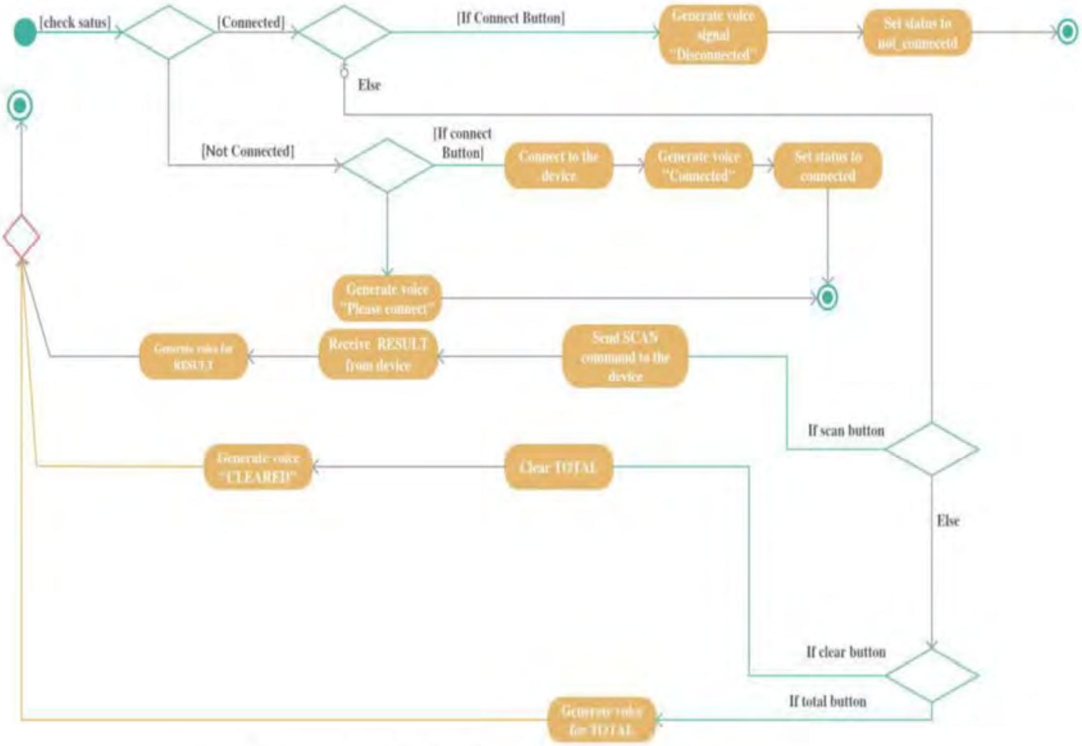

Figure 4.3.4: Android App Activity diagram

5. System Implementation

The Smart Eye Wallet comprises of three units, a currency identifier, a counterfeit detector and a notification unit. Implementing the design of the device involves the implementation of the three units in an integrated manner. The currency identifier contains a pair of TCS3200 colour sensors, six white LEDs and four UV LEDs which are interfaced directly with the Arduino. The counterfeit detector uses the same hardware and circuitry as that of the currency identifier. The notification unit has a Bluetooth interface for connecting the Smart Eye Wallet with a Smartphone, a vibration motor and an android app to act as the interface to the device. Figure 4.1 shows the implantation of the Smart Eye Wallet as a single unit.

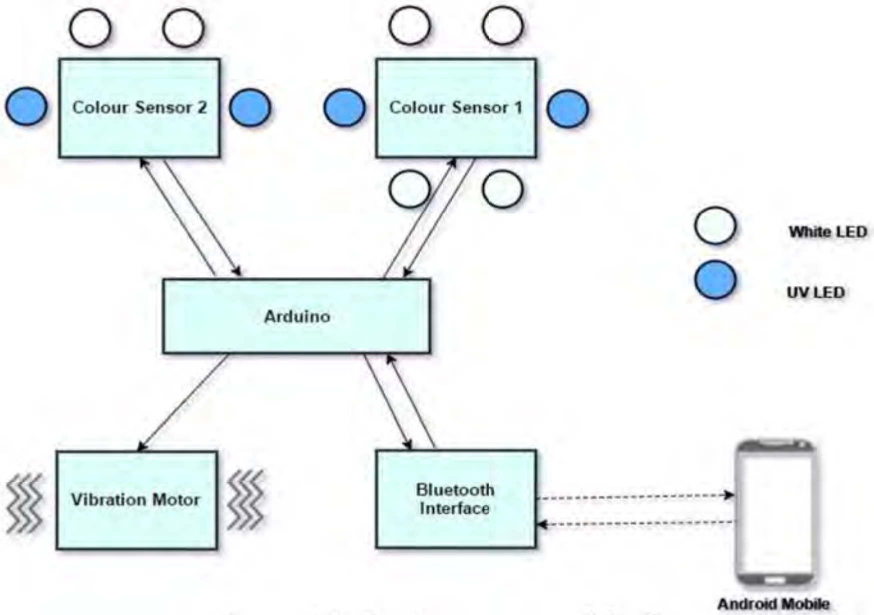

Figure 5.1: Implementation of the Smart Eye Wallet

The module used here is a three-layer multilayer perceptron consisting of two hidden layers and one output layer. The network uses the nonlinear sigmoid function as the activation function. The input layer consists of 16 different inputs, represented as 4 sets mentioned above. The first hidden layer consists of 16 perceptrons and second hidden layer consist of 28 perceptrons to differentiate the denominations. The output layer consists of total 28 perceptrons; each perceptron represents a denomination.

Indian currency presently has 7 denominations. In order to increase the accuracy of detection even further four perceptrons in the output layer represents a single currency note, each corresponding to different orientations of the same currency. The proposed multilayer perceptron for identifying the denominations of the currency is shown in figure 5.2.

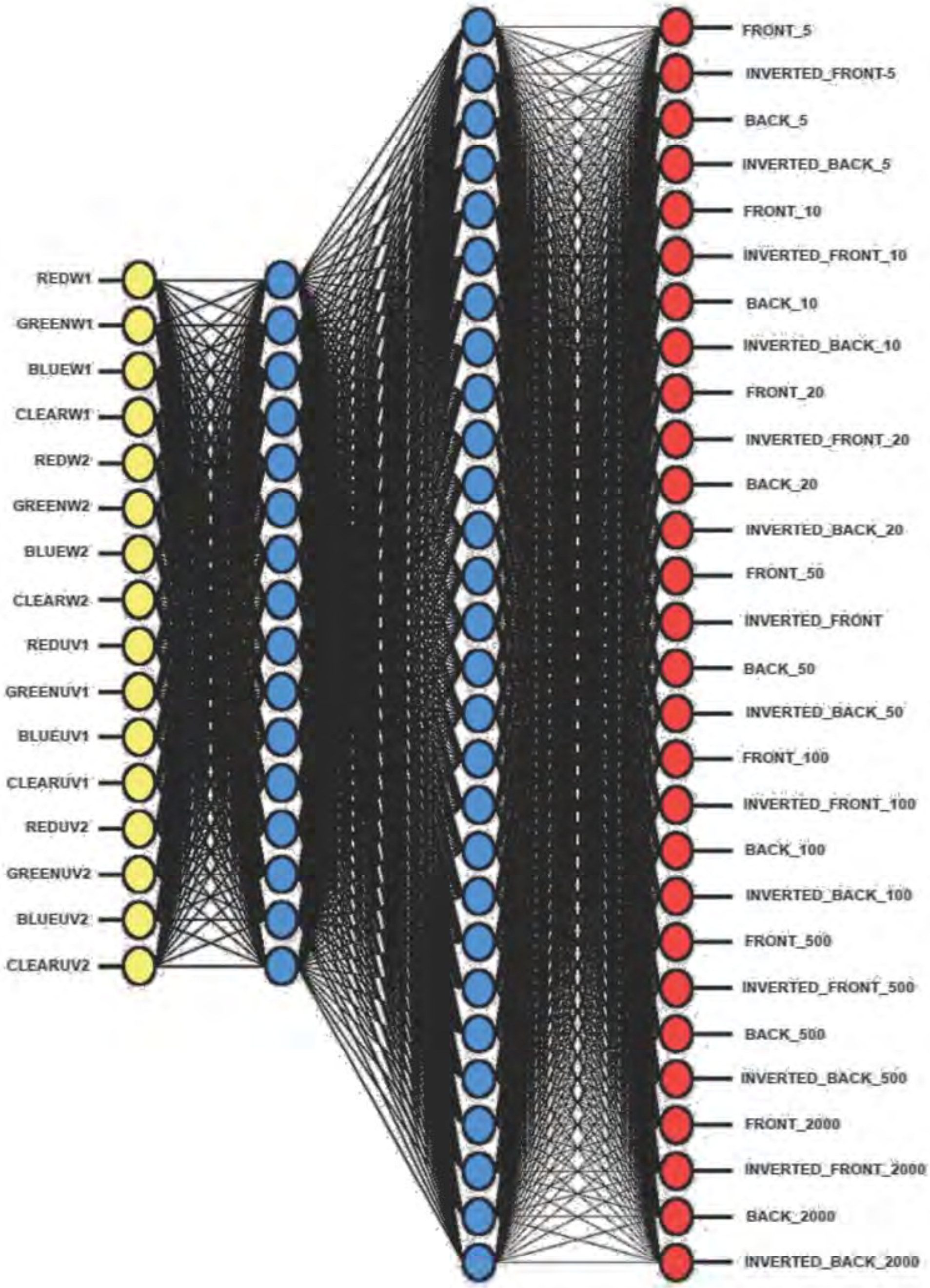

Figure 5.2: The proposed multilayered perceptron

6. Results and Discussion

The artificial neural network chosen here is the multi layered perceptron. In order to train the network, inputs from twenty-five currency notes of each denomination was chosen as the training set. The inputs from a single currency includes, the filtered and unfiltered frequency of reflected light from it when it is placed in four different orientations i.e., when the currency is placed with its front facing the sensor, when it is placed with its inverted front portion facing the sensor, when the back portion faces the sensor and when the inverted back portion faces the sensor.

After the training process was completed, currencies that was not used in the training was used as a means to test the network. The designing and training of the neural network was done with keeping in mind of the fact that there is always the probability of a visually impaired person placing the currency notes in any of the specified orientations.

Following are the graphical representations of the test set for the different denomination of the currency. 0 to 10 divisions in the x-axis shows the currency placed with its front facing the sensor, 10-20 with its inverted front portion facing the sensor, 20-30 with the back portion of the currency facing the sensor and 30-40 with its inverted back portion facing the sensor.

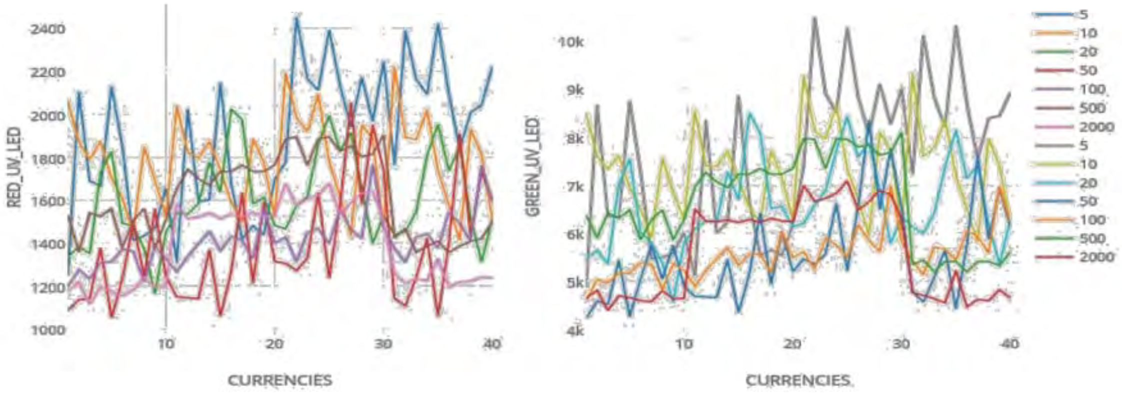

Figure 6.1: Test input of sensor 1 under white LED (RED and GREEN)

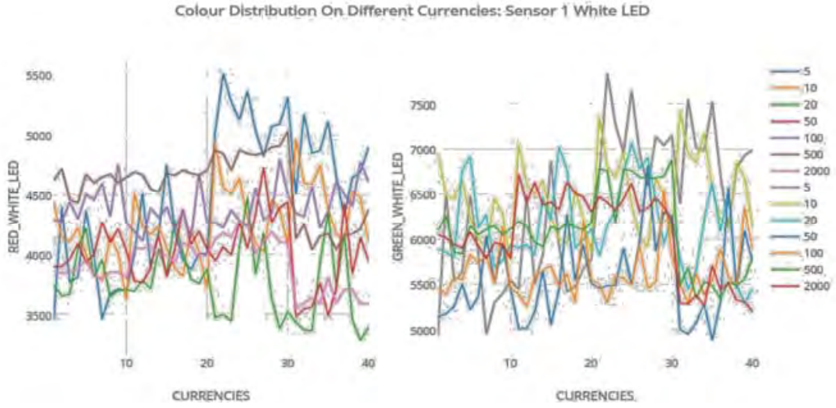

Figure 6.2: Test input of sensor 1 under white LED (BLUE and CLEAR).

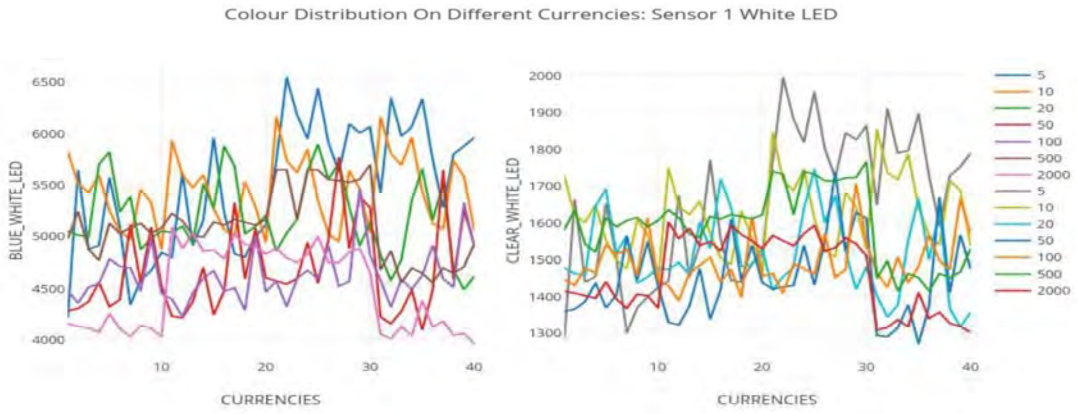

Figure 6.3: Test input of sensor 1 under UV LED (RED and GREEN)

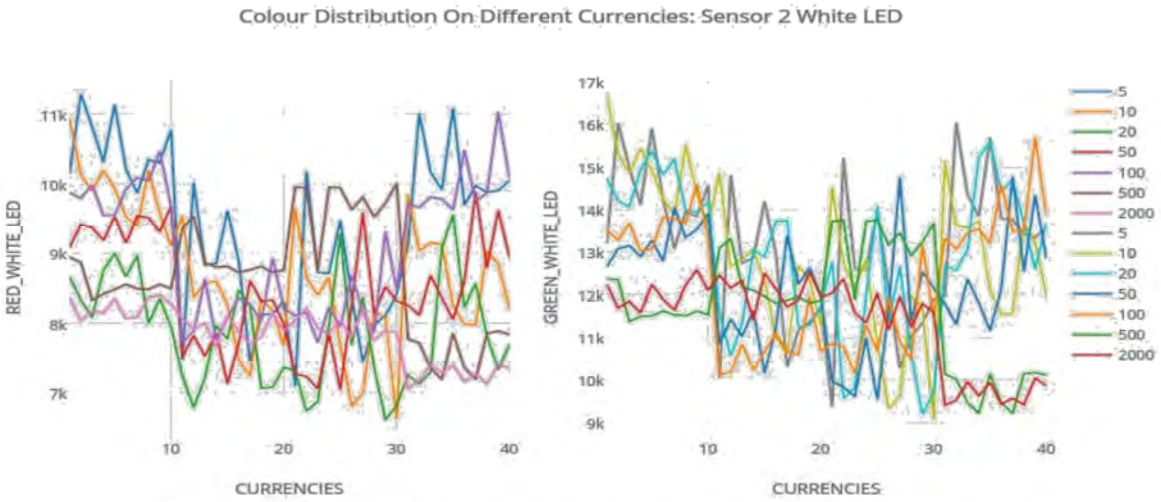

Figure 6.4: Test input sensor 2 under white LED (RED and GREEN)

6.1 Algorithm: Currency_Differentiation

1. Start
2. Read Sensor1 with White LED and store results on REDW1, GREENW1, BLUEW1 and CLEARW1.
3. Read Sensor2 with White LED and store results on REDW2, GREENW2, BLUEW2 and CLEARW2.
4. Read Sensor1 with UV LED and store results on REDUV1, GREENUV1, BLUEUV1 and CLEARUV1.
5. Read Sensor2 with UV LED and store results on REDUV2, GREENUV2, BLUEUV2 and CLEARUV2.

6. Introduce inputs REDW1, GREENW1, BLUEW1, CLEARW1, REDW2, GREENW2, BLUEW2, CLEARW2, REDUV1, GREENUV1, BLUEUV1, CLEARUV1, REDUV2, GREENUV2, BLUEUV2 and CLEARUV2 onto Neural Network and store results of each output layer into Output [] array.
7. Find the index of minimum value in the array Output [] into Currency_index.
8. Currency_no = Currency_index mod 4.
9. Return Currency_no.
10. End

6.2 Counterfeit Detection:

Counterfeit detection unit checks for the authenticity of the currency note and detects any counterfeits. This unit and the currency identifier is integrated into a single unit for the functional and design simplicity of the product. The basic principle behind the counterfeit detection is the fact that a genuine currency and a counterfeit behave differently under the UV light. The genuine currency is made of a unique material and has fluorescent ink, optical fibres in it. When UV light is shed across it, the genuine currency absorbs it while the counterfeit reflects it. The colour sensor senses the intensity and the composure of the reflected light and converts it into a frequency and is provided as the input to the programmed ATmega328P microcontroller.

This design does not make use of any additional hardware or physical unit. The hardware required is exactly the same as the one used in the previous unit. This has added advantages. The design of the system is kept simple, the cost of additional hardware is eliminated, the design workload is reduced, and the time is saved. The factors taken into account for counterfeit detection are the presence of fluorescent ink, optical fibres and the very nature of the material used in the currency. These factors altogether are extremely difficult to replicate, making it a robust counterfeit detecting mechanism. The Figure 5.2.1 shows the difference between frequency values for the genuine and fake currency.

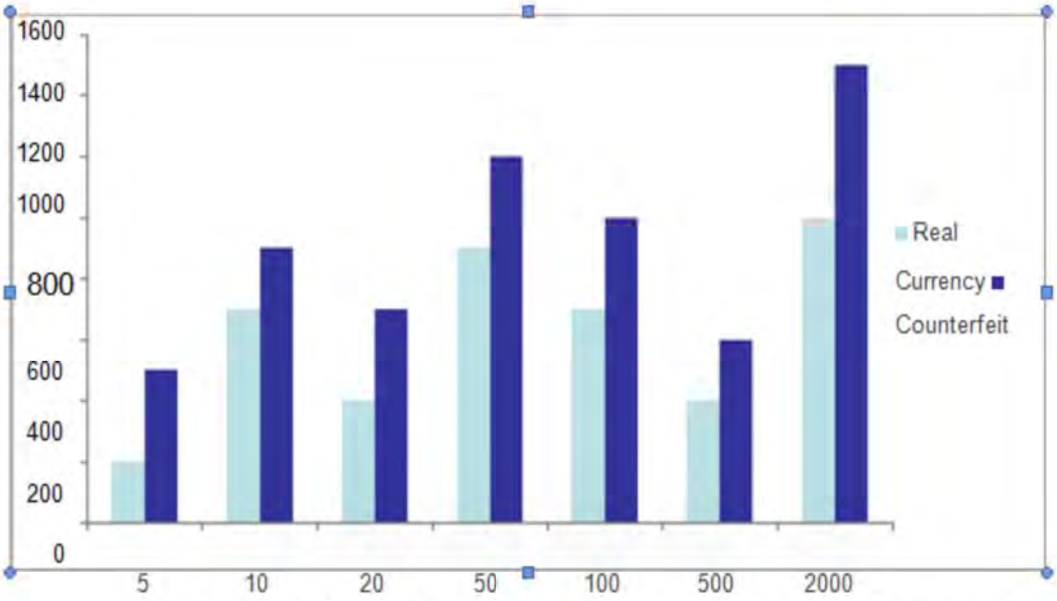

Figure 5.2.1: Frequency variation between genuine and fake currencies

Algorithm: Counterfeit_Detection

1. Start
2. Intialize Currency_Min_Val[][] array with minimum value of RED, GREEN, BLUE and CLEAR values of each currency.
3. Read Sensor1 with White LED and store results on REDW1, GREENW1, BLUEW1 and CLEARW1.
4. Read Sensor2 with White LED and store results on REDW2, GREENW2, BLUEW2 and CLEARW2.
5. Read Sensor1 with UV LED and store results on REDUV1, GREENUV1, BLUEUV1 and CLEARUV1.
6. Read Sensor2 with UV LED and store results on REDUV2, GREENUV2, BLUEUV2 and CLEARUV2.
7. Currency_no = Currency_Differentiation().
8. Check whether colour sensor outputs REDW1, GREENW1, BLUEW1, CLEARW1, REDW2, GREENW2, BLUEW2, CLEARW2, REDUV1, GREENUV1, BLUEUV1, CLEARUV1, REDUV2, GREENUV2, BLUEUV2, CLEARUV2 are less than minimum value of genie Currency which is stored in Min_Val[][].

```
9. If condition is TRUE return 1, indicating that Currency is counterfeit
10. Else return 0, indicating that Currency is genuine.
11. End
```

6.3 SIGNALING UNIT

One of the main reason that makes the visually impaired community unable to use the existing money counters is the way in which they notify their users about the counted sum or the detected counterfeit. Most of the devices use an LED or LCD display for the notification, hence a visually impaired person cannot efficiently use such a device. The signaling unit of the Smart Eye Wallet generates two kinds of outputs or notifications to their users, one a voice output and the other sequences of vibration.Voice output announces the denomination of the currency and hence is specifically designed for a visually impaired person. The vibration output generates a sequence of vibration for each denomination of the currency, and is specifically designed for the visually and hearing impaired community. The unit contains a vibration motor, HC05 Bluetooth interface, an android app designed specifically for the visually impaired community.

6.3.1 Algorithm: Bluetooth_Print

```
1. Switch ( Currency_no)
      i.    Case 0: Transfer „5‟ to Bluetooth Module.
      ii.   Case 1: Transfer „10‟ to Bluetooth Module.
      iii.  Case 2: Transfer „20‟ to Bluetooth Module.
      iv.   Case 3: Transfer „50‟ to Bluetooth Module.
      v.    Case 4: Transfer „100‟ to Bluetooth Module.
      vi.   Case 5: Transfer „500‟ to Bluetooth Module.
      vii.  Case 6: Transfer „2000‟ to Bluetooth Module.
      viii. Default: Transfer “COUNTERFEIT” to Bluetooth Module.
2. End
```

6.3.2 Algorithm: Vibration_Generate

```
1. Initialize array Pattern [][] with values {{5, 0}, {1, 1}, {2, 1}, {5, 1}, {1, 2},
   {5, 2}, {2, 3}}.
2. For i= 0 to Pattern[Currency_no][0]
      i.  Turn on Vibration Motor for 350ms.
      ii. Turn off Vibration Motor for 500ms.
3. For i= 0 to Pattern[Currency_no][1]
      i.  Turn on Vibration Motor for 200ms.
      ii. Turn off Vibration Motor for 500ms.
4. End.
```

7. Future Enhancement

Smart Eye Wallet is not a fully-fledged solution to the problem faced by the visually impaired, when dealing with money. Although it flawlessly identifies the denominations of the currency with an incredible precision, the accuracy of the device can be fine-tuned even further by choosing a more sensitive colour sensor. The same goes for counterfeit detection also, as of now we have only implemented the verification of one of many security features possible. Counterfeit detection can be strengthened to 99% and beyond by including the authentication of additional security features.

8. Conclusion

The project Smart Eye Wallet was our effort to help the visually impaired and the hearing impaired community achieve a sense of confidence and self-reliance when using the Indian currency. The Smart Eye Wallet is a simple device that is able to identify the denomination of a currency and to check its authenticity. It generates a voice message indicating the denomination, which enables the visually impaired person to know the value of the currency note. It also vibrates in different sequences, extending the use of the device to the hearing and visually impaired.

The device is “Smart” in the sense that it is precise, efficient and reliable. It identifies the denomination of the currency using only the frequency of reflected light from the currency and nothing else. These patterns of frequencies are given as input to the Artificial Neural Network (ANN) and that identifies the correct denomination by analyzing this complex pattern of frequencies. This device is a "wallet" in the sense that it can be carried around much like one. The Smart Eye Wallet hence, achieves its purpose. However, it is not a complete solution to the problems faced by the visually impaired when dealing with money. It can be improved even further. It is a fine example of one of the many powerful applications of the Artificial Neural Networks. This device gives an insight into a new and improved money counter and counterfeit detector, one which is portable, affordable, efficient and more importantly can enable the visually impaired community to use and handle money like any other ordinary person.

References

1. www.wikipedia.com
2. www.rhydolabz.com
3. www.nskelectronics.com
4. www.mitappinventor.com
5. https://www.rbi.org.in/currency
6. Simon Monk (2012) Programming Arduino. McGrawHill Education,Second Edn London
7. Michael Wright (2016) Hc-05 Bluetooth + Arduino.
8. C. RajaRao, Mahesh Boddu, Soumitra Kumar Mandal,(2015) Single Sensor Color Filter Array Interpolation Algorithms, Springer India
9. Michael McRobert (2010) Beginning Arduino, APress.

Nottingham | UK | 9–11 September 2019

Comparative study of companies with different focus on product longevity

Deepti Mahajan[1], Tim Cooper[2], David Smith[2]

[1,2] Nottingham Trent University, UK

[1]deepti.mahajan@.ntu.ac.uk

Abstract

Companies producing consumer durables for which high performance levels have been achieved may or may not opt to focus on product lifetime extension. Some companies have responded by promoting their products' reliability and durability by providing manufacturer guarantees, extended warranties and even lifetime warranties. Companies producing three types of products (large kitchen appliances, bicycles and clothing) with different foci on product longevity are studied in this paper. It reports on a comparison of warranties offered by these companies to address longevity in the products and highlights the commonalities and contrasts in their internal processes and in communicating this information. The findings suggest that the price points at which companies operate and warranties offered are not always comparable. Companies that are working towards differentiating products on longevity and companies that sell at the lowest price points use similar terminology as those used by companies that have longevity in their ethos, but have different meanings. Future interviews with key informants will be used along with this data to explore the role of business strategies to increase the uptake of longer lasting products.

Keywords: Product longevity, lifespan, consumer durables, warranties, product quality

1. Introduction

The objectives of a circular economy are to minimise resource depletion, keep resources in use as long as possible, manage waste appropriately and create less waste. Lately there has been increasing focus, by academics, on the transition of business into circular economy [1–3] which has shown that workable solutions are available. Academics have categorised various models practiced by companies in creating sustainable business and drivers for business model innovation [4], and have also suggested new models [1, 5]. According to Hockerts [6] the business case is the primary concern for companies in seeking corporate sustainability. Corporate sustainability leads to brand building, which may allow a company to charge a premium price. In the lifecycle of energy-using products, the use phase often has the most significant contribution to environmental impacts. Advancements in efficiency of the use phase has resulted in a greater focus on the production phase to reduce their environmental impact [7]. This can be adopted as a criteria to identify companies that manufacture products for longer lifespan. Some companies have responded by promoting their products' durability. Other companies, new and old, have gained attention and traction in the markets because their ethos is centred around product longevity and efforts are towards sufficiency (that is, consuming less) [8]. Consumer goods markets thus include a mix of companies with different levels of focus on product lifespans: (A) companies with product longevity as a core characteristic of their products, with longevity in their ethos, (B) companies that deliver some premium range products that are differentiated by longer lifespan or durability, and (C) companies that deliver some premium range products but without a specific focus on longevity, durability or reparability.

Product quality combines a variety of dimensions of a product, namely its performance, aesthetics, durability, reliability, upgradability, repairability, conformance and features. All of these may indicate the product's longevity, either in its technical specifications or through consumer attachment (or 'emotional durability') [9]. Together they form a complex array of specifications that may make it hard to judge the quality of a product, not least by consumers. Consumers need some indicator to simplify the process of identifying better products. Cues such as price and brand are often used by them to judge the quality of products [10]. Warranties may play the role in giving consumers confidence that producers and retailers stand by their products. Traces of companies' attempts to sell products on the grounds of their lifespan are sometimes evident in marketing. When developing and marketing products some companies focus on their core functionality, while others differentiate them by longevity.

A company which has product longevity in its ethos will be confident about its products and, we argue, would show this to its consumers by providing a warranty that is transferable, has no charges for returning, reinstalling or repairing, provides discretion of replacing or refunding to the consumer in the case of faults, and requires no effort by the customer beyond informing the company [11, 12]. Consumer durable companies, in general, provide warranties that are limited in one or more of these parameters.

2. Methods

Data used in this study were collected using a systematic process. The following parameters were considered to identify a specific product in each product category:

1. The product has minimal impact from fashion: in general, fashion restricts how long a product can be used.
2. Use variability is low, so that different brands and companies use similar price points for the same product as far as possible: this applies to shirts for office wear, for instance, whereas dresses were not considered suitable because they can be designed for office use, wedding, party, casual wear and so on, and thus price points vary.
3. The product is used on a regular basis such that the use frequency is high.
4. Consumers may have considered the lifespan of the product in their decision making and intend to use it for many years, as in the case of large kitchen appliances.
5. The market share for the specific product was utilised when data was available. For example, hybrid and road bikes together constitute about 36% of the UK bicycle market.

The specific product chosen for clothing was shirts, for large kitchen appliances it was washing machines and for bicycles, road and hybrid bikes. Companies in each product sector were listed from their industry association and those that sell the specific product were identified. Information for minimum and maximum price points at which the specific products are sold were listed from the company websites. Each company was then studied and evaluated for its degree of focus on longevity. Three focus levels were identified and are referred to below as company categories A, B and C.

A. Companies with product longevity as a core characteristic of their products, with longevity in their ethos,
B. Companies that deliver some premium range products that are differentiated on longer lifespan or durability
C. Companies that deliver some premium range products but without a specific focus on longevity, durability or reparability.

The criteria to classify companies in company categories A, B and C for product categories (large kitchen appliances, bicycles and clothing) evolved during the process of studying the companies in detail. Tables 1 and 2 list the criteria specific to product category.

3. Results

For large kitchen appliances: washing machines

Ideally, a washing machine should be able to work until eventually its mechanical parts wear-out due to material aging and fatigue and faulty parts can no longer be repaired or replaced [13]. A product's life is the life of its shortest-lived component. A company that has longevity in its ethos may thus provide warranty on the whole product and not on certain parts. Products that are manufactured for a longer lifespan typically have higher quality components and materials [7], and aim for emotional and economic durability [14].

Table 1: Criteria to classify companies for LKA

	A	B	C
Manufacturer's guarantee: 1. Full duration of ownership 2. Transferable 3. Free 4. If not repair, replacement or refund options both are available 5. No work for the consumer	All 5	Any 3	<3
Extended warranty: 1. Full duration of ownership 2. Transferable 3. Free 4. If not repair, replacement or refund options both are available 5. No work for the consumer	All 5	Any 3	<3
Spare parts availability	Lifetime	Declared	No mention
Guarantee on repair	Lifetime	Limited period	No mention
Promote second-hand market for their products	Yes	No	No

Almost all companies provide a manufacturer's guarantee of up to 2 years. Looking deeper into their warranties (both manufacturers' and extended) shows that most of the companies do not provide the five essentials of warranties and hence offer limited warranties. If warranties indicate companies trust their products, then limited warranties can imply that they do not believe in their products. Companies such as Miele claim that their washing machines are designed to work for 20 years, which is above the average lifespan of about 12.5 years [13], while Samsung, which sells some of its washing machines at comparable price points, has a warranty scheme of different durations for its components. Difference is warranties for products sold at similar price points shows that companies differ in their commitments towards consumers and confidence in their products. Companies in category C experiment with various options such as extended warranty for no fee on certain products only, or on particular parts. Companies, such as Indesit, provide extended warranties that offer consumers to not pay for parts but bear the cost of labour, which is generally high.

For bicycles: road and hybrid

In general, companies provide a guarantee for between 2 and 5 years but this may not be for all products offered by the company, and sometimes not for the full product but only on parts. Most provide a lifetime warranty on certain parts such as frames. Some companies also provide warranties on their second hand bikes such as Islabikes. Most bicycle companies are classified as B category. In category C, companies provide a limited warranty for their products. Almost all companies clearly specify that manufacturers' guarantees are non-transferable (whereas for washing machines this information is generally not provided explicitly).

Table 2: Criteria to classify companies for clothing

	A	B	C
Warranty	Lifetime warranty on all products (full product) or certain parts of all products	Lifetime warranty on some products (full product) or parts of some products but not all	As per minimum country requirements or no warranty
Promote second-hand market such as providing guarantee (lifetime or otherwise) for second owners	Yes	No	No
Repair services	Lifetime	Yes, but consumer pays for transport	No

For clothing: men and women shirts

For clothing, a different set of parameters evolved while studying the companies. Some companies provide a lifetime warranty and repairs for their products, such as Tom Cridland and Eileen Fischer. Eileen Fischer also provides free repairs for life and Tom Cridland provides three decades of free mending, Although their price points vary considerably, both companies provide free mending services for thirty years or lifetime. Most of the clothing companies do not provide any information about warranties and their sustainability efforts are generally focussed on transparent and environmentally responsible supply chain.

4. Discussion and Conclusion

Companies in category A are leaders in promoting longevity. Some of them are pioneers and, with their focus on longevity, are creating an example for other companies. Companies in category B are generally open to experimenting and may be struggling to create a business case for longevity. Companies in category C are followers and generally use terms related to longevity figuratively such as Hotpoint and Indesit, which claim to provide free replacement parts with the condition that the fitting is done by their own repair engineers.

In conclusion, the observations from this study indicate that there may not be a connection between the price points at which companies sell and their commitments towards producing longer lasting products. The next stage in this research is to confirm these observations in interviews with key informants in marketing and after-sales departments.

Acknowledgments

The research is a part of a PhD being undertaken at the Nottingham Trent University under the supervision of Prof. Tim Cooper and Prof. David Smith. The research is financially supported by the RCUK and University Alliance DTA-Energy.

References

1. Bocken NMP, Ritala P, Huotari P (2017) The Circular Economy: Exploring the Introduction of the Concept Among S&P 500 Firms. J Ind Ecol 21:487–490.
2. Schaltegger S, Burritt R (2018) Business Cases and Corporate Engagement with Sustainability: Differentiating Ethical Motivations. J Bus Ethics 147:241–259.
3. Boons F, Montalvo C, Quist J, Wagner M (2013) Sustainable innovation, business models and economic performance: an overview. J Clean Prod 45:1–8.
4. Bocken NMP, Short SW, Rana P, Evans S (2014) A literature and practice review to develop sustainable business model archetypes. J Clean Prod 65:42–56.
5. Beltramello A, Haie-Fayle L, Pilat D (2013) Why New Business Models Matter for Green Growth. OECD Green Growth Papers, 2013-01, OECD Publishing, Paris
6. Hockerts K (2014) A Cognitive Perspective on the Business Case for Corporate Sustainability.
7. Stamminger R, Tecchio P, Ardente F, et al (2018) Towards a durability test for washing-machines. Resour Conserv Recycl 131:206–215.
8. Bocken NMP, Short SW (2016) Towards a sufficiency-driven business model: Experiences and opportunities. Environ Innov Soc Transitions 18:41–61.
9. Haines-Gadd M, Chapman J, Lloyd P, et al (2018) Emotional durability design Nine-A tool for product longevity. Sustain 10:1–19.
10. Rao AR (2005) The Quality of Price as a Quality Cue. J Mark Res 42:401–405.

11. The European Parliament and the Council (1999) Directive 1999/44/EC of the European Parliament and of the Council of 25 May 1999 on certain aspects of the sale of consumer goods and associated guarantees.
12. United States Congress (1975) Magnuson-Moss Warranty-Federal Trade Commission Improvement Act. https://www.ftc.gov/enforcement/statutes/magnuson-moss-warranty-federal-trade-commission-impfrovements-act
13. Alfieri F, Cordella M, Stamminger R, Bues A (2018) Durability assessment of products: analysis and testing of washing machines. Publications Office of the European Union, Luxembourg
14. Cooper T (2004) Inadequate Life? Evidence of Consumer Attitudes to Product Obsolescence. J Consum Policy 27:421–449

ICESF 2019

Proceedings of

The International Conference on Energy and Sustainable Futures (ICESF 2019)

Edited by

Amin Al-Habaibeh, Abhishek Asthana, Vladimir Vukovic

The global warming and the increasing level of pollution and energy poverty in many areas worldwide give research in energy and sustainability a vital role in enhancing people's future. The International Conference on Energy and Sustainable Futures (ICESF 2019) is organised by Nottingham Trent University (NTU) in collaboration with Doctoral Training Alliance for Energy (DTA-Energy) and University Alliance. The conference is attended by experts in energy and sustainability from industry and academia, research students and early career researchers. The proceedings includes multi-disciplinary papers focused on academic research, industrial applications, and energy innovations and comprises a wide range of energy and sustainability themes such as renewable and clean energy, energy storage, energy management, transportation technology, internet of things, sustainable and resilient cities, condition monitoring and artificial intelligence.

NOTTINGHAM TRENT UNIVERSITY

ICESF
Nottingham | UK | 9–11 September 2019

DTA
Doctoral Training Alliance
Energy

University Alliance
Doctoral Training Alliance

ISBN 978-1-912253-01-2 (paperback)
ISBN 978-1-912253-02-9 (eBook)